Bio Thermo Kinetics

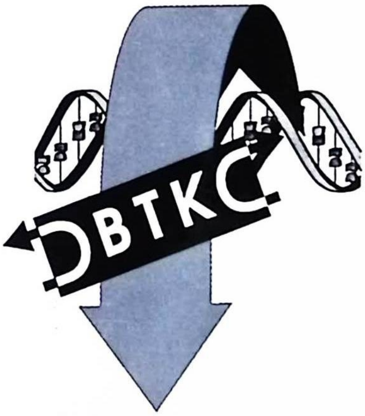

In The Post Genomic Era

BioThermoKinetics

In The Post Genomic Era

Edited by

Christer Larsson
Göteborg University
Inga-lill Påhlman
Göteborg University
Lena Gustafsson
Göteborg University

BioThermoKinetics In The Post Genomic Era
Edited by Larsson, C., Påhlman, I.-L. and Gustafsson, L.
Proceedings of the 8th international meeting on Biothermokinetics,
held July 2-5 1998 in Fiskebäckskil, Sweden

ISBN 91-630-7048-0

Printed by: Chalmers Reproservice
Göteborg 1998

Contents

Opening of the 8^{th} BTK Meeting

BTK traditions and perspectives: Complex biothermokinetics and control analysis 1
Westerhoff H.V., van Rotterdam B.J., van Heeswijk, Somsen O., Kholodenko, B.N.

Session 1: Control Analysis: Theory & Applications

Control analysis of adenylate-conserving cycles in the absence or presence of adenylate kinase 7
Hofmeyr J.S., Rohwer J.M.

Synthetic promoters for experimental control analysis 11
Andersen H.W., Schurmann R., Madsen K., Pedersen M.B., Koebmann B.J., Piskur J., Hammer K., Ruhdal Jensen P.

Mild mitochondrial transition pore opening during perfusion: top-down control analysis of mitochondria and organ ^{31}P-NMR analysis 18
Leducq N., Delmas-Beauvieux M.-C., Bourdel-Marchasson I., Dufour S., Gallis J.-L., Canioni P., Diolez P.

Metabolic control analysis of the Leloir pathway in *Saccharomyces cerevisiae* 22
Östergaard S., Olsson L., Nielsen J.

Relation between flux control coefficients and enzyme concentrations in states of minimized total amount of enzyme 27
Klipp E.

Evolutionary implications of metabolic control analysis for maximisation of rates of enzymes, pathways and physiological processes by natural selection 31
Brown G.C.

The influence of the LLD-ACV: BisACV ratio on a MCA of the penicillin biosynthetic pathway in *Penicillium chrysogenum* 35
Theilgaard H.A., Nielsen J.

Changes in enzyme expression and the control of metabolic flux 41
Fell D.A., Thomas S.

Using co-response coefficients and sensitivity analysis to explore physiological flux control and metabolite concentration regulation 46
Thomas S., Fell D.A.

The analysis of control distribution for catalytic cycle of inorganic pyrophosphatase of *Escherichia coli* 50
Nartisissov Ya.R., Kholodenko B.N.

An application of a flux control mapping to the kinetic model of a single enzyme 54
Nartisissov Ya.R.

Changes in energy metabolism of primary rat osteoblasts during differentiation 58
Komarova S.V., Rabkin B.A., Booker J.D., Ataullakhanov F.I., Globus R.K.

Regulation of glycolytic and oxidative phosphorylation pathways in mature osteoblasts 62
Komarova S.V., Rabkin B.A., Booker J.D., Ataullakhanov F.I., Globus R.K.

Metabolic control analysis reveals that glucose transport incompletely controls the glycolytic flux in *Trypanosoma brucei* 66
Bakker B.M., Mensonides F.I.C., ter Kuile B.H., Michels P.A.M., Opperdoes F.R., Westerhoff H.V., Walsh M.C.

Dynamics of coupled glycolytic oscillators 71
Wolf J., Heinrich R.

Separable matrices and unification of concepts in metabolic control analysis 76
Giersch C.

Functional interpretation of the flux control coefficient and excess capacity of cytochrome *c* oxidase at intracellular oxygen 81
Gnaiger E., Kuznetsov A.V., Lassnig B., Margreiter R.

High-resolution respirometry-optimum permeabilization of the cell membrane by digitonin 89
Gnaiger E., Kuznetsov A.V., Lassnig B., Fuchs A., Reck M., Renner K., Stadlmann S., Rieger G., Margreiter R.

Modelling calcium oscillations and coupling 96
Haberichter T., Hoefer T., Heinrich R.

Session 2: Metabolic Regulation, Control and Signaling

Yeast growth on mixed substrates. Repression or induction? 97
Somsen O.J.G., Snoep J.L., Westerhoff H.V.

Control analysis of cellular signal transduction pathways 102
Kholodenko B.N., Hoek J.B., Brown G.C., Westerhoff H.V.

Metabolic design: Engineering a living cell to desired metabolite concentrations and fluxes 108
Kholodenko B.N., Hoek J.B., Westerhoff H.V., Cascante M., Schwaber J.

CPT I: A reassesment of its role in control over ketogenic flux 113
New K.J., Eaton S., Elliott K.R.F., Quant P.A.

Growth of *Echerichia coli* on C_4-dicarboxylates is significantly controlled by the C_4-dicarboxylate transporter 117
Boogerd F.C., Boe L., Michelsen O., Ruhdal Jensen P.

Implications of the oxygen dependency of flux control of cytochrome *c* oxidase 123
Kunz W.S., Wiedemann F.R., Elger C.E.

Regulation analysis of mitogen T-cell activation – the effects of concanavalin A on thymocyte respiration 128
Krauss S., Buttgereit F., Brand M.D.

Autooscillation regimes and bistability in blood coagulation 132
Zarnitsina V.I., Ataullakhanov F.I.

Kinetic analysis of oxidative phosphorylation in rat liver and heart mitochondria after chronic alcohol feeding 137
Mildaziene V., Marcinkeviciute A., Hoek J.B., Kholodenko B.

Metabolic control by the redox-state of the Q-pool in the respiratory network of *Paracoccus denitrificans* 142
Otten M.F., Reijnders W.N.M., Bedaux J.J.M., Westerhoff H.V., Krab K., Van Spanning R.J.M.

The reversible effect of calcium overload on oxidative phosphorylation in heart mitochondria oxidizing different substrates 147
Mildaziene V., Marcinkeviciute A., Baniene R., Morkunaite S.

Polyunsaturated fatty acid deficiency and yield of oxidative phosphorylation: Role of adenine nucleotide carrier 152
Nogueira V., Piquet M.A., Devin A., Fontaine E.M., Sibille B., Filippi C., Brandolin G., Rigoulet M., Leverve X.M.

Hierarchical control of DNA supercoiling 157
Snoep J.L., van der Weijden C.C., Andersen H.W., Ruhdal Jensen P., Westerhoff H.V.

Cancer chemotherapy in terms of metabolic control analysis 163
Lankelma J., van der Wel H., Westerhoff H.V.

Control of the F_1F_0 ATP synthase on cell metabolism and growth in *Saccharomyces cerevisiae* 167
Raamsdonk L.M., Berden J.A., Westerhoff H.V., van Dam K.

Hierarchical control of the H^+-ATPase on cytochrome expression in *Escherichia coli* 171
Koefoed S., Ruhdal Jensen P., Egger L., Westerhoff H.V., Snoep J.L.

Kinetics of peroxidases in guinea pig bone marrow under immunostimulation 175
Keyhani E., Zarei M.A., Lashgarblooki-Livani T.

Session 3: Biological Energy Transformations & Non-Equilibrium Thermodynamics and Kinetics

Kinetics, thermodynamics and control analysis of ATP homeostasis in contracting skeletal muscle 179
Jeneson J.A.L., Wiseman R.W., Kushmerick M.J., Westerhoff H.V.

Flow-force relation of mitochondrial oxidative phosphorylation in rat fast-twitch skeletal muscle 183
Wiseman R.W., Jeneson J.A.L.

Optimal stoichiometric designs of ATP producing systems using genetic algorithms 186
Stephani A., Nuno J.C., Heinrich R.

Mitochondrial H^+/O ratio is independent of membrane potential and respiration rate in isolated hepatocytes 192
Ainscow E.K., Brand M.D.

Modelling of the fast phase of chlorophyll fluorescence induction 196
Lebedeva G.V., Belyaeva N.E., Riznichenko G.Yu., Demin O.V.

The regulation of mitochondrial ATP synthesis in skeletal muscle during the transition from exercise to rest 200
Kemp G.J., Roussel M., Bendahan D., Lefur Y., Cozzone P.J.

The glycolytic flux in *E.coli* appears to be controlled by the demand for ATP 205
Koebmann B.J., Nilsson D., Snoep J.L., Westerhoff H.V., Ruhdal Jensen P.

Antimycin induced change in catalytic mechanism of succinate ubiquinone reductase can be responsible for bell-shaped dependence of superoxide generation on [succinate]/[fumarate] ratio **211**
Vasenko A., Demin O.V.

Modeling of free-energy metabolism in *Lactococcus lactis* **215**
Pedersen M.B., Winterberg H., Ruhdal Jensen P.

Response times of muscle membrane potential to variations in potassium conductance depend on chloride transport **221**
Geukes Foppen R.J., van Mil H.G.J., Siegenbeek van Heukelom J.

ATP regulation of cytochrome oxidase in yeast mitochondria: Role of subunit VIa **226**
Beauvoit B., Bunoust O., Guérin B., Rigoulet M.

The oscillatory regime of the ATP synthesis reaction catalysed by the F_1F_0-ATPase of submitochondrial particles **231**
Bronnikov G.E., Vinogradova S.O.

Kinetics of KCN binding cytochrome *d* in *Salmonella typhimurium* **236**
Keyhani E., Minai-Tehrani D.

Session 4: Metabolic Pathways, Compartments and Channels & Transient Regulation of Metabolism

Regulation through moiety conservation: the role of product sensitivity in glycolysis of yeast and trypanosomes **240**
Teusink B., Menesonides F.I.C., Bakker B.M., Walsh M.C., Snoep J.L., van Dam K., Westerhoff H.V.

Correlation of glucose catabolism and the frequency of glycolytic oscillations in *Saccharomyces cerevisiae* **246**
Reijenga C.A., Teusink B., Van Verseveld H.W., Snoep J., Westerhoff H.V.

Control of glycolytic influx monitored through site-directed mutagenesis of yeast hexokinase PII **250**
de Winde H., Kraakman L., Winderickx J., Thevelein J.M.

Infrared thermographic analysis of yeast and adipocytes in microtiter plates **256**
Paulik M.A., Buckholz R.G., Lancaster M.E., Dallas W.S., Hull-Ryde E.A., Weiel J.E., Lenhard J.M.

Experimental strategies to analyse the control of glycolysis in *Lactococcus lactis* **261**
Andersen H.W., Pedersen M.B., Hammer K., Ruhdal Jensen P.

Role of mitochondrial acetaldehyde oxidation in respiratory metabolism of yeast *Saccharomyces cerevisiae* 268
Boubekeur S., Rigoulet M., Bunoust O., Castroviejo M., Guérin B.

Diffusion limitation of oxygen versus ADP in permeabilized muscle fibers 273
Kuznetsov A.V., Lassnig B., Margreiter R., Gnaiger E.

Influence of nutrient starvation on sugar uptake kinetics of *Saccharomyces cerevisiae* 277
Albers E., Walsh M.C., Sjöström S., Gustafsson L.

Control by water: The osmotic stress concept and its critics 282
Nicholls P.

Effect of pathological levels of hydrogen peroxide on control of ketogenic flux in hepatocytes isolated from neonatal rats 287
Patil K.K., Eaton S., Quant P.A.

Effects of membrane potential on the sensitivity of mitochondria from brown adipose tissue and liver to fatty acids 291
Matthias A., Cannon B., Nedergaard J.

A kinetic model of mitochondrial Ca^{2+} excitability 295
Selivanov V.A., Ichas F., Mazat J.-P.

Chloride in skeletal muscle fibres: Volume control or regulation? 300
Siegenbeek van Heukelom J., van Mil H.G.J., Foppen J.G.

Modelling and quantification of carbon fluxes in photosynthesizing cells of intact leaves *in vivo* 303
Keerberg O., Pärnik T.

An increase in NAD^+ concentration affects fluxes through glycolysis and neoglucogenesis in isolated rat liver cells 307
Devin A., Guérin B., Rigoulet M.

Aerobic-anoxic transitions and regulation of mitochondrial oxygen flux 312
Lassnig B., Kuznetsov A.V., Margreiter R., Gnaiger E.

Energy-dependent maintenance of cell redox potentials 317
Berry M.N., Grivell A.R., Grivell M.B., Phillips J.W.

Is the glycolytic flux conditionally controlled by the ATP concentration in *Saccharomyces cerevisiae*? 323
Larsson C., Nilsson A., Påhlman I.-L., Blomberg A., Gustafsson L.

Modulation of rats digestive glands resistance to action of ionizing radiation by means of sodium alfa-ketoglutarate 329
Kurgaliuk N., Goryn O.

Session 5: Metabolic Modeling & Applications

Elementary modes analysis illustrated with human red cell metabolism 332
Schuster S., Fell D.A., Pfeiffer T., Dandekar T., Bork P.

Retro-regulation of the bacterial phosphotransferase system: A kineticmodel 340
Rohwer J.M., Hofmeyr J.-H. S., Postma P.W.

Numerical optimisation and simulation for rational metabolic engineering 345
Mendes P., Kell D.B.

A kinetic model of interleaflet transport of lipids mediated by pore-forming proteins 350
Frickenhaus S., Heinrich R.

Combined effects of Ca-dependent potassium channels and adenylate metabolism in human erythrocytes volume stabilization 355
Martinov M.V., Vitvitsky V.M., Ataullakhanov F.

Can deficiency of non-key glycolytic enzymes in erythrocytes lead to hemolytic anemia?: A mathematical model 360
Vitvitsky V.M., Martinov M.V., Plotnikov A.G., Ataullakhanov F.I.

How do mitochondrial enzymes control the respiration and superoxide production rates 365
Demin O.V., Westerhoff H.V., Hoek J.B., Kholodenko B.N.

Heart and non-synaptic brain mitochondrial H_2O_2 production does not increase in proportion to O_2 consumption during the state 4 to state 3 transition. Main free radical generation at complex I 370
Herrero A., Cadenas S., Barja G.

Simulation of the epidermal growth factor signal transduction pathway 375
Brightman F.A., Fell D.A.

The control of glucose transport on glycolysis in the yeast *Saccharomyces cerevisiae* 378
Diderich J.A., Valkier J., Anjos J., Spencer-Martins I., van Dam K., Walsh M.C.

Modeling the fluxes of reducing equivalents in microaerobic RQ-controlled continuous cultures of *Saccharomyces cerevisiae* 383
Franzén C.-J., Niklasson C.

Mathematical modelling of biochemical pathways 388
Nielsen J.

Preface

BTK'98, the eigth meeting of the international Study Group for BioThermoKinetics

A main purpose of the international Study Group for BioThermoKinetics is to promote "*an extensive exchange of information and a closer collaboration between those scientists who try to assess biological processes by means of thermodynamics and/or kinetics. It should provide a forum for open discussions in a relatively small group of interested people; in particular young scientists should have the opportunity to present their ideas without the stress of appearance on an international congress. The subject to be discussed should include open problems, work in progress and unpublished material which requires that such information is not 'abused' or made available to persons not being member of the group*". This declaration is quoted from a letter (dated June 18, 1981) of the first acting chairman, Dieter Walz. The history and intentions, including this quotation, of the BTK Study Group is nicely described in the Introduction of the Proceedings of the BTK'96 by the now acting chairman Hans V. Westerhoff. I have repeated this declaration in order to remind us all of that the international Study Group for BTK are heading to arrange meetings where not resolved questions are openly discussed and where questions about biological processes may be reformulated because of lively discussions among interested people.

The invitation to the BTK'98 therefore reads:

The international study group on BioThermoKinetics - BTK - invites everyone to present her/his most recent and exciting results concerning the Thermodynamics, Kinetics, Regulation, or Control of Biological Systems. In particular contributions are encouraged that promote synthesis between theoretical and experimental approaches, or that examine the above topics quantitatively. BTK meetings are aimed at promoting (i) understanding of the quantitative sciences that are relevant to the field, (ii) rapid progress in the research in the field through synergism between the work of participants, and (iii) applications in medical and biotechnological contexts. Since the primary aim of the meeting is to encourage discussions between the most active scientists in the BTK field, sessions are organised so as to include a final discussion of each session's main topic with reference to the poster presentations. Accordingly, much attention will be given to the poster presentations. Lectures mainly serve to present an overview of a topic and provoke discussion of unresolved issues. All participants are requested to contribute with a poster, also presented as a mini-paper in the BTK proceedings, which will be available to the participants during the meeting.

The BTK'98 meeting with the notion "*In The Post Genomic Era*" is indicating the new powerful tools that are now available to reach a new level of understanding of the regulation or control of biological processes. The different sessions of the BTK'98 meeting has been organised as to promote discussions between people that have assessed different approaches to resolve questions of biological processes. Session 1, "*Control Analysis": Theory and Applications*", is arranged to confront advanced experimental and theoretical approaches in the field of control analysis. Session 2, "*Metabolic Regulation, Control and Signalling*", is to promote discussions of the whole metabolic process, from signalling to regulation and control. Session 3, "*Biological Energy Transformations & Non-equilibrium Thermodynamics and Kinetics*", is devoted to thermodynamic and kinetic approaches of biological energy transformations. Is there a contradiction? Session 4, "*Metabolic Pathways, Compartments and Channels & Transient Regulation of Metabolism*", is trying to address the whole complexity of biological systems. Not only are many biological systems facing a varying environment, but are also challenged with cross-talking between metabolic pathways and compartments involving channels and/or other communicative ways. Session 5, "*Metabolic Modelling & Applications*", is addressing advanced modelling work in order not only to describe metabolic processes in mathematical terms but also to simplify the interpretation of attained experimental data and to question our way of believed logical thinking! This session is last but not least devoted to discussions about the relevance of our work to applied processes.

The BTK'98 meeting has been organised by a local committee consisting of Eva Albers, Anders Blomberg, Christer Larsson, Gunnar Lidén, Annika Nilsson; IngaLill Påhlman, Hadi Valadi, Lena Gustafsson (all from Göteborg) extended by the acting chairman of BTK, Hans Westerhoff (Amsterdam). This committee is grateful for the support gained by the international advisory committee of the meeting consisting of David Fell (Oxford), Erich Gnaiger (Innsbruck), Reinhart Heinrich (Berlin), Jacqueline Hoerter (Chatanay Malabry), Jannie Hofmeyr (Stellenbosch), Douglas Kell (Aberystwyth), Jean-Pierre Mazat (Bordeaux), Jens Nielsen (Copenhagen), Michel Rigoulet (Bordeaux), Stefan Schuster (Berlin), Jacky Snoep (Amsterdam) and Karel van Dam (Amsterdam).

This book has been prepared (the proceedings) by Christer Larsson and the other editors, with help in the reviewing procedure by the chairpersons of each session (Jannie Hofmeyr, Reinhart Heinrich, Jean-Pierre Mazat, Stefan Schuster, Hans Westerhoff, Erich Gnaiger, Lena Gustafsson, Jacqueline Hoerter, Gunnar Lidén and Karel van Dam) and their groups and some other people. Not to forget anyone, the organising committee gratefully acknowledge all people that have helped us in this work. Thank you all.

To be judged from the proceedings, we can all be looking forward to a stimulating meeting. I hereby wish all participants most welcome to Göteborg – Gullmarsstrand on July 2. The BTK'98 meeting will continue directly after the EBEC Conference that will last during the period June 27 to July 2 in Göteborg, from where will together continue to Gullmarsstrand located in a nice environment at the sunny West coast of Sweden.

Göteborg, June 22, 1998

Lena Gustafsson

Lena Gustafsson

1

BTK TRADITIONS AND PERSPECTIVES: COMPLEX BIOTHERMOKINETICS AND CONTROL ANALYSIS

Hans V. Westerhoff[1,2], *Bart J. van Rotterdam*[2], *Wally C. van Heeswijk* [1], *Oscar Somsen*[1], *Boris N. Kholodenko*[3]

E.C. Slater Institute[1] and Institute for Molecular Biological Sciences[2], BioCentrum Amsterdam, Faculty of Biology, Free University, De Boelelaan 1087, NL-1081 HV Amsterdam, The Netherlands, and Department of Pathology, Anatomy and Cell Biology, Thomas Jefferson University, Philadelphia[3].

INTRODUCTION

Biology is subject to all principles of physics and chemistry. Yet, it is in biological systems that we recognize a degree of sophistication that is unsurpassed by almost all other systems. Faced with solving the Schrödinger equation for four interacting particles, and not being able to do so analytically, some physicists used to conclude that biology is 'complicated', and in fact, more complicated than to be amenable to the methods of physics. Because the four atoms in the example, and the billions and billions of atoms in biological systems were expected to be just more of the same as compared to the system of three particles that could be solved analytically, biology was not even going to be fundamentally interesting. This physicists' view of biology has disappeared, with the increased interest in mathematical complex systems. In the latter it was most impressive that very simple systems of equations could give rise to highly complex patterns in time and space. Neither the sets of equations nor the physical systems they might represent were complicated in the sense of consisting of many components or of many interactions. Yet they could be called '*complex*' in the sense of consisting of closely connected parts, where the connectedness rather than the parts individually gave rise to the complex behavior.

As compared to the simple systems of equations that have become a strange attractor to many scientists, biology has the disadvantage that it is not only complex, but also complicated. In recent years, this disadvantage has faded; the composition of certain entire living cells is largely known. Experimentation now allows one to manipulate and study the living cell. Moreover, computer hardware and software have improved such that cell behavior can be simulated in the computer. Accordingly the live cell is ready for students of complexity.

What is BioComplexity research? BioComplexity research focuses on the mechanisms by which in biological systems, due to the interaction of parts of the system, new behavior arises that is relevant for its biological function. The emergence of new behavior can be characterized in either of two ways: (i) the difference between the behavior of the system on the one hand and the sum of the behaviors of the components in the absence of the interactions on the other hand, or, (ii) the difference between the behavior of a component in the presence and in the absence of its interactions with the other components.

Here we introduced the term '*Bio*Complexity', to emphasize that the scientific topic of *biological* complex systems differs from that of Complex Systems more in general. BioComplexity is tied to understanding the mechanisms involved in attaining biological function. BioComplexity research will deal with real systems that may be low on the scale of complexity, but high on the scale of functionality. Here we will try to catalyze this area of research a little by giving a few examples of perhaps the simplest cases of BioComplexity. We will show that Mosaic Non Equilibrium Thermodynamics and Metabolic/Hierarchical Control Analysis already embody important aspects of BioComplexity research. We will also review and suggest extensions to MCA that may remove some of its limitations in view of other aspects.

Back pressure on light-driven systems

The free energy contained in a photon vastly exceeds the proton electrochemical potential difference across energy coupling membranes ($\Delta\tilde{\mu}_{H^+}$): Physical chemically, light driven proton pumping need not be sensitive to back pressure exerted by $\Delta\tilde{\mu}_{H^+}$. Accordingly the light-driven proton pumps might be the most likely exceptions to the proposition that all bio-molecules *in vivo* are subject to their BioComplex environment.

Through a Mosaic Non Equilibrium Thermodynamic (MNET) analysis it has been shown that the proton pumping by Bacteriorhodopsin *is* sensitive to such back pressure [1]. However, the more abundant light driven proton pumping in Nature is catalyzed by the chlorophyll based photosynthetic reaction centers of plants, algae, and most photosynthetic Bacteria. As had been done for Bacteriorhodopsin, bacterial photosynthetic reaction centers were incorporated into liposomes and the transmembrane electric potential difference was measured as a function of light intensity (I) and proton permeability (L_H^l). Plotting the inverse of minus the (negative) $\Delta\tilde{\mu}_{H^+}$ versus the inverse of the illumination intensity at various concentrations of protonophore, a behavior was found that differed from that of Bacteriorhodopsin [2]. The previous description did not account for the possibility that independently of $\Delta\tilde{\mu}_{H^+}$ the photochemical reaction cycle of the reaction centers might saturate at high light intensities. Allowing for such saturation (and a corresponding half maximum light intensity, $I_{0.5}$), the following equation was derived [Van Rotterdam *et al.*, in preparation] and shown to be fully consistent with the experimental observations:

$$\frac{1}{-\Delta\tilde{\mu}_{H^+}} = \frac{\gamma}{a_v} + \frac{L_H^l}{l_v \bullet a_v} \bullet \left(\frac{I_{0.5}}{I} + 1\right) \qquad \text{Eq. 1}$$

Here l_v represents the concentration of the light driven proton pump, a_v the (light intensity independent) thermodynamic driving force of the photon and γ quantifies the back pressure effect; γ equals zero in the absence of back pressure and is highly positive if the back pressure effect is strong. The lines in the above mentioned plots intersected in the second quadrant [Van Rotterdam *et al.*, in preparation], revealing that γ exceeded zero hence that the photosynthetic reaction centers were subject to back pressure by $\Delta\tilde{\mu}_{H^+}$. This observation indicates that even the light driven proton pumps that are at the origin of bioenergetics, do not function irrespectively of their biological environment. They too are BioComplex.

Transitions in Control through tight binding

Ammonia assimilation in *E. coli* is subject to appreciable regulation. A dual, twolegged cascade of regulatory proteins manages both the transcription and the covalent modification of glutamine synthetase. We have been interested in the control on signal transduction exerted by the presumably pivotal protein PII, which sits where the two legs of the cascade diverge. Previously we found that PII does not control GS demodification in cells that had been grown in the absence of ammonia, because of the presence of its twin protein GlnK. When cells were grown in the presence of ammonia, GlnK was absent. When they were then depleted of the ammonia, PII still did not control GS demodification. When PII concentration was reduced however, its control *abruptly* increased to close to 0.8 [3].

GS demodification is catalyzed by the bifunctional enzyme adenylyltransferase (ATase). The concentration of this protein is about three times that of the wild type concentration of PII. Because PII is a trimer, this implies that at the wild type level, the cellular amounts of PII and ATase are stoichiometric. If the dissociation constant of the ATase-PII complex were much smaller than the total concentration of ATase and if active ATase had full control on GS demodification rate, then the *abruptness* of the increase in control could be understood, because the fraction of ATase activated by (modified) PII, should be given by:

$$\frac{[ATase-PII_{complex}]}{[ATase_{total}]} \cong \frac{[PII_{total}]}{[ATase_{total}]} \quad for \quad \frac{[PII_{total}]}{[ATase_{total}]} < 1, \quad else \quad \cong 1 \qquad \textbf{Eq. 2}$$

If this explanation is correct, then the implication is that in the intact cell, the regulatory protein PII is fully complexed with the protein it regulates; protein-protein associations and corresponding biocomplex behavior, dominate control and regulation. Metabolic Control Analysis does not naturally take this type of feature into account. The importance of protein protein association also increases the likelihood that there is a strong difference between control and regulation inside the living cell and control and regulation in dilute solution biochemistry. The latter may not always mimic the high protein concentrations *in vivo*. It may prove important to adjust the conditions for *in vitro* biochemistry so as better to mimic the crowded *in vivo* conditions. At least in some cases it seems that the *in vitro* conditions can be mimicked by adding polyethylene glycol to simulate macromolecular crowding [4].

Complex Control Analysis

Metabolic Control Analysis (MCA) has been developed most extensively for fluxes and concentrations in metabolic pathways with unique, asymptotically stable, steady states [1]. Gratifying are the summation laws, in which the principle of the, possibly distributed, total flux control of 1, replaces that of the single rate-limiting step, and the connectivity laws relating control properties in a fluxing system to enzyme properties. These laws can be summarized as:

$$\mathbf{C} = \mathbf{E}^{-1} \qquad \textbf{Eq. 3}$$

Here **E** is a matrix of elasticity coefficients and some coefficients that reflect the structure of the pathway [5]. **C** is a matrix of control coefficients. Elasticity coefficients are kinetic properties of enzymes. Control coefficients quantify the extent to which an enzyme in the pathway controls a flux or concentration. Let us briefly illustrate this for the simplest possible metabolic pathway (which has been analyzed before, but not precisely from this perspective):

$$S \xleftrightarrow{e_1} X \xleftrightarrow{e_2} P \qquad \text{Eq. 4}$$

$$\mathbf{C} = \begin{pmatrix} C_1^J & C_2^J \\ C_1^X & C_2^X \end{pmatrix} = \begin{pmatrix} \frac{\varepsilon_X^2}{\varepsilon_X^2 - \varepsilon_X^1} & \frac{-\varepsilon_X^1}{\varepsilon_X^2 - \varepsilon_X^1} \\ \frac{1}{\varepsilon_X^2 - \varepsilon_X^1} & \frac{-1}{\varepsilon_X^2 - \varepsilon_X^1} \end{pmatrix} = \begin{pmatrix} 1 & -\varepsilon_X^1 \\ 1 & -\varepsilon_X^2 \end{pmatrix}^{-1} = \mathbf{E}^{-1} \qquad \text{Eq. 5}$$

so that, for instance:

$$C_1^X = \frac{1}{\varepsilon_X^2 - \varepsilon_X^1} \neq \frac{1}{-\varepsilon_X^1} \qquad \text{Eq. 6}$$

Eq. 6 demonstrates that the control coefficient of an enzyme with respect to a metabolite concentration is *not* just equal to the inverse of an elasticity coefficient of that enzyme with respect to that metabolite concentration, but rather to an element of the inverse of an entire matrix of elasticity coefficients of all enzymes in the systems with respect to all metabolites. This is a signature of the complexity of the control of metabolic pathways: control by an enzyme is a function of the kinetic properties of all enzymes in the pathway not just of that enzyme by itself. This conclusion is well known to experts of Metabolic Control Analysis, but is here highlighted as an indication that Metabolic Control Analysis can be an important tool in the analysis of BioComplexity.

Continuing in the formalism of Reder [6], we shall directly discuss the system in terms of the independent variables (as denoted by superscript 0). The matrix of elasticity coefficients of reactions with respect to the independent metabolic variables is denoted by $\tilde{\varepsilon}^0$, the matrix of concentration control coefficients with respect to the independent reaction rates **v**, as $\tilde{\mathbf{C}}^0$. The ~ on top of the coefficients implies that they correspond to the absolute rather than the log-log derivatives. The network stoichiometry matrix ($\mathbf{N}^0$) is defined by the second and third term of the equation that applies to any parameter variation for which the system reattains steady state:

$$0 = d\frac{d\mathbf{X}^0}{dt} = \mathbf{N}^0 \cdot \mathrm{d}\mathbf{v} = \mathbf{N}^0 \cdot \mathbf{dv} + \mathbf{N}^0 \cdot \tilde{\varepsilon}^0 \cdot \tilde{C}^0 \cdot \mathbf{dv} \qquad \text{Eq. 7}$$

Since this is true for an *arbitrary* modulation of the reaction rates, Reder found the following expression for the concentration control coefficients in terms of the elasticity coefficients:

$$\tilde{C}^0 = -\left(\mathbf{N}^0 \cdot \tilde{\varepsilon}^0\right)^{-1} \cdot \mathbf{N}^0 = -(\mathfrak{J})^{-1} \cdot \mathbf{N}^0 \qquad \text{Eq. 8}$$

$\mathfrak{J}$ is called the Jacobian of the system. For the pathway of Eq. 4 this reads as:

$$\tilde{C} = \begin{pmatrix} \frac{1}{\tilde{\varepsilon}_X^2 - \tilde{\varepsilon}_X^1} & \frac{-1}{\tilde{\varepsilon}_X^2 - \tilde{\varepsilon}_X^1} \end{pmatrix} \qquad \text{Eq. 9}$$

which is consistent with Eqs. 5 and 6. In the case of a simple metabolic pathway, the elasticity of enzyme 1 with respect to its product X is negative and the elasticity of reaction 2 with respect to its substrate X is positive. Accordingly, the Jacobian of the system, *i.e.*, $\Im = \tilde{\varepsilon}^1_X - \tilde{\varepsilon}^2_X$ is negative.

Here we are interested in cases where the latter condition is not necessarily met, for instance because enzyme 1 is product stimulated. With increasing strength of this product stimulation $\tilde{\varepsilon}^1_X$ becomes more and more positive, such that ultimately, but not immediately the Jacobian becomes equal to zero (*i.e.*, when $\tilde{\varepsilon}^1_X = \tilde{\varepsilon}^2_X$). At that bifurcation point the concentration control coefficients become infinite. This reflects that the system has become structurally unstable, *i.e*, that a small change in enzyme activity value can cause an infinitely larger change in metabolite concentration. In mathematical analyses this point is eliminated because it is demanded that the Jacobian not equal zero.

Our interest continues to the situation 'past' this bifurcation point, *i.e.*, where the Jacobian becomes positive. Just using the equations derived by Metabolic Control Analysis, one then calculates control coefficients such that enzyme 1 exerted negative control on metabolite X and enzyme 2 positive control on metabolite X. It is not clear how much of a warning such results would give to the user of Metabolic Control Analysis; the implication of a non-negative Jacobian is that the fixed point is a unstable. Because of the fluctuations of the system, such a state that is steady in the mathematical sense, will not be steady in the physical/chemical/biological sense.

Bifurcations of the above type are important for biological systems. They are often accompanied by the phenomenon of multiple fixed points. For a given set of parameters, a system may have three fixed points, one unstable, and two stable steady states. The actual state assumed by that system then depend on the initial conditions of the metabolic variables. Through a minor and temporary modulation of the independent variables, the system can be driven into either of the two stable steady states. Thus, a biological structure in development can become a wing or a leg, depending perhaps on such a minor and temporary modulation of a metabolic variable. Such phenomena certainly belong to BioComplexity and it should be worthwhile to examine to what extent MCA can address such cases.

To examine this issue, we make explicit the modulation that corresponds to the definition of a control coefficient. A parameter is modulated that selectively affects a reaction rate. A metabolic variable is noted to change in time. In the case of asymptotically stable steady states, the variable relaxes to a new steady state value. The alteration in the parameter value causes an instantaneous change δ**v** in the reaction rate vector **v**. The vector of metabolite concentrations will subsequently vary with time as follows [7, 8]:

$$\mathbf{X}^0_r(t) = \mathbf{X}^0(t) - \mathbf{X}^0(0) = -(\mathbf{I} - e^{\Im \cdot t}) \cdot \Im^{-1} \cdot \mathbf{N}^0 \cdot \delta \mathbf{v} \qquad \textbf{Eq. 10}$$

Earlier [1, 8] we defined the time dependent control coefficient as the time dependence of the change in concentration of a metabolite after a change in activity of an enzyme, divided by that infinitesimal change in activity of that enzyme. For this control coefficient Eq. 10 implies [8]:

$$\tilde{\mathbf{C}}^0(t) = -(\mathbf{I} - e^{\Im \cdot t}) \cdot \Im^{-1} \cdot \mathbf{N}^0 \qquad \textbf{Eq. 11}$$

This equation is now valid for both stable and unstable steady states. For the case of asymptotically stable steady states this control coefficient approaches the traditional one as time passes [*cf.*, 1,8]:

$$\lim_{t\to\infty}\tilde{\mathbf{C}}^0(t) = \lim_{t\to\infty} -(\mathbf{I}-e^{\mathfrak{I}\cdot t})\cdot\mathfrak{I}^{-1}\cdot\mathbf{N}^0 = -\mathfrak{I}^{-1}\cdot\mathbf{N}^0 = \tilde{\mathbf{C}}^0 \quad \text{if } \mathfrak{I} \quad \text{negative definite} \qquad \textbf{Eq. 12}$$

For non stable steady states, the expression for the control coefficient given by this equation will go to infinity. This can be envisaged most clearly for the case where the vector of independent metabolite concentrations is one dimensional and the Jacobian is positive, as in the above example.

In the case in which there are two independent metabolite concentrations, the time dependent control coefficient has a two dimensional time dependence. If the Jacobian then has *complex* eigenvalues, the control coefficient becomes a periodic function of time. If the real part of the eigenvalues is negative, the (real) control coefficient converges in an oscillating way to its traditional magnitude. If the real part of the eigenvalues is positive, the control coefficient diverges as time progresses and becomes ill defined [9]. This by itself does not constitute a Metabolic Control Theory for oscillating systems in the sense that we avail of a Metabolic Control Theory for systems at steady state. It does however clarify how traditional Metabolic Control Analysis would reflect that a system is oscillatory in nature. For a more complete Metabolic Control Theory of oscillating systems we refer to other recent theoretical developments [9, 10].

We have shown here that the control coefficients can be made to deal with oscillating systems, reminiscent of the cell cycle, of Calcium or glycolytic oscillations. It is in the cases of oscillations that 'Complex' Control Analysis obtains a double meaning.

REFERENCES:

1. Westerhoff, H.V. & Van Dam, K. (1987) Thermodynamics and Control of Biological Free Energy Transduction, Elsevier, Amsterdam.
2. Van Rotterdam, B. J., Westerhoff, H. V., Bloch, D. A., Hellingwerf, K. J., Jones, M. R., & Crielaard, W. (1996) In BioThermoKinetics of the Living Cell (Westerhoff, H. V., Snoep, J. L., Sluse, F. E., Wijker, J. E., & Kholodenko, B. N., Eds.), pp. 231-236, BTK Press, Amsterdam.
3. Van Heeswijk, W.C. (1998) Ph D Thesis, University of Amsterdam.
4. Rohwer, J. M., Postma, P. W., Kholodenko, B. N., & Westerhoff, H. V. (1998). Proc. Natl. Acad. Sci. USA, in the press.
5. Westerhoff, H. V., Hofmeyr, J.-H. S. & Kholodenko, B. N. (1994) Biophys. Chem. 50, 273-283.
6. Reder, C. (1988) J theor Biol. 135, 175-202
7. Kahn, D., & Westerhoff, H. V. (1993) In Modern Trends in Biothermokinetics (Schuster S., Mazat, J.-P. & Rigoulet M., Eds.), pp. 199-204, Plenum Press, New York.
8. Heinrich, R. & Reder, C. (1991) J theor Biol. 151, 343 - 350.
9. Kholodenko, B. N., Demin, O. V., & Westerhoff, H. V. (1997) J. Phys. Chem. B 101, 2070-2081.
10. Demin, O. V., Kholodenko, B. N., & Westerhoff, H. V. (1996) Biochemistry (Moscow) 61, 435-450.

Session 1

Control Analysis: Theory and Applications

2

CONTROL ANALYSIS OF ADENYLATE-CONSERVING CYCLES IN THE ABSENCE OR PRESENCE OF ADENYLATE KINASE

Jan-Hendrik S. Hofmeyr and Johann M. Rohwer*

Dept. of Biochemistry, Univ. of Stellenbosch, Private Bag X1, 7602 Matieland, South Africa
*Corresponding author. Tel.: +27-21-8083039, Fax: +27-21-8083022, Email: jhsh@maties.sun.ac.za

Adenylate-conserving cycles form a central axis in the energy metabolism of all living organisms. Although the individual processes that form and consume ATP have been thoroughly studied, the important matter of the control distribution between ATP-supply processes and the different ATP-demand processes (and the accompanying question of which properties of these processes determine this control of the steady-state flux and concentrations of adenylates), has only recently been tackled experimentally [1,2].

We have shown [3,4] how supply-demand control analysis of linear systems such as that depicted in Fig. 1, especially graphical analysis in the form of rate characteristics, can afford insight into the regulation of such systems.

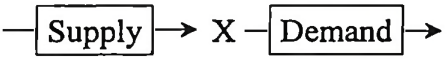

Figure 1. A simple linear supply-demand system for metabolite X. The supply and demand blocks can be single reactions or groups of reactions. The control analysis given in the text requires that the blocks can communicate through X only.

The control coefficients of the supply and demand blocks have the following simple and easily interpretable expressions in terms of the block elasticity coefficients [3]:

$$C^J_{\text{demand}} = \frac{-\varepsilon_x^{\text{supply}}}{\varepsilon_x^{\text{demand}} - \varepsilon_x^{\text{supply}}} \quad (1) \qquad C^J_{\text{supply}} = \frac{\varepsilon_x^{\text{demand}}}{\varepsilon_x^{\text{demand}} - \varepsilon_x^{\text{supply}}} \quad (2)$$

$$C^x_{\text{demand}} = \frac{-1}{\varepsilon_x^{\text{demand}} - \varepsilon_x^{\text{supply}}} \quad (3) \qquad C^x_{\text{supply}} = \frac{1}{\varepsilon_x^{\text{demand}} - \varepsilon_x^{\text{supply}}} \quad (4)$$

Adenylate-conserving cycles can also be regarded as supply-demand systems (Fig. 2) [3,5]. If an active adenylate kinase is present (Fig.2B), it equilibrates the three members of the adenylate pool: ATP, ADP and AMP (in reality AMP is also formed and consumed by other processes, but if these are slow in comparison with the adenylate kinase reaction near-equilibrium still exists).

A control analysis of the moiety-conserved cycle in Fig. 2A leads to expressions such as

$$C^{J}_{\text{demand}} = \frac{-\left(\frac{1}{[\text{ATP}]}\varepsilon^{\text{supply}}_{\text{ATP}} - \frac{1}{[\text{ADP}]}\varepsilon^{\text{supply}}_{\text{ADP}}\right)}{\left(\frac{1}{[\text{ATP}]}\varepsilon^{\text{demand}}_{\text{ATP}} - \frac{1}{[\text{ADP}]}\varepsilon^{\text{demand}}_{\text{ADP}}\right) - \left(\frac{1}{[\text{ATP}]}\varepsilon^{\text{supply}}_{\text{ATP}} - \frac{1}{[\text{ADP}]}\varepsilon^{\text{supply}}_{\text{ADP}}\right)} \qquad (5)$$

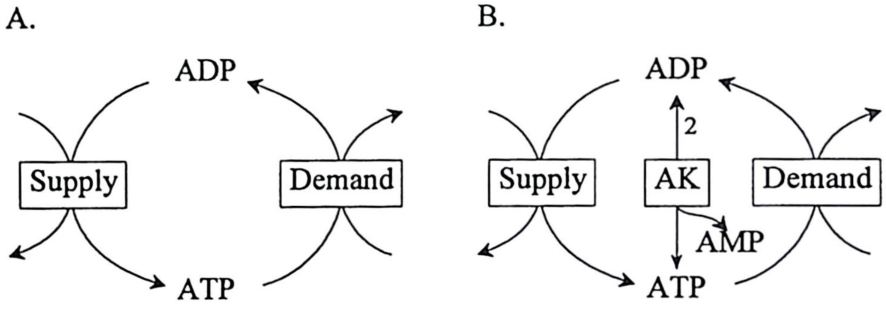

Figure 2. Adenylate-conserved cycles with (A) and without (B) an equilibrating adenylate kinase.

which seems considerably more complicated than its counterpart in the linear system (eqn. 1); an equivalent expression for the system in Fig. 2B is obviously even more complex. Simplifications are possible: (i) the inverse concentration factors unscale the fractional concentration change in the derivative so that each term is a half-scaled elasticity ($\partial \ln v / \partial x$); (ii) the bracketed terms (or rather the terms that would result if both numerator and denominator are multiplied with [ATP] to give, for example, $\varepsilon^{\text{supply}}_{\text{ATP}} - \varepsilon^{\text{supply}}_{\text{ADP}} \cdot [\text{ATP}]/[\text{ADP}]$) have been called 'apparent' or 'effective' elasticities [6,7,8]: for the system in Fig. 2A the simple form of eqn. 1 is regained if effective elasticities are used.

We have found an alternative approach to be very useful: it is based on the recognition that the cycles in Fig. 2 are moiety-conserved (a moiety-conserved cycle interconverts different forms of a chemical moiety, the sum of which remains constant [9,10]). If, in the case of Fig. 2A, the value of the sum [ATP]+[ADP] is known, one concentration can be calculated given the other—there is only one independent concentration. Atkinson [11] proposed the *energy charge* as the appropriate choice of independent variable for such a system. For the system in Fig. 2A the energy charge (*ec*) is simply the mole fraction of ATP (the mole fraction of ADP then being $1-ec$):

$$ec = \frac{[\text{ATP}]}{[\text{ATP}]+[\text{ADP}]} \qquad (6) \qquad\qquad 1-ec = \frac{[\text{ADP}]}{[\text{ATP}]+[\text{ADP}]} \qquad (7)$$

The term *ec* can be regarded as the *charged* fraction of the adenylate pool, while $1-ec$ is the *uncharged* fraction. In these terms the system transforms into that depicted in Fig. 3A. Formally, however, it remains a cycle and its control analysis is not simplified by the transformation. A great simplification results from the realisation that, instead of working with an independent and a dependent concentration variable as above, it is possible to consider only one independent variable, namely the concentration ratio [ATP]/[ADP], which can be seen to be equivalent to the ratio

$$\frac{\text{charged adenylates } (c)}{\text{uncharged adenylates } (u)} = \frac{ec}{1-ec} = \frac{[\text{ATP}]}{[\text{ADP}]} \tag{8}$$

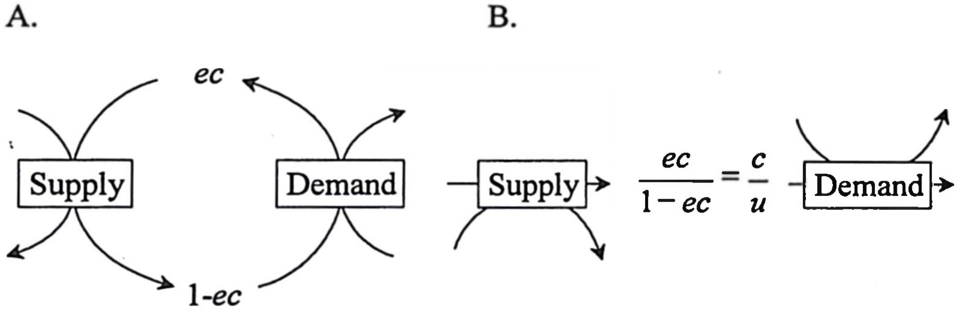

Figure 3. A generalised representation of the adenylate-conserving systems depicted in Fig. 2. Cyclic representation of supply-demand interconversion between charged fraction (*ec*) and uncharged fraction (1-*ec*). B. Linear representation of supply and demand of the ratio (*c/u*) of charged and uncharged fractions.

In terms of this ratio the system transforms to that given in Fig. 3B, which is formally equivalent to the linear system in Fig. 1.

Control analysis using metabolite ratios such as [ATP]/[ADP] is not a new idea and has been utilised before [e.g. 10,12]. However, its abstraction to the ratio *c/u* allowed us to extend the treatment to more complex adenylate cycles in the presence of adenylate kinase (Fig. 2B), which maintains an equilibrium distribution of AMP, ADP and ATP within the constant sum of their concentrations. The ATP-ADP cycle is no longer moiety-conserved and the [ATP]/[ADP] ratio no longer the appropriate variable; the conserved sum of adenylates now includes the concentration of AMP. Even so, there is still only one independent concentration variable (given the values of any one of the three concentrations, their sum, and the equilibrium constant of the adenylate kinase reaction, the other two concentrations can be calculated). For such systems, Atkinson [11] showed that the *energy charge* is given by the expression in eqn. 9 (the uncharged fraction then being that in eqn. 10).

$$ec = \frac{[\text{ATP}] + \frac{1}{2}[\text{ADP}]}{[\text{ATP}] + [\text{ADP}] + [\text{AMP}]} \tag{9}$$

$$1 - ec = \frac{[\text{AMP}] + \frac{1}{2}[\text{ADP}]}{[\text{ATP}] + [\text{ADP}] + [\text{AMP}]} \tag{10}$$

Analogous to eqn. 8 we now write

$$\frac{\text{charged } (c)}{\text{uncharged } (u)} = \frac{ec}{1-ec} = \frac{[\text{ATP}] + \frac{1}{2}[\text{ADP}]}{[\text{AMP}] + \frac{1}{2}[\text{ADP}]} \tag{11}$$

This unfamiliar ratio can be interpreted as follows: due to the stoichiometry of the adenylate kinase reaction half of the ADP pool is available (theoretically) to donate a phosphoryl group, and is therefore charged and added to the fully charged ATP, while the other half is available to accept a phosphoryl group, and is therefore uncharged and added to the fully uncharged AMP.

It can now be seen that the schemes depicted in Fig. 3 are quite general and, with the appropriate choice of *ec* and the ratio *c/u*, represent both Figs. 2A and 2B. The form that uses *c/u* as variable is, however, the most elegant in that it is formally equivalent to the linear system in Fig. 1, and therefore has the same simple control analytic expressions:

$$C^J_{\text{demand}} = \frac{-\varepsilon^{\text{supply}}_{c/u}}{\varepsilon^{\text{demand}}_{c/u} - \varepsilon^{\text{supply}}_{c/u}} \quad (12) \qquad C^J_{\text{supply}} = \frac{\varepsilon^{\text{demand}}_{c/u}}{\varepsilon^{\text{demand}}_{c/u} - \varepsilon^{\text{supply}}_{c/u}} \quad (13)$$

$$C^{c/u}_{\text{demand}} = \frac{-1}{\varepsilon^{\text{demand}}_{c/u} - \varepsilon^{\text{supply}}_{c/u}} \quad (14) \qquad C^{c/u}_{\text{supply}} = \frac{1}{\varepsilon^{\text{demand}}_{c/u} - \varepsilon^{\text{supply}}_{c/u}} \quad (15)$$

As with linear systems, the elasticities in these expressions can easily be visualised as the slopes at the intersection point of curves of rate of supply and rate of demand against *c/u* in log-log space (an example of this use of so-called rate characteristics is given in [4]). We therefore propose this cyclic-to-linear transformation as an elegant method to treat and present the experimental results of studies on moiety-conserved systems such as adenylate-conserving cycles (and, equally, pyridine nucleotide-conserving cycles).

REFERENCES

[1]Buttgereit, F. and Brand, M. (1993) Biochem. J.312, 163-167.

[2]Jeneson, J. A. L., Wiseman, R. W., Westerhoff, H. V. and Kushmerick, M. J. (1996) J. Biol. Chem 271, 27995-27998.

[3]Hofmeyr, J.-H. S. and Cornish-Bowden, A. (1991) Eur. J. Biochem. 200, 223-236.

[4]Hofmeyr, J.-H. S. (1995) J. Bioenerg. Biomembranes 27, 479-490.

[5]Hofmeyr, J.-H. S. (1998) in *New Beer in an Old Bottle: Eduard Buchner and the Growth of Biochemical Knowledge* (Cornish-Bowden, A., ed.), in press.

[6]Fell, D. A. and Sauro, H. M. (1985) Eur. J. Biochem. 148, 555-561.

[7]Cascante, M., Franco, R. and Canela, E. I. (1989) Math. Biosci. 94, 289-309.

[8]Kholodenko, B. N., Sauro, H. M., Westerhoff, H. V. and Cascante, M. (1995) Biochem. Mol. Biol. Int. 35, 615-625.

[9]Reich, J. G. and Sel'kov, E. E. (1981) *Energy metabolism of the cell,* Academic Press, London.

[10] Hofmeyr, J.-H. S., Kacser, H. and Van der Merwe, K. J. (1986) Eur. J. Biochem. 155, 631-641.

[11] Atkinson, D.E. (1977) *Cellular energy metabolism and its regulation,* Academic Press, London.

[12] H. V. Westerhoff and K. van Dam (1987) *Thermodynamics and control of free-energy transduction,* Elsevier, Amsterdam.

SYNTHETIC PROMOTERS FOR EXPERIMENTAL CONTROL ANALYSIS

Heidi W. Andersen, Regina Schürmann, Katrine Madsen, Martin B. Pedersen, Brian J. Koebmann, Jure Piskur, Karin Hammer and Peter Ruhdal Jensen

Department of Microbiology, Technical University of Denmark, Building 301, DK-2800, Lyngby, Denmark. Tel. +45 45252510. Fax. +45 45932809.
E-mail. prj@im.dtu.dk

INTRODUCTION

The experimental determination of control coefficients through modulated gene expression is a clean and promising approach, and in the future the advances in molecular genetics will allow for the perturbation of many biological processes that would otherwise be inaccessible to the experimenter. Ideally, one should change the expression of the enzymes under study around the normal level present in the cell, and measure the effect hereof on the relevant steady state variables in the system, i.e. fluxes, metabolite concentration and the concentration of enzymes that are subject to regulation. However, the tools for modulating gene expression is not well developed for many biological systems, and in many cases this is not really an experimental option. In some bacteria, such as *E. coli*, there are inducible systems available that allow one to adjust the expression of a gene or an operon by adding different amounts of an inducer. The best known example is the *lac* promoter system from *E. coli* and promoters derived from this system. These promoters are all silenced by the binding of the *lac* repressor protein, unless an inducer binds to the repressor and releases it from the DNA. The frequency of transcription initiation from these promoters can then be modulated by varying the concentration of the inducer, usually IPTG (isopropyl-β-D-thiogalactoside). Although this is in principle an attractive method, the method has several pitfalls: i) the active accumulation of IPTG by the lactose permease causes the induction curve to become very steep, and ii) a steady expression level in the batch cultures is sometimes difficult to obtain, because the expression changes with increasing cell concentrations. While the former problem was alleviated by inactivating the gene encoding the lactose permease (Jensen *et al.*, 1993), the latter problem persisted, and the experiments had to be done at very dilute cell concentrations (where a steady state could indeed be obtained). In addition, the modulation with IPTG is less practical for large scale fermentation.

If a library of promoters was available to choose from, then an alternative way to modulate gene expression would be to clone a number of promoters of different strength in front of the gene to be modulated. In order to be suitable for Metabolic Control Analysis, such a library should cover a broad range of promoter activities, and the strength of the individual promoters should only differ by a small factor, to allow for fine modulation of gene expression. In this paper we present a method for obtaining such promoter libraries, which should be applicable to many biological systems. The method will be illustrated through examples which include bacteria and yeast. Finally we present a strategy that reduces the cloning work considerably for many applications.

CONSTITUTIVE SYNTHETIC PROMOTERS FOR BACTERIA

The gram positive bacterium, *Lactococcus lactis*, which is used extensively as a starter culture in the dairy industry, is one of the systems to which we apply experimental MCA (see also Andersen *et al.*, Pedersen *et al.*, Koebmann *et al*, these BTK proceedings). Besides funding, this organism has the interesting property of a relatively simple free-energy metabolism: *Lactococcus lactis* does not benefit from oxidative phosphorylation and the habitat to which this organism has been adapted for thousands of years (milk substrates) supplies an excessive amount of nutrients. This allows for an almost perfect splitting of the metabolism into a catabolic module (ATP supply by substrate phosphorylation through glycolysis) and an anabolic module (ATP demand for polymerization of macromolecules, etc.).

The genetic tools on the other hand, for modulating gene expression in this organism, are not well developed. One exception is the nisin system developed by de Ruyter *et al.* (1996) which allows one to induce gene expression by changing the concentration of nisin in the growth medium. It is not yet clear whether this system also allows for a steady state gene expression. This is a crucial point in the determination of control coefficients in biological systems, where homeostatic control at the level of gene expression may affect the control exerted by the modulated enzyme.

We therefore took on the task of developing a library of synthetic promoters for use in *Lactococcus lactis*. This was done by synthesizing a degenerated oligonucleotide, which contained the consensus motifs for this organism (-35, -10 sequences, etc.), but in which the *spacers* between these motifs were randomized (see Jensen and Hammer, 1998a; 1998b, for further details):

```
  1    MCS          .         .         . -35     .          .
5'CGGGATCCTTAAGAATATTATGCATNNNNNAGTTTATTCTTGACANNNNNNNNNNNNNNT

  .   -10     .  +1     .     MCS .         .
  GRTATAATANNWNAGTACTGTTAACTGCAGCTGAATTCGG 3'
```

The oligonucleotide, which also encoded multible cloning sites (MCS), was converted into double stranded DNA fragments, using Klenow polymerase and a short 3' complementary primer, and cloned into a promoter cloning vector, pAK80 (Israelsen *et al.*, 1995), containing a promoterless β-galactosidase reporter gene. Somewhat surprisingly, the result was a library of promoters which differed in strength over some 3-4 orders of magnitude, in both *E. coli* and *L. lactis,* see figure 1.

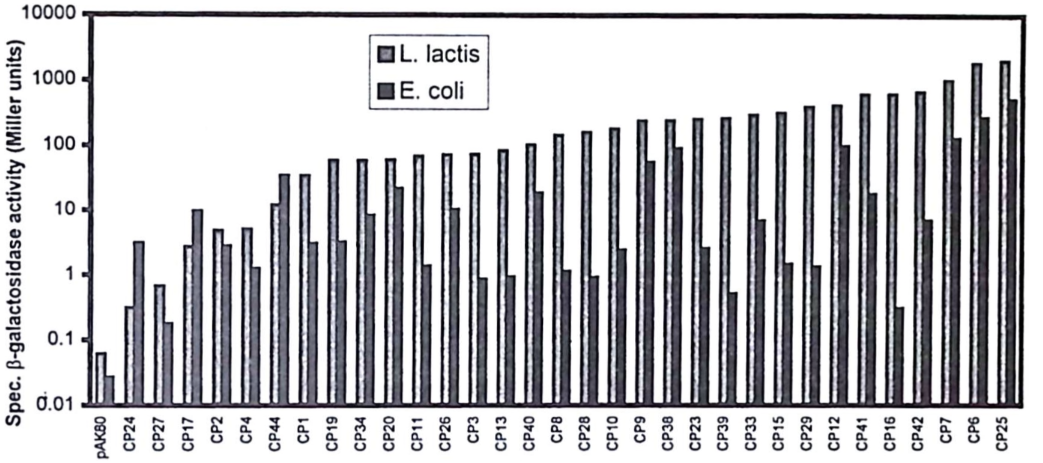

Figure 1. Synthetic promoters for modulating gene expression in *Lactococcus lactis* and *Escherichia coli*, cloned into the promoter cloning vector, pAK80, kindly provided by Dr. E. Johansen (data from Jensen and Hammer, 1998a)

The entire range was covered in relatively small steps of activity increase which makes these promoters well suited for MCA studies. Another important feature of these promoters is that they are perfectly constitutive with respect to the growth phase in batch culture (data not shown). We also tested the promoters for use in *E. coli* and also here the promoters gave rise to a broad range of β-galactosidase activities, see figure 1. In an accompanying paper we show that the CP promoters were useful for modulation of the expression of an uncoupled ATPase in *E. coli* (Koebmann *et al.*, these BTK proceedings).

REGULATED PROMOTERS FOR BACTERIA

For practical applications it is sometimes useful to be able to activate gene expression at a particular point in time during a fermentation process. We therefore decided to see if we could equip the synthetic promoters with regulatory features, i.e. to generate a library of promoters of different strength which were all regulated by the same external parameter. The model system that we chose to work with was the CIRCE element, a short inverted repeat found upstream of heat-shock regulated promoters in gram positive bacteria (Zuber and Schumann, 1994). Again we synthesized an oligonucleotide which specified promoters for *L. lactis* and this time incorporated the CIRCE element from this organism some 5 bp upstream of the -35 consensus sequence (Jensen, 1998):

```
1         MCS         .     →  .         .   ←    .        -35 .
CGGGATCCAAGCTTAATATTAATTAGCACTCNNNNNNNNNGAGTGCTAATTTTTTTGACA

61        .          -10        +1        MCS         .
NNNNNNNNNNNNNNNTGRTATAATANNWNAGTACTGCAGCTGTCTAGAATTCGG
```

Since we wanted to study promoter regulation we decided to integrate these promoters directly into the chromosome of *Lactococcus lactis*, to avoid interference from variations in plasmid copy number, etc. This was done using the promoter cloning vector, pLB85i (L. Brøndsted, personal communication), which contains a promoterless *gusA* gene, encoding β-glucoronidase activity. Figure 2 shows the activity of some of the putative heat shock regulated promoters at two temperatures, 30°C and 37°C. The activities of these promoters were generally 1.5 to 2.5 fold higher at the higher temperature. We also sub-cloned two of the promoters from the constitutive series (see above) into this reporter system, for comparison. The expression from the latter promoters was independent of temperature, see figure 2. Two fold regulation may not seem like a very strong regulation, but newer the less it is in the same order of magnitude as the regulation found for the naturally occurring heat-shock regulated promoters, which has to do with the transient nature of this response.

Synthetic promoters for bakers yeast.

We believe that the approach for generating synthetic promoters that has been presented above should be generally applicable to prokaryotic organisms. An exciting question is then whether the approach could also be extended to eukaryotic systems. We therefore looked into the litterature on promoters for *Saccharomyces cerevisiae*, and found that the promoter of the ARG8gene is located on a relatively small piece of DNA. This promoter contains regulatory sequences, like the TATA box, UAS_{GCN4p} motif, and the argR binding site (Crabeel *et al.*, 1995). Based on this information we designed a degenerated oligonucleotide containing consensus features of the ARG8 promoter, regulatory motifs and randomized spacers:

```
  1 EcoRI  UASGCN4p   .         .         .         .         .
   CAGAATTCGTGACTCANNNNNNNNNNNNNNNNNNNNNNNNNNNNNNNNNNNNNNNNNNNN

 61         .      TATA-box     .         .         .         .
   NNNNNNNNNNNNNNNNTATAAANNNNNNNNNNNNNNNNNNNNNNNNNNNNNNNNNNNNNN

121   TI box/argR-binding       .         .         .         .
   NCTCTTAAGTGCAAGTGACTGCGAACATTTTTTTCGTTTGTTAGAATAATTCAAGAATCG

181         . BamHI
   CTACCAATCATGGATCCCG
            ARG8start
```

This oligonucleotide was converted to double stranded DNA and cloned in front of a promoter-less β-galactosidase on the vector, pYLZ-2, a shuttle vector for *E. coli* and *S. cerevisiae* (Hermann *et al.*, 1992). The actual cloning step was performed in *E. coli*, and subsequently a selection of the resulting plasmids was transformed into various *S. cerevisiae* strains for measuring the promoter activities (Jensen, 1998; Jensen and Piskur, *manuscript in preparation*). Promoters of different strength had indeed been generated, see figure 3.

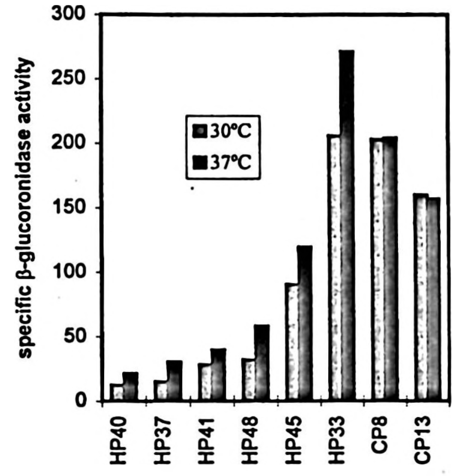

Figure 2. Synthetic heat-shock regulated promoters (HP-series) for *Lactococcus lactis.* Temperature regulation was estimated from the activity of β-glucoronidase expressed from the *gusA* integrated in the *attB* site on the chromosome. Two synthetic constitutive promoters were analysed for comparison (CP-series). Data from P.R. Jensen (manuscript in preparation).

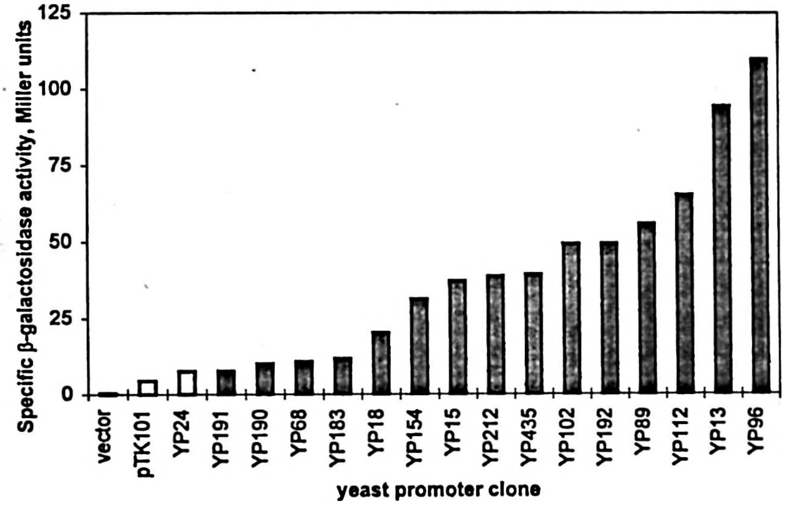

Figure 3. Synthetic promoters for *Saccharomyces cerevisiae.* Data from Jensen and Piskur (manuscript in preparation).

In principle, these synthetic yeast promoters should exhibit two different regulatory features: the promoters should be down-regulated i) specifically by the presence of arginine (mediated by argR), and ii) generally by the presence of amino acids in the growth medium (mediated by GCN4 protein), as has been observed for the wild-type ARG8 promoter (Crabeel *et al.,* 1995). In general, the promoters were found to possess the expected regulatory features.

Experimental modulation of a particular gene using synthetic promoters.

We have described a method that can be used for generating synthetic promoters. The *in vivo* activity of the promoters that we have generated differed over several logarithms of relative activity among the individual promoters, and should be suitable for MCA in many biological systems.

There are at least two technically different ways by which one may implement the promoters, to obtain the relevant levels of expression of the studied enzyme (encoded by geneX). One option is to choose from a pre-made promoter library, promoters that result in e.g. 25%, 50%, 200% and 400% of the normal expression level of the enzyme. This strategy assumes that the strength of the wild-type promoter of gene X is already known. Otherwise a broader range of promoter activities may be more appropriate, or one should start with just one promoter and then measure the expression relative to the normal expression before choosing the rest of the promoters. Alternatively it may be useful to start up by cloning the wild-type promoter of gene X in the same vector system that was used to characterise the artificial promoters in the first place. In some cases it may be necessary to fine-tune the expression further or to expand the range of promoter activities. This strategy assumes that the relative strength of the individual promoters in a promoter library is *independent of the context* in which it is placed, “and it ain’t necessarily so”. Another option is to always make a brand new promoter library directly in front of the gene to be modulated, see figure 4. At first sight, this may seem quite laborious, and in some cases the strategy described above may indeed be the fastest. But in other cases, particularly those where an assay allows one to readily screen for the clones which have the appropriate expression levels, the construction of a new library in front of the gene may actually be much easier. In prokaryotic systems, it may then be helpful to place a reporter gene, such as *lacZ* encoding β-galactosidase, downstream of the gene to be modulated for monitoring the relative transcription through the latter gene.

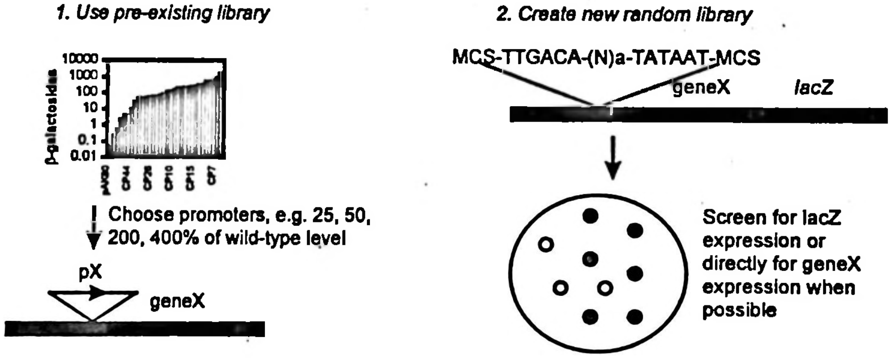
1. Use pre-existing library
β-galactosidase
10000
1000
100
10
1
0.1
0.01
CP44
CP26
CP10
CP15
CP7
Choose promoters, e.g. 25, 50, 200, 400% of wild-type level
pX
geneX
2. Create new random library
MCS-TTGACA-(N)a-TATAAT-MCS
geneX
lacZ
Screen for lacZ expression or directly for geneX expression when possible

Figure 4. Two different strategies for modulating the expression of geneX using synthetic promoters. The first strategy uses promoters from a pre-made library and the second one creates a new library in front of the geneX.

With respect to *Metabolic Optimization*, the synthetic promoters have several advantage, compared to using the inducible systems described above. One advantage is that after the optimal promoter activity has been determined, the strain is in principle ready for use in the industrial fermentation process. Another important feature, on a longer time scale, is the option to simultaneously modulate, to different extent, the expression of several individual genes or operons located on different positions of the genome in the same strain. With the existing systems now available, one would then quickly run out of expression systems to use, but with our method, one can in principle continue the optimization numerous times. It may also be necessary to perform additional rounds of optimization of the first enzyme after a second enzyme has been optimized, particularly when the optimization of the second enzyme has been successful with respect to increasing a pathway flux.

ACKNOWLEDGEMENT.

This work was supported by the Danish Centre for Advance Food Studies (LMC)

REFERENCES.

Crabeel, M., M. de Rijcke, S. Seneca, H. Heimberg, L. Pfeiffer, A. Matisova. Yeast **11**, 1367-1380 (1995)
de Ruyter, P.G., O.P. Kuipers, W.M. de Vos. Appl. Environ. Microbiol. **62**, 3662-3667 (1996)
Jensen, P. R., H.V. Westerhoff, O. Michelsen. Eur. J. Biochem. **211**, 181-191 (1993)
Jensen, P.R. International Patent Application, No. PCT/DK97/00342, publication number WO 98/07846 (1998)
Jensen, P.R., K. Hammer. Applied and Environmental Microbiology, **64**, 82-87 (1998a)
Jensen, P.R., K. Hammer. Biotechnology and Bioengineering. **58**, 191-195 (1998b)
Hermann, H., U. Hacker, W. Bandlow, V. Magdolen. Gene **119**, 137-41 (1992)
Israelsen, H. Appl. Environ. Microbiol., **61**, 2540-2547 (1995)
Zuber, U., W. Schumann, J. Bacteriol. **176**, 1359-1363 (1994)

MILD MITOCHONDRIAL TRANSITION PORE OPENING DURING REPERFUSION: TOP-DOWN CONTROL ANALYSIS OF MITOCHONDRIA AND ORGAN ^{31}P-NMR ANALYSIS.

Nathalie Leducq, Marie-Christine Delmas-Beauvieux, Isabelle Bourdel-Marchasson, Sylvie Dufour, Jean-Louis Gallis, Paul Canioni and Philippe Diolez

Résonance Magnétique des Systèmes Biologiques, UMR 5536, CNRS / Université Victor Segalen-Bordeaux 2, 146 rue Léo-Saignat, F-33076 Bordeaux cedex, France. Tel: 33 5 57 57 10 18; Fax: 33 5 56 96 13 41; diolez@rmsb.u-bordeaux2.fr

INTRODUCTION

The role of mitochondrial dysfunction in primary graft nonfunction following transplantation is of fundamental importance. ATP content has been well correlated with organ viability [1] and mitochondrial function is crucial in phosphate potential recovery after ischemia-reperfusion. However, it is still unclear to which extent organ dysfunction is linked to mitochondrial dysfunction. Furthermore, in perfused organs, no direct study of the effect of *in situ* mitochondrial permeability transition pore (MTP, see [2]) opening during reperfusion [3, 4] on mitochondrial function and energetic metabolism has been described. The aim of this work was to use cyclosporin A to evidence the role of MTP opening on mitochondrial dysfunction and intact organ capacity to maintain high ATP content, continuously assessed by ^{31}P-NMR on a model system of perfused rat liver. Mitochondrial damages occurring in perfused rat liver during cold ischemia, reperfusion and transition to normothermia were characterized using top down control analysis [5].

METHODS

Perfused rat livers were submitted to different treatments modeling the preservation phase (hypothermic ischemia) and the subsequent reperfusion occurring during transplantation process, in the absence or the presence of cyclosporin A (specific MTP inhibitor). A cold reperfusion phase was added before normothermia in order to assess a possible mitochondrial dysfunction during hypothermic ischemia. After excision, livers were perfused 20 min with 4°C Krebs-Henseleit medium, then kept at 4°C under ischemic conditions. After 0, 1 or 24 hours, livers were first submitted to a 20 min reperfusion at 4°C, then 1 hour 37°C reperfusion. When added, cyclosporin A (0.2 μM) was present during both cold and normothermic reperfusions. Phosphorylated metabolites of the perfused organ were followed and quantified at all phases by ^{31}P-NMR [6] and mitochondria were isolated at key stages. Top down metabolic control analysis [7] was applied to the study of oxidative phosphorylation in isolated mitochondria as previously described [8].

RESULTS AND DISCUSSION

Livers were subjected to ^{31}P-NMR analysis all along the different protocols until homogeneization for mitochondrial preparation. Figure 1 presents the evolution of perfused liver ^{31}P-NMR spectrum. Spectrum *a* was recorded during the first phase of hypothermic perfusion (before ischemia) and used as a reference for the quantitation of ATP levels (NTP peak). After 24 hour hypothermic ischemia (spectrum *b*), no ATP was detectable and a huge amount of inorganic phosphate was present. The subsequent hypothermic reperfusion, which triggered ATP synthesis, led to a progressive increase in ATP content of the liver and a recovery of about 50 % (spectrum *c* and *d*).

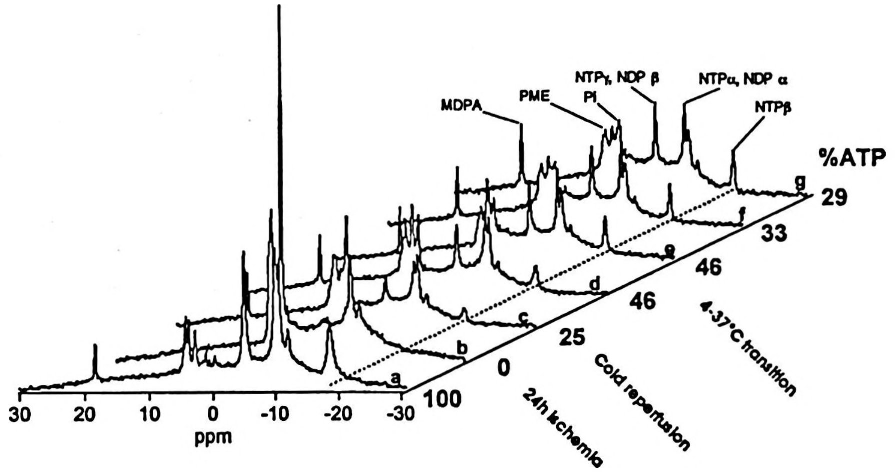

Figure 1. Typical evolution of rat liver ^{31}P-NMR spectrum during the basic protocol of ischemia-reperfusion, in the absence of cyclosporin A.

The three last spectra (*e-g*) illustrate the decrease in ATP content following normothermic reperfusion. In the experiment presented, stabilization of ATP content occurs at about 30 % (spectrum *g*). The apparent increase in the amplitude of the peak is misleading and is only a consequence of the effect of temperature on ^{31}P-NMR [6].

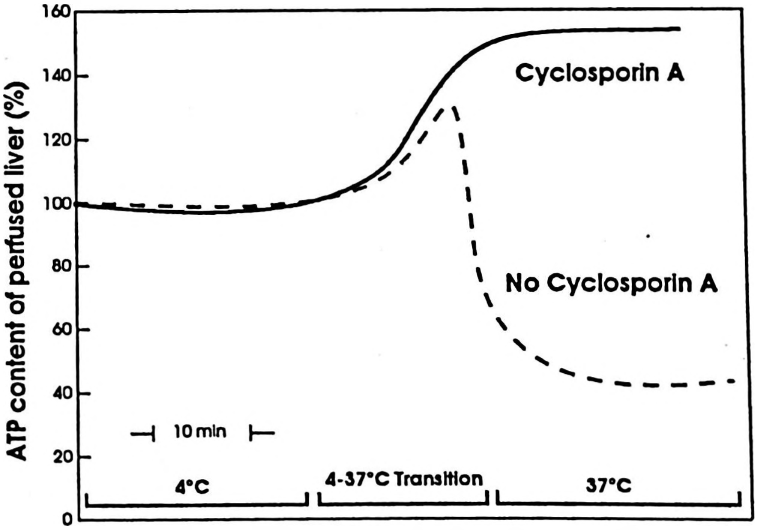

Figure 2. Evolution or rat liver ATP content during the transition to normothermia: Effect of cyclosporin A.

The effect of Cyclosporin A on the kinetics of ATP content of the liver during the transition to normothermia is presented in Figure 2. In the absence of Cyclosporin A a rapid fall in ATP was observed during normothermic transition, and a value of 46 ± 9% (n=3) of the initial ATP content was observed in the typical experiment presented here. This decline was completely prevented in the presence of 0.2 μM Cyclosporin A and the ATP content reached a plateau of 139 ± 4% (n=3) of the initial value.

In all conditions, isolated mitochondria were relatively well coupled and presented high values of membrane potential. No difference in proton leakage activity was observed between control mitochondria and mitochondria from livers submitted to the different protocols, indicating that membrane properties were affected neither by cold ischemia nor by temperature transition. Some significative modifications could however be noticed after normothermic reperfusion, but not after cold ischemia or reperfusion, even after 24 hours. A decrease in phosphorylation rate (about 25%), prevented by cyclosporin A, was effectively observed, but the full analysis of these data required the use of control analysis.

Thus, a complete top down control analysis was carried out on mitochondria isolated from livers after the various treatments. Over the entire range of phosphorylating conditions (from state 4 to state 3), no significant difference was found between mitochondria from livers which did not undergo normothermic reperfusion, whatever the treatment. The control pattern was identical to that obtained with mitochondria extracted from fresh livers and can therefore be called 'normal'. Interestingly, a distinct control pattern was observed after normothermic reperfusion, whatever the length of the preceding ischemic period. This 'pathological' pattern was characterized almost exclusively by a decrease in the control exerted by phosphorylation subsystem over the fluxes through the two other subsystems (respiratory chain and proton leak) and the intermediate (membrane potential, Fig. 3). Figure 3 also shows that the 'normal' control pattern was observed when cyclosporin A was present during the normothermic transition.

CONCLUSION

The data presented in this paper indicate that the damaging phase for organ energetics during the transplantation process is the temperature transition occurring during the normothermic reperfusion, not the reperfusion in itself. Damages have been correlated with mitochondrial dysfunction, revealed by a distinct -'pathological' - control pattern. This 'pathological' pattern was characterized by a decreased response of oxidative phosphorylation to the cellular ATP demand and may explain the impairement of organ ATP content. In the present study, the analysis smoothed the differences measured by the classical parameters of oxidative phosphorylation and gave a black and white picture: control patterns were 'normal' or not. The main differences in control pattern were observed under intermediate phosphorylating conditions, not accessible through classical parameters analysis, but likely to be close to *in situ* conditions.

Protection by Cyclosporin A of both mitochondrial and organ dysfunctions implies MTP opening. It is now well established that complete MTP opening is responsible for a mitochondrial burst [9, 10]. In the present study, the mitochondrial fraction that did not undergo such an irreversible process was also damaged and protected by Cyclosporin A. Thus, our results suggest a 'mild' opening of the MTP that would be responsible for mitochondrial damages to the phosphorylation system, diagnosed by top down control analysis, and sufficient to impair organ energetics. Since a simple inhibition of enzymes would not modify the control pattern [8], these data suggest a more fundamental change in the phosphorylation system that remains to be investigated.

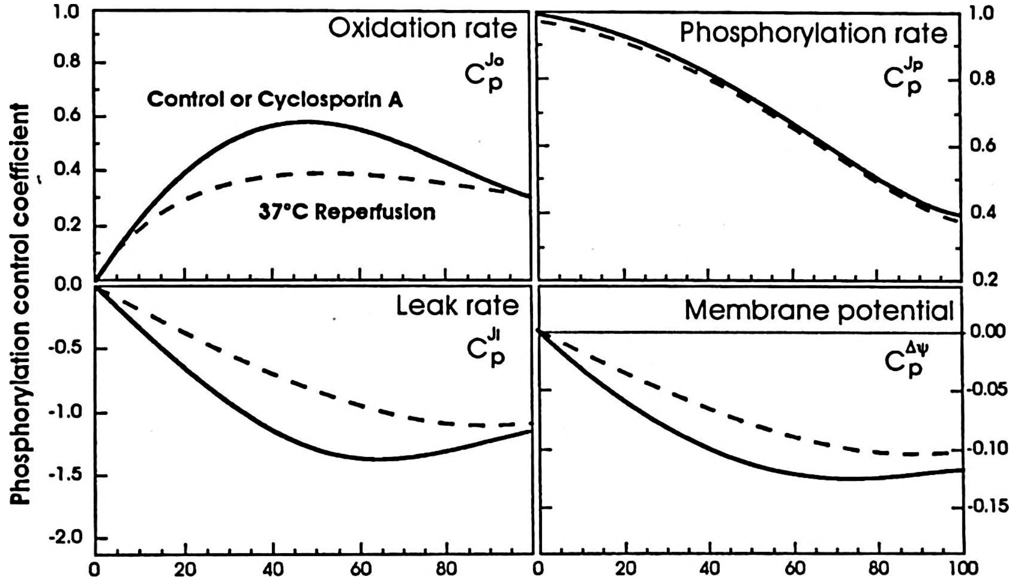

Figure 3. Effect of Cyclosporin A on the control pattern of the phosphorylation subsystem over the oxidation $C_p^{J_o}$, phosphorylation $C_p^{J_p}$ and leak rates $C_p^{J_l}$, and membrane potential value $C_p^{\Delta\Psi}$.

ACKNOWLEDGEMENTS

This work was supported by grant PARMIFR 9613, INSERM, France and the Etablissement Français des Greffes.

REFERENCES

1 Marabuyashi, S., Takenaka, M. and Dohi, K. (1980) Transplantation 30, 294-296.

2 Bernardi, P. (1996) Biochim. Biophys. Acta 1275, 5-9.

3 Griffiths, E.J. and Halestrap, A.P. (1993) J. Mol. Cardiol. 25, 1461-1469.

4 Nicolli, A., Costantini, P., Basso, E., Colonna, R., Petronilli, V. and Bernardi, P. (1995) Transplant. Proc. 27, 2825-2826.

5 Hafner, R.P., Brown, G.C. and Brand, M.D. (1990) Eur. J. Biochem. 188, 313-319.

6 Dufour, S., Thiaudière, E., Vidal, G., Gallis, J.-L., Rousse, N. and Canioni, P. (1996) J. Magn. Reson. 113, 125-135.

7 Brown, G.C., Hafner, R.P. and Brand, M.D. (1990) Eur. J. Biochem. 188, 321-325.

8 Dufour, S., Rousse, N., Canioni, P. and Diolez, P. (1996) Biochem. J. 314, 743-751.

9 Halestrap, A.P., Woodfield, K.-Y. and Connern, C.P. (1997) J. Biol. Chem. 272, 3346-3354.

10 Zoratti, M. and Szabo, I. (1995) Biochim. Biophys. Acta 1241, 139-176.

5

METABOLIC CONTROL ANALYSIS OF THE LELOIR PATHWAY IN *SACCHAROMYCES CEREVISIAE*

Simon Østergaard, Lisbeth Olsson and Jens Nielsen

Center for Process Biotechnology, Department of Biotechnology, Building 223, Technical University of Denmark, DK-2800 Lyngby, Denmark.

Telephone: +45 45 25 26 83, Fax: +45 45 88 41 48, E-mail: sios@ibt.dtu.dk

INTRODUCTION

The *GAL*-genes encoding the enzymes responsible for the consumption of galactose, are subjugated glucose repression which is of major importance for the utilisation of galactose industrially. The *GAL*-genes in *Saccharomyces cerevisiae* serve as one of the best studied models of genetic regulation in eukaryotic systems, which was extensively reviewed by Johnston and Carlson (1992). The *GAL*-genes comprise both regulatory and structural genes. The structural genes encode the enzymes responsible for the uptake of extracellular galactose and subsequent conversion of intracellular galactose to glucose-6-phosphate, known as the Leloir pathway (depicted in figure 1). The enzymes galactose permease, galactokinase, galactose-1-phosphate uridylyltransferase, UDP-glucose 4-epimerase and phophoglucomutase are designated Gal2p, Gal1p, Gal7p, Gal10p and Gal5p, respectively.

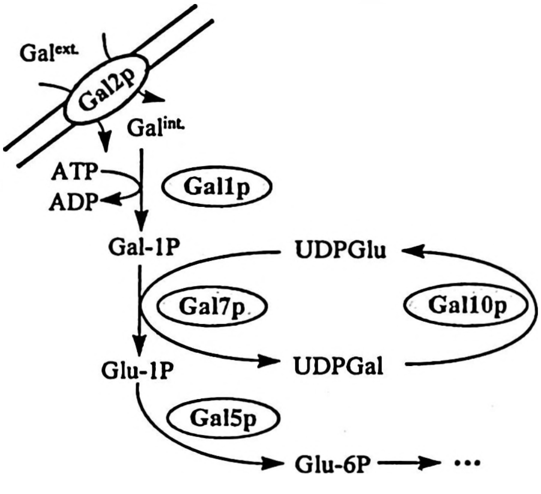

Figure 1 The Leloir Pathway

In this study the concepts of Metabolic Control Analysis (MCA) [Kacser and Burns, 1973 and Heinrich and Rapoport, 1974] was applied in order to identify potential rate-controlling step(s) in the Leloir pathway. Thus, a kinetic model of the enzymes encoded by the structural genes was established to evaluate the control of flux at steady state through the pathway. The flux control coefficients were determined using an indirect method where the elasticity coefficients were calculated from steady state measurements of the intracellular pool levels, and subsequently the flux control coefficients were deduced by application of the flux-control summation theorem and the flux-control connectivity theorem.

METHODS

The industrial strain of *Saccharomyces cerevisiae*, DGI342 (Danisco Distillers, Copenhagen, Denmark), was grown as continuous cultivations in an MBR bioreactor AG Switzerland, with a working volume of 3 litre. The cultivation conditions were controlled by an IMCS-2000 control unit of AG Switzerland. The chemostat experiments were carried out at a dilution rate of 0.1 h^{-1} with a mineral medium according to the method of Verduyn *et al.* (1990). The galactose concentration in the feed medium was 25 g/L for the galactose-limited chemostat, and 40 g/L for the nitrogen-limited chemostat. The rapid sampling technique as described by Theobald *et al.* (1993) was applied for withdrawing samples for determination of the intracellular metabolite levels. The intracellular concentrations of the sugar phosphates were determined by the method of Smits *et al.* (1998).

RESULTS AND DISCUSSION

Description of the kinetic model

The system examined comprised the four reactions catalysed by Gal2p, Gal1p, Gal7p and Gal10p, and hence, the reaction catalysed by Gal5p was not included in the kinetic model. This enabled us to deduce the flux control coefficient from the theorems of MCA. Leaving Gal5p out of the model seemed reasonable because glucose-1-phosphate, glucose-6-phosphate and fructose-6-phosphate constitute a single metabolic pool in which the pool can be replenished by any of the pool components, suggesting that Gal5p is present in excess [Zubay, 1988]. Furthermore, *GAL5* exhibits an unusually high basal level of expression independent of the positive transcriptional activator protein Gal4p [Oh and Hopper, 1990]. Thus, the reaction catalysed by Gal5p is not likely to present a rate-controlling step of the Leloir pathway.

The analytical rate expression of Gal2p, Gal1p, Gal10p and Gal7p are depicted in figure 2. The reactions catalysed by Gal2p, Gal1p and Gal10p were assumed to react according to reversible Michaelis-Menten kinetics where K_{eq} in the kinetic expression designates the relation between the product and the substrate concentration at steady state. The two-substrate reaction catalysed by Gal7p was assumed to occur with an ordered single-displacement mechanism.

$$V = V_{\max}\frac{C_{substrate} - \dfrac{C_{product}}{K_{eq}}}{C_{substrate} + \dfrac{C_{product}}{K_{eq}} + K_m^{substrate}} \qquad V = V_{\max}\frac{1}{\dfrac{K^{*}_{\mathrm{Gal1P}}\,K_m^{\mathrm{UDPGlu}}}{C_{\mathrm{Gal1P}}\,C_{\mathrm{UDPGlu}}} + \dfrac{K_m^{\mathrm{UDPGlu}}}{C_{\mathrm{UDPGlu}}} + \dfrac{K_m^{\mathrm{Gal1P}}}{C_{\mathrm{Gal1P}}} + 1}$$

Figure 2. Analytical rate expressions for Gal2p, Gal1p, Gal10p (left) and Gal7p (right).

The kinetic constants of the model are taken from Reifenberger *et al.* (1997) (Gal2p), Schell and Wilson (1977) (Gal1p), Fukasawa *et al.* (1980) (Gal10p), and Segawa and Fukasawa (1979) (Gal7p). K_{eq} in the rate expression of Gal1p was estimated as the ratio between the cytosolic ATP and ADP level, under the assumption that this ratio is the same as was determined in a glucose-limited chemostat at a dilution rate of 0.1 h^{-1} by Theobald *et al.* (1997). The binding constant of galactose-1-phosphate in the rate expression of Gal7p was unknown. It is most likely to be in the µM-range which had no impact on the MCA, so the term including K^{*}_{gal1P} in the denominator of the Gal7p rate expression, was excluded.

Steady state levels of the intracellular metabolites.

The intracellular pool levels of the metabolites of the Leloir pathway were determined from a galactose-limited and a nitrogen-limited chemostat both with a dilution rate of 0.1 h^{-1} (table 1). The intracellular level of galactose was the only component not determined.

Table 1 Intracellular pool levels

Metabolite	*Gal.-limited [mM]*	*N-limited [mM]*
Galactose$^{ext.}$	1.0	52.4
Galactose-1P	0.082	0.947
UDPGlucose	0.615	0.679
UDPGalactose	0.645	0.267
Glucose-1P	0.008	0

Results of the MCA

The elasticities were calculated as shown in figure 3, and subsequently, the flux control coefficients were determined by use of the flux-control summation theorem and the flux-control connectivity theorem, as depicted by matrix notation in figure 3. The indices of the flux control coefficients (*i*=1,..,4) refer to the reactions catalysed by Gal2p, Gal1p, Gal7p and Gal10p, respectively. The flux control coefficients are shown in figure 4 as a function of the intracellular galactose concentration. In the case of the galactose-limited steady state, the control of flux is exerted by the galactose permease at an intracellular galactose concentration below 0.35 mM. Above this concentration, the galactokinase takes over the control of flux. Recent results by Teusink *et al.* (1998) claim that the intracellular glucose concentration was less than 0.1 mM when the extracellular glucose concentration was at or below the affinity of the transport system. Assuming the same to be the case for galactose, the intracellular galactose concentration should be approximately 0.1 mM, and the control of flux is then mainly exerted by galactose permease. As illustrated, the intracellular level of galactose has a crucial effect on the control of flux according to this model. Physiologically intracellular galactose plays a pivotal role being the signal molecule for induction of the *GAL*-genes [Yano and Fukasawa, 1997].

$$\varepsilon_J^I = \left(\frac{\partial V_I}{\partial X_J} \frac{X_J}{V_I} \right)_{J=1,\dots,4,\, I=1,\dots,4}$$

$$\begin{bmatrix} 1 & 1 & 1 & 1 \\ \varepsilon_1^1 & \varepsilon_1^2 & 0 & 0 \\ 0 & \varepsilon_2^2 & \varepsilon_2^3 & 0 \\ 0 & 0 & \varepsilon_3^3 & \varepsilon_3^4 \end{bmatrix} \begin{bmatrix} C_1 \\ C_2 \\ C_3 \\ C_4 \end{bmatrix} = \begin{bmatrix} 1 \\ 0 \\ 0 \\ 0 \end{bmatrix}$$

Figure 3 Determination of the elasticities and the flux control coefficients.

Teusink *et al.* (1998) reported in the case of a high extracellular glucose concentration (*e.g.* a nitrogen-limited steady state), that the intracellular glucose pool was in the range of 2-3 mM, which is much higher than in most earlier reports. If the intracellular galactose concentration in the nitrogen-limited steady state is in the range of 2-3 mM, the control of flux is only exerted by galactose permease, as seen in figure 4. The flux control coefficient of Gal7p (C_3) is hardly zero for any of the two steady states, as is the case for the flux control coefficient of Gal10p (C_4) in both cases. Thus, the model described in this study states that galactose permease appears to be the rate-controlling step of the Leloir pathway under the physiological conditions examined.

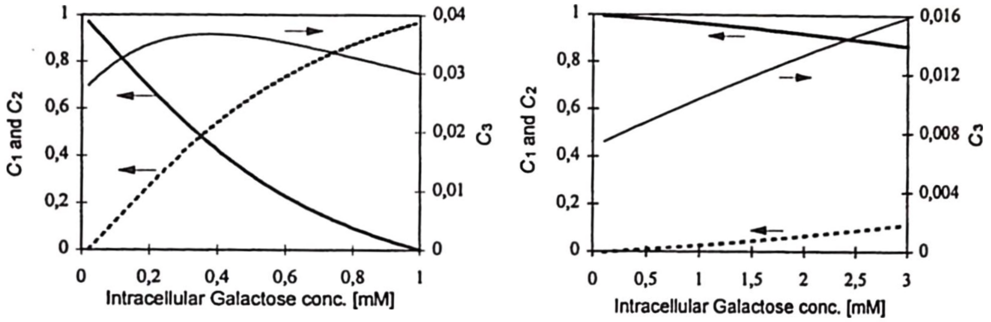

Figure 4. The flux control coefficients versus the intracellular galactose concentration for the galactose-limited chemostat (left) and the N-limited chemostat (right). C_4 was equal to zero in both cases.
C_1: (————); C_2: (··············); C_3: (————)

ACKNOWLEDGEMENT

Jens Dynesen and Hans Peter Smits are thanked for measuring the pool levels of the sugar phosphates.

REFERENCES

Fukasawa, T.; Obonai, K.; Segawa, T.; Nogi, Y. (1980). The enzymes of the galactose cluster in *Saccharomyces cerevisiae*. II. Purification and characterisation of uridine diphosphoglucoe 4-epimerse. *J. Biol. Chem.* **255**: 2705-2707

Heinrich, R.; Rapoport, T. A. (1974). A linear steady-state treatment of enzymatic chains. *Eur. J. Biochem.* **42**: 89-95

Johnston, M.; Carlson, M. (1992). Volume II. *The molecular and cellular biology of the yeast Saccharomyces: Gene expression.* © 1992 Cold Spring Harbor Laboratory Press.

Kacser, H.; Burns, B. A. (1973). The control of flux. *Symp. Soc. Exp. Biol.* **27**: 65-104

Oh, D.; Hopper, J. E. (1990). Transcription of a yeast phosphoglucomutase isozyme gene is galactose inducible and glucose repressible. *Mol. Cell. Biol.* **10** (4): 1415-1422

Reifenberger, E.; Boles, E.; Ciriacy, M. (1997). Kinetic characterisation of individual hexose transporters of *Saccharomyces cerevisiae* and their relation to the triggering mechanisms of glucose repression. *Eur. J. Biochem.* **245**: 324-333

Schell, M. A.; Wilson, D. B. (1977). Purification and properties of galactokinase from *Saccharomyces cerevisiae. J. Biol. Chem.* **252**: 1162-1166

Segawa, T.; Fukasawa, T. (1979). The enzymes of the galactose cluster in *Saccharomyces cerevisiae*. I. Purification and characterisation of galactose-1-phosphate uridylyltransferase. *J. Biol. Chem.* **254** (21): 10707-10709

Smits, H. P., Cohen, A.; Buttler, T.; Nielsen, J.; Olsson, L. (1998). Clean-up and analysis of sugar phosphates in biological extracts by using solid phase extraction and anion-exchange chromatography with pulsed amperometric detection. Accepted in *Anal. Biochem.*

Teusink, B.; Diderich, J. A.; Westerhoff, H. V.; Dam, K.; Walsh, M. C. (1998). Intracellular glucose concentration in derepressed yeast cells consuming glucose is high enough to reduce the glucose transport rate by 50%. *J. Bacteriol.* **180** (3): 556-562

Theobald, U.; Mailinger, W.; Reuss, M.; Rizzi, M. (1993). *In-vivo* analysis of glucose-induced fast changes in yeast adenine nucleotide pool applying a rapid sampling technique. Anal. Biochem. **214**: 31-37

Theobald, U.; Mailinger, W.; Baltes, M.; Rizzi, M.; Reuss, M. (1997). In vivo analysis of metabolic dynamics in *Saccharomyces cerevisiae*: I. Experimental observations. *Biotech. Bioeng.* **55** (2): 305-316

Verduyn, C.; Postma, e.; Scheffers, W. A.; van Dijken, J. P. (1990). Physiology of *Saccharomyces cerevisiae* in anaerobic glucose-limited chemostat cultures. *J. Gen. Microbiol.* **136**: 395-403

Yano, K.; Fukasawa, T. (1997). Galactose-dependent reversible interaction of Gal3p with Gal80p in the induction pathway of Gal4p-activated genes of *Saccharomyces cerevisiae. Proc. Natl. Acad. Sci. USA* **94**:1721-1726

Zubay, G. (1988). Biochemistry, 2. Ed., Macmillan Publishing Company, New York.

RELATIONS BETWEEN FLUX CONTROL COEFFICIENTS AND ENZYME CONCENTRATIONS IN STATES OF MINIMIZED TOTAL AMOUNT OF ENZYME

Edda Klipp

Theoreticl Biophysics, Institute of Biology, Humboldt University Berlin, Invalidenstr. 42, 10115 Berlin, Germany, phone +49 30-2093 8383, fax +49 30-2093 8813,
e-mail: edda=klipp@rz.hu-berlin.de

INTRODUCTION

Modelling of cellular metabolism is often done as simulation of the behaviour of the system assuming that one knows the structure of the system, the pattern of influences and the quantitative strength of these influences. Another approach is the prediction of features of metabolic systems (e.g. the number of reactions of a pathway, enzyme concentrations, values of kinetic constants) as a conclusion from optimality principles. These optimality principles can be regarded as an expression of the observation that biological systems are under evolutionary pressure. Several attempts have been made to derive conclusions from the demand for maximal flux through a pathway: the prediction of optimal kinetic constants for a single enzyme or for successive enzymes of a linear pathway, the prediction of the distribution of a given amount of enzyme over a linear pathway [1], the prediction of the distribution of ATP-consuming and –producing reactions in an ATP-producing pathway [2].

Here, we use the principle that the total amount of enzyme in a cell can be considered as limited or even minimized [3]. This can be explained by the fact that cellular metabolism is characterized by the necessity of parsimony in the use of resources. The synthesis of enzyme in the cell costs energy and material. The capacity of the cell to store enzyme (i.e. protein) is limited due to osmotical reasons.

Steady states of metabolic systems can be described in terms of metabolic control analysis. One can ask whether an optimized state is characterized by a special distribution of flux control. In unbranched chains of enzymic reactions in states of minimal total enzyme concentration at given flux the distribution of the flux control coefficients is identical to the distribution of the relative concentrations of the individual enzymes [1]. Reactions catalysed by those enzymes that must be present in a high concentration compared to the total amount of enzyme to maintain the given flux also exert a strong flux control and *vice versa*. That differs remarkably from non-optimized situations.

RESULTS AND DISCUSSION

Let us consider metabolic networks with linearity between reactions rates and enzyme concentrations. At fixed steady state fluxes $\boldsymbol{J} = \boldsymbol{v}(\boldsymbol{S}(\boldsymbol{E}), \boldsymbol{E})$ with

$$\mathrm{d}\boldsymbol{J} = \frac{\partial \boldsymbol{v}}{\partial \boldsymbol{S}} \frac{\partial \boldsymbol{S}}{\partial \boldsymbol{E}} \mathrm{d}\boldsymbol{E} + \frac{\partial \boldsymbol{v}}{\partial \boldsymbol{E}} \mathrm{d}\boldsymbol{E} = \boldsymbol{0} \tag{1}$$

the principle of minimized total enzyme concentration can be expressed as

$$\mathrm{d}E_1 + \mathrm{d}E_2 + \ldots + \mathrm{d}E_r = 0 \quad \text{or} \quad \mathit{1}^{\mathrm{T}}\mathrm{d}\boldsymbol{E} = 0. \tag{2}$$

Its application yields the following relations between optimized enzyme concentrations and flux control coefficients:

$$\mathbf{C}^{\mathrm{T}}\,\mathrm{E} = \mathrm{E} \tag{3}$$

where **C** represents the matrix of normalized flux control coefficients, T indicates the transpose and $\boldsymbol{E}$ is the vector of optimized enzyme concentrations. This distribution of flux control can be derived as follows. The matrix of flux control coefficients can be written as

$$\mathbf{C} = (\mathrm{diag}\,\mathrm{J})^{-1}\left(\mathbf{I} - \frac{\partial \mathrm{v}}{\partial \mathrm{S}}\left(\mathrm{N}\frac{\partial \mathrm{v}}{\partial \mathrm{S}}\right)^{-1}\mathrm{N}\right)(\mathrm{diag}\,\mathrm{J}) \tag{4}$$

were $(\mathrm{diag}\,\boldsymbol{J})$ represents a square matrix containing the steady state fluxes in the main diagonal, $\partial \boldsymbol{v}/\partial \boldsymbol{S}$ is the matrix of unscaled elasticities, and **N** the stoichiometric matrix.

The eigensystem of $\dfrac{\partial v}{\partial S}\left(\mathrm{N}\dfrac{\partial v}{\partial S}\right)^{-1}\mathrm{N}$ consists of the eigenvalues

$$\lambda_i = 1, \qquad i = 1,..,n \tag{5a}$$

$$\lambda_j = 0, \qquad j = n+1,..,r \tag{5b}$$

($\boldsymbol{n}$ is the number of independent internal metabolits, $\boldsymbol{r}$ is the number of reactions) with the corresponding eigenvectors

$$y_i = \frac{\partial v}{\partial S}\left(\mathrm{N}\frac{\partial v}{\partial S}\right)^{-1} \tag{6a}$$

$$y_j = \mathbf{K} \tag{6b}$$

were **K** is the nullspace matrix of the stoichiometric matrix **N**.

Let us return to the steady state condition (1). Because of the assumed linearity between reaction rates and enzyme concentrations the matrix $\partial \boldsymbol{v}/\partial \boldsymbol{E}$ can be expressed as $(\mathrm{diag}\,\boldsymbol{J})(\mathrm{diag}\,\boldsymbol{E})^{-1}$. Expression $\partial \boldsymbol{S}/\partial \boldsymbol{E}$ can be rewriten as $-(\mathrm{N}\,\partial \boldsymbol{v}/\partial \boldsymbol{S})^{-1}\mathrm{N}\,\partial \boldsymbol{v}/\partial \boldsymbol{E}$. Introducing these expressions into the steady state condition (1) yields

$$(\mathrm{diag}\,\boldsymbol{J})(\mathrm{diag}\,\boldsymbol{E})^{-1}\mathrm{d}\boldsymbol{E} = \left(\frac{\partial v}{\partial S}\left(\mathrm{N}\frac{\partial v}{\partial S}\right)^{-1}\mathrm{N}\right)(\mathrm{diag}\,\boldsymbol{J})(\mathrm{diag}\,\boldsymbol{E})^{-1}\mathrm{d}\boldsymbol{E} \tag{7}$$

or the fact that the vector $(\mathrm{diag}\,\boldsymbol{J})(\mathrm{diag}\,\boldsymbol{E})^{-1}\mathrm{d}\boldsymbol{E}$ represents an eigenvector y_i of

$\frac{\partial v}{\partial S}\left(\mathrm{N}\frac{\partial v}{\partial S}\right)^{-1}\mathrm{N}$ corresponding to the eigenvalue $\lambda_i = 1$. With

$$\boldsymbol{1}^{\mathrm{T}}\mathrm{d}\boldsymbol{E} = \boldsymbol{1}^{\mathrm{T}}(\mathrm{diag}\,\boldsymbol{E})(\mathrm{diag}\,\boldsymbol{J})^{-1}\,\boldsymbol{y}_{\mathrm{i}} = 0 \tag{8}$$

one can easily show the validity of equation (3) in states of mimimal total enzyme concentrations or, in other words,

$$\sum_{j=1}^{r} C_{v_i}^{J_j} E_j = E_i \qquad \text{for } i = 1,\ldots,r \tag{9}$$

For an unbranched chain this formula (3 or 9) is equivalent to the statement of proportionality between flux control coefficients and optimized enzyme concentrations. For branched systems a matching between the control coefficients and the optimized enzyme concentration can be concluded, too. Enzymes of reactions which excert more control over the fluxes in the system than others are present in a higher concentration in states of minimized total enzyme.

Eqn. (3) offers a set of relations between the control coefficients in addition to the well-known summation and connectivity theorems. For the matrix of scaled elasticities $\boldsymbol{\varepsilon}$ it follows from eqn. (3) under consideration of the connectivity theorem for systems without conservation relations ($\mathbf{C}\boldsymbol{\varepsilon} = \boldsymbol{0}$) that

$$\boldsymbol{\varepsilon}^{\mathrm{T}}\,\boldsymbol{E} = \boldsymbol{0}. \tag{10}$$

For practical purposes the use of equations (3) or (10) may allow the calculation of control coefficients if one knows fewer elasticities than would be necessary using only the summation and connectivity theorems since they supply as many new relations as there are independent internal metabolites included in the system.

Hitherto, optimization principles have been applied assuming that during evolution the cellular systems have had enough time to adopt to given conditions and that changes have been fixed by mutation and selection. However, it is known that organisms are able to change gene expression patterns remarkably with changing environmental conditions (e.g., in yeast cells one can observe the change of the m-RNA level of roughly 2000 genes during the diauxic shift switching from enzymes necessary for the degradation of glucose to ethanol to enzymes of the lower part of glycolysis and of gluconeogenesis) [4]. The distribution and the total amount of enzyme present in a cell are well regulated and quickly adapted to the environmental conditions. Hence, the enzyme distribution can be understood only in the context of genetic regulation.

References:

[1] Heinrich, R., Klipp, E., Control analysis of unbranched enzymatic chains in states of maximal activity, J. theor. Biol. 182 (1996) 243-252.

[2] Heinrich, R., Montero, F., Klipp, E., Waddell, T.G., Meléndez-Hevia, E., Theoretical approaches to the evolutionary optimization of glycolysis. Thermodynamic and kinetic constraints, Eur. J. Biochem. 243 (1997) 191-201.

[3] Brown, G.C., Total cell protein concentration as an evolutionary constraint on the metabolic control distribution in cells, J. theor. Biol. 153 (1991) 195-203.

[4] DeRisi, J.L., Iyer, V.R. & Brown, P.O., Exploring the metabolic and genetic control of gene expression on a genomic scale, Science, 278 (1997) 680-686.

7

EVOLUTIONARY IMPLICATIONS OF METABOLIC CONTROL ANALYSIS FOR MAXIMISATION OF RATES OF ENZYMES, PATHWAYS AND PHYSIOLOGICAL PROCESSES BY NATURAL SELECTION.

Guy C. Brown

Department of Biochemistry, University of Cambridge, Tennis Court Road, Cambridge
CB2 1QW, UK. Phone: 44 1223 333342, Fax: 44 1223 333345
e-mail: gcb@mole.bio.cam.ac.uk

INTRODUCTION

I am going to suggest that evolution by natural selection acts to equalise the control coefficients of steps within molecular, cellular and physiological processes. This is because a selection pressure is only felt by steps that have a significant control coefficient, and beneficial mutations in such steps tend to lower the control coefficient of that step. Further, steps which do not have a significant control coefficient over a selected characteristic will not feel any selection pressure, and therefore are likely to be subject to detrimental mutations, which will in turn tend to increase the control coefficient of that step. The net effect is to equalise the control coefficients of steps over a selected characteristic, and this has a number of implications for evolution and metabolic control. The analysis will be restricted to unbranched pathways.

One important selection pressure on biochemical and physiological processes during evolution is to maximise the rates of these processes for a given amount of protein [1]. Thus, for example there may be evolutionary selection pressure to increase the rate of single enzymes, metabolic pathways, and physiological processes (such as the maximal exercise rate or growth rate) without increasing the protein levels. Each of these processes consists of multiple components, which may (in principle) be independently varied by mutation, gene expression, or physiological regulation. If the overall rates are to be maximised during evolution, then this must occur via changes in the kinetics of the component steps by mutations to genes. But as these processes consist of multiple steps, changes acting at different steps may not have equivalent effects on the overall rate, because the extent to which these different steps limit the overall rate may differ. That is, some of the steps may be rate limiting for the overall rate, in which case changing the kinetics of these steps will change the overall rate, whereas other steps may not be rate limiting and thus changing the rate of these steps will have no effect on the overall process. Thus selection pressure will be exerted exclusively on the step (or steps) that is rate limiting, whereas steps that are not rate limiting will have no selection pressure exerted on them (except for large decreases in rate).

Within the theory of Metabolic Control Analysis (reviewed in [2]) the extent to which a step limits the steady-state rate of the overall process is quantified as a flux control coefficient (C). This coefficient is approximately equal to the percentage increase in the steady-state rate of the overall process brought about by a 1% increase in activity of the step. A step with a control coefficient of 1 is rate limiting, while a step with a control coefficient of 0 has no effect on the rate of the process. An important property of these flux control coefficients is that (if the system has certain common properties) the sum of the control coefficients is equal to 1. Thus in an unbranched system if one step has a control coefficient of 1, then normally all the other steps must have control coefficients of 0. Also, if the system is not branched, the control coefficients of all components will normally lie between 0 and 1. This has further important implications: (a) if the system has multiple component steps, most of steps must have control coefficients close to 0, and (b) if the control coefficient of one step changes, then the control coefficient of at least one other step must change as well (if all the coefficients are to still sum to 1).

We can define appropriate control coefficients for molecular [3], cellular [2], or physiological processes [4]. Note that if the control coefficients are defined appropriately then the control exerted by a rate constant over a physiological process may be calculated at the product of the control exerted by the rate constant over the molecular process ($C^{m,k}$), the control exerted by the molecular process over the cellular process ($C^{c,m}$), and the control exerted by the cellular process over the physiological process ($C^{p,c}$), i.e. $C^{p,k} = C^{m,k} \times C^{c,m} \times C^{p,c}$. Thus, if the individual molecular, cellular and physiological control coefficients are much less than one, which they usually will be, then in general the control exerted by a rate constant over a physiological process will be very small. The implication of this is that most mutations (natural or engineered), unless they cause a dramatic decrease in molecular rate, will have very little effect on physiological function. Consequently, normally there will be very little selection pressure on molecular steps.

The flux control coefficient acts as factor relating the selection pressure exerted on the overall process to the selection pressure exerted on the component step. We can quantify the control exerted by a process over evolutionary fitness as a fitness control coefficient (F) defined (for example) as the percentage change in the steady-state population of organisms carrying the relevant gene after unit time caused by a 1% change in the activity of the process. Thus, if the flux control coefficient of a component step i over a process j is $C^{j,i}$, and the control coefficient of the process over fitness if Fj, then the control coefficient of the step i over fitness is given by $C^{j,i} \times F^{j}$. Because for most steps in a linear process $C^{j,i}$ must be substantially less than one, it follows that the control exerted by most steps over fitness must be small.

If evolution were to start from a system where a single step was rate limiting, then selection pressure would only be applied to this step to increase its rate. However, if the rate of this step was substantially increased, then it would no longer be rate-limiting (its control coefficient would decrease) because it will no longer be the slowest step [5,6]. And consequently some other step (or steps) must become partially rate limiting, and thus these steps in turn will become subject to selection pressure to increase their rate, which in turn will cause other steps to become partially rate limiting. Furthermore, steps that are not rate limiting will have no selection pressure to prevent them undergoing genetic drift and mutation to forms with lower rates, thus in general they will drift to lower rates [7]. When the rate is low enough, the step will become partially rate limiting and selection pressure will again be applied to increase the rate or prevent it falling further. Thus, during the process of evolution by natural selection to a higher rate there is a strong tendency for most or all steps to become partially rate limiting, in fact for the control coefficients of all steps to become equal. This is because selection pressure is only felt by those steps that are rate limiting, and this selection tends to decrease the control exerted by that step and increase that of others; whereas steps without control have no selection pressure preventing them back mutating to lower rates and thus increasing their control. Thus, the process of natural selection itself causes an equalisation of control coefficients. However, there are other factors that may prevent such an equalisation. For example, changing the rate of each step is not likely to be equally easy; some steps will be difficult to increase the rate of whereas other steps will be relatively easy.

SINGLE ENZYMES AND OTHER MOLECULAR PROCESSES

Metabolic control analysis can be used to analyse control and rate limitation within molecular processes, such as single enzymes (reviewed in [3]). Catalysis of a reaction by an enzyme involves a cycle of component reaction steps, including binding of the substrates, catalysis, release of substrates, and any conformational changes involved. And the extent to which each step or rate constant limits the overall rate of the enzyme can be quantified within Molecular Control Analysis. Analysis of the control distribution within a number of enzymes and transporters has shown that control and rate limitation is generally distributed among a number of steps, rather than a single rate-limiting step, particularly at physiological levels of substrates and products [3]. The above reasoning may act as one explanation as to why the control coefficients are approximately equal, that is, evolution by natural selection towards higher rates tends to equalise the control coefficients of component steps. A control distribution where a single step is rate limiting may be difficult to obtain by natural selection, because once a step has low control over the selected function of the enzyme, then it does not feel any selection pressure and therefore has no pressure to preventing it back mutating to a lower rate, and thus gaining some level of control again.

A number of researchers have suggested that there is an evolutionary optimum distribution of rate constants within an enzyme in order to obtain a maximum rate (reviewed in [1]). However, a set of rate constants and substrate and product concentrations determines a unique distribution of control coefficients of the steps or rate constants. Thus, a distribution of rate constants within an enzyme which is "optimum" from a kinetic point of view may not be feasible in terms of the mechanism of evolution, because, for example, it may not be possible to evolve towards a set of rate constants where the control coefficients of one or more rate constants or steps is very close to zero (because selection pressure can not be applied to steps that have zero control).

METABOLIC PATHWAYS AND OTHER CELLULAR PROCESSES

Experimental measurement of the control coefficients of enzymes and transporters within metabolic pathways has shown in general that many enzymes share the control over pathway rates, and thus most control coefficients are small (reviewed in [2]). One explanation of this finding may be that evolution by natural selection tends to equalise control coefficients for the reasons outlined above. I have also previously argued that there may be a tendency for the control coefficients to be proportional to the specific activity of the enzymes involved if there is a strong pressure to minimise total protein levels in cells [8]. The relative activity of different enzymes in a pathway may also be varied by differential gene expression and by regulation, as well as by mutation. But it remains true that enzymes that have negligible control over the pathway flux will have no selection pressure to prevent them back mutating to lower rates, and enzymes that have significant control will be selected for higher rates, and therefore will in general lose control.

MAXIMAL METABOLISM AND OTHER PHYSIOLOGICAL PROCESSES

Metabolic control analysis can be applied to physiological processes using for example Physiological control analysis [4]. A physiological process such as maximal exercise or growth, involves the interaction of multiple organs and tissues, each of which may limit the overall rate to different extents. Tissues that are involved in the process but have no significant control over its rate will not feel any selection pressure to optimise their function with regard to that process, and therefore this function will in general degrade over time, due to genetic drift or selection for other functions. Those organs that are limiting for a selected physiological function will feel the selection pressure and therefore increase their rate, resulting in a decrease in their control.

The principle of symmorphosis has been suggested explain the evolutionary design of physiological processes such as maximal metabolic rate [9]. According to this principle, the organs or component activities of a physiological process are present at a level or activity just sufficient to only partially limit or not limit the overall rate of physiological process, because this represents the most efficient design as no component is present in excess. Thus, for example, the lungs, heart, vascular system, and muscles are present at levels where no one system is in excess for maximal metabolic rate or exercise. This seems a reasonable principle, but we could invert this reasoning and suggest that none of these organs is present in excess because evolution by natural selection tends to equalise the control distribution for the reasons outlined above.

ACKNOWLEDGEMENTS

This work was supported by the Royal Society, London.

REFERENCES

1. Heinrich, R., Schuster, S. & Holzhutter, H-G. (1991) Eur. J. Biochem. 201, 1-21.
2. Fell, D. (1992) Bichem. J. 286, 313-330.
3. Brown, G. C., Westerhoff, H. V. & Kholodenko, B. N. (1996) J. theor. Biol. 182, 389-396.
4. Brown, G. C. (1994) Biochem. J. 297, 115-122.
5. Fell, D. A. & Thomas, S. (1995) Biochem. J. 311, 35-39.
6. Kholodenko, B. N. & Brown, G. C. (1996) Biochem. J. 314, 753-760.
7. Hartl, D. L. & Taubes, C. H. (1996) J. theor. Biol. 182, 303-309.
8. Brown, G. C. (1991) J. theor. Biol. 153, 195-203.
9. Taylor, C. R. (1987) Annu. Rev. Physiol. 49, 135-146.

THE INFLUENCE OF THE LLD-ACV:BISACV RATIO ON A MCA OF THE PENICILLIN BIOSYNTHETIC PATHWAY IN *PENICILLIUM CHRYSOGENUM*

Hanne Aae Theilgaard and Jens Nielsen

Center for Process Biotechnology, Department of Biotechnology. Building 223, Technical University of Denmark, DK-2800 Lyngby, Denmark.
Telephone: +45 45 25 26 81, Fax: + 45 45 88 41 48, E-mail: ht@ibt.dtu.dk

INTRODUCTION

Metabolic control analysis (MCA) is an excellent tool to evaluate the distribution of metabolic flux control within biochemical pathways. With knowledge of the kinetics of the individual reactions in a linear pathway the elasticity coefficients can be calculated and thereafter the flux control coefficients (FCC) by using the summation and connectivity theorems (Fell and Sauro, 1985; Westerhoff and Kell, 1987). This approach requires detailed knowledge of the pathway biochemistry and well determined kinetic parameters. The penicillin biosynthetic pathway in *Penicillium chrysogenum* has been subject to several studies using MCA [Nielsen and Jørgensen (1995), Pissara *et al.* (1996) and Nielsen (1997)]. In this paper the original model of Nielsen and Jørgensen (1995) based on the kinetics of the first two reactions of the pathway is extended with the formation of bisACV from the pathway intermediate LLD-ACV and their parallel inhibition of the enzyme ACVS.

Biosynthetic pathway

Figure 1 depicts the first two steps of the penicillin biosynthetic pathway together with the formation and reduction of bisACV. The third step of the pathway (not depicted) is the final conversion of isopenicillin N to penicillin V catalysed by acyl-CoA:isopenicillin N acyltransferase (AT). In this step the α-aminoadipic acid side chain of isopenicillin N is exchanged with the precursor side chain phenoxyacetic acid or phenylacetic acid to give penicillin V or G, respectively.

As the first intermediate LLD-ACV possesses a free cysteine thiol, it can exist either in a reduced monomeric form or as an oxidised dimer: the disulfide bisACV, which is not a substrate for IPNS. During fed-batch cultivation of a high-yielding strain of *P. chrysogenum*, ACV (determined as a total of both the oxidized and reduced form) has been observed to accumulate throughout the cultivation to an intracellular pool level of about 6 mM (Nielsen and Jørgensen, 1995). Since the purified ACVS of *P. chrysogenum* is subject to feed-back inhibition of both the reaction product LLD-ACV (as shown below) and bisACV (Theilgaard *et al.* 1997), there is a significant inhibition of the first step during fed-batch cultivations.

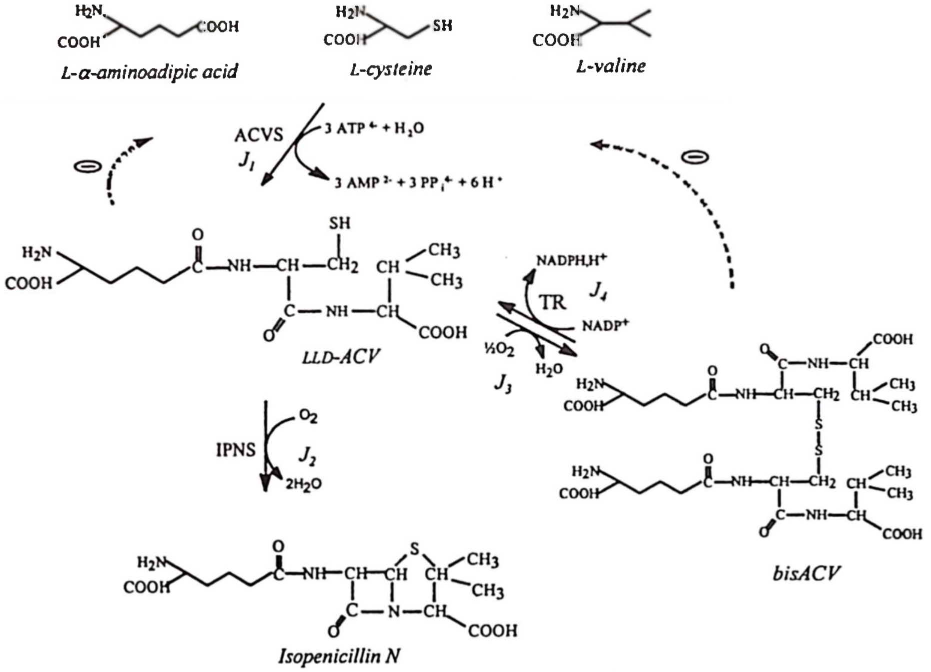

Figure 1 The first two steps in the penicillin biosynthetic pathway in *P. chrysogenum* together with the formation and reduction of bisACV.

Reduction of bisACV to LLD-ACV is catalysed by a specific thioredoxin reductase system (TR) which has a K_m value of 125 μM. This enzyme was purified by Cohen *et al.* (1993) together with another very similar disulphide reductase system: the glutaredoxin reductase system (GR). Both systems are located in the cytoplasm and can partially substitute each other. Besides keeping the LLD-ACV in its reduced

TR system is most likely supporting the β-lactam biosynthesis modulating the thiol-disulfide redox state of the functionally important cysteine residues in ACVS and IPNS (Cohen *et al.* 1993).

In both prokaryotic and eucaryotic organisms the GR is thought to govern the general thiol-disulfide redox balance by acting on the level of glutathione, which is kept almost entirely in its reduced monomeric state (Kosower and Kosower 1978). In *E. coli* the ratio of GSH:GSSG is reported to be 50:1 - 200:1 (Hwang *et al.* 1992). However the measurement of the *in vivo* GSH:GSSG ratio is difficult and in eucaryotic cells the problem of compartmentalisation is adding further complexity, and it is therefore difficult to draw any solid conclusions. The level of oxidative stress experienced by the cell will also affect the ratio as it has been reported by Emri *et al.* (1997). To examine whether the TR system together with the GR system is able to preserve the reductive environment during the production phase of penicillin V the ratio of ACV:bisACV has been measured during continuous cultivation and the result has been used to inspect the distribution of flux control in the penicillin biosynthetic pathway.

METHODS

The high penicillin yielding strain of *Penicillium chrysogenum* (obtained from Novo Nordisk A/S, Bagsværd, Denmark) was grown as a constant-mass continuous cultivation in a 9 L Chemap bioreactor (Christiansen *et al.* 1995). To measure the intracellular ratio of LLD-ACV:bisACV samples were withdrawn from the culture medium during the period of high penicillin productivity (Theilgaard *et al.* 1997). To extract and measure the two metabolites the method of Fariss and Reed (1987) was adopted: 2 g of frozen mycelium was ground to a fine powder in a mortar in liquid nitrogen. 5 ml of 10% perchloric acid with 1 mM bathophenanthroline-disulfonic acid was added and ground into the mycelium. The suspension was allowed to thaw and then centrifuged at 15,000g for 15 min. To block the free thiol groups and perform the derivation of the amino groups with 1-fluoro-2,4-dinitrobenzene the procedure of Fariss and Reed (1987) was used.

Kinetic model

The *in vitro* activity of the AT was shown to be orders of magnitude larger than the activity required to maintain the flux through the pathway (Nielsen and Jørgensen, 1995) and it was concluded that the degree of pathway control exerted by the AT could be neglected in MCA. The kinetics of ACVS and IPNS are as proposed by Nielsen and Jørgensen (1995), but the expression for the ACVS is revised to contain terms for feed-back inhibition of both LLD-ACV and bisACV (figure 2). The spontaneous oxidation of LLD-ACV to bis-ACV is assumed to follow second order kinetics with respect to LLD-ACV. The kinetics of the reverse reaction, i.e. the reduction of bisACV to LLD-ACV catalysed by the TR system, is assumed to follow Michaelis-Menten type kinetics. The v_{max} of the three enzyme catalysed reactions are function of various effectors which may include NADP(H), ATP etc. The kinetic constants necessary to calculate the elasticity coefficients are given in table 1.

$$r_{ACV} = \frac{v_{ACVS}}{1 + K_{aaa} c_{aaa}^{-1} + K_{cys} c_{cys}^{-1} + K_{val} c_{val}^{-1}} \cdot \frac{1}{1 + c_{ACV} K_{ACV}^{-1}} \frac{1}{1 + c_{bisACV} K_{bisACV}^{-1}} \qquad r_{OX} = k_{OX} \cdot c_{O_2}^{1/2} \cdot c_{ACV}^{2}$$

$$r_{IPN} = \frac{v_{IPNS} \cdot c_{ACV}}{c_{ACV} + K_{m,ACV} (1 + c_{glut} K_{i,glut}^{-1})} \cdot c_{O_2} \qquad r_{RED} = \frac{v_{RED} \cdot c_{bisACV}}{K_{m,bisACV} + c_{bisACV}}$$

Figure 2. The four kinetic expressions from which the elasticity coefficients are derived.

Table 1. Model parameters

Parameter	*Value*	*Reference*
c_{ACV} (total)	1.76 mM	Henriksen et al. (1997)
c_{GSH}	4.76 mM	-
K_{ACV}	0.54 mM	This reference
K_{bisACV}	1.4 mM	Theilgaard et al. (1997)
K_{aaa}	45 µM	-
K_{cys}	80 µM	-
K_{val}	80 µM	-
$K_{m,ACV}$	0.13 mM	Ramos et al. (1985)
$K_{i,GSH}$	8.9 mM	Nielsen and Jørgensen (1995)
$K_{m,bisACV}$	125 µM	Cohen et al. (1993)

Results

To investigate the proposed feedback inhibition of LLD-ACV on purified ACVS the standard ACVS assay (Theilgaard *et al.* 1997) was carried out with addition of LLD-ACV to a final concentration of 0-3 mM and the results were depicted in a Lineweaver-Burk plot (figure 3). The inhibition parameter K_{ACV} is determined to be 0.54 mM. The sensitivity of the HPLC method was sufficient for the detection of the reaction product LLD-ACV. The inhibition parameter for bis-ACV was earlier determined to be 1.4 mM (Theilgaard, *et al.* 1997). The results of the extraction and measurement of the LLD-ACV:bisACV ratio in *P. chrysogenum* are summarised in table 2. A LLD-ACV: bisACV ratio of 1:5 indicates that the intracellular reductive state is not preserved during the production phase of penicillin V fermentations. The ratio is used in the MCA based on the extended model of the first two steps of the penicillin biosynthetic pathway.

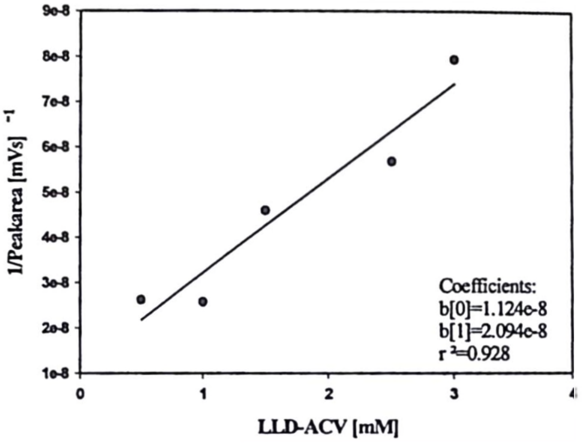

Figure 3. Lineweaver-Burk plot for the determination of the inhibition constant of LLD-ACV on purified ACVS.

Table 2. Determination of the LLD-ACV:bisACV ratio in *P. chrysogenum*. The result indicated at each measurement is the average of three independent derivations carried out with the same cell extract.

Measurement	*LLD-ACV (rt. 20.23)*	*bisACV (rt. 19.87 & 21.22)*	*ratio LLD-ACV: bisACV*
SAMPLEI Area (μVs)	113.144	592.796	~1:5
SAMPLEII Area (μVs)	137.925	706.124	~1:5

Metabolic control analysis

The model given in figure 1 contains 4 fluxes and two intermediate metabolites: LLD-ACV and bisACV. Two constrains are given at steady state: $J_1 = J_2$ and $J_3 = J_4$. J_1 and J_3 are chosen as dependent fluxes. As the number of metabolites in a branched pathway is smaller than the number of fluxes it is necessary to add structural relationships to be able to calculate the FCC. Based on the equations derived by Stephanopoulos *et al.* (1998) for branched pathways the expression given below relating the FCC and concentration control coefficients (CCC) with the elasticity coefficients and fractional fluxes is found. Here f_{12} and f_{34} specify the relative fluxes J_2/J_1 and J_4/J_3, respectively, and with the above mentioned constraints $f_{12} = f_{34} = 1$:

$$\begin{bmatrix} 1 & 0 & -\varepsilon^{ACV}_{IPNS} & 0 \\ 0 & 1 & 0 & -\varepsilon^{bisACV}_{RED} \\ f_{12} & 0 & -\varepsilon^{ACV}_{ACVS} & -\varepsilon^{bisACV}_{ACVS} \\ 0 & f_{34} & -\varepsilon^{ACV}_{OX} & 0 \end{bmatrix} \begin{bmatrix} C^{J_2}_{ACVS} & C^{J_2}_{IPNS} & C^{J_2}_{OX} & C^{J_2}_{RED} \\ C^{J_4}_{ACVS} & C^{J_4}_{IPNS} & C^{J_4}_{OX} & C^{J_4}_{RED} \\ C^{ACV}_{ACVS} & C^{ACV}_{IPNS} & C^{ACV}_{OX} & C^{ACV}_{RED} \\ C^{bisACV}_{ACVS} & C^{bisACV}_{IPNS} & C^{bisACV}_{OX} & C^{bisACV}_{RED} \end{bmatrix} = \begin{bmatrix} 1 & 0 & 0 & 0 \\ 0 & 1 & 0 & 0 \\ 0 & 0 & 1 & 0 \\ 0 & 0 & 0 & 1 \end{bmatrix}$$

The elasticity coefficients are easily derived from the kinetic expressions given in figure 2 and the constants in table 1, and the FCC and the CCC can then be found by matrix inversion.

Due to the constraints on the fluxes the FCCs with respect to J_1 and J_3 will be identical with the FCCs with respect to J_2 and J_4, respectively. In figure 4 and 5 the FCCs with respect to the fluxes $J_2 (= J_1)$ and $J_4 (= J_3)$ are depicted as function of different values of the LLD-ACV:bisACV ratio. When the pathway is extended with the formation of bisACV two sets of FCCs characterise the system: the oxidation/reduction of bis-ACV and the pathway towards IPN. As opposed to Henriksen *et al.* (1997) where an almost equal sharing of flux control between the ACVS and IPNS was found, the incorporation of the bis-ACV formation almost completely shifts the flux control towards the ACVS reaction and it can be concluded that the LLD-ACV branch point must be termed as strongly rigid as the LLD-ACV:bisACV ratio only has a minor influence on the flux control of the pathway. Regarding the oxidation-/reduction of bisACV the flux control is pronounced at the IPNS when the LLD-ACV: bisACV ratio is below 1 as it consumes the LLD-ACV. For high levels of LLD-ACV the flux control mainly resides at the oxidation reaction consuming the LLD-ACV.

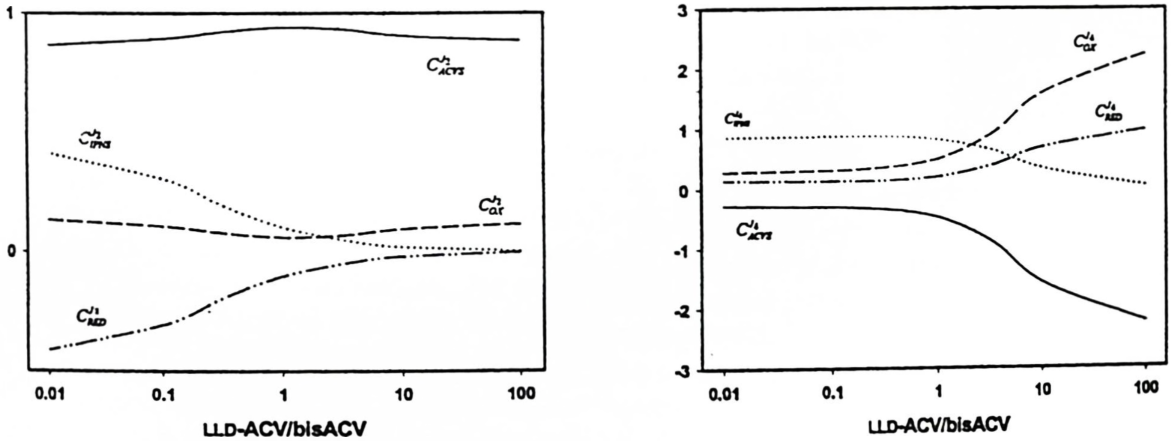

Figure 4 and 5. FCCs with respect to J_2 ($=J_1$) and J_4 ($=J_3$) as function of the LLD-ACV:bisACV ratio. The total ACV concentration was 1.76 mM (Henriksen *et al.* 1997).

REFERENCES

Christiansen, L.H.; Henriksen, C.M.; Nielsen, J. and Villadsen, J. and Egel-Mitani, M. (1995) J. Biotechnol. **42**: 95-107

Cohen, G.; Argaman, A.; Schreiber, R.; Mislovati, M. and Aharonowitz, Y. (1994) J. Bacteriol. **176** (4): 973-984

Emri, T.; Pócsi, I. and Szentirmai, A. (1997) Free Radical Biol. Med. **23**

Fariss, M.W. and Reed, D.J. (1987) Meth. Enzymol. **143**:101-107

Fell, D.A. and Sauro, H.M. (1985) Eur. J. Biochem. **148**:555-561

Henriksen, C.M.; Nielsen, J. and Villadsen, J. (1997) Biotechnol. Prog. **13**:776-782

Hwang, C.; Sinsky, A.J.; and Lodish, H.F. (1992) Science **257**: 1496-1502

Kosower, N.S. and Kosower, E.M. (1987) Int. Rev. Cytol. **54**:109-160

Nielsen, J. (1997) Biochem. J. **321**:133-138

Nielsen, J. and Jørgensen, H.S. (1995) Biotechnol. Prog. **11**:299-305

Pissara, P.d.N.; Nielsen, J. and Bazin, M.J. (1996) Biotechnol. Bioeng. **51**:168-176

Stephanopoulos, G.; Nielsen, J. and Aristodou, A. *Metabolic Engineering*. Academic Press, San Diego (1998)

Theilgaard, H.B.Aa.; Kristiansen, K.N.; Henriksen, C.M. and Nielsen, J. (1997) Biochem. J. **387**:185-191

Westerhoff, H.V. and Kell, D.B. (1987) Biotechnol. Bioeng. **30**:101-107

CHANGES IN ENZYME EXPRESSION AND THE CONTROL OF METABOLIC FLUX

David A. Fell & Simon Thomas

School of Biological and Molecular Sciences, Oxford Brookes University, Gipsy Lane, OXFORD, OX3 0BP, Great Britain, Tel: +44 1865 483247, Fax: +44 1865 484017 email: daf@bms.brookes.ac.uk

Metabolic Control Analysis has disproved the concept of the necessary existence of the rate limiting step, but leaves unanswered the question of how cells change the flux in metabolic pathways. We have argued [1-4] that the biochemical evidence is not consistent with large changes in metabolic flux resulting from control at a single site, as promoted by Krebs amongst others [5], instead requiring simultaneous action at several or many sites (multisite modulation) by analogy with the Universal Method [6]. Previously we have concentrated on the evidence that short term alterations in metabolic flux involve multiple control sites. Here we add that long-term adjustments in metabolic flux typically involve changes in the activity of most, if not all, the enzymes of the pathway.

INTRODUCTION

One perceived difficulty of Metabolic Control Analysis is that it is not an accurate predictor of the consequences of large parameter perturbations. Strictly this is true, but there are still lessons to be learnt about the characteristics of large flux changes that have been induced by different means. An example is the finite change analysis of Small & Kacser [5], which shows that the yield in terms of the relative increase in flux obtained by activating a single enzyme is poor unless its flux control coefficient is close to 1.

Another area where Control Analysis illustrates the properties of control mechanisms concerns their relative effects on fluxes and metabolite concentrations, since the differences between some of the predictions and experimental observations is so large that they cannot be attributed to the uncertainty in extrapolating from infinitesimal to finite changes. For example, in muscle glycolysis, of the order of 100-fold stimulations of glycolytic flux have been associated with negligible changes in glycolytic intermediates [2,4]. If such a large change in glycolytic rate could be produced by activation of a single enzyme, its concentration control coefficients would have to be significantly smaller than its flux control coefficient. Yet it can be shown that this is not usually the case [2,3]: concentration control coefficients are often larger than the flux control coefficients, and even where mechanisms such as feedback inhibition make the concentration control coefficients smaller, the difference is still not very large. Thus despite not being able to make accurate predictions of the effects of large changes in phosphorylase activity in muscle, we can be certain that its activation on contraction cannot be a sufficient explanation of the activation of glycolysis.

DEFINITIONS

The flux, J, and metabolite, S_j, response coefficients to an external parameter, such as an effector X, are:

$$R_X^J = \sum_i C_i^J \pi_X^i; \qquad R_X^{S_j} = \sum_i C_i^{S_j} \pi_X^i, \qquad (1)$$

where π_X^i is the elasticity of the step i to X. Normally these would only be valid for small changes, but in the case that the π_X^i are all identical, we will have:

$$R_X^J = \pi_X^i \sum_i C_i^J \Rightarrow \pi_X^i; \qquad R_X^{S_j} = \pi_X^i \sum_i C_i^{S_j} \Rightarrow 0. \qquad (2)$$

Under these circumstances, even the effects of a large change in X are predictable because only the flux is affected; no metabolite concentrations change.

Since we are interested in the relative sizes of the flux and concentration responses, we define the co-response of S_j and J to X as:

$$R_X^{S_j:J} = \frac{R_X^{S_j}}{R_X^J} = \frac{\partial \ln S_j}{\partial \ln X} \Big/ \frac{\partial \ln J}{\partial \ln X} = \frac{\partial \ln S_j}{\partial \ln J}, \qquad (3)$$

for which there are two simple cases. If X acts specifically on a single step k, then from eqn. (1), $R_X^{S_j:J}$ equals the ratio of the control coefficients of enzyme k, the co-response coefficient of enzyme k, $O_k^{S_j:J}$, by the original definition of Hofmeyr et al [7]. If X acts equally on all the steps, then eqn. (2) applies and $R_X^{S_j:J} = 0$. Unfortunately, if X acts on more than one step but with unequal effects, there is no simple expression for $R_X^{S_j:J}$. Finally, we should note that when looking at the biochemical literature, we may only be able to calculate a finite approximation:

$$R_X^{S_j:J} = \frac{\Delta \ln S_j}{\Delta \ln J} \qquad (4)$$

SHORT TERM CHANGES IN FLUX.

In support of our proposal for multisite modulation, the finite change values for $R_X^{S_j:J}$ for glycolytic and TCA cycle metabolites relative to flux, where 'X' is the rest to exercise transition, are typically in the range between 0.02 and -0.02 even for flux stimulations of 100 fold [2,4]. Insulin stimulation of rat muscles gives a co-response value for glucose 6-phosphate to glycogen synthesis flux of 0.15 to 0.30, quoted by Shulman & Rothman [8] in support of their argument that the predominant role of the covalent modification of glycogen synthase is homeostasis of the glucose 6-phosphate concentrations. Similarly, in hepatocytes, a 2 fold stimulation of glycogen synthesis by glutamine involves no measurable change in glucose 6-phosphate [9], a co-response of zero.

The significance of these small co-responses comes from the fact that in a linear pathway with simple kinetics, stimulation of the flux by activation of an enzyme with a finite control coefficient will give values for metabolite:flux co-responses greater than 1 for downstream metabolites [2]. This too is a typical result from engineering changes in the amount or kinetics of a single target enzyme: the metabolite concentration effects are usually larger than the flux changes. Cooperativity improves homeostasis of metabolite levels during flux changes [2,3,10,11], but can generally only reduce $O_k^{S_j:J}$

to $1/n_H$ at best, the reciprocal of the Hill coefficient for substrate or effector cooperativity. How the multiplicity of interactions between glycolysis and ATP demand might generate smaller co-responses is discussed in our poster [12].

Korzeniewski et al [13] used top-down analysis to study stimulation of oxidative phosphorylation in hepatocytes by lactate plus pyruvate or vasopressin. There was a discrepancy between the value expected for the co-response of the protonmotive force and respiration flux if either just the respiration block or just the phosphorylation block had been stimulated and the much smaller observed value, which they used to calculate a proportional activation factor that showed both blocks were near-equally stimulated.

CHANGES IN ENZYME EXPRESSION

There is little experimental data where the activities of all the enzymes in a pathway, the change in flux, and the metabolite levels are measured. Hence we have to rely mainly on indirect evidence.

Strategy	Relative activity					Flux, J	Metabolite:flux co-response (finite approximation)			
	E1	E2	E3A	E4A	E5A		S1:J	S2:J	S3A:J	S4A:J
Wild type	1	1	1	1	1	1.00				
"Opposition" - E1	5	1	1	1	1	1.02	20.5	20.8	5.3	5.3
"Opposition" - E3A	1	1	5	1	1	1.08	0.3	-0.1	5.2	5.0
"Opposition" - E1 & E3A	5	1	5	1	1	1.10	4.4	4.2	5.3	5.3
Evasion (Universal Method)	3	3	5	5	5	5.00	0.0	0.0	0.0	0.0
"Suppression" - E1	*	1	1	1	1	1.17	24.9	24.6	6.2	6.0
"Suppression" - E3A	1	1	*	1	1	1.29	0.2	-0.2	11.3	11.1
"Suppression" - E1 & E3A	*	1	*	1	1	1.31	14.3	13.9	24.7	24.7
"Subversion" - demand	1	1	1	1	5	4.13	0.4	-0.2	0.9	-0.4

Table 1. Relative changes in metabolite concentrations and fluxes in a simulated branched pathway on enzyme activity changes. The results are recalculated from [14]. The pathway has two branches each with three enzymes (3A-5A, 3B-5B); enzymes 1 and 2 are common to both. Enzyme 1 is feedback inhibited by metabolite 2 and enzyme 3A by metabolite 4A. '*' indicates that the feedback was abolished with enzyme activity unchanged.

An illustration of the different consequences of various patterns of changed enzyme expression can be seen in the simulated results of Cornish-Bowden et al for a branched pathway [14] (Table 1). Only two strategies give low metabolite:flux co-responses: the Universal Method, as expected, and activation of demand where the strong feedback effects assist the flux stimulation.

We have been measuring co-responses in the glycolytic pathway of rat 3T3 fibroblasts on stimulation with foetal calf serum. Initially, the 2-fold stimulation of lactate production represents short-term changes, but by 24 hrs, enzyme induction has resulted in all enzymes increasing significantly (except for GAPDH). Even so, the co-responses seem constant throughout, and for the hexose phosphates are less than 0.4; indeed the co-responses for the fructose phosphates can be less than 0.1. Many of the

3C glycolytic metabolites show negative co-responses.

We have previously cited lipogenesis in the *obese* mouse and urea synthesis in response to dietary nitrogen [3] as two of many examples where long term changes in total activity of all the enzymes of a pathway are involved in the change of flux. To a first approximation, this supports the multisite modulation/Universal Method proposal about the way cells change flux. However, in the case of the enzymes of nucleotide metabolism in a hepatic cancer cell line, Weber's group [15] showed that the changes in enzyme activity were not uniform; although all the enzymes were affected, there was a gradient whereby the least active enzymes showed the largest changes and the most active enzymes the least. We have recently found that this seems to be a consistent phenomenon in over 20 other examples, comprising different pathways, tissues, organisms and stimuli. Thus the multisite modulation mechanism implemented in cells on changes in enzyme expression seems to be a modified version of the Universal Method.

CONCLUSION

The challenges in applying Control Analysis to physiologically interesting biochemical situations only partly come from the need to deal with large perturbations. Of more importance is the fact that physiological control mechanisms are truly systemic so that there are many contributions with a variety of mechanisms to any observed outcome. Because metabolic research has been guided by the opposite paradigm - the search for a single dominant controller - it is likely we are ignorant of some of the important contributing mechanisms.

ACKNOWLEDGEMENTS

We thank Oliver Chow Worn and Janet Evins for able technical support. Financial support from the Wellcome Trust (Grant no. 04728), the Leverhulme Trust and Oxford Brookes University is gratefully acknowledged.

REFERENCES

[1] Fell, D. A. and Thomas, S. (1995) Biochem. J. 311, 35-39.
[2] Thomas, S. and Fell, D. A. (1996) J. Theor. Biol. 182, 285-298.
[3] Fell, D. A. (1997) Understanding the Control of Metabolism. Portland Press, London.
[4] Thomas, S. and Fell, D. A. (1997) Advan. Enzyme Regul. 38 (in press)
[5] Krebs, H. A. (1957) Endeavour 16, 125-132.
[6] Kacser, H. and Acerenza, L. (1993) Eur. J. Biochem. 216, 361-367.
[7] Hofmeyr, J.-H. S.,Cornish--Bowden, A. and Rohwer, J. M. (1993) Eur. J. Biochem. 212, 833-837.
[8] Shulman R. G. and Rothman D. L. (1996) Proc. Natl. Acad. Sci. 93, 7491-7495.
[9] Lavoinne, A., Baquet, A. and Hue, L. (1987) Biochem. J. 248, 429-437.
[10] Hofmeyr, J.-H. S. and Cornish--Bowden, A. (1991) Eur. J. Biochem. 200, 223-236.
[11] Hofmeyr, J.-H. S. (1995) J. Bioenerg. Biomembr. 27, 479-489.
[12] Thomas, S. and Fell, D. A. (1998) this volume.

[13] Korzeniewski, B., Harper, M.-E. and Brand, M. D. (1995) Biochim. Biophys. Acta. 1229, 315-322.

[14] Cornish-Bowden, A., Hofmeyr, J.-H. S., and Cárdenas, M. L. (1995) Bioorg. Chem. 23, 439-449.

[15] Weber, G. (1996) Advan. Enzyme Regul. 36, 33-55.

10

USING CO-RESPONSE COEFFICIENTS AND SENSITIVITY ANALYSIS TO EXPLORE PHYSIOLOGICAL FLUX CONTROL AND METABOLITE CONCENTRATION REGULATION

Simon Thomas & David A. Fell

School of Biological and Molecular Sciences, Oxford Brookes University, Gipsy Lane, OXFORD, OX3 0BP, Great Britain, Tel: +44 1865 483964, Fax: +44 1865 484017, email: simon@bms.brookes.ac.uk, daf@bms.brookes.ac.uk

INTRODUCTION

Metabolic Control Analysis (MCA) has provided a powerful tool for theoreticians and experimentalists alike to investigate the behaviour of metabolic pathways. In particular, the summation and connectivity theorems [1], and their methodological developments, such as the matrix method [2, 3] enable the rôles of individual components in the behaviour of pathways to be elucidated. However, newcomers to the field can, understandably, be immediately deterred by the enormous complexity of the expressions for control coefficients for enzymes from even relatively simple pathways. We have favoured the use of sensitivity analysis of control coefficients to identify those variables whose values are critical in determining the different aspects of a pathway's behaviour [4, 5], an illustration of which we provide here.

Our current interest is the homeostasis of metabolic intermediates in pathways undergoing flux change. We have previously described how multiple enzyme activation in a pathway can give rise to good metabolite homeostasis [6, 7], but an additional factor that must be considered is the interaction between pathway intermediates and members of conserved moieties such as the adenine nucleotides: changes in the concentrations of the latter can affect concentrations of pathways intermediates via the action of bimolecular reactions, such as those catalysed by kinases, as well as by allosteric interactions.

We use co-response coefficients [8], which quantify the relative magnitudes of changes in fluxes and metabolite concentrations in response to enzyme activation(s), as the most direct means of studying homeostatic phenomena. Thus, if activation of an enzyme, *E*, causes simultaneous changes in a flux, *J*, and a metabolite concentration, *M*, good homeostasis is indicated by a large value of $|O_E^{J,M}|$, where $O_E^{J,M}$ could be positive or negative. Furthermore, because co-response coefficients are quotients of the relevant control coefficients (e.g. $O_E^{J,M} = C_E^J/C_E^M$), they are amenable to the same sensitivity analysis.

METHOD

To illustrate the method, consider the pathways in Scheme 1, a representation of glycolysis from F6P to pyruvate, plus general cellular ATP hydrolysis (ATPase) and adenylate kinase (AK). 'PGK' is a composite step, representing the steps aldolase to enolase inclusive. 'F16BP', is a composite metabolite, representing the glycolytic intermediates from F16BP to 2-phosphoglycerate.

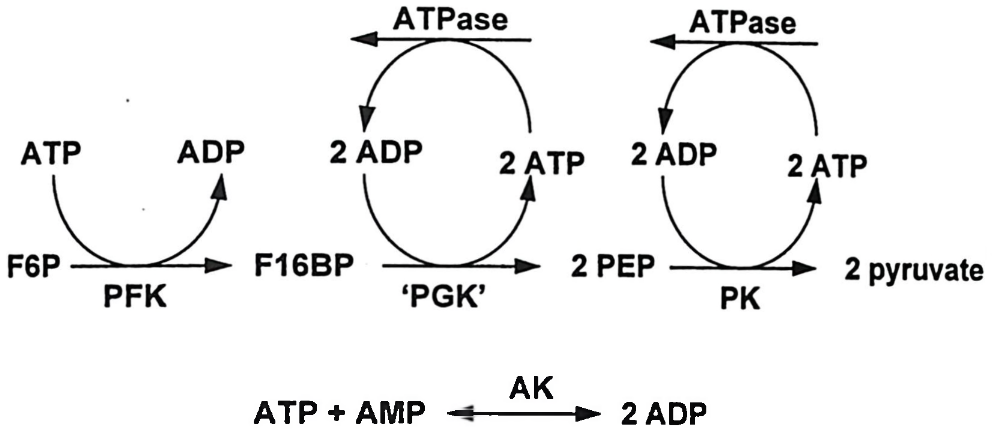

Scheme 1

Although the system in Scheme 1 is highly simplified, the equations for flux- and concentration control coefficients are nevertheless complex, involving 16 elasticities plus ratios of the adenine nucleotide (AN) concentrations, [ATP]/[AMP] and [ADP]/[AMP]. For example:

$$\frac{C^{J}_{ATPase}}{Den} = \varepsilon^{PGK}_{F16BP} \cdot \varepsilon^{PK}_{PEP} \cdot \begin{pmatrix} \varepsilon^{PFK}_{ADP} \cdot \left(\frac{ATP}{AMP} \cdot \varepsilon^{AK}_{AMP} - \varepsilon^{AK}_{ATP}\right) + \varepsilon^{PFK}_{AMP} \cdot \left(\frac{ADP}{AMP} \cdot \varepsilon^{AK}_{ATP} - \frac{ATP}{AMP} \cdot \varepsilon^{AK}_{ADP}\right) \\ +\varepsilon^{PFK}_{ATP} \cdot \left(\varepsilon^{AK}_{ADP} - \frac{ADP}{AMP} \cdot \varepsilon^{AK}_{AMP}\right) \end{pmatrix} +$$

$$\varepsilon^{PFK}_{F16BP} \cdot \varepsilon^{PK}_{PEP} \cdot \left(\varepsilon^{PGK}_{ADP} \cdot \left(\varepsilon^{AK}_{ATP} - \frac{ATP}{AMP} \cdot \varepsilon^{AK}_{AMP}\right) + \varepsilon^{PGK}_{ATP} \cdot \left(\frac{ADP}{AMP} \cdot \varepsilon^{AK}_{AMP} - \varepsilon^{AK}_{ADP}\right)\right) +$$

$$\varepsilon^{PFK}_{F16BP} \cdot \varepsilon^{PGK}_{PEP} \cdot \left(\varepsilon^{PK}_{ADP} \cdot \left(\frac{ATP}{AMP} \cdot \varepsilon^{AK}_{AMP} - \varepsilon^{AK}_{ATP}\right) + \varepsilon^{PK}_{ATP} \cdot \left(\varepsilon^{AK}_{ADP} - \frac{ADP}{AMP} \cdot \varepsilon^{AK}_{AMP}\right)\right)$$

where J is the flux through PK and *Den* is the common denominator of all control coefficients for the pathway [2, 3]. However, appropriate approximations to the elasticities and AN concentrations can be made. For initial values we chose: $\varepsilon^{PGK}_{Fru1,6P2} = \varepsilon^{PGK}_{ADP} = 5$, $\varepsilon^{PGK}_{PEP} = \varepsilon^{PGK}_{ATP} = -4$; $\varepsilon^{PK}_{PEP} = \varepsilon^{PK}_{ADP} = 0.7$, $\varepsilon^{PK}_{ATP} = -0.1$; $\varepsilon^{AK}_{AMP} = \varepsilon^{AK}_{ATP} = 50$, $\varepsilon^{AK}_{ADP} = 2 - 2 \times \varepsilon^{AK}_{AMP} = -98$; $\varepsilon^{PFK}_{Fru1,6P2} = 0$, $\varepsilon^{PFK}_{AMP} = 0.14$, $\varepsilon^{PFK}_{ADP} = 0.14$, $\varepsilon^{PFK}_{ATP} = -0.1$; $\varepsilon^{ATPase}_{ATP} = 0.5$, $\varepsilon^{ATPase}_{ADP} = -0.5$; [ATP]/[ADP] = 50, [ATP]/[AMP] = 0.98·([ATP]/[ADP])^2 = 2450. Substituting these values gives flux control coefficients of: $C^{J}_{PFK} = 0.55$, $C^{J}_{ATPase} = 0.45$, $C^{J}_{PGK} = 0$, $C^{J}_{PK} = 0$ and $C^{J}_{AK} = -0.0015$. As we are interested in flux control, we shall limit further discussion to those steps with significant flux control coefficients, namely PFK and ATPase. Co-response coefficients over flux and F16BP are: $O^{JF16BP}_{PFK} = 0.20$, $O^{JF16BP}_{ATPase} = -0.34$). Thus, a small flux change brought about by a change in PFK would entail a five-fold greater relative increase in F16BP, whereas that brought about by changing ATPase activity would give a three-fold greater relative decrease. Thus, a combination of activation of PFK and ATP hydrolysis could generate a flux increase with good homeostasis of glycolytic intermediates.

Obviously, the use of approximate values for elasticities and AN concentrations could be detrimental to the accuracy of the calculated control- and co-response coefficients. However, one benefit of the algebraic formalism of MCA is that algebraic expressions can be automatically generated for the sensitivities of the coefficients with respect to the variables, namely $\partial \ln C / \partial \ln v$, where C is any control coefficient, and v is any variable defined in the matrix method equations [2, 3].

RESULTS

Applying sensitivity analysis to the control coefficients for the pathway in Scheme 1 generates exact values for the sensitivities of the control coefficients, *at the given values of the elasticities and AN concentrations used in the analysis*. Again, restricting consideration to PFK and ATPase, only five of the variables have any significant influence on the values of their flux control coefficients. The relevant sensitivities, plus those to C^{F16BP}_{PFK} and C^{F16BP}_{ATPase} are listed in Table 1, all other sensitivities of C^{J}_{PFK} and C^{J}_{ATPase} being at least one order of magnitude smaller than those listed.

Table 1: Sensitivities of control coefficients to elasticities.

	$\varepsilon^{ATPase}_{ATP}$	$\varepsilon^{ATPase}_{ADP}$	ε^{PFK}_{AMP}	ε^{PFK}_{ADP}	ε^{PFK}_{ATP}
C^{J}_{PFK}	0.009	0.443	-0.297	-0.151	-0.002
C^{J}_{ATPase}	-0.011	-0.537	0.364	0.183	0.003
C^{F16BP}_{PFK}	-0.006	-0.269	-0.297	-0.151	-0.002
C^{F16BP}_{ATPase}	-0.011	-0.537	-0.599	-0.301	-0.004

Thus, from the complex expressions for the control coefficients, the control and regulatory properties in which we are interested can be considered in terms of only five important variables (or even three, noting that all the sensitivities to $\varepsilon^{ATPase}_{ATP}$ and ε^{PFK}_{ATP} are one to two orders of magnitude less than those to $\varepsilon^{ATPase}_{ADP}$, ε^{PFK}_{AMP} and ε^{PFK}_{ADP}).

Regarding the physiological relevance of the control coefficients and the sensitivities in Table 1, the following points can be deduced:

1. The distribution of flux control depends primarily on ADP inhibition of ATPase, and on the activation of PFK by AMP: increase in ADP inhibition of ATPase increases the control on PFK ($\partial \ln C^{J}_{PFK} / \partial \ln \varepsilon^{PFK}_{AMP} > 0 \Rightarrow \partial C^{J}_{PFK} / \partial \varepsilon^{PFK}_{AMP} < 0 \Rightarrow \partial C^{J}_{PFK} / \partial |\varepsilon^{PFK}_{AMP}| > 0$); increase in AMP activation of PFK increases control on ATPase ($\partial \ln C^{J}_{ATPase} / \partial \ln \varepsilon^{PFK}_{AMP} > 0$).
2. In addition to altering the relative degrees of flux control invested in PFK and ATPase, ADP inhibition of ATPase and AMP activation of PFK have pronounced effects on the homeostatic properties of the system. Stronger ADP inhibition of ATPase results in improved homeostasis of glycolytic metabolites in response to

PFK activation ($\partial \ln O^{J16BP}_{PFK} / \partial \ln \varepsilon^{ATPase}_{ADP} = \partial \ln C^{J}_{PFK} / \partial \ln \varepsilon^{ATPase}_{ADP} - \partial \ln C^{F16BP}_{PFK} / \partial \ln \varepsilon^{ATPase}_{ADP} > 0$), whereas stronger activation of PFK by AMP improves the homeostasis in response to ATPase activation ($\partial \ln O^{JF16BP}_{ATPase} / \partial \ln \varepsilon^{PFK}_{AMP} = \partial \ln C^{J}_{ATPase} / \partial \ln \varepsilon^{PFK}_{AMP} - \partial \ln C^{F16BP}_{ATPase} / \partial \ln \varepsilon^{PFK}_{AMP} > 0$).

3. Increased inhibition of ATPase by ADP, and increased activation of PFK by AMP have no effect on the homeostasis of glycolytic intermediates in response to activation of ATPase and PFK respectively ($\partial \ln C^{J}_{ATPase} / \partial \ln \varepsilon^{ATPase}_{ADP} - \partial \ln C^{F16BP}_{ATPase} / \partial \ln \varepsilon^{ATPase}_{ADP} = 0$; similarly $\partial \ln C^{J}_{PFK} / \partial \ln \varepsilon^{PFK}_{AMP} - \partial \ln C^{F16BP}_{PFK} / \partial \ln \varepsilon^{PFK}_{AMP} = 0$).

Additional results arise from this analysis. First, PFK exerts greater flux control than does ATPase over approximately 50% of the parameter space studied, but its control is sufficiently high to achieve sizeable flux increases over less than 20% of that space. Second, flux control by altering PFK activity results in poor glycolytic metabolite homeostasis over the entire parameter space studied. In contrast, over a large proportion of the parameter space, control by activation of ATPase can lead to large flux changes (i.e. high flux control) coupled with excellent glycolytic metabolite homeostasis, similar to that observed in working muscle.

DISCUSSION

The results are additional evidence of the potential for physiological ATP demand to exert control over glycolytic flux, but additionally show that the known effector interactions, in addition to their previously known role in ATP regulation [9], could contribute to the remarkable homeostasis of glycolytic metabolite levels observed *in vivo*. They further indicate that quantitative characterisation of likely domains of behaviour of metabolic systems can be achieved by an algebraic analysis that is not highly dependent on a full and precise knowledge of the molecular details of the kinetic/regulatory properties of the enzymes.

This work was supported by a Leverhulme Trust Special Research Fellowship awarded to ST, and a Wellcome Trust Sir Henry Wellcome Commemorative Award for Innovative Research (04728) to DAF and ST.

REFERENCES

1 Kacser, H., Burns, J.A. and Fell, D.A. (1995) Biochem. Soc. Trans. 23, 341-366.
2 Fell, D.A. and Sauro, H.M. (1985) Eur. J. Biochem. 148, 555-561.
3 Sauro, H.M., Small, J.R. and Fell, D.A. (1987) Eur. J. Biochem. 165, 215-221.
4 Small, J.R. and Fell, D.A. (1990) Eur. J. Biochem. 191, 413-420.
5 Thomas, S. and Fell, D.A. (1994) J. theor. Biol. 167, 175-200.
6 Fell, D.A. and Thomas, S. (1995) Biochem. J. 311, 35-39.
7 Thomas, S. and Fell, D.A. (1996) J. theor. Biol. 182, 285-298.
8 Hofmeyr, J.-H.S., Cornish-Bowden, A. and Rohwer, J.M. (1993) Eur. J. Biochem. 212, 833-837.
9 Sel'kov, E.E. (1975) Eur. J. Biochem. 59, 151-157.

THE ANALYSIS OF CONTROL DISTRIBUTION FOR CATALYTIC CYCLE OF INORGANIC PYROPHOSPHATASE OF ESCHERICHIA COLI.

Nartsissov Ya.R.[1], *Kholodenko B.N.*[2]

[1]-Medical Scientific & Production Complex "Biotics", P.O. Box 39, Moscow, 113452 Russia. phone/fax : (095) 322-0074; E-mail: yarosl@biotic.dol.ru
[2]-Department of Pathology, Anatomy and Cell Biology, Thomas Jefferson University, Philadelphia, USA.

INTRODUCTION

Inorganic pyrophosphatase (EC 3.6.1.1) is found nearly in all types of cells. It is highly specific for pyrophosphate (PP) hydrolysis. Two families of enzymes, cytosolic and mitochondrial are known. They have some differences in structures and functional properties. In this study we consider the enzyme of Eschrichia coli (*E. coli*).

$$EM_n \underset{k_{-1}}{\overset{k_{+1}}{\rightleftarrows}} EM_n(M_2PP) \underset{k_{-2}}{\overset{k_{+2}}{\rightleftarrows}} EM_n(MP)_2 \underset{k_{-3}}{\overset{k_{+3}}{\rightleftarrows}} EM_n(MP) \underset{k_{-4}}{\overset{k_{+4}}{\rightleftarrows}} EM_n$$

Figure 1. The kinetic scheme of catalytic cycle for pyrophosphatase from E. coli. The letters M, P and PP indicate magnesium ions, inorganic- and pyro- phosphate, respectively. The number of magnesium ions (n) is equal to 1 or 2.

The catalytic mechanism of cytosolic pyrophosphatase extracted from microorganisms has been studied in detail [1,2]. It is commonly accepted that the hydrolysis of pyrophosphate is accomplished by the direct transfer of phosphate into water in the presence of magnesium ions. There is no phosphorylated enzyme's intermediate during the process. A corresponding kinetic scheme of this reaction is shown on Fig.1. A particular feature of microbial pyrophosphatase is the presence of three or four magnesium ions surrounding PP in the active center. The synthesis and

Table 1 The set of kinetic constants, determined for the wild type[1], and the mutant strain [2] of E-coli. The measurements were carried out at pH=7.2 and 20 mM of magnesium ions.

constants \ *E. coli*	wild type	mutant E20D
k_{+1} (mM^{-1}s^{1})	135000	49000
k_{-1} (s^{1})	12	160
k_{+2} (s^{-1})	400	150
k_{-2} (s^{-1})	81	13
k_{+3} (s^{-1})	390	180
k_{-3}(mM^{-1}s^{1})	130	22
k_{+4} (s^{-1})	600	74
k_{-4} (mM^{-1}s^{1})	1300	27

hydrolysis of PP are accompanied by the fast exchange of oxygen between water and phosphate molecules. Although the oxygen exchange does not play a physiological role this process makes it possible to determine the values of kinetic constants for the kinetic scheme of Fig. 1 [1,2].

METHODS

The kinetic scheme on Fig.1 is nearly identical to *uni-bi* mechanism, as described in [3], but in the pyrophosphatase reaction there is additional step of transition from enzyme-substrate to enzyme-product complexes. The steady state rate (V) of pyrophosphate hydrolysis can be expressed as:

$$V = (\omega 1/\omega 2)\cdot e$$

Here e denotes the total enzyme concentration, and $\omega 1$, $\omega 2$ are functions of the rate constants and substrates' concentrations, which are expressed as the following:

$$\omega 1(S,P) = A_1 \cdot PP - A_2 \cdot P_i^2;$$
$$\omega 2(S,P) = B_0 + B_1 \cdot PP + B_2 \cdot P_i + B_3 \cdot P_i^2;$$

$$A_1 = k_1 \cdot k_2 \cdot k_3 \cdot k_4; \quad A_2 = k_{-1} \cdot k_{-2} \cdot k_{-3} \cdot k_{-4};$$
$$B_0 = k_4 \cdot (k_{-1} \cdot (k_{-2} + k_3) + k_2 \cdot k_3);$$
$$B_1 = k_1 \cdot (k_2 \cdot (k_3 + k_4) + k_{-2} \cdot (k_4 + k_{-3} \cdot P_i) + k_3 \cdot k_4);$$
$$B_2 = k_{-1} \cdot k_{-2} \cdot (k_{-3} + k_{-4}) + k_{-4} \cdot k_3 \cdot (k_{-1} + k_2) + k_1 \cdot k_2 \cdot k_{-3});$$
$$B_3 = k_{-4} \cdot k_{-2} \cdot (k_{-3} + k_{-1} + k_2);$$

where S and P are pyrophosphate (PP) and inorganic phosphate (P_i) concentration respectively. The extent to which a step within an enzyme or a transporter limits the steady-state rate is quantified as a flux control coefficient of that step [4-6].

$$C_i^V = \frac{k_{+i} \cdot \partial V}{V \cdot \partial k_{+i}} \,\Big|_{k_{+i}/k_{-i} = const}$$

For unbranched mechanisms the flux-control coefficient of any step can assume any value between 0 and 1. For any mechanism the sum of the control coefficients over all the steps is equal to 1 [4,5].

RESULTS AND DISCUSSION

The dependencies of the flux control coefficients of individual reaction steps on pyrophosphate concentrations are shown in Fig.2. At fixed concentration of inorganic phosphate (P_i = 4 mM) and low PP concentrations the main amount of control resides on the binding of pyrophosphate to a free enzyme (step 1), and the other steps have

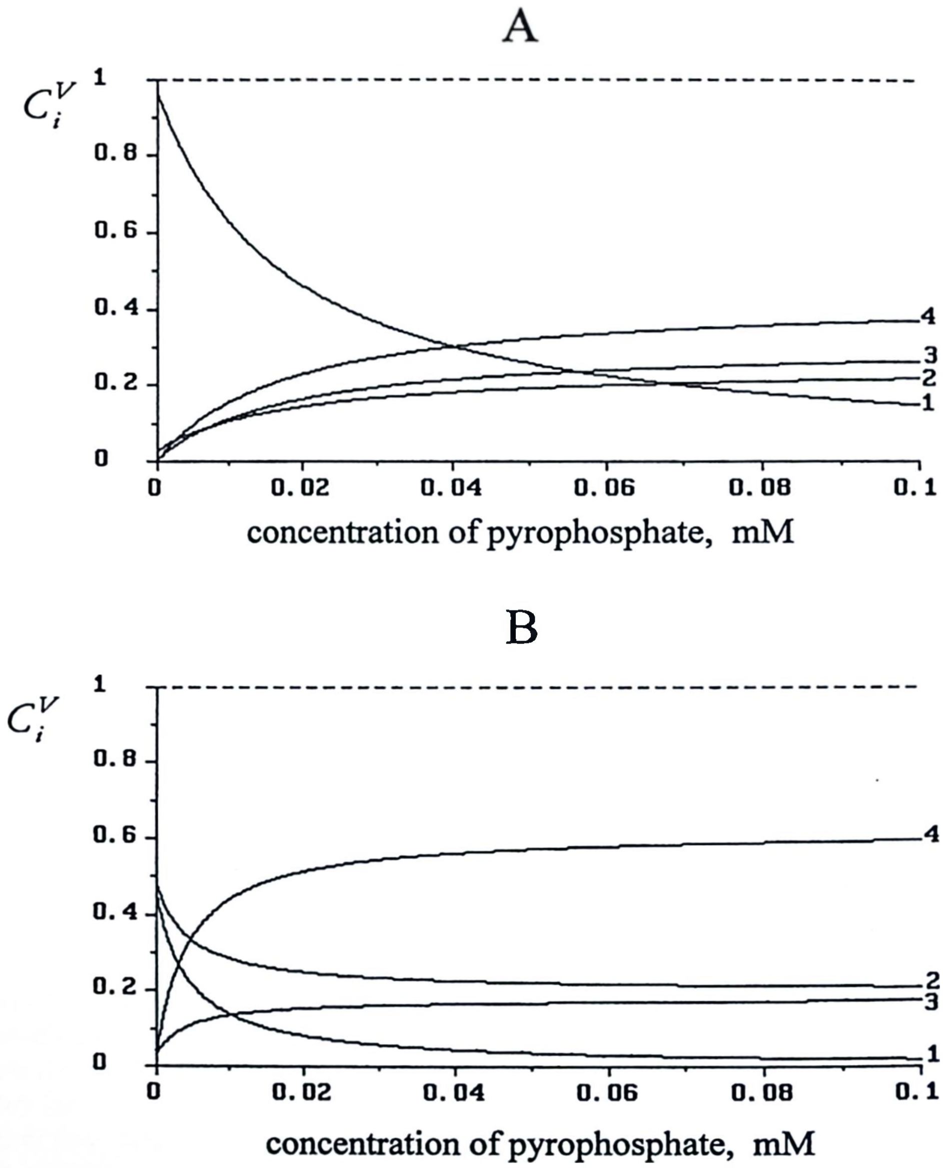

Figure 2. The dependence of flux control coefficients on pyrophosphate concentration for enzyme isolated from E.coli (A- wild type; B- mutant E20D). The concentration of inorganic phosphate is kept constant ([P_i]=4 mM) The numbers on the plots indicate steps of the reaction as shown in Fig.1.

a small contribution to the steady-state flux regulation. An increase in PP concentration brings about dramatic changes in the regulation properties of the reaction. Step 1 looses its flux control gradually, and the control exerted by the other steps increases. At high PP concentration (greater than 60 μM) the step of reversible dissociation of the second P_i from enzyme-P_i complex (step 4) has the largest control coefficient (C_i^V).

Interestingly, at low PP concentration, e.g., 0.01 mM, step 1 has the largest contribution to the control of pyrophosphatase flux, although the product of the second order rate constant k_{+1} and 0.01 mM of PP is much greater than any other forward rate constant (see Fig. 1.). Thus, the results of the present study indicate that the step having the fastest forward rate constant can have the largest flux control coefficient.

The substitution of Glu20 to Asp (mutant E20D) in the active site of the pyrophosphatase from E. coli leads to the changes in the distribution of the flux control. In this mutant, the steady-state rate of PP hydrolysis is controlled mostly by step 4. Also the control exerted by step 2 significantly differs from that of the wild type enzyme (the difference is up to 450% at the low pyrophosphate concentration). Glutamic acid 20 is an evolutionarily conserved residue, which contributes to the structural stability of the quaternary structure of the enzyme. For a wild type E. coli enzyme, it was previously shown that conversion of PP to P_i proceeds via enzyme-substrate complex that bound four Mg^{2+} ions [2]. However, for mutant E20D the number of bound four Mg^{2+} ions is five. The presence of five Mg^{2+} ions per the molecule of the enzyme E20D substantially reduces the energy barrier with respect to PP binding [2]. This suggestion is also supported by a marked decrease of the flux control coefficient of step 1 for the mutant enzyme (Fig.1). The substantial increase in the control coefficient of step 2 for low pyrophosphate concentrations suggests that Glu20 is essential for the transformation of PP into $2P_i$ in the active site of the enzyme. This means that a point mutation alters both kinetic and control properties of the enzyme.

ACKNOWLEDGMENT.

We acknowledge NIH grant AA11689 for the support of this work.

REFERENCES

[1] Smirnova, I.N., Kasho, V.A., Volk, S.E., Ivanov, A.H., and Baykov, A.A. (1995) Arch. Biochem. Biophys. 318, 340-348

[2] Volk, S.E., Dudarenkov, V.Yu., Käpylä, J., Kasho, V.N., Voloshina, O.A., Salminen, T., Goldman, A., Lahti, R., Baykov, A.A., and Cooperman, B.S. (1996) Biochemistry 35, 4662-4669.

[3] Cleland, W.W. (1963) Biochim. Biophys. Acta 67, 104-137.

[4] Brown, G.C. and Cooper, C.E. (1993) Biochem.J. 294, 87-94.

[5] Kholodenko, B.N. and Westerhoff, H.V. (1993) FEBS Lett. 320, 71-74.

[6] Kholodenko, B.N. and Westerhoff, H.V. (1994) Biochim. Biophys. Acta 1208, 294-305.

12

AN APPLICATION OF A FLUX CONTROL MAPPING TO THE KINETIC MODEL OF A SINGLE ENZYME.

Nartsissov Ya.R.

Medical Scientific & Production Complex “Biotics” P.O. Box 39, 113452 Moscow, Russia. phone/fax : (095) 322-0074; E-mail: yarosl@biotic.dol.ru

INTRODUCTION

It is well known that the solving of metabolic control analysis (MCA) problem is the finding of flux control coefficients. The last ones can depend on several parameters of a metabolic system. If the classical kinetic model of a single enzyme is considered concentrations of substrates and products are used as parameters. This assumption leads to the sophisticated analysis of coefficients’ dependencies. In this case it is tempting to suppose that there is a universal approach for representation of modeling results.

In the present study a way of simplification for MCA application to a single enzyme is described for instance of Na,K-ATPase. The sodium pump is one of the important membrane enzymes. It exchanges 3 endogenous sodium ions with 2 exogenous potassium ions. The enzyme consist of α and β subunits which form an octomer [1]. There are some differences in catalytic subunit’s content depending on type of tissue. [2,3]. These differences lead to alteration of enzyme activity but as a whole the mechanism of ions’ transport is the same for any kind of cells. Na,K-ATPase belongs to a family of P-type cation ATPase (E_1 -E_2 type). During the catalytic act the transition of conformation between E_1 and E_2 forms occurs. Each form can bind Na^+ and K^+ respectively. The binding and the following hydrolysis of ATP occur in E_1Na. The conservative residue of Asp is phosphorylated and enzyme turns into E_2 conformation.

If there is no exogenous K^+ situation becomes more simple [4]. Assuming the existence of the E_2 form it is supposed that this one can return to E_1 with or without previous binding of ATP to a low affinity regulatory site (Fig.1).

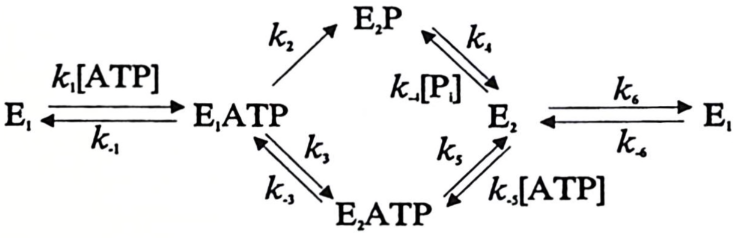

Figure 1. The scheme of Na-cycle for Na,K-ATPase. The rate constants for the enzyme partially purified from pig kidney are equal to [4]: k_1=0,025 $ms^{-1}\mu M^{-1}$; k_{-1}=0,009 ms^{-1}; k_2=0,199 ms^{-1}; k_3=1,95e-8 ms^{-1}; k_{-3}=0,054 ms^{-1}; k_4=0,0019 ms^{-1}; k_{-4} = $6 \cdot 10^{-5}$ $ms^{-1}\mu M^{-1}$; k_5=0,16 ms^{-1}; k_{-5}=0,0016 $ms^{-1}\mu M^{-1}$; k_6=0,1 ms^{-1}; k_{-6}=$1 \cdot 10^{-5}$ ms^{-1};

Some aspects of MCA application to Na-cycle of Na,K-ATPase have been described before [5]. Another part of this problem is considered in the present study.

METHODS

Taking into account the scheme of sodium cycle written on Fig.2 it was easy to obtain an analytical function of flux for ATP hydrolysis. This function can be written by the following equation:

$$\frac{d[ATP]}{dt} = \frac{\omega 1([ATP])}{\omega 2([ATP],[P_i])};$$

$$\omega 1([ATP]) = A_1 \cdot [ATP] + A_2 \cdot [ATP]^2;$$

$$\omega 2([ATP],[P_i]) = B_0 + B_1 \cdot [ATP] + (B_2 + B_3 \cdot [ATP]) \cdot [ATP] + (B_4 + B_5 \cdot [ATP]) \cdot [P_i];$$

$$A_1 = \left(k_{-6} \cdot k_{-3} \cdot k_{-5} + k_{+6} \cdot k_{+1} \cdot \left(k_{-3} + k_{+5}\right)\right) \cdot k_{+2} \cdot k_{+4}; \quad A_2 = k_{+1} \cdot k_{-3} \cdot k_{+4} \cdot k_{-5} \cdot k_{+2};$$

$$B_0 = k_{+4} \cdot \left(k_{+6} + k_{-6}\right) \cdot \left(k_{+5} \cdot k_{+3} + \left(k_{-1} + k_{+2}\right) \cdot \left(k_{-3} + k_{+5}\right)\right);$$

$$B_1 = \left(k_{+6} \cdot k_{+4} \cdot \left(k_{-3} + k_{+5}\right) + k_{+3} \cdot k_{+4} \cdot \left(k_{+6} + k_{+5}\right) + k_{+2} \cdot \left(k_{-3} + k_{+5}\right) \cdot \left(k_{+6} + k_{+4}\right)\right) \cdot k_{+1};$$

$$B_2 = \left(k_{-6} \cdot \left(k_{+4} \cdot \left(k_{-3} + k_{+3}\right) + k_{-3} \cdot (k_{+2} + k_{+4}) + k_{+4} \cdot \left(k_{-1} + k_{+2}\right)\right) + k_{-3} \cdot k_{-1} \cdot k_{+4}\right) \cdot k_{-5};$$

$$B_3 = \left(k_{-3} \cdot \left(k_{-1} + k_{+2}\right) + k_{+4} \cdot \left(k_{+3} + k_{+2}\right)\right) \cdot k_{+1} \cdot k_{-5};$$

$$B_4 = \left(k_{+5} \cdot k_{+3} + k_{-1} \cdot k_{-3} + k_{-1} \cdot k_{+5} + k_{+2} \cdot \left(k_{-3} + k_{+5}\right)\right) \cdot k_{-4} \cdot k_{-6};$$

$$B_5 = \left(k_{+5} \cdot \left(k_{+2} + k_{+3}\right) + k_{-3} \cdot k_{+2}\right) \cdot k_{+1} \cdot k_{-4};$$

Then the flux control coefficients of single steps were calculated. The control coefficient of a step (i) is just the percentage change in the reaction rate (V) brought about by 1% change in the forward (k_{+i}) and reverse (k_{-i}) rate constants of that step [6,7].

$$\overset{V}{\underset{i}{}} = \frac{k_{+i} \cdot \partial V}{V \cdot \partial k_{+i}} \Big|_{k_{+i}/k_{-i} = const}$$

After calculation of the functions for coefficients a novel method of *flux control mapping* was applied to the model. The base of this method is the following [8]. Consider some two parameters of the metabolic system. Then there is a two-dimensional space in which values of the parameters are lied on the axes. The lines of the fixed flux control should be depicted on the space in order to represent the regulation properties of the system. The set of these lines forms the *flux control map* for each step of the catalytic cycle. The obvious profit of this approach is an ability to analyze two dependencies at once. It should be stressed that there are a lot of reactions in which two general metabolites can be considered as the space parameters.

RESULTS AND DISCUSSION

The flux control maps for Na- cycle of Na,K-ATPase are shown in Fig.2. The main part of control at physiological concentration of ATP belongs to the step of reversible

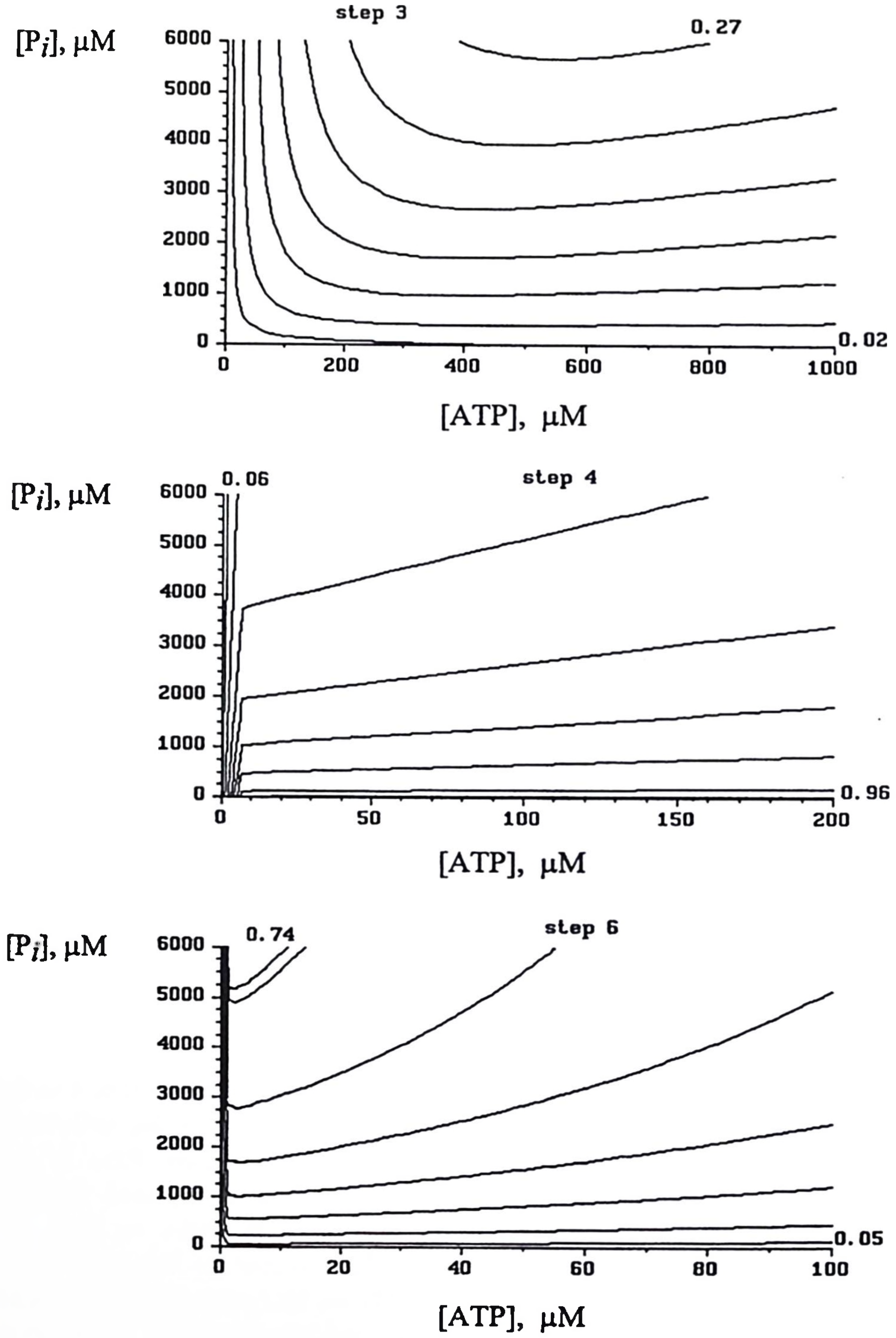

Figure 2. The flux control maps for Na-cycle of Na,K-ATPase. Numbers on the plots indicate value of flux control lines (e.g. for STEP 4 "0.96" indicates the line on which $C_4^V = 0.96$. The maps for steps with the control coefficients < 0.2 are not shown.

removing of inorganic phosphate from E_2 form of enzyme. However the whole type of control critically depends on P_i concentration. At the low P_i amount the above process takes almost all control (~92%) of ATP hydrolysis. If the concentration of inorganic phosphate is high (6mM) no more than 56% of control is kept on the step 4 (see Fig.2) and at the same time the influence of enzyme's isomerisation without ATP hydrolysis (the steps 3 and 5) on the flux is increased. It is remarkable, that the flux control coefficients of these steps have a maximum at ATP concentration approximately 600 μM. The extremum was found for the control coefficients of step 6 too. Furthermore, attention should be paid to the type of flux control maps. They also demonstrate the points of inflection. It means that the existence of extremum for flux control over two concentrations will lead to the close lines on the map for the step.

REFERENCES

[1] Skou, J.C. (1990) FEBS Lett. 268, 314-324.

[2] Hsu, Y.-M. and Guidotti, G. (1989) Biochemistry 28, 569-573.

[3] Munzer, J.S., Daly, S.E., Jewell-Motz, E.A., Lingrel, J.B. and Blostein, R. (1994) J.Biol.Chem. 269, 16668-16676.

[4] Campos, M. and Beaugé, L. (1994) J.Biol.Chem. 269, 18028-18036.

[5] Nartsissov, Ya.R., Lopina, O.D., and Kholodenko, B.N. (1997) FASEB J. 11, 1078

[6] Brown, G.C., and Cooper, C.E. (1994) Biochem. J. 300,159-164.

[7] Kholodenko, B.N., and Westerhoff, H.V. (1994) Biochim. Biophis. Acta 1208, 294-305.

[8] Nartsissov, Ya.R. (1998) Biophysics, in press.

CHANGES IN ENERGY METABOLISM OF PRIMARY RAT OSTEOBLASTS DURING DIFFERENTIATION.

Komarova S.V., Rabkin B.A.*, Booker J.D.*, Ataullakhanov F.I.#, Globus R.K.**

* NASA Ames Research Center, M-S 236-7, Moffett Field, CA 94035-1000
Tel: (650) 604-6390, Fax: (650) 604- 5931, e-mail: skomarova@mail.arc.nasa.gov.
# National Research Center for Hematology, Moscow, 125167 Russia.

INTRODUCTION

Cellular bioenergetics reflect various normal cell activities such as proliferation and differentiation as well as environmental stresses. The differentiation of bone-forming cells, osteoblasts, entails a step-wise and progressive sequence of precursor cell proliferation, production of an abundant extracellular matrix, and finally matrix mineralization [1-3]. These events are predicted to place unique and fluctuating demands on the energy production apparatus of the cell. Glycolysis was shown to play a major role in aerobic ATP production by bone cells [4-6] (as well as various other cell types [6-8]), while oxidative phosphorylation also occurs [9, 10]. However, very little is known about how the metabolic status of osteoblasts is regulated during progressive differentiation.

The aim of the present study is to investigate changes in energy metabolism during the proliferation and differentiation of cultured osteoblasts which are induced to mature by the addition of ascorbic acid (AA) [1-3]. AA promotes collagen synthesis and is required for the differentiation of primary osteoblasts *in vitro*. Akaline phosphatase activity was measured as a standard marker of osteoblast differentiation [1-3]. The rates of glucose and oxygen consumption and lactate production were measured to provide information on the oxidative and glycolytic components of energy metabolism. Cellular levels of ATP were measured as an indicator of the bioenergetic status of the cell.

MATERIALS AND METHODS.

Rat calvarial osteoblast-like cells were isolated from 21-day old fetal rat calvaria and plated at a density 36,000 cells/cm^2 as previously described [11]. Cells were incubated in α-MEM, supplemented with 10% serum at 5% CO_2 in air at 37°C for 14 days, and media was changed every 2-3 days. After the cell layer achieved confluence (day 3 in culture) half of the wells were used to induce cell differentiation by the addition of freshly prepared ascorbic acid (50 μg/ml) and β-glycerophosphate (3 mM) to the culture medium [11]. Preliminary experiments demonstrated that the addition of β-glycerophosphate alone does not affect glycolysis or ATP levels in osteoblasts during 14 days in culture.

To determine cell numbers, cultures were treated sequentially with PBS, containing 10 mM of EGTA, 20 mM HEPES, pH 7.4 for 20 min and collagenase (572 U/ml) for 60 min at 37°C. An equal volume of 0.25% trypsin was added to the collagenase and cells were incubated an additional 30 min. Detached cells were counted using a hemacytometer. Exclusion of 0.1 % trypan blue was used to determine cell viability.

Concentrations of glucose and lactate were measured in media using YSI Model 2700 Select Analyzer (Yellow Springs, Ohio).

O_2 consumption was measured at 37°C using a polarographic oxygen electrode (Radiometer, Copenhagen) modified to provide a gas-impermeable seal of the well.

Alkaline phosphatase activity and ATP levels were measured in the supernatant from 1 % Triton-X100 cell extracts that were sonicated and centrifuged at 10,000g for 3 min. Alkaline phosphatase activity was measured spectrophotometrically by the hydrolysis of p-nitrophenol phosphate (Sigma, USA). ATP was measured enzymatically using phosphoglycerate phosphokinase assay (Sigma, USA)

Values are expressed as mean ± standard error. They were compared using Students t-test.

RESULTS AND DISCUSSION

Figure 1 shows changes in cell numbers and alkaline phosphatase activity during 14 days of growth in culture. The most rapid proliferative phase for cells occurs prior to day 7. However, the rate of growth for cells induced to differentiate with AA was ~ 3 times higher than for undifferentiated cells and the final cell density was ~ 2 times higher. Treatment with AA caused a progressive increase in alkaline phosphatase activity to levels 7-fold higher than undifferentiated cells by day 14. Thus, proliferation occurs during the first week (days 3-7) of culture while differentiation, as assessed by alkaline phosphatase activity, steadily increased throughout the 2 week culture period.

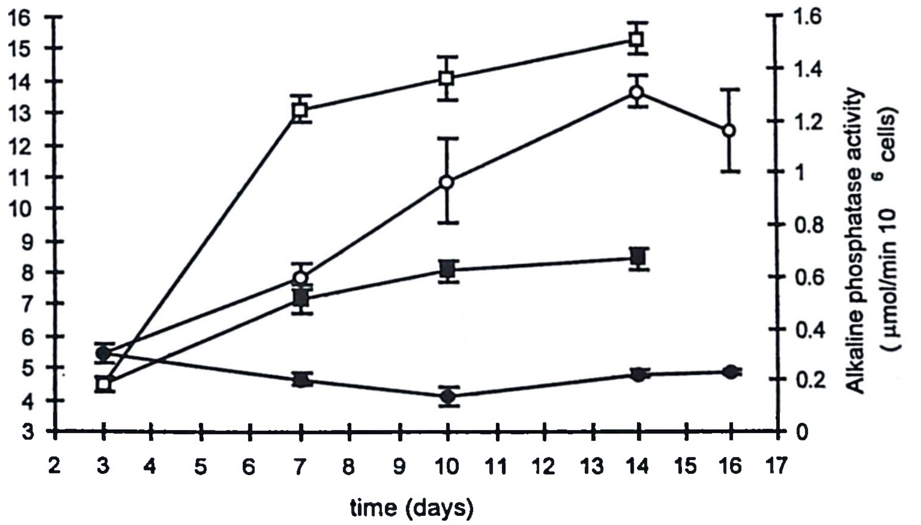

Figure 1. Changes in cell numbers (squares) and alkaline phosphatase activity (circle) during 14 days of culture. Cells treated with AA (open symbols), cells grown without ascorbate (closed symbols).

The rates of glucose consumption (V(glu)) and lactate (V(glu)) production in immature cells transiently declined over the 14 day culture period. In contrast, cells treated with AA to induce differentiation showed a progressive increase in glucose consumption to levels 2-fold higher than immature cells on day 14. The rate of lactate production by osteoblasts treated with AA transiently decreased (30 - 40%) relative to immature cells at 7-10 days in culture. Furthermore, the V(lac)/V(glu) ratio in osteoblasts treated with AA was 50-70% lower than in osteoblasts grown without AA. A decrease in the ratio V(lac)/V(glu) may reflect an increase in the production of pyruvate, which provides substrates for the Krebs cycle and oxidative phosphorylation.

The rate of O_2 consumption was 3-4 fold higher in cells treated with AA than in immature cells between days 7-14, showing that the activity of oxidative phosphorylation increased as cells progressively differentiated (Table 1). The rate of oxygen consumption by immature cells was relatively low and did not show significant changes during 14 days of culture.

In cells treated with AA, the ATP level increased after day 7 in culture and reached a maximum value by day 10. In cells grown without AA, the ATP level in osteoblasts transiently declined at day 7 then remained constant during the 14 days. Thus, the differentiation of osteoblasts caused as much as a 4-fold increase in the size of the ATP pool (corrected by cell number) relative to undifferentiated cells.

Table 1. Changes in the rates of glucose and oxygen consumption and lactate production during 14 day of culture.

day	AA	rate of glucose consumption	rate of lactate production	V(lac)/V (glu) ratio	rate of oxygen consumption	[ATP]
		nmol/hr 10^6 cells			nmol O_2/hr 10^6 cells	nmol / 10^6 cells
3	-	326 ± 56	654 ± 62	2.01	36 ± 10	86.3 ± 7.5
7	-	234 + 26	291 ± 15	1.24	42 ± 7	48.3 ± 3.9
	+	192 ± 10	142 ± 9*	0.74	166 ± 26*	63.9 ± 13.3
10	-	198 + 26	249 ± 33	1.26	72 ± 14	38.4 ± 3.2
	+	288 ± 27	140 ± 13**	0.49	194 ± 33*	212 ± 50*
14	-	248 ± 31	438 ± 32	1.77	41 ± 16	36.7 ± 3.1
	+	444 ± 31*	648 ± 44*	1.46	127 ± 32**	183 ± 12*

Significantly different from untreated control *P< 0.001, **P<0.05

These results demonstrate that significant changes in cellular energy metabolism occured when osteoblasts underwent the transition from an initial proliferative stage to progressively more mature stages of differentiation. During the first period of culture (day 3-7) when cells actively proliferated, the V(lac)/V(glu) ratio decreased and oxidative phosphorylation increased. As cells further matured (day 10-14), glycolysis was activated and ATP levels rose while oxidative phosphorylation did not change. Thus, to better understand the regulation of energy metabolism in osteoblasts, it is critical to take into consideration their stage of cellular differentiation.

REFERENCES

[1.] Quarles, L.D., Yohay, D.A., Lever, L.W., Caton, R., and Wenstrup, R.J. (1992) J. Bone Min. Res. 6, 683-692.

[2.] Franceschi, R.T., Wilson, J.X. and Dixon, J. (1995) Am. J. Phisiol. 268, C1430-39, 1995

[3.] Owen, T.A., Aronow, M., Shalhoub, V., Barone, L.M., Wilming, L., Tassinari, M.S., Kenndey, M.B., Pockwinse, S., Lian, H.B. and Stein, G.S. (1990) J. Cell Physiol.

143, 420-430.

[4.] Shapiro, I.M. and Haselgrove, J.C. (1990) Bone, ed.B.K.Hall, CRC Press, London.

[5.] Adamek, G., Felix, R., Guenther, H.L. and Fleisch, H. (1987) Biochem. J. 248, 129-137.

[6.] Cohn, D.V. and Forscher, B.K. (1962) Biochim.Biophys.Acta 65, 20-26.

[7.] Neermann, J. and Wagner, R. (1996) J. Cell Physiol. 166, 152-169.

[8.] Freinkel, R.K. and Traczyk, T.N. (1976) J. Invest. Dermatol. 67, 577-581.

[9.] Tuncay, O.C., Ho, D. and Barker, M.K. (1994) Am. J. Orthod. Dent. Orthop. 105, 457-463.

[10.] Schirrmacher, K., Lauterbach, S. and Bingmann, D. (1997) J.Orthop.Res. 15, 558-562.

[11.] Moursi, A.M., Damsky, C.H., Lull, J., Zimmerman , D., Doty, S.B., Shin-Ichi, A. and Globus, R.K. (1996) J. Cell Science, 109, 1369-1380.

REGULATION OF GLYCOLYTIC AND OXIDATIVE PHOSPHORYLATION PATHWAYS IN MATURE OSTEOBLASTS.

Komarova S.V.[*], *Rabkin B.A.*[*], *Booker J.D.*[*], *Ataullakhanov F.I.*[#], *Globus R.K.*[*]

[*] NASA Ames Research Center, MS 236-7, Moffett Field, CA 94035-1000
Tel: (650) 604-6390, Fax: (650) 604- 5931, e-mail: skomarova@mail.arc.nasa.gov.
[#] National Research Center for Hematology, Moscow, 125167 Russia.

INTRODUCTION

Cellular ATP in bone-forming cells, osteoblasts, is derived from glycolysis and oxidative phosphorylation. The contribution of these two processes to total ATP production and their relationship to one another differs according to cell type and metabolic state. Oxidative phosphorylation provides 17 times more ATP per mole of glucose than anaerobic glycolysis, and it is the main energy-producing mechanism for many cell types [1-3]. However in a variety of cells, including cultured bone cells, glycolysis was shown to play a major role in aerobic ATP production [4-8]. Evidence for the importance of oxidative phosphorylation for osteoblasts also exists [9, 10]. To elucidate the importance of different pathways of energy metabolism in mature osteoblasts, the effects of inhibitors of glycolysis and oxidative phosphorylation on ATP concentration and energy metabolic fluxes were studied. We measured the rates of oxygen and glucose consumption and lactate production in the presence of various metabolic inhibitors to provide information on oxidative and glycolytic components of energy metabolism. Sodium fluoride was used to inhibit glycolysis, arsenic acid was used as an uncoupler of glycolysis [11] and KCN and NaN_3 were used as inhibitors of oxidative phosphorylation [1, 2].

MATERIALS AND METHODS.

Rat calvarial osteoblast-like cells were isolated from 21-day old fetal rat calvaria and plated at a density 36,000 cells/cm^2 as previously described [12]. Cells were incubated in α-MEM, supplemented with 10% serum at 5% CO_2 at 37 C for 14 days, and media were changed every 2-3 days. After the cell layer achieved confluence (day 3 in culture), incubation media were supplemented with 50 μg/ml of freshly prepared ascorbic acid and 3 mM of β-glycerophosphate [12].

Effects of inhibitors of glycolysis and oxidative phosphorylation were studied in mature osteoblasts on day 14. Cells were pre-incubated with medium containing one of the inhibitors for 1 h, then the medium was refreshed and supplemented with inhibitor, then measurements of glucose, lactate or O_2 consumption were made during 2 - 4 hr. After 4 h of incubation with inhibitor, cell extracts for measurements of ATP concentration were prepared.

Concentrations of glucose and lactate were measured in media using YSI Model 2700 Select Analyzer (Yellow Springs, Ohio).

O_2 consumption was measured at 37 C using polarographic oxygen electrode (Radiometer, Copenhagen) modified to provide a gas-impermeable seal of the well.

ATP levels were measured enzymatically by phosphoglycerate phosphokinase assay (Sigma, USA) in supernatants of 1 % Triton-X100 extracts that were sonicated and centrifuged at 10,000g for 3 min.

Values are expressed as mean ± standard error. They were analyzed statistically using Students t-test.

RESULTS

The rate of glucose consumption (V(glu)) in mature osteoblasts is 440 ± 30 nmol/hr 10^6 cells, the rate of lactate production (V(lac)) is 650 ± 44 nmol/hr 10^6 cells and the rate of oxygen consumption is 130 ± 30 nmol O_2/hr 10^6 cells. The level of ATP is 180 ± 12 nmol/10^6 cells.

The addition of NaF to mature osteoblasts caused a dose-dependent decrease in the rates of glucose consumption and lactate production (Table 1). Maximum inhibition was 70% at 30 mM of NaF. At concentrations of 10 mM and higher, NaF affected V(lac) to a greater extent than V(glu). Therefore, NaF (>10 mM) caused a decrease in the ratio V(lac)/V(glu). However, there were no significant changes in the rate of O_2 consumption. The ATP level in osteoblasts declined with increasing concentrations of NaF.

Table 1. Effect of sodium fluoride on the energy metabolism of mature osteoblasts.

[NaF] mM	Rate of glucose consumption % of control	Rate of lactate production % of control	Rate of oxygen consumption % of control	ATP concentration % of control
5	60 ± 3 *	72 ± 5*	100 ± 10	83 ± 14
10	43 ± 3*	43 ± 5*	79 ± 13	74 ± 9
20	34 ± 7*	41 ± 7*	71 ± 25	69 ± 8**
30	27 ± 5*	31 ± 3*	73 ± 27	39 ± 4*

Significantly different from untreated controls at *P<0.001, **P<0.01

The effects of arsenic acid on ATP, V(glu) and V(lac) are shown in Table 2. The addition of arsenic acid caused a dose-dependent decrease in ATP concentration. Both V(glu) and V(lac) increased to 150% of controls using 1 mM of arsenic acid, and decreased at higher concentrations of arsenic acid. The rates of glucose consumption and lactate production using 10 mM of arsenic acid were similar to control cells, although the level of ATP was 70% lower than controls.

Table 2. Effects of arsenic acid on the energy metabolism of mature osteoblasts.

Arsenic acid mM	Rate of glucose consumption % of control	Rate of lactate production % of control	ATP concentration % of control
1	135 ± 6**	179 ± 15*	84 ± 9
2	122 ± 9	170 ± 8*	60 ± 6
5	97 ± 7	121 ± 9	49 ± 19**
10	104 ± 8	149 ± 4*	28 ± 6*

Significantly different from controls at *P<0.001, **P<0.01

Table 3. Effects of inhibitors of oxidative phosphorylation on the energy metabolism of mature osteoblasts.

Inhibitor concentration mM	Rate of glucose consumption % of control	Rate of lactate production % of control	Rate of oxygen consumption % of control	ATP concentration % of control
NaN_3				
1	177 ± 15*	256 ± 11*	48 ± 14	91 ± 8
2	208 ± 15*	260 ± 9*	35 ± 11**	105 ± 6
4	213 ± 8*	286 ± 10*	0*	96 ± 6
8	205 ± 9*	285 ± 9*	0*	81 ± 3
KCN				
4	235 ± 29*	255 ± 9*	0*	91 ± 8

Significantly different from controls at *$P<0.001$, ** $P<0.01$

The addition of NaN_3 caused a dose-dependent inhibition of O_2 consumption by osteoblasts (Table 3). Complete inhibition of O_2 consumption was achieved at 4 mM of NaN_3. In the presence of of NaN_3 (1 - 8 mM)$_3$ V(glu) increased by 200% and V(lac) rose by 250%. V(lac)/V(glu) increased in the presence of inhibitor and reached 2 at all concentrations of NaN_3. The cellular levels were not significantly affected after 4 hr of incubation with NaN_3. Addition of KCN (Table 3) showed similar results (increase in rates of glucose consumption and lactate production and absence of a significant effect on ATP levels).

DISCUSSION

Total ATP production in mature osteoblasts can be estimated from the assumption that anaerobic glycolysis produces 2 moles of ATP from 1 mole of glucose and reduction of 1 mole of O_2 is coupled to the production of 6 moles of ATP. Calculations show that the total rate of ATP production is about 900 nmol/hr 10^6 cells by glycolysis and 800 nmol/hr 10^6 cells by oxidative phosphorylation. Thus, glycolysis provides more than 50% of the energy requirements of mature osteoblasts. In addition, inhibition of oxidative phosphorylation by NaN_3 or KCN led to a rapid two-fold increase in the rate of glucose consumption by osteoblasts. The rate of lactate production increased to a greater degree, reflecting a decline in the production of pyruvate, which provides substrates for the Krebs cycle and oxidative phosphorylation. The activation of glycolysis in the presence of inhibitors of oxidative phosphorylation prevented a decrease in ATP level for at least 4 h. On the other hand, inhibition (or uncoupling) of glycolysis led to a decline in ATP levels, while the rate of oxygen consumption did not significantly change under these conditions. Thus, we conclude that although oxidative phosphorylation is an important energy source for osteoblasts, acute changes in the production of ATP are accomplished by the regulation of glycolysis while oxidative phosphorylation remains unaffected.

References

[1.] Kane, M.T. and Buckley N.J. (1977) J. Reprod. Fert. 49, 261-266.

[2.] Matsui, Y., Kitade, H., Kamiya, T., Kanemaki, T., Hiramatsu, Y., Okumura, T. and Kamiyama, Y. (1994) In Vitro Cell. Dev. Biol. 30A, 609-614.

[3.] Olivotto, M., Arcangeli, A., Caldini, R., Chevanne, M., Cipolleschi, M.G., and Dello Sbara, P.. (1984) Toxicol. Pathol. 12 (4), 369-373
[4.] Cohn, D.V. and Forscher B.K. (1962) Biochim. Biophys. Acta 65, 20-26.
[5.] Neermann, J. and Wagner, R. (1996) J. Cell Physiol. 166, 152-169.
[6.] Freinkel, R.K. and Traczyk, T.N. (1976) J. Invest. Dermatol. 67, 577-581.
[7.] Shapiro, I.M. and Haselgrove, J.C. (1990) Energy metabolism in bone. in: Bone, ed.B.K.Hall, CRC Press, London.
[8.] Adamek, G., Felix, R., Guenther, H.L. and Fleisch, H. (1987) Biochem. J. 248, 129-137.
[9.] Tuncay, O.C., Ho, D. and Barker, M.K. (1994) Am. J. Orthod. Dentofac. Orthop. 105, 457-463.
[10.] Schirrmacher, K., Lauterbach, S. and Bingmann, D. (1997) J. Orthop. Res. 15, 558-562.
[11.] Ataullakhanov, F.I., Vitvitsky, V.M., Zhabotinsky, A.M., Pichugin, A.V., Platonova, O.V., Kholodenko, B.N. and Ehrlich, L.I. (1981) Eur. J. Biohem. 115, 359-365.
[12.] Moursi, A.M., Damsky, C.H., Lull, J., Zimmerman, D., Doty, S.B., Shin-Ichi, A. and Globus, R.K. (1996) J. Cell Science, 109, 1369-1380.

METABOLIC CONTROL ANALYSIS REVEALS THAT GLUCOSE TRANSPORT INCOMPLETELY CONTROLS THE GLYCOLYTIC FLUX IN *TRYPANOSOMA BRUCEI*

Barbara M. Bakker[1,2,3], *Femke I.C. Mensonides*[2], *Benno H. ter Kuile*[4], *Paul A.M. Michels*[5], *Fred R. Opperdoes*[5], *Hans V. Westerhoff*[1,2] *and Michael C. Walsh*[2]

[1] Molecular Cell Physiology, BioCentrum, Vrije Universiteit, De Boelelaan 1087, NL-1081 HV Amsterdam, The Netherlands. E-mail: hw@bio.vu.nl. Tel.: +31 20 4447228. Fax: +31 20 4447229
[2] E. C. Slater Institute, BioCentrum, University of Amsterdam
[3] Kluyver Laboratory of Biotechnology, Delft University of Technology, Julianalaan 67, NL-2628 BC Delft, The Netherlands (present address)
[4] The Rockefeller University, New York
[5] Research Unit for Tropical Diseases, Christian de Duve Institute of Cellular Pathology, Brussels

INTRODUCTION

Trypanosoma brucei is the parasite that causes the African sleeping sickness. When living in the mammalian bloodstream this unicellular eukaryote depends solely on glycolysis for its ATP supply [1]. Its glycolysis lacks branches through which a substantial flux runs, such as a citric acid cycle or the synthesis of storage carbohydrates. Therefore, trypanosome glycolysis must be fully controlled by its own enzymes and transporters and, possibly, by the processes utilizing the produced ATP. This feature makes *T. brucei* an interesting model organism to study the control of glycolysis.

It has been assumed that the transport of glucose into the cell is the rate-limiting step of trypanosome glycolysis [2-5]. However, compelling evidence has been lacking [6]. From a detailed kinetic model of trypanosome glycolysis we calculated that trypanosome glycolysis may be only one of the controlling steps [7] and furthermore, that the distribution of control may depend on the blood glucose concentration, which can vary between 4 and 8 mM. The calculated flux control coefficient of the glucose transporter depended strongly on the exact kinetics of the enzymes and the transporter itself and could therefore not be predicted reliably [7].

The control exerted by a glucose transporter on the glycolytic flux has not been determined directly in any eukaryotic cell, *i.e.* by varying the amount or activity of the transporter. In perfused rat heart the control of glucose utilization was determined indirectly from *in vivo* concentrations of glycolytic intermediates and *in vitro* enzyme kinetics. The glucose transporter (Glut4) did have substantial flux control in the absence of insulin, but lost control upon stimulation by this hormone [8]. Direct measurement of the control exerted by glucose transport is complicated by the many different glucose-transporter genes in most eukaryotes. Furthermore, inhibitors of glucose transport, if available, are often competitive and their direct effect on the transporter does not only depend on the extracellular glucose concentration, but also on the intracellular glucose concentration. Here we devise a method to deal partly with these complications. We have used phloretin, a competitive inhibitor of glucose transport, to measure the flux control coefficient of the glucose transporter in bloodstream form *T. brucei.* A method was developed to deal with the influence of intracellular glucose on the transport kinetics.

MATERIALS AND METHODS

T. brucei strain 427 was isolated from a male Wistar rat four days after infection. All measurements were performed at 37 °C under aerobic conditions. Oxygen consumption was measured by using a Clark type electrode. The rate of zero-*trans* influx of D-[U-^{14}C] glucose was measured by a filtration technique, modified from a method to measure glucose uptake in *S. cerevisiae* [11]. Phloretin (3-[4-hydroxyphenyl]-1-[2,4,6-trihydroxyphenyl]-1-propanone) was from SIGMA.

The flux control coefficient $C^J_{transport}$ of the glucose transporter is defined by:

$$C^J_{transport} = \frac{(d\ln J / dp)_{ss}}{\partial \ln v_{transport} / \partial p}$$

in which J denotes the steady-state flux, p a parameter that specifically affects the glucose transporter (phloretin) and $v_{transport}$ the rate of glucose transport. The subscript ss indicates that the effect of phloretin on the flux was measured after relaxation to a new steady state. The effect of phloretin on the transport rate was determined at a constant concentration of intracellular glucose.

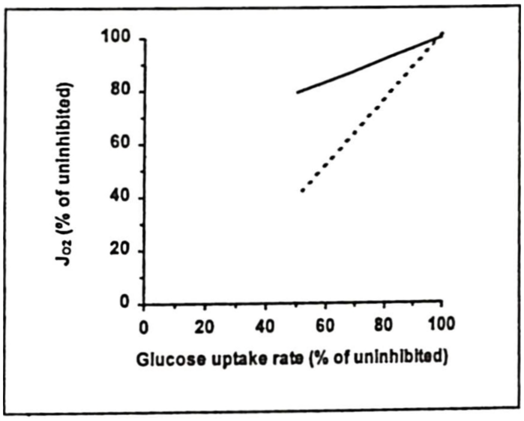

Figure 1 At 0.5 mM glucose (dashed line) the flux was much more sensitive to inhibition of glucose transport than at 5 mM glucose (full line). The effect of intracellular glucose on glucose uptake rate was neglected. The lines represent the tangents to the data points, obtained by linear regression through the linear part of the dataset.

RESULTS AND DISCUSSION

The rate of glucose transport was modulated by titrating with the inhibitor phloretin. Bloodstream form *T. brucei* oxidizes the NADH generated in glycolysis via a mitochondrial glycerol 3-phosphate : dihydroxyacetone phosphate shuttle with the concomitant utilization of one oxygen molecule per glucose. Therefore, the oxygen consumption flux was taken as a measure of the glycolytic flux. The effect of phloretin on the transporter itself was determined by measuring the uptake of radiolabelled glucose over 5 s.

How should we deal with the competitiveness of the inhibitor? In a first approximation intracellular glucose was neglected and the flux control coefficient was determined from a plot of the glycolytic flux against the rate of zero-*trans* uptake of glucose (Fig. 1). At 0.5 mM glucose the transporter had a control coefficient of 1.2, but at 5 mM glucose (the most common blood glucose concentration) only 0.4.

In a second approximation the effect of intracellular glucose was included in the analysis. Glucose transport into trypanosomes occurs via facilitated diffusion [12, 13]. This process can be described by a 4-state model [14]. The trypanosome glucose transporter is almost symmetrical, implying that the V_{max} for influx and efflux are almost identical, as are the K_m's [3, 6]. Since phloretin binds to the transporter on the outside [15] it breaks the symmetry (Fig. 2). The reaction scheme of Fig. 2 yields the following overall rate equation:

$$v = \frac{V^{f}_{max} \cdot \frac{[S]_{out}}{K_{m,out}} - V^{r}_{max} \cdot \frac{[S]_{in}}{K_{m,in}}}{1 + \frac{[S]_{out}}{K_{m,out}} + \frac{[S]_{in}}{K_{m,in}} + \alpha \cdot \frac{[S]_{out}}{K_{m,out}} \cdot \frac{[S]_{in}}{K_{m,in}}}$$

in which the factor α was 0.75 [6] and V^{f}_{max} and $K_{m,out}$ were measured. In the following it will be assumed that the carrier is symmetrical, *i.e.* $V^{f}_{max} = V^{r}_{max}$ and $K_{m,out} = K_{m,in}$.

$[Glc]_{out}$ (mM)	K_{i2}/K_{i1}	$C^{J_{O2}}_{glucose\ transport}$
0.5	1	1.2
0.5	100	1.2
5	1	0.40
5	100	0.51

Table 1 The ratio K_{i2}/K_{i1} was varied and the effect of phloretin on the transport rate was calculated at the measured intracellular glucose concentration (0.04 mM at 0.5 mM outside and 0.4 mM at 5 mM outside [4]). Together with the measured effect of phloretin on the flux these data yielded the control coefficients. If K_{i2}/K_{i1} was increased further, the results were identical.

By using the King-Altman method [16] it was derived that an inhibitor binding on the outside could affect all kinetic parameters in this equation, except the forward V_{max} (Bakker *et al.*, manuscript in preparation). Of two inhibition constants, only one (K_{i1}) had been measured in the zero-*trans*-uptake experiment. Consequently, the other (K_{i2}) had to be estimated. For a symmetrical carrier the ratio K_{i2}/K_{i1} can assume any

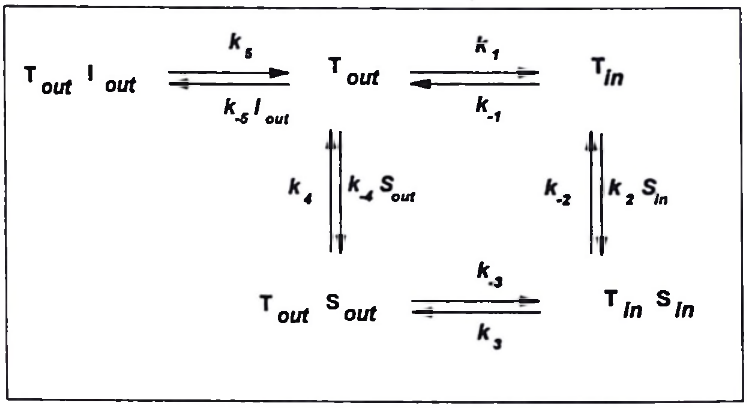

Figure 2 The mechanism of facilitated diffusion of glucose into cells. The transporter (T) can bind the substrate glucose (S) either on the inside or on the outside. The inhibitor phloretin (I) competes with glucose only on the outside.

value between 0.5 and infinity. Luckily however, the effect of this uncertainty on the calculated flux control coefficient was relatively small. Table 1 lists the flux control coefficients, when the measured intracellular glucose concentration was taken into account, for two extreme values of K_{i2}. Irrespective of the assumptions, glucose transport exerted only part of the control at 5 mM glucose. Since the sum of all flux control coefficients should be 1, it follows that other steps also have some control under physiological conditions. When the glucose concentration was decreased, the transporter assumed all flux control (Table 1), in agreement with previous model calculations.The finding that the flux control coefficient exceeded 1 under these conditions, may well be due to experimental error. These results prove that glucose transport is not *the* rate-limiting step of trypanosome glycolysis.

We here showed that competitive inhibitors can be used to determine to which extent a step in a metabolic pathway controls the flux. It is required then that some kinetic information is available and that the implications of uncertainties in kinetic parameters are examined.

One of the applications of this study is to identify promising targets for antitrypanosomal drugs. Since glucose transport exerts part of the flux control in the parasite, it should be an effective target. The perspectives for optimization of drug selectivity will, in part, depend on the flux control exerted by glucose transporters in the different tissues of the mammalian host.

ACKNOWLEDGEMENTS

We would like to thank M. Hendrix in Amsterdam and J. van Roy in Brussels for taking care of the animals and for cultivating the trypanosomes, and B. Teusink for valuable discussions and careful reading of the manuscript. This study was supported by the Netherlands Organization for Scientific Research (NWO) and the Netherlands Association of Biotechnology Research Schools (ABON).

REFERENCES

1 Opperdoes, F.R. (1987) Ann. Rev. Microbiol. 41, 127-151.
2 Gruenberg, J., Sharma, P.R. and Deshusses, J. (1978) Eur. J. Biochem. 89, 461-469.
3 Eisenthal, R., Game, S. and Holman, G.D. (1989) Biochim. Biophys. Acta 985, 81-89.
4 Ter Kuile, B.H. and Opperdoes, F.R. (1991) J. Biol. Chem. 266, 857-862.
5 Seyfang, A. and Duszenko, M. (1991) Eur. J. Biochem. 202, 191-196.
6 Bakker, B.M., Westerhoff, H.V. and Michels, P.A.M. (1995) J. Bioenerg. Biomembr. 27, 513-525.
7 Bakker, B.M., Michels, P.A.M. and Westerhoff, H.V. (1996) in BioThermoKinetics of the Living Cell (Westerhoff, H.V., Snoep, J.L., Sluse, F.E., Wijker, J.E. and Kholodenko, B.N., eds.), pp. 136-142, BioThermoKinetics Press, Amsterdam.
8 Kashiwaya, Y.K., Sato, K., Tsuchiya, N., Thomas, S., Fell, D.A., Veech, R.L. and Passonneau , J.V. (1994) J. Biol. Chem. 269, 25502-25514.
9 Bringaud, F. and Baltz, T. (1994) Mol. Biol. Evol. 11, 220-230.
10 Bringaud, F. and Baltz, T. (1993) Mol. Cell. Biol. 13, 1146-1154.

11 Walsh, M.C., Smits, H.P., Scholte, M. and Van Dam, K. (1994) J. Bacteriol. 176, 953-958.
12 Ter Kuile, B.H. (1994) J. Bioenerg. Biomembr. 26, 167-172.
13 Tetaud, E., Barrett, M.P., Bringaud, F. and Baltz, T. (1997) Biochem. J. 325, 569-580.
14 Stein, W.D. (1986) Transport and diffusion across cell membranes, Academic Press, London.
15 Krupka, R.M. and Devés, R. (1980) Biochim. Biophys. Acta 598, 134-144.
16 King, E.L. and Altman, C. (1956) J. Phys. Chem. 60, 1375-1378.

DYNAMICS OF COUPLED GLYCOLYTIC OSCILLATORS

Jana Wolf and Reinhart Heinrich

Humboldt University, Institute of Biology, Theoretical Biophysics, Invalidenstr. 42,
D-10115 Berlin, Germany, phone +49-30-20938694, fax +40-30-20938813
e-mail: jana=wolf@rz.hu-berlin.de, reinhart=heinrich@rz.hu-berlin.de

INTRODUCTION

In the last decades a variety of metabolic oscillations was discovered in various cell types. One of the best studied examples is that of glycolytic oscillations, occuring for instance in yeast cell suspensions as well as in cell extracts, muscle and heart cells. The underlying mechanism of this behaviour was clarified experimentally and in mathematical models.

In yeast cell suspensions it has been shown that the oscillating cells interact via an exchange of metabolites. To study the effects of intercellular interactions on the dynamical behaviour of whole suspension we analyzed a minimal model [1, 2]. Each cell contains a two-variable system with a simple feedback mechanism giving rise to oscillations for suitable sets of parameter. The interaction is mediated via the diffusion of a cellular metabolite. The resulting dynamics of the cell suspension depends on the kinetic parameters and is determined either by a stable steady state or by a limit cycle. Moreover, we found different types of limit cycles, leading to synchronous or asynchronous oscillations of the cells. We showed, that the existence of regular asynchronous oscillations could explain experimental results concerning glycolytic oscillations in yeast cell suspensions. In particular, in the asynchronous states the individual cells oscillate out of phase whereas the external concentration of the coupling substance oscillates only slightly. In this way cellular oscillations may remain unobservable by studying only mean concentration values of the whole suspension (hidden oscillations). We could demonstrate that one and the same coupling substance (for example acetaldehyde [3, 4]) may act as a 'synchronizer' as well as 'desynchronizer' of the oscillations depending on the kinetic parameters.

The question arises, whether regular asynchronous oscillations may occur in glycolytic oscillations in yeast cell populations, or whether this is a special characteristic of the simple two-component model. We therefore extend the model describing the glycolytic pathway by a detailed multi-variate system.

THE MODEL

We consider the anaerobic energy metabolism in yeast. In this case respiration is inhibited and alcoholic fermentation takes place.The reaction scheme for a single cell is presented in Fig. 1. It contains the main reactions of glycolysis and adjacent reactions producing ethanol and glycerol.

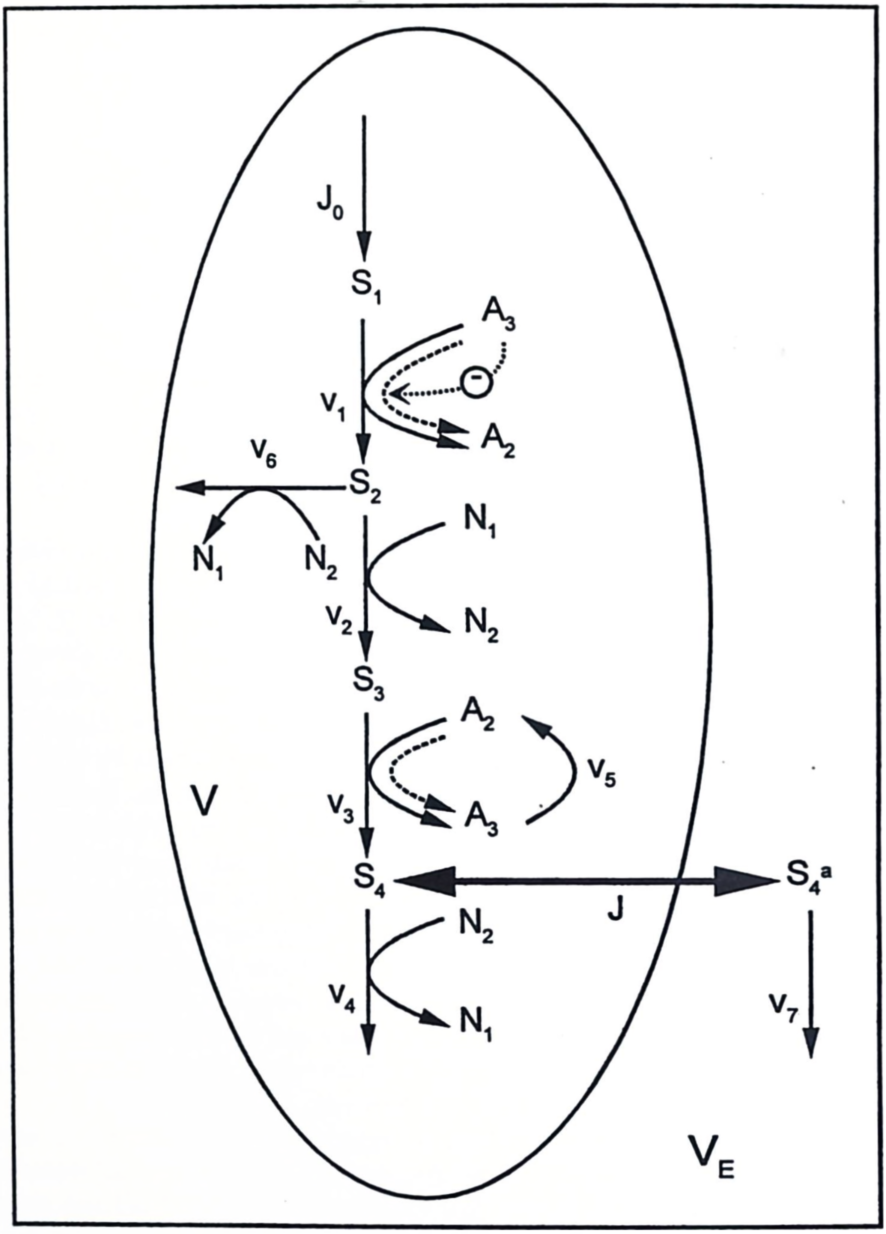

Figure 1. Reaction scheme for a single cell. Flux J_0: input of glucose, reaction 1: lumped reactions of hexokinase, phosphoglucoisomerase and phosphofructokinase, reaction 2: glycerinaldehyde-3P-dehydrogenase reaction, reaction 3: lumped reactions of phosphoglycerate-kinase, phosphoglucoisomerase, enolase and pyruvate-kinase, reaction 4: alcoholdehydrogenase-reaction, reaction 5: nonglycolytic ATP-consumption, reaction 6: glycerol-formation from triosephosphates, reaction 7: degradation of the coupling substance in the extracellular medium, flux J: transmembrane flux of the coupling substance. V, V_E: cellular and extracellular volume.

According to the fact that several reactions are lumped and others are omitted, some variables represent pools of metabolites rather than single intermediates. In detail the variables denote the concentrations of the following compounds: S_1 - glucose, S_2 - pool of triosephosphates glyceraldehyd-3-phosphate (GAP) and dihydroxyacetonphosphate (DHAP), S_3 - 1.3-biphosphoglycerate (1.3-DPG), S_4 - pool of pyruvate (Pyr) and acetaldehyde (AA), S_4^a - S_4 in the extracellular solution, A_2 - ADP, A_3 - ATP, N_1 - NAD^+ and N_2 - NADH. The assumption that the pool of pyruvate and acetaldehyde mediates the coupling between the cells corresponds to the experimental results of Richard et al. [4]. The arrows with the broken lines in reactions 1 and 3 indicate that in these lumped reactions two molecules of adeninnucleotides are converted corresponding to the overall stoichiometry in the upper and lower part of glycolysis. In reaction 1 two molecules triosephosphates are produced per molecule hexosephosphate. Reaction 7 was included to cope with the experimental situation where the inhibitor of the respiraory chain cyanide reacts with acetaldehyde.

For the mathematical description all reactions and the input flux of glucose are considered to be irreversible and simple rate laws are used. The activities of the enzymes are described by linear and bilinear functions of their substrate concentrations. An exception is the HK-PFK-reaction, which is described by the rate equation $v_1 = k_1 S_1 A_3 f(A_3)$. The factor $f(A_3) = \left[1 + (A_3/K_i)^n\right]^{-1}$ characterizes the substrate inhibition of PFK by ATP, where K_i and n denote the inhibition constant and the cooperativity coefficient of that regulation, respectively.

For the fluxes in and out of the cell we use $J_0 = const$ and $J = \kappa\left(S_4 - S_4^a\right)$. The kinetic constant κ (coupling strength) is related to the permeability P of the membrane to the coupling substance, to the membrane surface A_S, and to the cellular volume V as $\kappa = A_S P/V$.

The reaction scheme of Fig. 1 is used for all cells in the suspension. Moreover, the cells are considered to be identical with respect to the kinetic parameters and the input flux J_0. Taking into account $N = N_1 + N_2$ as well as $A = A_2 + A_3$ as conserved moieties the differential equation system has 6 variables per cell and 1 variable for the external concentration of the coupling metabolite.

RESULTS AND DISCUSSION

The model for the single cell situation shows a steady state in a realistic range of the metabolite concentrations. This state may be stable or unstable depending on the kinetic parameters. Using the degradation rate constant k_7 as bifurcation parameter one observes for small values of k_7 a stable stationary state which becomes unstable via a subcritical Hopf-bifurcation. This may lead to the coexistence of a stable limit cycle, an unstable limit cycle and a stable steady state in a certain range of parameters.

In the case of two interacting cells the stability of the steady state can be analyzed by introducing mean values and differences of corresponding metabolite concentrations in both cells as new system variables. Analogous to the previous system one may factorize the characteristic polynomial of the multivariate model into two parts. This gives rise to two lines of Hopf-bifurcations H_{syn} and H_{as}, keeping or destroying the symmetry of the steady state. In the present system the situation is complicated by the fact, that both Hopf-bifurcations are subcritical. This has the effect, that the parameters where limit cycles emerge are located within the region of stable steady states. These critical parameter points are determined by saddle-node-bifurcations. The situation is represented in Fig. 2 showing bifurcation lines in the k_7-J_0-parameter plane. The corresponding calculations have been performed by the software package AUTO [5]. At increasing values of k_7 the stable steady state becomes unstable at the line H_{syn}. The bifurcation line H_{as} lies in the region of instability. T_{syn} and T_{as} denote saddle-node bifurcations leading to synchronous and regular asynchronous oscillations of the cells. For a given parameter only one of these oscillations is stable. This means, for the set of parameters in Fig. 2, that for $J_0 < 4.76$ synchronous oscillations occur, whereas for $4.76 < J_0 < 5.0$ regular asynchronous oscillations arise.

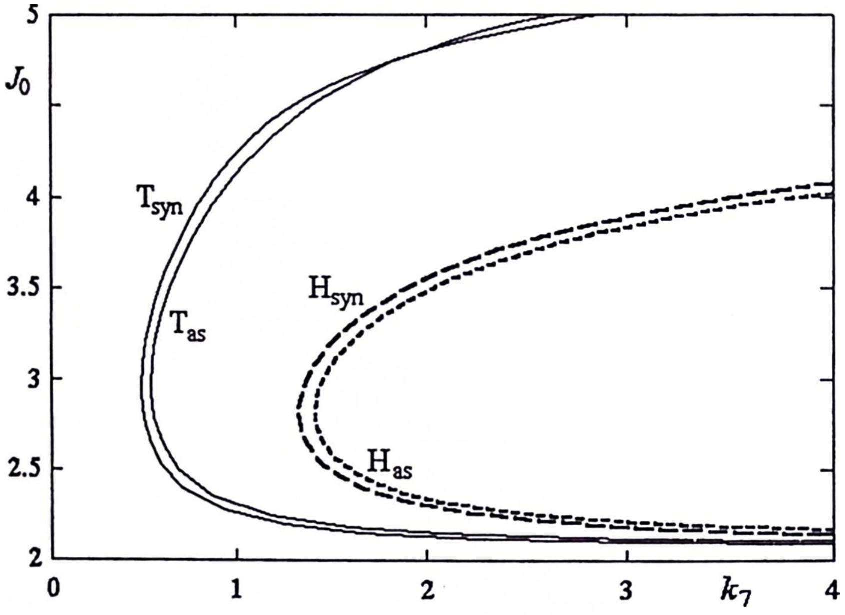

Figure 2. Bifurcation lines in the k_7-J_0-parameter plane for two interacting cells. H_{syn} and H_{as} denote the lines of Hopf bifurcation, keeping or destroying the symmetry of the steady state, respectively. T_{syn} and T_{as} are the saddle-node bifurcations of the limit cycle, leading to synchronous or regular asynchronous oscillations of the cells, respectively.

We conclude that not only for the simple two-component system studied in [2] but also in the present multivariable system synchronous as well as regular asynchronous oscillations occur. A third kind of limit cycles (not shown here) originate via a higher bifurcation of limit cycles. On these limit cycles the metabolites of one cell oscillates much stronger than that of the other cell.

The model predicts, in accordance with the experimental data, (1) upper and lower limits for the input flux and (2) a lower limit for the degradation rate constant k_7 for the occurence of oscillations (see Fig. 2).

The authors are grateful to Prof. H. Westerhoff and J. Passarge (Free University Amsterdam) for interesting discussions and for comments concerning experiments on oscillations in yeast cell populations.

REFERENCES

[1] J. Wolf, R. Heinrich (1996), in: BioThermoKinetics of the Living Cell, pp. 372-374, BTK Press, Amsterdam.
[2] J. Wolf, R. Heinrich (1997), BioSystems 43, 1-24.
[3] A.K. Ghosh et al. (1971), Arch. Biochem. Biophys. 145, 319-331.
[4] P. Richard et al. (1996), Eur. J. Biochem., 238-241.
[5] E. Doedel, J. Kernévez (1986), Technical report, California Institute of Technology, Applied Mathematics.

SEPARABLE MATRICES AND UNIFICATION OF CONCEPTS IN METABOLIC CONTROL ANALYSIS

Christoph Giersch

Institut für Botanik der TU Darmstadt, Schnittspahnstr. 3-5, D-64287 Darmstadt, Germany, Phone: +49 6151 16 4024; Fax: +49 6151 16 4630
e-mail: giersch@bio.tu-darmstadt.de

SUMMARY

A central quantity for calculating control coefficients is the Jacobian **H** for the pathway. For a simple metabolic chain, **H** is tridiagonal. Its inverse $\mathbf{H}^{-1}$, which is required to calculate control coefficients, is semi-separable. A semi-separable $n \times n$ matrix (a_{ij}) has the characteristic property that it is decomposable into two triangles for each of which there are vectors $\boldsymbol{r} = (r_1,...,r_n)$ and $\boldsymbol{t} = (t_1,...,t_n)$ with $a_{ij} = r_i t_j$. Owing to the semi-separability of $\mathbf{H}^{-1}$, the determinants of all 2×2 sub-matrices of elements located within one of the triangles are zero. The flux control coefficient matrix $\mathbf{C}^J$ is separable and the concentration control coefficient matrix $\mathbf{C}^S$ is semi-separable. $\mathbf{C}^S$ has in addition the peculiarity that the row vector is the same for both its upper and lower triangle. A feedback loop gives rise to a new sub-region of vanishing 2-minors, thereby disturbing the semi-separability of the upper triangle of $\mathbf{C}^S$. The notion of (semi-)separability allows assessment of all mutual dependences of control coefficients for metabolic pathways.

The separability of $\mathbf{C}^S$ and $\mathbf{C}^J$ gives rise to certain invariance properties of the ratios of control coefficients that can be expressed as relations among co-response coefficients. The concept of monovalent functional units seems to be related to the separability properties of $\mathbf{C}^S$ and $\mathbf{C}^J$, and also the combinatorial rules for selecting the right modulations originate from the fact that these matrices are separable. Thus, interdependence of control coefficients has its mathematical basis in the notion of (semi-)separability of the control coefficient matrices and can be expressed alternatively as superimposability of co-response profiles, as combinatorial rules, or as monovalent functional units.

INTRODUCTION

Recently designed approaches in metabolic control analysis allow the determination of the complete enzyme kinetics of metabolic pathways under *in-vivo* conditions. These methods require certain (Giersch, 1994) or all (Hofmeyr et al., 1993) of the pathway enzymes to be modulated in their activities. In the course developing the approaches it has been noted that modulations can be dependent or independent of each other, and that determination of elasticities requires the modulations to be independent (Giersch & Cornish-Bowden, 1996). These authors defined combinatorial rules to identify such sets of independent modulations. On the other hand, the mutual dependences of modulations can be interpreted as an invariance property of the metabolic system. Related to this latter view is the notion of superimposability of co-response profiles (Cornish-Bowden & Hofmeyr, 1994). Rohwer et al. (1996) formalized and extended the concept of superimposability by defining monovalent functional units.

Such an unit is characterized as a subsystem of the pathway reactions with the property that the co-response of two control coefficients outside the subsystem to a perturbation of a subsystem reaction does not depend on which of the subsystem reactions is modulated.

From early stages of the work it was evident that the three concepts (superimposability of co-response profiles, monovalent functional units, combinatorial rules) are somehow interrelated: The combinatorial rules are based on the independence of modulations, while the other two approaches are centered around the complementary aspect of mutually dependent modulations. Likewise, it was clear that there was no direct correspondence between the approaches, as the combinatorial rules consider independence also of more than two reactions, while the concept of co-response profiles is restricted to the ratio of two quantities. It was noted that the definition of the monovalent functional units involves variables not located within the unit so that the size of the "unit" can depend on outside quantities.

In this contribution it is shown that there is a common basis of these three concepts. The common basis is that the inverse $\mathbf{H}^{-1}$ of the system's Jacobian $\mathbf{H}$ has a certain pattern of linearly dependent rows or columns which to mathematicians is known as "semi-separability" of $\mathbf{H}^{-1}$. Also the control coefficient matrices $\mathbf{C}^S$ and $\mathbf{C}^J$ are semi-separable and separable, respectively, and the (semi-)separability can be expressed alternatively as superimposability of co-response profiles or as combinatorial rules.

RESULTS AND DISCUSSION

(a) Jacobi matrix H of the simple chain, and its inverse $\mathbf{H}^{-1}$

A quantity central to the analysis of metabolic systems is the Jacobian $\mathbf{H} = \mathbf{N}(\partial v/\partial x)$, since determining control coefficients requires calculation the inverse of $\mathbf{H}$ (Heinrich & Schuster, 1996). For the simple chain, $\mathbf{H}$ is tridiagonal: only entries to the principal diagonal and the adjacent diagonals are non-zero, and for a tridiagonal $\mathbf{H}$ one might be inclined to expect some regular pattern also for $\mathbf{H}^{-1}$. This is indeed the case: $\mathbf{H}^{-1}$ is "semi-separable", that is, $\mathbf{H}^{-1}$ can be decomposed in two triangular matrices for each of which the elements can be written as the product of a row vector and a column vector: for matrix $\mathbf{H}^{-1} = (h_{ij})$ there are four n-tuples q_i, r_i, s_i, τ_i, $i = 1,..,n$ with $q_i r_i = s_i \tau_i$ and

$$h_{i,j} = \begin{cases} q_i r_j \text{ if } i \leq j \\ s_i \tau_j \text{ if } i \geq j \end{cases}$$

A theorem holds that a semi-separable matrix is the inverse of a tridiagonal matrix, and that a tridiagonal matrix is the inverse of a semi-separable matrix (Ikebe, 1979). Also the $n \times (n+1)$ matrix $\mathbf{C}^S$ of concentration control coefficients, although not semi-separable *sensu stricto*, is denoted here as semi-separable to indicate that it exhibits two triangular regions of vanishing 2-minors [see eqn (1) below].

(b) Concentration control coefficients

The concentration control coefficient matrix $\mathbf{C}^S$ is given by $\mathbf{C}^S = -\mathbf{H}^{-1}\mathbf{N} = -[\mathbf{N}(\partial v/\partial x)]^{-1}\mathbf{N}$. If both $\mathbf{N}$ and $\partial v/\partial x$ were invertible (which they are not), we would have

$\mathbf{C}^S = -(\partial v/\partial x)^{-1}$. Following this notion, attempts are made to represent **N** and $\partial v/\partial x$ as modifications of invertible matrices, and to express the inverse of the product $\mathbf{N}(\partial v/\partial x)$ as the product of the inverses of these modified matrices (Elsner & Giersch 1998): The stoichiometry matrix **N** is written as a column vector attached to a square matrix $\tilde{\mathbf{N}}$, the elasticity matrix $\partial v/\partial x$ is decomposed into a row vector and a square matrix $\widetilde{\mathbf{B}}$. The matrix $\mathbf{C}^S$ can then be expressed by essentially $\tilde{\mathbf{N}}$, $\tilde{\mathbf{N}}^{-1}$ and $\widetilde{\mathbf{B}}^{-1}$. The calculation reveals that $\mathbf{C}^S$ is semi-separable and that one and the same row vector defines both the upper and lower triangle of $\mathbf{C}^S$. This corresponds to $r_i = \tau_i$, $i = 1,..,n$, in the above definition of semi-separability. Thus, if we denote this row vector as $c = (c_1,..,c_n)$, there are numbers t_i and u_i, $i = 1,..,n$, and a number d so that

$$\mathbf{C}^S = \begin{pmatrix} t_1c_1 & u_1c_2 & u_1c_3 & \cdots & u_1c_n & u_1d \\ t_2c_1 & t_2c_2 & u_2c_3 & \cdots & u_2c_n & u_2d \\ \vdots & \vdots & & & \vdots & \vdots \\ t_{n-1}c_1 & t_{n-1}c_2 & t_{n-1}c_3 & & u_{n-1}c_n & u_{n-1}d \\ t_nc_1 & t_nc_2 & t_nc_3 & \cdots & t_nc_n & u_nd \end{pmatrix} \qquad (1)$$

This representation has the invaluable advantage that it provides all the information on mutual dependences of concentration control coefficients. Thus it is evident from (1) that the determinants of all 2x2 submatrices located completely within one of the triangles are zero. Moreover, since the rows for *both* triangles are defined by vector c, also some of the 2-minors with elements from different triangles are zero [for instance, $(u_2c_3)(t_nc_n) - (t_nc_3)(u_2c_n) = 0$]. Such minors vanish if both rows of the 2x2 submatrix in question are completely located on one side of the diagonal of $\mathbf{C}^S$. Representation (1) contains the complete information on the positions of vanishing 2-minors in $\mathbf{C}^S$. The flux control coefficient matrix $\mathbf{C}^J$ is not only semi-separable but even separable (Elsner & Giersch, 1998)

A vanishing 2-minor in (1) means that two co-response coefficients (Hofmeyr et al., 1993) are equal. Thus, the regions of vanishing 2-minors can be translated into lists of co-response coefficients that all have the same value. Since $C_p^{S_r}$ (control coefficient of metabolite S_r towards reaction v_p) is the element in row r, column p of $\mathbf{C}^S$, it follows from eqn (1) that, for example, $C_1^{S_1}C_2^{S_2} \neq C_1^{S_2}C_2^{S_1}$, or that

$$C_3^{S_1}C_n^{S_2} = C_3^{S_2}C_n^{S_1} \text{ or } C_3^{S_1}/C_3^{S_2} = C_n^{S_1}/C_n^{S_2},$$

which in terms of co-response coefficients means $O_3^{S_1S_2} = O_n^{S_1S_2}$. In other words, the ratio C^{S_1}/C^{S_2} does not depend on whether it is expressed by modulating reaction 3 or reaction n. Independence of the ratio of two control coefficients from the reaction [i.e., from the column nuber in eqn (1)] has been termed superimposability of co-response profiles (Cornish-Bowden & Hofmeyr, 1994), and from eqn (1) it is evident that the ratios of control coefficients in any two rows within a region of vanishing 2-minors are superimposable. Also superimposable are the ratios of control coefficients in any two columns within the regions, which means for instance that the ratio C_1/C_2 is the same whether it refers to S_2 and S_3.

c) Determination of elasticities and the minor structure of $\mathbf{H}^{-1}$

Elasticities $\partial\mathbf{v}/\partial\mathbf{S}$ can be determined by means of modulating individual independent reactions (Giersch, 1994). The following system of linear equations allows calculation of the elasticities (Giersch & Cornish-Bowden, 1996):

$$\left(\frac{\partial \mathbf{S}}{\partial \mathbf{p}}\right)^{T}\left(\frac{\partial \mathbf{v}}{\partial \mathbf{S}}\right)^{T} = \left[{}^{?}\left(\frac{\partial \mathbf{J}}{\partial \mathbf{p}}\right)_{?}\right]^{T}, \qquad (2)$$

where $\mathbf{p}$ is a vector of specific parameters p_k, and $\partial\mathbf{S}/\partial\mathbf{p}$ and $\partial\mathbf{J}/\partial\mathbf{p}$ are matrices of the dependence on $\mathbf{p}$ of steady state metabolite concentrations $\mathbf{S}$ and flux rate $\mathbf{J}$, respectively. The elements of these two matrices can be determined experimentally. The question marks preceding and following $\partial\mathbf{J}/\partial\mathbf{p}$ indicate that the elements on the principal diagonal of $\partial\mathbf{J}/\partial\mathbf{p}$ may be unknown, since the extent to which a modulation perturbes a reaction rate has not to be kown. The relation between eqns (2) and (1) comes from the fact that the matrix $\partial\mathbf{S}/\partial\mathbf{p}$ has exactly the same structure of vanishing (and non-vanishing) 2-minors as the matrix $\mathbf{C}^S$ of concentration control coefficients [see eqn (5) in Giersch & Cornish-Bowden (1996)].

The combinatorial rules to identify minimal sets of independent modulations are derived by solving the linear system of eqn (2) for the unknown elasticities. $(\partial\mathbf{S}/\partial\mathbf{p})^T$ has the role of contributing non-vanishing minors (that is, non-singular sub-determinants) that will allow the calculation of the elasticities. Thus, the minor structure (or semi-separability) of $\mathbf{C}^S$ is the basis also for the combinatorial rules. For a given reaction, the algorithm of eqn (2) transforms the two-dimensional minor structure of $\partial\mathbf{S}/\partial\mathbf{p}$ into a one-dimensional pattern, namely that of the individual pathway reactions (Giersch, 1997). Therefore, the combinatorial rules can be formulated with reference to the one-dimensional pathway. To derive them, one needs to know (*i*) the positions of non-zero elements in $\partial\mathbf{v}/\partial\mathbf{S}$ and (*ii*) the minor structur of $\partial\mathbf{S}/\partial\mathbf{p}$ or $\mathbf{C}^S$.

The concept of monofunctional units (Rohwer et al., 1996) is related to that of superimposability of co-response profiles. Rohwer and coworkers attempted to decompose a given pathway into subsystems in such a way that the co-response of two variables outside a given subsystem to a modulation of a subsystem reaction does not depend on which subsystem reaction is modulated. It is tempting to identify the subsystems with the independent regions of $\mathbf{C}^S$. However, if this identification is made, the sizes and numbers of "units" depends on the variables outside the units, and, conversely, given reactions constitute a "unit" for certain variables but not for others. Thus the possibility cannot be excluded that the concept of monovalent units somehow tacitly implies the unjustified assumption that there is a one to one correspondence between the two-dimensional pattern of vanishing 2-minors of $\mathbf{C}^S$ and the one-dimensional metabolic pathway.

The separability analysis is not restricted to the simple metabolic chain. Regulatory loops cause the column vector for the semi-separable matrix to be disturbed, thereby giving rise to additional independent triangular regions within matrix $\mathbf{C}^S$ (Elsner & Giersch, 1998). For more complex pathways, there will be more than two independent regions of vanishing minors, and with the appearance of branches and additional regulatory loops the sizes of the regions will diminish and the complementary regions of independent elements will grow. It is evident that the notion of (semi-)separability and the mathematical method to calculate the separability properties dramatically simplify the analysis of metabolic systems with respect to the mutual dependences of control coefficients and of modulations of pathway reactions.

REFERENCES

Cornish-Bowden, A. & Hofmeyr, J.-H. S. (1994). Determination of control coefficients in intact metabolic systems. *Biochem. J.* **298**, 367-375.

Elsner, L. & Giersch, C. (1998) Metabolic control analysis: Separable matrices and interdependence of control coefficients. *J. theor. Biol.*, in press

Giersch, C. (1994). Determining elasticities from multiple measurements of steady-state flux rates and metabolite concentrations: Theory. *J. theor. Biol.* **169**, 89-99.

Giersch, C. & Cornish-Bowden, A. (1996) Extending double modulation: Combinatorial rules for identifying the modulations necessary for determining elasticities in metabolic pathways. *J. theor. Biol.* **182**, 361-369.

Giersch, C. (1997). Co-response coefficients, monovalent units, and combinatorial rules: Unification of concepts in metabolic control analysis. *J. theor. Biol.* **189**, 1-9.

Heinrich, R. & Schuster, S. (1996) *The Regulation of Cellular Systems*, pp. 138-148. New York: Chapman & Hall.

Hofmeyr, J.-H. S., Cornish-Bowden, A. & Rohwer, J. M. (1993). Taking enzyme kinetics out of control; putting control into regulation. *Eur. J. Biochem.* **212**, 833-837.

Ikebe, Y. (1979). On inverses of Hessenberg matrices. *Linear Algebra Appl.* **24**, 93-97

Rohwer, J.M., Schuster, S. & Westerhoff, H. V. (1996). How to recognize monofunctional units in a metabolic system. *J. theor. Biol.* **179**, 213-228.

FUNCTIONAL INTERPRETATION OF THE FLUX CONTROL COEFFICIENT AND EXCESS CAPACITY OF CYTOCHROME C OXIDASE AT INTRACELLULAR OXYGEN

Erich Gnaiger, Andrey V. Kuznetsov, Barbara Lassnig, Raimund Margreiter

Department of Transplant Surgery, D. Swarovski Research Laboratory, University Hospital Innsbruck, A-6020 Innsbruck, Austria, Fax: +43 512 504 4625
E-mail: erich.gnaiger@uibk.ac.at

INTRODUCTION: Regulation and control in the respiratory cascade

Metabolic rate is regulated by a hierarchy of behavioural, physiological and biochemical mechanisms in the dynamic range between minimum and maximum activity of an organism. Such regulation operates at time scales as low as seconds, e.g. in rest-work transitions of muscle. Biochemical regulation of metabolic flux represents a classical topic of enzyme kinetics, relating to down-regulation of key enzymes in metabolic pathways (e.g. [1]) and up-regulation of enzyme cascades. On the other hand, control of metabolic capacity for maximum flux is distributed over a large number of steps, as studied with the tool of flux control analysis [2,3]. Enzyme capacities and distribution of control change over the life span during development and ageing, by acclimation and pathological defects. Biochemical adaptations yield distinct metabolic strategies under selective pressure over evolutionary time [4].

Evolutionary optimisation of organismic form and function results in matched capacities for oxygen supply to mitochondria in the respiratory cascade and respiratory capacity of mitochondria, as summarised by the concept of symmorphosis [5,6] (Fig. 1). With the exception of excessive lung structure, such close matching is actually observed [6,7]. In the mitochondrial respiratory chain, however, cytochrome *c* oxidase appears to be expressed in excess over the capacity for mitochondrial oxygen flux [7-10]. Here we report results on oxygen kinetics in isolated mitochondria and cytochrome *c* oxidase, (i) providing a new perspective on the respiratory cascade and symmorphosis by relating mitochondrial oxygen affinity to intracellular oxygen pressure, and (ii) proposing a functional role of excess capacity of cytochrome *c* oxidase in terms of "synkinetic" regulation of high mitochondrial oxygen affinity.

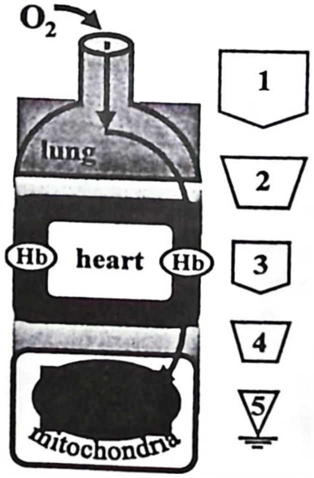

Figure 1. The respiratory cascade with critical steps for the control of oxygen flux. (1) Ventilation by the lung from atmospheric oxygen supply, (2) oxygen diffusion to the blood, (3) circulation of haemoglobin through the cardiovascular system, (4) oxygen diffusion to mitochondria, (5) mitochondrial oxygen consumption (after Ref. [6]). Mitochondrial oxygen kinetics yields a new perspective on respiratory control [10]: High intracellular oxygen pressure, p_{O_2}/p_{50} >>10 indicates that oxygen supply (1-4) exceeds mitochondrial capacity (5) and the mitochondrial flux control coefficient is high in the respiratory cascade. At low $p_{O_2}/p_{50} \leq 1$, mitochondrial capacity is in excess and the mitochondrial flux control coefficient is close to zero. Intracellular p_{O_2}/p_{50} ratios ≈ 5-10 indicate matching of capacities of mitochondria (5) and oxygen supply (1-4), consistent with symmorphosis, at a fairly low but non-zero flux control coefficient of mitochondria in the respiratory cascade.

MATERIALS AND METHODS

We studied oxygen kinetics of mitochondria isolated from rat heart and liver with the OROBOROS *Oxygraph* and DATLAB software (OROBOROS, Innsbruck, Austria) [10,11]. The incubation medium contained 200 mM sucrose, 20 mM HEPES, 0.5 mM EGTA, 1 g/l bovine serum albumin (essentially fatty acid free), 3 mM $MgCl_2$, 20 mM taurine and 10 mM KH_2PO_4, osmolarity ~300 mosm, pH 7.1 at 30 °C. 10 mM succinate was added for measurement of flux through the respiratory chain in the presence of 0.5 µM rotenone. For measurement of cytochrome *c* oxidase, 0.5 mM TMPD and 2 or 5 mM ascorbate were added in the presence of 2.5 µM antimycin A. Active or state 3 respiration was studied at 1 mM Mg-ATP and 1 mM Mg-ADP. ADP but not ATP was excluded for state 4. Instrumental background [11] and oxygen flux due to autooxidation of TMPD and ascorbate [12] were determined as a function of oxygen concentration and subtracted from total volume-specific oxygen flux.

RESULTS AND DISCUSSION

Mitochondrial oxygen kinetics and the organismic respiratory cascade: Symmorphosis

Mitochondrial oxygen flux, J_{O_2}, was a hyperbolic function of oxygen pressure, p_{O_2}, in the relevant oxygen range <1.1 kPa [11],

$$\frac{J_{O_2}}{J_{max}} = \frac{p_{O_2}/p_{50}}{1+p_{O_2}/p_{50}} \qquad (1)$$

The p_{O_2} at 50% of oxygen-saturated flux, p_{50}, was 0.035 and 0.057 kPa (0.3 and 0.6 µM) in heart and liver mitochondria, respectively (see also Lassnig et al. and Kuznetsov et al., this volume [10,12]). The elasticity of mitochondrial oxygen flux with respect to oxygen pressure is related to the hyperbolic dependence of flux on p_{O_2} (Fig. 2; [10]). From Eq.(1), the elasticity is [13],

$$\varepsilon^{J}_{O_2} = \frac{1}{1+p_{O_2}/p_{50}} = 1-\frac{J_{O_2}}{J_{max}} \qquad (2)$$

At intracellular p_{O_2} of 0.3 kPa (3 µM [14-16]), mitochondrial respiration at state 3 in heart is oxygen limited by a factor of 0.10, equivalent to the elasticity (Eq. 2; Fig. 2). At identical p_{O_2}, mitochondrial respiration in liver is more oxygen limited with an elasticity of 0.16 (Eq. 2).

Several important conclusions are drawn from relating mitochondrial oxygen affinity (Fig. 2) to the respiratory cascade (Fig. 1). (i) A negligible role is frequently assumed for intracellular oxygen pressure in the regulation of mitochondrial respiration in tissue. This assumption requires revision since intracellular p_{O_2} can be maintained high and without regulatory effect on maximum respiration only under the condition of excess capacities for oxygen supply (Fig. 1; steps 1-4) relative to mitochondrial respiratory capacity (step 5), $I_{max,supply} >> I_{max,mito}$ [nmol $O_2 \cdot s^{-1}$]. Oxygen supply capacity, however, is well matched with the mitochondrial capacity in muscle [6,7], $I_{max,mito}$, which is the product of maximum respiratory flux per unit mitochondria, J_{max} [nmol $O_2 \cdot s^{-1} \cdot mg^{-}$

^{1}], and mitochondrial mass, m_{mito} [mg of mitochondrial protein in the tissue] (system-related extensive flow, I, and size-specific flux, J [17]),

$$J_{\mathrm{max}} = \frac{I_{\mathrm{max,mito}}}{m_{\mathrm{mito}}} \qquad (3)$$

At excessive oxygen supply capacity, the mitochondrial flux control coefficient would approach 1 (Fig. 2), whereas mitochondrial capacity slightly exceeds maximum oxygen consumption of the heart [18], and flux control is distributed over several steps in the respiratory cascade [6,15]. Therefore, the flux control coefficient of mitochondria in the respiratory chain is <1, and intracellular oxygen is regulatory to a significant degree, $\varepsilon^{J}_{\mathrm{O_2}} > 0$ (Fig. 2).

(ii) Mitochondrial respiratory capacity is to be evaluated at average intracellular oxygen pressure, $p_{\mathrm{O_2,i}}$, yielding oxygen-limited respiration, $J_{\mathrm{O_2,i}} < J_{\mathrm{max}}$ (Fig. 2). At steady state, oxygen flow is equal through each step in the respiratory cascade,

$$I_{\mathrm{supply}} = I_{\mathrm{mito}} = J_{\mathrm{O_2,i}} \cdot m_{\mathrm{mito}} \qquad (4)$$

Mitochondrial capacity at kinetic oxygen saturation, therefore, must be higher than oxygen supply capacity to the tissue and maximum respiration in vivo at $p_{\mathrm{O_2,i}}$, $I_{\mathrm{max,mito}} > I_{\mathrm{max,supply}}$. The mitochondrial "oxygen-kinetic excess capacity", 4_{mito}, expressed relative to maximum flux at intracellular $p_{\mathrm{O_2}}$, is functionally necessary in the context of the respiratory cascade (from Eq. 1),

$$4_{\mathrm{mito}} \equiv \frac{J_{\mathrm{max}} - J_{\mathrm{O_2,i}}}{J_{\mathrm{O_2,i}}} = \frac{1}{p_{\mathrm{O_2,i}} / p_{50}} \qquad (5)$$

Comparison with Eq.(2) shows that at high $p_{\mathrm{O_2,i}}/p_{50} > 10$, the oxygen-kinetic excess capacity of mitochondria (Eq. 5) is approximately equal to the elasticity for O_2 (Fig. 2). 4_{mito} calculated for heart is c. 0.1 (Fig. 2), in agreement with measurements of maximum mitochondrial respiration, $I_{\mathrm{max,mito}}$, at 10-20 % above maximum oxygen consumption of the heart [18].

(iii) Oxygen gradients are necessary for oxygen transport by diffusion (Fick's law). Intracellular $p_{\mathrm{O_2}}$, therefore, is low relative to atmospheric $p_{\mathrm{O_2}}$, particularly at step 4 (Fig. 1) which is dominated by extracellular oxygen gradients and includes an intracellular component. $p_{\mathrm{O_2,i}}$ is maintained low by combination of a low mitochondrial p_{50} (0.2 to 0.3 % of atmospheric oxygen) with a small mitochondrial excess capacity, leading to a moderately low elasticity at maximum work load (Fig. 2).

(iv) Due to excessive lung structure, the flux control coefficient of step 1 is ≈0, but all other steps contribute to changes in respiratory capacity in organisms of various size and athletic versus sedentary type [6]. If flux control is distributed evenly over steps 2-5, then the flux control coefficient is 0.25 for mitochondria (summation theorem [2,3]). A linear model may be an oversimplification, however, since mitochondrial capacity contributes to the heart pumping capacity (step 3) and mitochondrial density influences intracellular diffusion distances (step 4).

(v) A large mitochondrial excess capacity is hypothetically assumed for explaining large threshold values for mitochondrial DNA mutations in human degenerative diseases and ageing [19]. The inevitable consequence of a large mitochondrial excess, as is readily apparent now, is a low intracellular $p_{\mathrm{O_2}}/p_{50}$ ratio and limitation by oxygen supply (Fig. 2).

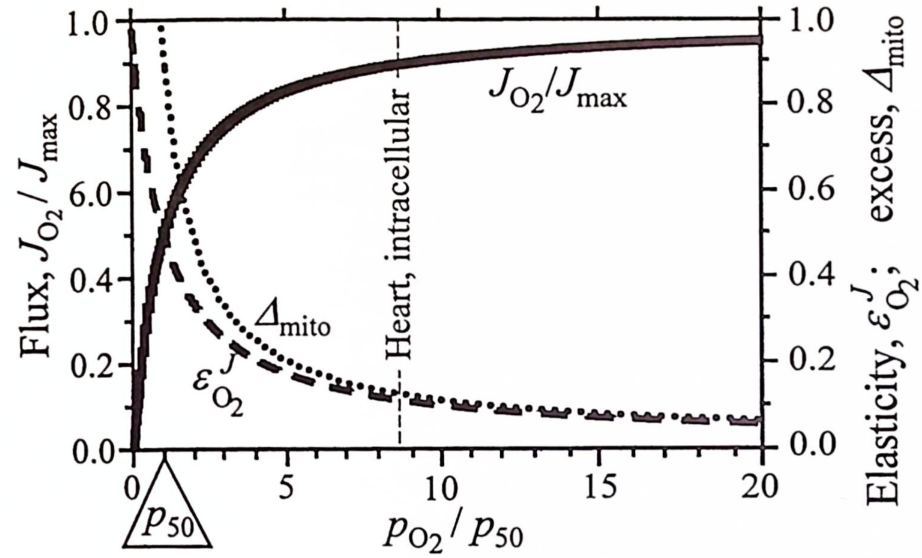

Figure 2. Oxygen flux relative to maximum flux at kinetic oxygen saturation, J_{O_2}/J_{max} (full line; Eq. 1), elasticity of mitochondrial oxygen flux (stippled line; Eq. 2), and oxygen-kinetic excess capacity, Δ_{mito} (dotted line; Eq. 5), as a function of oxygen pressure, p_{O_2}, expressed relative to the mitochondrial p_{50}. The $p_{O_2,i}/p_{50}$ ratio is shown (vertical line) for intracellular p_{O_2} in heart of 0.3 kPa and p_{50} in state 3. Without any oxygen limitation, the elasticity would approach zero and the flux control coefficient of mitochondria in the respiratory cascade (Fig. 1) would be one (connectivity theorem [2,3]).

An alternative explanation for the threshold effect is based on considering excess capacities of mitochondrial enzymes with low flux control coefficients for maximum mitochondrial respiration [8,9,20]. 50% lower COX activity in copper deficient mice yields unchanged maximum oxygen flux in permeabilized muscle fibers [21]. Since the early quantitative studies on flux control of oxidative phosphorylation, it is known that distribution of flux control depends on experimental conditions [22]. The flux control coefficient of cytochrome *c* oxidase for state 3 respiration of liver mitochondria increases from 0.1 to 0.5 when sucrose medium is replaced by media with physiological K^+ concentration [23]. Therefore, extrapolations to in vivo conditions must be viewed critically. In particular, physiological intracellular oxygen levels must be taken into account in mitochondrial bioenergetics [11,24,25].

While capacities of highly integrated components of the respiratory cascade are matched (Fig. 1), excess capacities of single enzymes appear to contradict the concept of optimum design of the respiratory chain. We address this apparent discrepancy with respect to the terminal enzyme in the mitochondrial electron transport chain and the functional relation between mitochondrial oxygen affinity and excess capacity of cytochrome *c* oxidase (COX).

Oxygen kinetics of COX and the mitochondrial respiratory chain: Synkinetics

Oxygen-saturated oxygen flux, V_{max}', measured for COX at state 3 and 0.5 mM tetramethyl-*p*-phenylenediamine (TMPD, below saturation concentration) was higher than oxygen-saturated oxygen flux, J_{max}, for the mitochondrial respiratory chain at state 3 with succinate. The relative excess capacity of COX, Δ_{COX}, was higher in heart than liver mitochondria,

$$\Delta_{\mathrm{COX}} \equiv \frac{V_{\mathrm{max}}' - J_{\mathrm{max}}}{V_{\mathrm{max}}'} \qquad (6)$$

The corresponding apparent turnover number of COX, k_{cat}' [nmol O_2·nmol aa_3^{-1}·s^{-1}], was 9.5±0.9 s^{-1} and 10.8±1.8 s^{-1} in heart and liver mitochondria, respectively (±SD, $N = 8$ and 6; estimated from the hyperbolic oxygen dependence at p_{O_2}<1.1 kPa; 16 and 7 % lower than initial maximum turnover rates measured at high p_{O_2} [12]). Like k_{cat}', the K_{m}' for oxygen of COX was not different between heart and liver mitochondria at an average of 0.063 kPa. The affinity of the single step, K_{m}', therefore, cannot explain the lower p_{50} of heart mitochondria.

Fast haem-haem electron transfer, k_{et}, to the binuclear haem iron-copper centre of COX yields kinetic trapping of oxygen as a basis for the low K_{m}' of COX [26-28],

$$K_{\mathrm{m}}' \approx \frac{k_{\mathrm{in}}}{k_{\mathrm{et}}} \cdot K_{\mathrm{eq}} \qquad (7)$$

k_{in} is the small, hence rate-limiting rate constant for electron input into COX, and K_{eq} is the equilibrium constant of oxygen binding. Consistent with Eq.(7), the K_{m}' decreased when k_{cat}' or k_{in} was suppressed at lower TMPD (0.3 mM) and no addition of ADP (Fig. 3; open symbols, substituting for J_{max} in Eq. 6 the oxygen-saturated V_{max}' of COX at states 3 or 4).

K_{m}' increases with COX turnover rate which is limited by k_{in} (Eq. 7). Reduction of COX turnover provides the key for a direct functional role of COX excess capacity which causes down-regulation of mitochondrial p_{50} by limitation of k_{in} from the respiratory chain [10]. Excess capacity of COX limits the COX turnover rate in maximally active mitochondria relative to k_{cat}', and thus lowers the mitochondrial p_{50} relative to K_{m}' (Fig. 3; closed versus open symbols). Regulation by COX turnover rather than adenylate binding to COX [29] decreases the p_{50} in state 4 compared to state 3 [10,12,30], when Δ_{COX} increases to 0.9 by ADP limitation of the respiratory chain with low electron input into COX (Fig. 3). Owing to the higher COX excess capacity, mitochondrial COX turnover is slower in heart than in liver, which is the synkinetic mechanism for the more effective down-regulation of mitochondrial p_{50} in heart.

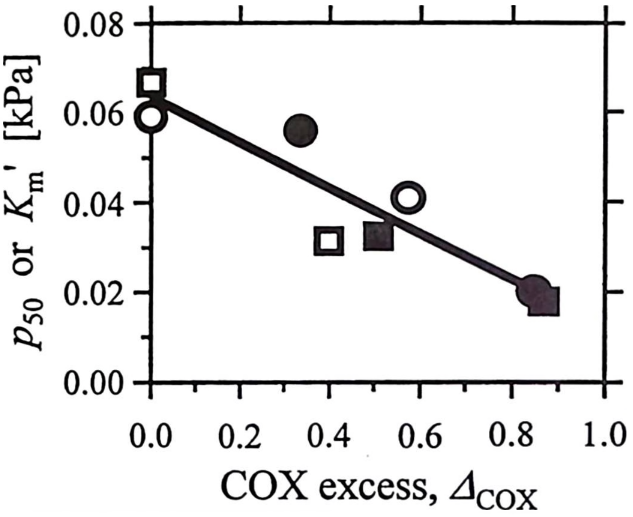

Figure 3. Mitochondrial p_{50} or K_m' for oxygen, as a function of relative COX excess capacity, Δ_{COX}. Open symbols: K_m' for COX measured at maximum COX turnover and Δ_{COX} of zero (0.5 mM TMPD, 1 mM ADP), and for limited COX turnover (0.3 mM TMPD, 0 mM ADP). Closed symbols: p_{50} at state 3 with Δ_{COX} of 0.33 and 0.50 (Eq. 7), and at state 4 with maximum Δ_{COX}. Squares and circles: heart and liver mitochondria, respectively.

CONCLUSIONS

Oxygen affinity of mitochondrial respiration is a function of both oxygen kinetics of cytochrome *c* oxidase as studied at the level of the single enzyme step, and excess capacity of COX which is a synkinetic characteristics of the tissue-specific mitochondrial multi-enzyme system. High oxygen affinity is achieved by down-regulation of COX turnover rate at excess capacity of COX relative to the respiratory chain. This functional interpretation of COX excess capacity depends on the physiological significance of mitochondrial oxygen affinity in the intracellular low-oxygen environment at the terminal level of the respiratory cascade.

ACKNOWLEDGEMENTS

Supported by a research grant of the University of Innsbruck to E.G. and an OROBOROS Research Award to A.K. The manuscript was completed while E.G. was visiting professor at the University of Bordeaux II, CJF-INSERM 97-05 with Prof. J.-P. Mazat, whom we thank for valuable comments.

REFERENCES

[1] Hand, S.C. and Gnaiger, E. (1988) Science 239, 1425-1427.
[2] Kacser, H. and Burns, J.A. (1973) Symp. Soc. Exp. Biol. 32, 65-104.
[3] Heinrich, R. and Rapoport, T.A. (1974) Eur. J. Biochem. 42, 97-105.

..[4] Hochachka, P.W. and Somero, G.N. (1984) Biochemical adaptation, Princeton Univ. Press.

[5] Weibel, E.R. (1984) The pathway for oxygen. Structure and function in the mammalian respiratory system. Harvard Univ. Press, Cambridge, Mass.

[6] Weibel, E.R., Taylor. C.R. and Hoppeler, H. (1991) Proc. Natl. Acad. Sci. USA 88, 10357-10361.

[7] Schwerzmann, K., Hoppeler, H., Kayar, S.R. and Weibel, E.R. (1989) Proc. Natl. Acad. Sci. USA 86, 1583-1587.

[8] Mazat, J.-P., Letellier, T. and Malgat, M. (1993) in Modern Trends in BioThermoKinetics (Schuster, S., Rigoulet, M., Ouhabi, R. and Mazat, J.-P., eds.), pp. 343-346, Plenum Press, New York.

[9] Letellier, T., Heinrich, R., Malgat, M. and Mazat, J.-P (1994) Biochem. J. 302, 171-174.

[10] Gnaiger, E., Lassnig, B., Kuznetsov, A.V., Rieger, G. and Margreiter, R. (1998) J. Exp. Biol. 201, 1129-1159.

[11] Gnaiger, E., Steinlechner-Maran, R., Méndez, G., Eberl, T. and Margreiter, R. (1995) J. Bioenerg. Biomembr. 27, 583-596.

[12] Lassnig, B., Kuznetsov, A.V., Margreiter, R. and Gnaiger, E. (in prep.).

[13] Fell, D. (1997) Understanding the control of metabolism. Portland Press, London.

[14] Wittenberg, B.A. and Wittenberg, J.B. (1989) Annu. Rev. Physiol. 51, 857-878.

[15] Wagner, P.D. (1996). Annu. Rev. Physiol. 58, 21-50.

[16] Helmlinger, G., Yuan, F., Dellian, M. and Jain, R.K. (1997) Nature Medicine 3, 177-182.

[17] Gnaiger E. (1993) Pure & Appl. Chem. 65, 1983-2002.

[18] Mootha, V.K., Arai, A.E. and Balaban, R.S. (1997) Am. J. Physiol. 272, H769-H775.

[19] Wallace, D.C., Shoffner, J.M.,Trounce, I., Brown, M.D., Ballinger, S.W., Corral-Debrinski, M., Horton, T., Jun, A.S. and Lott, M.T. (1995) Biochim. Biophys. Acta 1271, 141-151.

[20] Letellier, T., Malgat, M. and Mazat, J.-P. (1993) Biochim. Biophys. Acta 1141, 58-64.

[21] Kuznetsov, A., Clark, J.F., Winkler, K. and Kunz, W.S. (1994) in What is controlling life? (Gnaiger, E., Gellerich, F.N., Wyss, M., eds.), pp. 275-277, Modern Trends in BioThermoKinetics 3. Innsbruck Univ. Press, Innsbruck.

[22] Groen, A.K., Wanders, R.J.A., Westerhoff, H.V., van der Meer, R. and Tager, J.M. (1982) J. Biol. Chem. 257, 2754-2757.

[23] Devin, A., Guérin, B. and Rigoulet, M. (1997) Biochim. Biophys. Acta 1319, 293-300.

[24] Steinlechner-Maran, R., Eberl, T., Kunc, M., Margreiter, R. and Gnaiger, E. (1996) Am. J. Physiol. 271, C2053-C2061.

[25] Korzeniewski, B. and Mazat, J.-P. (1996) Acta Biotheoretica 44, 263-269.

[26] Chance, B. (1965) J. Gen. Physiol. 49, 163-188.

[27] Riistama, S., Puustinen, A., García-Horsman, A., Iwata, S., Michel, H. and Wikström, M. (1996) Biochim. Biophys. Acta 1275, 1-4.

[28] Verkhovsky, M.I., Morgan, J.E., Puustinen, A. and Wikström, M. (1996) Nature 380, 268-270.

[29] Napiwotzki, J., Shinzawa-Itoh, K., Yoshikawa, S. and Kadenbach, B. (1997) Biol. Chem. 378, 1013-1021.

[30] Gnaiger, E., Lassnig, B., Kuznetsov, A. and Margreiter, R. (1998) Biochim. Biophys. Acta, EBEC issue (in press).

HIGH-RESOLUTION RESPIROMETRY – OPTIMUM PERMEABILIZATION OF THE CELL MEMBRANE BY DIGITONIN

Erich Gnaiger, Andrey V. Kuznetsov, Barbara Lassnig, Anita Fuchs[a], *Michael Reck*[a], *Kathrin Renner, Sylvia Stadlmann, Gunde Rieger, Raimund Margreiter*

Department of Transplant Surgery, D. Swarovski Research Laboratory, University Hospital Innsbruck, A-6020 Innsbruck, Austria;
[a] OROBOROS, Bioenergetics and Biomedical Instruments, Schoepfstr. 18, A-6020 Innsbruck, Austria, Fax: +43 512 504 4625; [a]+43 512 566796; E-mail: erich.gnaiger@uibk.ac.at

INTRODUCTION

Permeabilization of the cell membrane is becoming an established alternative to the isolation of mitochondria in bioenergetic studies of cultured cells and biopsy samples of muscle. Depending on cell type, 5 to 50 million cells are required for a respirometric measurement of endogenous and permeabilized-cell respiration [1,2], using conventional oxygen monitoring instruments. An order of magnitude less cells are required when using high-resolution respirometry [3] (Tab. 1), which provides an up-to-date standard for general and clinical bioenergetics, including the diagnosis of mitochondrial defects, testing of drugs, oxidative stress and hypoxia-reoxygenation injury [4-6].

We provide an overview of (i) the specific features of high-resolution respirometry, (ii) test experiments for instrumental evaluation, and (iii) digitonin titrations for determining optimum concentrations for cell membrane permeabilization in cultured cells.

High-resolution respirometry: OROBOROS *Oxygraph* and DATLAB software

High-resolution respirometry is based on (i) the OROBOROS® *Oxygraph*, (ii) DATLAB for on-line display, data acquisition and analysis, and (iii) calibration of parameters for signal correction [3]. In addition, the OROBOROS® Titration-Injection microPump (TIP) provides the option for automatic titrations and steady-state injections. This combination yields the high sensitivity required in studies of biopsies with minimum amount of sample, pathological effects resulting in reduced respiration, cell cultures with limited number of cells, mutants with diminished respiratory capacity, and for inhibitor titrations in metabolic control analysis, resolution of changes in oxygen flux over incubation time, and measurement at low oxygen.

The OROBOROS *Oxygraph for high-resolution respirometry*

The OROBOROS® *Oxygraph* is a two-chamber titration-injection respirometer (Fig. 1) with the following features [3]: (i) Artefacts due to oxygen diffusion are minimised by using appropriate materials, glass for chambers and titanium for stoppers and injection cannulas. Avoiding perspex chambers is essential but not sufficient. Viton O-rings and butyl india rubber sealings are used with zero oxygen diffusion.

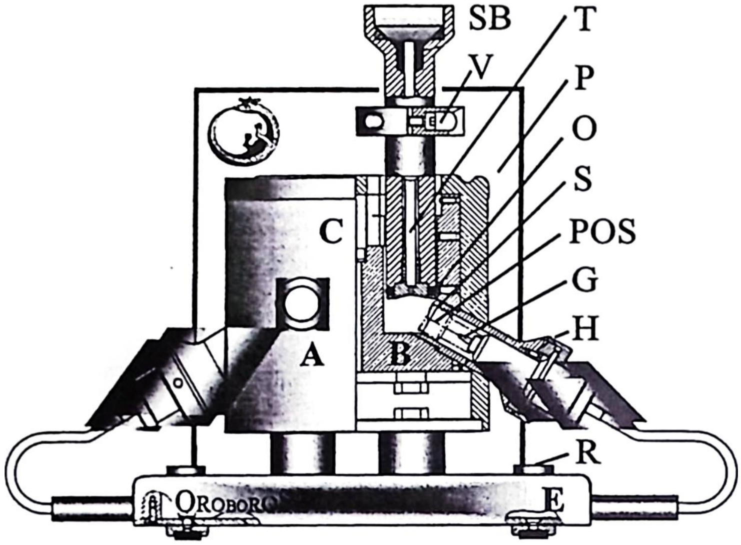

Figure 1. The OROBOROS® *Oxygraph* (Paar, Austria). **A**, window into chamber A; **B**, glass chamber B; **C**, copper block, temperature-regulated and insulated; **E**, base with electronics for signal amplification and rotating electromagnetic field for driving the PEEK stirrer bars (not shown); **G**, gold connection to POS; **H**, holder of POS; **O**, Viton O-ring on stopper; **P**, plate with heat dissipator in thermal contact with th peltier thermopiles between the copper block and P; **POS**, polarographic oxygen sensor; **R**, switch for stirrer B; **S**, sleeve for sealing POS against glass chamber, butyl india rubber; **SB**, stopper of chamber B with conical titanium plate at the bottom (no shown for chamber A); **T**, titanium cannula; **V**, adjustable sleeve for setting the chamber volume.

PEEK stirrer bars (polyetheretherketone) replace the conventional teflon stirrers. Teflon is an effective O_2 buffer with 10-fold higher oxygen solubility compared to incubation medium (Tab. 2; [7]). Oxygen leaks back from a teflon stirrer bar at up to -30 pmol $O_2 \cdot s^{-1} \cdot cm^{-3}$ at zero p_{O_2} [8]; –5 pmol $O_2 \cdot s^{-1} \cdot cm^{-3}$ is reported in one of the few cases in the literature [9], compared to –1.5 to –2 pmol $O_2 \cdot s^{-1} \cdot cm^{-3}$ with PEEK stirrers (Fig. 2). This residual oxygen diffusion is probably mainly due to oxygen leakage from the electrolyte reservoir of the sensor into the sample medium. After some hours of equilibration at minimum oxygen levels, oxygen stores for back-diffusion are depleted and diffusion is zero over days recorded in the OROBOROS *Oxygraph*. Oxygen diffusion increases, however, by a factor of >10 when choosing a wrong material for sealings.

(ii) Each chamber is equipped with a polarographic oxygen sensor (POS) with a large cathode (2 mm diameter; Orbisphere Model 2120). Sensitivity and signal to noise ratio increase and signal drift at zero oxygen decreases with increasing cathode area [7]. By angular insertion of the POS into the glass chamber (Fig. 1) dead space is minimized and the cathode is placed into an optimum position for stirring [8], contrary to the customary central insertion where the cathode is exposed to minimum water current.

Table 1
Where high resolution counts: high accuracy with minimum amount of sample

Sample	Concentration		Volume	Temp.	Ref.
Heart mitochondria	0.01	mg protein·cm^{-3}	2.0 cm^3	30 °C	[14]
Permeabilised muscle fibers	1.5	mg wet weight·cm^{-3}	1.5 cm^3	30 °C	[15]
Endothelial cells	0.2	10^6 cells·cm^{-3}	2.0 cm^3	37 °C	[12]
T-lymphocytes	1	10^6 cells·cm^{-3}	1.5 cm^3	37 °C	[6]

Table 2
Oxygen solubility in pure water, incubation medium and Teflon. The comparison illustrates the importance of eliminating Teflon (Teflon-coated magnetic stirring bars), for minimizing background distortion of oxygen flux

Compound	Oxygen solubility at 25 °C, S_{O_2} [µmol·dm^{-3}·kPa^{-1}]
Water	12.6
Incubation medium	10.7 to 11.6
Teflon, polytetrafluoroethylene	106.0

(iii) A paradigm shift from minimum to optimum volume of the *Oxygraph* chamber is based on considerations of the surface to volume ratio, which increases with decreasing volume. Boundary effects, therefore, entail larger errors at smaller volume, in particular binding of inhibitors to surfaces and oxygen diffusion. While the rate of oxygen depletion per unit amount of sample increases linearly with decreasing chamber volume, side effects may increase to a larger extent. Accuracy but not necessarily reproducibility is lost with decreasing chamber size. The optimum chamber volume of the OROBOROS *Oxygraph* is 1.5 to 2.0 cm^3 and is variable up to 8 cm^3. The large inner diameter of the cylindrical chambers (16 mm) provides space for additional electrodes, light guides and mechanical transducers.

(iv) Temperature is regulated electronically by a built-in peltier thermostat with accuracy better than ±0.05 °C in the range 2 to 50 °C (at room temperature). Superior temperature stability, higher safety and comfort are obtained by replacing the conventional water jacket and elimination of tubings connected to a water bath. The compact design provides for two independently operated respirometer chambers at minimum bench space (Fig. 1). The microprocessor controls independently the variable speed of the two built-in electromagnetic stirrers. A slow-start function prevents decoupling of the stirrer magnet.

(v) An A/D converter transmits the signal of each chamber independently through an RS232 port at 1 s intervals (minimum is 200 ms), after time-averaging 30 readings. The digital limit of resolution is <0.001 kPa (<0.005 % air saturation). Barometric pressure is digitally recorded from a pressure transducer for automatic calibration of oxygen by DATLAB.

DATLAB *for high-resolution respirometry*

Simultaneous on-line recording of oxygen concentration, c_{O_2}, and oxygen flux, J_{O_2} (per amount of sample) or r_{O_2} (per chamber volume), and digital data analysis are a prerequisite for high-resolution respirometry. Linear slopes of oxygen concentration over time are obtained only at constant flux (Fig. 3), but may be artifacts of low resolution with linear fitting on chart recorder traces, belonging to the past. Stability or small changes of oxygen flux can be evaluated and are resolved only by analysis of the time derivative of oxygen concentration as a function of time (Fig. 3). This is achieved on-line by DATLAB, displaying oxygen concentration and flux independently for the two *Oxygraph* chambers on one screen. Subsequently, sections of the experiment are selected for averaging and tabulating oxygen flux. Graphically supported DATLAB ANALYSIS is optimized specifically for *Oxygraph* high-resolution respirometry, combining speed and flexibility in a user-friendly analysis [10] (Fig. 2 and 3).

Oxygen flux is routinely recorded over large ranges of oxygen concentration, from air saturation to zero oxygen levels. A full-scale screen displays an overview of the experiment, but flexible zooming into particular windows of oxygen and time is crucial for high resolution during experiment and analysis.

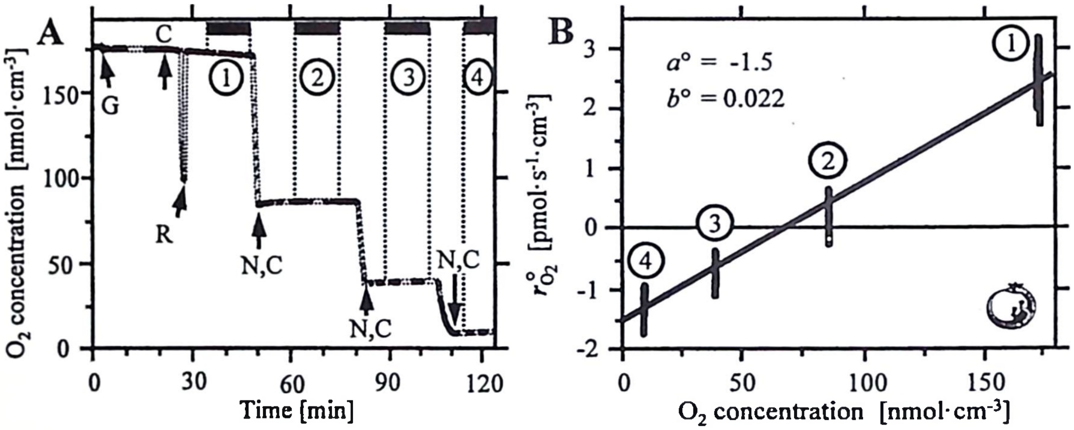

Fig. 2. Standard background test, with air calibration of the polarographic oxygen sensor (POS), calibration of the POS time constant, and background oxygen flux measured at four oxygen concentrations. **G**, electronic gain setting, after air equilibration of the stirred incubation medium (2 cm^3 RPMI, 37 °C, 95.5 kPa barometric pressure) with air introduced by partial insertion of the stopper (Fig. 1). See Fig. 3 for zero oxygen calibration. **C**, Closing the chamber containing incubation medium without sample. **R**, Rotation of the stirrer is shortly switched off and on, to calibrate the response time of the signal for dynamic correction [3]. **N,C**, Opening the stopper partially to purge argon into the gas phase; at the desired oxygen level, the chamber is closed for recording instrumental background. Numbers in circles: Four sections of the background experiment are selected (**A**) for plotting the volume-specific background rate, $r_{O_2}°$, as a function of oxygen concentration (**B**). The linear regression is shown with intercept, $a°$, and slope, $b°$ (**B**).

Automatic air calibration is based on digitally recorded barometric pressure and temperature. If the oxygen solubility of the incubation medium is not known, it may be selected according to general guidelines. Automatic calibration of the time constant of the oxygen sensor and deconvolution of the signal yield the high time resolution required in kinetic analyses [3]. Various options for smoothing are available, selected according to the requirements of time resolution and signal stability. Specific corrections are made for calculating oxygen flux when the TIP is used for continuous steady-state injections into the *Oxygraph* [11].

OROBOROS T*itration*-I*njection micro*P*ump (*TIP*)*

The electronically controlled TITRATION-INJECTION MICROPUMP (TIP) provides highest accuracy in automatic titrations. Continuous injection by TIP allows operation at quasi steady-states, with a new flexibility in experimental design by combining the advantages of closed and open systems approaches. Titration volumes are programmable between 0.05 to 250 mm^3, and injection flows can be set between 0.01 and 35 $mm^3 \cdot s^{-1}$ over selected periods of time. Setup programs can be saved with variable sequences of titrations and injections [11].

Instrumental test experiments

Oxygen consumption by the polarographic oxygen sensor and back-diffusion at low oxygen pressure contribute to background effects, correction of which sets a standard in high-resolution respirometry. Determination of the background flux over the experimental oxygen range provides a general test of instrument function (Fig. 2A). This is advantageous even in cases when experimental oxygen flux is high and, therefore, background correction is not more than 1-5 % of experimental flux.

The polarographic oxygen sensor produces an electrical signal by consuming oxygen proportional to the partial pressure of oxygen in the medium (Fig. 2B). On the other hand, the rate of diffusion into the chamber depends linearly on the oxygen pressure difference between the oxygen source and the medium, being largest in the hypoxic region and decreasing linearly with increasing oxygen pressure (Fig. 2B). Correction for calibrated background parameters (Fig. 2B) is performed automatically by DATLAB over the entire experimental oxygen range [3]. Sensitivity is better than ±1.5 pmol $O_2 \cdot s^{-1}.cm^{-3}$ with background correction, as judged from measurement of background rates at air saturation and zero oxygen of 2.85 (±0.64 SD) and -1.50 (±0.28 SD) pmol $O_2 \cdot s^{-1} \cdot cm^{-3}$, respectively, and respiration of endothelial cells inhibited by rotenone and antimycin A, averaging 2.5 (±1.0 SD, n=7) pmol$\cdot s^{-1} \cdot 10^{-6}$ cells at densities varied to a minimum of $0.2 \cdot 10^6$ cells$\cdot cm^{-3}$ [12].

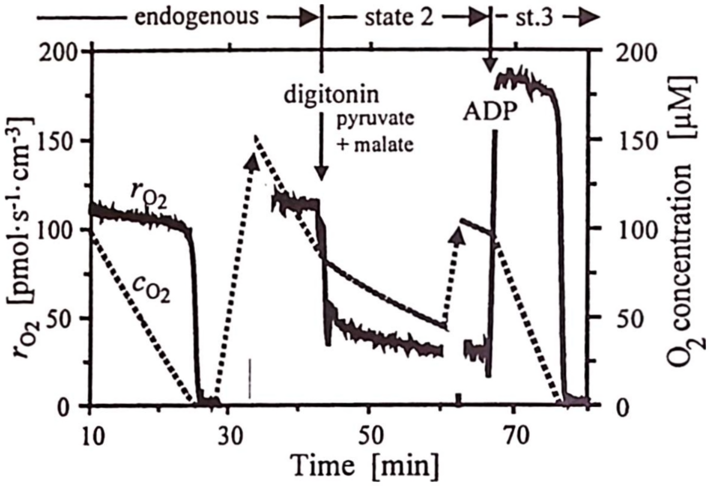

Fig. 3. Respiration of endothelial cells (continuous line; rate of oxygen consumption per volume, r_{O_2} [pmol·s^{-1}·cm^{-3}]) calculated on-line from oxygen concentration (dotted line; c_{O_2} [nmol·cm^{-3}]), at a density of 2.9·10^6 cells·cm^{-3}. Cellular respiration depleted oxygen to zero, which is used for zero calibration. Measurement was continued after opening the chamber shortly for re-oxygenation (dotted arrow lines). Permeabilization of cells by digitonin (10 μg·10^{-6} cells) induced a reduction of flux to state 2, independent of oxygen concentration as shown by a short re-oxygenation. Addition of ADP (1 mM) increased oxygen flux to state 3. Note the decline of flux after maximum ADP stimulation. Aerobic-anoxic transitions yield the oxygen kinetics.

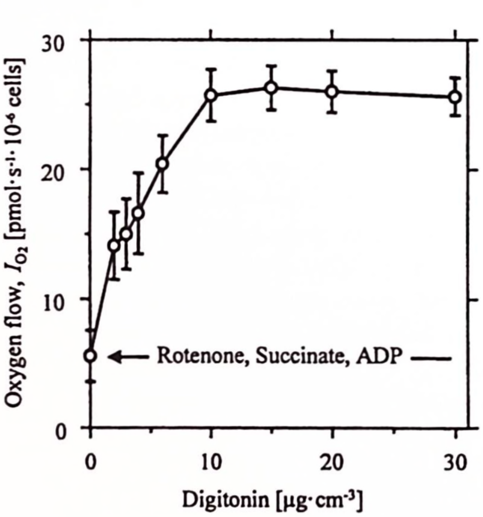

Fig. 4. Titration of digitonin during measurement of respiration in endothelial cells in mitochondrial medium, in the presence of 10 m succinate, 0.5 μM rotenone and 1 m ADP. Time intervals between titration were 12-14 min up to 3 μg·cm^{-3} and 4-min at higher digitonin concentrations Cell density: 1.02 (±0.16)·10^6·cm$^-$ (*N*=6; ±SD). Permeabilization wit digitonin concentration of 10 μg·10$^-$ cells is optimum for ADP-stimulate respiration.

Permeabilization of endothelial cells: Test for optimum digitonin concentration

Stimulation of mitochondria by ADP after permeabilization of cells with digitonin yields occasionally oxygen flux which is lower than endogenous respiration of intact cells [13]. Optimum conditions must be tested rigorously, therefore, for mitochondrial integrity and permeabilization of the cell membrane with digitonin, as a basis for conclusions to be drawn on the function of various components of the mitochondrial respiratory chain. A suitable test is shown in Figure 4, applicable to cells which are impermeable for succinate when the plasma membrane is intact [4,5].

Endogenous respiration of intact cells (human umbilical vein endothelial cells, transformed by lung carcinoma) is not stimulated by addition of succinate and ADP, and is strongly inhibited by rotenone (Fig. 4; zero digitonin concentration). Importantly, this is a quantitative quality control of suspended cells [4]. Subsequent stepwise digitonin titration yields gradual permeabilization of the cell membrane, shown by the increase of respiration up to state 3 (Fig. 4; at 10 $\mu g \cdot 10^{-6}$ cells). Combination of respiratory measurement in intact cells and mitochondria after permeabilization (Fig. 3) provides a link between bioenergetics and physiology.

REFERENCES

[1] Hofhaus, G., Shakeley, R.M. and Attardi, G. (1996) Methods Enzymol. 264, 476-483.

[2] Ouhabi, R., Boue-Grabot, M. and Mazat, J.-P. (1994) in What is Controlling Life? (Gnaiger, E., Gellerich, F.N., Wyss, M., eds.), pp. 141-144, Modern Trends in BioThermoKinetics 3. Innsbruck Univ. Press, Innsbruck.

[3] Gnaiger, E., Steinlechner-Maran, R., Méndez, G., Eberl, T. and Margreiter, R. (1995) J. Bioenerg. Biomembr. 27, 583-596.

[4] Steinlechner-Maran, R., Eberl, T., Kunc, M., Schröcksnadel, H., Margreiter, R. and Gnaiger, E. (1997) Transplantation 63, 136-142.

[5] Gnaiger, E., Rieger, G., Kuznetsov, A.V., Fuchs, A., Stadlmann, S., Lassnig, B., Hengster, P., Eberl, T. and Margreiter, R. (1997) Transplant. Proc. 29, 3524-3526.

[6] Knoblechner, A., Steinlechner, R., Schirmer, M., Gellerich, F.N., Margreiter, R., Konwalinka, G. and Gnaiger, E. (1994) in What is Controlling Life? (Gnaiger, E., Gellerich, F.N. and Wyss, M., eds.), pp. 294-296, Modern Trends in BioThermoKinetics 3. Innsbruck Univ. Press, Innsbruck.

[7] Gnaiger, E. and Forstner, H., eds. (1983) Polarographic oxygen sensors. Aquatic and physiological applications. Springer, Berlin, Heidelberg, New York: 370 pp.

[8] Haller, T., Ortner, M. and Gnaiger E. (1994) Analyt. Biochem. 218, 338-342.

[9] Robiolio, M., Rumsey, W. L. and Wilson, D. F. (1989) Am. J. Physiol. 256, C1207-C1213.

[10] Gnaiger, E. and Reck, M. (1997) High resolution of data in the lab - DATLAB Handbook. OROBOROS, Innsbruck, 5th ed.

[11] Gnaiger, E. (1997) TITRATION-INJECTION MICROPUMP – TIP operation manual. OROBOROS, Innsbruck, 3rd ed.

[12] Steinlechner-Maran, R., Eberl, T., Kunc, M., Margreiter, R. and Gnaiger, E. (1996) Am. J. Physiol. 271, C2053-C2061.

[13] Guan, M.-X, Fischel-Ghodsian, N. and Attardi, G. (1996) Hum. Molec. Genet. 5, 963-971.

[14] Gnaiger, E., Lassnig, B., Kuznetsov, A. and Margreiter, R. (1998) Biochim. Biophys. Acta, EBEC issue (in press).

[15] Gellerich, F.N., Steinlechner, R., Wyss, M., Eberl, T., Müller, L.C., Skladal, D., Sperl, W., Dapunt, O., Margreiter, R. and Gnaiger, E. (1994) in What is Controlling Life? (Gnaiger, E., Gellerich, F.N. and Wyss M., eds.), pp. 263-267, Modern Trends in BioThermoKinetics 3. Innsbruck Univ. Press, Innsbruck.

20

MODELLING CALCIUM OSCILLATIONS AND COUPLING

Thomas Haberichter, Thomas Hoefer, Reinhart Heinrich

Theoretical Biophysics, Institute of Biology, Humboldt University, Invalidenstr. 42, D-10115 Berlin, Germany, haberich@bp.biologie.hu-berlin.de
hoefer@bp.biologie.hu-berlin.de, reinhart=heinrich@rz.hu-berlin.de

Intracellular calcium transients play a central role in many signal transducing cascades. Recent experiments show that calcium signals can also propagate from one cell to another in a variety of cell populations; examples include hormone-evoked calcium oscillations in hepatocytes and glia-to-neuron signalling in response to neurotransmitters. The coupling mechanisms that can support such intercellular signals remain unclear. Potential candidates are diffusion of the calcium-releasing messenger, inositol 1,4,5-triphosphate through gap junctions, gap junctional diffusion of calcium ions, and paracrine signalling.

To investigate the different ways of coupling we introduce a model of three variables which employs the calcium-induced calcium release mechanism:

$$[Ca^{2+}]_{cytosol} \qquad \dot{x} = v_0 - k_1 x - k_1{}' x + k_2 y + k_3 \frac{x^4}{K_1{}^4 + x^4} \frac{y^4}{K_2{}^4 + y^4}$$

$$[InsP_3] \qquad \dot{y} = -y + \alpha + \beta \frac{x^2}{K_3{}^2 + x^2}$$

$$[Ca^{2+}]_{store} \qquad \dot{z} = k_1 x - k_2 y - k_3 \frac{x^4}{K_1{}^4 + x^4} \frac{y^4}{K_2{}^4 + y^4} \quad .$$

We extend this model to a system of several gap junction-coupled cells. In the case of identical cells and coupling through diffusion of a substance X proportional to the respective concentration gradients, $\frac{dX^{(i)}}{dt} = \ldots + c_{ij}\,(X^{(j)} - X^{(i)})$, stability analysis can be simplified by transformation to suitable variables. Thereby the Jacobian is turned into block structure,

$$\left| \begin{array}{cccc} \langle\ldots\rangle^{(1)} & & & \\ & \langle\ldots\rangle^{(2)} & & \\ & & \ddots & \\ & & & \langle\ldots\rangle^{(N)} \end{array} \right|_{(3N\times 3N)} ,$$

where the $\langle\ldots\rangle^{(i)}$ differ from the one cell Jacobian only in that linear combinations of the coupling constants c_{ij} are added in the diagonal. Thus the respective characteristic polynomial is a product of N polynomials of order three. We give an explanation for synchronisation of oscillations when coupling via calcium diffusion and discuss preliminary results of calculations concerning systems of non-identical cells.

Session 2

Metabolic Regulation, Control and Signaling

YEAST GROWTH ON MIXED SUBSTRATES. REPRESSION OR INDUCTION?

Oscar JG Somsen[1,2], *Jacky L Snoep*[1], *and Hans V Westerhoff*[1].

Depts. of Molecular Cell Physiology[1] and Biophysics[2], IMBS, BioCentrum Amsterdam, Free University, De Boelelaan 1087, 1081 HV Amsterdam.

ABSTRACT

The yeast *Saccharomyces cerevisiae* can metabolize both glucose and ethanol. Depending on environmental conditions, it either prefers the glucose or metabolizes the substrates simultaneously. Experimentally it has been established that the metabolism of the organism always follows the strategy that is 'best for the cell'. With a simple simulation, we compare two straightforward biochemical mechanisms that may bring about such relatively intelligent regulation in the living cell. We discuss how this could be investigated in more detail.

INTRODUCTION

Under aerobic conditions the yeast *S. cerevisiae* can grow on glucose as well as ethanol. When both substrates are abundant, glucose is preferred. However, when both substrates are limiting in a chemostat, they are metabolized simultaneously [1]. While this may benefit the cell, it also requires a complex regulation, with two or more distinct strategies. When the ethanol/glucose ratio is low, the ethanol is fed into the TCA cycle, which must be regulated to avoid accumulation. At high ratios, the ethanol is also used to construct building blocks for biosynthesis. For this, a reverse catabolic (glyoxylate- and gluconeogenesis-) pathway is needed. To avoid loss of ATP, the forward and reverse pathways should not be active simultaneously (futile cycling).

A sharp transition between the two strategies has been observed [1], *i.e.* the reverse catabolic enzymes are absent at low ethanol/glucose ratios, and each enzyme is induced only when it is required to sustain the maximal flux of biosynthesis. A possible mechanism for this tight regulation, is repression by glucose, which has indeed been observed [2], but may be restricted to short timescales [3]. On the other hand, the reverse enzymes could be induced by metabolites of the TCA cycle, since these would accumulate in the absence of reverse enzymes.

We present a simple model for growth on mixed substrates, differing from previous models that do not include the reverse pathway [4, and references therein], and study which of the two mechanisms reproduces the observed tight regulation. We discuss how this may be investigated in more detail.

MODEL

Figure 1 shows the simplest model for a yeast cell that metabolizes glucose and ethanol simultaneously. Two metabolites (A and B) represent respectively the (C6 and C3) intermediates of glycolysis and the (C2) intermediates of the TCA cycle. They enter the cell with a fixed flux determined by the chemostat and the total cellular volume. A forward catabolic pathway (J_f) converts A to B, and A and B are used in a fixed ratio for biosynthesis. A reverse pathway is necessary for high J_B/J_A ratios. ATP is not considered separately, but included in A and B as a building block for biosynthesis. Its inhibiting effect on glycolysis is partly represented by product inhibition of the forward pathway. Loss processes are not included either.

The rate (v_f) of the forward catabolic pathway is modeled as a single Michaelis-Menten reaction, which is irreversible, but potentially inhibited by its product:

$$v_f = V_f \frac{A/K_f}{1 + A/K_f + B/L_f}$$

with parameters V_f, K_f and L_f. The reverse pathway is accounted for by an analogous expression, except that V_r is multiplied by a scaling factor E_r to describe the regulation. We include both mechanisms that were proposed in the introduction, by expressing:

$$E_r = \frac{K_{Rep}}{K_{Rep} + A} \frac{B}{K_{Ind} + B}$$

The parameters K_{Rep} and K_{Ind} determine respectively the extent of repression by A, and induction by B. The overall biosynthesis is a complex network of reactions. For our present purposes, however, it can be modeled as a two-substrate reaction, that requires A and B in a fixed ratio, *i.e.* any one of them alone does not suffice. Only the substrate with a low concentration influences the rate (assuming a sequential substrate binding model):

$$v_{bs} = V_{bs} \frac{1}{1 + K_A/A + K_B/B}$$

K_A and K_B are Michaelis-Menten constants for the respective substrates.

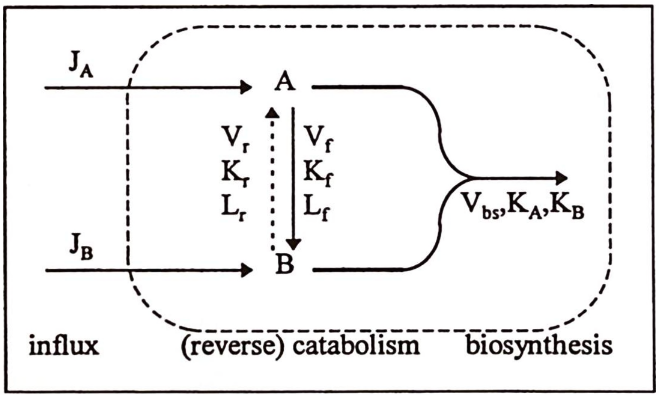

Figure 1. A simple model for simultaneous metabolism of glucose and ethanol in a yeast cell. A and B represent the intermediates of glycolysis and the TCA cycle respectively. The arrow pointing from A to B represents glycolysis, the dashed arrow in the opposite direction the glyoxylate cycle, and gluconeogenesis. Biosynthesis requires both A en B. Influxes occur at a fixed flux, determined by the chemostat.

PARAMETERS

Below, we shall investigate how the steady state of our model depends on the relative magnitudes of J_A and J_B, with $J_A + J_B = 1$. The variables are normalized, *i.e.* scaled to order unity. For accounting purposes, the concentrations and fluxes are measured in the number of carbon atoms ('C-moles').

The forward and reverse catabolic pathways have identical parameters, with intermediate velocity ($V_f = V_r = 1$), and Michaelis-Menten constants ($K_f = K_r = 1$), and weak product inhibition ($L_f = L_r = 10$). For the biosynthesis reaction, the Michaelis-Menten constants must be lower, to avoid strong sensitivity to the substrate concentrations, which may otherwise cause a breakdown of this reaction (results not shown). Thus: $V_{bs} = 2$, and $K_A = K_B = 0.1$. We consider the case where the biosynthesis reaction consumes A and B in equal amounts.

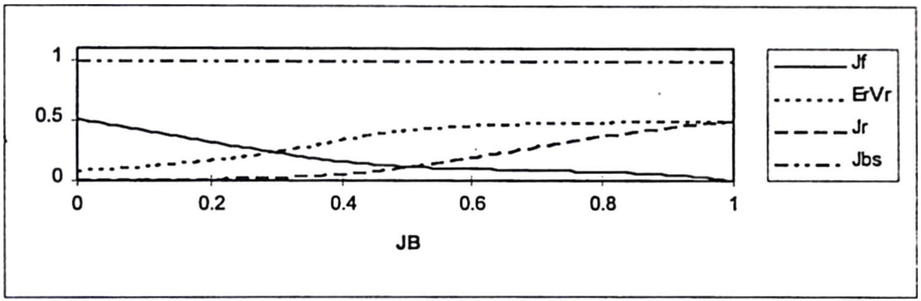

Figure 2. Calculated steady-state fluxes, with strong repression by A: $K_{Rep} = 0.1$ (see text). Other parameters: $V_f = V_r = 1$, $K_f = K_r = 1$, $L_f = L_r = 10$, $V_{bs} = 2$, and $K_A = K_B = 0.1$. $J_A = 1 - J_B$.

SIMULATIONS

First, we consider the case where, the reverse pathway is regulated only through repression by A (induction by B is switched of by setting $K_{Ind} = 0.001$). For a tight regulation, the repression should be strong, *i.e.* K_{Rep} should be low. We use $K_{Rep} = 0.1$.

Figure 2 shows how the metabolite concentrations and fluxes J_f, J_r and J_{bs} (the steady-state values of v_f, v_r and v_{bs}) vary with J_B. The forward catabolic flux is large ($J_f = 0.5$), for growth on substrate A only ($J_B = 0$), but decreases with increasing J_B, because more B enters the cell directly. Near $J_B = 0.5$, the reverse catabolic pathway (J_r) becomes active.

The regulation behaves well in the sense that the maximal flux of biosynthesis (J_{bs}) is maintained through the entire range of J_B. However, some amount of futile cycling (given by the smallest of J_f and J_r) does occur. Indeed, the activity (E_rV_r) of the reverse pathway, does not show the experimentally observed tight regulation, *i.e.* it is already significant for J_B as low as 0.2.

The regulation characteristics can be improved by choosing a stronger repression, *i.e.* a lower K_{Rep}. However, this creates a different problem; Low concentrations of A are then required which lead to a breakdown of the biosynthesis reaction as J_B approaches 1 (not shown). This can only be avoided by changing more parameters.

Figure 3 shows the case where the reverse pathway is regulated only through induction by B (repression by A is switched of by setting $K_{Rep} = 10$). The other parameters are the same as used in figure 2. For a tight regulation, the induction should be weak, *i.e.* K_{Ind} should be high. We use $K_{Ind} = 2$.

The fluxes in figure 3 are qualitatively similar to those in figure 2, *i.e.* J_f decreases with increasing J_B and is replaced by J_r around $J_B = 0.5$. The maximal flux of biosynthesis is again maintained. However, futile cycling is less than in figure 2, and the activity (E_rV_r) of the reverse pathway is in qualitative agreement with the observed tight regulation [1]. It is small for $J_B < 0.5$ and increases linearly with J_B for higher values. The tightness could be further improved by choosing a weaker induction, *i.e.* a higher value for K_{Ind}, but this would lead to an undesirable further accumulation of B.

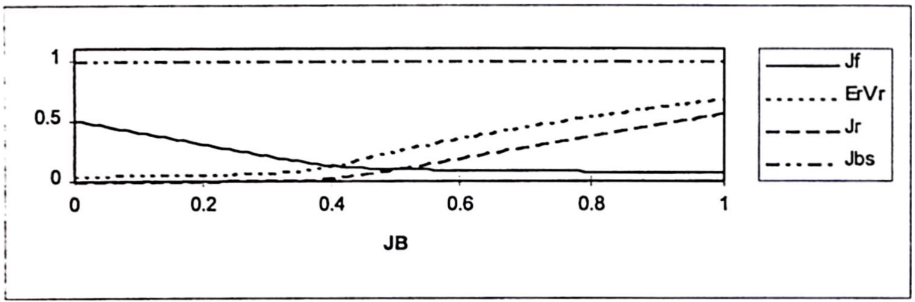

Figure 3. Calculated steady-state fluxes with weak induction by B: $K_{Ind} = 2$ (see text). Other parameters: See figure 2.

DISCUSSION

With a simple model, we studied the simultaneous metabolism of glucose and ethanol by the yeast *S. cerevisiae*. Since the catabolic pathway supplies both the Gibbs energy and the building blocks for biosynthesis, a complex regulation is required with distinct strategies for low and high ethanol/glucose ratios. The latter requires a reverse catabolic pathway to rebuild the larger building blocks. An abrupt transition between these strategies has been observed [1], and seems useful as it prevents futile cycling.

We considered regulation of the reverse pathway, either through strong repression by intermediates of the glycolytic pathway (A), or through weak induction by intermediates of the TCA cycle (B). In both cases, the maximal flux of biosynthesis could be maintained, but the latter case shows less futile cycling, and is in better agreement with the observed abrupt transition. This is related to the fact that the concentration of A decreases gradually as J_B increases, while B accumulates quite suddenly near $J_B = 0.5$, making it a more suitable candidate to reproduce the observed regulation.

A significant role is played, in our present model, by the biosynthesis reaction. For practical reasons, we set its Michaelis constants smaller than those of the forward and reverse catabolic pathways. As a side-effect, the concentration of either A or B is always low. This causes the abruptness of the transition. It also reduces futile cycling, even if both catabolic pathways are constitutively present (not shown), which makes the question, why the reverse pathway is so tightly regulated, even more interesting. To determine, whether these phenomena do indeed occur, it would be useful to measure how the substrate concentrations vary with the ethanol/glucose ratio.

In both our simulations, the induction of the reverse pathway is not as sharp as observed experimentally [1]. This can be improved by further decreasing the Michaelis constants of the biosynthesis reaction or by a more cooperative regulation, as will be discussed in a forthcoming paper.

An interesting phenomenon is, that the net catabolic flux approaches zero at intermediate substrate supply ratios. In *S. cerevisiae*, this could happen for the pyruvate dehydrogenase enzyme. Since the forward catabolic pathway is constitutively present [1], it would be useful to determine whether the flux does indeed vanish, and if so, whether this is due to allosteric regulation or to changing substrate and product concentrations. This has important implications, because the substrate (pyruvate) of this reaction is also a substrate for biosynthesis.

REFERENCES

1. de Jong-Gubbels, P, P vanRolleghem, S Heijnen, JP van Dijken, and JT Pronk. 1995. Regulation of Carbon Metabolism in Chemostat Cultures *of Saccharomyces cerevisiae* Grown on Mixtures of Glucose and Ethanol. *Yeast* 11:407-418.
2. Entian, KD and JA Barnett. 1992. Regulation of sugar utilization by *Saccharomyces cerevisiae*. *TIBS* 17:506-510.
3. Boles, E. 1996. Redundant regulatory mechanisms enable yeast cells without fructose-2,6-bisphosphate to sustain glycolytic flux and to prevent energy-wasting cycling at the phosphofructokinase/fructosebisphosphatase enzyme pair. *In*: BioThermokinetics of the Living Cell (Westerhoff *et al* eds.). BioThermokinetics Press, Amsterdam.
4. Narang, A. 1998. The Steady States of Microbial Growth on Mixtures of Substitutable Substrates in a Chemostat. *J.Theor.Biol.* 190:241-261.

22

CONTROL ANALYSIS OF CELLULAR SIGNAL TRANSDUCTION PATHWAYS.

Boris N. Kholodenko[1], Jan B. Hoek[1], Guy C. Brown[2], Hans V. Westerhoff[3,4]*

[1]Department of Pathology, Anatomy and Cell Biology, Thomas Jefferson University, 1020 Locust St., Philadelphia, PA 19107, USA, [2]Department of Biochemistry, University of Cambridge, Tennis Court Road, Cambridge, UK, [3]Department of Microbial Physiology, Free University, [4]E.C.Slater Institute, Biocentrum, University of Amsterdam, The Netherlands
*Corresponding author, E-mail: kholode1@jeflin.tju.edu, FAX: (1 215) 923-2218

INTRODUCTION

Considerable attention has been focused on molecular mechanisms of signal transduction during the past decade. However, the control of signaling pathways remains poorly understood. We have adapted Metabolic Control Analysis (see [1-4] for reviews) to quantify the signal transfer from a signal molecule to a cellular target. There are several quantitative aspects of signal transduction that are of interest, e.g., A) How does a receptor at the top of a signal transduction cascade control the activation state of the target at the bottom of a cascade? B) How does the response of a single cascade level to the immediately preceding level depend on the kinetics of the components involved? C) How do the control properties depend on the kinetic properties of each signaling level and the pathway structure, e.g., on branches and feedback regulatory loops between various levels of a cascade?

RESULTS AND DISCUSSION

A signal transduction pathway can be considered as a cascade of reaction modules, or cycles. Usually, each module consists of two or more interconvertable forms of a signaling intermediate (e.g., a phosphorylated and dephosphorylated protein), and one (or more) of these forms affects the next level down the cascade (Fig.1).

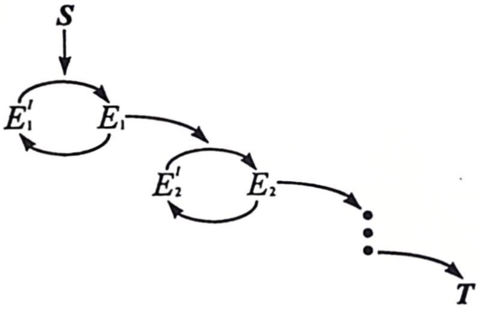

Figure 1. A scheme of a linear signal transduction pathway. At each cascade level only two interconvertable forms are shown. Superscript I denotes inactive forms, e.g., E^I_1 and E_1 stand for inactive and active receptor, respectively. The active form (E_i) at each level affects the activating and/or inactivating conversion at the subsequent level (i+1).

The control of the steady-state signal transfer from a signal (S) to a target (T) is quantified as the steady-state fractional change in the activated target divided by the fractional change in the signal (in the limit of infinitesimally small changes):

$$R_S^T = \lim_{\Delta S \to 0}\left(\left(\Delta T/T\right)/\left(\Delta S/S\right)\right) = d \ln T / d \ln S \qquad (1)$$

R is the sensitivity of the target to the signal, known as the response coefficient in Metabolic Control Analysis. The signal may be a hormone, growth factor, cytokine or neurotransmitter, and the cellular target may be a channel conductivity, rate of transcription or phosphorylation state of some protein at the other end of the pathway.

When a single cascade module is considered "in isolation" from the entire pathway, the response of a signaling protein at this module (E_i) to the immediately preceding module (E_{i-1}) is quantified as the *local* response coefficient:

$$r_{i-1}^{i} = d \ln E_i / d \ln E_{i-1} \mid_{E_j = const} \qquad (2)$$

The local response coefficient ($r^{i}{}_{i-1}$) quantifies the relative amplification or suppression of a signal at the module i of the cascade (when the activities of signaling intermediates at any other levels (E_j) are kept constant).

Linear pathways

For a linear cascade without branches and feedback loops (Fig. 1), the response coefficient (i.e., the overall sensitivity) of a cascade is equal to the PRODUCT of the local responses at each level of cascade [5,6]):

$$R_S^T = r_S^1 \cdot r_1^2 \cdot \ldots \cdot r_{n-1}^T = \prod (\text{path}) \qquad (3)$$

Branched pathways

If the signal and target are linked by more than one independent pathway (e.g., the signal has multiple receptors each with a different signal transduction pathway), then the total response is given by the sum of the products of local responses over each pathway [6]:

$$R_S^T = \prod (\text{path I}) + \prod (\text{path II}) \qquad (4)$$

Thus, the extent to which a signal controls a target through different pathways can be quantified and compared.

If two signals, S_1 and S_2, affect T through two different routes, which may converge at a common intermediate X and then have a common part from X to T, the total response of the target to simultaneous changes in both signals, $\Delta S_2/S_2 = \alpha \cdot \Delta S_1/S_1$, is given by:

$$R_{12}^T = R_{S_1}^T + \alpha R_{S_2}^T = \left(\prod (\text{path S}_1 \text{ to } X) + \alpha \prod (\text{path S}_2 \text{ to } X)\right) \cdot \prod (\text{path } X \text{ to } T) \qquad (5)$$

How does the local response depend on the kinetics of a particular level

We shall consider a simple kinase/phosphatase cycle (i), where the active form of a signaling molecule is phosphorylated form (E_i) and the inactive form is dephosphorylated form (E^I_i). The local response coefficient, r^i_{i-1}, of cycle (i) to the preceding cycle (i-1) is expressed through the elasticities of the kinase (κ) and the phosphatase (ρ) with respect to the E^I_i and E_i. If only the rate of the activation conversion is affected by E_{i-1}, and E_{i-1} is the kinase, then [7]:

$$r^i_{i-1} = 1/\left(\rho_{E_i} + \left(E_i/E^I_i\right)\cdot\kappa_{E^I_i}\right) \quad (6)$$

If only the rate v_{Ii} of the inactivation conversion is affected by E_{i-1}, so that E_{i-1} is the phosphatase, then the local response coefficient, r^i_{i-1}, has the opposite (negative) sign. Eq. 3 shows that the total response of the target to the signal is positive, if the number of cascade levels with negative local responses is even.

When both protein kinase and phosphatase follow Michaelis-Menten kinetics and are far from equilibrium, the magnitudes of the elasticities, κ and ρ are between 1 and 0 (see, e.g. [8]):

$$\kappa_{E^I_i} = 1/\left(1 + E^I_i/K_{mK}\right); \qquad \rho_{E_i} = 1/\left(1 + E_i/K_{mP}\right)$$

Here K_{mK} and K_{mP} are the Michaelis constants of the protein kinase and phosphatase. If at any level both protein kinase and phosphatase are saturated with E^I_i and E_i , so their elasticities κ and ρ are low, the local response r^i_{i-1} at this level, is high. For a monocyclic cascade this phenomenon is known as "zero-order ultrasensitivity" [9,10]. In general, when the total concentration of interconvertable enzyme is more than twice the affinities of the inactive and active forms for the catalysts, the dependence of the local response on the activity (E_{i-1}) of the preceding level follows a bell-shaped curve [6].

In a signal transduction pathway some cascade levels may include more than two interconvertable forms of a single molecule, e.g., sequential binding of multiple adapter proteins and/or phosphorylation at multiple residues. In this case, the local responses (r^i_{i-1}) will differ from those given by Eq. 6. However, for any kinetic scheme of the transformations at a particular level, these responses can be obtained using methods developed in [8,11]. Importantly, the general equations above, which relate the total response of a target(s) to the pathway structure and local responses at each module do not change. As an illustration, we consider a cycle of three interconvertable forms of a signaling protein (E_i): inactive dephosphorylated (I) and singly phosphorylated (P) forms and an active doubly phosphorylated (E) form (Fig. 2):

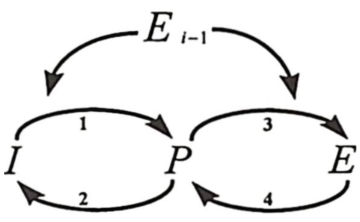

Figure 2. A double phosphorylation cycle. The active form, E_{i-1}, of a protein of the preceding cycle (i-1) is the kinase, that phosphorylates inactive forms, I and P, at the module i. E is the active, doubly phosphorylated form of a signaling protein of the module i. The numbering of the reactions of the module i is indicated.

Such cycles occur, for instance, in the mitogen activated protein kinase (MAPK) cascades. MAPK kinase kinase (MAPKKK) activates MAPK kinase (MAPKK) by phosphorylation at two serine residues. Doubly phosphorylated MAPKK-PP activates MAPK by phosphorylation at threonine and tyrosine residues. Therefore, both MAPKK and MAPK cycles consist of three interconvertable forms of these proteins. Assuming, that the cycle rates, v_1, v_2, v_3, v_4 (Fig.2), do not depend explicitly on their products, and the protein of the preceding level (E_{i-1}) catalyzes the activation conversions v_1 and v_3, and does not influence v_2 and v_4, the local response (r^i_{i-1}) of this cycle (i) to the cycle (i-1) is given by:

$$r^{i}_{i-1} = (I\cdot(\kappa^{3}_{P}+\rho^{2}_{P})+P\cdot\kappa^{1}_{I})\Big/\left(I\cdot\rho^{2}_{P}\cdot\rho^{4}_{E}+P\cdot\kappa^{1}_{I}\cdot\rho^{4}_{E}+E\cdot\kappa^{1}_{I}\cdot\kappa^{3}_{P}\right) \tag{7}$$

Here κ and ρ denote the elasticities of the activating (kinase) and the inhibiting (phosphatase) reactions of the module i, respectively.

Using Eq.7 one can show that for a three-form cycle, the dependence of the local response on the signal is a bell-shaped curve, provided the concentrations of interconvertable forms exceed the corresponding affinities for the kinases and phosphatases. In contrast to the two-form cycle, the local response of the three-form cycle is around 2 and not near 1, when the signal is low (i.e., when I is the prevailing form and P and E are very low). Therefore, for a three-form cycle the output-input relation (i.e., the dependence of E on E_{i-1}) is more sigmoidal at low signals than for a two-form cycle.

In a recent simulation of the steady-state kinetics and behavior of the MAPK cascade by Huang and Ferrell [12], the total MAPKKK concentration varied from 0.6 nM to 15 nM, whereas the K 's for the kinase and phosphatase varied from 60 to 1500 nM. For this range of parameters Eq.6 shows that the local response of the first (MAPKKK) level is always less than 1, decreasing from 1 to 0 with increase in the signal. In other words, the MAPKKK cycle responds to the signal like a Michaelian enzyme. At the second and third levels of MAPKK and MAPK interconversions, the total MAPKK and total MAPK concentrations varied from 240 nM to 6000 nM, whereas the K 's for the kinases and phosphatases varied from 60 to 1500 nM. Eq.7

shows that the local responses of MAPKK and MAPK cycles to the active MAPKKK and MAPKK, respectively, should vary with the signal as bell-shaped curves, assuming maximal values of more than 2 (depending on the total concentrations and K_m values selected). Importantly, Huang and Ferrel [12] found a successive increase in the steepness of the plots of activated MAPK cascade components at successively lower levels of the cascade. This is explained by our result that the total sensitivity of the cascade equals the product of the local sensitivities at each level (cf. [13, 14]).

Pathways with feedback.

We shall now describe the dependence of the overall response on the local responses for pathways with feedback loops. For any particular mechanism of the target influence on the receptor, the feedback can be described in terms of the local response (r_T^1) as follows:

$$r_T^1 = d\ln E_1 / d\ln T|_{E_f = const}$$

In the case of activation of the receptor, r_T^1 is positive, and r_T^1 is negative in the case of inhibition.

Feedback changes drastically the total response of a target to a signal. For a linear cascade that feeds back on itself, the total response to a signal is given by [6]:

$$R_S^T = \Pi(\text{path}) / \left(1 - \left(r_T^1 / r_S^1\right) \cdot \Pi(\text{path})\right) \qquad (8)$$

As expected, a positive feedback amplifies the control exerted by a receptor on a target and a negative feedback decreases the control.

In the absence of feedback different pathway branches add independently to the total response. Feedback loops change this simple picture. If a signal has two receptors each with a different signal transduction pathway to one target, which feeds back on one or both receptors, then the total response to the signal is given by [6]:

$$R_S^T = \frac{\Pi(\text{path I}) + \Pi(\text{path II})}{1 - \left(r_T^1(\text{I}) / r_S^1(\text{I})\right)\Pi(\text{path I}) - \left(r_T^1(\text{II}) / r_S^1(\text{II})\right)\Pi(\text{path II})} \qquad (9)$$

This equation shows that even when only one pathway has a feedback (e.g. r_T^1(II)=0), these two pathways no longer add independently to the total response. Signal transduction by the two pathways is integrated by the feedback.

Theories of information transfer (such as information theory) have been developed previously for the analysis of the transfer of digital information, and thus are not appropriate for signal transduction pathways in living cells. The theory outlined here, which we call Signal Transfer Analysis, is similar to the Modular Control Analysis, but aimed explicitly at an analysis of the transfer of analogue information within and between cells.

ACKNOWLEDGMENT.

We acknowledge NIH grants AA11689, AA07186, AA07215 and NWO for the support of this work.

REFERENCES

1. Fell, D.A. (1992) Biochem. J. 286, 313-330.
2. Kholodenko, B.N. and Westerhoff, H.V. (1995) Trends Biochem. Sci., 20, 52-54.
3. Brand, M.D. (1996) J. theor. Biol. 182, 351-360.
4. Brown, G.C., Westerhoff, H.V. and Kholodenko, B.N. (1996) J. theor. Biol. 182, 389-396.
5. Kahn, D and Westerhoff, H.V. (1991) J. theor. Biol., 153, 255-285.
6. Kholodenko, B.N., Westerhoff, H.V. Brown, G.C. (1997) FEBS Lett. 414, 430-434.
7. Small, J.R. and Fell, D.A. (1990) Eur. J. Biochem. 191, 405-411.
8. Kholodenko, B.N. (1988) Molec. Biol. (USSR) 22, 1238-1256 (Engl. transl. 22 (1989) 990-1005).
9. Goldbeter, A. and Koshland, D.E., Jr. (1981) Proc. Natl. Acad. Sci. USA, 78, 6840-6844.
10. Koshland, D.E., Jr., Goldbeter, A. and Stock, J.B. (1982) Science, 217, 220-225.
11. Kholodenko, B.N. (1988) FEBS Lett. 232, 383-386.
12. Huang, C.-Y. F. and Ferrell, J.E., Jr. (1996) Proc. Natl. Acad. Sci. USA, 93, 10078-10083.
13. Ferrel, J. E. (1997) Trends Biochem. Sci. 22, 288 – 299.
14. Brown, G. C., Hoek, J.B. & Kholodenko, B. N. (1997) Trends Biochem. Sci,. 22, 288.

METABOLIC DESIGN: ENGINEERING A LIVING CELL TO DESIRED METABOLITE CONCENTRATIONS AND FLUXES.

Boris N. Kholodenko[1,2], *Jan B. Hoek*[1], *Hans V. Westerhoff*[2], *Marta Cascante*[3], *Jim Schwaber*[4]

[1]Department of Pathology, Anatomy and Cell Biology, Thomas Jefferson University, 1020 Locust St., Philadelphia, PA 19107, USA, [2]Departments of Microbial Physiology and Mathematical Biochemistry, BioCentrum, Amsterdam, The Netherlands, [3]Department de Bioquimica i Biologia Molecular, Universitat de Barcelona, Marti i Franques 1, Barcelona, Spain, Central Research Department, [4]DuPont Experimental Station, Delaware, USA.
Corresponding author. E-mail: kholode1@jeflin.tju.edu, FAX: 1 215 923 22 18.

INTRODUCTION

The power of molecular genetics makes it possible to modulate the concentrations of selected enzymes in a cell, that potentially, allows one to design the metabolism of an organism. Yet, to the extent to which the biotechnology has been successful, it has used various qualitative and ad hoc rules to enhance specific product yield [1]. A "universal method" to increase a desired flux in a pathway without changing any of the intermediate concentrations has been devised by Kacser and Acerenza [2]. However, often the aim of metabolic engineering is to increase the concentrations of particular compounds, rather than a flux through a pathway. It would also be useful if one could design alternative ways to increase the flux, perhaps allowing some but not all of the metabolite concentrations to change (the viability of an organism strongly requires certain key metabolite concentrations to be maintained within narrow limits). Based on rate equations, Small and Kacser [3] devised a method for increasing the concentration of a metabolite, while leaving other metabolites and the reaction rates unperturbed. However, this method cannot be applied if one wishes to increase a flux also, or in case when some concentrations are constrained by moiety conservation (such as in coenzyme and substrate cycles). For the case of (infinitesimally) small changes, Westerhoff and Kell [4] elaborated a solution, but because the required changes in the enzyme activities were expressed via the control coefficients, predictions about what will happen during large modulations of the cell enzymes are limited. Apart from these restrictions, the existing methods fail to indicate that certain, potentially valuable changes in flux distributions and intermediate concentrations cannot be achieved, due to limitations caused by the pathway structure or kinetics. The "universal method" by Acerenza and Kacser [2], and the engineering of metabolite concentrations by Small and Kacser [3] and by Westerhoff and Kell [4] are both special cases of the so-called perturbation method applied to metabolic networks [5,6]. Here we will apply this perturbation method to show how one can modulate the enzyme concentrations so as to obtain any predefined change in metabolic fluxes and concentrations that is compatible with maintenance of a steady state.

METABOLIC DESIGN ANALYSIS.

We consider an arbitrary metabolic pathway including m metabolite concentrations (x_i) which are determined by the rates (v_j) of n enzyme reactions:

$$dx_i/dt = \sum_{j=1}^{n} N_{ij} v_j \qquad i = 1, \ldots, m \qquad (1)$$

N_{ij} is the stoichiometric coefficient of x_i in the jth reaction. We assume that any reaction rate (v_j) is proportional to the concentration (e_j) of the enzyme that catalyzes it:

$$v_j = e_j \omega_j(x) \qquad (2)$$

where ω_j is the function of metabolite concentrations ($\mathbf{x} = x_1, \ldots, x_m$) that defines the specific rate (i.e., the rate per unit of enzyme concentration). Note, that the specific rate differs from the turnover number, which stands for the maximum rate per unit of enzyme concentration at saturating concentrations of substrate(s) and zero product concentrations. At steady states, the reaction rate, v_j, will be referred to as the flux, J_i, through the ith reaction,

$$v_i^{st.st.} = J_i \qquad (3)$$

Perturbation method.

Let us assume that a metabolic network under consideration is in a steady state characterized by metabolite concentrations x_i and fluxes J_i. The question we wish to address is which perturbation in parameters, e.g. enzyme activities, will bring the system to a new steady state with the reaction rates J_i shifted by ΔJ_i and metabolite concentrations x_i shifted by Δx_i . Importantly, we do not assume the changes to be small, usually the desired change is large. We first note that, large or small, the changes in metabolic fluxes (ΔJ_i) and concentrations (Δx_i) cannot be arbitrary. The requirement that the cells remain at steady state imposes restrictions on the reaction rates, hence restrictions on ΔJ_i , caused by the structure of the metabolic network (i.e., the stoichiometries of reactions). For example, in a linear pathway of sequential reactions all ΔJ_i must be equal, since all the reactions must have the same rate at steady state. In general, the changes ΔJ_i in the steady-state reaction rates should satisfy the following restrictions (see Eq.1):

$$\sum^{n} N_{ij} \Delta J_j = 0 \qquad i = 1, \ldots, m \qquad (4)$$

A general recipe to obtain all changes ΔJ_i, that satisfy Eq. 4 is simple. For any pathway branch or cycle the rate changes should be equal, and they should satisfy Kirchhoff's law at all branch points.

In most metabolic networks the changes in the concentrations of some intermediates are constrained by moiety conservation. For instance, in energy metabolism, the intermediate forms that shuttle free-energy equivalents (such as ATP, ADP and AMP, or creatine and phosphocreatine) sum to the conserved total concentrations (adenine nucleotides and total creatine, respectively). A cycle of interconversions between the different forms of the same chemical moiety is termed a moiety-conserved cycle. The requested changes (Δx_i) in the concentrations of intermediates should not violate moiety conservation relations. Therefore, (Δx_i) are to satisfy the following restrictions:

$$\sum_{k=1}^{m} \gamma_{ik} \Delta x_k = 0 \qquad i = 1, \ldots, m-r \qquad (5)$$

where, γ_{ik} is the stoichiometric coefficient of metabolite x_i in the ith moiety conserved sum, r is the rank of the stoichiometry matrix (**N**) of the pathway. In most cases, γ_{ik} can be interpreted as the number of moieties of type i in the molecule of metabolite x_i. Using the matrix **N**, existing software calculates the coefficients γ_{ik} for any metabolic network [7].

How to bring about the desired sustainable changes.

Now we shall determine which changes in enzyme concentrations will provide the desired changes in metabolite concentrations and reaction rates. The molecular biologist may primarily manipulate the concentration of pathway enzymes with the intention of influencing flux through the pathway and the concentration of intermediates. However, to prove our approach it is more convenient to begin by treating formally the enzyme concentrations (e_i) as the dependent (slave) variables and the metabolic fluxes and concentrations as independent (i.e., modulated) variables. Subsequently, we shall deduce the implications for the required modulation of enzyme concentrations in the biotechnological context. From Eq.2 it follows:

$$J_i + \Delta J_i = (e_i + \Delta e_i)\omega_i(x + \Delta x) = e_i\omega_i(x) + \Delta J_i \qquad (6)$$

where $\omega_i(x+\Delta x)$ is the specific rate of the i-th reaction at the desired concentrations $x+\Delta x$ of the metabolites, and ΔJ_i is the desired change in the flux. Using Eqs.6 and 2, the required changes in the enzyme concentrations can be presented as:

$$\Delta e_i / e_i = (1 + \Delta J_i / J_i)[\omega_i(x) / \omega_i(x + \Delta x)] - 1 \qquad i = 1, \ldots, n \qquad (7)$$

Eq.7 gives us the answer, we were looking for: for each enzyme it determines the modulation of its concentration which brings about the desired change in metabolic pattern. To calculate the required changes Δe_i, one first needs to evaluate how the desired changes (Δx) in metabolite levels would affect the reaction rates if the enzyme concentrations were not changed. In Eq.7 this is written as $\omega_i(x)/\omega_i(x+\Delta x)$ for each reaction (i). This ratio can be measured in crude extracts as the ratio of the reaction rates at the original and desired levels of metabolite concentrations in the wild type cell. In vivo the same ratio can be measured by manipulating branch pathways, or enzyme activities around the enzyme of interest such that the metabolite concentrations that affect the enzyme are changed from x to $x+\Delta x$. The ratio $\omega_i(x)/\omega_i(x+\Delta x)$ is then multiplied by the new desired reaction rate divided by the original rate. Subtraction of 1 then leads to the required relative change ($\Delta e_i/e_i$) in the concentration of enzyme i. For this procedure the reaction kinetics of the enzymes does not need to be known (see also modular/top down approach below). Alternatively, the ratio $\omega_i(x)/\omega_i(x+\Delta x)$ can be obtained from the enzyme rate equations. In this case the kinetics need to be known, but only to the limited extent of predicting the change in the rate for the desired change in metabolite concentrations. If the desired changes in metabolite concentrations do not involve the substrates, products or effectors of a particular enzyme, no kinetic information regarding that enzyme is required.

Eq.7 implies another limitation on possible changes (Δx). Since $e_i + \Delta e_i$ has to be positive, the desired changes in the intermediate concentrations and fluxes are restricted by the following inequalities:

$$(J_i + \Delta J_i) / \omega_i(x + \Delta x) > 0, \qquad i = 1,...,n \qquad (8)$$

To insure that the fluxes in a metabolic network do not change their direction, one should not increase the product and/or decrease the substrate concentrations of a reaction to the extent at which the mass-action ratio exceeds the equilibrium constant (which would be equivalent to a reversal in the flux) [3].

"Top down "/modular versus"bottom-up"approach.

To understand how a large number of interrelated biochemical processes can be regulated coordinately, it helps to analyze them in terms of subsystems or modules of cell metabolism. Such an analysis, referred to as modular or "top-down" approach overcomes the experimental limitations of "bottom-up" analysis (which requires kinetic studies of any pathway reaction) by grouping reactions into a few large integrated subsystems interacting through a small number of intermediates (see., e.g. [8-10]). For instance, to solve the problem of increasing the concentration of some amino acid one can conceptually divide an entire metabolic network into supply and demand blocks communicating via that amino acid, provided there are no other interactions between these blocks, or such interactions can be neglected. In some cases it is convenient to consider several supply and demand blocks, e.g., free amino acid is incorporated into newly synthesized proteins, it can be a precursor for the synthesis of some other amino acids or cofactors, etc. One can view the whole group of reactions in such a block as a single overall reaction and, hence, analyze a simpler system (consisting of a few overall reactions) than the original metabolic network. To increase the concentration of the amino acid of interest one can apply the strategy described above to this simpler system. However, this strategy requires the knowledge of the phenomenological kinetics of the overall reactions, i.e., the dependencies of the steady-state rates on the concentration of the amino acid. These dependencies have to be measured experimentally. Perturbing a single block by adding specific inhibitors or activators acting within that block, or changing the concentration of initial substrates of that block, one can measure the fluxes through other blocks at different concentrations of the amino acid of interest. Implementing these experimentally obtained dependencies into Eq. 7, one arrives at the fractional changes in the required overall maximal activities of the blocks (corresponding to proportional changes in the concentrations of all the enzymes within the block), which have to be made to get a desired increase in the concentration of interest.

DISCUSSION

In this paper we have shown that, in principle, it is possible to calculate the required changes in enzyme activities (with respect to a wild type cell) that bring about a desired pattern of steady-state metabolite concentrations and fluxes. Importantly, we specified the restrictions, which are imposed on an otherwise arbitrary choice of a desired metabolic pattern. The possibility to solve the problem is due to the fact that only n-r fluxes and r concentrations (i.e., in sum n values) out of the total number of n+m values for metabolite concentrations and fluxes can be chosen arbitrarily and there are n different enzymes catalyzing n network reactions. The simplicity of the solution obtained (Eq. 7) is related to the assumed proportionality of the reaction rates with respect to the enzyme concentrations.

The method developed here is more general than the earlier approaches [2,3] in that it is not limited to an increase in a flux at constant concentrations of all metabolites, or to a change in the concentration of a metabolite at constant fluxes. It also clarifies which changes cannot be obtained without changing the network structure. In the present method of designing the metabolism, one may specify an increase in a flux, an increase in one metabolite, a decrease in a second and constant magnitudes for all others. The required changes in enzyme concentrations are then calculated readily.

ACKNOWLEDGEMENT

We acknowledge NIH grant AA11689 and the Netherlands organization for Scientific Research (NWO) for the support of this work.

REFERENCES

1. Cornish-Bowden, A. 1995. In: G. Reed and T.W. Nagodawithana (vol. eds.). Biotechnology, v.XVI, pp.121-136.
2. Kacser, H., Acerenza, L. (1993) Eur. J. Biochem. 216, 361-367.
3. Small, R., Kacser, H. 1994. Europ. J. Biochem. 226:649-656.
4. Westerhoff, H.V., Kell, D. B. 1996. J. theor. Biol., 182:411-420.
5. Kholodenko, B.N. 1988. Molec. Biol. (USSR) 22:1238-1256 (Engl. transl. 22:990-1005).
6. Kholodenko B.N. 1990/1991. J. Nonlinear Biology, 1, 107-126.
7. Sauro, H.M. 1993. Computer Appl. Biosci. 9:441-450.
8. Brand, M.D. 1996. J. theor. Biol. 182:351-360.
9. Quant, P. A. 1993. Trends Biochem. Sci., 18:26-30.
10. Schuster, S., Kahn, D., Westerhoff, H.V. 1993. Biophys. Chem. 48, 1-17.

24

CPT I: A REASSESSMENT OF ITS ROLE IN CONTROL OVER KETOGENIC FLUX

Karen J NEW*, Simon EATON*, Keith R F ELLIOTT# and Patti A QUANT*

*Unit of Paediatric Surgery, Institute of Child Health and Great Ormond Street Hospital for Children NHS Trust, University College London Medical School, 30 Guilford Street, London WC1N 1EH, UK (Tel:0171-242-9789) and#School of Biological Sciences, University of Manchester, Stopford Building, Oxford Road, Manchester M13 9PT, UK
knew@ich.ucl.ac.uk, seaton@ich.ucl.ac.uk, pquant@ich.ucl.ac.uk, keith.elliott@man.ac.uk

INTRODUCTION

The aim of this study was to reassess the role of mitochondrial outer membrane carnitine palmitoyltransferase (CPT I) in control of hepatic ketogenesis in neonatal rat pups. Recent theoretical advances [1] and experimental work [2-3] have suggested that the traditional view, where CPT I has been considered the 'rate-limiting' step of ketogenesis [4], may no longer be valid. Here, we question whether CPT I should even be considered to be 'rate-controlling' over this pathway. Since our aim was to assess how much control CPT I exerts *in vivo,* rather than using isolated mitochondria, where we would need to make assumptions regarding the concentration of various effectors, our system consists of isolated hepatocytes, which are a complex, more 'physiological' system. In the preliminary series of experiments presented here, we have used metabolic control analysis to determine flux control coefficients for CPT I over ketogenesis from a variety of substrates: a long-chain fatty acid, palmitate; a medium-chain fatty acid, octanoate and a more 'physiological mix' consisting of 60% palmitate and 40% octanoate (the proportions of long:medium chain fatty acids found in maternal rat milk [5]). We independently manipulated CPT I using a range of etomoxir concentrations, which are converted *in situ* to etomoxir-CoA (a specific inhibitor of mitochondrial CPT I [6]).

METHODS

We prepared hepatocytes from Wistar rat pups (11-13d), which had been with their mothers and allowed to suckle *ad libitum* [7]. Cells were incubated in 25ml conical flasks at a density of approximately 3 x 10^6 cells in total volume of 3ml KRB. Flasks were gassed with 95%O$_2$:5%CO$_2$ and incubated for 30min at 37°C in a reciprocating water bath. Appropriate concentrations of etomoxir (0µM-100µM) were added to flasks. After 10min, for the single substrate experiments, either 1ml (2mM, 0.4µCi [1-^{14}C]palmitate in KRB, 2% BSA) or 1ml (8mM, 0.8µCi [1-^{14}C]octanoate in KRB, 2% BSA) was added to the flasks. For the 'mixed fat' experiments: 1ml (2mM, 0.4µCi [1-^{14}C]palmitate and 1.32mM octanoate in KRB, 2% BSA); 1ml (2mM palmitate and 1.32mM 0.8µCi [1-^{14}C]octanoate in KRB, 2% BSA) or 1ml (2mM 0.8µCi [1-^{14}C]palmitate, 1.32mM 0.4µCi [1-^{14}C]octanoate in KRB, 2% BSA) was added to the flasks. The flasks were regassed, resealed and the incubation continued for 60min. Reactions were terminated by the addition of 400µl of 20% perchloric acid to the incubation medium, via a syringe needle. Where [1-^{14}C]palmitate was used in the experiment (either alone or with unlabelled octanoate) the acidified incubation medium was centrifuged 0.4ml supernatant was used directly for assaying ketone body production (^{14}C-KB). Where [1-^{14}C]octanoate was used in the experiment (either alone or as part of a 'mixed fat' experiment) 1.5ml supernatant was added to 4.5ml heptane, vortexed and centrifuged to separate the layers. The upper heptane layer was discarded and a further 4ml heptane added to the tubes. After repeating this washing procedure 3 times, 1ml of the aqueous layer was used for assaying ketone body production. Data from the three sets of 'mixed fat' experiments were pooled as there was no significant difference in flux in experiments where one or both substrates were labelled. Duplicate sets of incubations containing no radiolabel were performed to measure the effects of increasing etomoxir concentration on CPT I activity in each cell preparation. These cells were pre-incubated with the appropriate fatty acid substrate(s) and exposed to etomoxir as described previously. Cells were then permeabilised by the addition of 1ml of digitonin in KRP and after 10s the suspension was diluted with ice cold KCl buffer and centrifuged. The permeabilized cells were collected as a pellet and resuspended in KCl medium. This suspension was used to measure CPT I activity using ^{3}H-carnitine and palmitoyl-CoA, in the presence of 1% BSA, and the amount of butanol-extractable ^{3}H-palmitoyl carnitine measured [8]. Etomoxir-CoA is formed and bound to CPT I during the preincubation and free etomoxir is lost during the permeablisation; therefore the CPT I activity measurements reflect binding of etomoxir-CoA to CPT I during the preincubation [9].

We calculated flux control coefficients for CPT I with respect to ketogenesis using data from the graphs in Figure 1, Equation 1 and the SIMFIT package [10] to apply tangents (at zero inhibitor) to the best-fit lines and to estimate errors on the flux control coefficients.

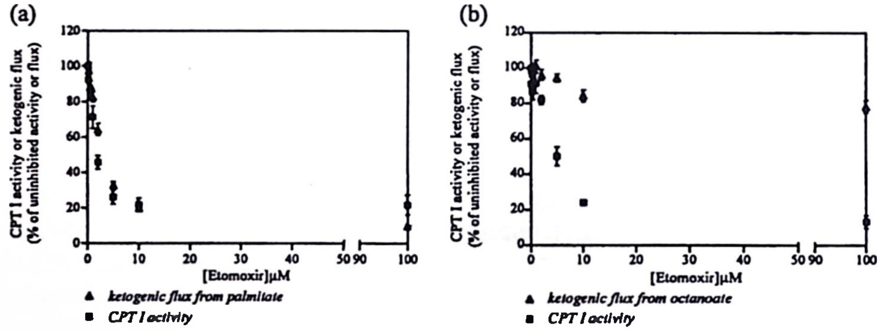

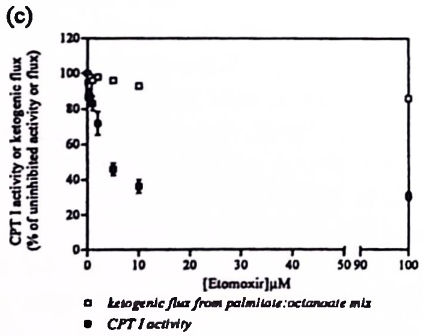

Figure 1 Inhibition of CPT I activity and ketogenic flux Values were normalised b expressing them as a percentage of those obtained i the absence of etomoxir. Errors expressed as SEM (a)palmitate: ketogenic flux (157+28nmol ketone bodies produced h^{-1} (10^{6}cells)$^{-1}$ n=28) and CPT I activity (142+18nmol h^{-1} (10^{6}cells)$^{-1}$ n=12) (b)octanoate: ketogenic flux (303+47nmol keton bodies produced h^{-1}(10^{6}cells)$^{-1}$ n=12) and CPT I activity (134+22nmol h^{-1} (10^{6}cells)$^{-1}$ n=12) (c)mix: ketogenic flux (86.63nmol ketone bodies produce h^{-1}(10^{6}cells)$^{-1}$ n= 27) and CPT I activity (105±4nmol h^{-1}(10^{6}cells)$^{-1}$ n=6)

EQUATION 1:

$$C^{J_{KB}}_{CPTI} = \left. \frac{\delta J_{KB}}{J_{KB}} \middle/ \frac{\delta vCPTI}{vCPTI} \right. (i = 0)$$

RESULTS AND DISCUSSION

Whilst metabolic control analyses have often supported intuitive assumptions, here, results from our analyses suggest that the widely-held view of CPT I as a rate-controlling enzyme over neonatal ketogenesis may be invalid.

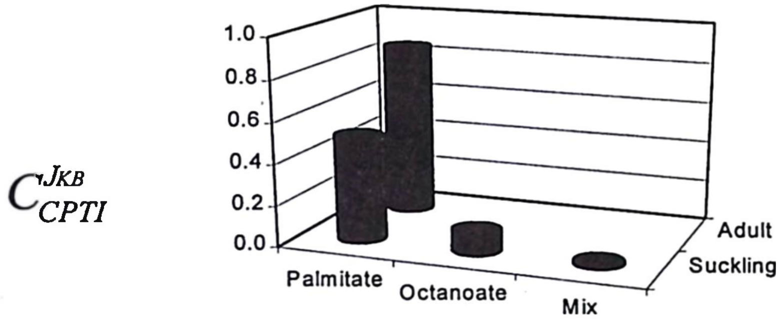

Figure 2 **Comparison of numerical values for** $C^{J_{KB}}_{CPTI}$ Adult data from *Drynan et al* [8]. Errors have been omitted for clarity but are detailed in text

We have previously shown [11] that whilst the control exerted by CPT I is lower in suckling rats than in adults ($_{palmitate}C^{J_{KB}}_{CPTI}$=0.85±0.2 (adults) [8], $_{palmitate}C^{J_{KB}}_{CPTI}$=0.55±0.03 (suckling rats) (Figure 2)), it still exerts significant control and although these results suggest that it is no longer appropriate to consider CPT I to be 'rate-limiting' under these conditions, it may be considered to be 'rate-controlling' [11,12]. However, the preliminary results from the more 'physiological' suckling system presented here ($_{mix}C^{J_{KB}}_{CPTI}$=0.02±0.00 (Figure 2)), suggest that CPT I cannot be considered to be 'rate-controlling' at this stage of development, in this system. Furthermore, these results suggest that the *in vivo* control exerted by CPT I over neonatal hepatic ketogenesis may be trivial.

REFERENCES

1. Mazat, J., Reder, C. and Letellier, T. (1996) J. Theor. Biol. 182 253-258
2. Krauss, S., Lascelles, C.V., Zammit, V.A. and Quant, P.A. (1996) Biochem. J. 319 427-433
3. Krauss, S. and Quant, P.A. (1996) J. Theor. Biol. 182 381-388
4. McGarry, J.D. and Foster, D.W. (1980) Annu. Rev. Biochem. 49 395-420
5. Girard, J., Ferré, P., Pégorier, J. and Duée, P. (1992) Physiol. Rev. 72 507-562
6. Declercq, P.E., Falck, J.R. Kuwajima, M. Tyminski, H., Foster D.W. and McGarry J.D. (1987) J. Biol. Chem. 262 9812-9821
7. Lorenzo, M., Roncero, C. and Benito, M. (1986) Biochem. J. 239 135-139
8. Drynan, L., Quant, P.A. and Zammit, V.A. (1996) Biochem. J. 317 791-795
9. Zammit, V.A. and Boon, M.R. (1988) Biochem. J. 249 645-652
9. Bardsley, W.G. and Prasad, N. (1997) Computers Chem. 21 71-82

10. New, K.J., Elliott, K.R.F. and Quant, P.A. (1997) Biochem. Soc. Trans. 25 418S
11. Fell, D.A. and Thomas, S. (1995) Biochem. J. 311 35-39

Abbreviations: BSA, bovine serum albumin; CPT I, mitochondrial outer membrane carnitine palmitoyltransferase; KB, ketone bodies; KRB, Krebs ringer bicarbonate; KRP, Krebs ringer phosphate

GROWTH OF ESCHERICHIA COLI ON C4-DICARBOXYLATES IS SIGNIFICANTLY CONTROLLED BY THE C4-DICARBOXYLATE TRANSPORTER

Fred C. Boogerd[1]*, *Lars Boe*[2]†, *Ole Michelsen*[2] *and Peter Ruhdal Jensen*[2]#

[1] Institute for Molecular Biological Sciences, BioCentrum Amsterdam, Free University, Amsterdam, The Netherlands

[2] Department of Microbiology, Technical University of Denmark, Lyngby, Denmark
* Tel. + 31 204447194, Fax: + 31 204447229, E-mail fcb@bio.vu.nl
# Tel. + 45 45252510, Fax. + 45 45932809, E-mail. prj@im.dtu.dk
† In remembrance of Dr. L. Boe.

INTRODUCTION

The C4-dicarboxylates, succinate, fumarate, and malate sustain the growth of wild type *Escherichia coli* strains under aerobic conditions. Complete dissimilation of these substrates to carbon dioxide via the TCA cycle results in the formation of ATP mainly via oxidative phosphorylation; the H^+-ATPase catalyses the phosphorylation of ADP to ATP using the proton-motive force as the driving force. Under these conditions, the H^+-ATPase plays a key role in the free energy transduction in *E. coli.* Nevertheless, it had zero control on the growth rate at the normal level of this enzyme, with succinate as sole carbon and free energy source (1). However, at much reduced enzyme concentrations in comparison with the wild type cell, the control by the H^+-ATPase increased towards 1.

The H^+-ATPase complex in *E. coli* is encoded by nine genes, located in the *atp* operon. Deletion of the entire *atp* operon results in an *E. coli* mutant that is devoid of the H^+-ATPase and therefore lacks any of its associated activities. Such strain has to rely solely on substrate-level phosphorylation to produce ATP. In comparison with the isogenic wild type strain, the growth rate and growth yield on glucose were indeed decreased, but not as much as expected for a shift from oxidative phophorylation to glycolysis alone (2). It was also found that the respiration rate was increased, which suggested that these cells supported uncoupled respiration in order to be able to profit from increased rate of substrate level phosphorylation. Furthermore, respiration also established the necessary energisation of the inner membrane, which would, under fermentative conditions, have been accomplished by the H^+-ATPase catalyzing the extrusion of protons at the expense of ATP hydrolysis.

With succinate or other C4-dicarboxylates, no growth of the *atp* deletion strain is observed however (suc$^-$ phenotype; 3). In the first instance, this seems not surprising, for the C4-dicarboxylates are so-called non-fermentable substrates. On the other hand, an *E. coli* strain devoid of the H^+-ATPase represents an interesting mutant, because it does possess an active TCA cycle but at the same time is deprived of oxidative phosphorylation and thus has only substrate level phosphorylation at its disposal to fuel anabolic processes. Substrate level phosphorylation could then in principle occur via the

TCA cycle or via acetate production and respiration could establish a proton-motive force. Why then, is the *atp* deletion strain unable to grow on the C4-dicarboxylates?

In this study, we characterize *E. coli* mutants that are capable of growth on the C4-dicarboxylates (suc$^+$) although they completely lack the H$^+$-ATPase, and demonstrate that the lack of growth of the *atp* deletion strain on the C4-dicarboxylates is a consequence of insufficient transport capacity for these substrates. Moreover, we show that growth of *E. coli* strains with functional H$^+$-ATPases is stimulated by moderate overexpression of the C4-dicarboxylate transporter.

METHODS

Bacterial strains and growth conditions

The wild type (LM1237) and the *atp* deletion strain (LM2800) of *E. coli* were used (2). One suc$^+$ mutant (LM3559) was obtained via transposon mutagenesis, using a Tn*5*-derived mini-transposon (4,5). A second suc$^+$ mutant (LM3305) was obtained as a spontaneous mutant of the *atp* deletion strain LM2800. Complementation tests were performed on AB minimal medium (6) supplemented with thiamine (2.5 mg/liter) and the indicated carbon source. Plates were incubated at 37° C and contained 2% agarose in place of the usual agar.

Expression vector

Plasmid pFH2106 is a pBR322-derived expression vector that harbors a synthetic *lacUV5* promoter, two *lacO* operator sites, a poly-linker region, and a strong transcriptional terminator. It further carries the *lacI* gene, encoding the lac-repressor protein that binds to both *lacO* operators, conferring a tight un-induced repression of the cloned gene of interest.

Cloning of the yhiD and yhiF genes into pFH2106

The two genes were individually amplified via PCR from chromosomal DNA isolated from strain LM1237. The fragments were ligated in pFH2106 and the resulting plasmids were transformed into *E. coli*. This yielded the plasmids pLAC-yhiD and pLAC-yhiF, in which the expression of the *yhiD* and *yhiF* genes have been placed under the control of the *lacUV5* promoter.

Cloning of the dctA gene into pFH2106

Plasmid pKAT204 carries a 2.5 kb insert, which harbors the entire wild type *dctA* gene from *E. coli* (7). The *dctA* gene fragment was cut out and subcloned into pUC19, resulting in the plasmid pUC-dctA. Subsequently, the *dctA* gene was inserted into pFH2106, resulting in the plasmid, pLAC-dctA, in which the expression of the *dctA* gene has been placed under the control of the *lacUV5* promoter.

RESULTS

Isolation of suc$^+$ mutants

The *E. coli* atp deletion strain LM2800 is unable to grow on minimal medium supplemented with succinate as the sole carbon and free energy source. However, when this strain was incubated on this medium, colonies began to appear after one week of incubation at 37° C, and turned out to be mutants able to grow on succinate (suc$^+$ phenotype) although at much lower growth rate than an atp$^+$ strain. One of these colonies was re-streaked to purity (LM3305) and used for further investigation. The relatively high frequency by which the spontaneous suc$^+$ mutant occurred indicated that the suc$^+$ phenotype could be the result of a gene inactivation, and it should then be possible to obtain the suc$^+$ mutant through transposon mutagenesis. Indeed, the screening of a mini-Tn*5* transposon library in strain LM2800 resulted in a transposon induced suc$^+$ mutant, LM3559.

Growth of suc$^-$ and suc$^+$ mutants

The *atp* deletion strain LM2800 and the two suc$^+$ mutant strains derived thereof, LM3305 and LM3559, grow similarly on plates with glycolytic substrates such as glucose, pyruvate, and lactate, but are unable to grow on acetate. However, only the latter two mutants grew on the C4-dicarboxylates succinate, malate, and fumarate (suc$^+$ phenotype). The transposon induced mutant LM3559 had a similar phenotype as the spontaneous mutant, LM3305, except that LM3305 yielded larger colonies than LM3559 on plates supplemented with the various C4-dicarboxylates when scored after the same incubation period.

The growth rate of LM3305, in liquid minimal medium supplemented with succinate as the sole carbon and free energy source, was 33% relative to the wild type control, while the yield of biomass on succinate was 30% of the wild type. The rate of succinate consumption and the rate of oxygen consumption was increased, to 115% and 132%, respectively, compared to the wild type.

Complementation with the yhiD gene in trans in the suc$^+$ mutants

The insertion point of the mini-Tn*5* on the *E. coli* chromosome in strain LM3559 was determined by cloning of the relevant part of the genome. Subsequent DNA sequencing revealed that the transposon was integrated in the *yhiD* gene, which encodes a putative 23.2 kD protein with unknown function. The insertion of the transposon probably leads to inactivation of the *yhiD* gene product, and it was therefore of interest to see if we could suppress the suc$^+$ phenotype by complementing with the wild type *yhiD* gene in *trans*. The growth of the suc$^+$ mutants harboring pLAC-yhiD was then compared on succinate plates in the presence and absence of IPTG. Surprisingly, the presence of the plasmid had no suppressive effect on the growth of colonies on succinate medium for either of the two suc$^+$ mutants. We therefore conclude that expression of the *yhiD* gene in *trans* does not suppress the suc$^+$ phenotype.

Complementation with the yhiF gene in trans in the suc^{+} mutants

From the genomic sequence of *E. coli*, it appears that *yhiF*, which encodes a hypothetical transcriptional regulator, is one of the flanking open reading frames. The growth of the two suc^{+} mutants harboring pLAC-yhiF was then compared on plates with succinate as substrate and in the absence or presence of IPTG. A strong decrease in colony size was observed on the IPTG containing plates. With malate as the substrate, a similar result was obtained, but with pyruvate no suppression of growth occurred on IPTG-containing plates. Finally, induction with IPTG did not have a significant effect on the colony size of either of the suc^{+} mutants when these were transformed with the vector pFH2106. We therefore conclude that expression of the *yhiF* gene in *trans* can suppress the suc^{+} phenotype.

Complementation with the dctA gene in trans in the atp deletion mutant

The above results indicated that the *yhiF* gene product might function as a negative transcriptional regulatory protein involved in C4-dicarboxylate metabolism. Furthermore, since the *atp* deletion mutant grows well on pyruvate but not on malate plates, it is likely that growth of the *atp* deletion mutant on malate is limited by transport of the C4-carboxylates into the cell. We therefore determined the effect of expression of the *dctA* gene (encoding the C4-dicarboxylate transporter) in *trans*, on the growth of the *atp* deletion strain, LM2800. Overexpression of the C4-dicarboxylate transporter was detrimental to the cells (7). However, at intermediate concentrations of IPTG, ranging from 3-15 M, the suc^{-} phenotype of strain LM2800 was converted to the suc^{+} phenotype, whereas both too low and too high concentrations of IPTG resulted in the suc^{-} phenotype. This demonstrates that the reason why the *atp* deletion strains fail to grow on the C4-dicarboxylates, is due to a lack of transport capacity for these compounds.

Introduction of the dcta gene in trans in atp^{+} strains

An *atp* deletion strain (atp^{-}/suc^{-} phenotype) is quite far from the wild type *E. coli* strain, and therefore the finding of a step which is limiting may not be too surprising. However, the introduction of the *dctA* gene in *trans* in strains that already had the capability to grow on the C4-dicarboxylates further stimulated the growth on these compounds. This was true for all three other possible combinations of phenotypes (atp^{-}/suc^{+}; atp^{+}/suc^{-}; atp^{+}/suc^{+}). In other words, not only the suc^{+} strains without the H^{+}-ATPase, but also the wild type strain gave bigger colonies when compared with the appropriate control strains after a certain period of incubation; even with the fast-growing strain LM3330, which arose from the wild type strain after P1 transduction of the suc^{+} phenotype, a stimulation of growth on the C4-dicarboxylates was observable.

DISCUSSION

The suc^{-} phenotype of *atp* mutants has traditionally been used to distinguish an *atp* mutant from a wild type strain (3). But still, the fact that an *E. coli atp* deletion strain cannot grow on C4-dicarboxylates as substrates is actually somewhat surprising. C4-dicarboxylates can be converted into pyruvate which can in turn be converted through either the TCA cycle to carbondioxide or via the phosphoroclastic cleavage to acetate, yielding one ATP in either case. In fact, pyruvate is quite a good substrate for growth the *atp* deletion mutant. Malate or fumarate will generate one additional molecule of NADH during dissimilation compared to pyruvate, but so does lactate and this compound does support the growth of the *atp* deletion mutant.

Two observations from this study seem to explain the absence of growth of the *atp* deletion mutant on succinate, malate or fumarate. First, the expression in *trans* of the *yhiF* gene, encoding a putative transcriptional regulator, suppressed the growth of the suc$^+$ mutants substantially. This indicates that the *yhiF* gene product may act as a negative transcriptional regulator of the *dctA* gene in *E. coli.* Secondly, the fact that the expression in *trans* of the *dctA* gene, the structural gene encoding the C4-dicarboxylate transporter, enabled the *atp* deletion strain to grow on the C4-dicarboxylates, shows that the transport step does limit the growth of the *atp* deletion mutant on these substrates. Our current working hypothesis is that the *atp* deletion strain cannot grow on C4-dicarboxylates, because expression of the negative transcriptional regulator *yhiF* prevents the synthesis of their specific transporter.

The mechanism by which the transposon insertion in strain LM3559 causes the suc$^+$ phenotype is not known yet. The insertion into the *yhiD* gene is likely to result in inactivation of its gene product, but still the introduction in *trans* of the wild type *yhiD* gene into the suc$^+$ mutant did not restore the suc$^-$ phenotype. The suppression of the suc$^+$ phenotype we found upon introduction of the wild type *yhiF* gene in *trans* in the suc$^+$ mutants, strongly suggests that this gene is no longer expressed in strains with the suc$^+$ phenotype. But it is unclear how the insertion of the mini-Tn*5* in the *yhiD* gene might have affected the expression of the adjacent *yhiF* gene.

Finally, the finding that moderate overexpression of the C4-dicarboxylate transporter stimulated the growth of *E. coli* strains on plates, irrespective of the absence or presence of a functional H$^+$-ATPase, strongly suggest that growth of *E. coli* on C4-dicarboxylates is significantly controlled by the C4-dicarboxylate transporter. Currently, we are quantifying the control of the C4-dicarboxylates carrier on the growth rate and the growth yield in liquid steady-state cultures in the suc$^+$ mutants as well as the wild type *E. coli* strain.

ACKNOWLEDGEMENTS

We thank V. Tjell, H. Winterberg Andersen and H.V. Westerhoff for helpful discussions. We are indebted to F.G. Hansen for providing the unpublished expression vector pFH2106 and to J. Neuhard for the gift of plasmid pKAT204.

REFERENCES

1. Jensen, P.R., Westerhoff, H.V. and Michelsen, O. (1993) The EMBO J. 12, 1277-1282.
2. Jensen, P.R. and Michelsen O. (1992) J. Bacteriol. 174, 7635-7641.

3. Butlin, J.D., Cox, G.B. and Gibson, F. (1971) Biochem. J. 124, 75-81.
4. de Lorenzo, V., Herrero M., Jakubzik, U. and Timmis K.N. (1990) J. Bacteriol. 172, 6568-6572.
5. Herrero, M., de Lorenzo, V. and Timmis, K.N. (1990) J. Bacteriol. 172, 6557-6567.
6. Clark, D.J. and Maaløe O. (1967) J. Mol. Biol. 23, 99-112.
7. Baker, K.E., Ditullio, K.P., Neuhard J. and Kelln, R.A. (1996) J. Bacteriol. 178, 7099-7105.

IMPLICATIONS OF THE OXYGEN DEPENDENCY OF FLUX CONTROL OF CYTOCHROME C OXIDASE

Wolfram S. Kunz, Falk R. Wiedemann and Christian E. Elger*

Department of Epileptology, University of Bonn Medical Center, Sigmund-Freud-Str. 25, D-53105 Bonn, and * Department of Neurology, University of Magdeburg, Leipziger Str. 44, D-39120 Magdeburg, Germany.

SUMMARY

The oxygen dependency of cytochrome *c* oxidase (COX) control on succinate oxidation was investigated in saponin-permeabilized human skeletal muscle fibers. For this cyanide titrations of the oxygen consumption in the presence of succinate + rotenone were performed at different oxygen concentrations in the medium. In analogy to data with mice skeletal muscle we observed below 50µM oxygen a flux control of COX close to unity. This result is in line with the high oxygen sensitivity of maximal respiration of saponin-permeabilized muscle fibers which is caused by oxygen diffusion gradients through the fiber lattice. In skeletal muscle fibers of a patient with COX deficiency we observed a flux control close to unity already below 100µM oxygen which can explain the pathological phenotype.

INTRODUCTION

The implication of mild cytochrome *c* oxidase deficiencies observed in mitochondrial and some neurodegenerative diseases [1] remains not understood. This is due to the fact that the activity of cytochrome *c* oxidase is between 2- and 3-fold higher than the activities of the other enzymes of respiratory chain [2]. Therefore, a rather low flux control coefficient of this enzyme on mitochondrial succinate oxidation rate (about 0.2) was observed [3]. A threshold value (at approximately 30% of its maximal activity) was detected [3], above which changes in cytochrome *c* oxidase activity should not affect ATP synthesis. Therefore, small activity changes should not contribute to the pathological phenotype, since the maximal mitochondrial ATP synthesis rate should remain unaffected. To resolve this apparent contradiction, we investigated the oxygen dependency of cytochrome *c* oxidase flux control in saponin-permeabilized human skeletal muscle fibers. Our results indicate that the actual flux control coefficient of cytochrome *c* oxidase does not only depend on the maximal activity of the enzyme but also on the oxygen availability within the tissue. This can serve as explanation for the pathological phenotypes of cytochrome *c* oxidase deficiencies in muscle and brain tissue.

MATERIALS AND METHODS

Preparation of muscle fibers: Muscle samples between 75 and 100 mg wet weight of M. vastus lateralis were obtained from biopsies of a patient with amyotrophic lateral sklerosis and orthopedic patients (controls, age between 50 and 70 years). About 50 mg of *m. quadriceps* tissue from C57BL/10ScSn mice (obtained from Harlan) were used for the preparation of mice skeletal muscle fibers. Bundles of muscle fibers containing usually about 3 single fibers were isolated by mechanical dissection. The saponin treatment was performed by incubation of the fiber bundles in a relaxing solution containing a 10 mM Ca-EGTA buffer (free concentration of calcium 0.1 µM), 20 mM imidazole, 20 mM taurine, 49 mM K-MES, 3 mM K_2HPO_4, 9.5 mM $MgCl_2$, 5 mM ATP, 15 mM phosphocreatine and 50 µg/ml saponin (pH 7.1) as described in [4].

Respiration measurements: The oxygen consumption of permeabilized fibers was measured at 25°C using an Oroboros oxygraph (Anton Paar, Graz) in a medium containing 5 mM $MgCl_2$, 60 mM KCl, 100 mM mannitol, 10 mM KH_2PO_4, 0.5 mM Na_2EDTA and 60 mM Tris-HCl (pH 7.4).

Determination of flux control coefficients: Using specific noncompetitive inhibitors, the flux control coefficient of an enzyme i can be determined experimentally according to the following equation:

$$C_i = - (dJ/J) / (dp_i/I_{max}) \qquad (1)$$

where J is the flux through the pathway, p_i the the concentration of a specific inhibitor of enzyme i and I_{max} is the maximal amout of inhibitor binding sites. Equation 1 was used for the calculation of flux control coefficients of cytochrome *c* oxidase. The maximal amount of cyanide binding sites in the samples (I_{max} , in nmol/mg protein or in nmol/mg dry weight) was determined from cyanide titration curves (performed under normoxic conditions) using nonlinear regression analysis, accounting for the dissociation equilibrium of the inhibitor as described in [4]. The initial slopes of the titration curves (dJ/dp_i) were obtained by linear regression of the first three points of the titration. Different oxygen concentrations were adjusted by argon/oxygen equilibration of the medium. In order to keep almost identical oxygen concentrations during the entire titration experiment, the potassium cyanide solutions used in the titrations, were made with oxygen equilibrated water (and kept in an oxygen atmosphere). The rate measurements were made after 2 min of equilibration with the inhibitor to reach a steady state.

RESULTS AND DISCUSSION

To study the metabolic consequences of the oxygen dependency of maximal respiration of saponin-permeabilized muscle fibers [4] we applied metabolic control analysis and determined the flux control coefficient of cytochrome *c* oxidase at different oxygen concentrations. For this we performed cyanide titrations of the succinate (+rotenone) oxidation rate in the presence of 1 mM ADP. To keep the concentration of oxygen in the measurement chamber at a constant value we used for the titration experiments oxygen equilibrated inhibitor solutions. Typical titrations of succinate respiration of saponin-permeabilized fibers from mice skeletal muscle at two different oxygen concentrations in the chamber are shown in Fig. 1. While under nearly normoxic conditions (190 µM oxygen, open circles) the initial slope of the titration curve is rather flat, indicating a low flux control coefficient, already at about 130 µM oxygen (filled circles) a steeper initial slope was detected. Moreover, the amount of cyanide, necessary to cause complete inhibition of respiration, decreased. For the calculation of flux control coefficients according to eq. 1 (cf. materials and methods) we determined the initial slopes of the titration curves by linear regression of the first 3 points and used the value for the maximal amount of cyanide binding sites calculated by nonlinear regression analysis of the complete titration curve under normoxic conditions. Using this procedure we observed at 177 µM oxygen a flux control coefficient of cytochrome *c* oxidase of 0.14 and at 95 µM oxygen a flux control coefficient of 0.38. Similar experiments were performed with human skeletal muscle fibers at different concentration of oxygen in the chamber.

From all titration curves we calculated the cytochrome *c* oxidase flux control coefficients and plotted the values versus the oxygen concentration (Fig. 2, filled circles). For saponin-permeabilized human fibers this dependency of cytochrome *c* oxidase flux control is very close to the oxygen dependency in mice skeletal muscle (compare with [4]). Already below 50 µM oxygen in the measurement chamber the flux control of cytochrome *c* oxidase approaches values of 1.

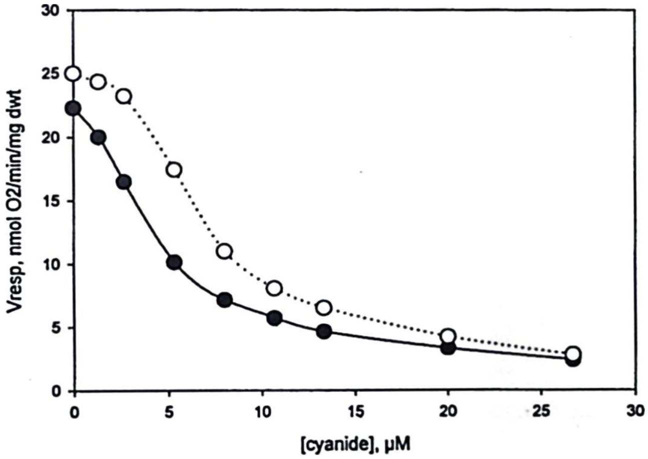

Figure 1. Titration of respiration of saponin-permeabilized mice muscle fibers with KCN KCN titrations of mice skeletal musle fibers oxidizing succinate. 0.8 mg dry weight saponin-permeabilized fibers at 177 µM oxygen (open circles) or at 95 µM oxygen (filled circles) in the medium for respiration containing additionally 10 mM succinate, 10 µM rotenone and 1 mM ADP. To keep the oxygen concentration in the chamber nearly constant oxygen equilibrated cyanide solutions were used for the titration experiments.

Fig. 2: Oxygen dependency of flux control of cytochrome *c* oxidase in human skeletal muscle fibers

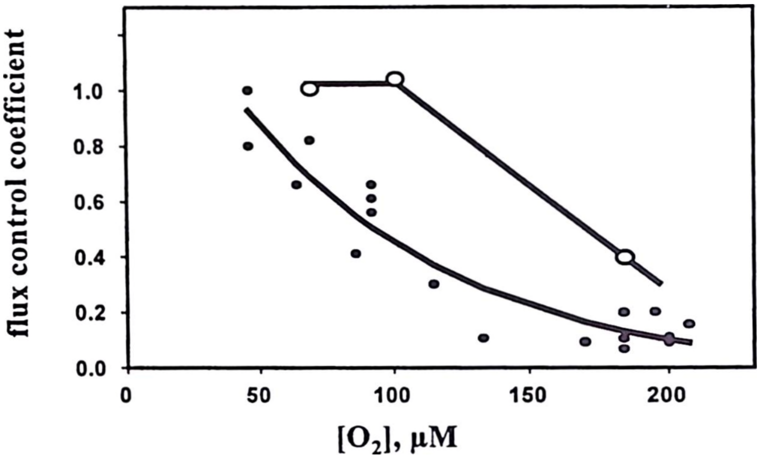

The flux control coefficients were calculated from cyanide titration experiments at different oxygen concentrations in the measurement chamber (cf. Fig. 1). The calculations were performed on the basis of eq. 1 as described in Materials and Methods. Filled circles: controls; open circles: patient with COX deficiency.

These data indicate that the influence of activity changes of cytochrome *c* oxidase on tissue energy metabolism should crucially depend on the oxygen concentration within the tissue. In agreement with earlier reports with isolated cardiac myocytes [5] we observed a strong oxygen dependency of maximal rates of respiration of saponin-permeabilized human muscle fibers. The phenomenon is most probably caused by oxygen diffusion gradients within the fiber lattice [5]. This possibility has been also predicted on the basis of theoretical considerations [6,7]. The oxygen dependency strongly affects the controlling influence of cytochrome *c* oxidase on mitochondrial oxidative phosphorylation at physiological oxygen concentrations in the muscle tissue. Below 50 µM oxygen the flux control coefficient of the enzyme becomes close to unity, e.g. cytochrome *c* oxidase is nearly exclusively rate controlling (cf. Fig. 2, filled circles). Since saponin-permeabilized muscle fibers are a model of mitochondrial function in skeletal muscle under *in situ* -like conditions [4], the observed oxygen dependency of cytochrome *c* oxidase flux control can explain the pathological phenotypes of cytochrome *c* oxidase deficiencies in muscle. As shown in Table 1 under normoxic conditions even rather severe deficiencies (about 30 % of citrate synthase normalized control activity) only slightly affect the maximal rate of respiration of saponin-permeabilized skeletal muscle fibers (82 % of citrate synthase normalized succinate oxidation rate of controls):

Table 1. Rates of fiber respiration and enzyme activities in the skeletal muscle biopsy of a patient with amyotrophic lateral sclerosis having a severe COX deficiency

	controls (n = 24)	Patient
succinate respiration	**10.3 ± 2.1**	**6.5 ± 1.0**
glutamate respiration	8.2 ± 0.9	5.2 ± 0.8
citrate synthase	11 ± 2.2	8.5 ± 0.4
COX	**7.1 ± 3.4**	**1.7 ± 0.2**
NADH:cyt c	3.5 ± 1.7	1.6 ± 0.3
succ:cyt c	1.7 ± 0.7	0.8 ± 0.2

Rates of respiration in nmol O_2/min/mg dry weight, enzyme activities in U/g wet weight.

However, as visible in Fig. 2, open circles, at lower physiological oxygen concentrations, when the flux control exerted by cytochrome *c* oxidase increases, deficiencies of this enzyme to a much larger extent affect the mitochondrial ATP production rate. Therefore, the availability of oxygen in the tissue should be considered as an important factor determining the pathophysiological consequences of a cytochrome *c* oxidase deficiency.

REFERENCES

1. Wallace, D.C. (1992) Annu. Rev. Biochem. 61: 1175-1212.
2. Letellier, T., Malgat, M., and Mazat, J.P. (1993) Biochim. Biophys. Acta 1141, 58-64.
3. Letellier, T., Heinrich, R., Malgat, M., and Mazat, J.-P. (1994) Biochem. J. 302, 171-174.
4. Wiedemann, F.R. and Kunz,W.S (1998) FEBS Lett. 422, 33-35.
5. Jones, D.P., and Kennedy, F.G. (1986) Am. J. Physiol. 250, C384-C390.
6. Gnaiger, E., Steinlechner-Maran, R., Mendez, G., Eberl, T., and Margreiter, R. (1985) J. Bioenerg. Biomembr. 27, 583-596.
7. Korzeniewski, B., and Mazat, J.-P. (1996) Biochem. J. 319, 143-148.

REGULATION ANALYSIS OF MITOGENIC T-CELL ACTIVATION - THE EFFECTS OF CONCANAVALIN A ON THYMOCYTE RESPIRATION

*Stefan KRAUSS**, *Frank BUTTGEREIT*† & *Martin D. BRAND**

*Department of Biochemistry, University of Cambridge, Tennis Court Road, Cambridge CB2 1QW, U.K., and †Medizinische Klinik m.S. Rheumatologie, Humboldt-Universität (Charité), Schumannstraße 20/21, 10117 Berlin, Federal Republic of Germany.

INTRODUCTION

The jack bean protein Concanavalin A (Con A) acts as mitogenic lectin in T-cells. Con A-induced stimulation of thymocyte respiration forms part of a prototypical range of biochemical events, including increased transport of ions, an acceleration of phospholipid turnover, increased rates of amino acid transport, protein synthesis, and respiration [1]. Up to 80% of a population of the cells isolated from rat thymus respond immediately and reproducibly to Con A with an increase in oxygen consumption of around 30 - 40% [2], depending on the conditions.

The top-down approach of metabolic control analysis provides an appropriate tool to handle the complex phenomenology of mitogenic activation. It allows us to explain in quantitative terms the overall effect of Con A on respiration at any chosen level of system resolution. We defined a conceptually simplified model system of rat thymocyte energy metabolism as described in [3] and used top-down regulation analysis [4] to address the question of how the system responses to Con A at different concentrations in the range 0 - 2 µg per 10^7 cells may be explained in terms of responses of the subsystems. The results show how the overall response of a particular subsystem can be dissected into direct responses to Con A and indirect ones via the other variables, and are in line with our previous observation of subsystem inhibition and stimulation patterns derived from elasticity analysis.

METHODS

Experimental

Thymocytes were isolated from female Wistar rats (4-7 weeks old) as described in [3]. Briefly, rats were killed by cervical dislocation. The thymus was pressed through a nylon mesh and the cells were washed twice by centrifugation, diluted to a final concentration of 4.5 - 5.5 x 10^7 cells ml^{-1} and kept at 37° C in RPMI 1640 with glutamine, without glucose, buffered with HEPES (pH 7.4). Oxygen consumption was measured in Clarke - type electrodes. Mitochondrial membrane potential within the cells ($\Delta\psi_m$) was estimated in situ using [^{3}H]TPMP. In a typical experiment, 1.7 ml of cell suspension were incubated for two minutes with different amounts of Con A (0, 0.15, 0.5, 0.8, 1.0 and 2.0 µg per 10^7 cells, respectively). During this time, the cells were kept under an atmosphere of CO_2/air (1:19) at 37° C in a plastic vial, mounted onto a submersible stirrer. Subsequently, carriers (TPMP, TPB) and inhibitors (myxothiazol, oligomycin or myxothiazol in the presence of a saturating oligomycin concentration) were added. 0.5 ml of cell suspension were transferred into a 1 ml thermostatted oxygen electrode chamber and [^{3}H]TPMP was added to the remainder of the cell suspension. The separated aliquots were constantly gassed with CO$_2$/air (1:19) and kept at 37° C for 20 min, then oxygen consumption was measured and [^{3}H]TPMP distribution and $\Delta\psi_m$ were determined by calculating [^{3}H]isotope spaces and using the equation given in [3].

Theoretical

The conceptually simplified model system of thymocyte respiration consisted of a substrate oxidation block (producing mitochondrial membrane potential, $\Delta\psi_m$) and the ATP turnover and proton leak blocks of reactions (consuming $\Delta\psi_m$). Partial responses of the three subsystems to Con A were calculated from group elasticities to Con A and group control coefficients [5,6]. (The total response of a subsystem to Con A equals to the sum of partial responses to Con A via all subsystems.) Elasticities to Con A were determined from flux data, and elasticities to $\Delta\psi_m$ were determined using the inhibitor titration data [5,6]. We made the practical assumption that each subsystem had a linear response to $\Delta\psi_m$ between adjacent measured values of $\Delta\psi_m$. Group flux control coefficients for the subsystems were then calculated from elasticities of the subsystems to the intermediate ($\Delta\psi_m$) and the system fluxes at the resting conditions [7]. The possibility of crosstalk between subsystems via ATP was excluded through appropriate control experiments. No significant glycogen levels were detectable in thymocytes.

Respiration data are presented as means ± SEM (n=4 independent experiments).

RESULTS

The effect of Con A in the range 0 - 2 μg per 10^7 cells on steady state thymocyte respiration is shown in Fig. 1. The stimulation of respiration is represented by a bell-shaped dose-response curve; respiration was maximally stimulated at a concentration between 0.5 and 1.0 μg per 10^7 cells. At higher [Con A], the stimulation in respiration decreased, but it remained above the quiescent level. A similar pattern was observed for the rate of ATP turnover reactions (Fig. 1b), whereas the leak rate was hardly affected (Fig. 1c).

Partial and overall response coefficients of the substrate oxidation and ATP turnover systems to Con A are presented in Fig. 2. From our data, we observe:

(i) The change in subsystem activities upon variation in [Con A] can be broken down into responses that are consequences of direct effects on the particular block and effects on other blocks, communicated by interaction with other blocks through the intermediate. The substrate oxidation and ATP turnover systems each display direct and indirect responses to Con A, whereas the leak does not respond directly to the mitogen (data not shown).

(ii) As a consequence of direct Con A effects, the substrate oxidation system displays small positive or (around [Con A] 0.8 μg per 10^7 cells) large negative partial response coefficients to changes in Con A. The direct response of the ATP turnover system to Con A is always positive and is maximal around 0.8 μg per 10^7 cells. These results tie in with conclusions drawn from elasticity analysis (data not shown) that Con A inhibits the substrate oxidation system, but stimulates ATP turnover. As there is no direct effect of Con A on the leak, the direct effects on the two affected subsystems superimpose and combine to similar overall response coefficient profiles.

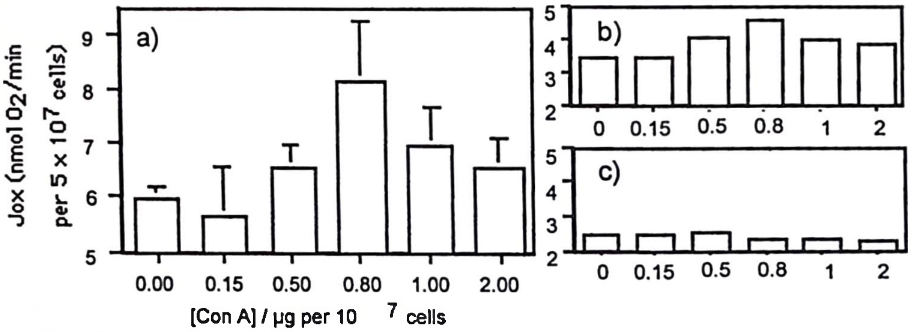

Figure 1. Thymocyte respiration in response to different [Con A]. a), total respiration (equivalent to the rate of substrate oxidation block of reactions); b), ATP turnover system; c), mitochondrial proton leak. No errors are shown for ATP turnover and proton leak rates, as these values were calculated (see [3]) and do not represent raw data.

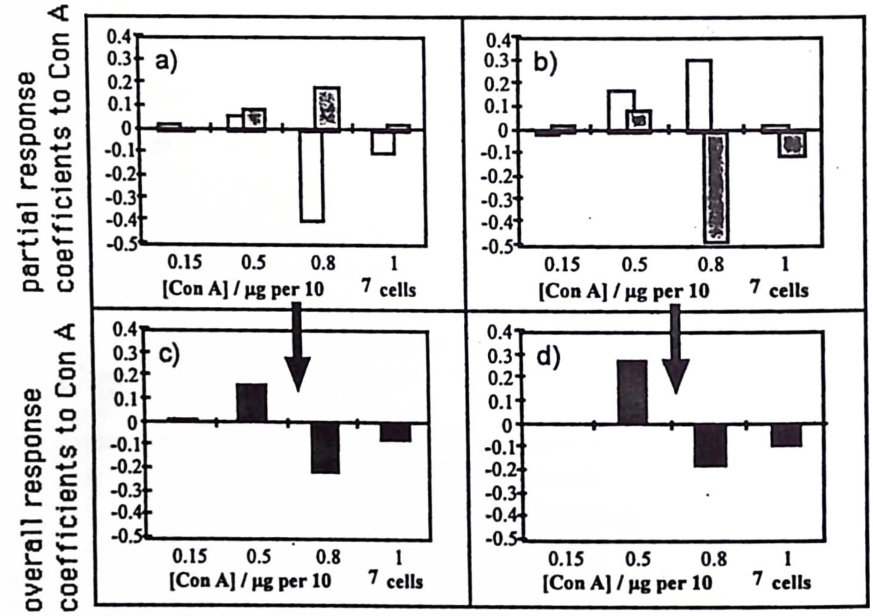

Figure 2. Partial and overall response coefficients of substrate oxidation (panels a,c) and ATP turnover reactions (panels b,d) to Con A. □, direct response of a subsystem to Con A, ▨, indirect response of the subsystem to Con A via the other subsystem. The partial response coefficients shown in pairs in a (or b) add to the overall responses shown in c (or d) (■). Note that proton leak is inelastic to Con A, therefore no effects are transduced via $\Delta\psi_m$ to the other systems; any responses of proton leak rate to Con A are secondary (data not shown).

ACKNOWLEDGEMENTS

This work was supported by a BBSRC research studentship to S.K. and grants from the Deutsche Forschungsgemeinschaft (Bu 1015/1-1) and the Deutscher Akademischer Austauschdienst (D/96/17655) to F.B. We thank Julie Buckingham for expert technical assistance.

REFERENCES

[1] Buttgereit, F., Brand, M.D. and Müller, M. (1992) Biosci. Rep. 12, 381-386.
[2] Buttgereit, F., Brand, M.D. and Müller, M. (1993) Biosci. Rep. 13, 41-52.
[3] Buttgereit, F., Grant, A., Müller, M. and Brand, M.D. (1994) Eur. J. Biochem. 223, 513-519.
[4] Brand, M.D. (1997) J. Exp. Biol. 200, 193-202.
[5] Kesseler, A. and Brand, M.D. (1994) Eur. J. Biochem. 225, 923-935.
[6] Kesseler, A. and Brand, M.D. (1994) Eur. J. Biochem. 225, 907-922.
[7] Hafner, R.P., Brown, G.C. and Brand, M.D. (1990) Eur. J. Biochem. 188, 313-319.

28

AUTOOSCILLATION REGIMES AND BISTABILITY IN BLOOD COAGULATION.

Veronika I. Zarnitsina, Fazoil I. Ataullakhanov

Scientific Center for Hematology, Novozykovsky 4a, Moscow 125167, Russia
Telephone: +7 095 212 55 31, Fax: +7 095 212 88 70, E-mail: fazli@bioscience.msk.su

INTRODUCTION.

In the site of blood vessel injury, the enzyme cascade of coagulation is triggered. Its operation culminates in the formation of a dense fibrin clot (thrombus) sealing the wound. The cascade structure of the activation signal transduction [1, 2] and the presence of strong positive feedbacks [3] results in strongly nonlinear behavior of the system. In [4], it was shown by means of mathematical modeling that the response of this system to increasing levels of activation changes in a threshold manner. This seems to be the most reliable protection of the body from the spontaneous thrombus formation. The reactions involving protein C constitute a negative feedback in the coagulation system [5]. We developed a mathematical model [6, 7] to analyze the effects of these reactions on the dynamics of the system and showed that the main effect is the repeating concentration spikes of activated factors [7]. In this study, these oscillations were analyzed using a simplified model, which was obtained by reduction of the model described in [6]. It was shown that the autooscillations in the blood coagulation system can exist in a wide range of parameters.

The model description.

In [6], the model describing the coagulation kinetics of contact-activated blood was proposed. Specifically, the kinetics of eight coagulation factors - IXa, Xa, IIa (thrombin), II (prothrombin), VIIIa, Va, APC (activated protein C), and fibrin - was considered. Analysis of the model showed that it can be reduced to a set containing only two variables, thrombin and APC, and that the model thus simplified retains all basic properties of the initial system.

The reduction resulted in the following set of equations:

$$\begin{cases} \dfrac{dIIa}{dt} = \dfrac{k_9 \cdot C0}{h_9 \cdot h_{10}} \cdot \left(k_{10} + \overline{k_{10}} \cdot \dfrac{k_{8,9} \cdot k_8}{h_{8,9}} \cdot \dfrac{IIa}{(h_8 + k_a \cdot APC)}\right) \cdot \\ \left(k_2 + \overline{k_2} \cdot \dfrac{k_{5,10} \cdot k_5}{h_{5,10}} \cdot \dfrac{IIa}{(h_5 + k_a \cdot APC)}\right) \cdot \left(1 - \dfrac{IIa}{Pt0}\right) - h_2 \cdot IIa \\ \dfrac{dAPC}{dt} = k_{apc} \cdot IIa - h_{apc} \cdot APC \end{cases}$$

The following values of the constants were used: $k_9=20\text{min}^{-1}$, $h_9=0.2\text{min}^{-1}$, $C0=0.3\text{nM}$, $k_8=10^{-5}\text{min}^{-1}$, $k_5=0.17\text{min}^{-1}$, $h_8=h_5=0.31\text{min}^{-1}$, $k_{10}=0.0033\text{min}^{-1}$, $\overline{k_{10}}=500\text{min}^{-1}$, $k_2=2.45\text{min}^{-1}$, $\overline{k_2}=2000\text{min}^{-1}$, $k_{5,10}=k_{8,9}=100\text{nM}^{-1}\text{min}^{-1}$, $h_{5,10}=100\text{min}^{-1}$ $h_{5,10}=100\text{min}^{-1}$, $k_a=1.2\text{nM}^{-1}\text{min}^{-1}$, $h_{10}=1\text{min}^{-1}$, $h_2=2.3\text{min}^{-1}$, $k_{apc}=0.0014\text{min}^{-1}$, $h_{apc}=0.1\text{min}^{-1}$.

Here, k_i and h_i are the kinetic constants for the corresponding reactions of the coagulation cascade. Their selection and estimation of the values were described in detail in [6]. C0 is the concentration of the upper-level factor of the coagulation cascade, which is used in the model to indicate the extent of activation of the system.

The active coagulation factors are formed from their plasma precursors. To simplify the analysis, we ignored their consumption. Thrombin undergoes the most profound concentration changes during coagulation. Therefore, the term (1-IIa/Pt0) was added in order to confine the concentration of thrombin by the concentration of its plasma precursor prothrombin, where Pt0=1000nM is the prothrombin concentration.

RESULTS.

Analysis of the model was performed within the framework of qualitative theory of dynamical systems. The phase portraits presented below show the major nullclines (indicated by thick solid lines): dIIa/dt=0 (the nullcline of vertical tangents to phase trajectories) and dAPC/dt=0 (the nullcline of horizontal tangents; this nullcline is a straight line). The number of points where these nullclines intersect varies from one to three, depending on the parameters of the system. These points correspond to the singular points.

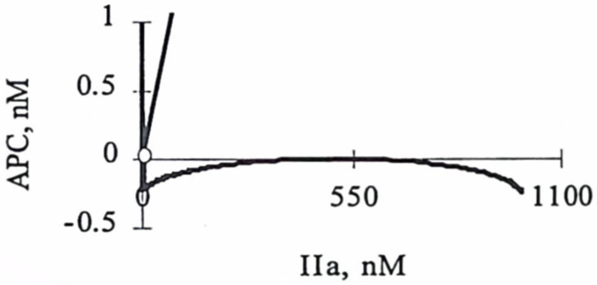

Fig. 1. Phase-plane diagram for the low-activated system (C0=0.00001nM and other parameters of the system are as indicated in the text). Part of the nullcline of the first equation is very close to the APC axis, but does not coincide with it.

First, let us consider how the phase portrait of the system changes with increasing activation (parameter C0 in the first equation). If activation is very low (Fig. 1), there exists only one singular point (a circle in the Fig), which is located near zero. The concentrations of activated factors are also very low in this state and the liquid state of blood is stable. No fluctuations result coagulation.

As the extent of activation increases, the nullcline of the first equation shifts upward. This leads to the appearance of three singular points (stable node, stable focus and an unstable saddle point between them; Fig. 2). The state of blood is bistable and depends on the initial concentration of active variables. Zero initial conditions result in that the system appears in the state that is characterized by low (underthreshold) concentrations of activated factors whose levels are determined by the presence of the stable singular point near zero. This state corresponds to liquid blood. However, from a certain initial level of thrombin, its concentration begins to increase sharply, and the system appears in the basin of attraction of the second stable point. This corresponds to the transition of the blood into the solid state. Figure 2 shows how low initial concentrations of thrombin could initiate the coagulation despite the underthreshold extent of activation (this phenomenon was found when the nonreduced model was analysed [6]).

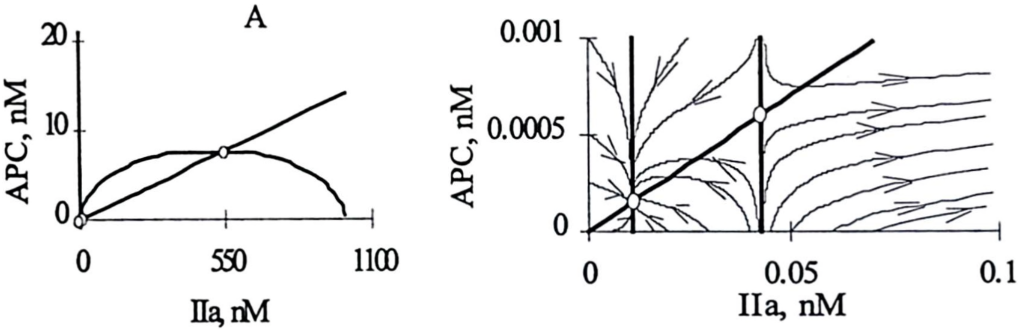

Fig. 2. Panel A: The appearance of three singular points as the extent of activation of the system increases (C0=0.005nM). Panel B: Two singular points (the same as in Panel A) in the vicinity of the origin of coordinates shown on a larger scale (the third point is beyond the plot on this scale). Thick and thin solid lines are the nullclines and phase trajectories, respectively.

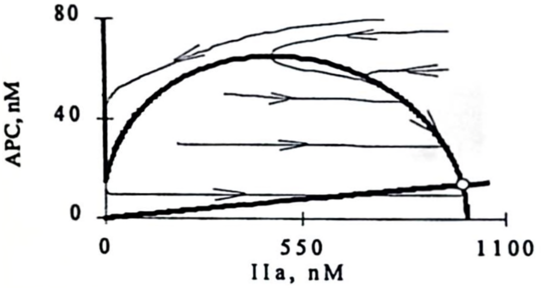

Fig. 3. Phase-plane diagram for the system activated with a suprathreshold signal (C0=0.3nM). Thick and thin solid lines are the nullclines and phase trajectories, respectively.

From a certain threshold level of activation, only one singular point remains in the system. This point is a stable node corresponding to large concentrations of activated factors (Fig. 3). It is the case when the blood will always be coagulated.

Thus, similar to earlier models [4], this model describes the threshold behavior of the system observed when the extent of activation increases. The first threshold value of activation corresponds to the transition of the system from a state with one singular point to the state with three singular points and allows the coagulation to be initiated at nonzero initial conditions. The second threshold value corresponds to the subsequent transition from three singular points to one stable point located far from zero. This means that plasma coagulates at any initial conditions.

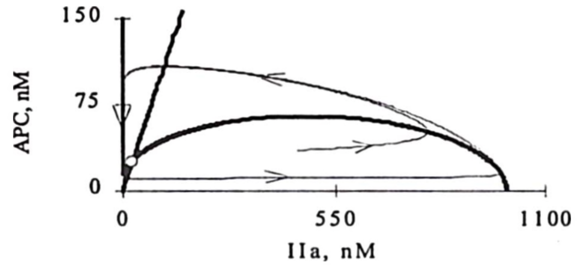

Fig. 4. Phase portrait for the system with a strengthened negative feedback through APC (k_{apc}=0.1min^{-1}, the extent of activation of the system C0=0.3nM is the same as in Fig.3)

The bifurcations occurring when the extent of activation of the system changes were described above under the assumption that the rate of APC formation is not modulated by the presence of any effectors. However, it is known that this rate can be higher by several orders in the presence of thrombomodulin [8]. In the model, the effect of thrombomodulin can be taken into account by the corresponding increase in the k_{apc} value. This changes the slope of the straight line (the nullcline of the second equation). The phase portrait changes as shown in Fig. 4. In all cases, only one steady state exists in the system. If the extent of activation is low, blood is liquid. The high extents of activation correspond to the solid state of the blood. Between these two extremes, a large range of activation values exist where the intersection point is on the ascending branch of the nullcline of the first equation. This single stationary solution is unstable (an unstable node), and the limit cycle exists in the system. Figure 5 shows the concentrations of both active variables plotted against time. This regime cannot exist endlessly in the real system. The oscillations will be damped. Nevertheless, analysis of the initial nonreduced model showed that the oscillatory regimes are possible in the coagulation system even if the depletion of the precursors is taken into account [7]. In this case, several damping pulses of the active factor concentrations are observed. Is this instability physiologically relevant? No direct experimental data exist to answer this question. However, our model study of spatial clot growth based on the equations of the nonreduced set [6] showed that this instability results in the appearance of several secondary waves of thrombin within the growing clot, with amplitudes increasing to the edge of the clot [7]. This consolidates the edge of the clot. It is of physiological importance, because the fragmentation of the clot with the consolidated edges is less probable that of the clot with loose edges.

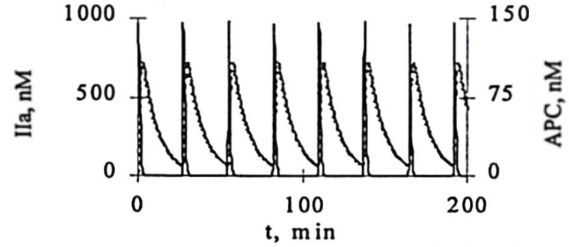

Fig. 5. Concentrations of IIa (solid line) and APC (dashed line) plotted against time (for the corresponding phase portrait Fig. 4).

REFERENCES.

1. Macfarlane R.G.(1964) Nature 202, 498-499.
2. Davie E.W. and Ratnoff O.D. (1964) Science 145, 1310-1312.
3. Mann K.G, Nesheim M.E., Church W.R., Haley P., and Krishnaswamy S. (1990) Blood 76, 1-16.

4. Khanin M.A., and Semenov V.V. (1989) J.Theor.Biol. 136, 127-134.
5. Marlar R.A., Kleiss A.J., Griffin J.H. (1982) Blood 59, 1067-1072.
6. Zarnitsina V.I., Pokhilko A.V., Ataullakhanov F.I. (1996) Thrombosis Research 84, 225-236.
7. Zarnitsina V.I., Pokhilko A.V., Ataullakhanov F.I. (1996) Thrombosis Research 84, 333-344.
8. Esmon C.T., Owen W.G. (1981). Proc.Natl.Acad.Sci. 78, 2249-2252

29

KINETIC ANALYSIS OF OXIDATIVE PHOSPHORYLATION IN RAT LIVER AND HEART MITOCHONDRIA AFTER CHRONIC ALCOHOL FEEDING

Vida Mildaziene[1,2], Ausra Marcinkeviciute[1,2], Jan B.Hoek[1] and Boris Kholodenko[1,]*

[1]Department of Pathology, Anatomy and Cell Biology, Thomas Jefferson University, 1020 Locust St., Philadelphia, PA 19107, USA, [2]Institute for Biomedical Research, Kaunas Medical Academy, Eiveniu 4, Kaunas 307-LT, Lithuania

[*] Corresponding author, E-mail: kholodel@jeflin.tju.edu, FAX: (1 215) 923-2218

INTRODUCTION

Long-term alcohol consumption causes mitochondrial dysfunction associated with morphological changes and alterations in the activities of mitochondrial enzymes (e.g., electron transport chain and ATP synthase) in multiple tissues, including liver and heart. The implications of these changes for physiological function are poorly understood, and their characterization requires integrated and quantitative approaches to the control of energy metabolism in the tissue, such as, e.g., Metabolic Control Analysis (MCA). The present work characterizes changes in the kinetics and control of mitochondrial oxidative phosphorylation in isolated mitochondria from rat heart and liver following chronic ethanol consumption. We use Modular, or Top-down MCA, a recently developed analytical tool that enables the identification of the control exerted by the functional units (blocks of reactions) of the oxidative phosphorylation machinery, or other complex enzymatic pathways (for a recent review see, e.g., [1]).

The importance of each step in controlling the pathway flux is given by a numerical value, referred to as the control coefficient of that step. This is defined as the fractional change in the steady-state flux divided by the fractional change in the activity of the step that caused the change in the flux, extrapolated to infinitesimally small change. Similarly, the control exerted by a block of reactions can be quantified as the (overall) control coefficient of the block (this is equal to the sum of the control coefficients of all the reactions of that block). Importantly, a control coefficient of a particular step or reaction block depends on the pathway structure and the kinetics of all the components of a system (rather than on the kinetics of that particular step or block). The kinetic properties, which ultimately determine the control distribution are given by the "local" sensitivities of individual steps or blocks of reactions to the relevant intermediates. These sensitivities are referred to as the elasticity coefficients.

Top-down MCA provides a simple experimentally-based overview of how a complex system is controlled. Top-down analysis groups reactions into the integrated subsystems connected by common intermediates. By measuring the fluxes through the subsystems and their overall elasticities to explicit intermediates, the top-down approach calculates the overall control coefficients of the integrated blocks and gives a picture of the behavior and the regulation of the whole system. In this context, the oxidative phosphorylation system is conceptually divided into three subsystems: the respiratory subsystem (R) producing the proton motive force Δp (substrate translocases, dehydrogenases of TCA cycle and the complexes of the electron transport chain) and the two blocks of reactions that consume Δp, either coupled to ATP synthesis (i.e. the phosphorylation subsystem (*P*), including the ATP synthase, ANT and phosphate carrier) or uncoupled respiration (proton leak (*L*) and any other cation cycling reactions). At steady state the flux through the respiratory subsystem (J_R) is equal to the sum of the rates of O_2 consumption needed to drive the phosphorylation subsystem (J_P) and the proton leak (J_L): $J_R = J_P + J_L$..

METHODS

Experiments were done on heart and liver mitochondria respiring on succinate from ethanol-fed rats and pair-fed control animals. Animals were fed a standard Lieber-DeCarli diet for 5-7 weeks, after which time the changes in respiratory activities in liver mitochondria are well-established. Heart and liver mitochondria were isolated in a Hepes (10 mM)-buffered mannitol (0.2M)-sucrose (0.05 M) (HMS) medium containing 0.1 mM EGTA from the same animal pairs by standard differential centrifugation procedures, with a final wash in EGTA-free HMS medium. Mitochondria were incubated at 30 °C with succinate in a Hepes-buffered KCl medium in the chamber of a polarograph (Rank Brothers) fitted with a TPP^+-electrode and an O_2 electrode for the simultaneous measurement of membrane potential and oxygen uptake rates. For determination of the proton motive force, Δp, the mitochondrial membrane potential was determined using a TPP^+-electrode, applying corrections for TPP^+ binding; ΔpH and mitochondrial volume was measured in a sample of the mitochondrial suspension incubated with ^3H_2O and ^{14}C-acetate or ^{14}C-sucrose [2].

The kinetic dependence of each block of reactions, *L, R* or *P,* on Δp was measured by the following procedures (under conditions where ΔpH was nearly constant, ΔΨ was monitored): (1) the dependence of J_L on ΔΨ was determined by titration of mitochondria oxidizing succinate with malonate under the complete inhibition of J_P by an excess of oligomycin (so that $J_R = J_L$). (2) the dependence of J_R on ΔΨ was determined in state 3 by titration with an inhibitor of the phosphorylation subsystem (carboxyatractiloside or oligomycin). (3) the dependence of J_P on ΔΨ was determined in state 3 by titration with an inhibitor of the respiratory subsystem (malonate) and measuring the flux J_R. The flux J_P was calculated at each ΔΨ value by substracting J_L (determined by procedure 1) from J_R ($J_P=J_R-J_L$).

RESULTS AND DISCUSION

In State 3 (maximal phosphorylation activity) liver mitochondria from chronically ethanol-fed rats respiring on succinate exhibit lower respiration rates (122 ± 5 natom O/min.mg) than mitochondria from pair-fed control animals (159 ± 5), whereas the membrane potential did not change significantly (142 ± 3 versus 138 ± 4 mV) (data from 3 pairs receiving ethanol for 5-6 weeks). In State 4 (resting state with minimal phosphorylation activity) both the respiration rate and the membrane potential did not differ between mitochondria from ethanol-fed and control animals. An explanation for these findings comes from Fig. 1, which presents the kinetic characteristics of the functional units of oxidative phosphorylation system. Fig. 1A shows the results of titration of mitochondrial succinate oxidation with malonate (an inhibitor of succinate dehydrogenase) in the presence of excess oligomycin to completely inhibit phosphorylation. Under these conditions the only load on the respiratory subsystem is the proton leak through the mitochondrial membrane. Clearly, in liver mitochondria the dependence of J_L on $\Delta\Psi$ was not affected by alcohol consumption.

Titration of mitochondria in State 3 with carboxyatractyloside (an inhibitor of the adenine nucleotide translocator), which inhibited the phosphorylation subsystem and thereby raised Δp, gave us the kinetic response of the respiratory subsystem to changes in $\Delta\Psi$ (Fig. 1B). In liver mitochondria from ethanol-fed animals oxidizing succinate the flux through the respiratory subsystem was significantly lower at $\Delta\Psi$ values corresponding to State 3 (high respiration rates), but did not differ from control preparations at $\Delta\Psi$ values corresponding to State 4 (low respiration rates). We note that in State 4 neither $\Delta\Psi$-supply (the respiratory subsystem), nor $\Delta\Psi$-consumption (uncoupled respiration) were affected by alcohol treatment, and hence both the respiration rate and the membrane potential were similar in control and alcoholic animals.

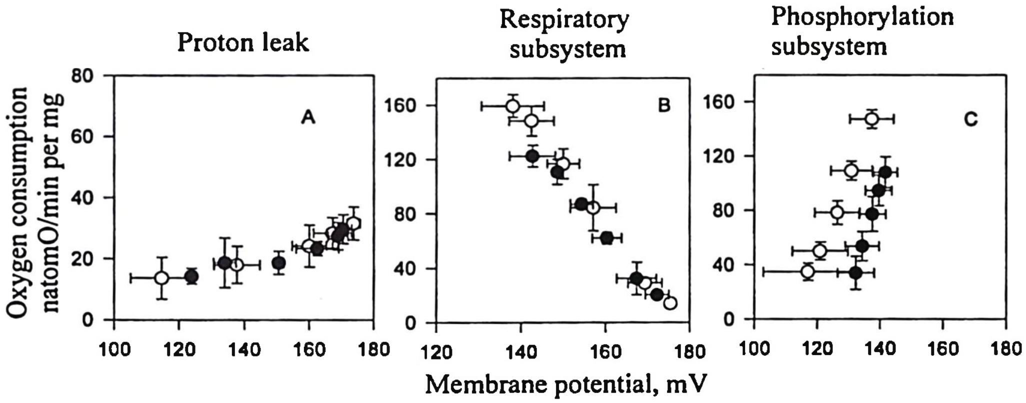

Figure. 1. Dependencies of fluxes through proton leak (J_L , panel A), respiratory subsystem (J_R, B), and phosphorylation subsystem (J_P,C) on the membrane potential in liver mitochondria oxidizing succinate (10 mM) in State 3 (rotenone 2μM). Control (○), ethanol-fed animals (●).

In Fig. 1C the flux through the phosphorylation subsystem was examined over a wide range of $\Delta\Psi$ values by titration with malonate of State 3 succinate oxidation. In State 3 the main $\Delta\Psi$-consuming system is the phosphorylation subsystem. Interestingly, in State 3 both respiratory chain and phosphorylation appeared to be inhibited by chronic alcohol feeding to almost equal degrees, resulting in significantly lower respiration activity of liver mitochondria, while maintaining practically the same $\Delta\Psi$ level as in control animals. Therefore, in normal conditions, i.e. in the absence of physiological stress, the ATP/ADP ratio would be practically the same in mitochondria oxidizing succinate from control and ethanol-fed animals. However, large differences between the fluxes through the phosphorylation subsystem are evident at low values of the membrane potential (Fig. 1C), clearly showing that the ability to phosphorylate and transport ATP can be significantly impaired in liver mitochondria from alcoholic animals under conditions of physiological stress. For instance, stress conditions that result in an increase in cytosolic Ca^{2+} concentrations decrease the membrane potential; under these conditions it would be more difficult for mitochondria from ethanol-fed animals to maintain the necessary rates of ATP production in liver cells.

The experiments carried out on heart mitochondria (3 pairs of animals receiving ethanol for 11 months) revealed dramatic differences between the functional consequences of chronic ethanol treatment for energy metabolism in heart and liver. In contrast to the liver, in heart mitochondria from ethanol-fed animals the respiration rates in State 3 were significantly higher than in control mitochondria (Fig. 2B). Moreover, this difference in respiration rate persisted at all the values of the membrane potential between States 3 and 4, and not only near State 3 as in liver mitochondria (Fig. 1).

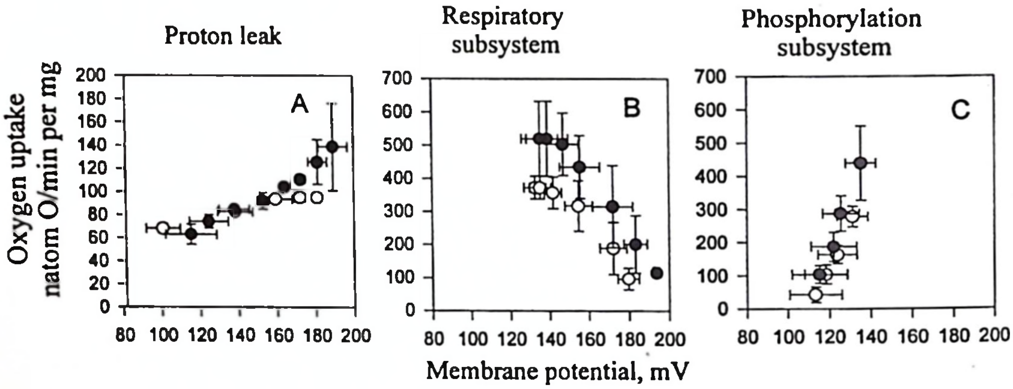

Figure 2. Dependencies of fluxes through proton leak (J_L , panel A), respiratory subsystem (J_R, B), and phosphorylation subsystem (J_P,C) on the membrane potential in heart mitochondria oxidizing succinate (10 mM) in State 3 (rotenone 2μM). Control (○), ethanol-fed animals (●).

A striking difference between heart and liver was found in the behavior of the proton leak (Fig. 2A) as a function of $\Delta\Psi$. In heart mitochondria proton leak increased much steeper with an increase in $\Delta\Psi$ in alcoholic animals than in pair-fed control animals. This increase in proton leak matches the increase in the activity of the respiratory chain found in State 4. On the other hand, the differences in the activity of the phosphorylation subsystems were quite modest in heart mitochondria from ethanol-fed and control animals compared to liver mitochondria (Fig. 2C and 1C).

From the kinetic dependencies shown in Figs. 1 and 2, the elasticities of three blocks of oxidative phosphorylation system on $\Delta\Psi$ were determined. These elasticities were used to calculate the control coefficients of every block over the fluxes through the system. Interestingly, both in heart and liver mitochondria (respiring on succinate in State 3), the distribution of control exerted by different reaction blocks over respiratory flux remained practically unchanged in spite of various changes induced by ethanol diet. This reflects the compensatory mechanisms involved in adaptation to alcohol, helping to maintain bioenergetic function of tissues under non-stress condition.

The findings reported in this study illustrate how mitochondria adapt to simultaneous changes in multiple components of the energy conversion system following chronic ethanol consumption. Previous studies in the literature (reviewed in [3,4]) had demonstrated that ethanol treatment causes tissue-specific decreases in electron transport chain complexes as well as ATP synthase subunits and also affects phospholipids in the mitochondrial inner membrane. MCA provides the tools to investigate systematically how such multiple changes affect the integrated function of the mitochondria. The top-down analysis employed here detected changes in mitochondrial energy conservation that are highly tissue-specific: (1) after two months of feeding an ethanol diet, the proton leak in liver mitochondria was not affected, whereas 11 months of ethanol feeding was associated with a 20-30% increase in proton leak in heart mitochondria; (2) the respiratory chain activity was inhibited in liver mitochondria in State 3, whereas the activity was increased in the heart; (3) the phosphorylation subsystem was inhibited in ;liver mitochondria over the entire range of respiration rates, whereas there were no pronounced ethanol effects on the phosphorylation subsystem in heart mitochondria. A more detailed analysis of the time dependence and tissue specificity will be presented in future papers.

ACKNOWLEDGMENT

We acknowledge NIH grants AA11689, AA01786, AA07215 and AA08714 for the support of this work..

REFERENCES

1. Brand, M.D. (1996) J. Theor. Biol. 182, 351-360.
2. Mildaziene, V., Baniene, R., Nauciene Z., Marcinkeviciute, A., Morkuniene, R., Borutaite, V., Kholodenko, B. and Brown, G.C. (1996) Biochem. J. 320, 329-334.
3. Hoek, J.B. (1994) Current Topics Bioenerg. 17, 197-241.
4. Cunningham, C. and Spach, P. (1994) Alc. Clin. Exp. Res., 16, 132-137.

METABOLIC CONTROL BY THE REDOX-STATE OF THE Q-POOL IN THE RESPIRATORY NETWORK OF PARACOCCUS DENITRIFICANS

Marijke F. Otten [1#], *Willem N.M. Reijnders* [1], *Jacques J.M. Bedaux* [2], *Hans V. Westerhoff* [1,3*], *Klaas Krab* [1], *and Rob J.M. Van Spanning* [1]

[1]Molecular Cell Physiology, Faculty of Biology, BioCentrum Amsterdam, Free University, De Boelelaan 1087, NL-1081 HV Amsterdam, The Netherlands

[2]Theoretical Biology, Faculty of Biology, Free University

[3]Mathematical Biochemistry, BCA, ECSI, University of Amsterdam
# Email: mfotten@bio.vu.nl Tel. +31 20 4447183 Fax. +31 20 4447229
* Email: hw@bio.vu.nl Tel. +31 20 4447230 Fax. +31 20 4447229

INTRODUCTION

Paracoccus denitrificans is a Gram-negative facultative anaerobic bacterium that is found in soil, sewage or sludge. Because its environment is subject to changes especially with respect to substrate availability and oxygen concentrations, it has evolved the capability of employing many compounds as electron donors to terminal electron acceptors of its electron-transfer chain. An example of variegated electron routing is the electron flow towards oxygen. Under aerobic heterotrophic growth conditions electrons can flow from NADH-dehydrogenase and succinate-dehydrogenase to three different types of terminal oxidase, two of which are cytochrome *c* oxidases (cytochrome aa_3 and cytochrome cbb_3), and one of which is a quinol-oxidase (cytochrome ba_3). There are two branch points, the first branch point is at ubiquinol (QH_2) where the electrons may flow to the quinol-oxidase or to cytochrome bc_1. The second branch point is at the level of cytochrome *c*, where the electrons may flow to either of the two cytochrome *c* oxidases (reviewed by [1]).

Because cellular control systems are hierarchical [2, 3], the control of the electron flux to the three terminal oxidases may be through adaptation of gene expression or metabolically. The distribution of electrons through the different pathways depends partly on the adaptation of gene expression: Cytochrome aa_3 is expressed at atmospheric oxygen tensions, while cytochrome cbb_3 is expressed predominantly at low oxygen tensions [4] . Little is known about the induction profile of cytochrome ba_3. So far, only the transcription regulator, FnrP, which is involved in the regulation of expression of the terminal oxidases, has been identified [5-7] . Metabolic control relies on the kinetic properties of individual components of the network.

We investigated whether or not the redox-state of Q could be involved in the metabolic control of the distribution of the electrons over the two quinol-oxidizing branches in *P. denitrificans*. By making correlations between the oxygen consumption rates and the fractions of reduced Q, we found that the quinol-oxidase pathway becomes active at higher Q reduction than the pathway involving cytochrome bc_1.

MATERIALS AND METHODS

The following strains of *P.denitrificans* were used: the wild-type strain Pd1222 [8] , the quinol-oxidase-negative mutant Pd2621 (*cyoB*::Km^r), devoid of cytochrome *ba*$_3$ [9] , and the *bc*$_1$-negative mutant Pd2421 (*fbcC*::Km^r), devoid of cytochrome *bc*$_1$ [10].

Cells grown aerobically on mineral batch medium for *P. denitrificans* [11, 12] , were harvested in the exponential phase. Cells were washed twice in 100 mM Tris/HCl, pH 7.5 at 4°C and suspended in the same buffer to an optical density of 50 cm^{-1} at 660 nm. For the isolation of membrane fractions, the cells were broken in a French Pressure Cell. Cell debris was removed and the supernatant was centrifuged. The pellet was resuspended in 0.1 M Tris/HCl pH 7.5, and will be referred to as "membrane fraction". Because the membrane fractions were isolated in similar ways, we considered that the membrane fractions were oriented in homogenous matter in all cases. Protein concentrations were determined by the modified Lowry procedure [13] with bovine serum albumin as a standard.

Oxygen consumption rates of membrane fractions and whole cells were measured polarographically with a Clark type oxygen electrode in 1 ml Tris/ HCl pH 7.5 at 25°C. Succinate was added to membrane fractions as electron donor. To inhibit the electron input rates, various concentrations of malonate were used.

In each assay, samples were taken for quinone and quinol extraction at steady states of respiration. Ubiquinone 10 and ubiquinol 10 were extracted from membrane fractions as described for plant mitochondria [14] . The fraction of quinone and the fraction of quinol in the Q-pool were determined by HPLC.

To compare sets of titration data, all sets were fitted with power functions

$$y = m_1 \, x^{m_2}$$

where y is the oxygen-consumption rate and x is the fraction quinol in the Q-pool.

RESULTS

By modulating specifically the activity of the quinone reducing pathways, the rate of electron transfer through the quinol-oxidizing pathways should vary only because of variation of the concentrations of substrates and products of the latter. By measuring both the steady state oxygen consumption rate and the fraction of reduced Q, the dependence of the QH_2 oxidation rate on the Q redox state could be determined, provided that the Q reduction and the QH_2 oxidation reactions only influence each other through that redox state. This method was applied to the wild-type, a *bc*$_1$-negative mutant which only has an electron transfer pathway towards the quinol-oxidase, and a quinol-oxidase-negative mutant. In membrane fractions, succinate was employed as the electron donor. The electron input rates were attenuated by titration with malonate, a competitive inhibitor of succinate dehydrogenase. The membrane fractions of the *bc*$_1$-negative mutant consumed oxygen at higher fractions of quinol in the Q-pool than did the membrane fractions of the wild-type strain (Fig. 1). These findings suggest that the apparent K_m for QH_2 of the quinol-oxidase is so high as to prevent flux through this branch in membranes of the wild-type cells. This prediction is confirmed by the kinetics of the membrane fractions of the quinol-oxidase-negative mutant: Oxidation of QH_2

occurred at equally low redox states of the Q-pool as do the membrane fractions of the wild-type.

DISCUSSION

The redox-state of Q regulates the distribution of electrons between the quinol-oxidase and the bc_1 pathway in *P. denitrificans.* We conclude this from the comparison of dependencies of the oxygen consumption rates on the redox-state of Q in membrane fractions of the wild-type, the quinol-oxidase-negative mutant, and the bc_1-negative mutant. We found that the flux through the electron transfer route to the quinol-oxidase in the membrane fractions of the bc_1-negative mutant became significant only at reduction levels of the Q-pool almost twice as high as compared with membrane fractions of the wild-type and the quinol-oxidase negative mutant (Fig.1). The kinetics of oxygen consumption relative to the redox-state of Q in the latter two strains was nearly identical, indicating that electron transfer routes in the wild-type strain are dominated by those terminating in cytochrome *c* oxidases. Flux in the wild-type membranes prefers the bc_1 dependent route. Although we were not able to determine for all respiratory chain compounds whether or not their amounts were identical in wild-type and mutant strains, we don't think that possible differences will have consequences on the interpretation of the results.

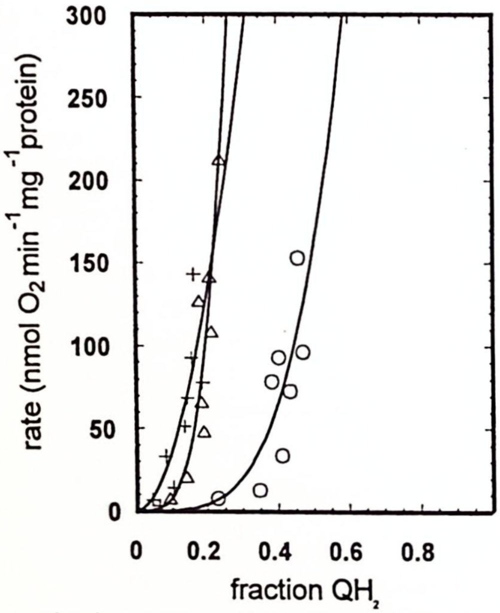

Figure 1. The oxygen consumption rates and the related fractions of QH_2 of membrane fractions of the wild-type strain (Δ), the bc_1-negative mutant (o), and the quinol-oxidase-negative mutant (+). The data points of each strain have been fitted with a power equation.

An other factor that determines the distribution of electrons in *P. denitrificans* is the membrane potential. The membrane potential during respiration in whole cells and membrane fractions is different. In whole cells the dependence of the QH_2 oxidation rate on the Q redox-state appeared to be much weaker than in the isolated membrane fractions (results not shown). The elasticity ("Hill") coefficient was 1 rather than 3.7. The quinol-oxidase-negative mutant cells and the bc_1-negative mutant cells exhibited quinol oxidation kinetics that were fairly similar to that in the wild-type cells. However, when we uncoupled the cells the correlations of the wild-type and the two mutants

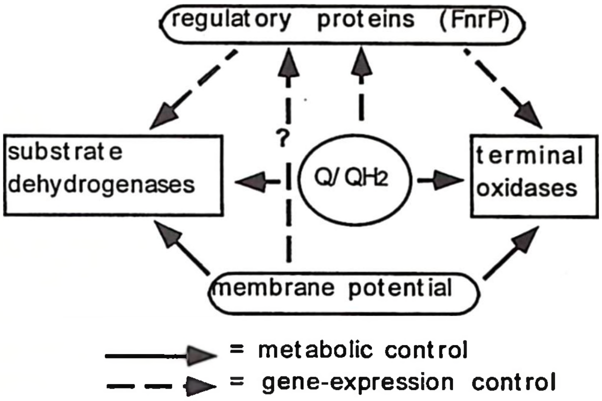

Figure 2. Model in which the redox-state of Q and the membrane potential are involved in both metabolic and gene-expression control of the respiratory network of *P. denitrificans*.

became more like those we found in the membrane fractions (results not shown). This suggests that part if not all of these different correlations were the result of differences in membrane potential.

It has been proposed that in *P. denitrificans* the redox potential of (one of the) components of the respiratory network upstream the *bc*$_1$ complex is sensed by the transcription regulator FnrP, and regulates its activity [6]. The redox-state of Q and also the membrane potential may be sensed by FnrP or other regulatory proteins, which results in enhanced or attenuated expression of respiratory enzymes. Here we have shown that QH_2/Q also engages in metabolic regulation. Consequently, the redox-state of Q and the membrane potential may be involved in both metabolic and gene-expression control of the respiratory network of *P.denitrificans*. Figure 2 shows a model of this metabolic and gene-expression control by the redox-state of Q and the membrane potential.

REFERENCES

1 Van Spanning, R.J.M., De Boer, A.P.N., Reijnders, W.N.M., De Gier, J.W.L., Delorme, C.O., Stouthamer, A.H., Westerhoff, H.V., Harms, N. and Van der Oost, J. (1995) J Bioenerg Biomembr. 27, 499-512

2 Wijker, J.E., Jensen, P.R., Snoep, J.L., Vaz Gomes, A., Guiral, M., Jongsma, A.P.M., De Waal, A., Hoving, S., Van Dooren, S., Van der Weijden, C.C., Van Workum, M., Van Heeswijk, W.C., Molenaar, O., Wielinga, P., Richard, P., Diderich, J., Bakker, B.M., Teusink, B., Hemker, M., Rohwer, J.M., Van der Gugten, A.A., Kholodenko, B.N. and Westerhoff, H.V. (1995) Biophys. Chem. 55, 153-165

3 Westerhoff, H.V., Jensen, P.R., Egger, L., Van Heeswijk, W.C., Van Spanning, R.J.M., Kholodenko, B.N. and Snoep, J.L. (1997) NATO/ESF Workshop Bioelelectron-Transfer Chains bb73

4 Bosma, G. (1989) PhD Thesis, Vrije Universiteit, Amsterdam

5 De Gier, J.W.L., Schepper, M., Reijnders, W.N.M., Van Dyck, S.J., Slotboom, D.J., Warne, A., Saraste, M., Krab, K., Finel, M., Stouthamer, A.H., Van Spanning, R.J.M. and Van der Oost, J. (1996) Mol. Microbiol. 20, 1247- 1260

6 Van Spanning, R.J.M., De Boer, A.P.N., Reijnders, W.N.M., Westerhoff, H.V., Stouthamer, A.H. and Van der Oost, J. (1997) Mol. Microbiol.23, 893- 907

7 Zickermann, I., Tautu, O.S., Link, T.A., Korn, M., Ludwig, B. and Richter, O.M.H. (1997) Eur. J. Biochem. 246, 618-624

8 De Vries, G.E., Harms, N., Hoogendijk, J. and Stouthamer, A.H. (1989) Arch. Microbiol. 152, 52-57

9 De Gier, J.W.L., Lubben, M., Reijnders, W.N.M., Tipker, C.A., Slotboom, D.J., Van Spanning, R.J.M., Stouthamer, A.H. and Van der Oost, J. (1994) Mol. Microbiol. 13, 183-196

10 De Gier, J.W.L., Van der Oost, J., Harms, N., Stouthamer, A.H. and Van Spanning, R.J.M. (1995) Eur. J. Biochem. 229, 148-154

11 Chang, J.P. and Morris, J.G. (1962) J. Gen. Microbiol. 29, 301-310

12 Lawford, H.G., Cox, J.C., Garland, P.B. and Hadock, B.A. (1976) FEBS Lett. 64, 369-374

13 Markwell, M.A.K., Haas, S.M., Bieber, L.L. and Tolbert, N.E. (1978) Anal. Biochem. 87, 206-210

14 Van Den Bergen, C.W.M., Wagner, A.M., Krab, K. and Moore, A.L. (1994) Eur. J. of Biochem. 226, 1071-1078.

THE REVERSIBLE EFFECT OF CALCIUM OVERLOAD ON OXIDATIVE PHOSPHORYLATION IN HEART MITOCHONDRIA OXIDIZING DIFFERENT SUBSTRATES

Vida Mildaziene[1,2], *Ausra Marcinkeviciute*[1], *Rasa Baniene*[1], *Sarune Morkunaite*[2]

[1]Institute for Biomedical Research, Kaunas Medical Academy, Eiveniu 4, 3007 Kaunas, Lithuania; E-mail: bioch@kma.lt, FAX: 370 7 796498;
[2]Kaunas Vytautas Magnus University, Daukanto 56, 3000Kaunas, Lithuania

INTRODUCTION

Calcium ions within the physiological range of concentration (reaching 1 μM with cytosolic Ca^{2+} pulse in heart and liver [1]) stimulates mitochondrial respiration and ATP synthesis effectively by acting in a coordinated manner on several steps [2]. Any disturbance of processes involved in maintaining of Ca^{2+} homeostasis within the cell leads to an increase of cytoplasmic Ca^{2+} concentration above the physiological level and the resulting Ca^{2+} overload has been assumed to be of key importance in deterioration of cell function in many conditions [3]. The main role in mitochondrial damage by Ca^{2+} overload is commonly prescribed to the opening of the mitochondrial permeability transition pore [1,4]. Our results show that Ca^{2+} accumulation reversibly and severely affects mitochondrial oxidative phosphorylation under conditions in which permeability transition pore remains closed [5]. We investigated the effect of increase in Ca^{2+} concentration from 1 μM to 30 μM on different parts of mitochondrial oxidative phosphorylation system using the kinetic elasticity analysis [6] and the results showed [5] that calcium uncouples oxidative phosphorylation and inhibits both the respiratory subsystem and the phosphorylating subsystem in heart mitochondria respiring on succinate. In this study, the relative importance of deleterious Ca^{2+} action on separate blocks of oxidative phosphorylation in the resulting overall inhibition is quantified and compared for oxidation of succinate and pyruvate+malate.

METHODS

Mitochondria were isolated from the hearts of several male Wistar rats. The tissue was cut into small pieces and homogenized in a buffer containing 160 mM KCl, 10 mM NaCl, 20 mM Tris-HCl, 5 mM EGTA and 1 mg/ml BSA (pH 7.7). The homogenate was centrifuged at 450 g, and the obtained supernatant was centrifuged at 6300 g. The mitochondrial pellet was resuspended in a buffer containing 180 mM KCl, 20 mM Tris-HCl and 3 mM EGTA (pH 7.35) to approximately 50 mg/ml protein and stored on ice. The protein concentration was determined by the biuret method.

Respiration and membrane potential of mitochondria were measured in a closed, stirred and thermostated 1.5 ml vessel fitted both by a Clark type oxygen electrode and a tetraphenyl-phosphonium (TPP^+) selective electrode. The experiments were performed at 37°C using 5 mM succinate (plus 1 μM rotenone) or 1 mM pyruvate + 1 mM malate as substrate, and 0.4 mg/ml mitochondria. Concentrations of free Ca^{2+} (1μM or 30 μM) and Mg^{2+} (1 mM) in the incubation media were stabilized by EGTA and nitrilotriacetic acid (NTA) buffers and calculated using the apparent stability constants for NTA [7] and EGTA [8], and the program published by Fabiato and Fabiato [8]. The free concentrations of Ca^{2+} in experimental solutions were verified by a fluorescent calcium indicator Calcium Green-5N (Molecular Probes) and were within a few percent of calculated values. The rate of mitochondrial respiration corresponding to the rate in state 3 was registered after addition of 1 mM ATP to the incubation medium containing 110 mM KCl, 10 mM NaCl, 30 mM Tris-HCl, 5 mM KH_2PO_4, 1 mM EGTA, 5 mM NTA, 1 mM dithiotreitol, 50 mM creatine, excess of creatine kinase, and 0.875 mM $CaCl_2$ (1 μM free Ca^{2+}) plus 5.17 mM $MgCg_2$ (1 mM free Mg^{2+}) either 1.5 mM $CaCl_2$ (30 μM free Ca^{2+}) plus 4.8 mM $MgCl_2$ (1 mM free Mg^{2+}), pH 7.2. The reversibility of Ca^{2+} effect was tested by addition of 2 mM EGTA (equilibrated by Trizma base to pH 7.2) to mitochondria already preinhibited by 30 μM Ca^{2+}.

RESULTS AND DISSCUSION

Heart mitochondria sustain an exposure to much higher external Ca^{2+} concentration than liver mitochondria do. At 30 μM external Ca^{2+} and in the presence of succinate (+ rotenone) or pyruvate+malate and Mg^{2+}, ATP, ADP they are still capable to phosphorylate and to maintain the membrane potential. Although the permeability transition pore remains closed [5], Ca^{2+} overload severely affects mitochondrial oxidative phosphorylation. The rate of respiration in state 3 with succinate is inhibited by 25%, whereas with pyruvate+malate by 61%. After addition of 2 mM EGTA to mitochondria already inhibited by 30 μM Ca^{2+} the rate of respiration with both substrates in state 3 was slowly restored and this restoration was abolished by 200 μM diltiazem indicating that $2Na^+/Ca^{2+}$ efflux is responsible for the reversal.

The elasticity kinetic analysis was applied to distinguish which blocks of reactions (inner membrane permeability to ions, respiratory subsystem or phosphorylation subsystem) are effected by Ca^{2+} in heart mitochondria oxidizing succinate and pyruvate+malate. For this, we determined the dependencies on mitochondrial membrane potential ($\Delta\Psi$) of a) the flux through the respiratory subsystem (J_C) which includes substrate transporter, succinate dehydrogenase and complexes of the respiratory chain, b) the flux through the phosphorylation system (J_P) and c) membrane leak (J_L) by titrating the rate of respiration and $\Delta\Psi$ with a) an inhibitor of phosphorylation subsystem (oligomycin), b) with an inhibitor of the respiratory chain (malonate or rotenone) and c) an inhibitor of the respiratory chain (malonate or rotenone) in the presence of an excess of oligomycin, respectively (as described in more detail by Hafner et al. [6]). One could measure changes in Δp as changes in $\Delta\Psi$ without introducing a significant error under the conditions when ΔpH values and changes are small. Measurement of ΔpH in our experiments [5] confirmed that this was so.

For both substrates, Ca^{2+} overload resulted in inhibition of both the respiratory subsystem and the phosphorylation subsystem and in partial uncoupling of mitochondria. By measuring the kinetics of the separate subsystems of the oxidative phosphorylation machinery we showed that the strongest effect of Ca^{2+} on succinate oxidation is the inhibition of the phosphorylation (-86% at 151 mV) respiratory subsystem is inhibited moderately (-12% at 164 mV), and permeability to ions substantially increases (+216% at 164 mV). As a result, $\Delta\Psi$ in State 3 increases from 151±2 to 164±3 mV. The effect of Ca^{2+} on the kinetics of the membrane permeability is completely abolished by addition of 0.5 μM ruthenium red to mitochondria which were preincubated already for 3 minutes with succinate at 30 µM Ca^{2+} (for accumulation of Ca^{2+} inside and uncoupling). Therefore we conclude that the increased rate of Ca^{2+} cycling across the inner mitochondrial membrane at 30 µM Ca^{2+} is responsible for partial uncoupling of oxidative phosphorylation. Our results show that the rate of Ca^{2+} cycling at 30 µM Ca^{2+} accounts for 53% of the respiration rate (i.e., 89 natom O/min per mg) in state 3. In other words, the cycling of Ca^{2+} becomes significant enough to be considered as the third component of the ΔΨ-consuming system in addition to the proton leak and the phosphorylation subsystem.

For pyruvate + malate, inhibition of the respiratory subsystem is much more pronounced (-72% at 137 mV) than that for succinate and therefore ΔΨ in State 3 decreases from 137±1 mV to 125±4 mV, although phosphorylation is also considerably inhibited (-78% at 125 mV) and membrane permeability to ions increased (+50% at 137 mV). The results are summarised in table 1.

Table 1. The effect of Ca^{2+} concentration on 5 mM succinate + 2 µM rotenone and 1 mM pyruvate + 1 mM malate oxidation in heart mitochondria (state 3).

Substrate	succinate		pyruvate + malate	
Ca^{2+} concentration	1 µM Ca^{2+}	30 µM Ca^{2+}	1 µM Ca^{2+}	30 µM Ca^{2+}
J_C, natom O/min per mg	346±11	258±12*	329±14	129±6*
J_L, natom O/min per mg	34±4	129±11*	33±5	62±4*
J_P, natom O/min per mg	312±8	129±10*	296±15	66±4*
ΔΨ, mV	151±2	164±3*	137±1	125±4*

*- statistically significant effect of Ca^{2+} ($p<0.05$).

The relative Ca^{2+} effect (in %) on respiration of mitochondria in state 3 both with succinate and pyruvate + malate stays of the same magnitude regardless to the presence of cytochrome c (30 µM) in the medium indicating that Ca^{2+} inhibition of the respiratory subsystem is not due to facilitated by Ca^{2+} cytochrome c release from mitochondria.

The determined flux dependencies of proton leak, respiratory chain and phosphorylation subsystem on ΔΨ at two concentrations of Ca^{2+} were used to calculate elasticities and control coefficients (shown in table 2) of these three blocks of reactions using equations described by Hafner et al. [6].

Table 2. The control coefficients of membrane leak, respiratory chain and phosphorylation subsystem over the rate of heart mitochondrial respiration ($C_L^{J_o}, C_C^{J_o}, C_P^{J_o}$) and phosphorylation ($C_L^{J_P}$, $C_C^{J_P}$, $C_P^{J_P}$) with succinate and pyruvate + malate in state 3 at two different Ca^{2+} concentrations.

Substrate	succinate		pyruvate+malate	
Ca^{2+} concentration	1 μM Ca^{2+}	30 μM Ca^{2+}	1 μM Ca^{2+}	30 μM Ca^{2+}
$C_L^{J_o}$	0.010±0.005	0.26±0.05*	0.03±0.01	0.30±0.02*
$C_C^{J_o}$	0.88±0.02	0.43±0.06*	0.74±0.01	0.37±0.06*
$C_P^{J_o}$	0.11±0.02	0.31±0.06*	0.23±0.01	0.33±0.05
$C_L^{J_P}$	-0.10±0.02	-0.27±0.05*	-0.09±0.01	0*
$C_C^{J_P}$	0.94±0.04	0.50±0.06*	0.77±0.02	0*
$C_P^{J_P}$	0.16±0.03	0.77±0.01*	0.32±0.01	1*

*- statistically significant effect of Ca^{2+} ($p<0.05$).

The results show that at 1 μM of external Ca^{2+} the main control over the respiration and phosphorylation rates for both substrates (in state 3) is exerted by the respiratory subsystem with the contribution of phosphorylation subsystem being slightly higher in the case of pyruvate + malate. Increase of Ca^{2+} concentration to 30 μM leads to severe changes in the kinetics of all three subsystems and these changes are qualititatively similar for both substrates, however some components of the respiratory subsystem involved only in pyruvate + malate oxidation are much more sensitive to inhibition by Ca^{2+}. For both substrates, 30 μM Ca^{2+} induced an essential shift in the distribution of the rate control from the respiratory chain to the leak and to the phosphorylation subsystem. Although the control coefficients of the leak and phosphorylation subsystem increased significantly, the respiratory chain still retained the main part of the control over the rate of respiration. However, the control over phosphorylation flux was more prominently shifted by Ca^{2+} to the prevailing role of the phosphorylating subsystem.

The results obtained allow to estimate the relative contribution of the inhibition of $\Delta\Psi$-producing block and of $\Delta\Psi$-consuming block to the overall inhibition of mitochondrial respiration rate by Ca^{2+}. In the framework of Metabolic Control Analysis such a contribution is quantified as a partial response coefficient of a particular subsystem to Ca^{2+} [9,10]. The calculated contribution of $\Delta\Psi$-producing and $\Delta\Psi$-consuming blocks of reactions to the response of mitochondrial respiration to Ca^{2+} overload is 45% and 55% for succinate oxidation, 72% and 28% for pyruvate + malate oxidation, respectively.

REFERENCES

[1] Gunter, T.E., Gunter, K.K., Sheu, S.-S. and Gavin, C.E. (1994) Am. J. Physiol. 267, C313-C339.

[2] Mildaziene, V., Baniene, R., Nauciene, Z., Marcinkeviciute, A., Morkuniene, R., Borutaite, V., Kholodenko, B., Brown, G.C. (1996) Biochem J. 320, 329-334.

[3] Nicotera, P., Bellomo, G. and Orrenius, S. (1990) Chem. Res. Toxicol. 3, 484-494.
[4] Nazareth, W., Nasser, Y. and Crompton, M. (1991) J. Mol. Cell. Cardiol. 23, 1351-1354.
[5] Mildaziene, V., Marcinkeviciute A., Baniene, R., Mazat, J.-P. (1996) In: Biothermokinetics of the Living Cell (H.V. Westerhoff, J. L. Snoep, J. E. Wijker, F. E. Sluse and B.N. Kholodenko, eds.) Biothermokinetics Press, Amsterdam, 168-173.
[6]Hafner, R.P., Brown, G.C. and Brand, M.D. (1990) Eur. J. Biochem. 188, 313-319.
[7] Dipenaar S. and Brand M.D. (1982) Biochem. J. 202, 731-737.
[8] Fabiato, A. and Fabiato, F. (1979) J. Physiol. (Paris) 75, 463-505.
[9] Kholodenko, B.N. (1988) FEBS Lett. 232, 383-386.
[10] Brand MD. (1996) J Theor Biol. 182, 351-360.

POLYUNSATURATED FATTY ACID DEFICIENCY AND YIELD OF OXIDATIVE PHOSPHORYLATION : ROLE OF ADENINE NUCLEOTIDE CARRIER.

V. Nogueira[a], *M.A. Piquet*[a], *A. Devin*[b], *E.M. Fontaine*[a], *B. Sibille*[a], *C. Filippi*[a], *G. Brandolin*[c], *M. Rigoulet*[b], *X.M. Leverve*[a].

[a]Laboratoire de Bioénergétique Fondamentale et Appliquée. Université J. Fourier, BP 53X, 38041 Grenoble-Cedex, France. Tel. : 33(0)476514386, Fax : 33(0)476514218
e-mail : Xavier.Leverve@ujf-grenoble.fr
[b]IBGC-CNRS, 1 rue Camille Saint-Saëns, 33077 Bordeaux-Cedex , France.
[c]URA 1130 CNRS, DBMS, Centre d'Etudes Nucléaires de Grenoble, France.

INTRODUCTION

Mitochondrial adenine nucleotide carrier (ANC) is a key energetic link between the mitochondrial and the cytosolic compartments of aerobic eukariotic cells. It catalyzes an electrogenic exchange of ATP and ADP across mitochondrial membrane, driven by the , and the control exerted by this step depends on tissue and metabolic conditions (*e.g.* rate of respiration and ADP-regenerating system used).

In isolated mitochondria, polyunsaturated fatty acids (PUFA) deficiency leads to an increase in non ohmic proton leak and in redox slipping [1]. But, these results obtained on isolated mitochondria cannot be directly extrapolated to oxidative phosphorylation in intact cells. Indeed, in hepatocytes from PUFA-deficient rats as compared to controls, we have previously reported a significant increase in oxygen uptake associated with a decreased cytosolic ATP/ADP ratio while mitochondrial ATP/ADP ratio was unaffected [2].This could be explained either by a decrease in the protonmotive force related to the uncoupling effect, or by an increase in kinetics constraints at the level of the adenine nucleotide carrier or by both. The aim of this work was to further investigate the consequences of polyunsaturated fatty acids deficiency on control of respiration of isolated rats liver cells and mitochondria.

MATERIALS AND METHODS

Hepatocytes were isolated [3, 4] from male Wistar rats fasted for 20-24 h. The deficiency in PUFA was obtained in male weanling Wistar rats (60 g), fed for at least 6 weeks a control or a PUFA deficient diet [1]. Liver cells (10-12 mg dry cells/ml) were incubated at 37°C in 2.5 ml of Krebs-Ringer-bicarbonate buffer (pH 7.4) saturated with O_2/CO_2 (19:1) in presence of dihydroxyacetone (20 mM), octanoate (4 mM) and with or without 50 μM 2,4-dinitrophenol (DNP). After 25 min of incubation, oxygen consumption was measured polarographically at 37°C by using a Clark electrode and 2 ml of the cell suspension. After two minutes, myxothiazol (2 μg/ml) was additioned in the oxygraph vessel, in order to abolish mitochondrial respiration activity. Mitochondrial respiration in intact cells was the oxygen consumption sensitive to myxothiazol. In addition, at the same time (25 min) 300 μl of the cell suspension were taken and mitochondrial and cytosolic contents were separated by using the digitonin fractionation method [5]. ATP and ADP were measured by HPLC as described in [6] and Pi as described in [7].

Livers cells were incubated for 25 min in a Krebs-bicarbonate medium containing 20 mM dihydroxyacetone, 4 mM octanoate additionned or not by 50 µM DNP, and in presence of radiolabelelled probes : (i) cell and mitochondrial matrix volumes were determined by subtracting either [^{14}C]-carboxymethylinulin or [^{14}C]-mannitol spaces respectively from water space determined by ^3H_2O, (ii) mitochondrial membrane electrical potential difference measurement in intact cells were performed by using distribution of [^{3}H]-TPMP$^+$ [8].

Rat liver mitochondria were isolated as described in [9], and incubated in a medium containing 250 mM sucrose, 1 mM EGTA, 10 mM Tris-HCl (pH 7.2), 5 mM Tris-Pi, 6.25 mM glutamate, 1.25 mM malate and 1 mM ADP at 37°C. The respiratory rate was modulated by addition of carboxyatractyloside (a quasi-irreversible inhibitor of the ANC).

ATPase activity was measured at 37°C in a medium containing 250 mM sucrose, 1 mM EGTA, 10 mM Tris-HCl (pH 7.2), 5 mM succinate, 5 mM ATP, 2 µg/ml myxothiazol and 0.4 µM CCCP. ATP hydrolysis was quantified by determination of Pi production [7].

Western blot analysis were performed on isolated mitochondria with rabbit antibodies raised against an 11-residue synthetic peptide corresponding to the C-ter sequence of the ANC [10]. After incubation with peroxydase-labeled protein A, the immunoreactive proteins were detected by autoradiography.

Results are expressed as mean±S.E.M., statistical analysis were done by using ANOVA.

RESULTS AND DISCUSSION

Comparison between DNP-uncoupling and effect of PUFA deficiency.

Condition	Control		PUFA deficiency		Control+DNP	
	cyto	mito	cyto	mito	cyto	mito
JO_2	30.30±1.14		40.10±1.51$^{\bullet}$		40.80±1.52$^{\bullet}$	
Volume	0.98±0.06	0.31±0.02	0.69±0.09$^{\bullet}$	0.63±0.03$^{\bullet}$	0.95±0.08$^{\$}$	0.33±0.01$^{\$}$
ATP/ADP	6.17±0.53	2.08±0.11	4.23±0.11$^{\bullet}$	1.96±0.03$^{\bullet}$	1.46±0.18$^{\bullet\$}$	1.66±0.12$^{\bullet\$}$
Pi (mM)	4.59±0.73	15.68±0.34	8.46±1.35$^{\bullet}$	7.39±0.35$^{\bullet}$	5.14±0.90$^{\$}$	14.88±0.63$^{\$}$
ΔG'p	51.70±0.39	45.60±0.08	49.21±0.40$^{\bullet}$	47.40±0.12$^{\bullet}$	47.63±0.64$^{\bullet\$}$	45.15±0.18$^{\bullet\$}$
ΔΨ (mV)	-176±4		-147±8$^{\bullet}$		-151±8$^{\bullet}$	
$\frac{\Delta G'p\ cyto}{\Delta G'p\ mito}$	1.1338±0.0079		1.0383±0.0088$^{\bullet}$		1.0552±0.0168$^{\bullet}$	

Table 1: Hepatocytes from control and PUFA deficient rats were incubated as described in Materials and Methods. Oxygen uptake are expressed in natom O/min/mg dry mass, volume in µl/mg dry mass. ΔG'p (kJ/mol) were calculated from ATP, ADP and Pi concentrations in cytosolic and mitochondrial compartments. Results are mean±S.E.M. (n=8). $p<0.05$: $^{\bullet}$ vs control, $^{\$}$ vs PUFA deficiency.

As already described in [2], Table 1 shows that hepatocyte oxygen uptake was significantly increased (by 30%) in the PUFA-deficient group compared to controls as well as the mitochondrial volume while the the cytosolic space was significantly reduced. Measurements of cytosolic and mitochndrial ATP, ADP and phosphate led us to calculate cytosolic and mitochondrial ΔG'p. Cells from PUFA exhibited a significant decrease in cytosolic ΔG'p whereas ΔG'p increases in mitochondria. The ratio of cytosolic ΔG'p over mitochondrial ΔG'p (ΔG'p ratio) is the consequence of both the electrogenic nature of the ANC and the degree of displacement from equilibrium. This ratio as well as the electrical potential difference across the mitochondrial membrane (ΔΨ) were lower in the PUFA deficient group. Protonophore (2,4-dinitrophenol or DNP) was added (50 µM) in order to mimic precisely the effect of PUFA deficiency on respiration. Table 1 shows that for similar respiratory rate and ΔΨ, cytosolic and mitochondrial ΔG'p were significantly higher in PUFA deficient than in DNP-uncoupled controls. So we can concluded that PUFA deficiency does not behave as a slight « *protonophoric like* » effect. While, a classical protonophore uncoupling is accompagnied by a decrease in the three forces involved in the oxidative phosphorylation pathway (*i.e.* mitochondrial redox potential, ΔG'p and the protonmotive force) [11], two of these forces are not affected by PUFA deficiency : mitochondrial redox potential (see [2]), and mitochondrial ΔG'p (see table1). Hence the value of the ΔG'p ratio in PUFA deficient cells is probably the result of kinetic changes at the level of enzymes involved in the phosphorylating pathway (ANC, ATPase or phosphate carrier), rather than a pure effect *via* protonmotive-force change.

Effect of PUFA deficiency on ANC

State 3 respiratory rate of liver mitochondria isolated from control and PUFA-deficient rats has been titrated with carboxyatractyloside (see Figure 1).

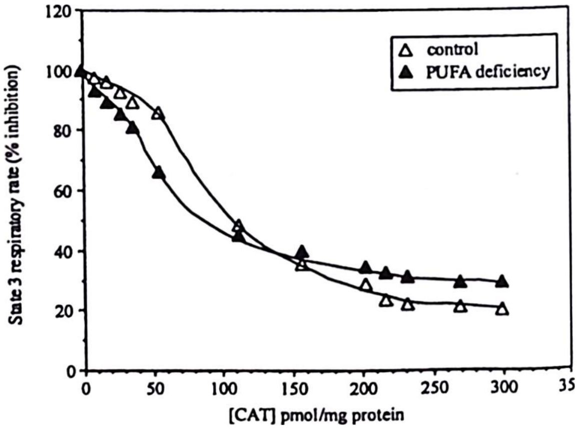

Figure 1. Titration of state-3 mitochondrial preparations in each respiration of liver mitochondria group isolated from control and PUFA-deficient rats by carboxyatractyloside (CAT).
Mitochondria were incubated as described in Materials and Methods. The respiratory rate, expressed as percentage of state 3 respiratory rate, was modulated by addition of CAT. One typical experiment is shown (similar results were obtained in seven other experiments from four rat liver mitochondrial preparations in each group).

ANC FLUX CONTROL AND CATMAXIMAL INHIBITION

Condition	$C^{JO_2}_{ANC}$	Imax
Control	0.29±0.04	144±11
PUFA deficiency	0.52±0.06$^{\bullet}$	109±12

Table 2. Imax (pmol/mg proteins) correspond to minimal inhibitor's quantity necessary for maximal inhibition of the respiratory rate. Results are mean±S.E.M. (n=8). $^{\bullet}$ p<0.01 vs control.

The flux control coefficient of ANC is significantly higher in PUFA deficiency while the maximal inhibition in state 3 respiration was obtained for a similar amount of inhibitor.

Moreover, western blot analysis have been performed on isolated mitochondria with anti-C-terminal peptide antisera against ANC. This antiserum labelled specifically a zone of molecular weight of about 30 000 and corresponding to the ANC protein [10]. Our results show that when the same concentration of mitochondria is used in blot, the quantity of immunoreactive ANC is almost unchanged in PUFA deficient *versus* control group (84±14 % of control group content, NS).

Hence, given the fact that CAT and ANC binding is in a one-to-one stoichiometry, the non significant change in Imax may be interpreted as a lack of effect of PUFA deficiency on ANC transcription. Moreover, the significant effect on ANC flux control coefficient is in favor of an effect on ANC activity. Given the large change observed in lipid content of the mitochondrial membrane in PUFA deficient cells [1], these results could be interpreted as an effect of membrane phospholipids on ANC activity [12].

Effect of PUFA deficiency on ATPase/ATP synthase

ATPase/ATPsynthase activity was significantly higher in PUFA deficient than in control group : 41±1 versus 30±1 nmoles Pi/min/mg proteins respectively (p<0.001). Such increase in ATPase activity could explain our previous report concerning the lack of change in state-3 $J_{AT}P$ together with a strong decrease in p in isolated mitochondria from PUFA-deficient rats [1]. Moreover the increase in ATPase/ATPsynthase activity may also explain the increase in mitochondrial ATP/ADP ratio, but the discrepancy in the change of cytosolic and mitochondrial G'p between DNP-uncoupled controls and PUFA-deficient cells remains to be explained.

In conclusion, PUFA deficiency induces several changes in oxidative phosphorylation which are much more complex than a single protonophoric effect. This effect of PUFA deficiency includes several membranal enzyme changes (glycerol-3-phosphate dehydrogenase [2], ATPase, ANC), as well as changes in ANC kinetic properties. The effect of PUFA-deficiency on Pi concentration (increase in the cytosol and decrease in the matrix) is in favor of an effect on the phosphate carrier. These modifications could be related to membrane lipid. Taken together, these results show that PUFA deficiency leads to an increased respiratory rate, a decrease in protonmotive force, an increase ATPase/ATPsynthase activity and an inhibition of ANC. Inhibition of

ANC together with activation of ATPase/ATPsynthase appear to play a crucial role for increasing mitochondrial phosphate potential. Studies are in progress in order to discriminate between an effect due to a change in protein transcription (change on isoform of ANC) or to an effect of membrane lipid composition. Hence it is not possible to propose that PUFA deficient cells are modified solely by one unique and well characterized alteration.

REFERENCES

[1] Fontaine, E.M., Moussa, M., Devin, A., Garcia, J., Ghisolfi, J., Rigoulet, M. and Leverve, X.M. (1996) Biochim. Biophys. Acta 1276, 181-187.

[2] Piquet, M.A., Fontaine, E., Sibille, B., Filippi, C., Keriel, C. and Leverve, X.M. (1996) Biochem. J. 317, 667-674.

[3] Berry, M.N.and Friend, D.S. (1969) J. Cell. Biol. 43, 506-520.

[4] Groen, A.K., Sips, H.J., Vervoorn, R.C. and Tager, J.M. (1982) Eur. J. Biochem. 122, 87-93.

[5] Zuurendonk, P.F. and Tager, J.M. (1974) Biochim. Biophys. Acta 333, 393-399.

[6] Argaud, D., Roth, H., Wiernsperger, N., and Leverve, X.M. (1993) Eur. J. Biochem. 213, 1341-1348.

[7] Summer, J.B. (1944) Science 100, 413-418.

[8] Espié, P., Devin, A., Guérin, B. and Rigoulet, M. (1997) J. Bioenerg. Biomembr. 29, 591-601.

[9] Klingenberg, M. and Slenczka, W. (1959) Biochem. Z. 331, 486-495.

[10] Brandolin, G., Boulay, F., Dalbon, P. and Vignais, P.V. (1989) Biochemistry 28, 1093-1100.

[11] Leverve, X., Sibille, B., Devin, A., Piquet, M.A., Espié, P. and Rigoulet, M. (1998) Molecular and Cellular Biochemistry (in press).

[12] Streicher-Scott, J., Lapidus, R., Sokolove, P.M. (1994) Arch. Biochem. Biophys., 315, 548-554.

HIERARCHICAL CONTROL OF DNA SUPERCOILING

Jacky L. Snoep[1], Coen C. van der Weijden[1], Heidi W. Andersen[2], Peter R. Jensen[2] and Hans V. Westerhoff[1]

[1] Molecular Cell Physiology, Free University, BioCenter Amsterdam, De Boelelaan 1087, 1081 HV Amsterdam, The Netherlands.
Tel# +31 20 4447192; Fax# +31 20 4447229; E-mail js@bio.vu.nl
2 Department of Microbiology, Technical University of Denmark, Building 301, DK-2800 Lyngby, Denmark

INTRODUCTION

DNA isolated from the prokaryotic cell is usually negatively supercoiled, i.e. the linking number of covalently closed DNA molecules is lower than it would be in the relaxed state [1]. There are at least two enzymes which have the potential to control the level of DNA supercoiling: topoisomerase I, a type I topoisomerase, which relaxes negatively supercoiled DNA, and DNA gyrase, a type II topoisomerase, which introduces negative supercoils in the DNA by coupling the reaction to ATP hydrolysis.

The genes encoding topoisomerase I (*topA*) and DNA gyrase (*gyrA* and *gyrB*) are among the genes that respond to changes in the level of DNA supercoiling: the expression of the DNA gyrase is highest when the level of DNA supercoiling is low [7] and the expression of topoisomerase I, is stimulated by high levels of negative supercoiling [8]. This feedback on the level of gene expression may contribute to a homeostatic control of DNA supercoiling [7].

Homeostatically controlled systems have not been widely studied in terms of control analysis. In traditional Metabolic Control Analysis [5;2] the levels of enzymes are considered to be parameters of the system i.e. fixed. If the control exerted by the topoisomerases on DNA supercoiling is attenuated through genetic feedback loops, then the concentrations of these two enzymes will not remain constant. Hierarchical Control Analysis [12], is the extension to Metabolic Control Analysis that does accept variations of enzyme concentrations as regulatory mechanisms.

Here we modulate the concentrations of DNA gyrase and topoisomerase I in growing *Escherichia coli* cells, and ask to what extent DNA gyrase and topoisomerase I control the steady state level of DNA supercoiling. Furthermore, using Hierarchical Control Analysis, we show the relationship between direct metabolic control (with constant enzyme levels) and hierarchical control (which does include regulation through transcription).

METHODS

Bacterial strains

Chromosomal promoters of the DNA gyrase and of the topoisomerase I were replaced by inducible promoters in *E. coli* MC4100 [4].

Plasmid extraction and supercoiling assay

Cell cultures were sampled into 80 °C phenol and plasmid DNA (pBR322) was extracted using standard isopropanol precipitation [3]. DNA samples were subjected to agarose electrophoresis in the presence of chloroquine. After electrophoresis, DNA was transferred to Hybond membranes and hybridised with digoxigenin labeled pBR322. Labeling and detection with CSPD was performed according to the Boehringer Mannheim recommendations. After digitizing the film, the average linking number was determined as described by Van Workum *et al* [7]. DNA supercoiling was assessed in terms of the active linking number aLk (i.e., the difference between the linking number of coumermycin/rifampicin treated cells and that of the cells under study).

DNA gyrase and topoisomerase I concentration

The DNA gyrase and topoisomerase I content of the cells was estimated by quantitative Western blotting using an antibody against the Gyr A subunit and topoisomerase I respectively.

RESULTS AND DISCUSSION

Control of gyrase on DNA supercoiling

In the controllable strain gyrase was manipulated from 5% to 250% of wild type and effects on DNA supercoiling were quantified. DNA supercoiling is expressed as the active linking number, the more negative the aLk, the more underwound, the more negatively supercoiled the DNA is. An increase in gyrase concentration is clearly correlated with an increase in negative supercoiling. Three different curves were fitted through the experimental data and from these curves the control coefficients were calculated by differentiation (Figure 1). The control of gyrase rapidly decreased with increasing concentrations of the enzyme but the control never became zero. Importantly at wild type levels of gyrase activity the enzyme has a control of 0.18. The independent fitting of several curves show only a small variation in this value (Fig 1). In addition to DNA supercoiling also growth rate, and ATP/ADP ratios were measured. There appeared to be no control on growth rate at wild type levels of gyrase and the ATP/ADP ratio was higher than 10 in the whole range (i.e. outside the range in which gyrase is sensitive towards changes in the ratio).

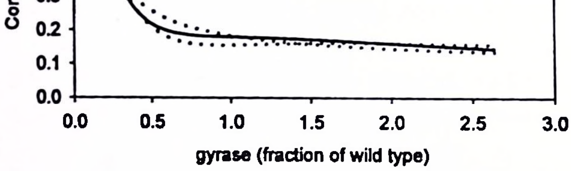

Figure 1: Control of DNA gyrase on DNA supercoiling.
Lines are derivatives of fitted curves through the experimental data. The fitted curve is an exponential decay curve: $y=a+b*\exp(-c*x)+d/(1+d*e*x)$. The values for a,b,c,d and e were respectively: -18.37, 8.951, 7.956, 9.437 and 0.072.
Several other curves were also fitted through the data points ; another decay function or a logaritmic polynomial (derivatives of functions are shown as dotted lines in the insert).

Control of DNA supercoiling by topoisomerase I

Preliminary experiments have been performed to determine the control of topoisomerase I on supercoiling. Again the expression of the enzyme of interest was modulated from the chromosome using a genetically modified strain. Expression levels ranged from 0.5 to 16 times the wild type level and effect on DNA supercoiling was determined (Figure 2).

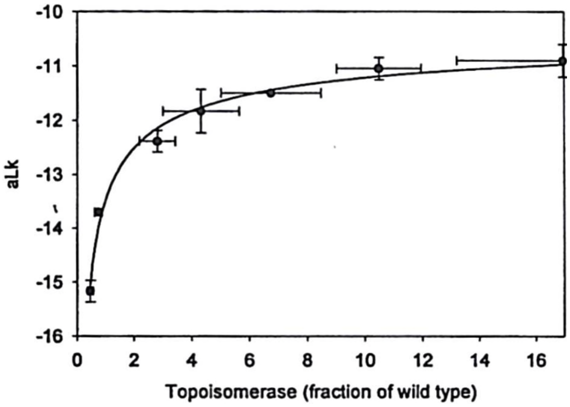

Figure 3: Dependence of DNA supercoiling on topoisomerase I expression.
Values are averages of three measurements. Fitted curve: y=a+b/x^(0.5), a=-10.17, b=-3.32

At wild type level the control of topoisomerase I on DNA supercoiling was estimated to be –0.12. Additional experiments with manipulation of the enzyme concentration closer to wild type have to be performed in order to come to a better estimation of the control coefficient.

Metabolic versus Hierarchical Control Analysis

The control exerted by DNA gyrase on supercoiling was lower than might have been expected for this far from equilibrium enzyme. Furthermore the sum of the control coefficients of the DNA gyrase and topoisomerase I appear not to add up exactly to zero. Since the degree of supercoiling can be seen as a concentration one would expect the control coefficients to add up to 0. The control by topoisomerase I was not determined very accurately and more experiments at lower concentrations of topoisomerase I are necessary.

We examined whether the low control of DNA supercoiling by gyrase could be attributed to the homeostatic control mechanism that has been proposed to exist for DNA supercoiling. Also the issue of the validity of the concentration summation theorem was raised in a theoretical analysis of this system.

The effect of DNA gyrase and topoisomerase I on DNA supercoiling is schematically represented in Figure 4.

Here X represents the degree of supercoiling and dashed arrows depict the interactions between the metabolic and the genetic level. In total there are three levels, a metabolic level with gyrase and topoisomerase I activity leading to supercoiling, and two genetic levels with transcription/translation and degradation for both DNA gyrase and topoisomerase I. These three levels are unconnected in the sense that there is no mass flow between them [9]. We will first treat each of these levels individually, leaving the regulatory interactions with the other levels out of consideration. This will lead to control coefficients that are local with respect to those levels. Such control coefficients will be denoted by lower case c, while the control coefficients that do take into account the regulatory interactions, i.e. the global control coefficients, will be denoted by capital C. The local control coefficients can be expressed readily into elasticity coefficients by standard methods. For the local control of gyrase on DNA supercoiling (metabolic level) or for the local control of the transcription of gyrase on the gyrase concentration (genetic level) one finds, (with X = -aLk):

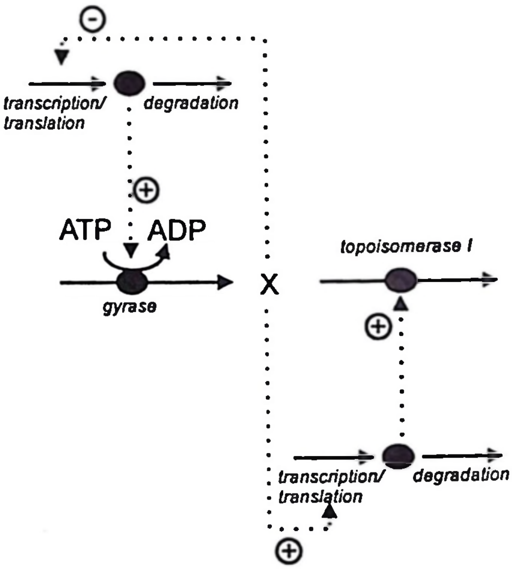

Figure 4: Model of the homeostatic control of DNA supercoiling by DNA gyrase and topoisomeraseI

$$c^{X}_{v\_gyr} = \frac{1}{\varepsilon^{v\_top}_{X} - \varepsilon^{v\_gyr}_{X}} \quad (1) \qquad c^{gyr}_{t\_gyr} = \frac{1}{\varepsilon^{d\_gyr}_{gyr} - \varepsilon^{t\_gyr}_{gyr}} \quad (2)$$

Assuming that transcription/translation is not product sensitive and protein degradation is first order, all of the elasticities on the genetic level become either 1 or 0 and the local concentration control coefficients become either 1 or –1:

$$c^{gyr}_{t\_gyr} = c^{top}_{t\_top} = -c^{gyr}_{d\_gyr} = -c^{top}_{d\_top} = 1$$

For the global control coefficients the interactions between the different levels becomes important [6;9]. For instance a direct change in transcription rate of gyrase will be affected by the resulting change in the degree of supercoiling. How such global control coefficients can be expressed in terms of local control coefficients, has been derived in [11]. For the global control coefficients of transcription rate of gyrase this results in:

$$C^{gyr}_{t\_gyr} = c^{gyr}_{t\_gyr} + \varepsilon^{t\_gyr}_{X} \cdot C^{X}_{t\_gyr} \text{(3)} \qquad C^{X}_{t\_gyr} = c^{X}_{v\_gyr} \cdot C^{gyr}_{t\_gyr} + c^{X}_{v\_top} \cdot C^{top}_{t\_gyr} \text{(4)}$$

$$C^{top}_{t\_gyr} = \varepsilon^{t\_top}_{X} \cdot C^{X}_{t\_gyr} \text{(5)}$$

These three equations contain three global control coefficients which can be expressed in terms of local control coefficients and thus in terms of elasticity coefficients:

$$C^{gyr}_{t\_gyr} = \frac{1 - \varepsilon^{t\_top}_{X} \cdot c^{X}_{v\_top}}{1 - \varepsilon^{t\_top}_{X} \cdot c^{X}_{v\_top} - \varepsilon^{t\_gyr}_{X} \cdot c^{X}_{v\_gyr}} = 1 - \frac{-\varepsilon^{t\_gyr}_{X}}{-\varepsilon^{t\_gyr}_{X} + \varepsilon^{t\_top}_{X} - \varepsilon^{v\_gyr}_{X} + \varepsilon^{v\_top}_{X}} \text{(6)}$$

With the same three equations the control of the transcription rate of the gyrase on the degree of supercoiling can be expressed in terms of elasticity coefficients:

$$C^{X}_{t\_gyr} = \frac{1}{-\varepsilon^{t\_gyr}_{X} + \varepsilon^{t\_top}_{X} - \varepsilon^{v\_gyr}_{X} + \varepsilon^{v\_top}_{X}} \text{(7)}$$

Similar expressions can be derived for the control by transcription of the topoisomerase I on topoisomerase concentration or degree of supercoiling:

$$C^{top}_{t\_top} = 1 - \frac{\varepsilon^{t\_top}_{X}}{-\varepsilon^{t\_gyr}_{X} + \varepsilon^{t\_top}_{X} - \varepsilon^{v\_gyr}_{X} + \varepsilon^{v\_top}_{X}} \text{(8)} \qquad C^{X}_{t\_top} = \frac{-1}{-\varepsilon^{t\_gyr}_{X} + \varepsilon^{t\_top}_{X} - \varepsilon^{v\_gyr}_{X} + \varepsilon^{v\_top}_{X}} \text{(9)}$$

For the control by the V_{max} of gyrase and topoisomerase (i.e. determined by a proportional modulation of both the forward and reverse V_{max} of this step without modulating the enzyme concentration) exactly the same expressions can be derived as for the respective transcription rates. This is due to the control of the transcription rates on the enzyme concentrations and the elasticity of the rate of enzyme activity to the enzyme concentration both being 1.

Equation (7) may help to understand why the control of gyrase on DNA supercoiling is relatively low: all the elasticities in the system contribute to the dynamic buffering of the degree of DNA supercoiling. The transcription rate sensitivity of both the DNA gyrase and the topoisomerase I add to the homeostatic effect that is already contained in the reaction rate sensitivities.

In relation to our second question concerning the validity of the concentration summation theorem it can be seen from equations (7) and (9) that the sum of the transcription rate control on X does sum up to 0. However in our experiments this is not measured, what we actually measure is a co-response coefficient: we manipulate the transcription rates and measure the covariance between the overexpressed enzyme concentration and the degree of supercoiling, i.e.:

$$^{t\_gyr}O^{X}_{gyr} = \frac{C^{X}_{t\_gyr}}{C^{gyr}_{t\_gyr}} = \frac{1}{\varepsilon^{t\_top}_{X} - \varepsilon^{v\_gyr}_{X} + \varepsilon^{v\_top}_{X}} \text{(10)}$$

and similarly for the topoisomerase I transcription rate:

$$ {}^{t\_top}O^{X}_{top} = \frac{C^{X}_{t\_top}}{C^{top}_{t\_top}} = \frac{-1}{-\varepsilon^{t\_gyr}_{X} - \varepsilon^{v\_gyr}_{X} + \varepsilon^{v\_top}_{X}} \quad (11) $$

These two co-response coefficients do not add up to zero unless absolute magnitudes of the elasticities of the transcription rate for X of the two enzymes equal one another. In the case of the experimentally determined control coefficients this appears to be almost the case. Interestingly in these co-response coefficients the elasticity of the transcription rate of the manipulated enzyme has canceled out. This is important as this elasticity can not be determined directly in the genetically engineered strains in which the native promoter has been replaced by an artificial promoter.

CONCLUSIONS

In this contribution we have shown how the control distribution in a hierarchically controlled system can be analyzed. Although the system that was chosen as an example, i.e. DNA supercoiling and the action of DNA gyrase and topoisomerase I, is relatively simple, its analysis quickly becomes complicated. With the use of Metabolic and Hierarchical Control Analysis the regulatory interactions can still be studied rigorously and quantitatively interpreted.

REFERENCES

[1] Drlica, K. (1984) Microbiol. Rev. 48, 273-289.

[2] Heinrich, R., and Rapoport, T.A. (1974) Eur. J. Biochem. 42, 89 - 95.

[3] Jensen, P. R., Westerhoff, H. V. and Michelsen, O. (1993) EMBO J. 12, 1277-1282.

[4] Jensen, P.R., Andersen, H.W., Van der weijden, C.C., Vad, A., Jensen, L.B., Snoep, J.L. and Westerhoff, H.V. (1996) *in* BTK of the living cell, pp 305-310.

[5] Kacser, H. and Burns, J. A. (1973) *in* Rate control of biological processes (D.D. Davies, Ed.). Symp. Soc. Exp. Biol., 27, 65-104. Cambridge University Press, Cambridge.

[6] Kahn, D. and Westerhoff, H.V. (1991) J. Theor. Biol. 153, 255-285.

[7] Menzel, R., and Gellert, M. (1983) Cell 34, 105-113.

[8] Tse-Dinh, Y.-C. (1985) Nucl. Acid Res. 13, 4751.

[9] Van der Gugten, A.A. and Westerhoff, H.V. (1998) BioSystems 44, 79-106.

[10] Van Workum, M. , van Dooren, S.J.M. Oldenburg, N. Molenaar, D. Jensen, P.R. Snoep, J.L. and Westerhoff, H.V. (1996) Mol. Microbiol., 20, 351-360.

[11] Westerhoff, H.V., Jensen, P.R., Snoep, J.L. and Kholodenko, B.N. (1998) Thermochim. Acta 309, 111-120.

[12] Westerhoff H.V., Koster J.G., Van Workum M., and Rudd K.E. (1990) *In* Control of Metabolic Processes (Cornish-Bowden A., ed.), pp. 399 - 412, Plenum, New York.

34

CANCER CHEMOTHERAPY IN TERMS OF METABOLIC CONTROL ANALYSIS.

Jan Lankelma[1,2], *Hanke van der Wel*[1] *and Hans V. Westerhoff*[2]

[1]Dept Medical Oncology, Free University Hospital, P.O. Box 7057, 1007 MB Amsterdam, the Netherlands, and [2]Dept Molecular Cell Physiology, Free University, Amsterdam, the Netherlands (e-mail: j.lankelma@azvu.nl).

INTRODUCTION

Cancer can be seen as the result of a micro-evolutionary process, in which genetic and epigenetic changes and selective pressure lead to cells that lack proper feed-back growth control. Most agents used in the treatment against cancer induce cellular damage. Provided that the integrated circuits that normally respond to this damage (repair with a proper halting of cell cycle progression) fail, the extra damage reverts the selection process, in favor of normal cells.

Present-day knowledge on the biology of the cell and state-of-the-art technology has revealed many details concerning the response of intact cells to damaging agents (O'Connor et al., 1997). In some ways the cancer cells can be considered as unicellular organisms, communicating with the outside world. This outside world is dynamic. The cell may face a DNA-damaging agent (doxorubicin) at varying concentrations, changes in concentrations of oxygen and nutrients (and waste products), as well as varying impacts of growth factors and mechanical factors (Fig.1).

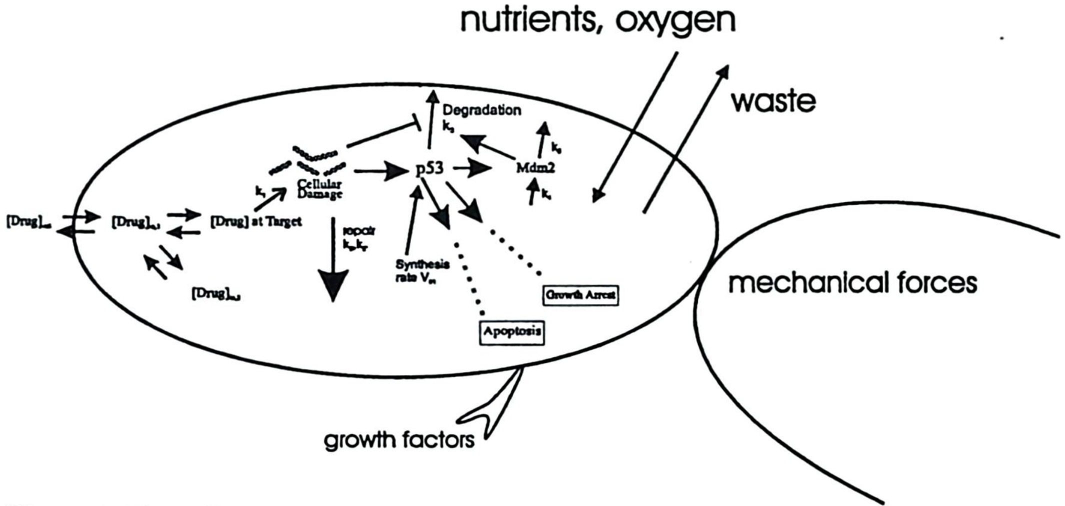

Figure 1. The cell and its dynamic environment.

Doxorubicin is one of the most effective anti-cancer agents. The transcription factor p53 plays a role in the cells' response to the induced damage (Hall, 1996). Changes in expression of p53 after transfection has dozens of downstream effects (Polyak, 1997 and http://welchlink.welch.jhu.edu/~molgen-g/P53-SAGE.HTM). Although in vitro tumor cell lines are not the same as cancer cells in their *in vivo* environment, some pathways and functional responses of the latter will remain intact *ex vivo*. Metabolic control analysis (MCA) has helped to elucidate what controls metabolic fluxes and why. We are examining whether MCA may play a similar role in cancer-cell biology. Here we present a first step in terms of the interpretation of the control of cell number by modulation of cellular p53 concentrations.

MATERIALS AND METHODS

Human MCF-7 breast cancer cells (with wild-type p53) were grown in Dulbecco's Modification of Eagle's Medium (ICN), supplemented with 7.5% fetal calf serum (Gibco BRL/Life Technologies).

Doxorubicin was purchased from Montedison Holland BV (Rotterdam, the Netherlands).

Western blot analysis was carried out after SDS-PAGE gel electrophoresis and blotting to PVDF (Transblot, Bio-Rad), using the DO-7 monoclonal antibody against p53 (DAKO). Protein/antibody detection was carried out with enhanced chemiluminescence (ECL+Plus kit) on Hyperfilm ECL (Amersham), and signals were analyzed using a densitometer 690 and Molecular Analyst software (Bio-Rad).

RESULTS AND DISCUSSION

The sensitivity of the cell killing process with regard to changes in doxorubicin concentration ([S]) is expressed by the response coefficient

$$R^N_S = \lim_{\Delta S \to 0} ((\Delta N/N)/(\Delta[S]/[S]))$$

in which: N = number of cells measured during/after drug exposure at the same time as the control; in the control the number of cells was measured after three doubling times (3-5 days); [S] = drug concentration.

To establish the role of p53 in this process we have defined the control coefficient as

$$C^N_{k_{tr}} = d(\ln N)/d(\ln k_{tr})$$

in which: k_{tr} = transcription rate constant induced by p53. The response of transcription to changes in p53 concentration may be quantified in terms of an elasticity coefficient $\varepsilon^{k_{tr}}_{[p53]}$.

The relative correlation between both growth inhibition and [p53], when doxorubicin concentration is modulated, may be quantified in terms of the co-response coefficient (Hofmeyr, 1993):

$$^{[S]}O^N_{[p53]} = R^N_S / R^{[p53]}_S$$

In a model in which doxorubicin affects the cell number only through the p53 concentration, this co-response coefficient should equal $^{[S]}O^N_{[p53]} = C^N_{k_{tr}} \varepsilon^{k_{tr}}_{[p53]}$.

For human MCF-7 breast cancer cells fig. 2 shows the measured growth after a 2hr doxorubicin exposure, as well as cellular p53 concentrations, at 4hr from the start of doxorubicin exposure, as determined by (semi-)quantitative Western blotting. At the latter time point no overt cellular toxicity of doxorubicin was observed. It can be concluded that around the IC_{50} the co-response coefficient ${}^{[S]}O^{N}_{[p53]}$ is maximal.

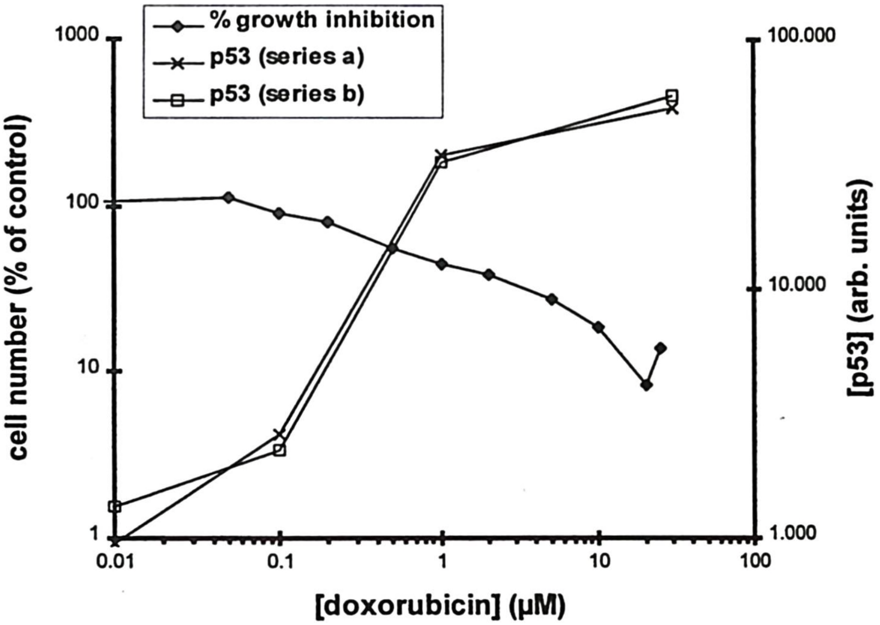

Figure2. Cell number (as % of control) after a 2h doxorubicin exposure at the indicated concentrations (left y-axis) and cellular p53 concentrations (arbitrary units, data from duplo samples, measured on two films a and b), measured at 4h after the start of doxorubicin exposure.

From the functioning of p53 as a tetramer (Jeffrey, 1995) a steep dependence of k_{tr} on the p53 concentration should be expected provided that most of p53 is present as the monomer with local elasticity (Kholodenko, 1997) $\varepsilon^{k_{tr}}_{[p53]}$ of approximately 4.

The log-derivative in Fig.2 gives around the IC_{50} R^{N}_{S} = -0.3 and $R^{[p53]}_{S}$ = 0.5-1.2 and a co-response coefficient ${}^{[S]}O^{N}_{[p53]}$ in the range of only -0.3 till -0.6. The absolute value is much smaller than 4, suggesting that most of p53 is present as tetramer in the p53 concentration range, as studied, or that p53 has low control over the cell number ($|C^{N}_{k_{tr}}| \ll 1$). The latter could result from the parallel activation of cell death pathways (the existence of which has been indicated in mutant-p53 cell lines). The direct involvement of p53 dimers would also decrease the value for $\varepsilon^{v_{tr}}_{[p53]}$. In the case of complete control $R_S^{[p53]}$ would then approach the measured value. Measurement of mRNA concentrations of genes directly downstream from p53 as a function of cellular p53 concentrations, may help sorting out the possible interpretations.

REFERENCES

O'Connor, P.M., Jackman, J., Bae, I., *et al.*, Cancer Res. (1997), **57**, 4285-4300.

Hall, P. A., Meek, D., and Lane., D.P., Int. J. Pathol. (1996), **180**, 1-5.

Polyak, K., Xia, Y., Zweier, J.L., *et al.* Nature (1997), **389**, 300-305.

Hofmeyr, J-H. S., Cornish-Bowden, A., and Rohwer, J.M., Eur. J. Biochem. (1993) **212**, 833-837.

Jeffrey, P. D., Gorina, S., Pavletich, N. P., Science. (1995) **267**, 1498-1502.

Kholodenko, B.N., Hoek, J.B., Westerhoff, H.V., Brown, G.C., FEBS Letters (1997) **414**, 430-434.

CONTROL OF THE $F_1 \cdot F_0$ ATPSYNTHASE ON CELL METABOLISM AND GROWTH IN *SACCHAROMYCES CEREVISIAE*

Léonie M. Raamsdonk, Jan A. Berden, Hans V. Westerhoff and Karel van Dam

E.C. Slater Institute, BioCentrum Amsterdam, University of Amsterdam, Plantage Muidergracht 12, NL-1018 TV Amsterdam, The Netherlands,
Telephone: +31 20 5255069, Fax: +31 20 5255124, E-mail: Leonie@chem.uva.nl

INTRODUCTION

The mitochondrial $F_1 \cdot F_0$ ATPsynthase plays a central role in free energy transduction. Under anaerobic conditions the yeast *S. cerevisiae* can produce ATP only via substrate level phosphorylation as no oxygen is present to act as the terminal electron acceptor in the respiratory chain. When yeast is grown aerobically on non-fermentable carbon sources (e.g. ethanol, lactate or glycerol), it solely depends on oxidative phosphorylation for the synthesis of ATP. However, when a fermentable carbon source is present in the medium (glucose, maltose etc.) ATP can be obtained *via* both substrate level phosphorylation and oxidative phosphorylation.

In galactose-grown yeast, about 20% of the metabolised galactose is completely oxidised to CO_2 and water, the remainder is fermented to ethanol. In glucose-grown yeast, the biogenesis of mitochondria is repressed. Under these conditions around 95% of the consumed glucose is fermented and only 3 to 5% is completely oxidised. This oxidation, however, may well account for almost 40% of the total ATP produced per glucose molecule consumed [1].

Yeast $F_1 \cdot F_0$ ATPsynthase consists of a proton-conducting F_0 unit and a catalytic F_1 unit, which are each built from several subunits. The catalytic sites are located on the β-subunits of the F_1 unit. To investigate the control of $F_1 \cdot F_0$ ATPsynthase on yeast metabolism, the *ATP2* gene, which encodes the β-subunit of the ATPsynthase, was deleted and the effect on cell metabolism and growth on glucose was examined. Subsequently, the *ATP2Δ* strain was complemented with the *ATP2* gene under the control of the MET25 promoter and the control of the $F_1 \cdot F_0$ ATPsynthase on cell metabolism and growth on non-fermentable carbon sources was investigated.

METHODS

The *Saccharomyces cerevisiae* wild-type strain CEN.PK113-12B (*MATa URA3 his3-Δ1 LEU2 trp1-289 MAL2-8c SUC2*) (obtained from Peter Kötter in Düsseldorf) and the *ATP2Δ* strain LRY7A (*MATa URA3 his3-Δ1 leu2-3 trp1-289 MAL2-8c SUC2 atp2Δ::LEU2*) were grown on YNB + 2% glucose and the required amino acids and samples were taken at $OD_{600} = 1$.

The *ATP2* complemented strain, equal to LRY7A plus a single copy plasmid with *ATP2* under the control of the MET25 promoter, was grown on YNB + 2% ethanol and 2% glycerol and the required markers to an $OD_{600} = 0.5$. Subsequently, methionine was added to a concentration of 1 mM and samples were taken every hour.

The cells were quenched in cold 50% (w/v) methanol (final concentration) and the intracellular metabolites were extracted as described in [2] and analysed for ATP and ADP. Samples were quenched in 5% (w/v) trichloroacetic acid (final concentration) and analysed for glucose. The oxygen consumption was directly measured in 1ml of culture with an oxygen electrode. The $F_1 \cdot F_0$ ATPsynthase activity was measured in concentrated cells ($OD_{600} = 50$) after treatment with glass beads at 4°C for 30 minutes [3]. The protein content of the culture was measured according to Lowry *et al.* [4].

RESULTS AND DISCUSSION

The *ATP2Δ* strain was not capable of growing on non-fermentable carbon sources and was devoid of any detectable level of $F_1 \cdot F_0$ ATPsynthase activity (Table 1.). No difference in growth rate on glucose was observed between the mutant strain and the wild-type. The yield of biomass, however, was about 30% lower in the ATPase deletion strain, which, since the specific growth rate was similar in both strains, may indicate a higher glycolytic flux in the ATPase deletion strain. Such a finding would contradict the general assumption that no Pasteur effect is present in growing *S. cerevisiae* cells [5,6], although Boumans *et al.* [7] demonstrated that batch grown *S. cerevisiae* cells can also exhibit the Pasteur effect.

	OD_{600}	Specific growth rate (h^{-1})	Intracellular metabolites			O_2 uptake µmol/min/g protein	Yield mg drw / g glc	$F_1 \cdot F_0$ ATPase mmol ATP/min /g protein
			ATP(mM)	ADP (mM)	ATP/ADP			
Wild-type	1.0	0.38	1.6	0.9	1.7	66	51	0.15
ATP2Δ	1.0	0.37	1.1	0.7	1.6	22	37	0.00

Table 1. Intracellular metabolites, oxygen consumption, yield and ATPsynthase activity in a wild-type strain and an *ATP2Δ* mutant (drw = dry weight; glc = glucose).

The rate of respiration measured during growth in the *ATP2Δ* strain was 66% lower than in the wild-type strain. This was remarkable as Jensen and Michelsen [8] showed that an *Escherichia coli* strain mutated in the $F_1 \cdot F_0$ ATPsynthase subunits had a 40% increased respiration rate and an 80% increased expression of the respiratory chain subunits compared with the wild-type strain. In this mutant strain, ATP/ADP ratios were also lower, whereas we found that in *S. cerevisiae* all the internal metabolites measured, including the concentrations of ATP and ADP, remained the same. The lower respiration rate may be caused by the sensitivity of the respiratory chain to a higher proton motive force in the absence of ATPsynthase activity. In *E. coli*, however, a higher proton motive force did not slow down the respiration rate [8]. Another explanation for the lowered oxygen consumption by the *ATP2Δ* strain may be a possible interaction between the respiratory units and the $F_1 \cdot F_0$ ATPsynthase. Boumans *et al.* [9] reported that, in contrast to mammalian systems, respiratory chain complexes in *S. cerevisiae* interact both functionally and physically and therefore behave as one unit. Consequently a deficiency in the bc_1 complex resulted in concomitant loss of cytochrome oxidase protein. Ozawa *et al.* (1985) [10] claimed to have isolated supramolecules consisting of both respiratory complexes and $F_1 \cdot F_0$ ATPsynthase. The possibility of stabilising interactions between respiratory chain complexes and the ATPsynthase will be further investigated.

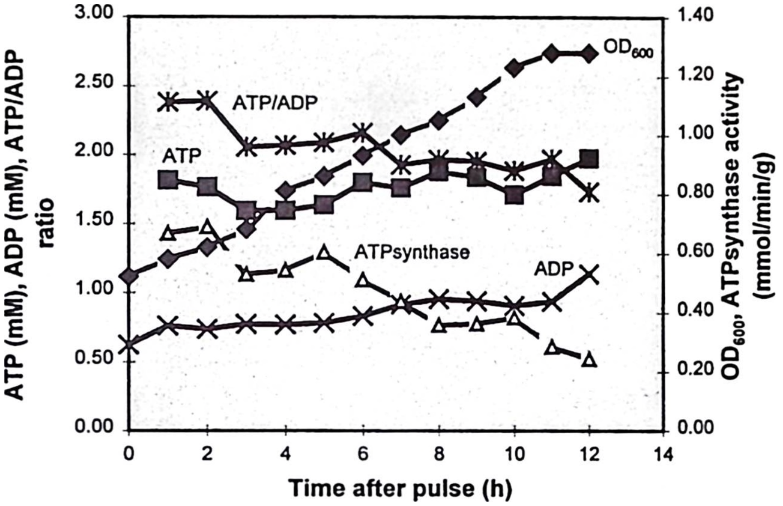

Figure 1:Results of a methionine pulse to the strain comprising *ATP2* under the control of the *MET25* promoter. At t=0 a methionine pulse (final concentration = 1mM) was given to exponential growing cells on YNB + 2% ethanol/glycerol medium. In this system methionine should repress the synthesis of the ATPsynthase. Every hour samples were taken to determine the OD_{600}, the intracellular ATP (mM) and ADP (mM) concentration and the ATPsynthase activity (mmol ATP/min/g protein).

To investigate the control of $F_1 \cdot F_0$ ATPsynthase on yeast metabolism and growth a strain was constructed in which the original gene encoding the β-subunit of ATPsynthase (*ATP2*) was deleted and was complemented by a single copy plasmid containing the *ATP2* gene behind the *MET25* promoter [11]. By varying the concentration of methionine in medium with non-fermentable carbon sources, we were able to reach wild-type growth rates in the absence of methionine down to no growth at all in the presence of 100 μM methionine (data not shown). Pulse experiments showed that after addition of 1 mM methionine to the mutant strain, the ATP and ADP concentrations were almost constant in time even when the level of ATPsynthase capacity was decreased to less than half of the wild-type level (Figure 1.). This suggests that the cell maintains the internal ATP concentration by decreasing the growth rate. The ATPsynthase could then exert control *via* a hypersensitivity of the growth for the level of ATP or the ATP/ADP ratio on non-fermentable carbon-sources.

ACKNOWLEDGMENTS

We would like to thank Michael C. Walsh for fruitful discussions and critical reading of the manuscript, and Monique van Gaalen for help with the methionine pulse experiments.

REFERENCES

[1] Lagunas, R. (1976) Biochim. Biophys. Acta. 440: 661-674
[2] Gonzalez, B., Francois, J., and Renaud, M. (1997) Yeast 13: 1347-1355
[3] Van der Bend, R.L. (1985) Thesis: 37-63
[4] Lowry, O.H., Rosenbrough, N.J., Farr, A.L. and Randall, R.J. (1951) J. Biol. Chem. 193: 265-275
[5] Lagunas, R. (1979) Mol. Cell. Biochem. 27: 139-146
[6] Lagunas, R. (1981) Trends Biochem. Sci. 6: 201-203
[7] Boumans, H., Berden, J.A., Grivell, L.A., and Van Dam, K. (1998a) Biochem. J. 331: 877-883
[8] Jensen, P.R. and Michelsen, O. (1992) J. Bac. 174: 7635-7641
[9] Boumans, H., Grivell, L.A., and Berden, J.A. (1998b) J. Biol. Chem. 273: 4872-4877
[10] Ozawa, T., Tanaka, M., and Suzuki, H. (1985) 13^e IUB Amsterdam
[11] Mumberg, D., Muller R., Funk, M. (1994) Nucleic Acids Res. 22: 5767-5768

36

HIERARCHICAL CONTROL OF THE H^+-ATPASE ON CYTOCHROME EXPRESSION IN *ESCHERICHIA COLI*

Sarah Koefoed[1], *Peter R. Jensen*[2], *Louis Egger*[1], *Hans V. Westerhoff*[1] *and Jacky L. Snoep*[1]

1 Department of Molecular Cell physiology, Biocentrum, Free University, De Boelelaan 1087, NL-1081 HV Amsterdam, The Netherlands, Phone: +31 20 4447192
Fax: +31 20 4447229, E-mail: saark@bio.vu.nl
2 Department of Microbiology, Technical University of Denmark, Building 301, DK-2800 Lyngby, Denmark

INTRODUCTION

Under aerobic growth conditions *Escherichia coli* synthesises ATP mainly via oxidative phosphorylation. Reduction equivalents, formed during catabolism, are oxidised via the respiratory chain, thereby pumping protons across the membrane. The resulting proton gradient is used by the H^+-ATPase for the synthesis of ATP, giving the H^+-ATPase a central role in energy metabolism in the cell. The H^+-ATPase has no control on growth rate in glucose grown cells, and very little control in succinate grown cells [1, 2]. Also the control on glycolytic flux was very small. An increase in cytochrome levels was observed when the *atp* operon was deleted, suggesting a homeostatic control mechanism [3, 4]. In this mechanism a decrease in H^+-ATPase would lead to an increase in H^+ and to an increase in turnover rate of this enzyme, masking its down modulation (figure 1). Here we present data on this regulatory loop. Our aim is to unravel the mechanism and strength of the regulation.

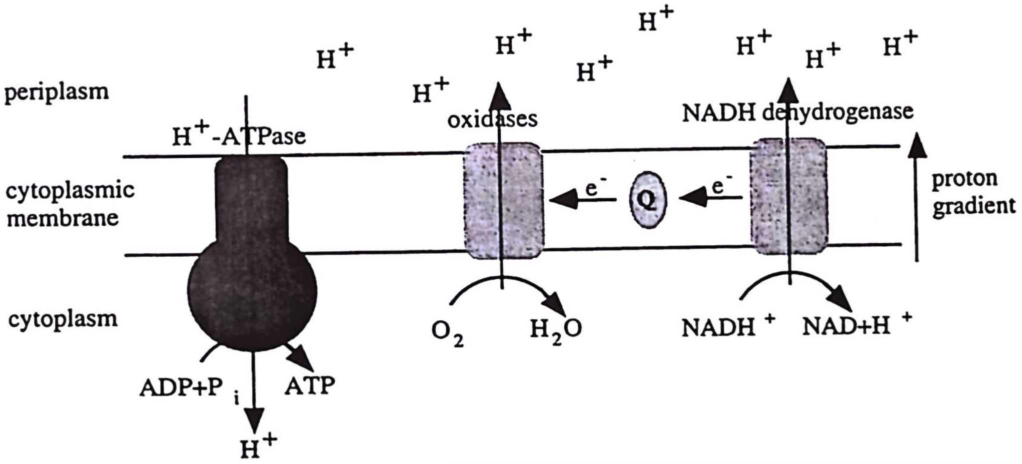

Figure 1. The respiratory chain of Escherichia coli. NADH is oxidised to NAD^+, with a transfer of electrons via Q to the terminal oxidases (cytochrome *bo* and *bd*) oxygen serving as terminal electron acceptor. During respiration a proton-gradient is generated which is subsequently used by the H^+-ATPase for ATP synthesis.

MATERIALS AND METHODS

Wild type *Escherichia coli* LM3118 and LM3113 where the *atp* operon is under the control of the *tacI* promoter have been described elsewhere [2]. SR13.1 is isogenic to LM3118 except that a part of the *lac*-operon has been deleted and a fusion of the *cyo* promoter to lacZ has been integrated into the *att* site. SR15.1 has the same *cyo* promoter-lacZ fusion in the *att* site but its chromosomal *atp* promoter has been replaced by the IPTG inducible *tacI* promoter. Cells were grown on minimal medium supplemented with 0.2 % glucose and 1 mg/l thiamine in shaking flasks. At an OD_{600} of 0.4, cells were harvested and washed with 50 mM phosphate (pH 7.5). Cells were resuspended to a high cell density (OD_{600}_50). Two spectra were taken at an Aminco DW2, reduced with dithionite and sparged with CO and subsequently reduced with dithionite. The cytochrome *o* heme content was determined by taking the CO reduced minus the reduced spectrum and measuring the absorption at 416 nm minus absorption at 400 nm [5]. Cytochrome *d* heme content was determined from the absorption of the reduced spectrum at 632 nm (figure 2). Cytochrome promoter activity was determined in duplo in a MUG assay according to Miller [6]. H^+-ATPase contents were determined on Western blots with an antibody specific to the ß subunit of the H^+-ATPase. All concentrations were calculated relative to the wild type level.

RESULTS AND DISCUSSION

Figure 2 shows that cytochrome *d* increased about ten times when H^+-ATPase concentration was down modulated to about 20 % wild type level.

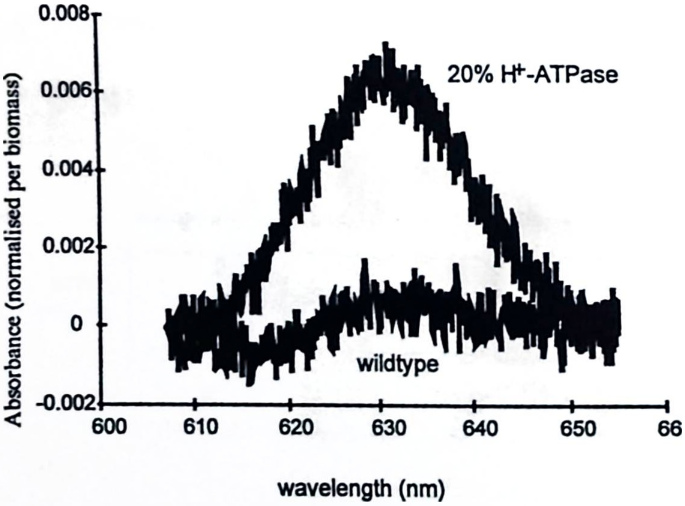

Figure 2. Increase of the *bd* type cytochrome upon down modulation of the H^+-ATPase. On the x-axis the wavelength and on the Y-axis the absorbance corrected for biomass.

Figure 3

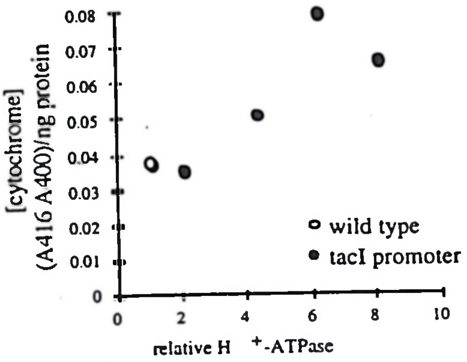

Figure 4

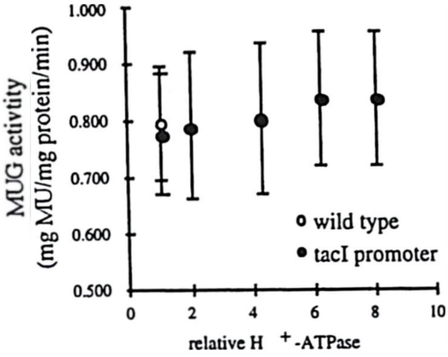

Figure 3 and 4. Response of cytochrome o and transcriptional cyo promoter activity to changes in H^+-ATPase levels in the cell. Open circles indicate the wild type levels, closed circles the mutant. X-abscise gives H^+-ATPase levels relative to wild type (set at 1), Y-ordinate gives heme incorporation, fig. 3 (derived from spectral analysis) or transcriptional activity (figure 4). Bars in figure 4 indicate standard deviation.

Figure 3 shows how differences in H^+-ATPase concentrations in the cell affected cytochrome *o* content. Spectral analysis showed an increase in cytochrome *o* heme content with an increase in H^+-ATPase, wild type *cyo* content was higher at the same H^+-ATPase levels. When *cyo* expression was monitored at a transcriptional level with promoter-*lacZ* fusion's, no significant effect on expression was observed (figure 4). However in the *atp* deletion strain an increase in heme concentration by 80% was observed [7]. The change in heme composition we observed upon changes in the H^+-ATPase concentration suggest a complex response of cytochrome *o* expression to modulations of H^+-ATPase in the cell. At this moment we are not able to decrease H^+-ATPase below wild type levels, these constructs will be made in the near future.

We have shown that the concentrations of terminal oxidases in *Escherichia coli* depend on H^+-ATPase levels. Thus the components of the respiratory network are coupled to each other, not only via the H^+ but also via transcription and translation. The differences in the heme measurements and the transcriptional activity of the *cyo* operon could be due to differences in heme incorporation in the cytochrome *o*. Also the position of the fusion on the chromosome could be of importance. We are currently investigating these options. One might speculate on the role of the decreasing cytochrome *bo* content while decreasing H^+-ATPase concentrations. This terminal quinol oxidase predominates at high oxygen tensions, and can translocate maximally 2 protons per electron [8], in contrast to the *bd* terminal oxidase which can translocate at the most 1 proton per electron [8]. If the cells uses the *bd* type oxidase instead of the bo type the Gibbs energy used for building up of the proton motive force stays the same, but as *bd* tranlocates only one proton the maximum attainable $\Delta\mu_{H^+}$ will be higher.

ACKNOWLEDGEMENTS

We wish to thank dr. O. Michelsen for stimulating discussions. This research was funded (SK) by the Netherlands Foundation for Chemical Research.

REFERENCES

[1] P.R. Jensen, O. Michelsen, H.V. Westerhoff, Proc. Natl. Acad. Sci. USA 90 (1993) 8068-8072.

[2] P.R. Jensen, H.V. Westerhoff, O. Michelsen, Eur. J. Biochem. 211 (1993) 181-191.

[3] P.R. Jensen, O. Michelsen, J. Bacteriol. 174 (1992) 7635-7641.

[4] P.R. Jensen, O. Michelsen, H.V. Westerhoff J. Bioenerg. Biomembr. 27 (1995) 543-554.

[5] W.J. Ingledew, R.K. Poole, Microbiological Reviews 48 (1984) 222-271.

[6] J.H. Miller in Experiments in Molecular Genetics, Chap. 3, 1972, pp. 43-80.

[7] P.R. Jensen, H.V. Westerhoff, O. Michelsen, EMBO J. 12 (1993) 1277-1283.

[8] A. Puustinen, M. Finel, T. Haltia, R.B. Gennis, M. Wikström, Biochemistry (1991) 3936-3942.

KINETICS OF PEROXIDASES IN GUINEA PIG BONE MARROW UNDER IMMUNOSTIMULATION

E. Keyhani(*), M.A. Zarei and T. Lashgarblooki-Livani

Institute for Biochemistry and Biophysics, University of Tehran, I.R. Iran
Tel: 00-98-21-611-3373; Fax: 00-98-21-640-4680
E-mail: keyhanie@ibb.ut.ac.ir or keyhanie@hemmat.ut.ac.ir

INTRODUCTION

Two peroxidases, eosinophil peroxidase and neutrophil peroxidase (myeloperoxidase: MPO) are present in bone marrow [1]. Eosinophil peroxidase (EPO) can injure cells and tissues directly in addition to its capacity to produce free radical species [2]. Eosinophils, like neutrophils, are cytotoxic to mammalian tumor cells and this cytotoxicity is mediated by the EPO-H_2O_2-halide system [3]. In contrast, human basophils do not contain EPO [4]. Both MPO and EPO have been purified by various authors and their properties have been investigated [5,6]. Inactivation of peroxidases in bone marrow by repeated administration of propylthiouracil has been reported [7]. Various methods for the mobilization of peripheral blood progenitor cells into circulation have also been described [8]. But, to our knowledge, stimulation of peroxidases in bone marrow and their kinetic properties has not yet been reported. Thus, the purpose of this research is to investigate the kinetic properties of peroxidases under immunostimulation in guinea pig bone marrow.

MATERIALS AND METHODS

1 ml sheep blood was injected subcutaneously to guinea pigs, daily, for 12 days. Front and hind legs were removed at times ranging from 4 to 30 days after the first injection, and smears were prepared from the bone marrow. The rest of the tissue was suspended in 9 $^0/_{00}$ NaCl, and pelleted at 3,000 rpm (1,000 g). The pellet was frozen at -20^{0}C for up to 48 hours. After 2 cycles of freeze-thawing, cells were suspended in 50 mM tris-HCl buffer (pH 7.4) containing 1 mM EDTA and 200 mg/l phenylmethylsulfonyl fluoride, and homogenized with 20 passes in a Potter homogenizer (with tight pestle). The homogenate was centrifuged at 20,000 g for 15 minutes and the pellet was discarded. Protein concentration was determined by the Biuret method. The isolation procedure gave reproducible results as the protein concentration in the samples was always about the same (2.28 +/- 0.12 mg/ml). Peroxidase activity was determined by o-dianisidine and guaiacol at 460 nm and 470 nm, respectively [8]; the extinction coefficients used were 11.3 $mM^{-1}.cm^{-1}$ for o-dianisidine and 26.6 $mM^{-1}.cm^{-1}$ for guaiacol. Assays were carried out at room temperature (~ 22-25^{0}C) using Aminco-DW2 and Milton-Roy spectrophotometers. Results were averages of 2 experiments (4 controls and 2 x 6 animals).

(*) also: Lab. for Life Sciences,Saadat Abade,Sarve Sharghi 34,19979 Tehran

RESULTS AND DISCUSSION

Fig. 1 shows variations in the percentage of various granules-containing cells in guinea pig bone marrow, at different times after immunostimulation. The percentage of basophil cells rose progressively with a 20-fold increase at day 12 after the 1st injection (from 0.5 % at day 0 to 10.5% at day 12); then the level dropped to roughly the initial control value. The percentage of eosinophil cells increased also, showing two peaks at day 8 and day 16. Thus a 2.5-fold increase in the percentage of eosinophil cells was seen at day 16 (from 15% at day 0 to 37% at day 16). Then the level dropped off but did not reach the initial control value at day 30. For neutrophil cells, there was a small and progressive decrease in the percentage, with a peak at day 16 (25% decrease), followed by an increase. The decrease in the percentage of neutrophil cells may not represent an actual situation in the bone marrow, since any increase in the percentage of eosino-basophil cells decreases the percentage of neutrophils.

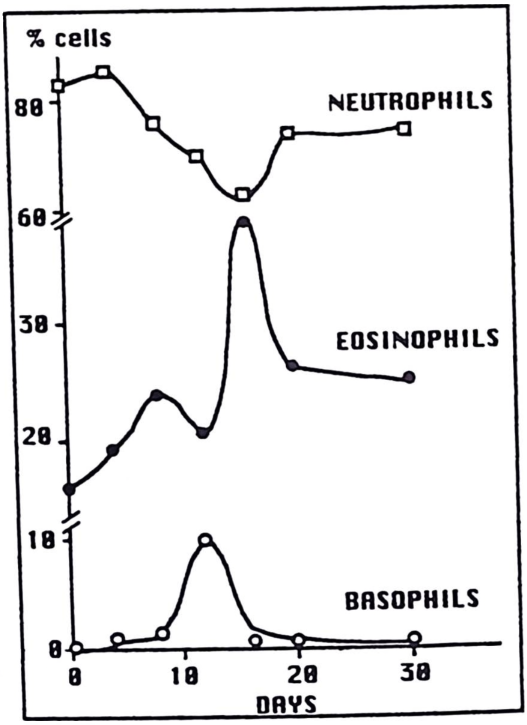

Fig. 1 - Changes in granulocytes populations in bone marrow after immunostimulation.

Figure 2 shows the actitivity of bone marrow peroxidases at different times after immunostimulation as measured by the peroxidation of o-dianisidine and guaiacol. Both substrates showed roughly the same pattern of enzyme activity. With o-dianisidine, peroxidase activity increased up to day 8, decreased slightly at day 12, increased again at days 16 and 20 and decreased at day 30. Thus 2 peaks of peroxidase activity at days 8 and 20 were seen and the maximum activity was nearly 7-fold that of the control at day 0 (~ 80 nmoles/sec/mg prot. for day 20 versus 12 nmoles/sec/mg prot. for day 0). With guaiacol as substrate, however, the maximum increase in activity at day 20 was over 30-fold the value of the control at day 0 (~ 27 nmoles/sec/mg prot. for day 20 versus 0.8 nmoles/sec/mg prot. for day 0). Since guaiacol was reported to be more sensitive than o-dianisidine to peroxidation by EPO [8], this differential increase indicated a preferential increase of EPO rather than MPO. This correlated with the results obtained when the peroxidases activity was assayed in the presence of 5 mM aminotriazole (AT) and reported in Table I. In the presence of guaiacol, inhibition was observed at days 0 and 12, when the peroxidative activity measured (preferentially due to EPO) was lowest. Interestingly, at day 20, when the EPO activity was highest, a stimulation was observed in the presence of AT. In contrast, at day 20, inhibition by AT was maximum when the peroxidative activity was measured by o-dianisidine.

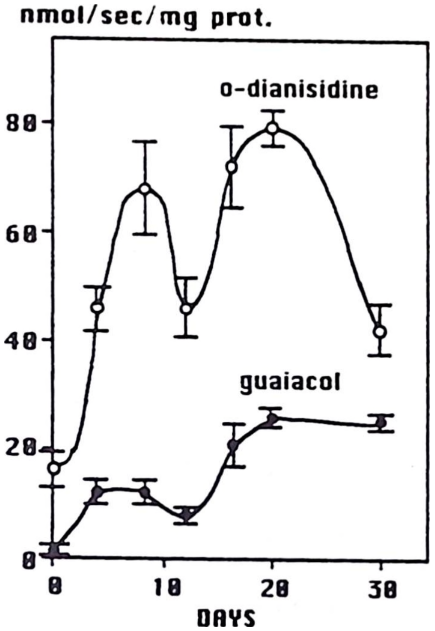

Fig. 2 - Determination of peroxidases activity in bone marrow at various times after immunostimulation. Activity was expressed as nmoles of substrate (o-dianisidine or guaiacol) peroxidized per sec. Values were averages of 2 experiments (2 animals); for each animal, measurements were done in triplicate.

Table II shows the values of V_{MAX} and K_M obtained with o-dianisidine. V_{MAX} was lowest at day 12 (21 nmol/sec/mg prot.) and highest at day 20 (48 nmol/sec/mg prot.). K_M was lowest for the control at day 0 (4 µM) and highest at day 4 (19 µM). As it was pointed out previously, there is no true V_{MAX} for peroxidase systems because the value depends upon the choice of H_2O_2 concentration [9]. Thus values of V_{MAX} and K_M obtained were not interpretable in terms of changes in the concentration of peroxidases under immunostimulation. In contrast, determination of k_4 as suggested in reference [9], may show a more accurate picture of the changes in peroxidases under immunostimulation. The reaction scheme is as follows:

$$E + H_2O_2 \xrightarrow{k_1} EO + H_2O$$
$$EO + \text{electron donor} \xrightarrow{k_4} E + \text{O-electron donor}$$

Table III shows changes in the value of k_4 under our experimental conditions for both o-dianisidine and guaiacol. With o-dianisidine, k_4 is similar at days zero (control) and 30, suggesting that the peroxidation of o-dianisidine is by the same kind of enzyme. In contrast, where under immunostimulation the amount of peroxidase increased, only one value of of k_4 was observed. With guaiacol, k_4 exhibited roughly similar values for

TABLE I

Effect of aminotriazole on the peroxidation of

	O-dianisidine		guaiacol	
	% inhib.	% stimul.	% inhib.	% stimul.(*)
Control	2	0	21	0
Day 4	3	0	5	0
Day 8	19	0	0	0
Day 12	14	0	26	0
Day 16	0	3	0	0
Day 20	17	0	0	10
Day 30	0	3	0	0

(*) inhib. = inhibition; stimul. = stimulation

TABLE II

	Control	Day 4	Day 8	Day 12	Day 16	Day 20	Day 30
VMAX (nmol/sec/mg prot.)	27.0 +/- 1.0	36.0 +/- 1.5	28.5 +/- 1.0	21.0 +/- 2.4	24.6 +/- 0.5	48.0 +/- 1.5	45.0 +/- 3.0
KM (µM)	4.0 +/- 0.5	19.0 +/- 3.0	10.5 +/- 1.5	8.5 +/- 1.0	16.0 +/- 2.0	8.5 +/- 1.0	9.0 +/- 1.0

days 4, 8 and 12 and higher but similar values for days 16, 20 and 30. Since guaiacol is more sensitive than o-dianisidine to peroxidation by EPO [8], the k_4 under our experimental conditions reflected changes in at least three EPO isoenzymes, one value for the control and two values for stimulation of EPO. On the other hand, o-dianisidine is more sensitive for the determination of MPO and showed possibly two isoenzymes with two different k_4, one for control and for day 30, and one for all others.

TABLE III

k_4

	0-dianisidine	guaiacol
	($x\ 10^5$)	($x\ 10^3$)
Control	13.0 +/- 2.0	0.045 +/- 0.005
Day 4	5.3 +/- 0.6	0.69 +/- 0.07
Day 8	5.4 +/- 0.5	0.68 +/- 0.06
Day 12	5.0 +/- 0.5	0.49 +/- 0.05
Day 16	3.0 +/- 0.6	1.17 +/- 0.12
Day 20	7.0 +/- 0.8	1.48 +/- 0.12
Day 30	13.8 +/- 1.6	1.46 +/- 0.15

(Enzyme concentration: mg prot./ml)

REFERENCES

1 Desser, R.K., Himmelhoch, S.R., Evans, W.H., Januska, M., Mage, M. and Shelton, E. (1972) Arch. Biochem. Biophys. 148, 452-465.
2 Spry, C.J.F., Kay, A.B. and Gleich, G.J. (1992) Immunology Today 13, 384-387.
3 Jong, E.C. and Klebanoff, S.J. (1980) J. Immunol. 124, 1949-1953.
4 Dvorak, A.M. (1994) J. Allergy and Clinical Immunol. 94, 1103-1134.
5 Sies, H. (1993) Eur. J. Biochem. 215, 213-219.
6 Lee, E., Hirauchi, M., Hosokawa, M., Sayo, H., Kohno, M. and Karya, K. (1988) Biochem. Pharmacol. 37, 2151-2153.
7 Brugger, W., Bross, K., Frisch, J., Dern, P., Weber, B., Mertelsmann, R. and Kanz, L. (1992) Blood 79, 1193-1200.
8 Cramer, R., Bisiacchi, B., De Nicola, G. and Patriarca, P. (1982) Exptl. Med.-Biol. 141, 91-99.
9 Pruitt, K.M., Kamau, D.N., Miller, K., Mansson-Rahemtulla, B. and Rahemtulla, F. (1990) Anal. Biochem. 191, 278-286.

Session 3

Biological Energy Transformations & Non-Equilibrium Thermodynamics and Kinetics

38

KINETICS, THERMODYNAMICS AND CONTROL ANALYSIS OF ATP HOMEOSTASIS IN CONTRACTING SKELETAL MUSCLE

J.A.L. Jeneson[1], *R.W. Wiseman*[1], *M.J. Kushmerick*[1,2] *and H.V. Westerhoff*[3,4]

Departments of Radiology[1], and Physiology and Biophysics[2], University of Washington School of Medicine, Seattle, WA 98195, U.S.A. Phone 1-206-685-2805, Fax 1-206-543-3495, email: utrecht@u.washington.edu); department of Microbial Physiology[3], Faculty of Biology, Free University, and E.C. Slater Institute[4], Biocenter, University of Amsterdam, Amsterdam, NL.

The study of biological energy transformations and its control has a rich history (1). Experimental work often focussed on skeletal muscle because of its intrinsic interest as a contractile organ; but because of the ~30-fold range in ATP flux that can be studied, skeletal muscle also constitutes a paradigm for testing principles of bioenergetics (2). Much of the work on muscle has focussed either on the 'ATP demand' side of energy balance, in particular on the dominant ATPase in muscle, actomyosin (AM) ATPase, or on the 'ATP supply' side, in particular the mitochondria. Here, we attempt quantitative integration of both facets to arrive at an understanding of the function of the muscle cell as a whole, and in particular observed limits to this function. The question will come up if a steady-state analysis of the ATPase network in muscle is a useful approach to address the limits of function.

Observations on limits to skeletal muscle function

The free energy level of skeletal muscle, ΔG_p (= $\Delta G_p^{o'}$ + RT ln([ADP][Pi]/ATP]), has been found to range between ~-64 kJ/mole in resting muscle and ~-54 kJ/mole in maximally activated muscle ((3) and Figure 1). Steady-states of energy balance outside this range have not been reported in the literature.

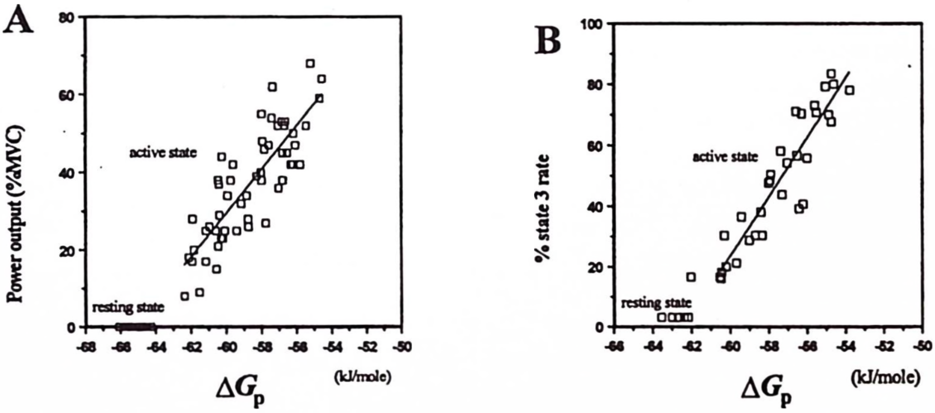

Figure 1. (A) relation between muscle power output during voluntary exercise, normalized to Maximum Voluntary Contraction (MVC) and the cytosolic phosphate potential ΔG_p for human forearm flexor muscle (4); (B) relation between mitochondrial ATP synthesis flux, normalized to the maximal rate (state 3 rate) and the cytosolic phosphate potential ΔG_p for human forearm flexor muscle (5).

The lower extreme of this free energy range, -66 - -64 kJ/mole (Fig. 1), is close to the static head potential generated by the mitochondria respiring on NADH-linked substrate (6), since the net ATP flux in resting muscle is only some 3% of state 3 rate (Fig. 1B). The upper extreme, ~-54 kJ/mole (Fig. 1), however, is less well explained. We found that at this ΔG_p value, corresponding to [ADP] = 0.085 mM and an ATP/ADP ratio of 95, mitochondria in human forearm flexor muscle were stimulated to 85% of maximum (state 3 rate) (Figure 1B). This upper extreme metabolic steady-state of the muscle was attained by voluntary exercise (bulb-squeezing at 0.33 Hz) at maximal steady-state workload (~60% MVC) (4) or by implementing a frequency of twitch contractions of 1.6 Hz (5). Increasing the workload of voluntary exercise above 60%MVC or, alternatively, increasing the frequency of muscle twitch contraction to 2.0 Hz did *not* result in a new steady-state of energy balance at which $|\Delta G_p| < 54$ kJ/mole and mitochondrial ATP synthesis flux > 85% state 3. Instead, this resulted in failure of the muscle to maintain function. The demanded sustained higher power-output could not be delivered. We found this same result in *in situ* studies of rat hindlimb muscle (*Wiseman and Jeneson, this Meeting*). This raises the question: which element(s) in the muscle is responsible for this energetic upper limit to cell function?

One school of thought in the literature that has addressed this issue from a perspective of understanding cardiac pump failure during hypoxia (3) and fatigue of skeletal muscle (7) has proposed a thermodynamic basis for this observed limit to muscle function. It is proposed that if $|\Delta G_p| < \sim 54$ kJ/mole, the free energy of ATP hydrolysis falls below the level required by the sarcoplasmic reticulum (SR) Ca^{2+}-ATPase to pump Ca^{2+} from the myoplasm back into the SR following a Ca^{2+} pulse upon muscle stimulation; consequently, the SR Ca^{2+} content would decrease, ultimately resulting in inactivation of the muscle (3,7).

A direct implication of this hypothesis of a thermodynamic basis for muscle fatigue is that a steady-state analysis of the network of ATPases in contracting muscle - i.e. a control analysis of ATP metabolism - should provide an adequate description and understanding of the full range of muscle function. Such an analysis is described below.

Control analysis of ATP homeostasis in contracting muscle

Methods. In our analysis, we modeled ATP metabolism in contracting skeletal muscle cells as a modular branched pathway, consisting of three enzyme modules (Table 1):

Table 1: overview of components in model of ATPase network in skeletal muscle

physiologic component	function in cell	Control Analysis equivalent	effect of ADP
mitochondria	ATP supply	module 1; flux J_1	stimulation
AM-ATPase	mechanical force generation	module 2; flux J_2	competitive inhibition
SR Ca^{2+}-ATPase	Ca^{2+} recovery by SR	module 3; flux J_3	mixed type inhibition

The common intermediate S_1 connecting the three ATPases is the cytosolic ATP/ADP ratio. The Ca^{2+} content of the SR was modeled as a system parameter - i.e. a constant. At steady-state, there are three fluxes in the pathway: J_1, J_2 and J_3 (Table 1) where the magnitude of flux J_1 is equal to that of the sum of J_2 and J_3. Using the summation, connectivity and branch theorems (8) for flux and metabolite control in this branched pathway, and the rate-dependent ATP/ADP elasticity of each module computed on basis of the steady-state kinetic equation, the control structure of the four system variables (fluxes J_{1-3} and the cytosolic ATP/ADP ratio) was solved as a function of respiration rate (*manuscript submitted*).

RESULTS AND DISCUSSION.

Over the physiological domain of steady-states of energy balance including the upper extreme steady-state at -54 kJ/mole (Figure 1), AM-ATPase and SR-ATPase each dominantly controlled their respective ATPase flux, as well as the mitochondrial ATPase flux. This means that over this sustainable range of muscle function, all ATPase fluxes in the cell associated with muscle contraction are only limited by external control (i.e. nerve stimulation), not by any internal control of ATP-supply limitation. Homeostasis of the cytosolic ATP/ADP ratio is achieved by means of equally shared control of the ATP/ADP ratio by the ATP consuming and ATP producing modules.

With respect to the flux control structure extrapolated for states outside the physiological domain of steady-states (corresponding to respiration rates exceeding 85% state 3 and cytosolic ATP/ADP ratios below 95), the analysis predicted that control of the activity of mitochondria maintaining the cytosolic ATP/ADP ratio, over mitochondrial flux J_1 and the SR ATPase flux J_3 would rapidly increase; for respiration rates greater than 95% state 3, the activity of mitochondria would in fact dominantly control these fluxes. However, force generation associated with AM-ATPase flux J_2 was predicted to remain insensitive to internal control of mitochondrial ATP/ADP ratio maintenance because of the very low ATP/ADP elasticity of AM-ATPase. As such, the analysis in this form did *not* predict loss of capacity of the muscle for force production by AM-ATPase at low free energy content. Does this now argue against a purely thermodynamic *viz.* steady-state approach to explain the empirical upper limit to muscle function on basis of a limiting free energy level of the cytosol?

A limitation in the present analysis was the constraint in the model that SR Ca^{2+} content was a system parameter, not a variable. However, removing this constraint may not be sufficient to properly amend the analysis. Instead we propose that in addition to the thermodynamics and steady-state kinetics of Ca^{2+} pumping by the SR Ca^{2+}-ATPase, the duty cycle and transient kinetics of muscle contraction *must* be considered to understand failure of sustained forearm flexor muscle function coinciding with the free energy level falling below 54 kJ/mole, and the twitch frequency approaching 2.0 Hz. The aspect of muscle twitch contraction of pulsed-activity (as opposed to a continuous activity) must be explicitly considered. For the time interval between subsequent twitches in combination with the particular cytosolic ATP/ADP ratio sensed by the enzyme will determine whether or not the SR Ca^{2+} content prior to a stimulation should be modeled as an invarying system parameter, or as a system variable. In fact, for the case of a sufficiently long time interval between subsequent twitches, SR Ca^{2+} recovery will be effectively *in*dependent of the ATP/ADP ratio. This introduction of a time dependence in the problem limits the value of steady-state arguments and analyses in the explanation of the upper limit to muscle function.

Supported in part by NIH Grants AR 41793 (to RWW) and AR 36281 (to MJK)

REFERENCES

1 Atkinson, D.E. (1977) *Cellular energy metabolism and its regulation*, Academic Press, San Diego
2 Kushmerick, M.J. (1995) *J. Bioenerg. Biomembr.* 27, 539-552
3 Kammermeier, H. (1988) *J. Mol. Cell. Cardiol.* 19, 115-118
4 Jeneson, J.A.L., Westerhoff, H.V., Brown, T.R., van Echteld, C.J.A., and Berger, R. (1995) *Am. J. Physiol.* 268, C1474-C1484
5 Jeneson, J.A.L., Wiseman, R.W., Westerhoff, H.V., and Kushmerick, M.J. (1996) *J. Biol. Chem.* 271, 27995-27998
6 Slater, E.C., Rosing J, and Mol, A. (1973) Biochim. Biophys. Acta 292, 534-553
7 Dawson, M.J., Gadian, D.G., and Wilkie, D.R. (1980) *J. Physiol.* 299, 465-484
8 Westerhoff, H.V. and van Dam, K. (1987) *Thermodynamics and control of biological free-energy transduction*, Elsevier, Amsterdam

FLOW-FORCE RELATION OF MITOCHONDRIAL OXIDATIVE PHOSPHORYLATION IN RAT FAST-TWITCH SKELETAL MUSCLE

RW Wiseman and JAL Jeneson

Department of Radiology, University of Washington Medical Center, Seattle, WA 98195 USA, phone: 206-685-1262, FAX: 206-543-3495, email: rwiseman@u.washington.edu)

INTRODUCTION

The relationship between oxidative phosphorylation flux and the cytosolic free energy of ATP hydrolysis has been described extensively [1, 2, 3]. In these models, the relationship has a near linear dependence over the operating range of the muscle where ATPase activity is well above the resting state [3, 4] corresponding to the quasi-linear NET range of the flow-force relation that is sigmoidal over its full range [5]. A second, much smaller quasi-linear domain exists, and corresponds to the near equilibrium region around the resting state. Near resting state, the metabolic load on the cell is largely limited to the cost of maintaining the membrane potential which is dominated by the activity of Na^+/K^+ ATPase. In contrast, in the mid-velocity domain in contracting skeletal muscle, an additional metabolic load, that being the activity of actomyosin ATPase and sarcoplasmic reticular Ca^{2+} ATPases (contractile ATPases). The metabolic demands over each of these domains are matched by mitochondrial oxidative phosphorylation and to a limited extent by glycolysis.

The purpose of this communication is to address the relationship between the phosphate chemical potential and contractile ATPase through the lower velocity range. To further our understanding of muscle function it is important to establish whether there are active states in muscle that do not correspond to either linear domains. More pointedly, do physical states exist at low velocities that deviate from the linearity established by the mid-velocity domain. If this were the case, it would argue that the control of the phosphate potential by the contractile ATPases is not dominant in these lower velocity regions. In contrast, if no such states exist, then it suggests that in any active working muscle the AM-ATPase dominates the control of phosphate potential. Essentially this argues for a switch-like behavior of the control structure of the muscle. Specifically, the onset of mechanical work activates actomyosin ATPase which was quiescent (comparable to adding a new enzyme to the control structure of the cell). We investigated this question using ^{31}P-NMR spectroscopy in a well-defined skeletal muscle system which we could electrically stimulate over the entire operating range thus controlling ATPase activity.

METHODS AND MATERIALS

Muscle Preparation and Stimulation Procedures: Animals were anesthetized with xylazine/ketamine and an intraperitoneal catheter was inserted through the abdominal wall permitting subsequent doses of anesthetic as needed during the experiment (judged by respiration rate). The right sciatic nerve was exposed, ligated and cut prior to placement into a bipolar cuff electrode for stimulation. In addition the knee joint was fixed in position with suture under the patellar tendon. The animal was then mounted in a custom built NMR probe at which time the achilles tendon was ligated and attached to a cantilever beam strain gauge to measure force output. This arrangement positioned the head of the gastrocnemius muscle directly over a three turn solenoidal surface coil (1 cm diameter) fashioned from 22 gauge copper wire. The tendon was passively loaded until stimulation gave a maximum output which was recorded using a Metrabyte DAS 1601G A/D board and monitored online using a Nicolet Storage oscilloscope.

NMR Spectroscopy: The probe was placed in a horizontal bore 4.7 T NMR spectrometer (Bruker Instruments). NMR spectra were acquired at 81 MHz after shimming on the available proton signal. For absolute quantification, fully relaxed phosphorus spectra were acquired with a 90° tip angle and 15s recycle delay. For spectroscopic measurements where higher time resolution was required spectra were acquired using a 45° tip angle and a 1.4 sec recycle delay (8 sec time resolution per 4 summed transients).

Experimental Protocol: Muscles were repeatedly stimulated for 10 minutes over a 5 Hz range of twitch frequencies. Briefly, after an initial baseline period, muscles were stimulated until a new steady-state of energy balance was attained and then allowed to recover to the resting state over a 15 min period. This cycle was repeated for a series of four stimulation frequencies and NMR spectra were continuously acquired. At the end of each experiment, muscles from both hindlimbs were removed and frozen for later analysis.

Mechanical Analysis: Digital force traces were analyzed using a commercially available PC program (DaDISP, DSP Development). After baseline correction, the tension-time integral (TTI) was determined for each force trace (in mN*sec). The TTI was constant during the stimulation period for each twitch over a range of 0.35-4.0 Hz.

Biochemical Analysis: Frozen muscles were pulverized in a liquid nitrogen cooled mortar. Tendon and connective tissues were then removed and the powdered muscle was placed in tared vials. Neutralized perchloric acid extracts were analyzed phosphocreatine and ATP by anion exchange HPLC whereas the free was analyzed by cation exchange HPLC in the same extract using methods we have previously reported [7,9].

NMR Data Analysis: Data acquired during rest-stimulation-recovery experiments were batch-processed using NMR1 software (New Methods Research, Inc.). Summed data transients were apodized using a matched Lorentzian filter, zero-filling to 4096 data points and Fourier transformed to the frequency domain. PCr, Pi and ATP were quantified by integration of each resonance. Intracellular pH (pH_i) was estimated from the chemical shift difference between the PCr and Pi resonances [8]. Analysis of the transient changes in PCr, Pi and pH_i during the time course of

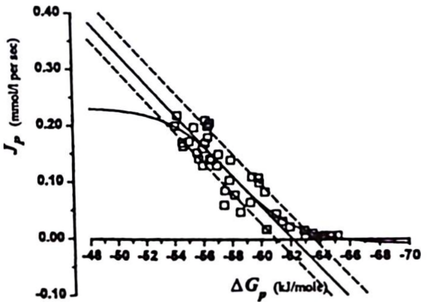

Figure 1. Flow-Force relation in rat fast-twitch skeletal muscle.The straight line is the Taylor expansion about the midpoint potential from the fitted sigmoid function. The dashed solid lines represent the 95% confidence interval of the Taylor expansion based on the extremes derived from the sigmoid fit.

contraction were analysed on a PC using Fig.P software (Elsevier Biosoft) for each twitch frequency. For analysis of metabolite content in each steady-state region for a given stimulation frequency, the corresponding FIDs were summed, and analysed in the time domain using Fitmasters software (Philips Medical Systems) [9].

RESULTS AND DISCUSSION

Figure 1 shows the resultant relation of Jp versus ΔGp over the entire operating range of the muscle.

Curve-fit analysis yielded a maximal flux of 0.231 +/- 0.05 mmoles ATP L^{-1} sec^{-1} and the mid-point potential was –58.1 +/- 0.9 kJ/mole in muscle cells. These values are not significantly different than those obtained from human forearm flexor muscles from previously reported studies [6].

Taylor expansion about the mid-point potential (linearization in mid-velocity range) is depicted as the solid straight line in Figure 1 which we have extrapolated to the x axis. The 95% confidence interval for the expansion is presented as dashed lines. We show that in the lower ATP synthesis domain (slightly above resting state) the confidence interval completely explains the observed data. Thus we are not able to statistically demonstrate there are active states in muscle that do not correspond to either NET quasi-linear domain. The implication for this result is that there is a rapid transition in the control state as contractile ATPases are activated and that this dominates the control of phosphate potential. Contributions from glycolytic ATP synthesis have not been corrected for and thus statistical validation will await further refinement of the analysis as this will influence both the slope and confidence interval of the present NET domain. Inspection of the data suggests that even with confidence intervals that are half the dimension of those presently shown, no active states would fall outside of this region. However, existence of transitional states is still important to establish as this would mean that activation of contractile ATPases gives rise to a gradual increase in their control over the phosphate potential. This would demonstrate that the shift in the control structure of the cell from other ATPases (such as Na+/K+ ATPase) to actomyosin ATPase was not switch-like but gradual and implies that the control of contractile ATPases over phosphate potential can vary over the operational range of working muscle.

REFERENCES

1 Connett, R.J. (1988) Am J Physiol 254, R949-R959.
2 Connett, R.J. and Honig, C.R. (1989) Am J Physiol 256, R898-R906.
3 Meyer, R.A. (1989) Am J Physiol 257, C1149-C1157.
4 Meyer, R.A. (1988) Am. J. Physiol. 254, C548-C553.
5 Wanders, R.J. and Westerhoff, H.V. (1988) Biochemistry 27, 7832-40.
6 Jeneson, J.A., Westerhoff, H.V., Brown, T.R., Van, E.-C.J. and Berger, R. (1995) Am J Physiol 268, C1474-84.
7 Wiseman, R.W., Moerland, T.S., Chase, P.B., Stuppard, R. and Kushmerick, M.J. (1992) Anal Biochem 204, 383-389.
8 Wiseman, R.W., Beck, T.W. and Chase, P.B. (1996) Am J Physiol 271, C878-86.
9 Wiseman, R.W. and Kushmerick, M.J. (1995) J Biol Chem. 270, 12428-12438.

OPTIMAL STOICHIOMETRIC DESIGNS OF ATP PRODUCING SYSTEMS USING GENETIC ALGORITHMS

Amadeus Stephani[1)], *Juan Carlos Nuño*[2)] *and Reinhart Heinrich*[1)]

[1)] Humboldt Universität zu Berlin, Institut für Biologie, Theoretische Biophysik, Invalidenstr. 42, D-10115 Berlin, Germany, Tel: +49 30 2093 8381, fax: +49 30 2093 8813, e-mail: amadeus=stephani@rz.hu-berlin.de

[2)] Universidad Complutense de Madrid, Facultad de Ciencas Químicas, Departamento de Bioquímica y Biología Molecular, E-28040 Madrid, Spain. Tel: +34 91 3944255, fax: +34 91 3944159, e-mail: juanca@solea.quim.ucm.es

INTRODUCTION:

In this contribution we continue the application of optimization principles in studying the standard design of metabolic systems ([1],[2],[3]). The main aim of the work is to reveal possible interdependences between stoichiometric and kinetic properties of energy metabolisms. The application of suitable optimization principles to (parts of) metabolic systems is motivated by the well known argument that in the course of evolution essential features of biological systems have been developed on account of a selective pressure they were subjected to.

Recently [4] we have proposed a model for the optimization of ATP producing unbranched pathways which is based on the following three assumptions: (i) All reactions involved in the system belong to one of the following five types (abbreviations in brackets): phosphorylation of a substrate by consumption of ATP (A), dephosphorylation of a substrate by production of ATP (a), phosphorylation of a substrate by an uptake of inorganic phosphate (P), dephosphorylation of a substrate by a release of inorganic phosphate (p), and an interconversion of a substrate into a product without any coupling to ATP or inorganic phosphate (U). (ii) The initial substrate and the end product of the pathway are nonphosphorylated, i.e. neither the first reaction can be a dephosphorylation reaction nor the last reaction can be a phosphorylation reaction. (iii) All substances involved in the pathway can be phosphorylated at most twice, i.e. there cannot take place more than two (de-) phosphorylation reactions one after the other.

Furthermore, the model has the following kinetic and thermodynamic properties: All rate equations are described by bilinear or linear functions of the reactant concentrations depending on whether a coupling to ATP occurs or not. An external ATPase is introduced to maintain a steady state for the concentration of ATP. This process is represented by the time constant $\tilde{\tau}_{\mathrm{ATPase}}$, which is a useful parameter to characterize the cellular demand on ATP. (The "~" denotes a reference state.) The kinetic equation as well as the values used for the time constants and the equilibrium constants (extracted from typical parameters of the standard glycolysis) are given in [4]. The overall change in standard free energy $\Delta G^0_{\mathrm{U,tot}}$ of all U-reactions is distributed uniformly among the n uncoupled U-reactions, i.e.:

$$\Delta G^0_{\mathrm{U}} = \Delta G^0_{\mathrm{U,tot}}/n\,. \tag{1}$$

Three examples for $n=4$ may elucidate the stoichiometric assumptions and notations: 1) $(\mathrm{U\,U\,U\,U})$ is the shortest pathway and no ATP is produced. 2) $(\mathrm{U\,U\,U\,P\,U\,a})$ is one of the shortest pathways producing ATP; notice that in this example the P-reaction as well as the a-reaction are located as far as possible at the end of the pathway. 3) In the pathway $(\mathrm{A\,A\,U\,U\,p\,a\,U\,P\,P\,a\,U\,P\,a\,a})$ all types of reactions are represented and a net production of two ATP molecules per consumed substrate takes place.

The optimization function is the ATP flux, i.e. we are searching for the stoichiometry which results in a maximum ATP flux for given thermodynamic and kinetic parameters.

For a given number n of U-reactions the number of pathways $R(n)$ can be calculated as follows [4]:

$$R(n)=\frac{1}{4}\left[(-11)^{n+1}+2\cdot(-7)^{n+1}+(29)^{n+1}\right] \tag{2}$$

One obtains, for example, $R(1)=265$, $R(4)=5.079.121$ and $R(7)=125.118.075.361$. An increase in n implies a strong growth in the number of possible pathways. For $n=4$ the optimization problem was solved by a systematic generation of pathways and calculation of their corresponding ATP fluxes [4]. From the numerical point of view this procedure is, however, rather inefficient. The expense in time combined with the discrete feature of the sequences justify the application of Evolutionary Algorithms, in particular Genetic Algorithms.

Using these algorithms the space of sequences can be scanned very efficiently to find the optimal pathway by means of a "cloud" of closely related sequences. In addition to the reduction of expended time a further advantage of the application of this kind of algorithm is that, once a steady state is reached, the distributions of suboptimal pathways give some interesting insights into alternative metabolic structures, which may exert relevant functions in contemporary cells or in paleometabolisms [3]. However, a disadvantage of any application of Evolutionary Algorithms is the uncertainty whether the optimal solution has actually been found. For this reason we have compared the results obtained for $n=4$ from the Genetic Algorithm with the systematic search carried out in [4]. This allows us to choose the best set of parameters for steering the Genetic Algorithm. In addition, all optimal solutions must fulfill some necessary conditions derived analytically in [4].

METHODS:

The implemented Genetic Algorithm works as follows:

0) At the beginning a population of N_{pop} arbitrary pathways is produced and their corresponding ATP fluxes are calculated.
1) Each pathway can be replicated according to an assessment by comparing its ATP flux with the ATP flux of the best pathway in the current generation. The probability, represented by the amplification factor A_i, of replication of the ith pathway reads:

$$A_i = \frac{J_{\text{ATP},i}/J_{\text{ATP,max}}}{1+\Omega\cdot\left(1-J_{\text{ATP},i}/J_{\text{ATP,max}}\right)} \qquad \text{with } \Omega \geq 0 \qquad (3)$$

The limiting cases are $J_{\text{ATP,i}} = J_{\text{ATP,max}}$. with $A_i = 1$ and $J_{\text{ATP,i}} = 0$ with $A_i = 0$. The number of sequences, which are replicated, is determined by the steering parameter Ω. If Ω is high, only sequences i with $J_{\text{ATP,i}}$ close to $J_{\text{ATP,max}}$ are replicated.

2) Crossover as well as mutation operators act on each pathway with probabilities P_{cross} and P_{mut}, respectively. P_{mut} is related to the quality factor Q as follows: $P_{\text{mut}} = (1-Q)$. It is important to take into consideration that many crossover and mutation operations on pathways lead to pathways contradicting the three assumption of the model (see above). Therefore, we implemented thorough checks in order to produce just "meaningful" new pathways.
3) Finally, in order to introduce a selective process in the population some pathways will be eliminated randomly (the population size N_{pop} must be kept constant).
4) The next generation starts at 1)

RESULTS AND DISCUSSIONS:

In Fig. 1 the fluxes of the optimal stoichiometries are depicted versus the time constant of the external ATP consuming process for the system sizes $n = 4$ and $n = 7$, respectively. The bars are labeled with the optimal stoichiometries in vertical direction.

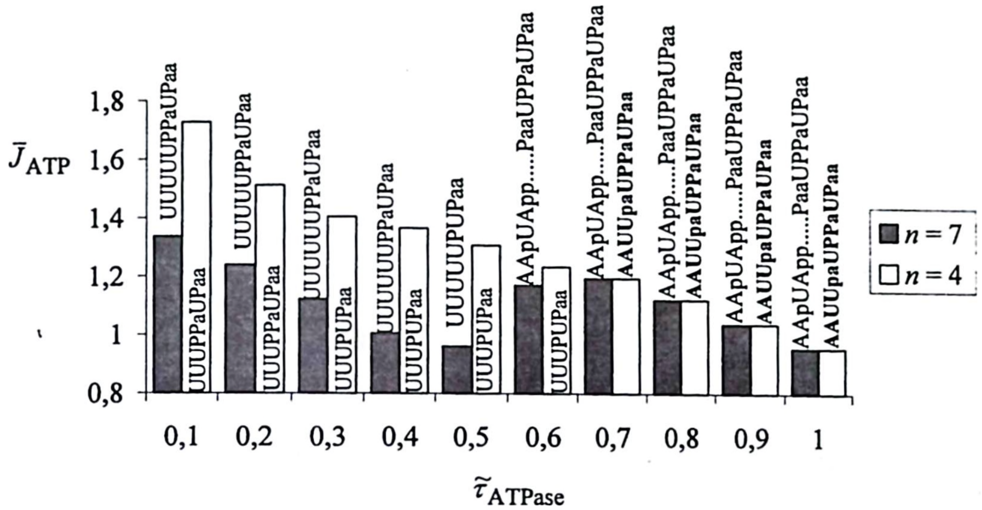

Figure 1. $\bar{J}_{ATP}$ in units of mMh^{-1}, $\tilde{\tau}_{ATPase}$ in units of h. Time constants of the ATP producing system are 1.0 h, equilibrium constant of the A-reaction: 1.962, equilibrium constant of P-reaction: 0.287, equilibrium constant of U-reaction: 7.3 for $n=4$ and 3.115 for $n=7$; concentrations of the external metabolites: 1.0 mM (for the choice of parameters see [4]), parameters of the Genetic Algorithm: $N_{pop}=100$, $Q=0.8$, $\Omega=500$, $P_{cross}=0$.

For $\tilde{\tau}_{ATPase} \leq 0.5$ no A-reaction is incorporated and for $\tilde{\tau}_{ATPase} \geq 0.7$ at least two A-reactions occur at the beginning of the optimal stoichiometries. These changes in the optimal stoichiometries can be explained if one takes into consideration that for increasing $\tilde{\tau}_{ATPase}$, i.e. for a lowering of the external ATPase activity, the ATP concentrations also increases. For low $\tilde{\tau}_{ATPase}$ the ATP concentration is low, which implies that the A-reaction, which has (by definition) ATP as a substrate, is very unfavorable. For higher $\tilde{\tau}_{ATPase}$ (higher ATP concentration) the situation occurs where an incorporated A-reaction at the beginning accelerates the ATP flux.

Furthermore, a monotonous decrease of $\bar{J}_{ATP}$ with increasing $\tilde{\tau}_{ATPase}$ for identical pathways can be observed. This can be explained by the fact that the number of ATP producing reactions is always greater than the number of ATP consuming reactions.

The optimal stoichiometry for $0.7 \leq \tilde{\tau}_{ATPase} \leq 1.0$ and $n=4$ corresponds to (A A U U p a U P P a U P a a) which has much in common with the design of standard glycolysis. This concerns, in particular, the location of the two ATP consuming reactions at the beginning and the number of ATP molecules consumed and produced per consumed external substrate. Differences in the number of P-reactions can be explained by the neglected splitting reaction catalyzed by the aldolase.

In the region $0.1 \leq \tilde{\tau}_{\text{ATPase}} \leq 0.5$ the ATP fluxes $\bar{J}_{\text{ATP}}$ is smaller for $n = 7$ (gray bars) compared with the case $n = 4$ due to a lengthening of the pathway by additional U-reactions. According to Eq. (1) their corresponding ΔG_{U}^{0} values are smaller than those of the case $n = 4$.

The points in the middle of the stoichiometries for $n = 7$ and in the region $0.7 \leq \tilde{\tau}_{\text{II}} \leq 1.0$ indicate a negligible influence of the reactions in the middle part on $\bar{J}_{\text{ATP}}$. This result has been already observed in [4] for $n = 4$: In the case of ATP consuming reactions located at the beginning the control of reactions on the flux are high in the upper and lower part of the pathway whereas the middle part has only a low influence on the ATP flux. A consequence of this fact is that many stoichiometries with almost equal fluxes (flat landscape) can be distinguished just very hardly using Evolutionary Algorithms.

Finally, it may be interesting to discuss the influence of the operators P_{cross} and Q on the dynamic of the implemented Genetic Algorithm. In Fig. 2 the generation, in which the optimal pathway (AAUUpaUPPaUPaa) is found for the first time, is plotted as a function of P_{cross} and Q. As can be seen for small Q (high mutation rate) the search in the space of solutions seems like a random aimless search. For high Q, the probability to be trapped in a local maximum is high. Depending on the resolution of the surface plot there is a minimum for the required generation at about $Q = 0.6..0.7$. Nevertheless an improvement due to the incorporated crossover operations has not been observed in these simulations.

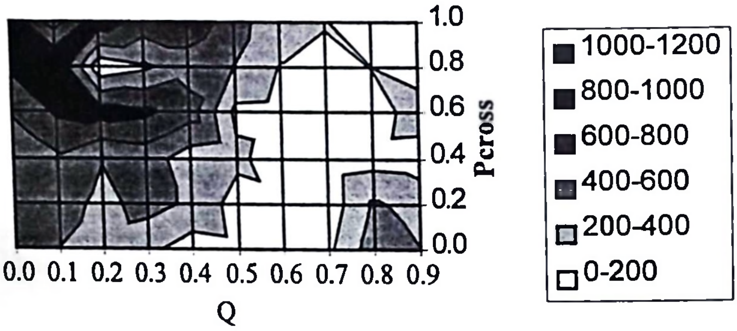

Figure 2. Generations, in which for $n = 4$ the optimal structure (AAUUpaUPPaUPaa) is found for the first time, versus Q and P_{cross}. $N_{\text{pop}} = 100$, $\Omega = 1000$, $\tilde{\tau}_{\text{ATPase}} = 1.0\,\text{h}$, other parameters as in Fig. 1. For each pair $(Q, P_{\text{cross}}) = (i \cdot 0.1, j \cdot 0.1)$ with $i, j = 0,1,...,9$ the generation of first appearance is averaged over 10 trials.

REFERENCES:

[1] Heinrich, R., Schuster, S., and Holzhütter, H.-G. (1991) Mathematical analysis of enzymic reaction using optimization principles, (review) *Eur. J. Biochem.*, **201**, 1-21.

[2] Heinrich, R., Montero, F., Klipp, E., Waddell, T.G., and Meléndez-Hevia, E. (1997) Theoretical approaches to the evolutionary optimization of glycolysis; Thermodynamic and kinetic constraints, Eur. J. Biochem., **243**, 191-201.

[3] Meléndez-Hevia, E., Waddell, T.G., Heinrich, R., and Montero, F. (1997) Theoretical approaches to the evolutionary optimization of glycolysis; Chemical analysis, Eur. J. Biochem., **244**, 527-543.

[4] Stephani, A. and Heinrich, R. (1998) Kinetic and thermodynamic principles determining the structural design of ATP producing systems; *Bulletin of Mathematical Biology*, (in press).

MITOCHONDRIAL H^+/O RATIO IS INDEPENDENT OF MEMBRANE POTENTIAL AND RESPIRATION RATE IN ISOLATED HEPATOCYTES

Edward K. Ainscow and Martin D. Brand

Department of Biochemistry, University of Cambridge, Tennis Court Road, Cambridge
CB2 1QW, U.K. Fax: +44 1223 333345; Tel: +44 1223 333648,
e-mail: m.d.brand@mole.bio.cam.ac.uk

INTRODUCTION

The non-linear relationship between respiration rate and mitochondrial proton motive force (Δp) in non-phosphorylating mitochondria is widely known [1]. The cause of the non-linearity has been the subject of much debate. Four mechanisms have been proposed to explain it: (i) non-ohmic proton conductance of the mitochondrial inner membrane at high Δp [1]; (ii) an increase in proton conductance of the mitochondrial membrane at high respiration rate [2]; (iii) a drop in the number of protons pumped per oxygen by the respiratory chain (H^+/O ratio) at high Δp [3]; (iv) a drop in the H^+/O ratio at high respiration rate [4]. The first two hypotheses propose that the proton pumps 'slip', i.e. there is some electron transfer without proton pumping.

A test has been used to distinguish between these hypotheses [5]. In isolated rat liver mitochondria, under physiological conditions, there was no evidence for any change in H^+/O ratio due to high Δp or respiration rate and no increase in membrane conductance at high respiration rate [6]. Hence, the mitochondrial inner membrane appears to display non-ohmic proton conductance at high Δp. Similar experiments on isolated hepatocytes have shown no evidence for any rate-dependency in proton conductance or H^+/O ratio but were inconclusive with regard to any change in H^+/O ratio at high mitochondrial membrane potential (Δψ) [7].

METHODS

Experimental

Liver cells were isolated from fed male Wistar rats (250-300 g) using the "two-step method" of Seglen [8] and stored on ice at approximately 25 mg dry mass.ml^{-1}. Viability was > 90% (trypan blue). Cells were incubated in medium containing 110 mM NaCl, 25 mM $NaHCO_3$, 10.8 mM glucose, 6.25 mM Na_2HPO_4, 5 mM KCl, 1.5 mM $CaCl_2$, 0.73 mM $MgSO_4$, 0.48 mM KH_2PO_4, 0.6 mM methyltriphenylphosphonium bromide, 60 mg/ml inulin and 1.35% (w/v) defatted bovine serum albumin at pH 7.2 at 10 mg dry mass.ml^{-1} in a shaking water bath at 37°C under 5% CO_2/95% air in sealed glass vials. Cells were pre-incubated for 10 min before further additions.

Intracellular mitochondrial membrane potential and cell volume were measured using the method of Brand [9]. The plasma membrane potential was assumed to be -30 mV under all conditions [10]. Oxygen consumption was measured using a Clark-type oxygen electrode. Non-mitochondrial oxygen consumption was determined as the myxothiazol-insensitive oxygen consumption and was subtracted from the total oxygen consumption to give mitochondrial respiration. Respiration rates and $\Delta\psi$ values were normalised to those measured for control cells in the absence of any inhibitors/uncoupler to decrease day-to-day variation in the experimental data.

Mitochondrial phosphorylation was fully inhibited with oligomycin (1 $mg.ml^{-1}$). A titration with myxothiazol (0.25-2.0 mM) gave the non-phosphorylating oxygen consumption rate at different values of $\Delta\psi$. The myxothiazol (0.25-1.0 mM) titration was repeated in the presence of excess oligomycin and two different concentrations (1 nM and 2.5 nM) of *p*-trifluoromethoxycarbonylcyanide phenylhydrazone (FCCP). Data for the two FCCP concentrations were obtained on separate days, but comparison of data obtained in the absence of FCCP (determined on all days) showed there to be no difference between the cells used.

Theory

Addition of sub-saturating concentrations of uncoupler to the cells will cause an increase in proton flux across the mitochondrial membrane. If the uncoupler is ohmic (as is the case for FCCP) then the extra proton flux will be proportional to Δp and the amount of uncoupler. If the H^+/O ratio of the mitochondria is constant, then the extra respiration used to drive the uncoupler-induced proton flux, calculated at a given Δp (ΔJ_o), will also be proportional to Δp and the amount of uncoupler. Hence, a plot of ΔJ_o against Δp divided by the [FCCP] should be linear if H^+/O is constant [5].

$$\frac{\Delta J_o}{[\mathrm{FCCP}]} = \frac{\Delta p . C^{\mathrm{FCCP}}}{H^+/O}$$

where C^{FCCP} is the proton conductance of FCCP (constant) and Δp is the proton motive force (assumed to be primarily composed of $\Delta\psi$ in hepatocytes [10]).

If there is a Δp-dependency of H^+/O then a plot of uncoupler induced respiration against $\Delta\psi$ will be non-linear [5]. Rate-dependence of H^+/O and endogenous membrane proton conductance can also be tested by adding different concentrations of uncoupler. If either endogenous proton conductance or H^+/O ratio depends on respiration rate then plots of ΔJ_o against $\Delta\psi$ will not superimpose for different FCCP concentrations [5].

RESULTS

Fig. 1 shows the relative non-phosphorylating respiration rates plotted against $\Delta\psi$ in the absence of FCCP and in the presence of 1 nM or 2.5 nM FCCP. On a given hepatocyte preparation the data have been normalised to the control mitochondrial oxygen consumption rate and $\Delta\psi$ value. Under control conditions, the average mitochondrial oxygen consumption was 12.6 ± 0.3 nmol O.(mg dry mass)$^{-1}$; non-mitochondrial oxygen consumption averaged 16.7 ± 0.5 % of total oxygen consumption. The average value of $\Delta\psi$ for cells in the standard condition was 146 ± 1 mV.

The data in Fig. 1 was then used to calculate ΔJ_o/[FCCP] for each of the FCCP data points. ΔJ_o was determined by calculating the difference in the observed respiration rates in the presence of FCCP and the interpolated respiration rate in the absence of FCCP at the same $\Delta\psi$ (see Fig. 1) assuming the curve in the absence of FCCP passed through the origin. The derived plots of ΔJ_o/[FCCP] against $\Delta\psi$ are shown in Fig. 2.

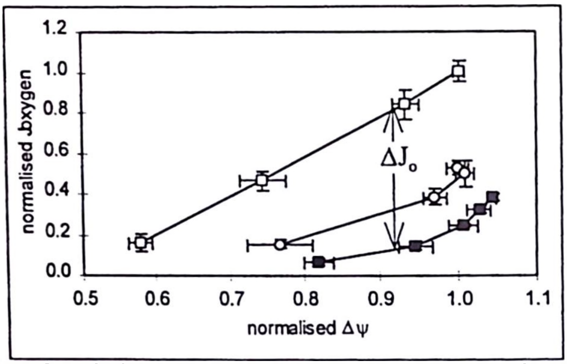

Figure 1. Non-phosphorylating respiration in the presence and absence of FCCP. Mitochondrial phosphorylation was inhibited by the addition of a saturating amount of oligomycin (1 $mg.ml^{-1}$). Non-phosphorylating respiration rate was titrated with increasing levels of myxothiazol in the absence of FCCP (■), mean ± s.e.m. n≥14, and in the presence of 1 nM (O) and 2.5 nM (□) FCCP, mean ± s.e.m. n≥5. Δψ and mitochondrial oxygen consumption are reported relative to the control values (absence of oligomycin). The extra respiration caused by FCCP (ΔJ_o) was calculated by interpolation (assuming the curve in the absence of FCCP passed through the origin).

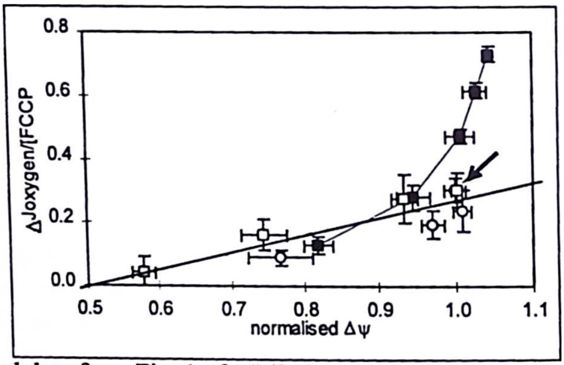

Figure 2. Replotted data from Fig. 1 of ΔJ_o/[FCCP] against Δψ.
The additional respiration caused by the presence of FCCP (ΔJ_o) was calculated as the difference between the respiration in the presence of the FCCP and the interpolated value at the same Δψ from the myxothiazol titration in its absence - see Fig. 1. There was no significant difference ($p = 0.1$) between regression lines fitted to the data from 1 nM FCCP (O) and 2.5 nM FCCP (□) and a regression line fitted to both data sets is shown. Regressions took account of errors in both x and y (using the ratio of these errors estimated from the error bars shown). Note that the data points indicated by the arrow represent two superimposing data points, one from each of the FCCP concentrations. The closed symbols show the result expected if the non-linearity of the endogenous respiration in Fig. 1 was caused by Δp-dependent slip. The curve was obtained by assuming the lowest two points of the myxothiazol titration in the absence of FCCP were due to an endogenous ohmic proton conductance equivalent to 0.52 nM FCCP [7].

The data show that there is a linear relationship between the extra respiration caused by the uncoupler and $\Delta\psi$. For comparison, a theoretical plot is also shown in Fig. 2, showing the predicted points if the non-linearity of the titration in Fig. 1 in the absence of FCCP had been due to slip in the proton pumps (assuming ohmic conductance of the mitochondrial membrane up to the lowest two data points of the titration). The replotted FCCP data show a linear relationship for ΔJ_o/[FCCP] against $\Delta\psi$ indicating that the H^+/O ratio is independent of $\Delta\psi$. There is no tendency for the data to fit the theoretical slip curve.

The data for the different concentrations of FCCP overlap indicating that there is no rate-dependency of H^+/O or of membrane conductance, as reported previously [7].

In theory, the straight line fitted to the experimental data of Fig. 2. should pass through the origin. The intercept with the $\Delta\psi$-axis (equivalent to 74 mV) has been reported previously and may be caused by relatively large errors in very low values of $\Delta\psi$ due to TPMP binding [6,7].

CONCLUSION

Of the four models proposed to explain the non-linearity of the plots of non-phosphorylating respiration against Δp, the results are only consistent with theory that the phenomenon is caused by non-ohmic proton conductance of the mitochondrial inner membrane. The results are in agreement with those obtained previously for isolated rat liver mitochondria [6]. Previous work on rat hepatocytes has not excluded the possibility of Δp-dependent changes in H^+/O ratio [7]. The linearity of the plots in Fig. 2 rule out any Δp-dependence of the H^+/O ratio, while the fact that replotted data for two different FCCP concentrations superimposes suggests no rate-dependence of either mitochondrial proton conductance or H^+/O ratio.

ACKNOWLEDGEMENTS

This work was supported by a grant from the Wellcome Trust (041431/Z/94/Z).

REFERENCES

[1] Nicholls, D.G. (1974) Eur. J. Biochem. 50, 305-315.
[2] Wrigglesworth, J.M., Cooper, C.E., Sharpe, M.A., Nicholls, P (1990) Biochem. J. 270, 109-118.
[3] Pietrobon, D., Azzone, G.F., Waltz, D. (1981) Eur. J. Biochem. 117, 389-394.
[4] Proteau, G., Wrigglesworth, J.M., Nicholls, P. (1983) Biochem. J. 210, 199-205.
[5] Brand, M.D., Chien, L.-F., Diolez, P. (1994) Biochem. J. 297, 27-29.
[6] Brand, M.D., Chien, L.-F., Ainscow, E.K., Rolfe, D.F.S., Porter, R.K. (1994) Biochim. Biophys. Acta 1187, 132-139.
[7] Porter, R.K., Brand, M.D (1995) Biochem. J. 310, 379-382.
[8] Seglen, P.O. (1976) Methods Cell Biol. 13, 29-83.
[9] Brand, M.D. (1994) in Bioenergetics - A Practical Approach (Brown, G.C. & Cooper, C.E. eds.), p. 39-62, Oxford University Press, Oxford.
[10] Nobes, C.D., Brown, G.C., Olive, P.N., Brand, M.D. (1990) J. Biol. Chem. 255, 1458-1464.

MODELLING OF THE FAST PHASE OF CHLOROPHYLL FLUORESCENCE INDUCTION.

G.V.Lebedeva[1], *N.E.Belyaeva*[1], *G.Yu.Riznichenko*[1], *O.V.Demin*[2,3]

[1]Department of Biophysics, Biological Faculty, Moscow State University, 119899, Vorobjovy Gory, Moscow, Russia; phone: +7 095 939 1963, fax: +7 095 939 1115, E-mail: lebed@biophys.msu.ru
[2]A.N.Belozersky Institute of Physico-Chemical Biology, Moscow State University, 119899, Vorobjovy Gory, Moscow, Russia, [3]M.M. Shemyakin and Yu.A. Ovchinnikov Institute of Bioorganic Chemistry, Moscow, Russia

INTRODUCTION

Fluorescence induction curves registered from plant samples are known to reflect the complex sequence of primary and secondary photosynthetic processes, taking place after an increase in light intensity [1]. One of the most well-studied induction effects is the fast fluorescence rise - OIDP-kinetics (Fig.1). OIDP-kinetics represents the increase in the photosystem II fluorescence yield from the origin level (O) to the peak level (P) in the interval about 1 s after the beginning of illumination. The fluorescence rise OP is multiphase and usually the transients ID may be observed. After the peak level of fluorescence is reached the slow relaxation to the steady-state level T takes place.

The models of fluorescence kinetics usually consider the fast (nano- and microsecond) processes of light absorption, transfer of excited states, charge separation [2] and (or) the slower (millisecond) processes of electron transfer through the two-electron-gate (redox-transformations of Q_AQ_B) [3, 4, 5]. The origin of nonmonotone behaviour of OIDP-kinetics is usually explained according to two basic hypothesis about the role of photosystem I (PS I) and heterogeneity of PS II units.

In this paper we present a model of primary events of photosynthesis, which includes detailed consideration of the light-driven electron transfer processes and takes into account the conversion of photosynthetic energy. We focus on the investigation of the effects of transmembrane electric potential formation and decreasing lumenal pH on the parameters of fluorescence kinetics.

MODEL DESCRIPTION

The proposed mathematical model of primary photosynthetic processes [6] takes into account strict compartmentalization of photosynthetic processes. We consider photosynthetic events in three different chloroplast compartments: the thylakoid membranes, intrathylakoid space (lumen) and stroma of the chloroplast. The volume ratio between these compartments was put equal 1:1:10.

The light-driven electron transfer in the thylakoid membranes is catalyzed by the complexes of photosystem II, cytochrome b6/f and photosystem I. The pool of the mobil electron carrier plastoqiunone is also located in the membrane. The thylakoid membrane processes were considered in details and included in the model after the proper reduction of the system according to the hierarchy of time scales. These processes generate $\Delta\mu H$ on the thylakoid membrane by transmembrane electron transfer and coupled uptake of protons into the thylakoid lumen. In the model the dependence of certain electron transfer stages on electric potential $\Delta\psi$ is introduced.

We also considered a number of processes, describing $\Delta\mu H$ consumption. ATP synthesis and ion fluxes of H^+, K^+ and Cl^- through the thylakoid membrane according to [7].

The fluorescence was assumed to be proportional to the total concentration of PSII excited states multiplied by the corresponding rate constants of their inactivation by fluorescence emission.

RESULTS

The model allows to give a realistic description of the time course of chlorophyll fluorescence after the change in light intensity: nonmonotone behaviour of the fast fluorescence rise OIDP and the subsequent decrease in fluorescence yield PT (Fig.1). Here we consider fluorescence changes observed in response to the illumination after the dark adaptation period.

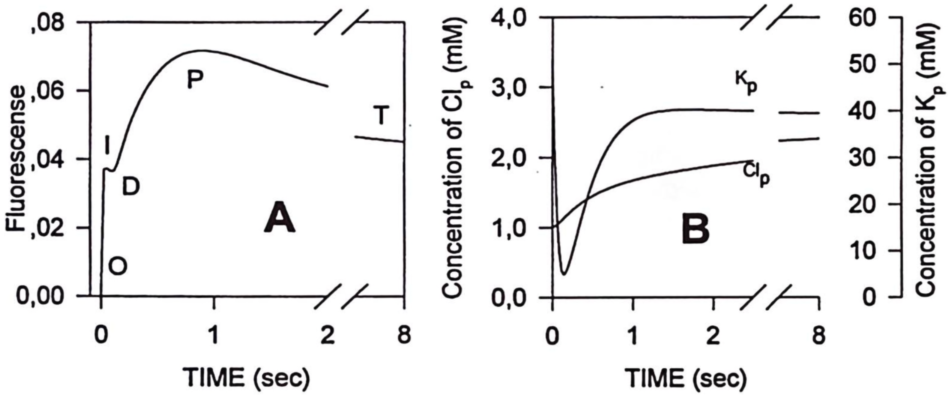

Figure 1. A. Calculated time course of fluorescence induction. **B.** Calculated kinetics lumenal ion concentartions (K_p, Cl_p).

In the dark all the PS2 and PS1 complexes are in the ground state and no excitation and charge separation processes occur. Plastoquinones Q_A, Q_B and all the mobile electron carriers of plastoquinone pool PQ and plastocyanin Pc were assumed to be fully oxidized in the dark. Concentrations of K^+ and Cl^- in the stroma and lumen have an equal value. In these conditions the level of fluorescence is minimal (0 in our model). Transmembrane electric potential $\Delta\psi$ and proton gradient ΔpH are also equal to zero.

Let us consider in more details the sequence of primary photosynthetic events after the beginning of illumination in the interval 0-1 s (Fig.2)

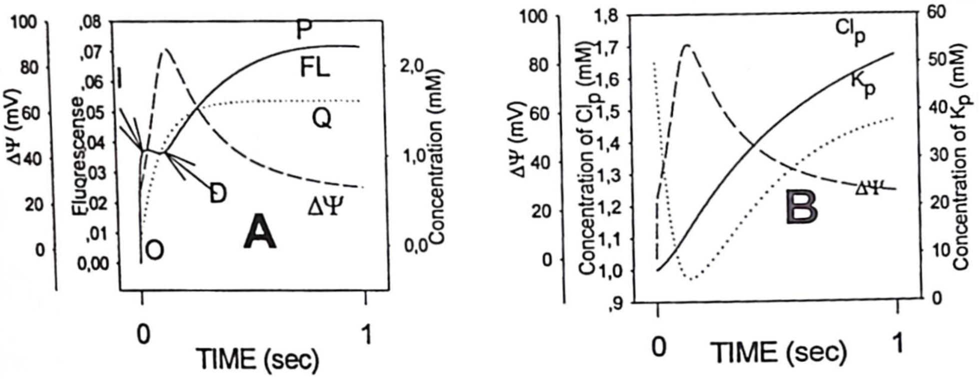

Figure 2. **A.** Simulated fast fluorescence induction (Fl) and time courses of electric potential ($\Delta\psi$) and total concentration of PS II states with non-oxidized Q_AQ_B (Q)
B. Calculated kinetics of lumenal ion concentration (K_p, Cl_p) and transmembrane electric potential $\Delta\psi$.

After the beginning of illumination the light-driven electron transfer across the thylakoid membrane is activated, which is coupled to the uptake of protons into the thylakoid lumen. This results in the fast (about 100 ms) increase of $\Delta\psi$ (Fig. 2) and ΔpH (not shown). The $\Delta\psi$ increase leads to the deceleration of electron transfer process due to the dependence of a number of its stages on electric potential. This results in the fast fluorescence rise OI. The maximal rate of $\Delta\psi$ increase corresponds to the appearance of the local maximum I on the fluorescence induction curve.

The H^+ uptake observed in the thylakoids in the light is possible due to the counterflow of other ions across the membrane. In the framework of our model we may suggest the following mechanism of this process. The $\Delta\psi$ increase results in the acceleration of the ion transfer across the thylakoid membrane and leads to the K^+ -efflux and influx of Cl^-.(Fig.2, B). In turn, these ion fluxes lead to the deceleration of $\Delta\psi$ rise and subsequent decrease of $\Delta\psi$ (Fig. 2, A). Deceleration of $\Delta\psi$ rise facilitates in some extent electron transfer processes and leads to a fall in fluorescence yield (ID transition). Further fluorescence increase DP is caused by the electron back-pressure due to the reduction of quinone acceptors Q_A and Q_B.(Fig. 2A). When $\Delta\psi$ starts to decrease the influx of K^+ may be observed.

CONCLUSIONS

The model appears to be realistic in describing some kinetic components of fluorescence induction. The process of the transmembrane electric potential formation as well as initiated ion fluxes were shown to play a significant role in the determination of the fast fluorescence rise pattern. The model needs further refinements to give a proper description of ΔpH formation and the slow phase of fluorescence induction.

ACKNOWLEDGMENT

We acknowledge RFFR grant N 98-04-48868 for the support of this work.

REFERENCES

[1] Dau, H. (1994) J.Photochem.Photobiol. B:26, 3-27.
[2] Leibl, W., Breton, J., Deprez, J. and Trissl, H.W. (1989) Photosynth.Res. 22, 257-275.
[3] Renger, G and Schulze, A. (1985) Photobiochem. Photobiophys. 9, 79-87.
[4] Baake, E. and Shloder, J.P. (1992) Bull. Math. Biol. 54, 999-1021.
[5] Van Kooten, O., Snel, J.F.H. and Vredenberg, W.J.(1986) Photosynth. Res. (, 211-227.
[6] Demin, O.V., Lebedeva, G.V., Riznichenko, G.Yu., Rubin, A.B. (1998) Biochemistry (submitted).
[7] Kholodenko, B.N. (1988) D.Sc. Thesis. Moscow State University.

THE REGULATION OF MITOCHONDRIAL ATP SYNTHESIS IN SKELETAL MUSCLE DURING THE TRANSITION FROM EXERCISE TO REST

GJ Kemp[1], *M Roussel*[2], *D Bendahan*[2], *Y Lefur*[2], *PJ Cozzone*[2]

[1]Dept of Orthopaedic & Accident Surgery, University of Liverpool, Liverpool L69 3GA, UK. Tel + 44 (151) 7064124, Fax +44 (151) 7065815, Email gkemp@liv.ac.uk.
[2]Centre de Resonance Magnetique Biologique et Medicale, UMR-CNRS #6612, Faculté de Médecine, 27 Bd. J. Moulin, 13005 Marseille-France.

INTRODUCTION

In skeletal muscle during recovery from exercise, phosphocreatine (PCr) resynthesis is entirely oxidative. The initial PCr resynthesis rate (V), a measure of oxidative ATP synthesis rate (Q), has a roughly hyperbolic relationship to [ADP] [1, 2]. However, re-analysis of data from aerobic exercise and mitochondria *in vitro* suggests that this ought more precisely to be sigmoid [3]. 'Undershoots' in ADP recovery [4] are incompatible with simple ADP-control of the mitochondrion, although the extent of the discrepancy has not been well defined. To elucidate mitochondrial regulation in the exercise-rest transition, we examined relationships between V, [ADP] and the Gibbs free energy of ATP hydrolysis (ΔG_{ATP}) after exercise of various durations.

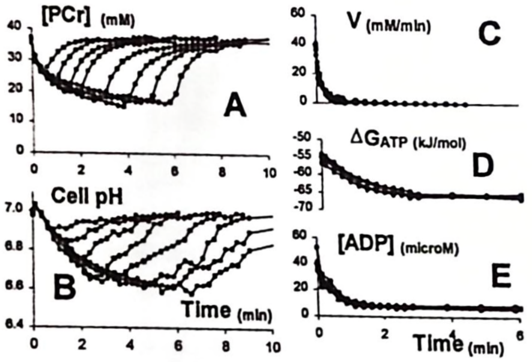

Figure 1. A & B show [PCr] & pH during exercise of differing duration (0.5-6 min) and recovery. C-E show the PCr resynthesis rate (V), ΔG_{ATP} and [ADP] during recovery after exercise.

SUBJECTS & METHODS

Ten males (25-45 y) performed finger flexion lifting 10% MVC at 0.7 Hz. 8-scan ^{31}P magnetic resonance spectra at 1.5 s i.p. delay were acquired from finger flexor muscle in a 4.7 T magnet using a double-tuned (^{1}H-^{31}P) 5 cm surface coil. Subjects exercised separately for 0.5, 1, 1.5, 2, 3, 4, 5 & 6 min, recovery data being acquired for 15 min. pH was calculated from the chemical shift of Pi, [Pi] and [PCr] from peak ratios, and [ADP] and ΔG_{ATP} as in [5].

RESULTS

At rest pH = 6.99±0.01, [PCr] = 37.0±0.6 mM, [ADP] = 8.5±0.3 μM and ΔG_{ATP} = -64.5±0.2 kJ/mol (mean±SEM). During exercise, power = 1.2±0.1 W and ATP turnover rate = 60±5 mM/min. Figs 1A & B show how PCr and pH changes during exercise roughly superimposed in the 7 data sets, recovery occurring from a succession of endpoints. [ADP] and ΔG_{ATP} rose in exercise: at 6 min, pH = 6.61±0.03, [PCr] = 17±2 mM, [ADP] = 40±5 μM and ΔG_{ATP} = -55±1 kJ/mol. Fig 1C shows the time course of

PCr resynthesis. Figs 1D and 1E show post-exercise [ADP] and ΔG_{ATP} recovery: both showed undershoot, reaching minima of 7.2±0.3 μM and -66.1±0.1 kJ/mol. Exercise duration had no effect on initial V (mean = 37±3 mM/min), implying that oxidative ATP synthesis was constant in exercise from 0.5 min. PCr recovery was near-exponential, and $t_{1/2}$ increased with exercise duration (from 0.50±0.03 to 0.71±0.06 min), and therefore also with decreasing end-exercise [PCr] and pH, as in other studies [4, 6, 7]. (Although PCr $t_{1/2}$ depends on mitochondrial function in theory [8, 9] and in fact [10], its dependence on end-exercise state makes interpretation difficult if end-exercise pH, for example, differs in patients and controls). Mitochondrial function is reflected by the kinetics of ADP [4], which can be thought of as an error signal in a feedback loop [9]: accordingly, exercise duration had no effect on ADP recovery $t_{1/2}$ (mean = 0.39±0.03 min). Exercise duration did not affect initial-recovery Q_{MAX} (mean = 56±5 mM/min), which is an estimate of 'mitochondrial capacity' calculated from initial V and end-exercise [ADP] [11], assuming for the sake of argument sigmoid kinetics with Hill coefficient = 2 [3] and Km = 25 μM, and basal Q of 2 mM/min. Fig 2 shows the dependence of V on [ADP] and ΔG_{ATP} throughout that phase of recovery in which V was measurable. These relationships were similar for all exercise durations, and Fig 2A shows the combined data. Calculating Q_{MAX} becomes unreliable as recovery proceeds, but clearly no single relationship describes the relation between V and [ADP] (Fig 2A), and the main cause is the ADP undershoot. This is unlikely to be a fibre-type inhomogeneity problem [4]. In other studies undershoot was greater at lower pH [4], although the mechanism remains unknown. The implications for mitochondrial control by [ADP] can be seen in Figs 2A & C. The sigmoid 'kinetic' relationships illustrated (passing through the initial-recovery point) can account for the low 'basal' value of Q in recovery i.e. that component which does not fund PCr resynthesis (in resting human muscle basal Q ≈ 1 mM min^{-1} [12]), but not for the ADP undershoot (Fig 2C). A similar discrepancy is seen in the quasi-sigmoid 'thermodynamic' relationship between V and ΔG_{ATP} (Figs 2B & 2D): theoretical lines through the initial-recovery point fails to fit well both near-resting data (Fig 2D) and the early-recovery points (Fig 2B).

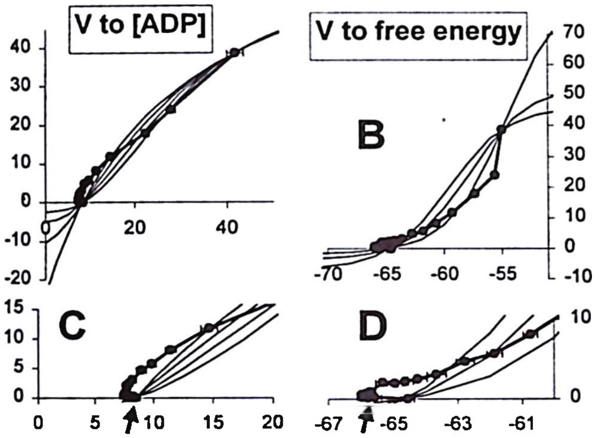

Figure 2. Relationships between post-exercise PCr resynthesis rate (V mM/min), [ADP] (μM) and ΔG_{ATP} (kJ/mol). Thick lines show combined (±SEM) data from experiments of different exercise duration (1-6 min). Thin lines are theoretical functions fitting the initial-recovery point: in A, Km = 25 μM, n=1.0-2.5 (based on [3]); in B, min/max Q = 0.05-0.10 (based on [13]). C & D are expansions of A & B (arrows show resting state)

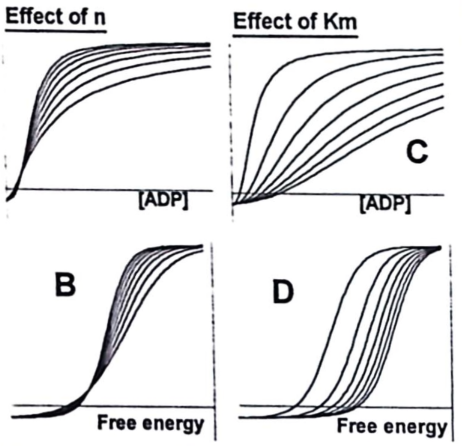

Figure 3. Relationships between oxidative ATP synthesis rate and [ADP] & ΔG_{ATP}, assuming 'kinetic' control, showing the effect of changing the Hill coefficient (A & B) and affinity for ADP (C & D). Based on [14], varying Km and n

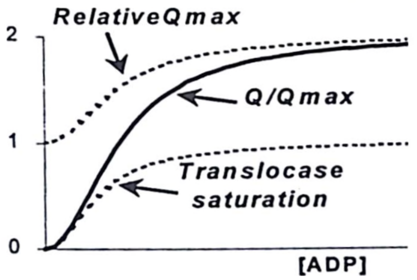

Figure 4. Relation between oxidative ATP synthesis (Q, relative to 'basal' Q_{MAX}) and [ADP] in the 'parallel activation' model: also shows apparent Q_{MAX}, and ADP-saturation of the translocase as labelled

DISCUSSION

In general, hyperbolic (Michaelis-Menten) kinetics imply sigmoid force-flow relationships for conserved systems [13], and the truth of this for mitochondrial ATP synthesis [14] is seen in aerobic exercise [15]. Here we make two theoretical comments. The classical analysis of this implication [14] must be modified in view of the new evidence that the 'kinetic' Q-to-[ADP] relationship is second-order [3]. Fig 3 shows how the form of this affects that of the 'force-flow' relationship to ΔG_{ATP}. Second, it has been argued that because large changes in Q can occur without large changes in [ADP], there must be a component of what is variously called 'open-loop' control [9], 'feed-forward' regulation, or 'parallel activation' [16]. Conversely, it is argued that this postulate is unnecessary in view of increased dynamic range afforded by the sigmoid response to ADP [3]. To make the parallel-activation proposal more precise, Fig 4 shows a simple and fairly general model of this. In this model, effective Q_{MAX} in exercise is taken to be a saturable function of a signal proportional to ATP turnover (this could be e.g. calcium). Fig 4 shows the resulting steady state transfer function relating Q to [ADP]. It can be seen that the effect of this mechanism is to alter the effective Km for ADP and increase the available dynamic range (compare Q with the 'translocase saturation' line in Fig. 4, which also shows the resulting relationship between 'stimulated' Q_{MAX} and ADP). In recovery from exercise however, as the presumed 'parallel activation' signal must decay rapidly, one might expect V largely to reflect 'unstimulated' Q_{MAX}. Alternatively, Q_{MAX} might decline rapidly after exercise, as decreasing blood flow reduces oxygen supply, to values lower than any seen during exercise. None of these possibilities can be excluded. However, this could not explain how oxidative ATP synthesis in excess of basal can occur despite sub-resting [ADP]. 'Basal' ATP turnover is probably higher in early recovery than at rest, due to the need to restore ionic gradients: but this works the wrong way to explain the ADP undershoot. Thus neither model fully explains the control of mitochondrial ATP synthesis in recovery, although the present work shows that the relationships upon which both are based are relatively independent of exercise duration despite substantial changes of pH. Because of the constraints of the creatine kinase equilibrium, large pH changes are necessary to distinguish these models [17], but clearly not sufficient. The effects of respiratory acidosis on oxygen consumption in stimulated rat muscle are more plausibly described as changing 'mitochondrial conductance' ($dQ/d\Delta G_{ATP}$) and 'mitochondrial potential' (ΔG_{ATP} at $Q=0$) than Q_{MAX} and Km [5]. It would be interesting to know its effects on the V-to-[ADP] and V-to-ΔG_{ATP} relationships in recovery from exercise.

REFERENCES

1. Kemp, G.J., Taylor, D.J. and Radda, G.K. (1993) Control of phosphocreatine resynthesis during recovery from exercise in human skeletal muscle. NMR in Biomed 6, 66-72.
2. Boska, M. (1994) ATP production rates as a function of force level in the human gastrocnemius/soleus group using ^{31}P MRS and ^{1}H MRI. Magn Res Med 32, 1-10.
3. Jeneson, J.A.L., Wiseman, R.W., Westerhoff, H.V. and Kushmerick, M.J. (1996) The signal transduction function for oxidative phosphorylation is at least second order in ADP. J Biol Chem 271, 27995-8.
4. Argov, Z., DeStefano, N. and Arnold, D.L. (1996) ADP recovery after a brief ischemic exercise in normal and diseased muscle - a ^{31}P MRS study. NMR in Biomed 9, 165-172.
5. Harkema, S.J. and Meyer, R.A. (1997) Effect of acidosis on control of respiration in skeletal muscle. Am J Physiol 272, C491-500.
6. Bendahan, D., Confort-Gouny, S., Kozak-Reiss, G. and Cozzone, P. (1990) Heterogeneity of metabolic response to muscular exercise in humans. New criteria of invariance defined by in vivo phosphorus-31 NMR spectroscopy. FEBS Lett 272, 155-158.
7. Walter, G., Vandenborne, K., McCully, K.K. and Leigh, J.S. (1997) Noninvasive measurement of phosphocreatine recovery kinetics in single human muscles. Am J Physiol 272, C525-34.
8. Meyer, R.A. (1988) A linear model of muscle respiration explains monoexponential phosphocreatine changes. Am J Physiol 254, C548-C553.
9. Kemp, G.J. (1994) Interactions of mitochondrial ATP synthesis and the creatine kinase equilibrium in skeletal muscle. J Theor Biol 170, 239-246.
10. Paganini, A.T., Foley, J.M. and Meyer, R.A. (1997) Linear dependence of muscle phosphocreatine kinetics on oxidative capacity. Am J Physiol 272, C501-10.
11. Kemp, G.J., Thompson, C.H., Taylor, D.J., Hands, L.J., Rajagopalan, B. and Radda, G.K. (1993) Quantitative analysis by ^{31}P MRS of abnormal mitochondrial oxidation in skeletal muscle during recovery from exercise. NMR in Biomed 6, 302-310.
12. Blei, M.L., Conley, K.E. and Kushmerick, M.J. (1993) Separate measures of ATP utilization and recovery in human skeletal muscle. J Physiol 465, 203-222.

13. Van der Meer, R., Westerhoff, H.V. and van Dam, K. (1980) Linear relation between rate and thermodynamic force in enzyme-catalyzed reactions. Biochim Biophys Acta 691, 488-493.
14. Westerhoff, H.V., van Echteld, C.J.A. and Jeneson, J.A. (1995) On the expected relationship between Gibbs energy of ATP hydrolysis and muscle performance. Biophys Chem 54, 137-42.
15. Jeneson, J.A.L., Westerhoff, H.V., Brown, T.R., van Echteld, C.J.A. and Berger, R. (1995) Quasi-linear relationship between Gibbs free energy of ATP hydrolysis and power-output in human forearm muscle. Am J Physiol 268, C1474-C1484.
16. Korzeniewski, B. (1998) Regulation of ATP supply during muscle contraction: theoretical studies. Biochem J 330, 1189-1195.
17. Connett, R. (1988) Analysis of metabolic control: new insights using a scaled creatine model. Am J Physiol 254, R949-R959.

THE GLYCOLYTIC FLUX IN E. COLI APPEARS TO BE CONTROLLED BY THE DEMAND FOR ATP.

Brian J. Koebmann, Dan Nilsson, Jacky L. Snoep, Hans V. Westerhoff and Peter Ruhdal Jensen

Department of Microbiology, Technical University of Denmark, Building 301, DK-2800 Lyngby, Denmark. Tel. + 45 45252510. Fax. + 45 45932809. E-mail. prj@im.dtu.dk.

INTRODUCTION

The glycolytic pathway of various organisms has been exploited for thousands of years for the production of alcohol and lactic acid. More recently, the fundamental question has been asked of what controls the flux through glycolysis, and much work has been done to determine the control by enzymes of the glycolytic pathway. Surprisingly, none of the glycolytic enzymes exerted a significant control on the pathway flux (Schaaff *et al.*, 1989). According to metabolic control theory (Kacser and Burns, 1973; Heinrich and Rapoport, 1974) the sum of control exerted on the glycolytic flux should add up to 1. But metabolic control theory also shows that flux control could reside in any of the enzymes in the system, i.e. also in the processes that consume the ATP generated in glycolysis (the ATP demand). It therefore becomes important to determine experimentally to what extent these processes control the glycolytic flux. However, to undertake the task of overexpressing all the enzymes involved in the anabolic processes and measuring their contribution to flux control is not realistic. Besides, the control of the glycolytic flux could easily be distributed over numerous anabolic processes and the control coefficients may then be too small to be measured accurately. A way to circumvent this problem would be to introduce an additional ATP consuming process. Such a process should not interfere with other aspects of metabolism. An ATPase that would simply hydrolyze ATP to ADP and P_i, without coupling to any energy conserving reaction, would be ideal for this purpose. One of the normal enzymes that comes closest to the ideal ATP-hydrolyzing enzyme is part of the membrane bound H^+-ATPase. This huge enzyme complex consists of two parts, the membrane integral part, F_0, which forms a proton channel, and the cytoplasmic part, F_1, which contains the catalytic site for conversion of ATP to ADP and P_i. In this paper we show that when parts of the F_1 part is overexpressed glycolysis is increased and growth decreased. Modulation of ATPase activity then allowed us to estimate the control exerted by the ATP demanding processes on the glycolytic flux, from the relative elasticities of demand and supply, with respect to ΔG_p.

MATERIAL & METHODS

Bacterial strain : Cloning, plasmid propagation as well as growth experiments were performed using *E. coli* K-12 strain BOE270, derived from MC1000 (Casabadan *et al.*, 1980), kindly provided by Dr. Lars Boe.

Enzymes : Restriction enzymes, Calf Intestine Phosphatase, and T4 DNA ligase from Pharmacia and New England Biolabs were used as recommended.

DNA techniques : DNA isolation, cutting with restriction enzymes, treatment with T4 DNA polymerase and calf intestine phosphatase were carried out as described by Maniatis *et al.*, (1982).

Cloning *E. coli atp* genes under the control of an inducible promoter : Details of this work will be given elsewhere (Koebmann *et al.*, manuscript in preparation). Shortly, the plasmid pBJC917 (von Meyenburg *et al.*,1984), which carries the entire *atp* operon was cut with proper restriction enzymes to get fragments containing different combinations of the *atp* genes that encode subunits of the F1 part, i.e. i) *atpAGDC* (subunits α, γ, β, ε), ii) *atpAGD* , iii) *atpDC* and iv) *atpD,* see Jensen (1998) for details. The fragments were cloned in pTTQ18 (Starck, 1987), resulting in the plasmids pTAC-AGDC, pTAC-AGD, pTAC-DC, and pTAC-D (figure 1), in which different combinations of the *atp* genes can be induced from a *tac* promoter.

Cloning of *atpAGD* under the control of artificial promoters : The *atpAGD* fragment from pTAC-AGD was cloned downstream of the CP promoters on the plasmids pCP32, pCP34, pCP41, and pCP44 (Jensen and Hammer, 1998), resulting in pCP32::*atpAGD*, pCP34::*atpAGD*, pCP41::*atpAGD*, and pCP44::*atpAGD* (figure 1), which express the *atpAGD* genes to different extents.

Growth experiment : Growth experiments were performed with strains having *atpAGD* under control of either an inducible *tac* promoter or a range of artificial promoters, i.e., CP32, CP34, CP41 and CP44. Strains with the respective expression vectors were used as control. The strains were inoculated from overnight-cultures at 30°C into shaking 100 ml ABT-medium supplemented with 0.04% glucose and 200 µg/ml erythromycin (pCP-vectors) or 100 µg/ml ampicillin (pTAC-AGD). For the strain containing pTAC-AGD we also added different concentration of IPTG. Regular measurements of OD_{450} were made and samples taken for measuring [ATP] and [ADP], as described by Jensen *et al.*, (1993).

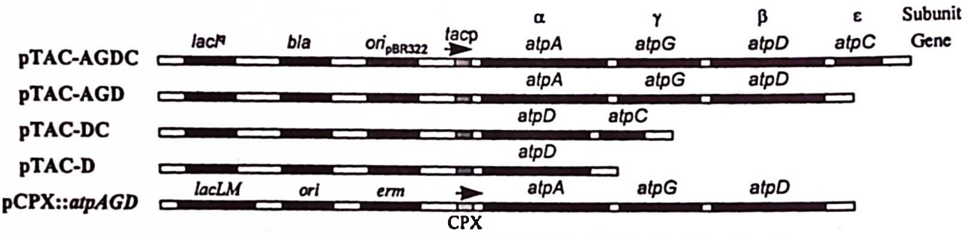

Fig. 1. Linear representation of the plasmids constructed for modulating the cellular ATP/ADP ratio in *E. coli* (not drawn to scale). See text for further details. X:= 32, 34, 41, 44.

RESULTS AND DISCUSSION

Expression of ATPase activity inhibits the growth of *E. coli.*

We constructed plasmids that express, from a *tac* promoter, combinations of the *E. coli* genes coding for the F_1 ATPase subunits (see figure 1). The strains containing one each of the four plasmids were streaked onto LB plates containing ampicilin (100 µg/ml) and varying amounts of IPTG, to induce the expression from the *tac* promoter. The strain carrying the genes for the four subunits α,γ, β and ε (pTAC-AGDC), was only very slightly affected in growth, even in the presence of 1 mM of IPTG, while the combination of F_1-subunits caused severe growth inhibition in the presence of 1 mM of

IPTG. At intermediate concentrations of IPTG the plasmids affected the growth of their host cell to different extents. These results are in accordance with reconstitution experiments, which showed that the complex $\alpha_3\gamma\beta_3$ was most active with respect to ATP hydrolysis *in vitro* (Dunn and Heppel, 1981). The observation that the overexpression of β-subunits alone caused severe inhibition of growth was somewhat surprising.
The effect of induction of ATPase was also studied with cells grown in liquid cultures. For this purpose we chose the strain PJ4333, carrying the plasmid pTAC-AGD, which appeared to be the most active plasmid with respect to the inhibitory effect on the growth of *E. coli*. PJ4333 was grown in minimal medium supplemented with a limiting concentration of glucose, without IPTG and in the presence of increasing concentrations of IPTG. Surprisingly, we observed that the growth rate first increased with increasing amounts of IPTG up to about 30 μM. At higher IPTG concentrations the growth of the cells was gradually more inhibited by IPTG. We attributed this to growth inhibition by the vector itself, which appeared to inhibit the growth by some 30%. Indeed, also the strain which carried the empty vector was stimulated in growth rate by the addition of IPTG. Perhaps the high expression of lactose repressor protein from this vector inhibited the growth, this effect being alleviated by the addition of IPTG. The yield of biomass on glucose decreased drastically with increased ATPase expression in the cells, which indicated that more and more ATP was being hydrolyzed.

Figure 2 : Measurements of the intracellular ATP/ADP ratio with increasing expression of *atpAGD* from a *tac* promoter (from Jensen, 1998).

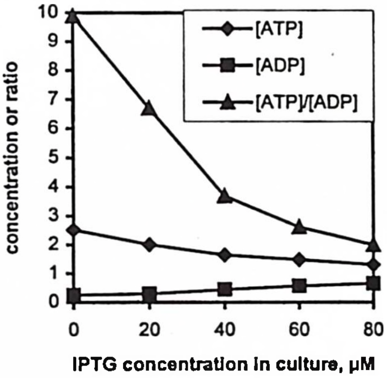

We then measured the concentration of ATP and ADP in cells growing at different expression levels of ATPase activity (figure 2). The intracellular ATP concentration decreased gradually and the ADP concentration increased, with increased expression of ATPase. Therefore, the [ATP]/[ADP]-ratio decreased with increased expression of
ATPase, which indicates that ATP was converted to ADP and P_i, as a result of ATPase expression.

Expression of F_1-ATPase activity from constitutive promoters in *E. coli*.

Due to the unexpected effect of low concentrations of IPTG on the growth of cells carrying the inducible *atpAGD* genes, we were unable to use these data for estimating the elasticities of the ATP demand and ATP supply towards the phosphorylation potential, ΔG_p. To remove the requirement for varying concentrations

of IPTG, the *E. coli atpAGD* genes were therefore cloned downstream of four constitutive promoters of moderate but different strengths and transformed into *E. coli.* The strains were subsequently characterized with respect to the specific growth rate, μ, yield on glucose, Y_{gluc}, and glycolytic flux, J_{gluc}. These results are shown in table 1.
The expression of the F_1-ATPase subunits had a slightly negative effect on the growth rate as its expression level was increased. At high expression level the drop in growth rate was more pronounced. The effect on the growth yield however was much stronger and at the highest expression level the growth yield had dropped to 35% of the initial value.

Table 1 : Expression of uncoupled F1-ATPase activity (α-, γ-, β-subunits) in *E. coli* (from Koebmann *et al.*, manuscript in preparation).

Strain	**Plasmid**	**Biomass yield** gdw/mmol glucose	**Growth rate µ** h-1	**Glucose flux** mmol glucose/h/gdw	**Biomass yield** %	**Growth rate µ** %	**Glucose flux** %
PJ4451	pCP41	0.067	0.47	6.9	100	100	100
BK1032	pCP41::*atpAGD*	0.047	0.42	9.1	69	90	131
PJ4444	pCP34	0.063	0.41	6.6	100	100	100
BK1017	pCP34::*atpAGD*	0.034	0.34	9.9	54	81	149
PJ4454	pCP44	0.067	0.44	6.5	100	100	100
BK1036	pCP44::*atpAGD*	0.027	0.30	11.2	40	69	172
PJ4442	pCP32	0.062	0.42	6.7	100	100	100
BK1048	pCP32:*atpAGD*	0.022	0.19	8.8	35	46	131

The ATPase activity is increased from top to bottom in the table.

The glycolytic flux was stimulated by 70%, but when the overexpression became to high, we observed a drop in the glycolytic flux, which coincided with a strongly reduced growth rate. Apparently, hydrolysis of ATP can only be complemented to a certain extent by an enhanced glycolytic flux. A further removal of free-energy will eventually kill the cell, as we had already seen with the IPTG induced ATPase expression (see above).

The glycolytic flux is controlled by the demand for ATP.

In a simple view, cellular free-energy metabolism is divided into supply and demand for ATP, where we have assumed that ATP production is strictly coupled to growth :

$$\text{Substrate} \xrightarrow{e_1} \Delta G_p \xrightarrow{e_2} \text{Growth}$$

Metabolic Control Analysis of this simple scheme allow us to express the flux control coefficients in terms of the elasticities of the two modules, i.e.:

$$C^J_{e_2} = \frac{-\varepsilon^{e_1}_p}{\varepsilon^{e_2}_p - \varepsilon^{e_1}_p} = \frac{-\frac{d\ln J_1}{d[\Delta G_p]}}{\frac{d\ln J_2}{d[\Delta G_p]} - \frac{d\ln J_1}{d[\Delta G_p]}} \qquad (1)$$

If we change ΔG_p by introducing a small amount of uncoupled ATPase, we should be able to calculate the two elasticities with respect to ΔG_p and from that we should be able to calculate the control coefficient, $C^J_{e_2}$. But since both elasticities are measured in one experiment where ΔG_p is perturbed only slightly, eq (1) reduces into (Westerhoff and van Dam, 1987):

$$C^J_{e_2} = \frac{-d\ln J_1}{d\ln J_2 - d\ln J_1} = \frac{1}{1-\frac{d\ln J_2}{d\ln J_1}} \qquad (2)$$

which becomes

$$C^J_{e_2} \approx \frac{1}{1-\frac{\Delta J_2\%}{\Delta J_1\%}} \qquad (3)$$

for small changes in the relative fluxes.

Using Eq. 3, we calculated the control by demand on the glycolytic flux, $C^{J_1}_{e_2}$, for each level of ATPase, and found 0.76, 0.72, 0.70 and 0.36 for the four increasing levels of ATPase expression, respectively. This demonstrates that in the wild type cell the control by demand on the glycolytic flux is at least 0.76, which indicates that the demand for ATP is strongly involved in the control of the glycolytic flux. This leaves only a small amount of flux control to the supply reaction and may therefore offer an explanation to why the individual glycolytic enzymes appear to have very little flux control in same system. In this paper, the change in ATP demand is only increased relative to the wild type level. In principle, one should also lower the ATP demand to calculate the control coefficient at the wild type level, but this is of course not feasible with the current approach. However, the relative constant control coefficients with respect to the extent of modifications indicates that the control coefficient may also be valid at the wild type level of demand. We are currently constructing plasmids that should allow us to make even smaller increases in the ATP demand.

It is interesting that the flux control was found to be relatively independent on which level of ATPase activity was being used in the calculation. Only at very high expression level the control by demand decreased significantly.

ACKNOWLEDGEMENTS

We thank Regina Schürmann and Anne Vad for excellent technical assistance. This work was supported by The Danish Academy of Technical Sciences (ATV) and Chr. Hansen A/S.

REFERENCES

1 Casabadan, M. J. and Cohen, S. N. (1980). *Journal of Molecular Biology* **138**, 179-207.

2 Dunn, S. D. and Heppel, L. A. (1981). *Arch. Biochem. Biophys.* **210**, 421-436.

3 Heinrich, R., Rapoport, T.A. (1974). *Eur. J. Biochem.* **42**, 89-95.

4 Israelsen, H., Madsen, S. M., Vrang, A., Hansen, E. B. and Johansen, E. (1995). *Appl. Environ. Microbiol.* **61**, 2540-2547.

5 Jensen, P. R., Westerhoff, H. W., Michelsen, O. (1993). *EMBO J.* 12, 1277-82

6 Jensen, P. R. (1998). International patent application number PCT/DK97/00373, publication number WO 98/10089.

7 Jensen, P. R. and Hammer, K. (1998). *Appl. Environ. Microbiol.* **64**, 82-87.

8 Kacser, H. and Burns, J. A. (1973). *Rate control of biological processes* (D.D. Davies, Ed.). Symp. Soc. Exp. Biol., 27: 65-104. Cambridge University Press, Cambridge

9 Maniatis, T., Fritsch, E. F., and Sambrook, J. (1982). *Molecular cloning.* Cold Spring Harbor Laboratory Press, Cold Spring Harbor, New York.

10 Starck, M. J. R. (1987). *Gene* **51**, 255-267.

11 von Meyenburg, K., Joergensen, B. B., and van Deurs, B. (1984). *EMBO J.* **3**, 1791-1797.

12 Yanisch-Perron, C., Viera, J., and Messing, J. (1985). *Gene* **33**, 103-109.

13 Schaaff, I., Heinisch, J., Zimmermann, F. K. (1989). *Yeast* **5**, 285-290.

14 Westerhoff, H. V., van Dam, K. (1987). *Thermodynamics and Control of Biological Free Energy Transduction.* Elsevier, Amsterdam.

ANTIMYCIN INDUCED CHANGE IN CATALYTIC MECHANISM OF SUCCINATE UBIQUINONE REDUCTASE CAN BE RESPONSIBLE FOR BELL-SHAPED DEPENDENCE OF SUPEROXIDE GENERATION ON [SUCCINATE]/[FUMARATE] RATIO.

Vasenko[1], A. and Demin[1,2], O.V.

[1]A.N. Belozersky Institute of Physico-Chemical Biology, Moscow State University, 119899, Vorobjovy Gory, Moscow, Russia, [2]M.M. Shemyakin and Yu.A. Ovchinnikov Institute of Bioorganic Chemistry, Moscow, Russia
fax: (095) 939 31 81, e-mail: bkhol@energ.genebee.msu.su

INTRODUCTION

The steady-state rate of the antimycin induced superoxide generation in beef heart submitochondrial particles was shown to be maximal at the [succinate]/[fumarate] ratio of about 1:5 and decays at both higher and lower redox potentials [1]. Concentration of protonated semiquinone at centre "o" of bc_1 complex (substance donating one electron to oxygen with superoxide formation) as well as upstream Q-cycle intermediate - ubiquinol, has to follow the same bell-shaped dependence. For submitochondrial particles respiring on succinate this paradoxical behaviour of steady-state ubiquinol concentration at succinate titration can be explained through the similar dependence of rate of succinate ubiquinone reductase (SUR) on the succinate concentration. The aim of the paper is to show that assumption that antimycin affects ubiquinone binding site of SUR would suffice to describe bell-shaped dependence of the rate on [succinate]/[fumarate] ratio. In contrast, inhibition of carboxylate binding site of SUR cannot provide such dependence.

MATHEMATICAL MODELS

A mathematical model of enzyme cycle of SUR includes 12 states of the enzyme (Scheme 1):

x_1=(|ox|Q), x_2=(|ox|), x_3=(|ox|QH_2);
y_1=(S|ox|Q), y_2=(S|ox|), y_3=(S|ox|QH_2);
z_1=(F|ox|Q), z_2=(F|ox|), z_3=(F|ox|QH_2);
w_1=(F|red|Q), w_2=(F|red|), w_3=(F|red|QH_2);

First and third positions inside the brackets mean carboxylate (i.e. succinate and fumarate) and ubiquinone binding sites, respectively. Second position determines redox state of the enzyme: "ox" stands for oxidised enzyme forms and "red" stands for reduced enzyme forms. Empty place at first or third position inside the brackets means empty binding site. x_i, y_i, z_i, i=1,2,3, correspond to oxidised enzyme states:
and w_i, i=1,2,3, correspond to reduced enzyme states:

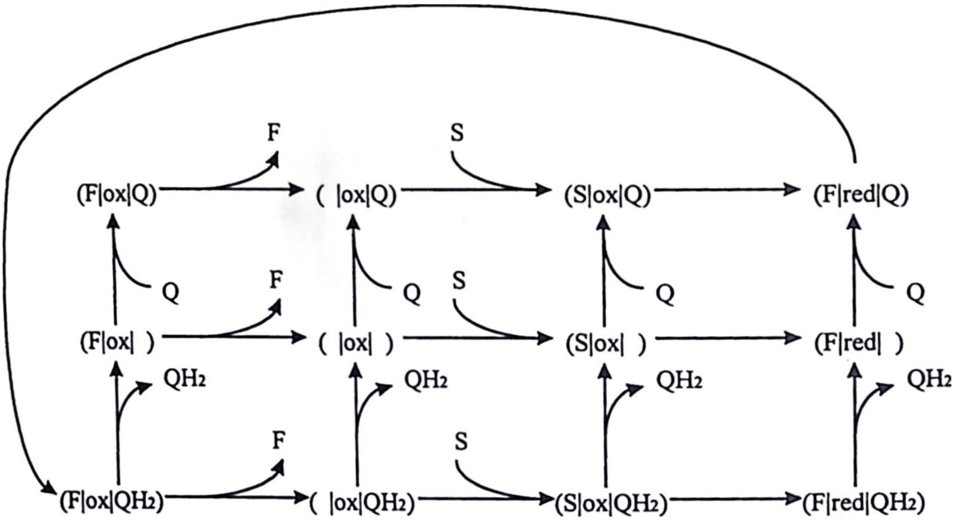

Scheme 1. Enzyme cycle of succinate ubiquinone reductase.

S, F, Q, QH_2 designate succinate, fumarate, ubiquinone and ubiquinol, correspondingly. Concentration of the species are parameters of the model. In accordance to experimental data [2] all substrates and products have different affinity towards oxidised and reduced enzyme. Other experimentally observed fact which we take into account is that fumarate cannot leave reduced enzyme. Values of all equilibrium constants were taken from [2].

RESULTS

Assumtion that succinate and ubiquinone association as well as fumarate and ubiquinol dissociation are quasi-equilibrium processes allows us to reduce scheme 1 to the simple two-state scheme (not shown). Using the two-state scheme we derived rate equation which described experimentally measured, monotonously increasing dependence on succinate concentration.

Then, we considered the case when antimycin (directly or through the bc_1 complex which is possibly connected to succinate dehydrogenase via special protein [2]) affected complex II in a such way to slow down operation carboxylate binding site. Consequently, all processes connected with succinate/fumarate association/dissociation cease to be quasi-equilibrium. This, in turn, reduce scheme 1 to scheme 2.

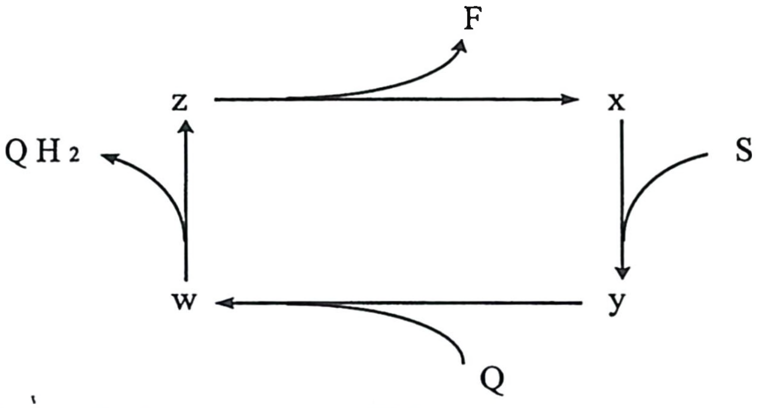

Scheme 2. Enzyme cycle of SUR which carboxylate binding site affected with antimycin.

Here,
$x=x_1+x_2+x_3$; $y=y_1+y_2+y_3$; $z=z_1+z_2+z_3$; $w=w_1+w_2+w_3$;
We found that rate equation corresponding to Scheme 3 is monotonous dependence on succinate.

Finally, we considered the case when antimycin inhibited ubiquinone binding site. Taking into account the fact that only processes of association/dissociation of succinate/fumarate are quasi-equilibrium we transformed Scheme 1 to Scheme 3.

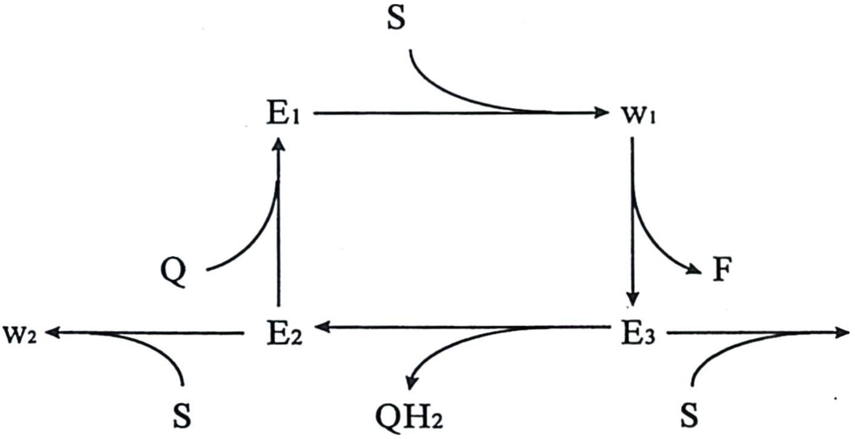

Scheme 3. Enzyme cycle of SUR which ubiquinone binding site affected with antimycin.

Here,
$E_1=x_1+y_1+z_1$; $E_2=x_2+y_2+z_2$; $E_3=x_3+y_3+z_3$;
Rate equation corresponding to Scheme 3 shows bell-shaped dependence on [succinate]/[fumarate] ratio (see Fig. 1). Indeed, increase in succinate concentration results in increase in rate of fumarate formation until sum of concentrations of appendix forms of SUR, i.e. w_2 and w_3, constitute the major portion of enzyme. Then, reaction rate decreases with increase in succinate.

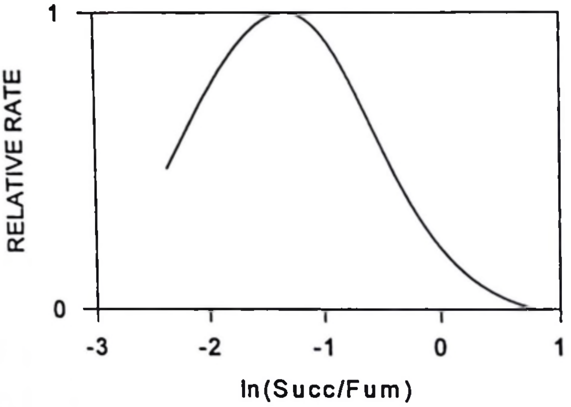

Figure 1. Dependence of relative rate of SUR which ubiquinone binding site affected with antimycin on [succinate]/[fumarate] ratio.

ACKNOWLEDGEMENT

We acknowledge RFFR grant N 98-04-48868, European Union (through its Copernicus program grant IC15-CT96-0307) and NWO for the support of this work.

REFERENCES

[1] Ksenzenko, M., Konstantinov, A.A., Khomutov, G.B., Tikhonov, A.N. and Ruuge, E.K. (1984) FEBS Lett., 175, 105-108.
[2] Vinogradov, A.D. (1986) Biochemistry (Moscow), 51, 1944 - 1973.

MODELING OF FREE-ENERGY METABOLISM IN LACTOCOCCUS LACTIS

Martin Bastian Pedersen, Heidi Winterberg Andersen and Peter Ruhdal Jensen.

Institute of Microbiology, building 301, Technical University of Denmark, DK-2800 Lyngby, Denmark. Phone: +45 4525 2510. Fax: +45 4593 2809. E-mail: prj@im.dtu.dk

INTRODUCTION

The lactic acid bacterium *Lactococcus lactis* is used extensively as a starter culture in the dairy industry, where the production of lactate is important. The sugar in milk is taken up and converted into pyruvate through glycolysis. This process generates two molecules of ATP and two molecules of NADH per glucose equivalent (see left part of Fig. 1). Since *L. lactis* does not benefit from oxidative phosphorylation, the NADH is oxidized back to NAD^+ by reduction of pyruvate to lactate by lactate dehydrogenase (LDH). Furthermore, the excretion of lactate from the cell and into the medium adds to the proton gradient and thereby to the total energy gain [11]. The fermentation pattern in which primarily lactate is formed is called homolactic fermentation.

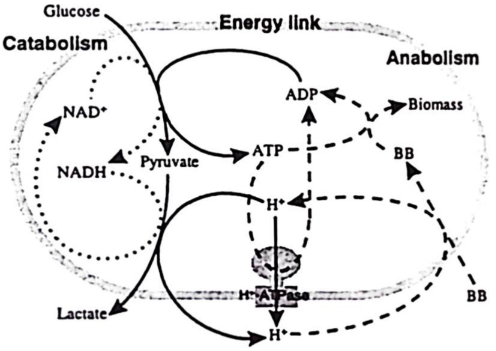

Figure 1. Partitioning of metabolism in *L. lactis*
Metabolism in *L. lactis* can be split up into three sections: catabolism, anabolism and an energy link between the two. Dotted, full and dashed lines signify redox, energy generating and energy consuming reactions, respectively. BB designates building blocks (e.g. amino acids).

Under conditions where the energy source is limited there is an alternative pathway for pyruvate, namely the conversion into formate, acetate and ethanol [5]. This fermentation pattern is named mixed acid fermentation and the committed step is conversion of pyruvate into formate and acetyl-CoA by pyruvate formate lyase (PFL). As can be seen from Fig. 2, the two molecules of NADH formed in glycolysis are still oxidized back into NAD^+ by conversion of one acetyl-CoA into ethanol by alcohol dehydrogenase (ADH). The other acetyl-CoA can be converted into acetate by acetate kinase (ACK), and an extra ATP is gained. Because of the redox constraint, the ACK and ADH fluxes are equal, and there is a net gain of 3 ATP per glucose equivalent in mixed acid fermentation, as opposed to a gain of only 2 ATP in homolactic fermentation (see Fig. 2). However, under most conditions where PFL is active, LDH is also active, and a combination of the two flux patterns is observed.

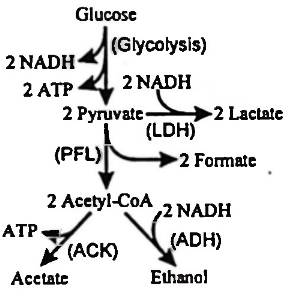

Figure 2. Homolactic and mixed acid fermentation
When primarily LDH is active, the fermentation pattern is homolactic. If PFL (and possibly also LDH) is active the cells exhibit a mixed acid fermentation pattern. See Fig. 3 for legend.

To get a better understanding of the regulation of the shift from homolactic to mixed acid fermentation in *L. lactis*, we have perturbed the metabolism both genetically and by adjusting fermentation parameters. From these experiments and from data found in the literature we have constructed a modular metabolic computer model of the free-energy metabolism in *L. lactis*.

The computer modeling was performed in WinModel 1.0 [12]. WinModel is a Windows 95 application, which encapsulates the DOS modeling program SCAMP 2.4gc [13] by an easy-to-use interface. Furthermore, there are additional features for finding syntax errors and drawing graphs directly in Gnuplot [16], which makes it possible to set up simple animations.

MATERIALS & METHODS

Strains and plasmids

Lactococcus lactis subsp. *cremoris* MG1363 was used for the fermentation experiments.

The *ldh* gene from pMU2901 [9] was engineered to contain a deletion. It was thereafter inserted into pG⁺host4, which is a temperature sensitive vector for gene replacement [2]. This construct was used to inactivate *ldh* in MG1363 by homologous integration followed by excision and screening for the *ldh⁻* phenotype [12]. The mutant was verified by DNA sequencing.

Cloning techniques

Standard cloning procedures were employed [10], in which *E. coli* was used as an intermediate host.

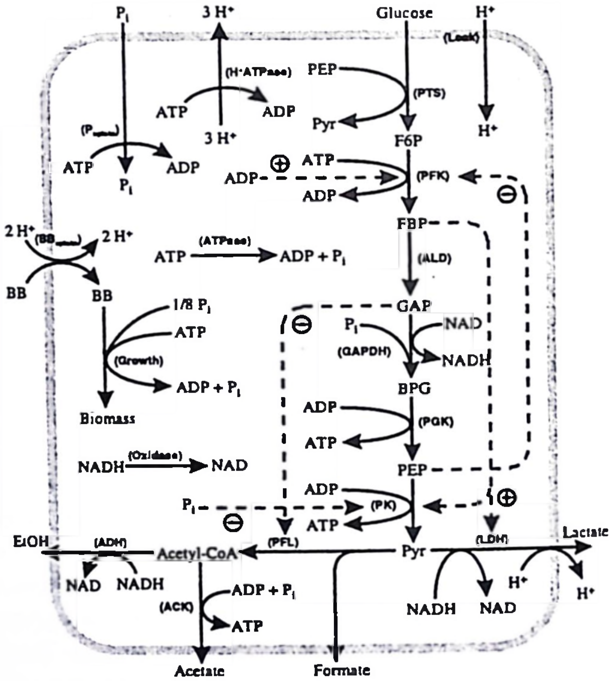

Figure 3. Modules in model of *L. lactis* metabolism
Dashed lines signify either positive or negative regulation as indicated by a plus (+) or minus (-) sign. **Modules:** PTS, phosphotransferase system; PFK, phosphofructokinase; ALD, aldolase; GAPDH, glyceraldehyde-3-phosphate dehydrogenase; PGK, phosphoglycerate kinase; PK, pyruvate kinase; LDH, lactate dehydrogenase; PFL, pyruvate formate lyase; ACK, acetate kinase; ADH, alcohol dehydrogenase. **Metabolites:** F6P, fructose-6-phosphate; FBP, fructose-1,6-biphosphate; GAP, glyceraldehyde-3-phosphate; BPG, 1,3-biphosphoglycerate; PEP, phosphoenolpyruvate; Pyr, pyruvate; BB, building blocks.

Growth of L. lactis

SA synthetic medium [7] with 2.5g/l of glucose was used for growth of *L. lactis*. pH was kept constant at 7.0 by automatic titration with 2.0M NaOH. The culture volume was 0.6l, and the agitation rate was 200rpm for batch and 750rpm for chemostat cultures, both of which did not cause vortex formation. No form of gas sparging was used in the cultures, but since the vessels were not sealed, oxygen from the atmosphere could freely enter the growth media.

Measurement of end metabolite concentrations

HPLC was used to measure glucose, lactate, formate, acetate and ethanol concentrations in the *L. lactis* culture medium. The column used was a Bio-Rad HPX-87H, and the mobile phase was 5mM H_2SO_4, with a flow rate of 0.5ml/min.

RESULTS

Growth of *L. lactis* in rich media can be viewed as the uptake of building blocks by the proton gradient followed by their incorporation into cell material at the expenditure of ATP (see right part of Fig. 1). As mentioned in the introduction, the redox balance closes in catabolism. Also, less than 5% of the sugar taken up from the medium is used for cell mass [1]. Consequently, the only link between anabolism and catabolism is ATP/ADP and the proton gradient (see middle part of Fig. 1). This partitioning of metabolism forms the basis of a modular kinetic model. The 17 modules have simplified kinetics where the parameters are based primarily on adjusting the model to exhibit behavior found in the literature with respect to 1) how metabolite concentrations and fluxes in *L. lactis* change according to growth conditions, 2) proposed regulative patterns, 3) the finding that control of glycolysis in *E. coli* is largely controlled by the ATP consuming processes (see Købmann et al., these BTK proceedings) and 4) results from own experiments.

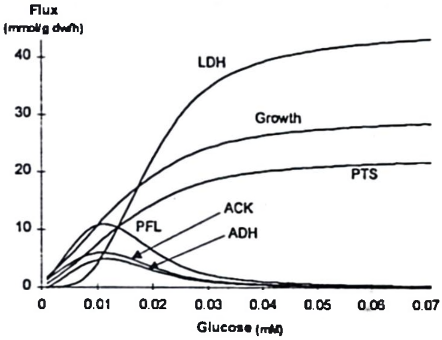

Figure 4. Main model fluxes as a function of the glucose concentration.
The shift towards mixed acid fermentation (signified by the PFL flux) is apparent as the glucose concentration decreases. See Fig. 3 for legend.

The 17 modules of the model that have been set up are shown in Fig. 3. As can be seen, the focus has been on catabolism and its regulation, particularly the shift from homolactic to mixed acid fermentation. Anabolism in the model consist only of two modules, namely uptake of building blocks by the proton gradient and their incorporation into cell material at the expenditure of ATP (see left part of Fig. 3). The reaction kinetics for each of the modules is of a reduced reversible Michaelis-Menten type. The general format of the rate equations is

$$v = K \cdot \frac{A^a}{I^i} \cdot \frac{k \cdot S_1 \cdot S_2 \cdot \ldots \cdot S_m - P_1 \cdot P_2 \cdot \ldots \cdot P_n}{1 + S_1 + S_2 + \ldots + S_m + P_1 + P_2 + \ldots + P_n}$$

although there are some deviations for certain modules. *K* signifies a constant with unit [mmol/g dw/h], S_m a substrate, *m* the number of substrates, P_n a product, *n* the number of products, *A* an activator with the exponent *a*, *I* an inhibitor with the exponent *i* and, finally, *k* is a constant.

The central point of the model is that it should simulate a shift from homolactic to mixed acid fermentation when the glucose concentration drops below about 0.05mM [1]. As can be seen from Fig. 4, the model has been developed to show this response. At glucose concentrations above 0.05mM only lactate is produced by LDH, but when the glucose concentration drops below 0.05mM we see a gradual shift towards mixed acid fermentation as indicated by formate production by PFL (see Fig. 4 and Fig. 2).

Two of the major factors in the shift from homolactic to mixed acid fermentation are believed to be the concentrations of fructose-1,6-biphosphate (FBP) and the triose phosphates (which are combined as glyceraldehyde-3-phosphate (GAP) in the model). FBP is believed to activate pyruvate kinase (PK) and LDH [14], whereas GAP inhibits PFL [5] (see Fig. 3). Both the FBP and GAP concentrations in the model behave quantitatively as stated in the literature, as does the ATP concentration (data not shown, [4, 5, 15]). The phosphoenolpyruvate (PEP), pyruvate (Pyr) and inorganic phosphate (P_i) concentrations of the model behave qualitatively as found in the literature.

Enzyme abbreviations are shown in Fig. 3. See text for details. About 15% of the carbon was not accounted for in the fermentations. This lost carbon was disregarded in the left graph. Notice the small deviation between the x-axis scales.

Both batch and chemostat fermentations were performed to obtain additional data for the model. The relative carbon fluxes (C-fluxes) for some of these fermentations are shown in the left part of Fig. 5. It was expected that the ACK and ADH fluxes should be equal as illustrated in the introduction, but this was not what was found. The ACK flux was several-fold higher than the ADH flux (see left part of Fig. 5). One reason for this could be NADH-oxidase activity due to aeration of the medium in the chemostat. This aeration could have been caused by the 750rpm of agitation, and the fact that the overflow pump constantly sucked fresh atmospheric air into the headspace of the vessel. Therefore, a NADH-oxidase was incorporated into the model, as shown in the left part of Fig. 3. By doing this, the ACK flux becomes relatively higher than the ADH flux, as found in the fermentations. The output from the model is shown in Fig. 4 and the right part of Fig. 5.

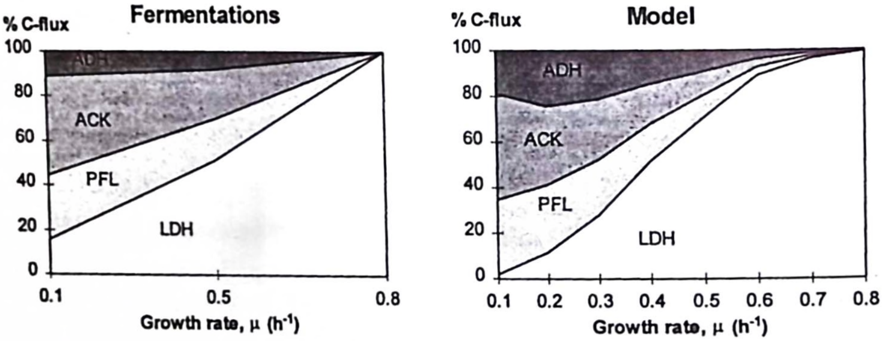

Figure 5. Relative C-fluxes for fermentations and model as a function of the specific growth rate.

We are currently in the process of constructing strains of *L. lactis* MG1363 with altered expression of the *pyk* and *ldh* genes which encode PK and LDH, respectively (see Andersen et al., these BTK proceedings). As indicated under materials and methods a *ldh* mutant has been engineered, which exhibits mixed acid fermentation [12]. Plasmids that have artificial constitutive promoters [8] upstream of the wild-type *ldh* gene are being constructed and will be integrated into the chromosome of the *ldh* mutant. When finalized, these strains will be investigated in fermentations. A similar approach is being used to investigate the effect of the expression of the *pyk* gene.

The presented model predicts that lowering the LDH activity should result in more mixed acid fermentation (data not shown). Intuitively, this is that we expect, since reducing the expression of *ldh* should result in a build-up of pyruvate (see lower right corner of Fig. 3) and thereby a relatively higher flux through PFL, which has a lower affinity for pyruvate than LDH, although this has been questioned [3]. The result of this would be a more pronounced shift towards mixed acid fermentation at a higher glucose concentration.

If we look at PK instead, the model predicts that lowering the PK activity should lead to less mixed acid fermentation (data not shown). A qualitative reasoning for this is that there would be a build-up of metabolites before PK, including FBP and GAP. This would activate LDH and inhibit PFL (see regulatory pattern in Fig. 3) and hence result in less mixed acid fermentation.

DISCUSSION

This paper explores an alternative way of doing metabolic modeling. An important difference compared to traditional modeling is that *in vitro* enzyme kinetics is not required. Instead, we start out with equations with simplified kinetics and continually refine the model by adjusting the overall elasticities of the modules to fit flux and metabolite behavior in the literature and our own fermentations. A drawback of this approach is that the starting point is not much more than a flux analysis model. However, we have chosen this approach anyway, because we believe that the control and regulation of a living cell is far too complex to be described accurately from *in vitro* kinetic data. The numerous regulatory mechanisms in a living cell, many of which run through the level gene expression and enzyme modification etc., will be very hard to incorporate quantitatively into a rate equation (this of course becomes even more complicated when a modular approach is used, where several reactions are combined into one rate equation). Moreover, even if it was possible, the *in vitro* kinetic data would probably be inaccurate *in vivo*, because the *in vivo* conditions are far too complex to be simulated in a test tube. We believe that one of the dangers of building models from *in vitro* kinetics is that one tends to accept the predictions of the model unconditionally, as a consequence of their objective origin.

The model predicts that reducing the LDH activity will enhance mixed fermentation, whereas lowering the PK activity will decrease mixed acid fermentation. When the engineered constructs with altered *pyk* and *ldh* expression have been completed, fermentations will be performed and the results can be compared to the predictions of the model. Flux control coefficients will also be calculated from the fermentation data. These *in vivo* coefficients are invaluable in the empirical modeling approach used here.

Data from Garrigues et al. [6] indicates that the shift from homolactic to mixed acid fermentation could be mediated by the redox balance of the cell as a consequence of the relative elasticities of the glyceraldehyde-3-phosphate dehydrogenase (GAPDH) and LDH enzymes towards NAD$^+$ and NADH. In our model, the redox balance plays only a minor role in the shift to mixed acid fermentation.

ACKNOWLEDGEMENTS

Parts of this work was supported by a grant from the Danish Dairy Board (MFF). We wish to thank Martin Willemoës for inspiring discussions and critical reading of this manuscript, and Tina Walther at the Institute of Biotechnology, DTU for measuring fermentation products by HPLC.

REFERENCES

[1] Benthin, S., Schulze, U., Nielsen, J., and Villadsen, J. (1994) Chemical Engineering Science 49, 589-609.
[2] Biswas, I., Gruss, A., Ehrlich, S. D., and Maguin, E. (1993) J. Bacteriol. 175, 3628-3635.
[3] Cocaign-Bousquet, M., Garrigues, C., Loubiere, P. and Lindley, N. D. (1996) Antonie van Leeuwenhoek 70, 253-267.
[4] Cook, G. M. and Russell, J. B. (1994) Current Microbiol. 28, 165-168.
[5] Fordyce, A. M., Crow, V. L., and Thomas, T. D. (1984) Appl. and Env. Microbiol. 48, 332-337.
[6] Garrigues, C., Loubiere, P., Lindley, N. D. and Cocaign-Bousquet, M. (1997) J. Bacteriol. 179, 5282-5287.
[7] Jensen, P. R. and Hammer, K. (1993) Appl. and Env. Microbiol 59, 4363-4366.
[8] Jensen, P. R. and Hammer, K. (1998) Appl. and Env. Microbiol 64, 82-87.
[9] Llanos, R. M., Hillier, A. J., and Davidson, B. E. (1992) J. Bacteriol. 174, 6956-6964.
[10] Maniatis, T., Fritsch, E. F. and Sambrook, J. (1982) Cold Spring Harbor.
[11] Otto, R., Sonnenberg, A. S. M., Veldkamp, H. and Konings, W. N. (1980) Proc. Natl. Acad. Sci. USA 77, 5502-5506.
[12] Pedersen, M. B. (1997) Master's thesis including WinModel 1.0 modeling software. Institute of Microbiology, Technical University of Denmark.
[13] Sauro, H. (1994) Scamp 2.4gc modeling software.
[14] Sjöberg, A. (1992) Ph.D. thesis. Lund University, Sweden.
[15] Sjöberg, A., Persson, I., Quednau, M. and Hahn-Hägerdal, B. (1995) Appl. Microbiol. Biotechnol. 42, 931-938.
[16] Williams, T. and Kelley, C. (1996) Gnuplot 3.0 plotting software.

47

RESPONSE TIMES OF MUSCLE MEMBRANE POTENTIAL TO VARIATIONS IN POTASSIUM CONDUCTANCE DEPEND ON CHLORIDE TRANSPORT.

Remco J. Geukes Foppen, Harald G.J. van Mil and Jan Siegenbeek van Heukelom.

Institute of Neurosciences, Cell Biophysics, Faculty of Biology, University of Amsterdam, Amsterdam, The Netherlands; Telephone: + 31 (0) 20 5257642;
Fax: + 31 (0) 20 6659125; e-mail: foppen@bio.uva.nl

INTRODUCTION

The role of chloride in skeletal muscle cellular physiology is to date not very well understood. The reason for this becomes clear if one knows the history of the findings in this field of research. It took until the late 1950's to acknowledge the fact that the Cl permeability, P_{Cl}, is actually very high in skeletal muscle [1]. Before that, it was thought that P_{Cl} was low, because reductions of extracellular Cl_o[a] never caused substantial changes in the membrane potential, V_m. In 1959 Hutter and Padsha provided the first evidence that P_{Cl} was high, when they did experiments in which they replaced Cl_o with nitrate and saw a two-fold increase in membrane resistance [1]. This was later confirmed by others [2]. The subsequent hypothesis was, that if P_{Cl} were indeed that high, then Cl must be in equilibrium ($V_m = E_{Cl}$[b]). Meanwhile, Palade and Barchi tested 25 carboxylic acids, and found that anthracene-9-carboxylic acid (9-AC) was the most potent inhibitor of P_{Cl} in skeletal muscle [3]. This pharmacological agent reduced the membrane conductance almost three-fold. With the use of this agent and the application of intracellular Cl-sensitive microelectrodes Aickin et al. found, that Cl was actively kept slightly above equilibrium, which means that $V_m < E_{Cl}$ [4].

The skeletal muscle fibres [5], as do many other cells, contain an electroneutral $Na^+/K^+/2Cl^-$-cotransporter [6]. It's activity ensures a small Cl accumulation. The driving force of the cotransporter, because of it's electroneutral behaviour, does not depend on the membrane potential, V_m, but only on the sum of the chemical gradients, $\Delta\mu$. Since two Cl ions are transported per turnover, $\Delta\mu_{Cl}$ has to be calculated twice. Therefore, the role of Cl_i is very important, because the driving force is related to $(Cl_i)^2$, whereas the effects of Na_i and K_i are linear. Cl_i is the balanced outcome of the Cl efflux through Cl channels, which is purely passive, and the Cl influx through the cotransporter, which is secondarily active draining on the Na gradient. The Cl channels rectify only slightly, meaning that they have an almost linear current-voltage relationship. However, since Cl is not the only ion transported through the cotransporter, the Cl fluxes depend on the fluxes of the other ions as well.

---

[a] Cl_i, Cl_o, K_i, K_o, Na_i and Na_o refer to the concentrations of the respective ions either in the cell (index"$_i$") or outside (index "$_o$") of the cell.

[b] E_{Cl} and E_K are the Nernst potentials of the ions.

The disequilibria of Na and K are primarily energised by the Na^+/K^+ pump. Potassium leakage out of the cell is large because of the ion channel, called the inward potassium rectifier (IRK). IRK is the major potassium channel in skeletal muscle, which makes V_m near E_K, because it is normally fully open. IRK's are strong inward rectifiers [7], meaning that the K current through these channels rapidly decreases at V_m positive to E_K. This strong rectification greatly affects cellular excitability. The conductance, which is the reciproke of resistance, of IRK varies with the square root of extracellular potassium, K_o, due to the properties of these channels [8].

We hypothesise that the combination of high P_{Cl} and a small electrochemical gradient for chloride across the membrane, must contribute largely to the rate change of V_m in response to potassium conductance, G_K, reductions. In other words, this particular combination would very impressively mask K fluxes across the membrane. Therefore, we set out to measure rate changes in V_m, when it depolarizes (~ 20 mV) due to the reduction of G_K. Variations in response times were induced either by modulating the chloride gradient with bumetanide and hypertonicity, or by lowering P_{Cl} with 9-AC. Additionally, low P_{Cl} values are charateristic for myotonia; a neuromuscular disease, which causes muscle stiffness [9].

MATERIALS AND METHODS

Lumbrical muscles were dissected from the hind foot of the mouse (Swiss White). The bundels, once dissected and freed from connective tissue, were pinned down in a perfusion chamber (volume 0.1 ml) with a constant temperature (35 °C). At a perfusion rate of 3.03 ml/min, the total volume of the chamber was changed within 5 s. Most experiments were carried out in the same cell to avoid diffusional artefacts occurring around the cell. The control solution contained (in mM): NaCl 117.5, KCl 5.7, $NaHCO_3$ 25.0, NaH_2PO_4 1.2, $CaCl_2$ 2.5, $MgCl_2$ 1.2 and glucose 5.6, saturated with humidified gas: 95 % O_2 + 5 % CO_2; pH = 7.35 - 7.45 with an osmolality of approximately 290 mOsm (mol/kg). Low potassium medium (K_o = 0.76 mM) was made by exchanging sodium for potassium equimolarly. Hypertonic solutions (~ 340 mOsm) were made adding 18 g/l poly-ethylene-glycol 400 (PEG 400). Barium (80 µM), bumetanide (75 µM) and 9-AC (75 µM) were added directly to the solution. Fine-tipped intracellular glass microelectrodes, back-filled with 3 M KCl and having a resistance of 25 - 80 M were used to measure V_m. Impalements were considered successful, if stable potentials were achieved at $V_m < -70$ mV.

RESULTS

Time course of the Barium induced depolarizations

Ba^{2+} is an established blocker of G_K [10]. Ba^{2+} is a very useful substance, because the time course of V_m change, induced by it, can be fit according to a single exponential (eq. 1) (figure 1). The timeconstant, , due to Ba^{2+} in 290 mOsm is considered the control value.

$$V_m(t) = V_{m\,(t=0)} + \Delta V_m * (1 - \exp(-t/\tau) \qquad \text{(eq. 1)}$$

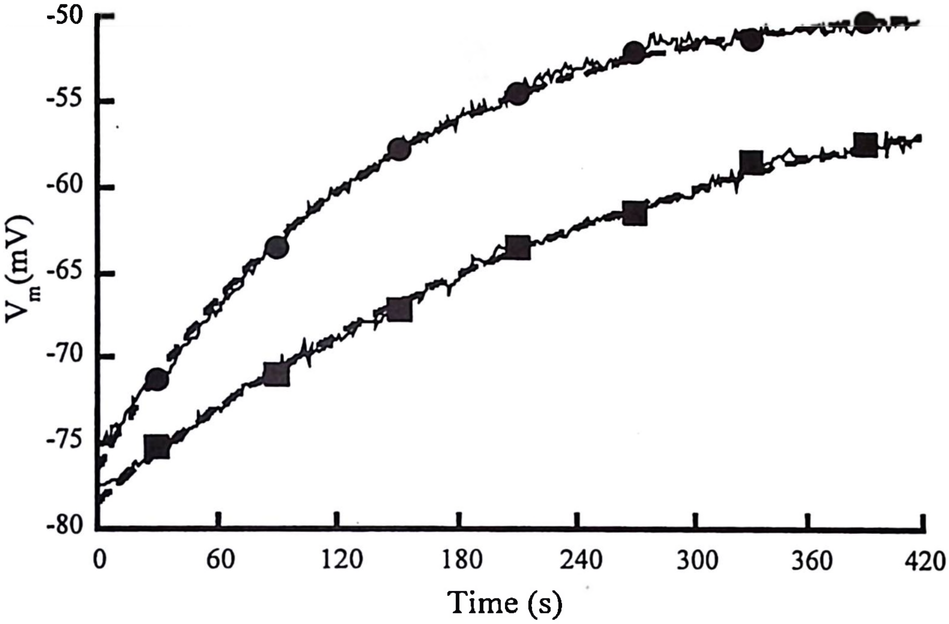

Figure 1. A typical experiment comparing the Ba^{2+} induced depolarization in the presence (squares in the drawn line) and absence of bumetanide (circles in the drawn line) in the same cell. The recordings are fit according to eq. 1 (dashed lines). The timeconstants of Ba^{2+} induced depolarizations in the presence and absence of bumetanide are 270 s and 138 s respectively. Both have regression coefficients of 0.999. The initial values in the presence and absence of bumetanide differ, because bumetanide hyperpolarizes $V_m \sim 3$ mV.

Differences in time courses induced by cotransport modulators

We have tested the influence of bumetanide as a blocker of $Na^+/K^+/2Cl^-$-cotransporter and hypertonicity (340 mOsm) as an activator of $Na^+/K^+/2Cl^-$-cotransporter [5]. The timeconstants of the Ba^{2+} depolarization caused by bumetanide and hypertonicity are displayed in table 1. Bumetanide delays the depolarization by approximately 50 s (38 %), and hyperosmolality accelerates the depolarization by approximately 40 s (30 %).

	Bumetanide	Control	Hyperosmolality
τ (s) ± SEM (n)	182 ± 23 (7)	132 ± 9 (18)	96 ± 6.9 (8)
P as compared to control	< 0.05		< 0.05

Table 1. Comparison of due to Ba^{2+} induced depolarizations in the presence of bumetanide, control and hyperosmolality. P-values were calculated using Student t test.

The presence of 9-AC accelerates the time course of V_m considerably

We set out to do test the combined effect of Ba^{2+} and 9-AC on the time course of V_m. However, this combination caused vigorous myotonic discharges, and thus movement artefacts, which dislodged the microelectrode out of cell very frequently. So, instead of reducing G_K with Ba^{2+}, we reduced G_K by lowering K_o to 0.76 mM [11]. This also caused myotonia, but to a much lesser extent, so that the cell impalement was lost less frequently.

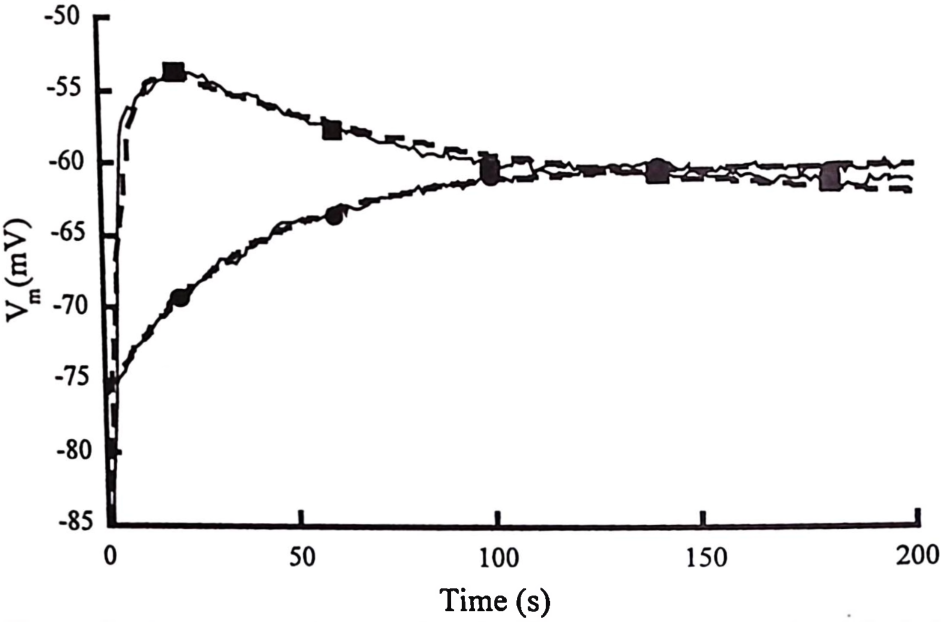

Figure 2. An experiment comparing the low potassium (0.76 mM) induced depolarization in the presence (squares in the drawn line) and absence of 9-AC (circles in the drawn line) in the same cell. The recording in the absence of 9-AC is fit according to eq. 1 (dashed line); $\tau = 37.2$ s and $R = 0.998$. The recording in the presence of 9-AC is fit (dashed line) according to the sum of two exponentials $V_m(t) = V_{m\,(t=0)} + \Delta V_{m,1} * (1 - \exp(-t/\tau_1)) + \Delta V_{m,2} * (1 - \exp(-t/\tau_2))$; $\tau_1 = 4$ s, $\tau_2 = 86.7$ s and $R = 0.973$. The initial values in the presence and absence of 9-AC differ, because 9-AC hyperpolarizes V_m.

Figure 2 displays the effect of lowering P_{Cl} on the change of V_m caused by low K_o. It clearly shows that the time course in control solution can be fitted by eq. 1, whereas it is composed of two exponentials once P_{Cl} is reduced. We propose that the first exponential is mainly due to the equilibration of cation fluxes (maybe contaminated by some Cl fluxes, since P_{Cl} is not entirely zero), and that the second exponential is due to Cl equilibration. This is in analogy to the interpretation given by Hodgkin and Horowicz for frog skeletal muscle [2]. They simultaneously reduced P_{Cl} by reducing Cl_o from the extracellular medium and increased P_K by increasing K_o, and also saw an instantaneous depolarizing transient followed by a relatively slow repolarization.

CONCLUSION

Our data clearly demonstrate that the $Na^+/K^+/2Cl^-$ cotransporter accelerates the rate change of V_m, and strongly support the interpretation that P_{Cl} damps the speed of

V_m responses to reductions in G_K. The fact that this damping stabilises V_m is also demonstrated. The occurrence of myotonia supports this analysis. A full fledged analysis of the results must wait for further measurements. Notwithstanding this damping by P_{Cl}, action potentials can still be generated, mainly because, we think, P_{Na} during the action potential is about 3 - 10 higher than P_{Cl}. These results emphasize the importance of the role of Cl in skeletal muscle. Additionally, these results were predicted by a model simulation [12]. Thereby showing a clear link between a theoretical approach using model simulations and experimental work.

REFERENCES

[1] O.F. Hutter, S.M. Padsha, J. Physiol. 146 (1959) 117 - 132.
[2] A.L. Hodgkin, P. Horowicz J. Physiol. 148 (1959) 127 - 160.
[3] P.T. Palade, R.L. Barchi, J. Gen. Physiol. 69 (1977) 879 - 896.
[4] C.C. Aickin, W.J. Betz, G.L. Harris, J. Physiol. 411 (1989) 437 - 455.
[5] H.G.J. van Mil, R.J. Geukes Foppen, J. Siegenbeek van Heukelom, Br. J. Pharmacol. 120 (1997) 39 - 44.
[6] E. Delpire, M.I. Rauchmann, D.R. Beier, S.C. Hebert, S.R. Gullans, J. Biol. Chem. 269 (1994) 25677 - 25683.
[7] C.G. Nichols, A.N. Lopatin, Ann. Revs. Physiol. 59 (1997) 171 - 191.
[8] B. Hille, Ionic Channels of Excitable Membrane. Sinauer Ass. Sunderland, Mass 1992.
[9] R.L. Barchi, Neurobiology of Disease 4 (1997) 254 - 264.
[10] H.G.J. van Mil, C.J.M. Kerkhof, J. Siegenbeek van Heukelom, Br. J. Pharmacol. 116 (1995) 2881 - 2888.
[11] J. Siegenbeek van Heukelom, J. Physiol. 434 (1991) 549 - 560.
[12] J. Siegenbeek van Heukelom, Biophys. Chem. 50 (1994) 345 - 360.

ATP REGULATION OF CYTOCHROME OXIDASE IN YEAST MITOCHONDRIA : ROLE OF SUBUNIT VIA

Bertrand Beauvoit, Odile Bunoust, Bernard Guérin, Michel Rigoulet

Institut de Biochimie et Génétique Cellulaires du CNRS, Université Victor Ségalen, Bordeaux II, 1 rue Camille Saint-Saens, 33077 Bordeaux cedex, France, Phone: +33 5 56 99 90 33, Fax: +33 5 56 99 90 59, E-mail: Bertrand.Beauvoit@ibgc.u-bordeaux2.fr

INTRODUCTION

Cytochrome oxidase is composed of three subunits encoded by mitochondrial genome and involved in catalysis, and several nuclear-encoded subunits whose composition varies with species. The functions of these supernumerary subunits are still a matter of debate. They may be involved in the assembly of the enzyme and/or in tissue-specific regulatory properties of cytochrome oxidase.

The rate of electron transfer through cytochrome oxidase is primarily controlled by the thermodynamic force across the complex, which contains two terms : (i) the difference in redox potential between oxygen and cytochrome c (i.e. ΔE_h) and (ii) the protonmotive force across the inner membrane (i.e. Δp) [1, 2]. In addition, the rate of electron flow through the enzyme depends secondly on effectors, encompassing adenylic nucleotides [1, 3]. With isolated yeast mitochondria, modifications of flow-force relationship were observed under conditions where the kinetic control exerted by the cytochrome oxidase was changed upon addition of external ATP, thus illustrating the inter-dependence between thermodynamic control and kinetic regulation [1].

Although the number and localization of binding-sites for nucleotides on the cytochrome oxidase are still a matter of debate [4, 5], there is strong structural, biochemical and functional evidence that subunit VIa bears an ATP-binding site on the C-terminal part facing the cytosol and an ADP-binding site on the matrix side of the transmembranous polypeptide [4-9]. To follow up earlier studies [1, 5, 7], we have re-examined the effect of ATP on the respiratory rate of mitochondria isolated from either subunit VIa-null mutant or the parental strain when the proton leak was modulated by adding different amounts of a protonophoric uncoupler, CCCP. The effect of ATP and the role of subunit VIa on the dependence of the electron flux through cytochrome oxidase on its associated thermodynamic forces - Δp and the redox state of cytochrome c and aa3 pools - has been investigated.

MATERIALS AND METHODS

The *Saccharomyces cerevisiae* haploid strains - the cox13 disrupted strain (JΔ6a-1) and its parent (JHRY1-2Cα) [5, 7] - were a gift from Dr Capaldi (University of Oregon). Aerobic cultures, mitochondria isolation, and steady state measurements of the respiratory rate and the cytochrome reduction level were carried out according to previously published techniques [1]. $\Delta\Psi$ was estimated by rhodamine 123 fluorescence quenching [10] after calibrating the signals as a function of the $\Delta\Psi$ measured by means of $^{86}Rb^+$ (in the presence of valinomycin).

RESULTS AND DISCUSSION

Effect of ATP on the respiratory rate of wild-type and subunit VIa null mutant

We investigated the effect of ATP (in the presence of oligomycin) on the electron flow over the entire respiratory chain or the functionally isolated complex IV (in the presence of antimycin) of the subunit VIa null mutant with respect to the wild-type (Table 1).

Table 1. Effect of ATP on maximal respiratory rate of mitochondria isolated from subunit VIa null mutant (ΔCOX13) and wild-type strain (WT)[a].

Strain	Ethanol		Lactate (plus antimycin)	
	+ATP (% of control)	+ATP +CAT (% of control)	+ATP (% of control)	+ATP +CAT (% of control)
JHRY1-2Cα (WT)	126 ± 5	135 ± 10	164 ± 2	166 ± 3
J 6a-1 (ΔCOX13)	81 ± 3	96 ± 4	79 ± 5	95 ± 4

[a] When added, ATP was 1 mM and carboxyatractylate (CAT) 1.25 µM. Control values were measured in the absence of ATP. Values are means ± SD of 6 to 9 independent experiments.

Adding ATP increased the fully uncoupled respiratory rate of mitochondria isolated from the wild-type when using ethanol or lactate (plus antimycin) as electron donors, suggesting that ATP was an effector - activator - of wild-type cytochrome c oxidase. In the case of the mutant, we measured a decrease by ATP of the maximal respiratory rate of isolated mitochondria utilizing either ethanol or lactate (plus antimycin), suggesting that ATP was still an effector - an inhibitor - of the subunit VIa null cytochrome oxidase. After adding carboxyatractylate to inhibit the ATP/ADP carrier and therefore to prevent ATP transport to the matrix, the ATP-induced inhibition of the null mutant was abolished, demonstrating that the ATP-inhibiting site was located on the matricial side of complex IV (table I). Moreover, for the wild-type, CAT addition further increased the ATP-induced activation suggesting the presence of stimulatory and inhibitory sites for ATP on the cytosolic and matricial side of complex IV, respectively (table I). Finally, evidence was found that protein phosphorylations are unlikely involved in these phenomena.

Effect of ATP on the flux-force relationships of wild-type and subunit VIa null mutant

The respiratory rate of mitochondria isolated from either the subunit VIa null mutant (ΔCOX13) or the wild-type (WT) strain was stimulated by a proton leak increase, using different amounts of an uncoupler (CCCP), in the presence of oligomycin and nigericin to collapse ΔpH and therefore to avoid any interference of the matrix pH on the cytochrome oxidase kinetics [11]. Figures 1 and 2 show that the respiratory rate was not uniquely dependent on both the ΔΨ value and the reduction level of cytochromes, with regard to : (i) the presence or not of ATP in the incubation medium, and (ii) the presence or not of subunit VIa. Indeed, at equivalent rate of electron flow, ATP increased the reduction level of cytochrome aa3 of the null mutant, without any change in ΔΨ, whereas the a+a3 redox state decreased for the wild-type, parallel to an increase in the ΔΨ value. These results point to changes in the kinetic behaviour of the cytochrome oxidase of mutant and wild-type mitochondria with respect to ATP regulation. Thus, the pattern of cytochrome aa3 redox state is consistent with an activation of the wild-type cytochrome oxidase by ATP [1], on one hand, and an inhibition by ATP of the cytochrome oxidase lacking subunit VIa, on the other.

Considering electron transport from cytochrome c to O_2, the net thermodynamic force across the complex is expressed as $-\Delta G/F = 2 \times \Delta E_h - (n+2) \times \Delta p$; where n is the $H^+/2e^-$ stoichiometry, ΔE_h, the difference in redox potential between cytochrome c and O_2. Under our conditions, Δp was expressed entirely as $\Delta\Psi$ and n value was assumed to be constant and equal to 2 [2]. Comparing the mutant and wild-type mitochondria on one hand, and steady states made in the presence or not of ATP on the other, there was no unique relationship between J_O and the net Gibbs energy across complex IV (figure 3).

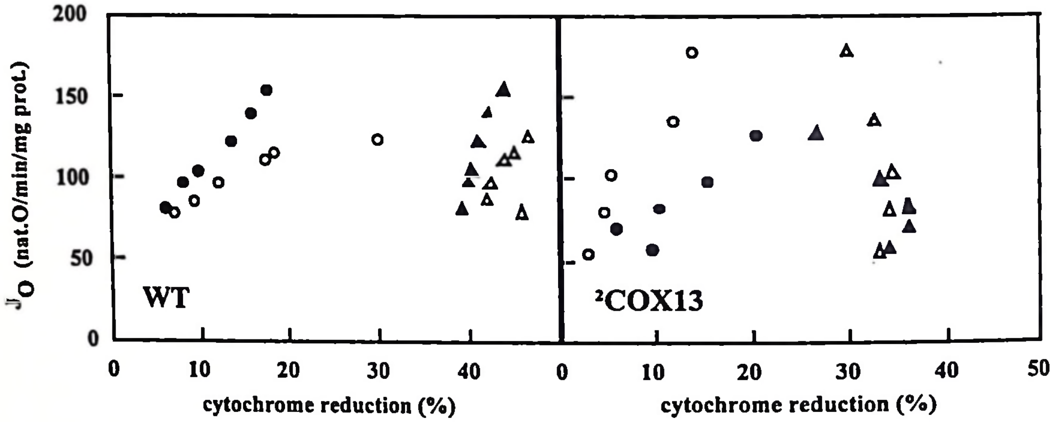

Figure 1. Effect of ATP on relationship between J_O and reduction level of cytochrome a+a3 (circles) and c+c1 (triangles) of mitochondria isolated from subunit VIa null mutant (ΔCOX13) and wild-type strain (WT).
J_O was modulated by using CCCP amounts up to 10 μM, in the presence of oligomycin, nigericin and ethanol as respiratory substrate. When added (closed symbols), ATP was 1 mM.

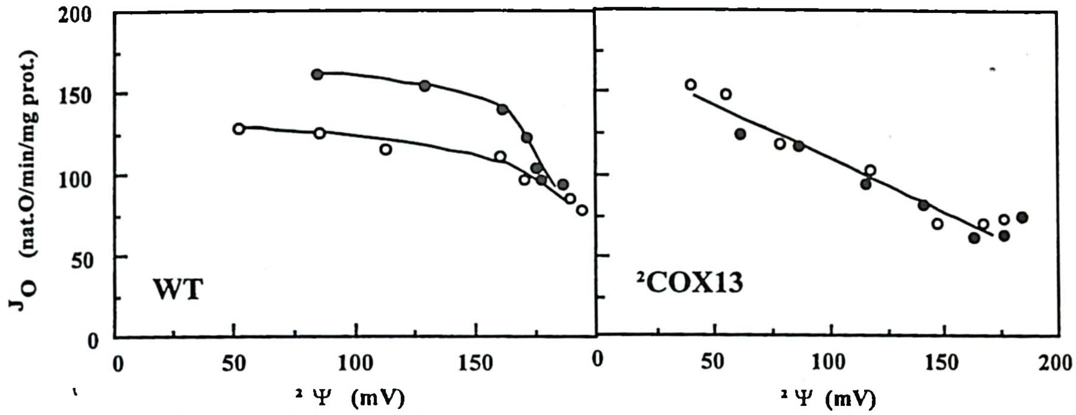

Figure 2. Effect of ATP on relationship between J_O and $\Delta\Psi$ of mitochondria isolated from subunit VIa null mutant (ΔCOX13) and wild-type strain (WT).
When added (closed circle), ATP was 1 mM.

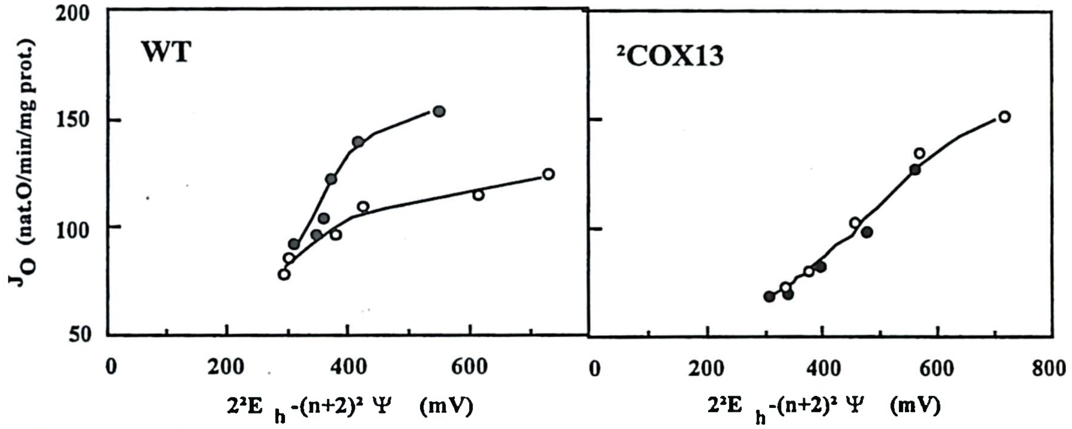

Figure 3. Effect of ATP on relationship between J_O and net thermodynamic force across cytochrome oxidase of mitochondria isolated from subunit VIa null mutant (ΔCOX13) and wild-type strain (WT).
When added (closed circle), ATP was 1 mM.

For instance, for the subunit VIa null mutant, ATP addition did not significantly modify the relationship between the rate of electron flow and the disequilibrium (i.e. -$\Delta G/F$) across complex IV (figure 3). In contrast, for the wild-type enzyme, ATP-induced activation of cytochrome oxidase changed the overall response of the enzyme upon changes in its net Gibbs energy. Such an ATP-induced change in flux-force relationship might be indicative of : (i) a decrease in the proton pumping efficiency and/or (ii) a change in the kinetic control (e.g. change in rate-constant) exerted by the individual reaction step within the catalytic cycle of the enzyme.

CONCLUSION

Taken together, our results demonstrate the existence of multiple ATP-binding sites on the cytochrome oxidase with respect to their localization and their kinetic effect. Firstly, subunit VIa is involved in the activation by ATP on the cytosolic side of the cytochrome oxidase. This is in agreement with the fact that subunit VIa possesses at least one ATP-binding site [4, 5, 7] which has been proposed to be involved in the tissue-specific effect of nucleotides on the kinetics of the reconstituted mammalian enzyme [6, 8]. In addition, we demonstrate that the subunit VIa null enzyme bears an inhibiting site for matricial ATP, whose location remains undetermined. Since all putative ATP-binding sites are present on the wild-type cytochrome c oxidase, there should be a balance between activation and inhibition with respect to the ATP concentration (or the ATP/ADP ratio) in the cytosol and matrix, on one hand, and to the nature (inhibiting vs.activating) and the location of the binding sites, on the other [3]. The question is therefore raised as to the physiological meaning of such multiple binding and regulating sites for adenylic nucleotides in the control and regulation of cellular energy metabolism.

ACKNOWLEDGEMENTS

The authors wish to thank Dr. R. A. Capaldi for the gift of J 6a-1 and JHRY1-2Cα strains and Dr. R. Cooke for editing the manuscript.

REFERENCES

[1] Rigoulet, M., Guérin, B. and Denis, M. (1987) *Eur. J. Biochem.* **168:** 275-279.

[2] Murphy, M. P. and Brand, M. D. (1987) *Biochem. J.* **243:** 499-505.

[3] Napiwotski, J., Shinzawwa-Itoh, K., Yoshikawa, S. and Kadenbach, B. (1997) *Biol. Chem.* **378:** 1013-1021.

[4] Rieger, T., Napiwotzki, J., Huther, F.-J. and Kadenbach, B. (1995) *Biochem. Biophys. Res. Comm.* **217:** 34-40.

[5] Taanman, J.-W., Turina, P. and Capaldi, R. A. (1994) *Biochemistry* **33:** 11833-11841.

[6] Anthony, G., Reimann, A. and Kadenbach, B. (1993) *Proc. Natl. Acad. Sci. U.S.A.* **90:** 1652-1656.

[7] Taanman, J.-W. and Capaldi, R. A. (1993) *J. Biol. Chem.* **268:** 18754-18761.

[8] Frank, V. and Kadenbach, B. (1996) *FEBS Lett.* **382:** 121-124.

[9] Tsukihara, T., Aoyama, H., Yamashita, E., Tomizaki, T., Yamaguchi, H., Shinzawa-Itoh, K., Nakashima, R., Yaono, R. and Yoshikawa, S. (1996) *Science* **272:** 1136-1144.

[10] Emaus, R. K., Grunwald, R. and Lemaster, J. J. (1986) *Biochim. Biophys. Acta* **850:** 436-448.

[11] Gregory, L. C. and Ferguson-Miller, S. (1989) *Biochemistry* **28:** 2655-2662.

49

THE OSCILLATORY REGIME OF THE ATP SYNTHESIS REACTION CATALYSED BY THE F_1F_O-ATPASE OF SUBMITOCHONDRIAL PARTICLES

Gennady E. Bronnikov[1, 2] *and Svetlana O. Vinogradova*[1]

(1) Institute of Cell Biophysics, Russian Academy of Sciences, 142292 Pushchino, Moscow Region, Russia; (2) The Wenner-Gren Institute, The Arrhenius Laboratories F3, Stockholm University, S-10691 Stockholm, Sweden; e.mail: gennady@molbio.su.se

INTRODUCTION

The ATP synthase complex catalyses ATP synthesis, driven by the transmembrane proton electrochemical gradient $\Delta\mu H^+$. The mechanism of ATP synthase function has been intensively studied using the water soluble F_1-ATPase which is only capable of ATP hydrolysis. The postulate advanced by Lardy and Wellman [1] more than 40 years ago, according to which the synthesis reaction is a reverse sequence of intermediate stages of the ATP hydrolysis reaction, underlies most of the suggested mechanisms for the ATP synthase function [2]. However, there are also experimental observations and interpretations in the literature [3-5] that could hardly be explained within the micro-reversibility of the ATPase reaction. The problem is to solve the question of whether the possible difference between the kinetics of the ATPase and the ATP synthase reactions is due to only the transmembrane potential or whether there are two H^+-ATPase functional forms, a synthase and a hydrolase.

Twenty years ago Vinogradov's group [6] discovered a phenomenon of turnover-dependent inactivation of the ATPase activity that was induced by ADP in the presence of Mg^{2+}. In the present report we, for the first time, describe a symmetrical situation, i. e. turnover-dependent inactivation of oxidative substrate-driven synthesis of ATP. An oscillatory regime of ATP synthase functioning is also demonstrated. We propose that both the inactivation of F_1F_O-ATPase and the oscillatory regime can be explained by the presence of two functional forms, a hydrolase and a synthase. The transition between these forms is not one of the stages of the catalytic act and lasts much longer than one enzyme turnover.

MATERIALS AND METHODS

Submitochondrial particles (SMP) were prepared according to Racker [7] by sonication of bovine heart mitochondria in the presence of 10 mM pyrophosphate (PP_i) and stored in 0.25 M sucrose, 10 mM Tris HCl, pH 7.8 in liquid nitrogen at 40 mg protein/ml. The SMP (10 mg protein/ml) were incubated in the presence of 20 mM succinate or 5 mM NADH throughout the experiment. The phosphorylation rate was measured by the incorporation of $^{32}P_i$ into ATP [8] in the following medium: 60 mM tricine KOH, pH 8.0; 4.5-18 mM K_2HPO_4, 1 mM dithiothreitol, 0.1 mM EDTA, 0.2% bovine serum albumin fatty acid free, 1.5 mM NADH, 6.5-9.5x10^5 cpm $^{32}P_i$; protein content (SMP) was 0.10-0.16 mg/ml; MgATP, MgADP and P_i were added as indicated on the Figures. A centrifuge microcolumn was used [9] to replace PP_i bound to SMP for P_i. Frozen SMP were diluted (1:3) with a buffer: 75 mM sucrose, 150 mM KCl, 2 mM $MgSO_4$, 10 mM Tris.HCl, pH 8.0 and incubated for 20 min with 5 mM PP_i or 50 mM K_2HPO_4. 30-40 µl of SMP suspension were passed through the microcolumn (250 µl Sephadex G-50) equilibrated with the same buffer containing 50 mM P_i [9]. The non-linear curve-fitting option of KaleidaGraph 3.0 for Macintosh was used.

RESULTS AND DISCUSSION

SMP from bovine heart isolated in the presence of 10 mM PP_i catalysed oxidative phosphorylation at [MgADP] > 1 mM with a constant rate for at least 12 min (Fig. 1A, Δ. When these SMP had been passed in the presence of 50 mM P_i through a microcolumn before the experiment, the kinetic curves of ATP synthesis at any of the concentration of MgADP tested were non-linear (Fig. 1A, O): the pretreatment of SMP with PP_i and P_i led to a turnover-dependent inactivation of oxidative substrate-driven synthesis of ATP. The inactivation was found to be dependent on medium concentration of ATP and ADP (Fig. 1B). The maximal ATP synthesis was approximately proportional to the total concentration of ATP and ADP. It was assumed that depletion of non-catalytic site(s) by successive treatment with PP_i and P_i was a reason for the turnover-dependent inactivation of the enzyme in the ATP synthesis, as earlier suggested for the ATPase reaction [10, 11]. The data is compatible with the existence of at least one binding site for ADP (h = 1.2) or two to three sites for ATP (h = 2.3) with K_m(app) of 1.7 mM for both nucleotides (Fig. 1B), the occupancy of which would prevent the ATP synthesis rate decay ($k_o = 1.2$ min^{-1}).

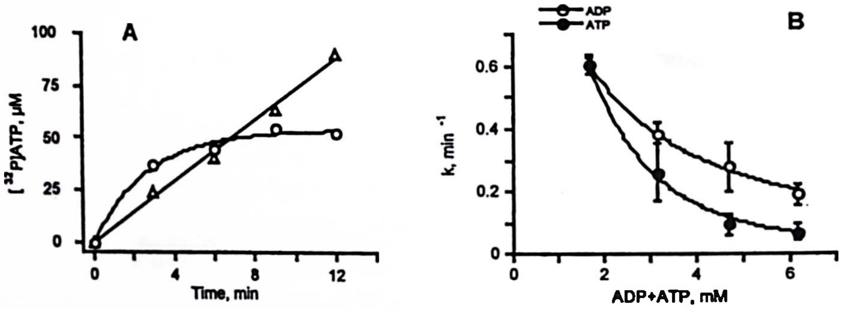

Figure 1. (A) Kinetics of ATP synthesis at 2.2 mM MgADP by non-treated SMP (Δ) and by SMP passed through a microcolumn (O). (B) Dependence of a rate constant (k) for the decay of ATP synthase activity on the concentration of adenine nucleotides (mean ± SE, n=3). Rate constants were estimated with first-order kinetic equation and data fitted by equation $k = k_o - k_o/(1+(K_m /AdN)^h)$. SMP had been preincubated with PP_i and passed through the microcolumn (50 mM P_i). Following concentrations were used: (-O-) 0.2 - 6.2 mM MgADP, (-●-) 0.2 mM MgADP + 0 - 6 mM; 9 mM P_i.

The further behaviour of the system after inactivation could be divided into two types: (i) after reaching some degree of substrate conversion the reaction completely ceased for the rest of the experiment (Fig. 1A) or (ii) the reaction changed its direction, hydrolysis of synthesised ATP took place and the process acquired a distinctly expressed oscillatory character (Figs. 2 & 3). These figures depict the non-regular character of the oscillations, the period of which ranged from 2 to 7 min. Effects of adenine nucleotides, phosphate and uncoupler on parameters of the oscillations were investigated. An increase in the ATP/ADP ratio or concentration of P_i did not affect the period of the oscillations or their appearance. The amplitude dependence on ATP/ADP was unclear and requires further investigation. The amplitude of the oscillations increased by 2.5-fold as P_i concentration decreased by 4-fold (Figs. 2 & 3). The ATP synthesis was inhibited and the ATPase activity of SMP was stimulated by the uncoupler (3 μM tetrachlorotrifluoromethylbenzimidazole, TTFB, not shown).

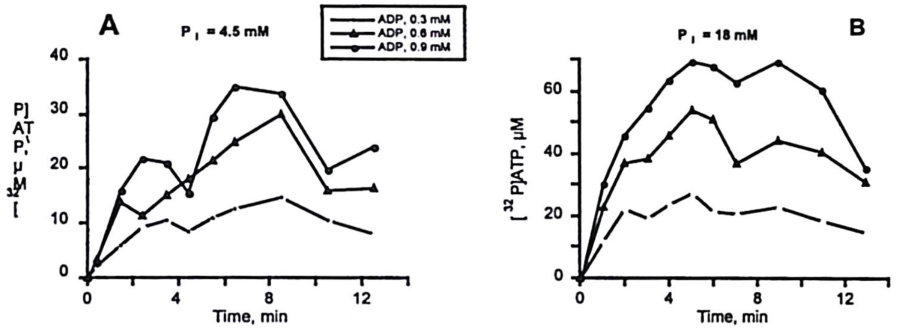

Figure 2. Non-linear regimes of ATP synthesis at different concentrations of the adenine nucleotides and inorganic phosphate.

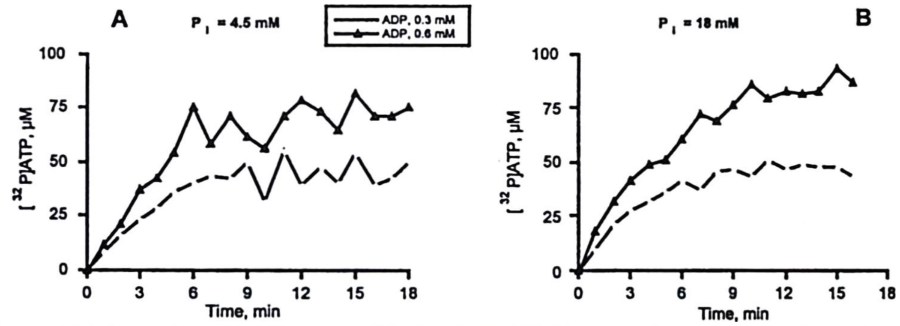

Figure 3. Dependence of the amplitude of oscillations on the concentration of inorganic phosphate. The reaction proceeded in an oscillatory regime (A) or the reaction ceased (B).

The origin of those phenomena lies outside of a trivial explanation. The physical nature of the initial rate decay described is surely not related to a net accumulation of ATP as a reaction product, the reaching of a threshold value of ΔG_p, or to participation in the regulation of a natural inhibitor protein. Appearance of both regimes, the turnover-dependent inactivation and oscillations, apparently depended on occupancy of non-catalytic sites of F_1: treatment of F_1 with PP_i and microcolumn in the presence of

P_i has been widely used for preparation of adenine nucleotide free F_1 [9]. Binding of either ATP or ADP prevented the non-linear kinetics, with a higher effect of ATP.

In our opinion the results of the present report have great similarity with the estimated mechanism of the turnover-dependent inactivation of the F_1-ATPase. Briefly, during the ATPase reaction an intermediate enzyme·product complex, F_1·MgADP, isomerizes slowly to the inactive complex with entrapment of the MgADP in a catalytic site [10]. These complexes, active and inactive, are in an equilibrium that can be shifted towards an active form with dissociation of the inhibitory MgADP by the binding of ATP [11] or PP_i [12] to the non-catalytic site(s). Sulphite, azide and P_i are able to affect the equilibrium between the active and inactive forms [13, 14].

We propose that the initial ATP synthesis rate decay can be well interpreted on the basis of a suggestion that is symmetrically opposite to the mechanism presented above: there is a slow conversion of an intermediate enzyme·product complex, ATP synthase·MgATP into an inactive form, ATP synthase*MgATP. Based on differential effects of ADP [14], sulphite and azide [5] on ATPase and oxidative phosphorylation in SMP, Vinogradov has hypothesised [3, 14] that F_1-ATPase can exist in two slowly interconverting forms and that ATP and ADP act as effectors controlling the equilibrium between the functional forms by binding at tight-affinity sites. We propose that either inactive form with the product entrapped in a catalytic center functionally is its opposite enzymatic form, i.e. slow inactivation actually is a transition of either active functional form into its active opposite enzymatic mode. A successive turnover-dependent inactivation of ATP synthesis and ATP hydrolysis with k ~ 0.1-1 min^{-1} provides the foundation for the oscillatory regime and other types of non-linear kinetics:

ATPase·MgADP ' ATP synthase·MgADP (i.e. ATPase*MgADP) (1)

and ATP synthase·MgATP ' ATPase·MgATP (i.e. ATP synthase*MgATP) (2)

The proper substrate of F_1-ATPase is MgATP; when MgADP, in the absence of P_i, is bound at the catalytic site, the complex is unstable and isomerizes slowly into the stable synthase form without any measurable ATPase activity (eq. 1). Now, after energization of SMP, entrapped MgADP can be dissociated (K_m(ADP) for synthase form ~ 10-100 μM) or phosphorylated. The correct substrate for the ATP synthase is MgADP; the ATP synthase·MgATP complex is unstable and loses its synthase activity due to a slow isomerization (eq. 2) into its opposite functional form. Entrapped MgATP can now be hydrolysed or dissociated from the ATPase active site after deenergization (K_m(ATP) ~ 100 μM).

Figs. 2 & 3 show that P_i affected the amplitude of the oscillations: the oscillations practically disappeared when the P_i concentration increased. As Yalamova et. al [14] reported, P_i accelerated the transition between the functional forms quickening the dissociation of tightly bound MgADP. Beharry and Bragg [15], studying ATP synthesis by F_1-ATPase in dimethylsulfoxid, found that the effect of medium phosphate was analogous to that occurring on membrane energization: P_i accelerated a transition from the ATPase form to a synthetically-competent enzyme. The existence of this conformational transition in bovine F_1-ATPase was shown by chemical modification and cross-linking [15]. In our opinion the non-linear kinetics are additional evidence for a lack of micro-reversibility in reactions of ATP synthesis and hydrolysis.

REFERENCES

[1] H.A. Lardy and H. Wellman, The catalytic effect of 2,4-dinitrophenol on adenosinetriphosphate hydrolysis by cell particles and soluble enzymes, J. Biol. Chem. 201 (1953) 357-370.

[2] P.D. Boyer, The ATP synthase - a splendid molecular machine, Annu. Rev. Biochem. 66 (1997) 717-749.

[3] A.D. Vinogradov, Catalytic properties of mitochondrial ATP synthase, Biochemistry (Russian) 49 (1984) 1220-1238.

[4] I.I. Lobysheva, M.G. Goldfeld, V.D. Mikoyan and L.A. Blumenfeld, Oscillatory phenomena in chloroplasts at acid-base shift. I. Kinetics of ATP formation, Biophysics (Russian) 33 (1988) 886-888.

[5] A.V. Syroeshkin, E.A. Vasilyeva and A.D. Vinogradov, ATP synthesis catalyzed by the mitochondrial F_1F_0-ATP synthase is not a reversal of its ATPase activity, FEBS Lett. 366 (1995) 29-32.

[6] A.F. Fitin, E.A. Vasilyeva and A.D. Vinogradov, An inhibitory high affinity binding site for ADP in the oligomycin-sensitive ATPase of beef heart submitochondrial particles, Biochem. Biophys. Res. Commun. 86 (1979) 434-439.

[7] E. Racker, Studies of factors involved in oxidative phosphorylation, Proc. Natl. Acad. Sci. USA 48 (1962) 1659-1663.

[8] G.E. Bronnikov and S.D. Zakharov, Microquantitative determination of P_i-ATP and ADP-ATP exchange kinetics using thin-layer chromatography on silica gel, Analyt. Biochem. 131 (1983) 69-74.

[9] F.A.S. Kironde and R.L. Cross, Adenine nucleotide-binding sites on beef heart F_1-ATPase. Conditions that affect occupancy of catalytic and noncatalytic sites, J. Biol. Chem. 261 (1986) 12544-12549.

[10] Y.M. Milgrom and P.D. Boyer, The ADP that binds tightly to nucleotide-depleted mitochondrial F_1-ATPase and inhibits catalysis is bound at a catalytic site, Biochim. Biophys. Acta 1020 (1990) 43-48.

[11] Y.M. Milgrom, L.L. Ehler and P.D. Boyer, ATP binding at noncatalytic sites of soluble chloroplast F_1-ATPase is required for expression of the enzyme activity, J. Biol. Chem. 265 (1990) 18725-18728.

[12] J.-M. Jault, S.R. Paik, N.B. Grodsky and W.S. Allison, Lowered temperature or binding of pyrophosphate to sites for noncatalytic nucleotides modulates the ATPase activity of the beef heart mitochondrial F_1-ATPase by decreasing the affinity of a catalytic site for inhibitory MgADP, Biochemistry 33 (1994) 14979-1485.

[13] E.A. Vasilyeva, I.B. Minkov, A.F. Fitin and A.D. Vinogradov, Kinetic mechanism of mitochondrial adenosine triphosphatase. Inhibition by azide and activation by sulphite, Biochem. J. 202 (1982) 15-23.

[14] M.V. Yalamova, E.A. Vasilyeva and A.D. Vinogradov, Mutually dependent influence of ADP and P_i on the activity of mitochondrial adenosine triphosphatase, Biochem Internat. 4 (1982) 337-344.

[15] S. Beharry and P.D. Bragg, Conformational change in beef-heart mitochondrial F_1-ATPase to ATP synthesis mode induced by dimethylsulfoxide and ATP revealed by sulfhydryl group labeling, FEBS Lett. 253 (1989) 276-280.

KINETICS OF KCN BINDING TO CYTOCHROME *d* IN *SALMONELLA TYPHIMURIUM*

E. Keyhani (*) and D. Minai-Tehrani

Institute for Biochemistry and Biophysics, University of Tehran, I.R. Iran
Tel: 00-98-21-611-3373; Fax: 00-98-21-640-4680
E-mail: keyhanie@ibb.ut.ac.ir or keyhanie@hemmat.ut.ac.ir

INTRODUCTION

Cytochrome *d* is one of the terminal oxidases in a number of gram-negative heterotrophic bacteria [1,2]. In *Escherichia coli* it was shown that under high aeration growth conditions, the cytochromes *bo* terminal oxidase complex predominated, whereas under low aeration conditions, the cytochromes *bd* complex predominated [3-7]. Antibodies raised against cytochrome *d* of *E. coli* showed that gram-negative bacteria such as *Serratia marcescens*, *Photobacterium phosphoreum*, *Salmonella typhimurium*, *Klebsiella pneumoniae*, and *Azotobacter vinelandii* contained cytochrome *d*- related material [8]. Cytochrome *o* belongs to the oxidases family containing a heme/copper binuclear oxygen reducing center and functioning as a proton pump [9]; cytochrome *d* has no copper [5] and does not pump protons [10]. Cyanide is a known respiration inhibitor and its interaction with oxidases of various respiratory chains has been reviewed in the past [11], including its interaction with cytochrome *d* of *E. coli* [3] and *Azotobacter vinelandii* [12,13]. However, virtually most studies, including recent ones [14,15], payed very little attention to other bacterial species. *Salmonella typhimurium* is a major threat to human health and, whether considering the biological aspect or the medical aspect of this bacterium, an important element of the bacterial metabolism is the mechanism of energy production catalyzed by the respiratory chain. In this research, we study some aspects of the kinetics of KCN with cytochrome *d*, one of the two terminal cytochromes of *Salmonella typhimurium*.

MATERIALS AND METHODS

Salmonella typhimurium was grown in a medium containing 7g peptone, 5 g yeast extract and 3 g NaCl per liter; the pH of the medium was adjusted to 7.0 with 10 M NaOH. To obtain a maximum amount of cytochrome *d*, the cells were harvested in the stationary phase of growth (47-72 hours). After two washes with phosphate buffer 0.1 M, pH 7.0, the cells were resuspended in buffer (0.1 M), either at pH 7.0 or at different pH values from 5.0 to 10.0 with unit increments.

Spheroplasts were prepared according to reference [16].

To prepare membrane fragments, the cells were suspended in phosphate buffer and equal amounts of glass beads were added. The mixture was

---

(*) also: Lab. for Life Sciences,Saadat Abade,Sarve Sharghi 34,19979 Tehran then vortexed 3 times for 30 seconds with intermittent cooling in an ice-water bath. The cells were centrifuged at 7,000 rpm for 15 minutes, the pellet discarded and the supernatant centrifuged at 30,000 rpm for 45 min. The pellet, consisting of membranes fragments, was suspended in phosphate buffer 0.1 M, pH 7.0. All assays were carried at room temperature (~ 22°C) and the spectra were obtained by Aminco DW2 spectrophotometer.

RESULTS AND DISCUSSION

Figure 1A shows the reduced-minus-oxidized difference spectrum of *S. typhimurium* The sample was reduced with dithionite and the reference was oxidized by addition of 3 µl of H_2O_2 according to reference [17]. The presence of catalase caused decomposition of H_2O_2, thus enough O_2 was present to keep the system in the oxidized state. In this spectrum, cytochrome *d* showed an absorption band at 630 nm and a through at 649 nm; the α absorption bands of cytochromes *b595* and *b560* were also seen. Fig. 1B shows the effect of KCN on cytochrome *d*. Both sample and reference were kept in the oxidized state by the addition of 3 µl of H_2O_2; then KCN (1 mM) was added to the sample and the complex of oxidized cytochrome *d*-KCN showed a through at 649 nm. Upon addition of dithionite to the sample, some reduction of cytochrome *d* was detected as the absorption band at 630 nm appeared (Fig. 1C).

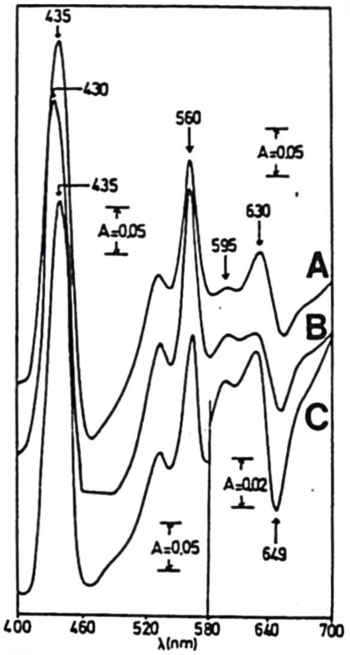

Fig. 1 - Intact cells; A and B: 26 mg prot./ml; C: 32 mg prot./ml. See text for details.

To obtain optimal conditions during kinetic studies of spectral changes of cytochrome *d* in the presence of cyanide, different amounts of H_2O_2 were added to both sample and reference in a preliminary experiment, to ensure that no endogenous or anaerobic reduction was taking place during the course of the experiment, since it was suggested that KCN only binded to the oxidized form of cytochrome *d* [3].

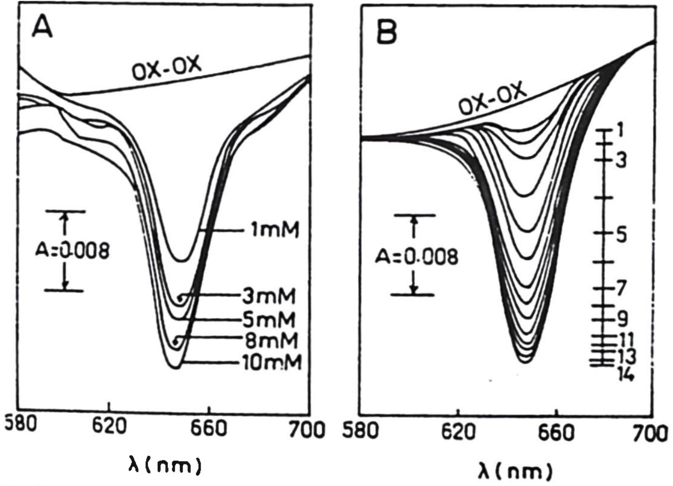

Fig.2-A and B:KCN-cyt. *d* in intact cells (24 mg prot./ml).

Fig. 2A shows that the addition of KCN to the H_2O_2 oxidized sample in intact cells (H_2O_2-oxidized-KCN minus H_2O_2-oxidized) produced a concentration-dependent through at 649 nm (each spectrum was taken after 30 min. incubation). In Fig. 2B, a single amount (5 mM) KCN was added to the sample and spectra were obtained at 2 min. intervals; results indicated that the interaction between KCN and cytochrome *d* in intact cells was a progressive process. Lineweaver-Burke plot (Fig.3) for the reaction between cytochrome *d* and KCN in intact cells, spheroplasts and membrane fragments showed that K_S for all three conditions was around 3 mM; in contrast, V_{MAX} was higher for membrane fragments (28 pmol/min/mg protein) than for spheroplasts (17 pmol/min/mg protein), and, finally, for intact cells it was the lowest (8.2 pmol/ min/mg protein). This indicated that the diffusion process from intact cells to cytochrome *d* was slower than from spheroplasts and membrane fragments. Indeed, in intact cells, KCN has to cross the outer- and inner- membranes as well as the periplasmic space to reach cytochrome *d* while in spheroplasts, it has to cross only the inner membrane, and in membrane fragments, KCN is readily accessible to cytochrome *d*. In contrast, the absence of change in the Ks value indicated that a single form of cytochrome *d* reacted with KCN in *S. typhimurium*.

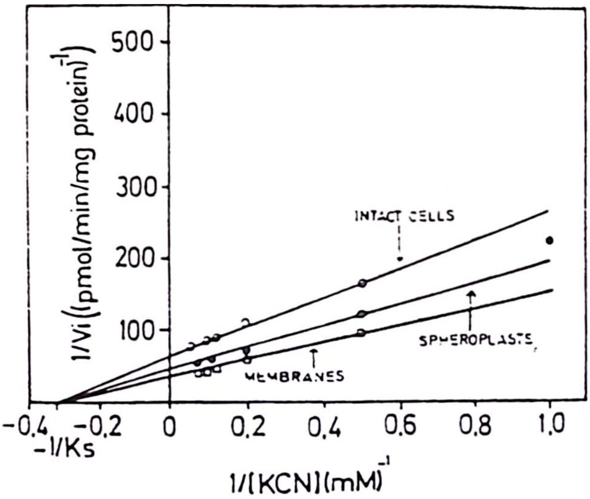

Fig. 3 - Lineweaver-Burke plot for the formation of KCN-cyt. *d* complex in intact cells, spheroplasts and membrane fragments.

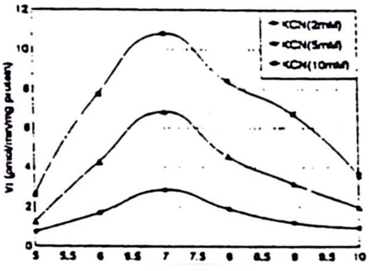

Fig. 4 - pH profile of KCN binding to cyt. *d*

The pH effect on the binding of KCN to cytochrome *d* in intact cells is shown in Fig. 4. For concentrations of 2, 5, and 10 mM KCN, binding was maximal at pH 7 and minimal for pH 5 and 10. This result again suggested that only one species

TABLE I

BUFFER (1)	V_{MAX} (2)	K_S (3)
MES	43	4.2
TRIS	32	3.7
TES	25	4.7
PIPES	22	4.6
HEPES	22	2.2
PHOSPHATE	12	3.0

(1) All buffers were 0.1 M, pH 7.0

(2) (pmol/min/mg protein); (3) (mM)

Session 4

Metabolic Pathways, Compartments and Channels & Transient Regulation of Metabolism

of cytochrome *d* was involved in KCN binding. Enzymes are pH sensitive and dual optima peaks in pH curves can be taken as indication that more than one enzyme species is present [18]. The effect of various buffer systems at pH 7 and concentration of 0. 1M on V_{MAX} and K_S is indicated in Table I. V_{MAX} was lowest for phosphate buffer and highest for MES buffer and the stability of the complex was (HEPES < phosphate < tris < MES < PIPES < TES) with a factor of 2 between the two extremes. Addition of NaCl (Fig.5) (0.1 to 1.0 M) decreased cytochrome*d*'s affinity for KCN (K_S increased 1.5 X) and the rate of formation of the complex in phosphate buffer (V_{MAX} decreased 4 X).

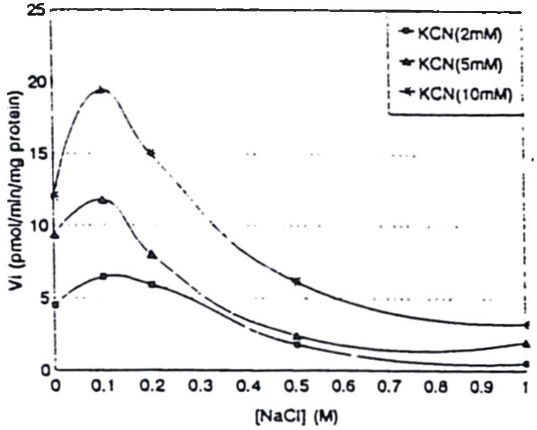

Fig. 5 - Effect of NaCl on KCN binding to cytochrome *d* in intact cells.

REFERENCES

1 Poole, R.K. (1983) Biochim. Biophys. Acta 726, 205-243.
2 Anraku, Y. (1988) Ann. Rev. Biochem. 57, 101-132.
3 Pudek, M.R. and Bragg, P.D. (1974) Arch. Biochem. Biophys. 164, 682-693.
4 Kita, K., Kasahara, M. and Anraku, Y. (1982) J.Biol.Chem. 257, 7933-7935.
5 Kita, K., Konishi, K. and Anraku, Y. (1984) J. Biol. Chem. 259, 3368-3374.
6 Kranz, R.G. and Gennis, R.B. (1984) J. Biol.Chem. 259, 7998-8003.
7 Georgiou,C.D., Fang,H. and Gennis,R.B.(1987) J.Bacteriol.169, 2107-2112.
8 Kranz, R.G. and Gennis, R.B. (1985) J. Bacteriol. 161, 709-713.
9 Saraste, M., Holm, L., Lernieux, L., Luhheen, M. and Oost, J. (1991) Trends Biochem. Sci. 19, 608-612.
10 Purustinen, A., Finel, M., Haltia, T., Gennis, R.B. and Wikstrom, M. (1991) Biochemistry 30, 3936-3942.
11 Lemberg, R. and Barrett, J. (1973) Cytochromes, pp. 43-47, Academic Press, London.
12 Kauffman, H.F. and Van Gelder, B.F. (1973) Biochim. Biophys. Acta 314, 276-283.
13 Kauffman, H.F. and Van Gelder, B.F. (1974) Biochim. Biophys. Acta 333, 218-227.
14 Krasnoselskaya, Arutjunjan, A.M., Smirnova, I., Gennis, R. and Konstantinov, A.A. (1993) FEBS Letters 327, 279-283.
15 Tsubaki, M., Hori, H., Mogi, T. and Anraku, Y. (1995) J. Biol. Chem. 270, 28565-28569.
16 Goodhew, C.F., Wilson, I.B.H., Hunter, D.J.B. and Pettigrew, G.W. (1990) Biochem. J. 271, 707-712.
17 Keyhani, E. and Keyhani, J. (1982) Biochim. Biophys. Acta 717, 355-368.
18 Fullbrook, P.D. (1996) in: Industrial Enzymology (T. Godfrey and S. West, Eds) 2nd edition, pp 508-510, Stockton Press, New York.

REGULATION THROUGH MOIETY CONSERVATION: THE ROLE OF PRODUCT SENSITIVITY IN GLYCOLYSIS OF YEAST AND TRYPANOSOMES

Bas Teusink[1], *Femke I.C. Mensonides*[1], *Barbara M. Bakker*[1,2], *Michael C. Walsh*[1], *Jacky L. Snoep*[2], *Karel van Dam*[1] *and Hans V. Westerhoff*[1,2]

[1] E.C. Slater Institute, BioCentrum Amsterdam, University of Amsterdam, Plantage Muidergracht 12, NL-1018 TV Amsterdam, The Netherlands
[2] IMBS, BioCentrum Amsterdam, Department of Microbial Physiology, Faculty of Biology, Vrije Universiteit, De Boelelaan 1087, NL-1081 HV Amsterdam, The Netherlands, Tel +31 20 5255069, Fax +31 20 525 5124, E-mail: a311bt@chem.uva.nl

INTRODUCTION

Many catabolic pathways invest free energy at the beginning of the pathway, after which subsequent metabolism yields a surplus of free energy (mainly ATP and reducing equivalents). The example used here is glycolysis, in which two ATP are invested at the hexokinase (HK) and phosphofructokinase (PFK) step, after which the phosphoglycerate kinase and pyruvate kinase steps produce 4 ATP (see Fig. 1A).

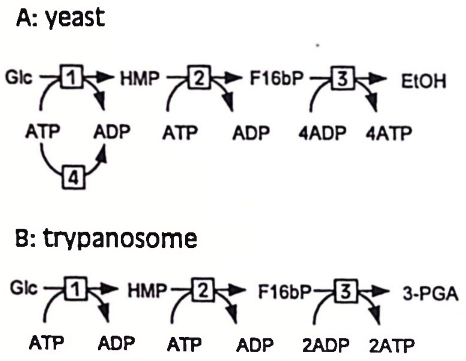

Fig 1. Schematic representation of glycolysis in yeast and in the glycosome of trypanosomes. HMP, hexose monophosphates; F16bP, fructose 1,6-bisphosphate; 3-PGA, 3-phosphoglycerate; 1, hexokinase (HK); 2, phospho fructokinase (PFK); 3, lower part glycolysis; 4, ATPase

This autocatalytic (or "turbo") design of glycolysis may be optimal with respect to the rate of ATP production [1, 2]. However, on the basis of mathematical modeling we have suggested that such designs require additional regulation to ensure proper steady states at highly variable extracellular substrate concentrations [3]. We found that feedback via the adenine nucleotides was incapable of adapting the HK activity to the capacity of the ATP producing steps. In this paper we will show experimentally that HK appears to be sensitive to its product, but that this (weak) product sensitivity alone is not strong enough to reach a steady state for all metabolic variables. Yeast appears to require additional regulation mediated by trehalose 6-phosphate synthase (see e.g. [4]). The need for product inhibition is here explained in terms of Metabolic Control Analysis. The metabolic danger of glycolysis' autocatalytic stoichiometry is further illustrated by comparison with the glycolytic design of *Trypanosoma brucei*, which is *not* autocatalytic [5]. In trypanosomes, glycolysis takes place in the glycosome, an organelle in which glycolysis proceeds only until 3-phosphoglycerate, and hence, only two ATP are produced per two ATP invested (Fig. 1B).

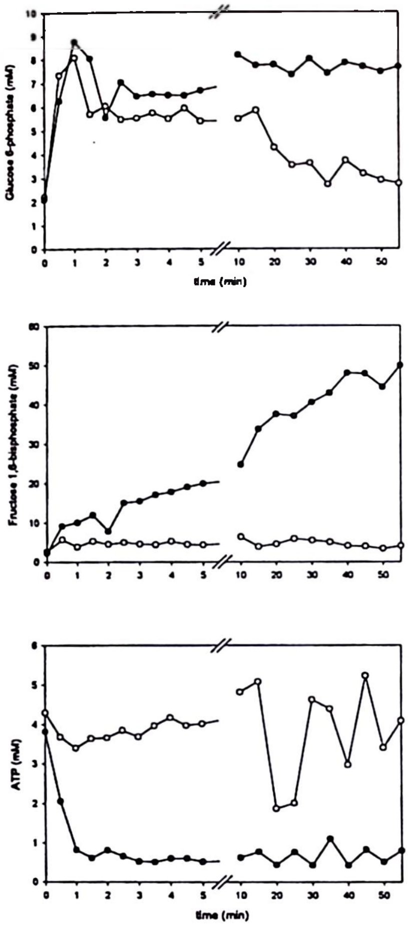

Fig 2. Time dependence of intracellular metabolite concentrations after addition (at t=0) of 50 mM glucose to galactose-grown yeast cells. Open symbols, wild type; closed symbols, tps1-Δ mutant. (Note that Fig. 2 is a combination of two independent experiments, done at different time-scales; see the time-axis)

METHODS

Computational

A core model has been constructed as described in Ref [3] (see also Fig 1A). This model consists of three ordinary differential equations (ODE's), describing the time-dependence of the three independent metabolites HMP, F16bP and ATP. Michaelis-Menten kinetics were used, except for PFK, for which a two-substrate Monod-Wyman-Changeux model with ATP inhibition was employed. For the glycosomal model (Fig. 1B), the same kinetics were used; the ATPase was omitted and the ODE for ATP was adapted to the different stoichiometry of ATP production. The differential equations were integrated using the metabolic modelling package SCAMP [6].

Experimental

A *tps1-Δ* mutant of *Saccharomyces cerevisiae* and its parent strain (M5) were grown in 2% galactose medium containing 0.17% YNB, 0.5% ammonium sulphate and the required auxotrophic markers, harvested at mid-exponential growth and resuspended in a 100 mM potassium phosphate buffer at pH 6.8. After addition of glucose (at 30°C), samples were taken and quenched in perchloric acid (5% final concentration). After neutralization with potassium carbonate, the samples were analyzed for metabolites by enzymatic determinations, essentially according to Bergmeyer [7].

RESULTS AND DISCUSSION

Introducing reversibility of the hexokinase (HK) step

Fig.2 shows a time course of glucose 6-phosphate, fructose 1,6 bisphosphate and ATP in a yeast *tps1-Δ* mutant and in the wild type, after addition of 50 mM glucose. In the mutant, the ATP concentration dropped quickly and remained constant while fructose 1,6-bisphosphate continued to accumulate throughout the 55 minutes of the experiment. Glucose 6-phosphate (and fructose 6-phosphate, not shown), however, reached a steady state within 3 minutes. (Note that Fig. 2 is a combination of two independent experiments, done at different time-scales; see the time-axis). This suggests that HK is product sensitive, allowing the rates of HK and PFK to adjust to one another. The continuous accumulation of F16bP suggests that, in the mutant, product inhibition of PFK is not very effective. In the model, introducing weak product inhibition of HK by replacing the irreversible MM equation by a reversible one ($K_{eq,\ HK}$ =4000; K_{ADP}=1mM; K_{HMP}=5mM), we could reproduce the experimental results for the mutant qualitatively (Fig 3A). Clearly, weak feedback inhibition of HK is not sufficient for a steady state to settle; the lower part of glycolysis appears unable to communicate its failure to cope with the flux through PFK. This is very different for the trypanosomal glycolysis. In Fig.3B a time course is shown for the model of glycosomal glycolysis (see Methods, Fig. 1B). Here, even though the same bottleneck in the ATP-producing (v_3) step was present, no accumulation was seen and the system reached a steady state. Apparently the communication via the adenine nucleotides was functional in the case of glycosomal glycolysis, which has no 'turbo' design.

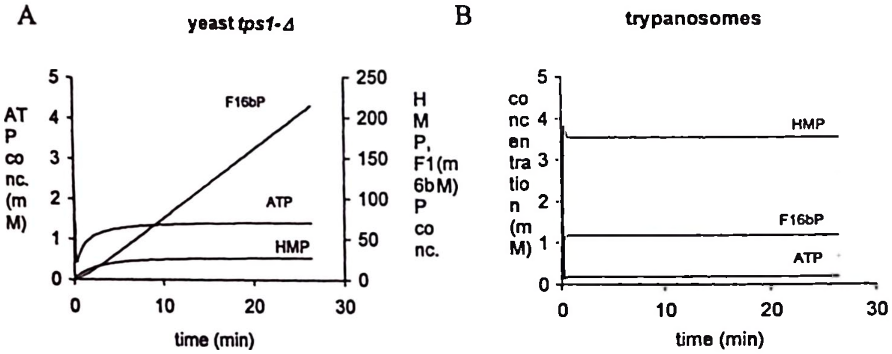

Fig 3. Time course of the variables of the two models. See text for explanation

The flux control of the ATP producing step in yeast and in the glycosome

A detailed kinetic analysis [3] revealed that the "bottleneck" in the ATP-producing part of glycolysis is not properly signaled through the adenine nucleotides because the concentrations of the adenine nucleotides and the hexose phosphates could vary independently. Consequently, after ATP had reached a stationary state the hexose phosphate continued to accumulate. The accumulation of hexose phosphates at a constant ATP concentration could be prevented by reducing the capacity of HK or by (strong) product inhibition. If the product inhibition of HK is weak, however, a steady state is not reached (Fig 2 and 3A): also PFK needs to be sensitive to its product fructose 1,6-bisphosphate. Apparently, feedback regulation of PFK via the adenine nucleotides fails, as it did for HK.

Here we wish to demonstrate the failure of the adenine nucleotide feedback with Metabolic Control Analysis. Using the summation and connectivity theorems of Metabolic Control Analysis [8-10], we have calculated the control of the ATP producing step (v_{lower}) on the flux through the system. For the glycolytic pathway of yeast:

$$\tilde{C}^{J}_{lower} = -\tilde{\varepsilon}^{HK}_{HMP}\tilde{\varepsilon}^{PFK}_{F16bP}(\tilde{\varepsilon}^{ATPase}_{ATP} - \tilde{\varepsilon}^{ATPase}_{ADP})/\Sigma_1 \qquad (1)$$

Where Σ_1 abbreviates a nonzero extensive sum of combinations of elasticities; we are only concerned with the numerator here. For the trypanosomal glycolysis:

$$\tilde{C}^{J}_{lower} = \left[\left(\tilde{\varepsilon}^{HK}_{HMP}\tilde{\varepsilon}^{PFK}_{FBP} + 2\tilde{\varepsilon}^{HK}_{HMP}\left(\tilde{\varepsilon}^{PFK}_{ATP} - \tilde{\varepsilon}^{PFK}_{ADP}\right) + \tilde{\varepsilon}^{PFK}_{FBP}\left(\tilde{\varepsilon}^{HK}_{ATP} - \tilde{\varepsilon}^{HK}_{ADP}\right)\right) - 2\tilde{\varepsilon}^{PFK}_{HMP}\left(\tilde{\varepsilon}^{HK}_{ATP} - \tilde{\varepsilon}^{HK}_{ADP}\right)\right] / \Sigma_2$$

(2)

Where Σ_2 is again a sum of combinations of elasticities. Note that unscaled control and elasticities have been used.

Comparing the two numerators, it is clear that in the case of yeast glycolysis (Eq. 1), *both* ATP-consuming kinases need to be sensitive to their *'carbon'*-product in order for the ATP producing step to have a nonzero flux control. If PFK is (modeled to be) carbon-product insensitive, a bottleneck in the lower part of glycolysis cannot be communicated to the upper part of glycolysis. It does *not* suffice for PFK to be sensitive to the adenine nucleotide product, ADP.

Carbon-product sensitivity of HK and/or PFK is not required in the glycolytic pathway of trypanosomes without 'turbo' design (Eq. 2). Even if both HK and PFK are product insensitive, the lower part of glycolysis can still control the glycolytic flux to some extent. The important difference with yeast is, that in the glycosomal case there are *two* moiety conservation cycles, not only ATP + ADP, but also HMP + 2F16bP + ATP. The latter expresses the conservation of phosphate in the system, as there is no ATPase releasing inorganic phosphate. (Saturation of phosphate was assumed in the yeast model.) The latter moiety conservation caused effective coupling of the concentration of adenine nucleotides with the hexose phosphates, which was absent from the turbo glycolysis.

Understanding the control by the ATP-producing step

It was not immediately obvious to us why the coupling of the upper part of glycolysis with the lower part cannot be brought about by the adenine nucleotides. We have therefore constructed a simplified version of the core model of yeast glycolysis (Fig 4A). X denotes a glycolytic metabolite separating the ATP consuming reactions from the ATP producing ones; Y denotes ADP (we have chosen ADP so that X and Y are both products of reaction 1 and substrates of reaction 2); reaction 3 is an ATPase, producing ADP. Control analysis of this system of Fig. 4A leads to the following expression for the control of reaction 2 on the flux through rate 1:

$$\tilde{C}^{J_1}_{2} = \frac{-\tilde{\varepsilon}^{3}_{Y}\tilde{\varepsilon}^{1}_{X}}{-\tilde{\varepsilon}^{1}_{Y}\tilde{\varepsilon}^{2}_{X} + \tilde{\varepsilon}^{2}_{Y}\tilde{\varepsilon}^{1}_{X} - \tilde{\varepsilon}^{3}_{Y}\tilde{\varepsilon}^{1}_{X} + \tilde{\varepsilon}^{3}_{Y}\tilde{\varepsilon}^{2}_{X}} \qquad (3)$$

Again, if rate 1 (the kinase) is carbon-product insensitive (i.e. ε^{1}_{X}=0) the flux control of step 2 is again zero: whether or not the coupling metabolite Y is a member of a moiety conserved cycle (which is not the case in Fig. 4A) does not appear to be crucial. What is important then? If rate 1 is insensitive to X, then rate 2 is the *only* rate that is still sensitive to X (as the ATPase is a function of Y only). When the activity of step 2 is increased, X will simply decrease, in order to reach a steady state in X. Variation of X does not affect the rates of ADP (Y) production, and Y will not change. This fate of step 2, i.e. being able merely to adjust the steady-state concentration of X, can be clearly illustrated by introducing a reaction 4 consuming X (Fig. 4B). Rate 4 could represent the glycerol branch in yeast glycolysis. The flux control coefficient of step 2 with respect to flux 1 is now:

$$\tilde{C}_2^{J_1} = \frac{-\tilde{\varepsilon}_Y^1(\tilde{\varepsilon}_X^1 - 2\tilde{\varepsilon}_X^4) - \tilde{\varepsilon}_X^1(\tilde{\varepsilon}_Y^3 + \tilde{\varepsilon}_Y^1)}{(\tilde{\varepsilon}_Y^2 + \tilde{\varepsilon}_Y^1)(\tilde{\varepsilon}_X^1 - 2\tilde{\varepsilon}_X^4) - (\tilde{\varepsilon}_Y^3 + \tilde{\varepsilon}_Y^1)(\tilde{\varepsilon}_X^2 + \tilde{\varepsilon}_X^1 - \tilde{\varepsilon}_X^4)} \quad (4)$$

If rate 1 is insensitive to X in this case, the flux control of rate 2 is *not* zero. Step 2 cannot affect the concentration of Y directly, but can do so by changing the distribution of X consumption over its own step and step 4. This change in flux distribution does have an effect on the net consumption of Y per X produced, and in this way step 2 can affect the steady-state concentration of Y (unless the branch (step 4) is insensitive to X, in which case we are back in situation 4A). Rather than introducing a branch in glycolysis, simply making the ATPase sensitive to X also works (not shown), but appears less realistic. Thus, paradoxically, introducing an extra degree of freedom by adding a branch leads to restoration of the coupling between the upper and lower part of glycolysis through the adenine nucleotides. Interestingly, it was found experimentally that overproducing the enzymes in the glycerol branch did suppress the *tps1-Δ* mutant's glucose-negative phenotype [11]. One may expect that increasing the activity of step 4 in our simple system increases the sensitivity of step 4 to X, and thus, increases the flux control by step 2.

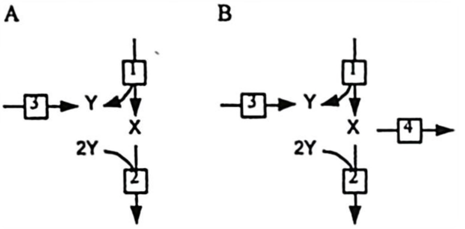

Fig 4. Minimal representation of glycolysis without (A) and with a branch (B).

The crucial factor for the absence of flux control by the ATP-producing step in Fig. 4A appears to be that this step is elastic to a metabolite for which only one elasticity is nonzero. This metabolite can then freely vary to adjust the rate of the enzyme sensitive to it. It follows directly from the connectivity theorems of metabolic control analysis that the step that is elastic to such a metabolite cannot control any metabolic variable except the concentration of that metabolite.

There is another interesting consequence of this analysis: most mathematical models of yeast glycolysis have a structure as depicted in Fig 1A, and most of the kinetic expressions for PFK deal with regulation by F6P, ATP and AMP only, i.e. PFK is taken to be F16bP insensitive. Following the analysis above, this implies that in those models flux control only resides in PFK and upstream steps, unless the glycerol branch is also included. This is indeed the conclusion in most of these studies: control appears distributed mainly between the glucose transporter, HK or PFK [12-14]. We wonder to what extent these results are a consequence of model limitations.

REFERENCES

1 Melendez-Hevia, E., Torres, N.V., Sicilia, J. and Kacser, H. (1990) Biochem. J. 265, 195-202.

2 Melendez-Hevia, E., Waddell, T.G., Heinrich, R. and Montero, F. (1997) Eur. J. Biochem. 244, 527-543.

3 Teusink, B., Walsh, M.C., Van Dam, K. and Westerhoff, H.V. (1998) Trends Biochem. Sci. 23, 162-169.

4 Thevelein, J.M. and Hohmann, S. (1995) Trends Biochem. Sci. 20, 3-10.

5 Bakker, B.M., Westerhoff, H.V. and Michels, P.A.M. (1995) J. Bioenerg. Biomembr. 27, 513-525.

6 Sauro, H.M. and Fell, D.A. (1991) Mathl. Comp. Modelling 15, 15-28.

7 Bergmeyer, H.U. (1974) Methods of enzymatic analysis, Verlag Chemie, Weinheim.

8 Kacser, H. and Burns, J.A. (1973) Symp. Soc. Exp. Biol. 27, 65-104.

9 Heinrich, R. and Rapoport, T. (1974) Eur. J. Biochem. 42, 89-95.

10 Westerhoff, H.V. and Chen, Y. (1984) Eur. J. Biochem. 142, 425-430.

11 Luyten, K., Albertyn, J., Skibbe, W.F., Prior, B.A., Ramos, J., Thevelein, J.M. and Hohmann, S. (1995) EMBO J. 14, 1360-71.

12 Cortassa, S. and Aon, M.A. (1997) Enzym. Microb. Technol. 21, 596-602.

13 Galazzo, J.L. and Bailey, J.E. (1990) Enz. Microbiol. Technol. 12, 162-172.

14 Schlosser, P.M., Riedy, G. and Bailey, J.E. (1994) Biotech. Prog. 10, 141-154.

CORRELATION OF GLUCOSE CATABOLISM AND THE FREQUENCY OF GLYCOLYTIC OSCILLATIONS IN *SACCHAROMYCES CEREVISIAE*

Corinne A. Reijenga[1,2], *Bas Teusink*[1,2], *Henk W. Van Verseveld*[1], *Jacky L. Snoep*[1] *and*
Hans V. Westerhoff[1,2]

[1] Department of Molecular Cell Physiology, Faculty of Biology, Free University, de Boelelaan 1087, 1081 HV Amsterdam, The Netherlands
Telephone: +31 20 4447195, Fax: +31 20 4447229, E-mail: reijenga@bio.vu.nl.
[2] E.C. Slater Institute, BioCenter, University of Amsterdam, Plantage Muidergracht 12, 1018 TV Amsterdam, The Netherlands

INTRODUCTION

During industrial production processes culture conditions in the fermenter are far from ideal. Due to large volumina and high cell densities mixing is a problem and homogeneity of the culture is poor. The organisms are subject to fluctuating substrate (glucose) and oxygen concentrations. At high cell densities the accumulation of products and cell-cell communication may affect the metabolism of the cell and the behavior of the culture. This paper addresses the effects of external conditions on some aspects of the dynamics of glycolysis in *Saccharomyces cerevisiae*. Important objects of study are the glucose transport system, communication between the cells and the occurrence of autonomous glycolytic oscillations.

Intact yeast cells transiently exhibit glycolytic oscillations when glucose is added to starved cells and respiration is inhibited (for review see [1]). Glycolytic oscillations have been monitored macroscopically through the NAD(P)H fluorescence of populations of yeast cells. Oscillations last longer at higher cell densities which indicates that there is a synchronizing mechanism that keeps the cells in phase. It appears that acetaldehyde is the synchronizing agent for the occurrence of sustained oscillations and that a subtle balance should exist between secretion of acetaldehyde by the cells and acetaldehyde trapping [2]. Cyanide appears to be essential for sustained oscillations and has a dual role in the inhibition of respiration and acetaldehyde trapping. Furthermore it was shown that the cellular make-up of the cells is very important for oscillations and that cells harvested around the growth phase transition show sustained oscillations [3].

Studies on regulation and control of glycolytic enzymes have suggested that the control of these enzymes on the steady state glycolytic flux is very small [4]. Although control on flux of these enzymes is small they still might have an important role in adaptation of yeast to changes in external conditions. Enzymes not yet tested for their control on flux are the glucose transporter and the ATP consuming reactions, making these possible candidates for a high control on flux. In *Saccharomyces cerevisiae* there is a large number of putative hexose transporter genes (*HXT1-17*) which together with a galactose permease gene (*GAL2*) and two putative regulatory genes (*RGT2, SNF3*) belong to a superfamily of monosaccharide facilitator genes [5]. The ability to induce sustained oscillations in intact yeast cells makes it possible to study a system that shows dynamics in flux, in a stationary situation. In this paper we test whether growth conditions of the cell affect the glycolytic oscillations. We measured the glucose consumption rate after addition of cyanide and monitored oscillations. Furthermore we determined the cyanide concentration needed for the induction of sustained oscillations after growing the cells under different conditions.

METHODS

The yeast *Saccharomyces cerevisiae* (MC996A, *MAT*a *ura3-52 his3-11,15 leu2-3,112 MAL2 SUC2 GAL MEL*) was grown under semi-aerobic conditions at 30°C on a rotary shaker in rich medium containing 1% glucose or galactose, 1% Difco yeast extract and 2% Difco Bacto Peptone. The cells were harvested at the diauxic shift by centrifugation or filtration, washed twice with 100 mM potassium phosphate, pH 6.8, resuspended and starved in the same buffer for 3 hours at 30°C on a rotary shaker. The cells were pelleted and resuspended in the same buffer to a protein concentration of approximately 4 $g.l^{-1}$ determined according to Lowry *et al.* [6]. Oscillations were induced in a thermostated cuvet at 25°C by adding 3 mM (glucose grown cells) or 1 mM (galactose grown cells) KCN to the cell suspension, 4 minutes after the addition of 20 mM glucose. Oscillations were monitored macroscopically by measuring the NADH fluorescence in a fluorimeter (excitation wavelength 351 nm, emission wavelength 462 nm). Glucose consumption was measured by sampling and quenching in perchloric acid (final concentration 5%). The glucose concentration was measured enzymatically [7].

RESULTS AND DISCUSSION

After addition of glucose to the starved cells a range of KCN concentrations was tested for induction of synchronized oscillations. In glucose grown cells sustained oscillations were induced by adding 3 mM of KCN while in galactose grown cells sustained oscillations were induced by adding 1 mM of KCN (fig. 1 and fig. 2).

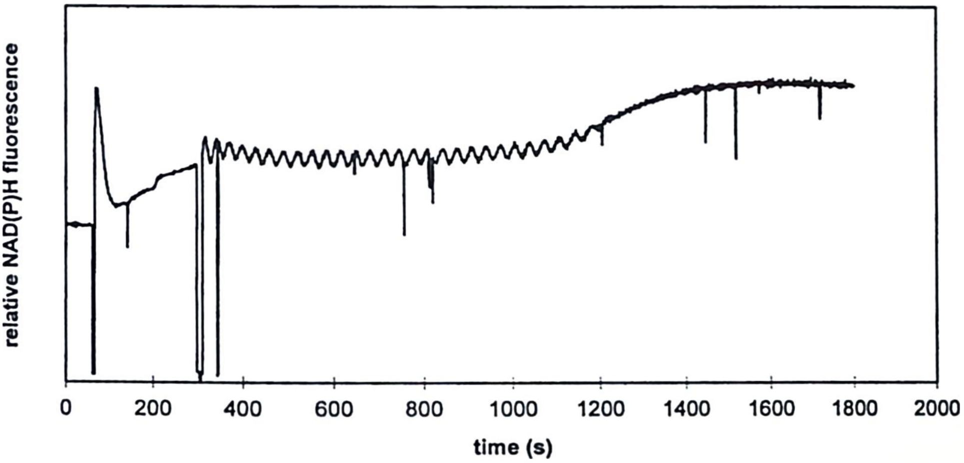

Figure 1. Oscillations in glucose grown cells. Cells were prepared and oscillations induced as described in Methods. 3 mM of KCN was added at t = 300 s. Protein concentration was approximately 4 $g.l^{-1}$.

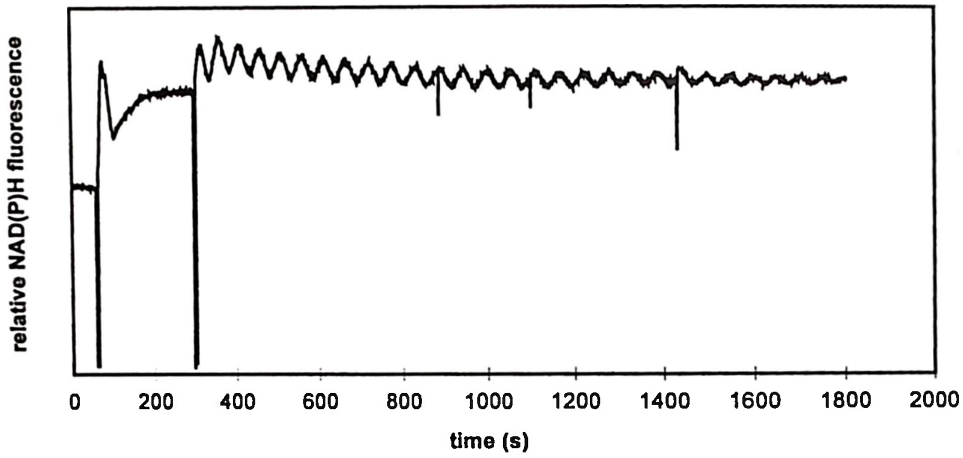

Figure 2. Oscillations in galactose grown cells. Cells were prepared and oscillations induced as described in Methods. 1 mM of KCN was added at t = 300 s. Protein concentration was approximately 4 g.l^{-1}.

When cells had been harvested in the exponential phase growing on glucose or galactose or after the diauxic shift no sustained oscillations were detected. The difference in cyanide concentration needed for inducing sustained oscillations in glucose and galactose grown cells is not yet understood. The different growth conditions may have influenced the cellular composition. An example of an enzyme that is likely to differ in activity between the two cell preparations and is thought to be important for induction of sustained oscillations, is alcohol dehydrogenase. This enzyme converts acetaldehyde to ethanol and is therefore important for the balance between secretion and trapping of acetaldehyde. Glucose induces the expression of ADH1 and represses the expression of ADH2. The enzymes will be present in different concentrations when comparing glucose and galactose grown cells. The difference in affinity of the two enzymes for acetaldehyde may account for the difference in cyanide concentrations needed for the occurrence of sustained oscillations. From experimental results on glycolytic oscillations in *Saccharomyces cerevisiae*, it was shown that the rate at which acetaldehyde was trapped was very important for the state of the system [2].

The glucose consumption rate was measured for both the glucose and the galactose grown cells after addition of cyanide. In the same batches of cells sustained oscillations were induced and monitored. The glucose consumption rate for the glucose grown cells was 0.26 μmol.min^{-1}.mg protein^{-1}. For the galactose grown cells the glucose consumption rate was 0.17 μmol.min^{-1}.mg protein^{-1}. The frequency of the oscillations was 1.8 min^{-1} for the glucose grown cells and 1.1 min^{-1} for the galactose grown cells (fig.1 and fig.2). A 1.5 fold increase in average glycolytic flux was accompanied by a 1.6 fold increase in frequency of oscillations, suggesting a co-response coefficient close to 1. The co-response coefficient quantifies how two variables are affected by a parameter change relative to one another. It is the ratio of the two individual response coefficients [8]. From these results we can conclude that it is possible to change the glucose consumption rate of the cells by growing them under different physiological conditions and to see an effect on the dynamics of glycolysis.

REFERENCES

[1] Hess, B. and Boiteux, A. (1971) Ann. Rev. Biochem. 40, 237-258

[2] Richard, P., Bakker, B.M., Teusink, B., Van Dam, K. and Westerhoff, H.V. (1996) Eur. J. Biochem. 235, 238-241

[3] Richard, P., Teusink, B., Westerhoff, H.V. and Van Dam, K. (1993) FEBS lett. 341, 80-82

[4] Schaaff, I., Heinisch, J. and Zimmerman, F.K. (1989) Yeast 5, 285-290

[5] Boles, E. and Hollenberg, C.P. (1997) Mic. Rev. 21, 85-111

[6] Lowry, O.H., Rosebrough, N.J., Farr, A.L. and Randall, R.J. (1951) J. Biol. Chem. 193, 265-275

[7] Bergmeyer, H.U. (1974) Methods of Enzymatic Analysis, Verlag Chemie, Weinheim

[8] Hofmeyr, J.-H.S., Cornish-Bowden, A., and Rohwer, J.M. (1993) Eur. J. Biochem. 212, 883-837

CONTROL OF GLYCOLYTIC INFLUX MONITORED THROUGH SITE-DIRECTED MUTAGENESIS OF YEAST HEXOKINASE PII.

*Han de Winde *, Leon Kraakman, Joris Winderickx and Johan M. Thevelein*

* Corresponding author: Laboratory for Molecular Cell Biology, Department of Biology, Katholieke Universiteit Leuven, Kardinaal Mercierlaan 92, B-3001 Leuven-Heverlee, Flanders, Belgium. phone: +32-16-321516 / fax: +32-16-321979
E-mail: han.dewinde@bio.kuleuven.ac.be

INTRODUCTION

The rate by which cells of baker's yeast *Saccharomyces cerevisiae* ferment glucose to ethanol is generally believed to be mainly controlled through the activity of glucose transport, of phosphofructokinase and pyruvate kinase, and through the rate of ATP consumption. Attempts to increase steady state glycolytic flux and glycolytic intermediate levels by overexpression of glycolytic enzymes have been unsuccessful [1, 2], underscoring a general lack of understanding of the metabolic regulation of yeast glycolysis. Recently, we have presented evidence that yeast hexokinase may be a rate limiting factor for the sugar influx into glycolysis during the onset of fermentative growth [3].

The yeast hexokinases PI (Hxk1) and PII (Hxk2) have been identified as central and essential components of several signal transduction pathways that are triggered by fermentable sugars. Activation of the yeast Ras-cAMP pathway, and subsequently of cAMP-dependent protein kinase A (PKA), during the transition from respiratory to fermentative growth is fully dependent on sugar phosphorylation by the hexokinases [4, 5]. Moreover, inactivation of gluconeogenic enzymes and shut down of the expression of genes involved in the utilization of non-fermentable carbon sources by the main glucose repression pathway are primarily dependent on active hexokinases [6, 7, 8]. In addition to this central role in sugar-induced signal transduction, the yeast hexokinases have been implicated in metabolic control of the upper part of glycolysis. Most notably, yeast hexokinase activity may be competitively inhibited *in vivo* by trehalose-6-phosphate [9, 10]. This regulation appears to be of vital importance for a strict control on sugar influx and onset of glycolysis, since deletion of *TPS1* encoding trehalose-6-phosphate synthase results in severe metabolic deregulation caused by unbridled hexokinase activity in the presence of fermentable sugar [3, 11, 12].

Despite extensive research efforts, the actual mechanisms by which the yeast hexokinases are themselves regulated, and by which they regulate glycolytic influx and sugar-induced signalling are at present unclear. In order to obtain more insight into the structural requirements of yeast hexokinase for sugar dependent regulatory mechanisms, we have undertaken site-directed mutagenesis of Hxk2. Amino acid residues were mutated that are important for binding of sugar and ATP, for efficient phosphoryl transfer and for controlled closure of the substrate binding cleft and conformational changes of the enzyme during catalysis. The effects of these mutations on hexokinase-mediated signal transduction are described in detail elsewhere [13]. In this paper we focus on the effects on the initiation of glycolysis during the transition from respiration to fermentation. Results indicate that yeast hexokinase presents an important control point for sugar influx into glycolysis during the onset of fermentation.

METHODS

Strains, constructs and growth conditions

Strains used in this study are all isogenic to W303-1A [14]. Site-directed mutagenesis of *HXK2* is described elsewhere [13]. Wild type and mutated alleles of *HXK2* were introduced into single copy vector YCplac33 [13], and transformed into YSH7.4-3C (*hxk1Δ::HIS3 hxk2Δ::LEU2 glk1Δ::LEU2*) [7]. Yeast cells were cultured in standard yeast nitrogen base/ammonium sulfate media with synthetic 'drop-out' amino acid/nucleotide mixture as required, and supplemented with 2% (w/v) galactose (SCGal), or with 2% (w/v) ethanol, 2% (w/v) glycerol and 0.1% (w/v) glucose (SCEGd). Wash and sample medium was standard complete YP (1% yeast extract and 2% peptone). Cultures were grown in an orbital shaker at 30°C and harvested by centrifugation.

Hexokinase activity and kinetic analysis

For determination of specific hexokinase activity, maximum phosphorylation rate V_{max} and substrate binding coefficient K_m, cells were grown in SCGal to mid-logarithmic growth phase and harvested by centrifugation at 4°C. Preparation of crude enzyme extracts and activity measurement were essentially as previously described [3, 12]. For kinetic analysis glucose concentrations in the hexokinase assay were between 0.05mM and 100mM, fructose concentrations between 1.0mM and 200mM, and ATP concentrations between 0.1mM and 10mM. Kinetic constants were calculated by non-linear least squares analysis, using the Excel template ANEMONA [15].

Determination of metabolites

For determination of glycolytic intermediates, cells were grown in SCEGd to mid-logarithmic growth phase, harvested by centrifugation at 4°C and washed twice in ice-cold YP medium. Subsequently the cells were resuspended in YP medium and pre-incubated at 30°C before addition of 100mM glucose or fructose. Sampling in cold methanol, preparation of extracts and measurement of metabolites were essentially as previously described [3, 12].

RESULTS AND DISCUSSION

To study structural requirements of Hxk2-mediated control, we have mutated the following amino acids. Lysine-111 is highly conserved among eukaryotic hexokinases and is specifically involved in glucose-enhanced binding of ATP [16]. Lysine-111 was mutated to arginine (K111R) and to valine (K111V). Aspartate-211 has been implicated in the nucleophilic attack of the glucose 6-OH group on the gamma-phosphate of ATP and hence was predicted to present the conserved catalytic center of eukaryotic hexokinases [17, 18]. Aspartate-211 was mutated to isoleucine (D211I) and to serine (D211S). Serine-158 is a conserved critical determinant of hexokinase conformation, sugar binding affinity and catalytic activity [19]. The central role of this amino acid in the phosphoryl transfer reaction was recently emphasized by the finding that it is autophosphorylated when Hxk2 is inhibited by non-phosphorylatable D-xylose [20]. Serine-158 was mutated to alanine (S158A). *HXK2* alleles carrying each of these mutations were introduced on single-copy plasmids into a yeast strain lacking the endogeneous *HXK1*, *HXK2* and *GLK1* genes. Stable and unperturbed expression of all mutant enzymes was verified by Western blot analysis (data not shown).

In Table 1, V_{max} and K_m values for glucose and fructose are depicted for wild type Hxk2 and mutant proteins. Mutation of Lys-111 partially decreased V_{max} but did not or only slightly affect sugar binding affinity for glucose and fructose. Accordingly, both Lys-111 mutations confered wild type growth on either carbon source [13]. In agreement with a specific role in ATP binding, both mutations increased the K_m for ATP. In line with a central role in catalysis for Asp-211, mutation of this amino acid virtually abolished enzyme activity. However, sugar binding affinity was even slightly enhanced compared to wild type. The Asp-211 mutants could not grow on fermentable carbon sources [13]. The Ser-158 mutation is remarkable in several aspects. The V_{max} for glucose is severely reduced. Accordingly, growth on glucose was retarded compared to wild type and severely inhibited in the presence of antimycin, indicating that sugar influx into glycolysis was strongly reduced [13]. Surprisingly, glucose binding affinity was dramatically enhanced, while ATP-affinity was severely decreased. This is indicative of a conformational distortion of the enzyme and a concomittant decrease in the efficiency of the phosphoryl transfer reaction [13], reflected in a lowered V_{max}. With fructose, the V_{max} was only lowered to about 50% of wild type, whereas sugar affinity was not affected. The affinity for ATP was however even more dramatically affected than with glucose. Apparently, the structural requirements of Hxk2 for phosphoryl transfer from ATP are different with different sugar substrates.

In vivo activity of the various *HXK2* alleles was monitored by measuring the accumulation of glycolytic intermediates upon addition of glucose (Fig.1) and fructose (data not shown; see [13]) to cells grown under respiratory conditions. For the Asp-211 mutants, like for the triple kinase deletion strain no accumulation of sugar phosphates could be detected. This was in agreement with the about 500-fold reduction of the k_{cat} measured *in vitro* (Table 1). Metabolic profiles for both Lys-111 mutants were comparable to wild type, including the rapid decrease in intracellular phosphate concomittant with the boost of sugar phosphates in the first minutes after glucose addition. Like in the wild type there was virtually no accumulation of intracellular glucose [3], indicating a rapid influx of sugar into glycolysis. Apparently, both Lys-111 mutants with decreased V_{max} as measured *in vitro* (Table 1), supported about normal *in vivo* sugar phosphorylation at the onset of glycolysis. Since fructose-1,6-bisphosphate levels were slightly lowered, the overall flux through the upper part of glycolysis may have been somewhat decreased.

Table 1. Michaelis-Menten kinetics for yeast Hxk2 wild type and mutant enzymes.

	V_{max} mU/mg	rel.V_{max} %	K_m mM	V_{max}/K_m	K_m^{ATP*} mM
Glucose					
HXK2	590 ± 50	100	0.22 ± 0.02	2680	0.16 ± 0.13
K111R	526 ± 30	90	0.21 ± 0.01	2505	0.31 ± 0.10
K111V	305 ± 20	50	0.15 ± 0.01	2033	0.38 ± 0.08
D211I	0.97 ± 0.09	0.16	0.16 ± 0.10	6.0	0.32 ± 0.09
D211S	0.72 ± 0.07	0.12	0.16 ± 0.10	4.5	0.31 ± 0.08
S158A	67 ± 4	10	0.025 ± 0.010	2680	1.31 ± 0.05
Fructose					
HXK2	600 ± 20	100	1.19 ± 0.02	505	0.088 ± 0.03
K111R	600 ± 20	100	1.70 ± 0.03	350	0.17 ± 0.06
K111V	365 ± 30	60	1.48 ± 0.06	245	0.23 ± 0.06
D211I	2.0 ± 0.2	0.33	2.20 ± 0.09	1.0	0.37 ± 0.10
D211S	1.2 ± 0.1	0.12	2.03 ± 0.10	0.6	0.35 ± 0.11
S158A	292 ± 20	50	1.21 ± 0.03	240	1.05 ± 0.04

* Kinetics for ATP were determined in the presence of 10 mM glucose or 50 mM fructose, respectively.

The Ser-158 mutation exhibited a severely inhibited accumulation of sugar phosphates upon addition of glucose which is fully in line with the about 10-fold reduction in specific activity measured *in vitro* (Table 1). Sugar mono-phosphate levels were clearly lower than for the wild type and Lys-111 mutants, and fructose-1,6-bisphosphate accumulation was poor and very short-lived. This indicates that the influx into and the flux through the upper part of glycolysis was indeed strongly inhibited, as already suggested by the poor growth on fermentable carbon sources (see above). Accordingly, intracellular phosphate levels did not rapidly decline and glucose accumulated intracellularly, albeit not as dramatic as in the triple kinase deletion strain in which glycolytic influx was completely blocked. Upon addition of fructose, sugar phosphate accumulation and decrease in intracellular phosphate of the S158A mutant were comparable to those of the K111R and K111V mutants (data not shown).This was not unexpected, since the V_{max} for fructose was not dramatically affected (Table 1).

These results indicate that accumulation of sugar phosphates and the influx of fermentable sugar into glycolysis can be modulated during the transition from respiration to fermentation, by specifically modulating Hxk2 enzyme activity. Hence, yeast hexokinase PII presents an important control point for sugar influx into glycolysis during the initiation of fermentation.

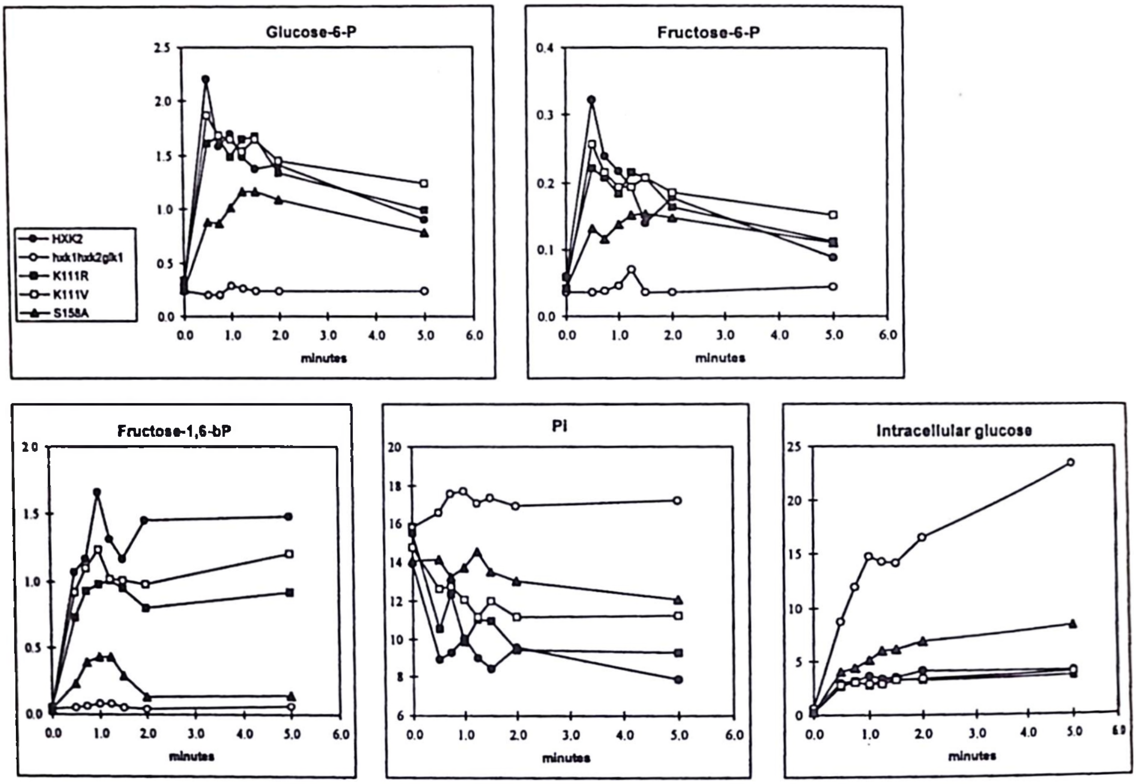

Figure 1. Intracellular concentrations of metabolites after the addition of 100mM glucose to SCEGd-grown yeast cells. Concentrations are indicated on the vertical axes in mM. Symbols for each of the strains investigated are indicated in the legend to the upperleft panel.

REFERENCES

1 Schaaff, I., Heinisch, J. and Zimmermann, F.K. (1989) Yeast 5, 285-290.
2 Davies, S.E.C. and Brindle, K.M. (1992) Biochem. 31, 4729-4735.
3 Ernandes, J.R., De Meirsman, C., Rolland, F., Winderickx, J., de Winde, J.H., Brandao, R.L. and Thevelein, J.M. (1998) Yeast 14, 255-269.
4 Beullens, M., Mbonyi, K., Geerts, L., Gladines, D., Detremerie, K., Jans, A.W.H. and Thevelein, J.M. (1988) Eur. J. Biochem. 172, 227-231.
5 Thevelein, J.M. (1994) Yeast 10, 1753-1790.
6 Entian, K.D. and Barnett, J.A. (1992) Trends Biochem. Sci. 17, 506-510.
7 De Winde, J.H., Crauwels, M., Hohmann, S., Thevelein, J.M. and Winderickx, J. (1996) Eur. J. Biochem. 241, 633-643.
8 Ronne, H. (1995) Trends Genet. 11, 12-17.
9 Blazquez, M.A., Lagunas, R., Gancedo, C. and Gancedo, J.M. (1993) FEBS Lett. 329, 51-54.
10 Thevelein, J.M. and Hohmann, S. (1995) Trends Biochem. Sci. 20, 3-10.
11 Hohmann, S., Neves, M.J., de Koning, W., Alijo, R., Ramos, J. and Thevelein, J.M. (1993) Curr. Genet. 23, 281-289.

12 Hohmann, S., Bell, W., Neves, M.J., Valckx, D. and Thevelein, J.M. (1996) Mol. Microbiol. 20, 981-991.

13 Kraakman, L.S., Winderickx, J., Thevelein, J.M. and de Winde, J.H. (1998) submitted for publication.

14 Thomas, B.J. and Rothstein, R.J. (1989) Cell 56, 619-630.

15 Hernandez, A. and Ruiz, M.T. (1998) Bioinformatics 14, 227-228.

16 Tamura, J.K., LaDine, J.R. and Cross, R.L. (1988) J. Biol. Chem. 263, 7907-7912.

17 Anderson, C.M., Stenkamp, R.E., McDonald, R.C. and Steitz, T.A. (1978) J. Mol. Biol. 123, 207-219.

18 Lange, A.J., Xu, L.Z., van Poelwijk, F., Lin, K., Granner, D.K. and Pilkis, S.J. (1991) Biochem. J. 277, 159-163.

19 Xu, L.Z., Harrison, R.W., Weber, I.T. and Pilkis, S.J. (1995) J. Biol. Chem. 270, 9939-9946.

20 Heidrich, K., Otto, A., Behlke, J., Rush, J., Wenzel, K.-W. and Kriegel, T. (1997) Biochem. 36, 1960-1964.

INFRARED THERMOGRAPHIC ANALYSIS OF YEAST AND ADIPOCYTES IN MICROTITER PLATES

Mark A. Paulik, [1]Richard G. Buckholz, Mary E. Lancaster, [2]Walter S. Dallas, Emily A. Hull-Ryde, James. E. Weiel, and James M. Lenhard**

Departments of Metabolic Diseases, [1]Molecular Endocrinology, and [2]Molecular Sciences, GlaxoWellcome Inc., 5 Moore Drive, Research Triangle Park, NC 27709
*corresponding authors, Ph. (919) 483-5854, Fax (919) 483-5691
E-mail: map16209@glaxowellcome.com, jml29514@glaxowellcome.com

INTRODUCTION

Although infrared thermography is used to measure heat dispersion from the skin of living animals [1, 2], similar techniques have not been developed for detecting temperature changes using isolated cells. Indeed, *in vivo* studies of thermogenesis are limited because of the contributions that multiple tissues make to energy expenditure. This report provides evidence that high resolution infrared thermography can be used non-invasively to measure the real time thermogenic effects of both anti-obesity (*e.g.*, CL316243) and anti-diabetic (*e.g.*, troglitazone) agents in cells cultured in microtiter plates. Furthermore, the infrared technology can be applied to study thermogenic proteins such as the uncoupling proteins (UCPs) which uncouple oxidative phosphorylation from respiration in mitochondria resulting in heat generation [3]. This novel approach provides the biologist with a rapid method for studying how multiple drug candidates and/or thermogenic proteins affect thermogenesis in isolated cells.

METHODS

A detailed description of the methods are described in Paulik et al. [4]. Briefly, yeast were transformed with uncoupling protein 2 (UCP2) or exposed to carbonyl cyanide p-(trifluoromethoxy)phenylhydrazone (FCCP) or rotenone. Adipocytes were prepared and processed as previously described [5,6]. Subsequently, the adipocytes were exposed to either rotenone, FCCP, cycloheximide, troglitazone, or CL316243. Thermogenesis was measured using infrared thermography.

RESULTS AND DISCUSSION

As part of the initial effort to validate the use of infrared thermography to monitor mitochondrial heat production, we treated human adipocytes cultured in 96-well microtiter plates and yeast suspended in 384-well microtiter plates with rotenone or FCCP. Rotenone is an inhibitor of mitochondrial electron transport [7] while FCCP is an uncoupler of mitochondrial respiration [8]. Subsequently, we measured the heat produced from the cells using an Agema Thermovision 900 Infrared Imaging System. As shown in the dose response assays in Fig. 1, rotenone treatment inhibited thermogenesis in human adipocytes (Fig. 1A) and yeast (Fig. 1B). In contrast, FCCP stimulated heat production in both cell types relative to untreated cells (Fig. 1).

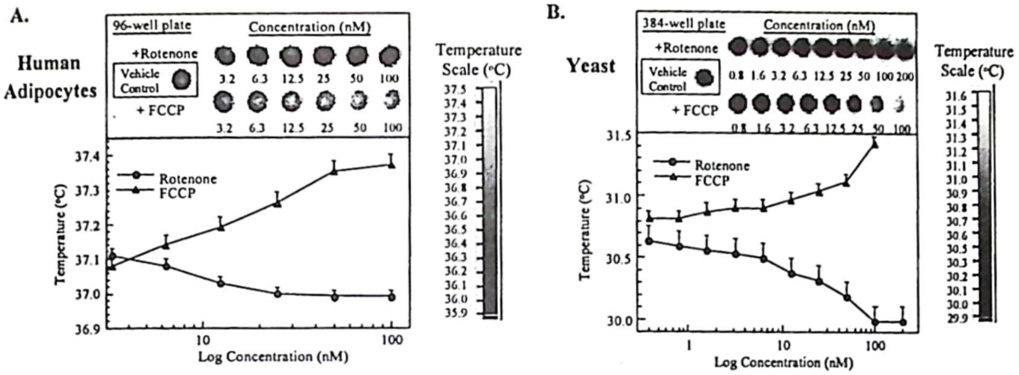

Figure 1. Infrared image of yeast and human adipocyte cultures treated with rotenone and FCCP. Dose responses are shown on the thermogenic effects of rotenone and FCCP on (**A**) human adipocytes and (**B**) yeast. The cells were treated for 10 minutes with either agent before the images were analyzed by infrared thermography. Representative data is presented from experiments performed in triplicate.

Kinetic analysis revealed that changes in heat production were detectable 10 minutes after treating the cells with either agent (data not shown). Shorter times could not be measured because the system required 10 minutes for temperature equilibration after treating the cells with either agent.

Although UCP1 regulates mitochondrial-mediated thermogenesis in rodent brown adipose tissue [3], there is no direct evidence that a protein homologoue, UCP2, plays a similar role. In order to evaluate UCP2's role in thermogenesis and further validate the use of infrared thermography, the UCP2 gene was cloned from a human cDNA library and expressed in yeast using a galactose-inducible expression system. As shown in Fig. 2A, expression of UCP2 in yeast resulted in increased thermogenesis relative to cells lacking UCP2. As expected, treatment of the cells with rotenone inhibited UCP2-mediated thermogenesis (Fig. 2A and 2B). For reference, we confirmed UCP2 was expressed in these cells by Western blot analysis (Fig. 2C). Peak expression and thermogenesis was observed 3-4 hours after inducing UCP2 synthesis with galactose (data not shown). Taken together, the results validate using infrared thermography as a tool to measure the effects of various molecules (*e.g.*, rotenone, FCCP, and UCP2) on mitochondrial-mediated thermogenesis.

We were interested in determining if infrared thermography could be used to analyze the pharmacological effects of drugs which alter fuel metabolism. Troglitazone is an antidiabetic agent that increases anabolism (*e.g.*, lipogenesis and mitochondrial mass) and decreases catabolism (*e.g.*, basal lipolysis and aerobic respiration) in C3H10T1/2 cells [6]. The effects of troglitazone on these cells is a result of activation of the transcription factor PPARγ which, in turn, induces differentiation of the stem cells into adipocytes [5,6]. Thus, infrared thermography was used to test the affects of troglitazone and 5 structurally related agonists on heat production in differentiating C3H10T1/2 cells (Fig. 3A).

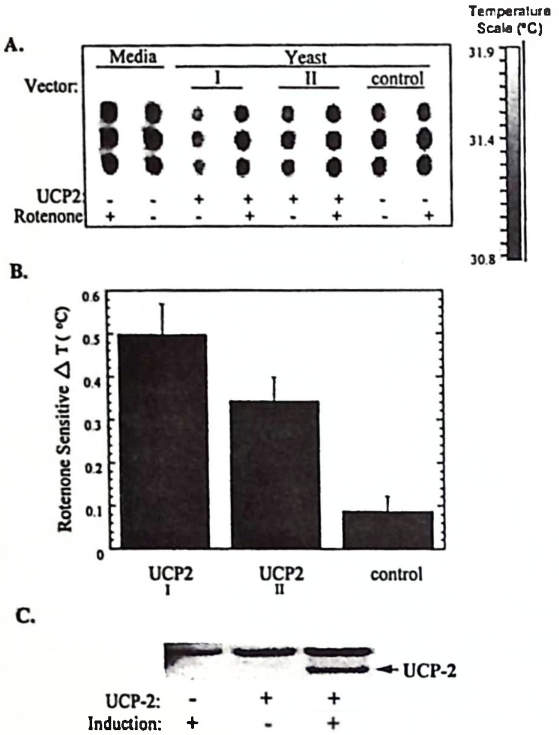

Fig. 2. Infrared thermographic analysis of yeast expressing UCP2. Yeast were transformed with two plasmids expressing UCP2 (isolates I and II) or vector lacking UCP2 (control). (A) As a control, the cells were treated with (+) or without (-) rotenone for 10 minutes prior to the plates being analyzed by infrared thermography. (B) The rotenone-sensitive thermogenic response (ΔT) was calculated by subtracting the temperature of the cells in the presence of rotenone from the temperature of the cells in the absence of rotenone. (C) For reference, Western analysis of UCP2 was performed on nontransfected cells (UCP2: -) or transfected cells (UCP2: +) which were treated with (induction: +) or without (induction: -) galactose. Representative data from three experiments is given. Each sample was repeated in triplicate for the given experiment.

Heat production decreased in cells treated with increasing concentrations of troglitazone or the other related PPARγ agonists (Fig. 3A), suggesting thermogenesis is suppressed as these cells differentiate into adipocytes. Further, the rank order potency of the various PPARγ agonists tested in the thermogenesis assay was BRL49653 ≥ GW1929 > troglitazone ≥ pioglitazone > ciglitazone > englitazone (Fig. 3A). These rank order of potencies correlated (r=0.9) with the minimal effective doses *in vivo* for the PPARγ agonists [9]. Since UCP expression increases as stem cells differentiate into adipocytes [5], these observations suggest that increased UCP expression is not sufficient for stimulation of thermogenesis in adipocytes. Moreover, these results indicate infrared thermography can be used to study the pharmacological effects PPARγ agonists on heat production during adipogenesis.

The β_3-adrenergic receptor (β_3AR) agonists are candidate therapeutic agents for the treatment of diabetes and obesity. The mechanism of action for these agents is thought to involve increased metabolic rate [10].

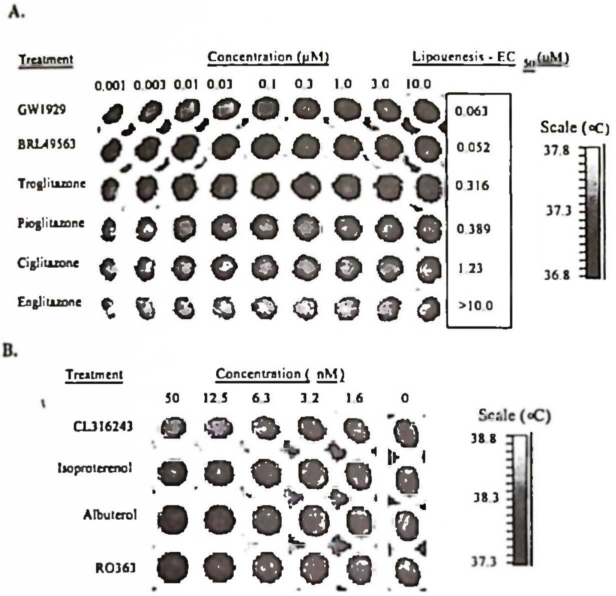

Fig. 3. (**A**) Infrared image of differentiating adipocytes. Confluent C3H10T1/2 stem cells were cultured in 96-well microtiter plates An infrared thermographic image was recorded one week after treating the cells with increasing concentrations of various PPARγ agonists in the presence of insulin and 9-*cis* retinoic acid. (**B**) Effect of β-AR agonists on thermogenesis in C3H10T1/2 adipocytes. Confluent adipocytes (50 μl/well) were incubated with various concentrations of the given β-AR agonists for 10 minutes and real time images were recoded by infrared thermography. Representative data are given from one of three separate experiments.

Therefore, we tested if infrared imaging could be used to monitor the effects of βAR-agonists on thermogenesis in cultured adipocytes. As shown in Fig. 3A, thermogenesis in C3H10T1/2 adipocytes was stimulated by treatment with the selective β_3AR agonist, CL316243, and the non-selective βAR agonist, isoproterenol. The β_1AR agonist, RO363, and the β_2AR agonist, albuterol, were less effective than CL316243 or isoproterenol at stimulating thermogenesis in these cells.

As a control, the effects of βAR agonists on lipolysis was measured. Dose response analysis revealed the various βAR agonists had similar EC_{50}s in both the thermogenesis and lipolysis assays (data not shown, [3]). A correlation coefficient of 0.99 was observed when the potencies of the various βAR agonists were compared in both assays, suggesting the same βAR signaling pathways mediate lipolysis and thermogenesis in adipocytes. Taken together, these observations indicate infrared thermography is useful for characterizing how anabolic (*e.g.*, troglitazone) or catabolic (*e.g.*, CL316243) drugs affect heat production in cell culture.

The pleiotropic effects of multiple tissues on heat dispersion *in vivo* necessitates the measurement of thermoregulatory properties of isolated cells. To address this problem, in part, microcalorimetry has been developed as a technique to measure the heat produced by isolated cells [11]. This technique has the advantage of measuring heat output quantitatively (*i.e.*, kJ/mol). However, this technique is limited because it can not be used to measure temperature gradations over fixed surface areas, such as those found in cell culture plates. Thus, we developed several applications for using infrared thermography to measure thermogenesis in cultured cells. Taken together, the data show infrared thermography can be used to measure changes in mitochondrial metabolism in yeast and the pharmacological effects of PPARγ and βAR agonists in adipocytes. We have observed that infrared thermography has several advantages when compared to other metabolic assays for PPARγ agonists (*e.g.*, lipogenesis assays) or βAR-agonists (*e.g.*, cAMP measurements). For example, this technique does not require any radioactive precursors, thereby eliminating unnecessary exposure to ionizing radiation. Further, it does not require consumable supplies (*e.g.*, substrates or buffers) outside of those needed to maintain cells in culture. Indeed, the non-invasive nature of infrared thermography allows for multiple serial measurements for as long as cells are maintained in culture. Finally, it is concluded that the sensitivity (0.002°C) and robustness (*i.e.*, 384-well format) of this detection system will make it a useful tool for analyzing the effects of a variety of agents on heat production in various cell types.

REFERENCES

1) H. Handelsman. Thermography for indications other than breast lesions. *Health Technol. Assess Rep.* **2**:1-32, 1989.

2) W. J. Yang and P. P. Yang. Literature survey on biomedical applications of thermography. *Biomed Mater. Eng.* **2**:7-18, 1992.

3) D. Ricquier, l. Casteilla, and . Bouillaud. Molecular studies of the uncoupling protein. FASEB J. **5**:2237-2242, 1991.

4) M. A. Paulik, R. G. Buckholz, M. E. Lancaster, W. S. Dallas, E. A. Hull-Ryde, J. E. Weiel, and J. M. Lenhard. Development of Infrared Imaging to Measure Thermogenesis in Cell Culture: Thermogenic Effects of Uncoupling Protein 2, Troglitazone, and β-Adrenoceptor Agonists. *Pharm. Res.* (In Press) 1998.

5) M. A. Paulik and J. M. Lenhard. Thiazolidinediones inhibit alkaline phosphatase activity while increasing expression of uncoupling protein, deiodinase, and increasing mitochondrial mass in C3H10T1/2 cells. *Cell Tissue Res.* **290**:79-87, 1997.

6) J. M. Lenhard, S. A. Kliewer, M. A. Paulik, K. D. Plunket, J. M. Lehmann, and J. E. Weiel. Effects of troglitazone and metformin on glucose and lipid metabolism: alterations of two distinct molecular pathways. *Biochem. Pharmacol.* **54**:801-808, 1997.

7) S. A. Ahmad-Junan, P. C. Amos, G. S. Cockerill, P. C. Levett., and D. A. Whiting. Synthetic studies on electron transport inhibitors related to natural products. *Biochem. Soc. Trans.* **22**:237-241, 1994.

8) H. Terada The interaction of highly active uncouplers with mitochondria. *Biochim. Biophys. Acta* **639**:225-242, 1981.

9) T.M. Willson, J.E. Cobb, D.J. Cowan, R.W. Wiethe, I.D.Correa, S.R. Prakash, K.D. Beck, L.B. Moore, S.A. Kliewer, J.M. Lehmann. The structure-activity relationship between peroxisome proliferator-activated receptor gamma agonism and the antihyperglycemic activity of thiazolidinediones. *J Med Chem* 1996 **2;39(3):665-668**

10) P. J. Scarpace. Thermoregulation with age: role of beta-adrenergic signal transduction. *Ann. N. Y. Acad. Sci.* **813**:111-116, 1997.

11) H. Bottcher and P. Furst. A new microcatheter enables microcalorimetric assessment of thermogenesis after stimulation in cell cultures. *J. Biochem. Biophys. Methods* **32**:191-194, 1996.

EXPERIMENTAL STRATEGIES TO ANALYSE THE CONTROL OF GLYCOLYSIS IN *LACTOCOCCUS LACTIS*

Heidi Winterberg Andersen, Martin Bastian Pedersen, Karin Hammer and Peter Ruhdal Jensen

Department of Microbiology, Technical University of Denmark, Building 301, DK - 2800 Lyngby – Denmark, Telephone: +45 45252510, Fax: +45 45932809
E-mail: PRJ@IM.DTU.DK

INTRODUCTION

Lactococcus lactis is used extensively in the manufacturing of fermented dairy products, mostly cheeses. The primary function of this organism is the homofermentative conversion of sugar through glycolysis to the major end product lactate and other minor products that contribute to preservation, texture and flavour of fermented dairy products.

The enzymes phosphofructokinase (PFK), pyruvate kinase (PK) and lactate dehydrogenase (LDH) which are involved in glycolysis (Fig. 1) posses interesting regulatory properties [1]. The 3 corresponding genes *pfk*, *pyk* and *ldh* [2,3] are organized in one operon (*las*), in contrast to the arrangement found in other organisms. This organization may provide the cell with a way to regulate the glycolytic flux without considerable influence on the concentration of the glycolytic intermediates, simply by changing the expression level of the *las* genes and thus affect enzyme activities both early and late in glycolysis (Fig. 1). This phenomenon may indicate that the *las* operon plays a central role in the regulation of the glycolytic flux. An interesting question is then whether these enzymes also *control* the glycolytic flux in *L. lactis*.

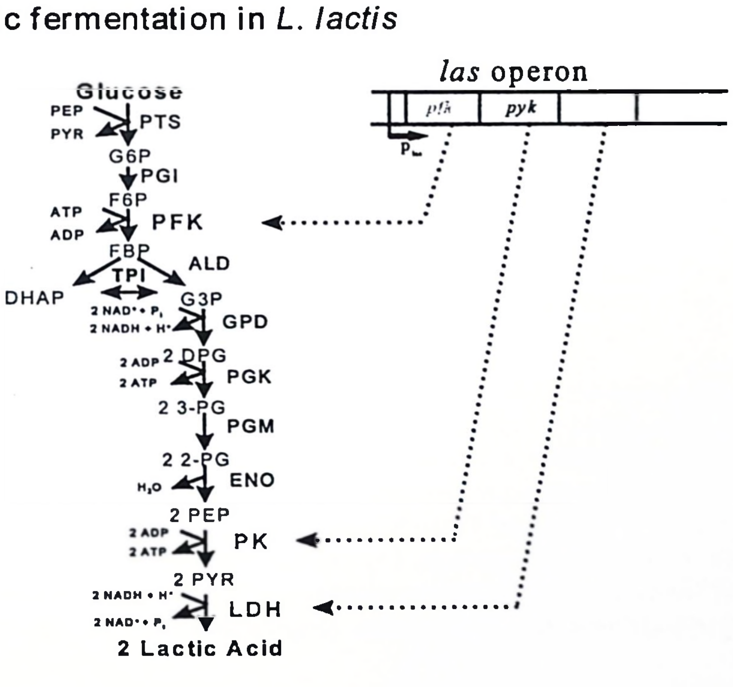
Homolactic fermentation in *L. lactis*

Figure 1. A scheme of the glycolytic pathway in *L. lactis* grown on excess of glucose. PFK, PK and LDH are the 3 enzymes encoded by the *las* operon.

In this paper, we present our experimental strategy to apply metabolic control analysis (MCA) on glycolysis and measure the concentration and flux control exerted by these key enzymes. We present work concerning the characterization of the promoter of the *las* operon (P_{las}) with respect to strength and regulation. Experimental strategies for construction of strains are outlined where the expression of either the entire *las* operon or the individual genes *pfk*, *pyk* and *ldh* are modulated. The latest progress on the construction of these strains is presented.

EXPERIMENTAL STRATEGY - RESULTS

Characterizing the promoter P_{las} of the *las* operon

For the purpose of experimental MCA (see later) we want to exchange the native promoter transcribing the *las* operon with synthetic promoters [4] on the chromosome to achieve different levels of constitutive expression. It is therefore necessary to determine the native activity of the *las* promoter in order to be able to select synthetic promoters with relevant strength.

Several DNA fragments up- and downstream of the promoter region were cloned in front of the reporter genes *lacLM* in the promoter probe vector pAK80 [5]. The pAK80 derivatives were introduced in MG1363 and the strength of the promoter regions was estimated from the specific activity of β-galactosidase in overnight cultures (Fig. 2).

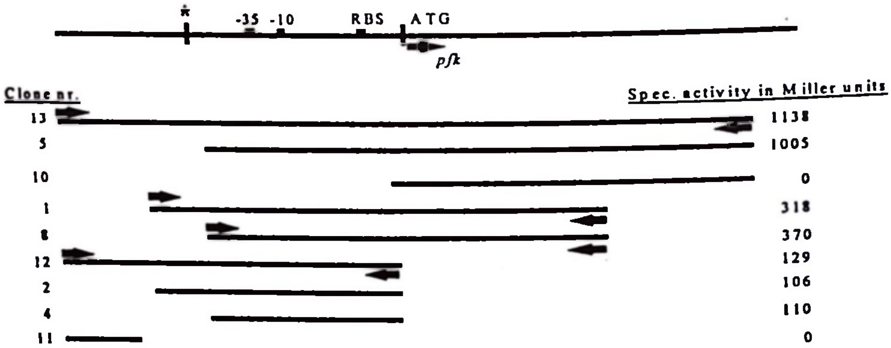

Figure 2. Different DNA regions up- and downstream from mRNA initiation of the *las* operon are cloned in the promoter probe vector pAK80. The sequence to the right of the asterix is published [2,3]. Regions amplified with PCR are indicated with arrows. The activity of the promoter clones in stationary phase is presented in Miller units.

Promoter clone 13 showed the highest activity of 1138 Miller units which is a relatively high promoter strength. A computer analysis of the sequence predicted the presence of putative conservative promoter sequences in the coding region of the *pfk* gene. However, from promoter clone 10 we observed no promoter activity in the region. When less downstream DNA was included the activity decreased approximately three fold, see Fig. 2 (clone nr. 5 vs. 8 vs. 4). The reason is probably differences in the mRNA stability of the different promoter clones. The pAK80 derivatives carrying the promoter regions showed a 10 fold higher β-galactosidase activity in the stationary phase compared to exponential phase. This is partly explainable from the plasmid copy number, which has been shown to increase three fold in stationary phase [6].

In order to avoid influence of the copy number we decided to use a single copy system to perform accurate studies on the regulation of the *las* promoter. Promoter clone 5 and 13 were cloned in front of the reporter gene *gusA* in the promoter probe vector, pLB85 [7] encoding β-glucuronidase. The plasmids were subsequently integrated by site-specific recombination between the attachment site of the TP901 phage (*att*P) and the *att*B site on the chromosome of MG1363. We investigated the influence of external factors on the transcription from the *las* promoter, i.e. growth phase, pH and other stress factors [8]. Both promoter clones 5 and 13 were induced 5.7 fold in the late exponential growth phase around OD_{600} ~1 and pH = 6.3 (Fig. 3) compared to a reference constitutive promoter [4].

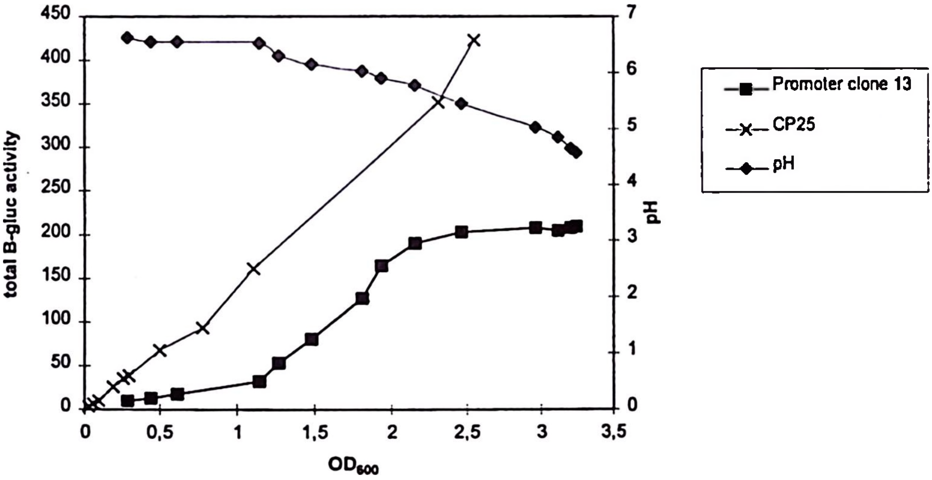

Figure 3. The total β-glucuronidase (B-gluc) activity and pH values are plotted against OD_{600} for promoter clone 13 and constitutive promoter 25 integrated on the chromosome of MG1363. The cultures were grown in rich media M17 + 1% glucose.

This regulation is not immediately understandable, because it takes place in the growth phase where the cells are about to grow slower, and this should require less ATP supply from glycolysis. One could speculate that either product inhibition by lactate or uncoupling by external lactate is the cause. However, in preliminary studies we adjusted the pH with different amounts of lactic acid to imitate the induction. The results showed a *lower* induction with lower pH and below a certain pH value no induction occurred. The mechanism for this regulation remains obscure. Furthermore the synthesis of β-glucuronidase was stopped completely late in the stationary growth phase indicating that the *las* promoter was no longer active. This part of the regulation makes some sense because the cell is in the state where it is no longer necessary to provide it with ATP for growth. The promoter clones were also affected by another stress factor, namely heat shock when transferred from 30°C to 37°C. The specific activity of β-glucuronidase was reduced which implies that the activity of the promoters were shut down.

Strategies for experimental MCA

The 3 genes *pfk*, *pyk* and *ldh* constituting the *las* operon are transcribed from P_{las} in the wild type MG1363 (Fig. 4A). In order to modulate the expression of the *las* operon the P_{las} is exchanged with synthetic promoters of different strength on the chromosome by homologous recombination (Fig. 4B). To modulate each gene individually, the genes preceded by synthetic promoters are integrated by site-specific recombination. Subsequently the original chromosomal copy of the gene will be deleted, here shown for *ldh* (Fig. 4C).

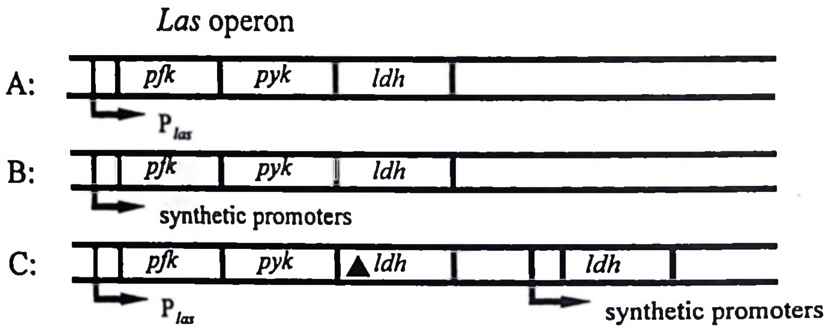

Strengh of promoters i.e.: 25, 50, 150 and 200 % of the wild type P_{las} level

Figure 4. The strategy for the genetic constructions. A: Wild type MG1363. B: Strains to modulate the expression level of the *las* operon. C: Strains to modulate the individual *pfk*, *pyk* and *ldh* genes. Here shown for *ldh* where the symbol ▲ indicates the deletion of the gene.

Modulating the expression of the *las* operon

Series of plasmids were constructed in which synthetic promoters were flanked by DNA fragments from each side of the native promoter P_{las}. By homologous recombination between these upstream and downstream regions and with selection for erythromycin resistance the type B strains will be isolated (Fig. 4B). We constructed a strain HWA182.4 in which the synthetic promoter CP25 was transcribing the *las* operon. The result was confirmed by Southern blotting and the strain had a lower expression level measured as phosphofructokinase activity (Table 1). A plasmid with a synthetic promoter was integrated by homologous recombination on the chromosome (strain HWA182.7), where P_{las} was still transcribing the *las* genes. A second cross-over event should place the *las* genes under control of the synthetic promoter. Further strains with different strengths of the synthetic promoters are under construction.

Table 1: Measurements of the specific activity of phosphofructokinase (PFK). Strain HWA182.7 where the plasmid is integrated on the chromosome and the wild type P_{las} is transcribing the *las* operon. Strain HWA182.4 where the synthetic promoter CP25 is transcribing the *las* operon

Strain	Promoter transcribing the *las* operon	Spec. activity of PFK U/mg protein
MG1363	wild type P_{las}	0.1128
HWA182.7	wild type P_{las}	0.1090
HWA182.4	CP25	0.0533

Modulating the expression of the *las* genes *pfk*, *pyk* and *ldh*

Using the site-specific recombination system, strains are under construction in which the expression of the individual *las* genes are modulated (Fig. 4C). The genes *pfk*, *pyk* and *ldh* were cloned separately in the integration vector pFB12α [7] harboring the *att*P site and in which the genes were transcribed from constitutive promoters. In order to control the expression level without influence from regulating factors and to be able to lower the expression level of the genes, the original chromosomal copy of the modulated gene will be deleted. A mutant with *ldh* inactivated was constructed and deletion mutants of *pfk* and *pyk* are under construction.

MATERIALS AND METHODS

Bacterial strain, culture media, and plasmids.

The plasmid-free *Lactococcus lactis* subsp. *cremoris* MG1363 [9] was used for studying promoter activities in *L. lactis*. It was routinely cultured in M17 [10] containing 1% glucose and incubated at 30°C.

The promoter probe vector pAK80 [5] was used for cloning P_{las} promoter fragments and synthetic promoters to predict the native activity of the *las* promoter. pAK80 is a shuttle vector between *E. coli* and *L. lactis* and carries the promoterless *lacL* and *lacM* genes, which encode the reporter β-galactosidase. Erythromycin at the concentration of 2μg/ml was used for selection of the pAK80 derivatives in *L. lactis*. The promoter probe vector pLB85 [7] was used for cloning of P_{las} promoter fragments and synthetic promoters in order to study the regulation of the *las* promoter. pLB85 is an *E.coli* vector that harbors the attachment site of the TP901 phage (*att*P) for recombination on the chromosome and the promoterless *gusA* gene [11] encoding β-glucuronidase. For site-specific recombination a plasmid encoding the enzyme integrase necessary for integration was added in trans to the strain. Therefore the pLB85 derivatives integrated on the chromosome were selected with chloramphenicol at the concentration of 5μg/ml and erythromycin at 2μg/ml.

Plasmids containing *pfk*, *pyk* and *ldh* were kindly provided by Dr. L. Hillier. The commercial pBluescript II SK (Stratagene) and pUC7erm [12] were used in the plasmid constructions to modulate the *las* operon. The unpublised DNA upstream of the *las* operon (approximately 1000bp) was obtained by inverse PCR [8]. The sequence was confirmed by sequencing 3 independent clones. In order to integrate the *las* genes on the chromosome by site-specific recombination we use the integration vector pFB12α [7] with an *att*P site.

The synthetic promoters were synthesized from degenerated oligonucleotides [4] with known consensus sequences kept constant and the sequences of the separating spacers were randomized. The promoter library covers the range of 0.3 up to 2,000 Miller units and here used for selecting promoters for the modulation of gene expression.

Enzyme assays.

Measurement of β-galactosidase activity in culture media was performed as described in [13] and modified by [5]. The assay condition for the β-glucuronidase measurement was the same as for the β-galactosidase, however *p*-nitro-β-D-glucuronic acid was used as the substrate [11]. Pyruvate kinase activity was conducted as described in [14].

DISCUSSION

The control and the regulation of metabolism in the bacteria *Lactococcus lactis* are of great interest, commercially as well as scientifically. The regulatory properties of the promoter of the *las* operon can be applied to construct starter cultures producing a specific product at a certain time. For instance, if the product is too toxic for the cell to be expressed during the entire fermentation period.

The goal of this study will be the determination of the control exerted by 3 different glycolytic enzymes on the glycolytic flux and we hope to achieve this goal by carefully tuning the expression of the genes around wild type level. The drawback of the chosen method is the time-consuming genetic work. However, we believe that this will pay back due to the ease at which steady state experiments can be performed with these presumed highly stable strains. The fact that the modulation of gene expression is achieved with synthetic promoters, allow us also to complement these modulations with the modulation of other enzyme activities more freely, and to perform accurate metabolic optimization of these bacteria [15].

ACKNOWLEDGEMENTS

We thank Katrine Madsen and Regina Schürmann for excellent technical assistance and Martin Willemöes for fruitful discussions. Integration vectors pLB85 and pFB12α were kindly provided by Dr. L. Brøndsted. This work is part of the FØTEX-programme supported by the Danish Dairy Research Foundation (Danish Dairy Board).

REFERENCES

[1] Thompson, J. (1987). FEMS Microbiol. Rev. 46, 221-231.
[2] Llanos, R.M., Hillier, A.J. and Davidson, B.E. (1992). J. Bacteriol. 174, 6956-6964.
[3] Llanos, R. M., Harris, C. J., Hillier, A. J. and Davidson, B. E. (1993). J. Bacteriol. 175, 2541-2551.
[4] Jensen, P.R. and Hammer, K. (1998). Appl. Environ. Microbiol. 64, 82-87.
[5] Israelsen, H., Madsen, S. M., Vrang, A., Hansen, E. B. and Johansen, E. (1995). Appl. Environ. Microbiol. 61, 2540-2547.

[6] Madsen, P. L. (1996). Transcription of the lactococcal temperate phage TP901-1. Ph.D. thesis. Department of Biological Chemistry, Institute of Molecular Biology, University of Copenhagen, Denmark.
[7] Brønsted, L. and Hammer, K. (1998). Manuscript in preparation.
[8] Andersen, H. W., Hammer, K and Jensen, P. R. (1998). Manuscript in preparation.
[9] Gasson, M.J. (1983). J. Bacteriol. 154, 1-9.
[10] Terzaghi, B. E. and Sandine, W. E. (1975) Appl. Microbiol. 29, 807-813.
[11] Platteeuw, C., Simons, G. and de Vos, W. M. (1994). Appl. Environ. Microbiol. 60, 587-593.
[12] de Vos, NIZO, the Netherlands.
[13] Miller, J. M. (1972). Cold Spring Harbor Laboratory, Cold Spring Harbor N.Y.
[14] Crow, V. L. and Pritchard, G. G. (1982). Methods Enzymol. 90, 165-170.
[15] Jensen, P.R. and Hammer, K. (1998). Biotech. and Bioengineering 58, 191-195

ROLE OF MITOCHONDRIAL ACETALDEHYDE OXIDATIONIN RESPIRATORY METABOLISM OF YEAST *SACCHAROMYCES CEREVISIAE*

Samira Boubekeur, Michel Rigoulet, Odile Bunoust, Michel Castroviejo and Bernard Guérin

Institut de Biochimie et Génétique Cellulaires, CNRS, 1 rue Camille Saint-Saëns 33077
Bordeaux Cedex, France, Phone: +33 556 99 90 33, Fax: +33 556 99 90 59
E-mail: samira.boubekeur@ibgc.u-bordeaux 2.fr

INTRODUCTION

Three major pathways of pyruvate in the yeast *Saccharomyces cerevisiae* have been described (1 for review). During fermentative growth, pyruvate is decarboxylated into acetaldehyde by pyruvate decarboxylase which is then reduced into ethanol in the cytosol by ADH 1, one of the four known alcohol dehydrogenase isoenzymes (2, 3); this sequence of reactions allows the reoxidation of NADH which is produced at level of the glyceraldehyde-3-phosphate dehydrogenase. During respiratory metabolism pyruvate can enter mitochondria by a specific carrier (4) and is decarboxylated and oxidized into acetyl-CoA by pyruvate dehydrogenase, a multienzyme complex located in the matrix (1). In addition, a pyruvate dehydrogenase bypass, located in the cytosol converts pyruvate into acetyl-CoA by the action of the following enzymes: pyruvate decarboxylase, cytosolic acetaldehyde dehydrogenase (5) and acetyl-CoA synthetases (6, 7); acetyl-CoA synthesized in the cytosol is either directly used for biosynthetic pathways or enters mitochondria via the carnitine acetyl transferase system (8).

We recently observed that permeabilized yeast cells oxidized pyruvate at a high rate while isolated mitochondria did not (9). It is shown in this paper that this respiration is due to the oxidation by mitochondria of acetaldehyde produced in the cytosol, and that this pathway can compensate for absence of functional pyruvate dehydrogenase.

MATERIAL AND METHODS

The *Saccharomyces cerevisiae* diploid Yeast Foam strain was used and grown in complete medium as in (10), mitochondria prepared as in (11) and spheroplasts permeabilized by nystatine as in (12). When indicated the strains listed in table 1 were used. For other methods see (12) and the legends of figure and tables.

Table 1. Genotypes and sources of *Sacccharomyces cereviciae* strains

Strain	Genotype	Activity lacking
YSH6.36.-3D	*MATa leu2-3/112ura3-52 trp1-92*	none (parental strain)
YSH4.136.-2D	*MATatrp1-92leu23/112ura352pdc1Δ::LEU2 pdc5Δ::URA3* (S.Hohmann)	Pyruvate decarboxylase
T2-3D	*HO/HO PDA1/PDA1*	none (parental strain)
T2-3C	*HO/HO pda1::Tn5ble/pda1::Tn5ble* (H.Y de Steenma)	Pyruvate dehydrogenase
RY601	*ura3-52 lys2-801 ade2-101 trp1-Δ63 his3-Δ200 leu2-Δ1*	none (parental strain)
RY271	*ura3-52 lys2-801 ade2-101 trp1-Δ63 his3-Δ200 leu2-Δ1 ald7::HIS3* (P.Meaden)	Mitochondrial acetaldehyde dehydrogenase

Table 2. Comparison of respiratory rates between isolated mitochondria and permeabilized spheroplasts incubated with different substrates [a].

	Respiratory rate (natom O/min^{-1}.mg $^{-1}$protein)					
	permeabilised spheroplasts			**isolated Mitochondria**		
Substrates	-ADP	+ADP	%	-ADP	+ADP	%
Ethanol	76±05	144±06	100	227±20	409±45	100
Succinat	67±03	151±07	104	147±15	250±11	62
Pyruvat	65±04	110±09	76	66±08	15±04	04
Malate	06±01	06±01	04	14±03	12±03	62
Pyruvate Malate	87±04	148±08	102	66±08	83±15	20

[a] Mitochondria 0.5 mg/ml were incubated in medium containing 0.65 M mannitol, 0.36 mM EGTA, 10 mM Tris-maleate, 5 mM phosphate, pH 6.8.For spheroplasts, 1 mg/ml were incubated in medium containiung 1M sorbitol, 0.5 mM EGTA, 2 mM $MgSO_4$, 1.7 mM NaCl, 10 mM KH_2PO_4 and 1% bovine serum albumin, pH 6.8. Permeabilisation of spheroplasts was performed by incubation with 20 mg/ml nystatin for 10 min.

Respiratory rate was measured after addition of various substrates. All the substrates were used at 10 mM except for ethanol : 109 mM. For ADP 2 mM were added. To compare the relative activities between spheroplasts and isolated mitochondria the respiratory values (+ADP) were expressed as a percent of ethanol respiratory rate.

RESULTS AND DISCUSSION

Respiration of isolated mitochondria and permeabilized spheroplasts on different substrates is presented in table 2. Mitochondria did not oxidize pyruvate unless malate was added in accordance with a catabolism via the pyruvate dehydrogenase and the tricarboxylic cycle. Oxidation of pyruvate by permeabilized spheroplasts, however, did not require malate addition although this dicarboxylate stimulated the respiration (see also 9). It was verified that spheroplast extracts did not contain malate in a sufficient amount to explain the respiration on pyruvate.

After centrifugation of the permeabilized spheroplasts the pellet containing the mitochondrial fraction did not oxidize pyruvate. This activity was restored in the presence of the soluble fraction which contained a non-dialysable and acid- or thermo-sensitive active molecule. We tried to purify this molecule as described in the legend of figure 1. It can be seen that the molecule co-purified with the pyruvate decarboxylase activity. Morever, respiration of isolated mitochondria with pyruvate as the sole substrate had been induced by addition of commercial pyruvate decarboxylase (data not shown) .These results lead to the conclusion that the active molecule is pyruvate decarboxylase.

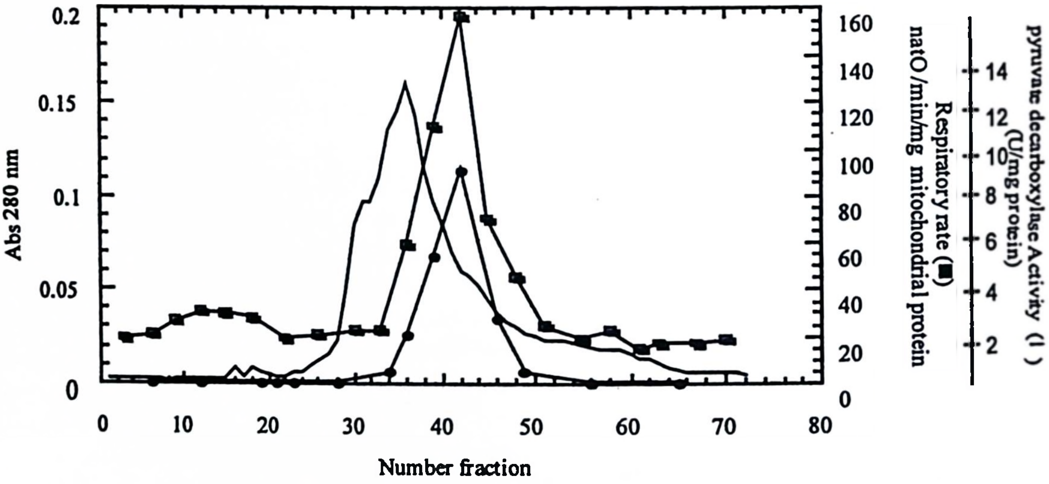

Figure 1. Characterization of the cytosolic active fraction.
Broken spheroplasts were centrifuged at 12 000g, proteins of the supernatant precipitated at 65 % ammonium sulfate saturation and solubilized in a phosphate buffer. After dialysis overnight against phosphate buffer, the extract was separated on monoQ column and eluted by a 0-1 M KCl gradient . A superose-12 column was loaded by the active fraction eluated from monoQ column. (-) absorbancy at 280 nm ; (l) pyruvate decarboxylase activity ;(n) respiratory rate of mitochondria on pyruvate (10 mM) in the presence of the different fractions.

This conclusion was confirmed and extended by the use of mutants (see table 3). It is clear that spheroplasts from the strain YSH4.136.-2D lacking pyruvate decarboxylase activity did not oxidize pyruvate, in contrast to its parental strain.

However, addition of malate induced a respiration on pyruvate indicating that the unique way of pyruvate oxidation is the pyruvate dehydrogenase- tricarboxylic cycle pathway. As expected, spheroplasts from the strain T2-3C lacking pyruvate dehydrogenase activity oxidized pyruvate, but the respiration was not stimulated by malate.

Table3. Comparison of respiratory rates of permeabiliazed spheroplasts between mutants and ther parental strains with various substrates ^{c}.

	Respiratory rate (natom $O.min^{-1} \cdot mg^{-1}$protein)					
Strains	YSH6.36.-3D	YSH4.136.-2D	T2-3D	T2-3C	RY601	RY271
Substrates						
Ethanol	125	112	150	120	104	100
Succinate	130	91	100	104	72	74
pyruvate	54	07	138	124	05	52
Malate	07	08	08	03	14	10
pyruvate-malate	64	40	162	120	56	40

^{c}Experimentals conditions are described in the legend the table 2.

Yeast cells contain two kinds of acetaldehyde dehydrogenase: the cytosolic $NADP^{+}$ dependent enzyme and the mitochondrial $NAD(P)^{+}$ dependent one. The former is thought to be involved in the cytosolic biosynthetic pathway since NADPH is not oxidized by mitochondria.The gene ALD7 coding for the mitochondrial enzyme was interrupted in the strain RY271. We verified that the mitochondrial acetaldehyde dehydrogenase was lacking. Table 3 shows that this strain did not oxidize pyruvate unless malate was added, pointing to an essential role of the mitochondrial acetaldehyde dehydrogenase in the pyruvate oxidation process.

The way of acetyl-coenzyme A synthesis in the cytosol from pyruvate is known as the pyruvate dehydrogenase 'by pass'. This is true for acetyl-coA formation. However, pyruvate dehydrogenase also catalyses the NAD^{+} reduction in the mitochondrial matrix; a possible alternative via the mitochondrial acetyl dehydrogenase is proposed in figure 2. This view is also supported by the observations that mutants lacking either pyruvate dehydrogenase or mitochondrial acetaldehyde dehydrogenase activities both grew on lactate as carbon source.

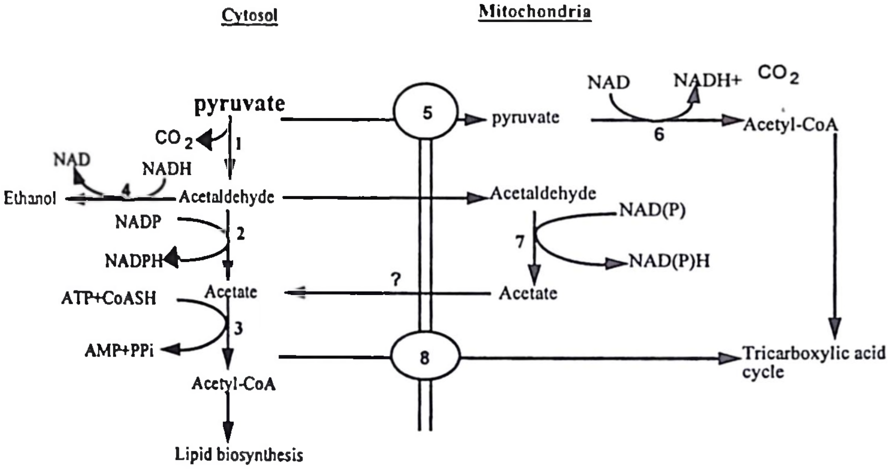

Figure 2. Key enzymatic reactions at the pyruvate branch-point *Saccomyces cerevisiae*. Numbered reactions are catalysed by the following enzymes: **1** pyruvate decarboxylase(PDC), **2** cytosolic acetaldehyde dehydrogenase NADP dependent (ACDH), **3** acetyl-CoA synthetase (ACS), **4** alcohol dehydrogenase (ADH), **5** mitochondrial pyruvate carrier, **6** pyruvate dehydrogenase complex(PDH), **7** mitochondrial acetaldehyde dehydrogenase, **8** carnitine acetyl transferase (CAT).

ACKNOWLEDGEMENTS

We wish to thank Dr Philip Meaden for the gift of the RY601 and RY271 strains, Dr H. Yde Steenma for the gift T2-3D and T2-3C strains and Dr Stephen Hohmann for the gift YSH6.36.-3D and YSH4.136.-2D strains.

REFERENCES

1) Pronk, J.T., Steensma, H. and van Dijken, J.P. (1996). Yeast, 12, 1607-1633.
2) Ciriacy, M. (1975). Mutat. Res. 29, 315-326.
3) Paquin, C. E. and Williamson, V. M.(1986). Mol. Cell Biol. 6, 70-79.
4) Nalecz, M. J., Nalecz, K. A. and Azzi, A. (1991). Biochim. Biophys. Acta 1079, 87-95.
5) Dickinson, F. M. (1996). Biochem.J., 315, 393-399.
6) Meaden, P.G., Dickinson, F. M., Mifud, A., Tessier, W., Westwater, J., Bussey,H.and Midgley, M. (1997). Yeast,13, 1319-1327.
7) van den Berg, M.A. and Steensma, H. Y. (1995) . Eur. J. Biochem., 231, 704-713.
8) van den Berg, M.A., de Jong-Gubbels, P., Kortland, C.J., van Dijken, J.P., Pronk, J.T.and Steensman, H.Y. (1996). J. Biol. Chem., 271, 28953-28959.
9) Averet, N. ,Fitton, V. ,Bunoust , O. ,Rigoulet ,M. and Guérin , B.(1998) Mol. cell.Biochem., in press
10) Arselin de Chateaubodeau, G.,Guérin, M. and Guérin, B. (1976).Biochimie(Paris) 58:601-610.
11) Guérin, B., Labbe, P. and Somlo, M. (1979).Methods in enzymology, 55, 149-159.
12) Fitton, V., Rigoulet, M., Ouhabi, R. and Guérin , B. (1994). Biochemistry.33,9692-9698

DIFFUSION LIMITATION OF OXYGEN VERSUS ADP IN PERMEABILIZED MUSCLE FIBERS

A.V. Kuznetsov, B. Lassnig, R. Margreiter, E. Gnaiger

Department of Transplant Surgery, D. Swarovski Research Laboratory, University Hospital Innsbruck, Anichstrasse 35, A-6020 Innsbruck, Austria
Tel: 43 512 504 4626, FAX: 43 512 504 4625, E-mail: Andrei.Kuznetsov@uibk.ac.at

INTRODUCTION

Regulation of oxygen consumption of oxidative muscle is exerted by various factors such as ADP, phosphorylation potential, phosphocreatine/ creatine ratio, intracellular Ca^{2+}, nitric oxide and oxygen [1-4]. Permeabilized muscle fibers and isolated cardiomyocytes display pronounced limitation for ADP transport when compared with isolated mitochondria [5]. Whereas the outer mitochondrial membrane is the proposed mechanism for transport limitation for the charged molecule ADP [6-7], biological membranes do not constitute any barrier for oxygen diffusion. Nevertheless, oxygen affinity is significantly reduced in respiration of permeabilized muscle fibers [8]. In the present study we addressed the problem of oxygen limited respiration by comparing the oxygen kinetics in permeabilized muscle fibers, collagenase-treated permeabilized muscle fibers and isolated mitochondria.

METHODS

Rat heart mitochondria were isolated using a trypsin method [9]. Permeabilized bundles of rat cardiac and skeletal muscle fibers (from endocardial surface of left ventricle and M. soleus) were prepared by incubation in relaxing solution with 50 µg/ml saponin for 30 min at 4 °C [10]. Oxygen kinetics was studied by high-resolution respirometry with the OROBOROS *Oxygraph* in transitions between aerobic and anoxic states [11]. The incubation medium (30 °C, pH 7.1) consisted of 200 mM sucrose, 0.5 mM EGTA, 3 mM $MgCl_2$, 20 mM taurine, 10 mM KH_2PO_4, 20 mM K-HEPES, 1 mg/ml BSA, and 10 mM pyruvate and 5 mM malate as substrates for complex I. The software DATLAB 2.1 (OROBOROS, Innsbruck, Austria) was used for data acquisition and specific oxygen kinetics analysis, including internal zero-oxygen calibration and corrections for response time and instrumental background [4].

RESULTS

Isolated mitochondria as well as permeabilized muscle fibers showed hyperbolic relations between oxygen flux and oxygen pressure. The apparent K_m for oxygen (p_{50}) in isolated cardiac mitochondria was not controlled by diffusion gradients but by metabolic state. p_{50} was 0.02 kPa at rest, and increased to 0.04 kPa in actively respiring isolated mitochondria, in the presence of 1 mM ADP (Fig. 1). In uncoupled mitochondria p_{50} was 0.02 kPa at a maximum flux identical to the active state. In contrast, permeabilized muscle fibers showed oxygen-dependent respiration over the entire experimental oxygen range used routinely in respirometry with permeabilized fibers. In soleus and cardiac muscle fibers, p_{50} increased from 1 kPa in resting states (without ADP) to 4 kPa (up to 7 kPa) in active states (with 1 mM ADP; Table 1). Addition of collagenase („Sigma", type II, final concentration 0.2 mg/ml) in the course of respiration measurements resulted in a dramatic increase of affinity for oxygen. The p_{50} decreased by almost two orders of magnitude to 0.04 ± 0.02 kPa in the active state, reaching an identical value as in isolated mitochondria (Fig. 2).

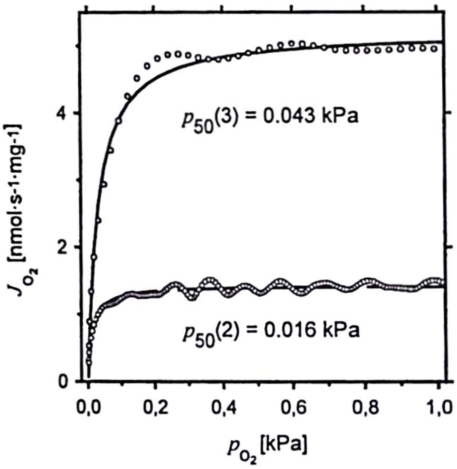

Figure 1. Hyperbolic relation of respiration, J_{O_2}, and oxygen pressure, p_{O_2}, in isolated heart mitochondria. (3) active; (2) resting state.

Table 1. Kinetic parameters for oxygen* and ADP in permeabilized muscle fibers and isolated mitochondria.

Preparation	RCI §	c_{50} for oxygen resting state §, μM	c_{50} for oxygen active state §, μM	K_m^{app} for ADP #, μM
Permeabilized muscle fibers Rat soleus	7.1 ± 1.5	11 ± 1.0	38 ± 17	330 ± 50 [7]
Permeabilized muscle fibers Rat heart	7.8 ± 1.3	9 ± 1.0	42 ± 27	260 ± 50 [5]
Isolated mitochondria Rat heart	8.4 ± 2.3	0.16 ± 0.07 [11]	0.35 ± 0.08 [11]	17.6 ± 1.0 [5]

* Half-saturating oxygen concentration, c_{50}, was calculated from p_{50} and the oxygen solubility of 10.07 μM/kPa.

§ with pyruvate/malate; RCI, respiratory control index was calculated as ratio between rates of respiration in active and resting state.

# with glutamate/malate.

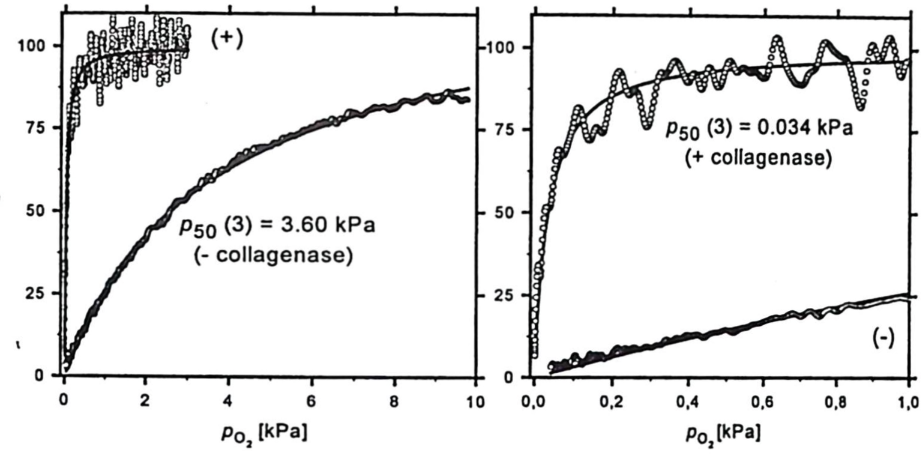

Figure 2. Hyperbolic relation of active respiration, J_{O_2}, and oxygen pressure, p_{O_2}. (-) in permeabilized rat skeletal muscle fibers (M. soleus); (+) after treatment of bundles of muscle fibers with collagenase.

DISCUSSION

Based on simple diffusion, the oxygen diffusion „gradient" between extracellular medium and the average mitochondrion can be calculated at half-maximum flux as the difference between the p_{50} of fibers and isolated mitochondria, i.e. 42 - 0.4 µM. By comparing diffusion coefficients of oxygen ($20 \cdot 10^{-6}$ $cm^2 \cdot s^{-1}$ [12]) and Mg-ADP ($4 \cdot 10^{-6}$ to $6 \cdot 10^{-6}$ $cm^2 \cdot s^{-1}$; [13,14]), the diffusion gradient for ADP between extracellular medium and mitochondria is calculated as 3 to 5 times the concentration gradient for oxygen. This value of c. 130 to 200 µM ADP, added to the mitochondrial $K_m{}^{app}$ for ADP of 20 µM (Table 1), yields a theoretical $K_m{}^{app}$ for ADP in permeabilized fibers of 150 to 220 µM. Therefore, diffusion limitation can explain part of the observed increase of the $K_m{}^{app}$ for ADP to 300 µM in permeabilized muscle fibers (Table 1). However, a more than 50 % contribution of diffusion limitation to total transport limitation is certainly an overestimation since a significant fraction of mitochondrially produced ATP is hydrolyzed and regenerates ADP locally. Moreover, the $K_m{}^{app}$ for ADP is not significantly lower in cardiomyocytes (c. 20 µm in diameter) than in permeabilized fiber bundles in spite of remarkably different sizes [5].

Evaluation of these results is of primary methodological importance for the application of permeabilized muscle fibers in the field of diagnosis of mitochondrial dysfunction. Respiratory flux of muscle fiber bundles is limited by oxygen diffusion at high oxygen concentration. This problem may be avoided by collagenase treatment, potentially offering a new approach in mitochondrial studies with permeabilized muscle fibers.

In addition, it remains to be shown whether the simple increase of diffusion distances can explain the observed decrease in oxygen affinity in permeabilized muscle fibers. Alternatively, other factors related to metabolic state may contribute to the decrease of oxygen affinity in permeabilized muscle fibers. Since p_{50} depends on metabolic state and coupling, oxygen affinity is a sensitive indicator of the functional state of isolated mitochondria and cells [15].

ACKNOWLEDGEMENTS

Supported by a research grant of the University of Innsbruck and by an OROBOROS Research Award.

REFERENCES

1 Chance, B., Leigh, J.S. Jr, Clark, B.J., Maris, J., Kent, J., Nioka, S., Smith, D. (1985) Proc. Natl. Acad. Sci. USA 82. 8384-8388.

2 Koretsky, A.P., Katz, L.A., Balaban, R.S. (1989) J. Mol. Cell. Cardiol. 21, 59-66.

3 Brown, G.C. McBride, A.G., Fox, E.J., McNaught, K.S., Borutaite, V. (1997) Biochem. Soc. Trans. 25, 901-904.

4 Gnaiger, E., Steinlechner-Maran, R., Mendez, G., Eberl, T., Margreiter, R. (1995) J. Bioenerg. Biomembr. 27, 582-596.

5 Saks, V.A., Belikova, Y.O., Kuznetsov, A.V. (1991) Biochim. Biophys. Acta 1074, 302-311.

6 Saks, V.A., Belikova, Yu.O., Vasilleva, E.V., Kuznetsov, A.V., Lyapina, S., Petrova, L., Perov, N.A. (1993) Biochim. Biophys. Acta 1144, 134-148.

7 Saks, V.A., Kuznetsov, A.V., Khuchua, Z.A., Vasileva, E.V., Belikova, Y.O., Kesvatera, T., Tiivel, T. (1995) J. Mol. Cel. Cardiol. 27, 625-645.

8 Gnaiger, E., Steinlechner, R., Keriel, C., Leverve, X., Rossi, A., Saks, V., Sibille, B., Kay, L., Novel, V., Daneshrad, Z., Gellerich, F.N., Eberl, T., Skladal, D., Sperl, W., Margreiter R. (1995) J. Molec. Med. 73, B39.

9 Saks, V.A., Kuznetsov, A.V., Kupriyanov, V.V., Miceli, M.V., Jacobus, W.E. (1985) J. Biol. Chem. 260, 7757-7764.

10 Veksler, V.I., Kuznetsov, A.V., Sharov, V.G., Kapelko, V.I., Saks, .A. (1987) Biochim. Biophys. Acta 892, 191-196.

11 Gnaiger, E., Lassnig, B., Kuznetsov, A., Rieger, G., Margreiter, R. (1998) J. Exp. Biol. 201, 1129-1139.

12 Grote, J., Thews, G. (1962) Pfluegers Arch. 276, 142-165.

13 Jacobus, W.E., Diffley, D.M. (1989) in Energy Transformations in Cells and Organisms (Wieser, W. and Gnaiger, E., eds.), pp. 28-35, Georg Thieme Verlag, Stuttgart, New York.

14 Hubley, M.J., Locke, B.R., Moerland, T.S. (1996) Biochim. Biophys. Acta 1291, 115-121.

15 Steinlechner-Maran, R., Eberl, T., Kunc, M., Margreiter, R., Gnaiger, E. (1996) Am. J. Physiol. 271, C2053-C2061.

INFLUENCE OF NUTRIENT STARVATION ON SUGAR UPTAKE KINETICS OF *SACCHAROMYCES CEREVISIAE*

Eva Albers[a,c] *, *Michael C. Walsh*[b], *Susanna Sjöström*[a], *and Lena Gustafsson*[c]

[a] Dept. Chemical Reaction Engineering, Chalmers University of Technology, SE-412 96 Göteborg, Sweden
[b] E.C. Slater Institute, Biocentrum Amsterdam, University of Amsterdam, NL-1018 TV Amsterdam, The Netherlands
[c] Dept. General and Marine Microbiology, Lundberg Laboratory, University of Göteborg, Box 462, SE-405 30 Göteborg, Sweden
* Corresponding author at address a. Tel. + 46 31 772 3096. Fax: + 46 31 772 3035.
e-mail: eva@cre.chalmers.se

INTRODUCTION

Periods of nutrient starvation often occur in industrial processes. One example is the production of Bakers' yeast, where periods of starvation may occur both in the production phase and during subsequent storage. Lack of one or several nutrients may occur. Starvation affects the quality of the yeast, and especially the important fermentative capacity of the cells may decrease. It has been shown that the fermentative capacity after nitrogen starvation was much lower compared to after carbon starvation [1]. The physiological state of the cells also plays a significant role. Yeast cells growing logarithmically on glucose were much more sensitive for carbon starvation than cells originating from the diauxic shift (transition from glucose to ethanol as the carbon source). After 7 days of starvation, log phase cells lost 80 % of the fermentative capacity. In contrast, cells harvested from the diauxic shift maintained their fermentative capacity during starvation [6]. Further investigations showed that the decrease in fermentative capacity did not correlate with the amount of glycolytic and fermentative enzymes [2]. Another explanation for the difference between carbon and nitrogen starved cells may be the activity of the glucose uptake system. It has been suggested that the transport step exerts a high level of control on the glycolytic flux in this yeast [3]. Former studies [4, 5] revealed that during nitrogen starvation, in the presence of a fermentable carbon source, the uptake systems of *S. cerevisiae* are irreversibly inactivated. In derepressed cells, which maintain a high fermentative capacity [6], mainly the high affinity uptake system (K_m 1-2 mM) was present [7, 8].

The aim of the present study was to investigate if the influence of starvation on the uptake capacity could possibly explain the lower fermentative capacity of nitrogen starved cells compared to carbon starved cells. Different methods to estimate the kinetic coefficients are also discussed.

METHODS

Uptake experiments

A wildtype diploid laboratory strain, X-2180, from Yeast Genetic Stock Center (Berkeley, California, USA) was used. The cells were grown in shake flask cultures (volume of liquid/flask ratio, 1:2) at 30 °C and 170 rpm in a rotary shaker with YNB

(Yeast Nitrogen Base, w/o amino acids and ammonium sulphate) medium. The medium contained 1.7 g/l YNB, 20 g/l glucose (monohydrate) as carbon source, 5 g/l ammonium sulphate as nitrogen source in 0.1 M potassium phthalate buffer, pH 5.0. The cells were grown until one hour after glucose depletion (giving transition phase cells), centrifuged (4 °C, 7 min, 5000 g) and resuspended in starvation medium (volume of liquid/flask ratio, 1:4). The starvation media lacked either the carbon or nitrogen source, or both the carbon and nitrogen sources, of the YNB medium. The medium for nitrogen starvation experiments contained 35 g/l glucose (monohydrate) which was sufficient to prevent depletion of glucose during the starvation period. The cells were starved for 24 h at 30 °C and 170 rpm in a rotary shaker. The cells were harvested by centrifugation as earlier and resuspended in a synthetic freshwater, S6, containing per litre; 84 mg $NaHCO_3$, 12 mg $NaNO_3$, 14.7 mg $CaCl_2{\cdot}2H_2O$, 12.3 mg $MgSO_4{\cdot}7H_2O$, 1.74 mg K_2HPO_4, 0.49 mg Na_2SiO_3.

The initial uptake rate of glucose was measured over 5 s as described by Walsh *et al.* [7] using glucose concentrations between 0.05-50 mM. Protein was determined according to the method of Lowry [9].

Evaluation

The uptake was assumed to follow Michaelis-Menten kinetics. To determine the V_{max} and K_m, the data were fitted to the Michaelis-Menten equation by regression of linearised variables. Three linearised equations were used, Eq. 1-3, all of which are common for the determination of enzyme kinetics. The variables are denoted; v, uptake rate, V_{max}, maximal uptake rate, S, substrate (glucose) concentration; and K_m, affinity constant.

Eadie-Hofstee
$$v = -K_m \cdot \frac{v}{S} + V_{\max} \tag{1}$$

Lineweaver-Burk
$$\frac{1}{v} = \frac{K_m}{V_{\max}} \cdot \frac{1}{S} + \frac{1}{V_{\max}} \tag{2}$$

Hanes (or Woolf)
$$\frac{S}{v} = \frac{1}{V_{\max}} \cdot S + \frac{K_m}{V_{\max}} \tag{3}$$

The Eadie-Hofstee method is widely used for determination of uptake kinetics, because multiple uptake systems can easily be detected from the resulting "bilinear-like" plot. However, if multiple uptake systems are detected, it is important to use an appropriate method for the determination of the kinetic coefficients of the different uptake systems (see discussion in *e.g.* [10]). A drawback with the Eadie-Hofstee rearrangement is that an error is introduced in the regressor variable, v/s, by the multiplication with v. One of the base assumptions made in linear regression, is of course that the regressor variable is known without error [11]. In the next equation (Lineweaver-Burk, Eq. 2), the error in the dependent variable, 1/v, has a non-constant variance. This is caused by the use of the reciprocal of v, which results in a larger influence of the lower rates on the estimated parameter values. Finally, in the Hanes method (Eq. 3), the variance of the error in the dependent variable, S/v, is almost constant and for this reason this equation may be preferable to Eq. 2 [12]. However, in the present case the dependent variable does not have a constant error. The sum of squares of the pure error (estimated from repeated experiments) was found to increase with increased substrate concentration. This means that a weighted linear regression has to be used. In the present work, the calculated pure errors for determination of weighting factors were used in the regression of Hanes equation [11].

RESULTS AND DISCUSSION

The experimental results of the uptake experiments (Fig. 1) clearly show a difference between the differently starved cells.

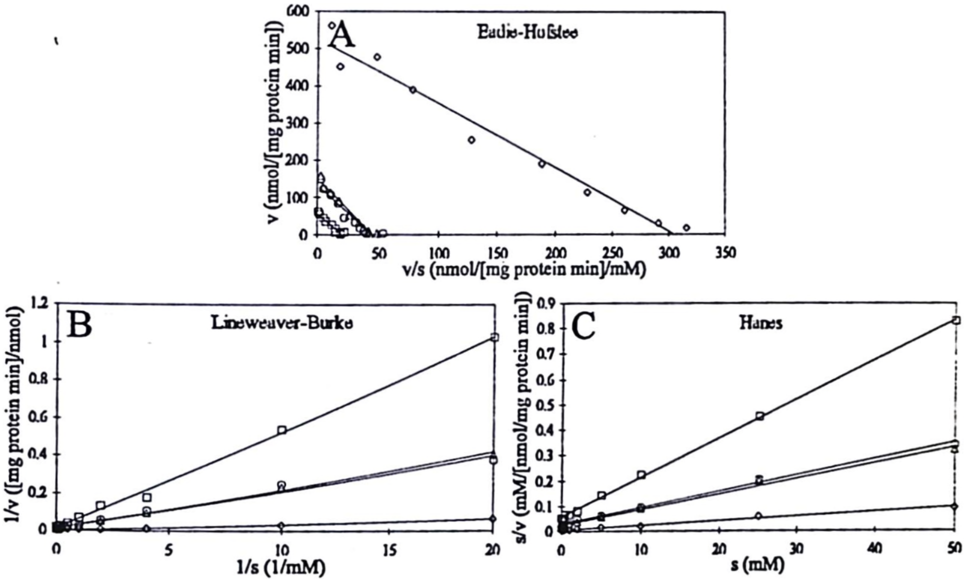

Figure 1. Plots of uptake rate (v) and glucose concentration (S) according to A, Eadie-Hofstee; B, Lineweaver-Burk; C, Hanes. Data are presented for cultivations with *S. cerevisiae*: not starved ◊, nitrogen starved □, carbon starved Δ, and both carbon and nitrogen starved O. Each point is the average of at least four determinations from at least two cultivations.

As seen in Tab. 1, the estimations of the kinetic parameters were influenced by the linearisation method used. For all cases the method of Lineweaver-Burk gave the lowest V_{max}, whereas the Hanes method gave the highest values. The Lineweaver-Burk method also resulted in the largest standard deviation of the V_{max} values for all types of starvation. This illustrates that this linearisation does not give a good fitting of the data. However, it is necessary to keep in mind that the standard deviation of the parameters determined for either of the unweighted linearisation methods is not correct, because the base assumptions of linear regression are not fulfilled. The K_m values also differed significantly, and the Hanes equation resulted in the largest values. For the nitrogen starved cells there was also a qualitative difference in the K_m, determined by the different methods. Compared to the carbon starved cells, the K_m was lower using both

Eadie-Hofstee and Lineweaver-Burk equations, whereas for the Hanes method the K_m of the nitrogen starved cells was higher. This shows the importance of taking into account how kinetic parameters have been determined when comparing data from the literature.

Table 1. Values of V_{max} and K_m determined from the three different types of linearised equations of the Michaelis-Menten equation for different types of starved cells of *S. cerevisiae*. The standard deviations of the parameters are given. The standard deviation was calculated using the error propagation formula with correlation corrections where necessary.

	V_{max} (nmol/ mg protein min)			
Type of starvation	Eadie-Hofstee	Lineweaver-Burk	Hanes	Hanes, weighted
Non	393±29	377±219	452±22	646±82
Nitrogen	32±4	21±19	57±4	75±10
Carbon	148±5	101±36	162±4	150±4
Dual	127±7	71±35	155±3	156±3

	K_m (mM)			
Type of starvation	Eadie-Hofstee	Lineweaver-Burk	Hanes	Hanes, weighted
Non	1.3±0.2	1.5±0.9	2.3±0.9	1.7±0.3
Nitrogen	1.2±0.3	1.6±1.5	5.7±1.3	3.6±0.7
Carbon	3.2±0.2	2.1±0.8	4.0±0.5	3.4±0.2
Dual	2.8±0.2	1.4±0.8	4.3±0.4	4.5±0.1

However, despite the differences in the estimated values of V_{max} and K_m, the results clearly showed that the starvation condition had a large influence on the uptake kinetics. For all types of cells the K_m values were in the region of 1 to 6 mM, of which the highest values of K_m were obtained from using the Hanes equation. However, with a proper regression it was possible to distinguish between differences in K_m at different conditions, *i.e.* when the weighted Hanes method was used. All types of starvation then resulted in an increased value of the K_m. Large differences were found in the V_{max} values, on which different starvation conditions apparently had a large effect. For nitrogen starved cells a V_{max} of about 10 % of the V_{max} for non-starved cell was estimated. Carbon and dual starvation resulted in an almost equal V_{max} of about 30 % of the value obtained for the non-starved cells. Conclusively, it seems that the presence of a (fermentative) carbon source is important for the inactivation of the uptake system during nitrogen starvation [4]. The clear difference between the carbon and nitrogen starved cells indicate that the uptake system at least to some part explains the former shown difference in fermentative capacity [1].

ACKNOWLEDGEMENTS

Professors K. van Dam and H.V. Westerhoff are gratefully acknowledged for that Eva Albers had the possibility to visit their laboratories and practise uptake measurements. The authors also would like to thank Dr. Gunnar Lidén for helpful comments on the manuscript. The Swedish National Board for Industrial and Technical Development (NUTEK) is acknowledged for the financial support.

REFERENCES

1 Larsson, C., Nilsson, A. and Gustafsson, L. (1994) Proceedings of the 6th BTK, Modern trends in BioThermoKinetics, pp. 232-237, Innsbruck University Press, Innsbruck, Austria.
2 Blomberg, A., Norbeck, J., Nilsson, A. and Gustafsson, L. (1996) Proceedings of the 7th BTK, BioThermoKinetics of the living cell, pp. 381-386, BioThermoKinetics Press, Amsterdam, The Netherlands.
3 Gancedo, C. and Serrano, R. (1989) in The yeasts (Rose, A.H. and Harrison, J.S., eds.), Vol. 3: Metabolism and physiology of yeasts, 2nd ed., pp. 205-259, Academic Press Ltd., London, U.K.
4 Busturia, A. and Lagunas, R. (1986) J. Gen. Microbiol. 132, 379-385.
5 Lagunas, R., Dominguez, C., Busturia, A. and Saez, M.J. (1982) J. Bacteriol. 152, 19-25.
6 Nilsson, A., Larsson, C. and Gustafsson, L. (1995) Thermochim. Acta 250, 233-245.
7 Walsh, M.C., Smits, H.P., Scholte, M. and van Dam, K. (1994) J. Bacteriol. 176, 953-958.
8 Bisson, L.F. (1988) J. Bacteriol. 170, 4838-4845.
9 Lowry, O.H., Rosebrough, N.J., Farr, A.L. and Randall, R.J. (1951) J. Biol. Chem. 193, 265-275.
10 Fuhrmann, G.F. and Völker, B. (1993) Biochim. Biophys. Acta 1145, 180-182.
11 Draper, N. and Smith, H. (1981) Applied regression analysis, 2nd ed., John Wiley & Sons, Inc., New York, USA.
12 Cornish-Bowden, A. (1995) Fundamentals of enzyme kinetics, Portland Press Ltd., London, UK.

CONTROL BY WATER: THE OSMOTIC STRESS CONCEPT AND ITS CRITICS

Peter Nicholls

Dept. of Biological Sciences, University of Essex, Colchester, CO4 3SQ UK

ABSTRACT

Theories of enzyme hydration include an 'osmotic stress' model, a 'dehydration' model, and a 'molecular crowding' model. Hexokinase changes its conformation on binding glucose. Polyethyleneglycols cause progressive decreases in the glucose binding constant (K_d). The K_d effect depends upon PEG size. The effect of osmolytes on adenosine deaminase suggests a hypersensitivity to decreasing water activity. Low levels of proteins affect activity of lactate dehydrogenase and DNA-protein binding is very osmolyte sensitive. All the results can be analysed using the osmotic stress concept with variable success. The three theories may not be mutually exclusive, but alternatives whose applicability depends upon the system examined. Concepts derived from all three models may be needed to explain the intracellular behaviour of proteins and enzymes.

INTRODUCTION AND ANALYSIS

Intracellular macromolecule environments differ from *in vitro* environments. The cell has a high osmolarity and high protein concentration. Test tube and cuvette osmolarities are often low. But most proteins hydrate to between 0.2 and 0.3 gm H_2O/gm protein (1). Changes in these waters affect protein behaviour and the control of that behaviour. When proteins interact with other molecules there are increases and decreases in amounts of bound waters. Such chemically necessary changes are potentially physiologically significant. Three theories of osmotic or hydration effects are available: (i) the 'osmotic stress' model (2,3), in which binding of a physiological ligand or substrate is directly accompanied by binding or release of a number of water molecules; (ii) the 'dehydration' model, in which enzyme function is impaired as a hydration layer is depleted of water by addition of osmolyte; and (iii) the 'molecular crowding' model, in which the solute affects the equilibrium between bound and free macromolecules because their covolume changes upon interaction.

Hexokinase undergoes a conformation change upon binding glucose, as monitored by changes in tryptophane absorbance or fluorescence. Increasing concentrations of osmolytes (polyethyleneglycols) induce a progressive decrease in the glucose binding constant (K_d). This has been analysed in terms of osmotic stress and uptake or release of bound waters (4). Adenosine deaminase seems to show hypersensitivity to decreasing water activity; this has been interpreted in terms of the dehydration model (7). Effects of low levels of proteins on lactate dehydrogenase activity, and macromolecular interactions involving DNA and proteins, have been interpreted in terms of the macromolecular crowding model (9).

All three types of result can however be analysed using any one of the three models. The present paper employs the osmotic stress method (2,3). Water movement from inaccessible fractions to bulk phase can occur in concert with binding of conventional ligands, e. g. glucose in hexokinase (4), and oxygen in haemoglobin (5). The numbers of such water molecules ('n' in Eq. [1]) may be positive (5) or negative (4).

$$P(H_2O)_m + L + nH_2O \text{ <-----> } P(H_2O)_{n+m}L \text{ complex} \qquad \text{..... [1]}$$

where P = protein and L = ligand.

Glucose binding by hexokinase involves loss of water from the protein (4, 6). The 'n' value is obtained by plotting the natural logarithm of the ratio of the K_d at a given osmolality to that at zero osmolality against the measured osmolality in atmospheres or dynes/cm^2. In the simplest thermodynamic treatment (2) this should be a straight line with slope = $\Delta V_w/RT$ where ΔV_w is the volume of water removed or added, as in Eq. [2].

$$\Delta V_w = \frac{\Delta RT \ln K_d}{\Delta P} \qquad \text{....[2]}$$

When base 10 logarithms, volumes in cm^3/mol, and pressures in atmospheres are used, and if water density does not change, Eq. [2] becomes:

$$n = \Delta V_w/18.1 \approx \frac{12650\Delta \log(K_d/K_d o)}{\Delta P} \qquad \text{....[3]}$$

Complications arise when the plots are not linear. Hexokinase challenged with large PEGs (M_w>1500) shows a non-linear response to π (6). Adenosine deaminase also shows a non-linear response to osmolarity change (7). Lactate dehydrogenase changes its activity in response to small amounts of inert protein (8) which cannot appreciably affect osmolarity, and protein-DNA binding is especially osmotically sensitive (9). But do these osmotic hypersensitivities require the abandonment of the "simple" osmotic model? The following analysis attempts to address this question.

The hexokinase case.

Initially Rand *et al.* (4) estimated a value of n (Eqs. 1-3 above) of ≈ 65. Later Reid & Rand (6) showed that a more complex model was needed as (i) the osmotic response was not completely independent of the molecular mass of the PEG; and (ii) plots of Ln (k/k(0)) vs. π are not linear (Eqs. 2 & 3 are not obeyed).

Fig. 1 contains a summary of the data for two PEGs, one with an average MW of 400, the other with an average MW of 8000. Each such plot may be fitted to a rectangular hyperbola of the form in Eq. 4:

$$\mathrm{Ln}(K_d/K_d0) = \mathrm{Ln}(K_d/K_d0)_{max} {}^{*}\pi/(\pi_{50}+\pi) \qquad \text{... (4)}$$

At low osmolarities Eq. (4) reduces to Eq. 5:

$$\mathrm{Ln}(K_d/K_d0) = \mathrm{Ln}(K_d/K_d0)_{max} {}^{*}\pi/\pi_{50} \qquad \text{... (5)}$$

which has the form of Eq. 3.

At high osmolarities Eq. 4 becomes Eq. 6:

$$\mathrm{Ln}(K_d/K_d0) = \mathrm{Ln}(K_d/K_d0)_{max} \qquad \text{... (6)}$$

That is, the ratio approaches a maximal value independent of π. The values for $\mathrm{Ln}(K_d/K_d0)_{max}$ {or $\mathrm{Ln}(K_{d(min)}/K_d0)$} and π_{50} obtained for PEGs of different molecular masses are plotted in Fig. 2.

The adenosine deaminase case

Dzingeleski & Wolfenden (7) have studied the effects of high concentrations of sucrose or ethanol on the activity of adenosine deaminase. They interpret their results, which show a marked inhibition of enzyme activity by the solute, in terms of a dehydration of an enzyme surface whose functionality requires the cooperative action of 10-20 water molecules. Fig. 1 includes a summary of their data replotted in the Ln (k/k_0) vs. π format. The effects of sucrose obey Eq. (2) but the ethanol plot is non-linear and requires the postulation of more than one process.

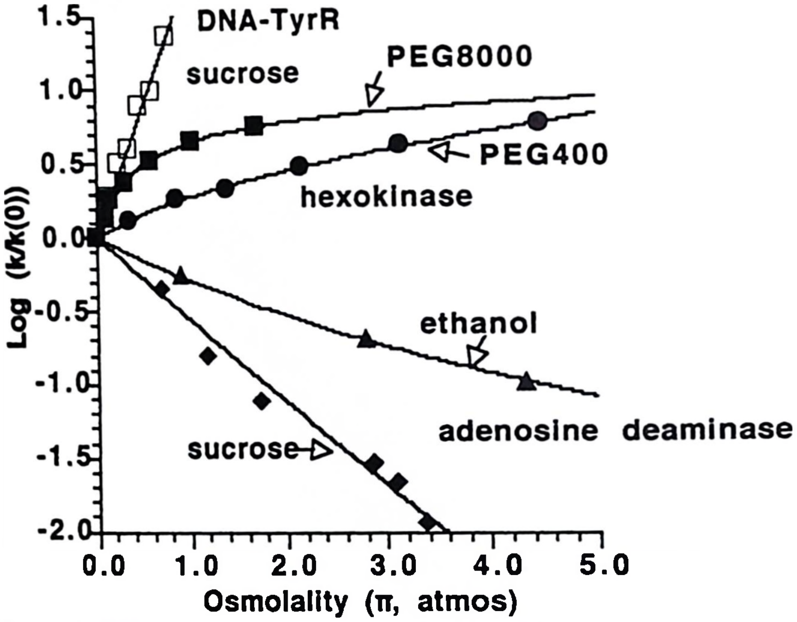

Figure 1. Effect of osmolarity on catalysis or binding by three enzymes or proteins. Adenosine deaminase activity was perturbed by sucrose or ethanol (ref. 7). Hexokinase K_d for glucose was perturbed by two PEGs (ref. 6). DNA-TyrR binding was perturbed by sucrose (ref. 9). Rand-Parsegian plots are of Log parameter ratio vs. osmolarity in atmospheres (cf. ref. 2).

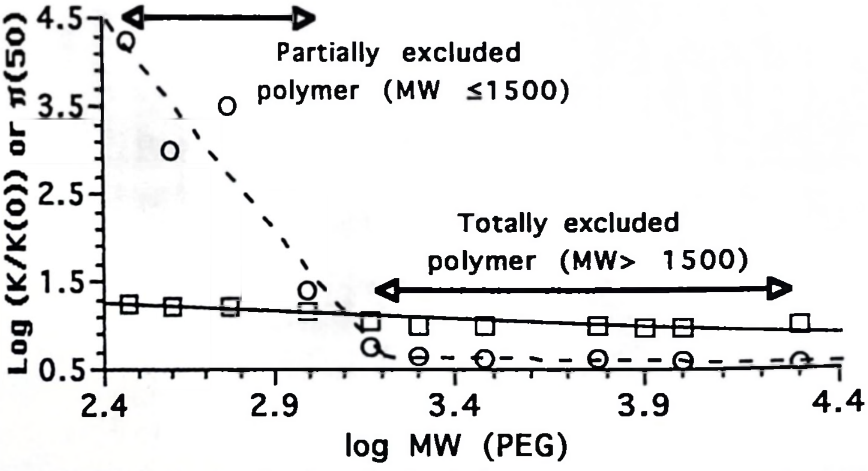

Figure 2. Effect of molecular size of polyethylene glycol upon the maximal K_d/K_{d0} ratio and the osmolarity (π) required for half maximal change of this ratio in hexokinase. , K_d/K_{d0} ratios; O, osmolarity (π) for half maximal change. Hexokinase data at pH 9.0 from Reid and Rand (6).

The lactate dehydrogenase and DNA-pTyrR binding cases

Winzor and coworkers (8, 9) use a 'crowding' (volume exclusion) model to analyse enzymes (lactate dehydrogenase, LDH) and protein-DNA binding. The LDH data cannot easily be interpreted thermodynamically but Fig. 1 also shows the data for the binding of the control protein pTyrR to DNA replotted as Ln (k/k_0) vs. π. As reported (9) this plot is linear and thus the reaction also obeys Eq. (1). Only the interpretation of the apparent volume changes is a subject of disagreement (6, 9).

DISCUSSION

Macromolecular processes have been analysed using both osmotic stress (2,3,10,11) and crowding (9, 12) ideas and in one case the surface dehydration idea (7). Are these real alternatives or different ways of looking at the same thing? Osmotic stress and crowding both predict that the processes will follow an equation like Eq. (2) although the interpretations are different and the magnitudes of the volume changes are not the same (values obtained using the osmotic stress method are about 4 times larger). Neither model has a simple explanation for the non-linearity seen in cases like hexokinase (Figs. 1 & 2) and adenosine deaminase with ethanol (Fig. 1). The dehydration model does not predict linearity of response nor equivalence of osmolytes but it requires a mechanistically implausible degree of cooperativity between water molecules on the enzyme surface.

From the slopes of the lines in Fig. 1 the water changes predicted according to the osmotic stress hypothesis are summarised in Table 1.

Enzyme/ protein	Osmolyte	n @ low π	n @ high π	Ref.
1. Hexokinase	PEG8000	1100	0 (0-25)	6
2. Hexokinase	PEG400	170	0 (0-25)	6
3. Ad. deaminase	ethanol	**-140**	**-40**	7
4. Ad. deaminase	sucrose	**-320**	--	7
5. DNA-TyrR	sucrose	1000	--	9

Table I. Bound waters (n) required for substrate interaction (negative values) or released upon substrate binding or interaction (positive values). cf. Fig. 1.
n = estimated moles water bound or released per mole enzyme or protein.

The small numbers of waters calculated in the original hemoglobin and hexokinase studies were consistent with the known changes of structure involved. But the larger values in Table I, such as the predicted values for the DNA-TyrR interaction and the low osmolality region of the PEG8000-hexokinase system, are hard to reconcile with physically plausible water movements. Thus there remains room for all three models in the interpretation of osmolyte effects on enzymes.

Do these phenomena have physiological relevance? Any complete analysis of events in cellular compartments must take into account osmolarities, protein concentrations and water activities. Although linked, these parameters are distinct. Each may contribute to changes in enzyme activity and binding behaviour under appropriate metabolic conditions.

REFERENCES

1. Belton, P. S. (1994) Prog. Biophys. Molec. Biol. **61,** 61-79.
2. Parsegian, V. A., Rand, R. P., Fuller, N. L. & Rau, D. C. (1986) Meth. Enzym. **127**, 400-416.
3. Rand, R. P. & Parsegian, V. A. (1989) Biochim. biophys. Acta **988,** 351-376.
4. Rand, R. P., Fuller, N., Butko, P., Francis, G. & Nicholls, P. (1993) Biochemistry **32,** 5925-5929.
5. Colombo, M. F., Rau, D. C., & Parsergian, V. A. (1992) Science **256**, 655-659.
6. Reid, C. & Rand, R. P. (1997) Biophys. J. **72,** 1022-1030.
7. Dzingeleski, G. D. & Wolfenden, R. (1993) Biochemistry **32,** 9143-9147.
8. Bergman, D. A. & Winzor, D. (1989) Eur. J. Biochem. **185,** 91-97.
9. Poon, J., Bailey, M., Winzor, D., Davidson, B.E., & Sawyer, W. H. (1997) Biophys. J. **73,** 3257-3264.

EFFECT OF PATHOLOGICAL LEVELS OF HYDROGEN PEROXIDE ON CONTROL OF KETOGENIC FLUX IN HEPATOCYTES ISOLATED FROM NEONATAL RATS

Patil, K. K., Eaton, S. & Quant, P. A.

Department of Paediatric Surgery, Institute of Child Health & Great Ormond Street Hospital for Children NHS Trust, University College London Medical School, 30 Guilford Street, London WC1N 1EH, U.K., Telephone: +44 (0) 171 242 9789 ext. 2136, Fax: +44 (0) 171 404 6181, E-mail: P.Quant@ich.ucl.ac.uk

INTRODUCTION

In the period immediately following birth ketone bodies, produced in liver from endogenous fat stores or exogenous dietary lipid, become the main oxidative fuels for the brain, heart and peripheral tissues [1] and provide carbon for myelinogenesis to encase the brain and nervous system in a protective sheath [2,3]. Therefore, it is essential, if neural dysfunction and infant morbidity are to be avoided, that neonatal hepatocytes have the capacity to oxidize fatty acids, in addition to glucose, to generate and export ketone bodies. Despite the clear importance of neonatal ketogenesis to metabolic adaptation to extrauterine life, the mechanisms regulating and controlling this pathway in both physiological and pathological conditions are poorly understood[4,5] However, we do know that control over this pathway is finely tuned and regulated and does not lie in a single enzyme or a rate-limiting step, but lies in multiple control sites both extra and intrahepatic. Indeed, control over ketogenesis appears to alter markedly with development, nutrition and clinical status [6].

Surgical infants, especially those who are preterm and/or receiving long-term total parenteral nutrition, are at increased risk of developing sepsis. Repeated episodes of sepsis can result in sequential liver dysfunction/failure, multi-organ failure and, in extreme cases, even death. We hypothesize that pathological levels of reactive oxygen species, e.g. H_2O_2, observed in such clinical infants (as a result of hypermetabolic response to sepsis secondary to respiratory burst by phagocytes) [7] impair ketogenesis and, hence, initiate the biochemical pathogenesis of liver dysfunction/failure.

In this paper we present our preliminary *in vitro* metabolic control analyses and transmission electron microscopy studies which support our hypothesis.

METHODS

As the research requires invasive experiments, which cannot be performed in at-risk infants, we designed an experimental *in vitro* model system (Fig.1). We isolated viable (>88%) neonatal (11d-13d) rat hepatocytes by collagenase digestion of excised livers and incubated the cells (3×10^6 cells in a total volume of 3 ml) for 1h at 37^oC respiring on $[1\text{-}^{14}C]$palmitate (4μCi, 0.5mm in 2% BSA). Top-down control analysis was applied to the isolated neonatal rat hepatocytes to assess quantitatively the effect of a range (0.5mM; 1mM; 1.5mM; 2mM) of hydrogen peroxide concentrations on control over flux to ^{14}C-ketone bodies by the system blocks of reactions [8].

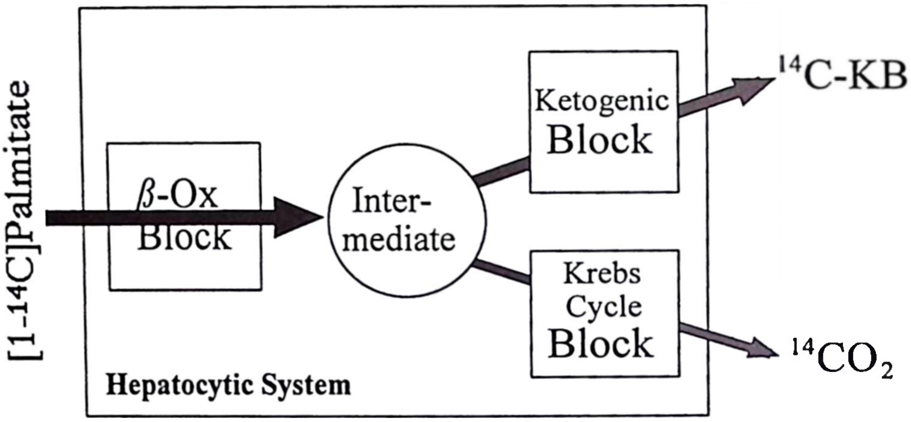

Figure 1. Experimental system

Abbreviations: KB, ketone bodies; CO_2, carbon dioxide; β-Ox, β-oxidation

We used transmission electron microscopy to assess gross changes in cellular morphology.

RESULTS AND DISCUSSION

Under our experimental conditions (in the absence or presence of 2mM (pathological levels) H_2O_2) the distribution of control, by the blocks of reactions over ketogenesis, is markedly altered (Fig. 2).

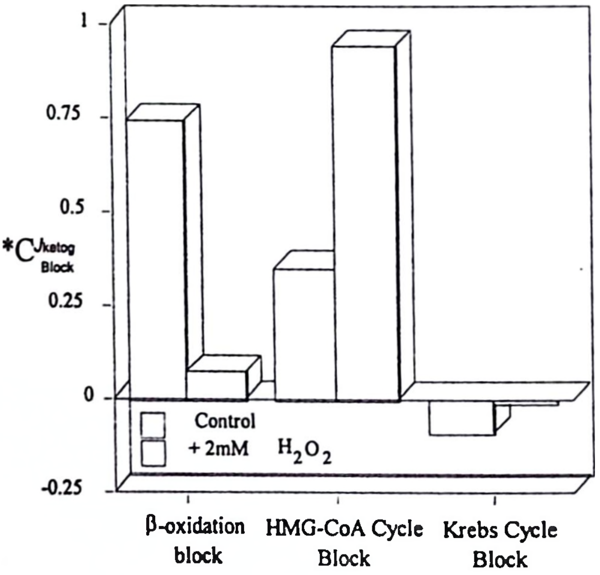

Figure 2. Group flux control coefficients for the three system blocks over flux through ketogenesis.

$^{*}C^{J_{ketog}}_{Block}$, group flux control coefficient for system blocks over ketogenesis

In the absence of hydrogen peroxide the control exerted by the β-oxidation block was greater than the HMG-CoA block, however, in the presence most of the control resided in the ketogenic block. The Krebs cycle block of reactions exerted negligible control over ketogenic flux under both sets of experimental conditions.

Electron micrographs of hepatocytes from control incubations in the absence of 2mM H_2O_2 demonstrated normal inner and outer mitochondrial membranes and cellular morphology (Fig.3). In hepatocytes which had been exposed to 2mM H_2O_2 the cellular architecture was disrupted with cell wall blebbing. Mitochondria from treated hepatocytes demonstrated structural heterogeneity and were significantly swollen with loss of cristae structure. Such severe changes in mitochondria would not be inconsistent with impaired ketogenesis. A population of damaged mitochondria was intermixed with intact ones. The presence of morphologically normal mitochondria in the treated cells may indicate that the hepatocyctes contain a mixed population of damaged and hyperfunctional mitochondria seen in *in vivo* models of sepsis [9]. These TEM data, therefore, suggest that our *in vitro* model of sepsis approximates *in vivo* conditions.

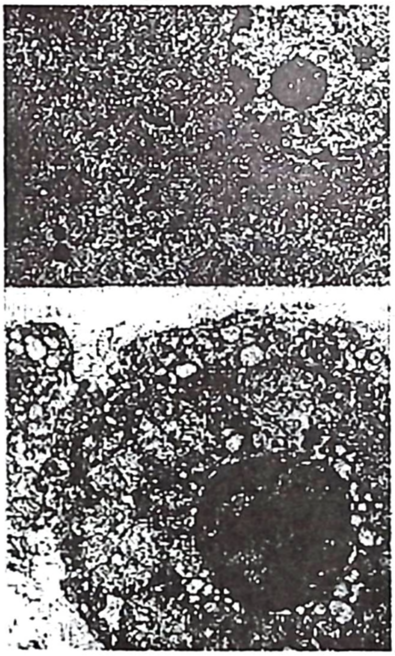

x 6000 to a scale 1µm - 5µm

Figure 3. Transmission electron micrograph of control or 2mM H_2O_2 treated hepatocytes isolated from neonatal rats

CONCLUSION

Our *in vitro* studies suggest that pathological levels of H_2O_2 have the potential to: (i) impair mitochondrial ketogenesis directly; (ii) disrupt metabolic control; (iii) damage cellular morphology and, therefore, (iv) initiate the biochemical pathogenesis of liver dysfunction associated with long-term total parenteral nutrition and/or sepsis in surgical neonates.

REFERENCES

[1] Girard, J. M., Ferré, P., Pégorier, J.-P. & Duée, P.-H. (1992) Adaptations of glucose and fatty acid metabolism during perinatal period and suckling-weaning transition Physiol. Rev. **72,** 507-562

[2] Hawkins, R. A., Williamson, D. H. & Krebs, H. A. (1971) Ketone- body utilization by adult and suckling rat brain in vivo Biochem. J. **122,** 13-18

[3] Nehling, A. & Pereira de Vasconcelos, A. (1992) Glucose and ketone body utilization by the brain of neonatal rats Prog. Neurobiol. **40,** 163-221

[4] Krauss, S., Lascelles, C.V., Zammit, V. A. & Quant, P. A. (1996) Flux exerted by overt carnitine palmitoyltransferase over palmitoyl-CoA oxidation and ketogenesis is lower in suckling than in adult rats Biochem. J. **319,** 427-433

[5] Krauss, S. & Quant, P. A. (1996) Regulation and control in complex, dynamicmetabolic systems: experimental application of top-down approaches of metabolic control analysis to fatty acid oxidation and ketogenesis J. theor. Biol. **182,** 381-388

[6] Quant, P. A., Lascelles, C. V., New, K. J., Patil, K. K., Azzouzi, N., Eaton, S. & Elliot, K. R. F. (1998) Impaired neonatal ketogenesis Biochem. Soc. Trans. (in press) **26,** 125-130.

[7] Vleissis, A. A., Goldman, R. K. & Trunkey, D. D. (1995) New concepts in the pathophysiology of oxygen metabolism during sepsis Brit. Jour. Surg. **82,** 870-876

[8] Quant, P. A. (1993) Experimental application of top-down control analysis to metabolic systems Trends in Biochemistry. **18,** 26-30.

[9] Kantrow, S. P., Taylor, D. E., Carraway, M. S, and Piantadosi, C. A. (1997) Oxidative metabolism in rat hepatocytes and mitochondria during sepsis archives of Biochemistry and Biophysics **345,** 278-288

EFFECTS OF MEMBRANE POTENTIAL ON THE SENSITIVITY OF MITOCHONDRIA FROM BROWN ADIPOSE TISSUE AND LIVER TO FATTY ACIDS

Anita Matthias, Barbara Cannon and Jan Nedergaard

The Wenner-Gren Institute, The Arrhenius Laboratories F3, Stockholm University,
S-106 91 Stockholm, Sweden, phone: +46 8 164122, Fax: +46 8 156756
E-mail: anita@zoofys.su.se

INTRODUCTION

Although fatty acids have been known for a long time to cause uncoupling in mitochondria [1], the mechanism through which this action occurs is still not fully understood. Several proteins have been suggested to be involved in this process including the uncoupling protein (UCP1), the adenine nucleotide translocator and two recently identified UCP1-related proteins: UCP2 and UCP3.

In order to investigate the effect of membrane potential ($\Delta\psi$) on the uncoupling action of fatty acids, two types of mitochondria - from BAT and liver - and two methods of uncoupling - GDP omission and FCCP addition - were selected. Due to the presence of UCP1 in BAT mitochondria, purine nucleotides are required for the formation of a high membrane potential. By decreasing the nucleotide concentration, $\Delta\psi$ can be lowered in these mitochondria in a pseudo-physiological manner and the effect of this on the fatty acid dose-response curve can be examined. By the use of an exogenous uncoupler (FCCP), $\Delta\psi$ can be altered in both types of mitochondria and in this way a distinction between UCP1-related and $\Delta\psi$-related effects can be made.

MATERIALS AND METHODS

Mitochondria were prepared from BAT and liver principally as described by Cannon and Lindberg [2] from adult female Sprague-Dawley rats which had been acclimated (one rat per cage) to 4°C (6 h light, 18 h dark) for 3 weeks. The rats had free access to food and water. Briefly, liver and BAT (pooled from the interscapular, periaortic, axillary and cervical deposits) was dissected out and homogenised in 40 ml of a 250 mM sucrose solution, filtered through gauze and centrifuged at 8500 × g for 10 mins. The pellet was resuspended in sucrose and centrifuged at 800 × g for 10 mins. The resulting supernatant was then centrifuged at 8500 × g for 10 mins and the resulting pellet was resuspended in 100 mM KCl + 20 mM Tris (pH 7.2) + 0.2% fatty-acid-free bovine serum albumin. After recentrifugation at 8500 × g for 10 min, the mitochondria were further washed and resuspended in KCl/Tris (without albumin). The mitochondrial protein concentration was measured with the fluorescamine method (Fluram from Fluka) and the suspension diluted to a stock concentration of 20 mg.ml^{-1}.

Membrane potential was monitored with the cationic, fluorescent dye Rhodamine 123, using the dual-wavelength mode (516 - 495 nm) on an Aminco DW-2 spectrophotometer. Membrane potential was calculated using the Nernst equation. $[K^+]_{IN}$ was calculated from calibration curves using a method similar to that used by Nedergaard [3].

All assays were conducted at 37°C in a medium consisting of 125 mM sucrose, 20 mM Tris (pH 7.2), 2 mM $MgCl_2$, 1 mM EDTA, 0.1% fatty-acid-free bovine serum albumin, 4 mM KPi, 5 μM rotenone, 0.6 μM Rhodamine 123 and 5 mM succinate (liver) or α-glycerophosphate (BAT).

The free concentration of oleate was calculated using the equation from Richieri et al. [4] for the binding of oleate to bovine serum albumin:

$[FFA] = 6.5\,\upsilon - 0.19 + 0.13\,e^{1.54\,\upsilon}$ where υ is the ratio of oleate to albumin. The molecular weight of albumin was taken as 60,000.

All data is expressed as means of 3 experiments.

RESULTS AND DISCUSSION

In liver mitochondria, alterations in the concentration of GDP had only a minor effect on $\Delta\psi$ (Table 1). The change in $\Delta\psi$ induced by a given concentration of oleate was also similar despite changes in the GDP concentration (Fig. 1). In BAT mitochondria, as expected, $\Delta\psi$ decreased as the GDP concentration was lowered (Table 1). In these mitochondria (Fig. 2), the change in $\Delta\psi$ due to the addition of each concentration of oleate was nucleotide concentration dependent. Some of the decreased response to a given concentration of oleate could be due to interaction of the fatty acid with the oxidative system.

Concentration	$\Delta\psi$ (mV) Liver	$\Delta\psi$ (mV) BAT
GDP (mM)		
1.000	-220	-212
0.500	-217	-204
0.150	-228	-180
0.050	-231	-150
FCCP (μM)		
0.00	-227	-216
0.11	-217	-207
0.25	-205	-203
0.41	-194	-188
0.50	-189	-157

Table 1: Basal $\Delta\psi$ of BAT and liver mitochondria in the presence of varying concentrations of GDP and FCCP.

Liver mitochondria were partially uncoupled by the addition of FCCP, as they were not when GDP concentrations were altered (Table 1). At higher concentrations of FCCP, the change in $\Delta\psi$ due to a given concentration of oleate was greater, indicating that the uncoupling ability of oleate had also increased (Fig. 3). In BAT mitochondria however, as $\Delta\psi$ was decreased by the addition of FCCP (Table 1), the effect of oleate appeared to be unchanged (Fig. 4). Thus, in both types of mitochondria, the results were the opposite to those seen when $\Delta\psi$ was altered by changing the GDP concentration.

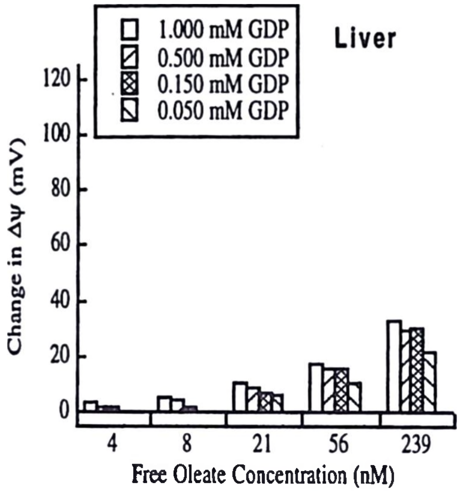

Figure 1: Effect on the oleate-induced uncoupling of liver mitochondria of different concentrations of GDP.

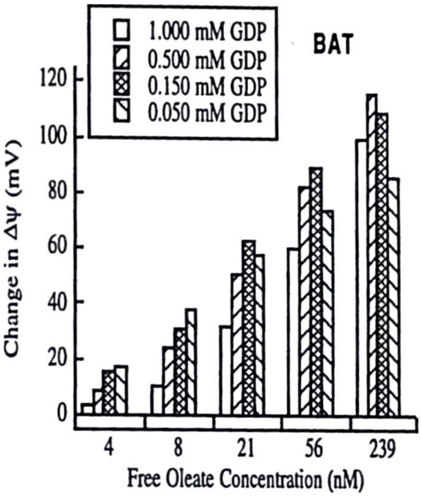

Figure 2: Effect on the oleate-induced uncoupling of BAT mitochondria by decrease of Δψ via removal of GDP.

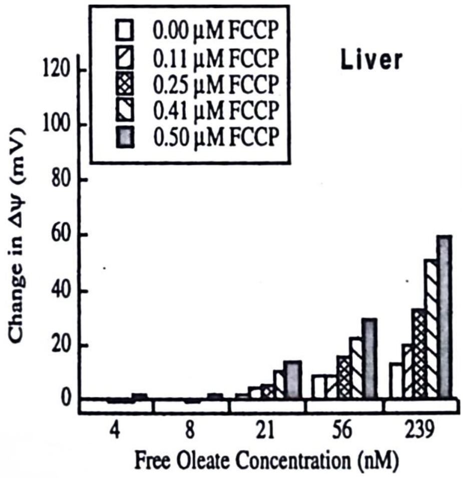

Figure 3: Effect on the oleate-induced uncoupling of liver mitochondria of lowering ψ by addition of an exogenous uncoupler FCCP. GDP = 1 mM.

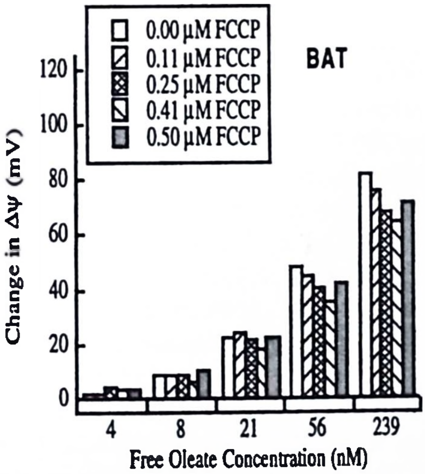

Figure 4: Effect on the oleate-induced uncoupling of BAT mitochondria of lowering Δψ by addition of an exogenous uncoupler FCCP. GDP = 1 mM.

In the present investigation, we have examined whether the uncoupling effect of fatty acids was dependent on the $\Delta\psi$. We found that the sensitivity of BAT and liver mitochondria to fatty acids was different and that in BAT mitochondria this sensitivity also depended on the method used to alter $\Delta\psi$. Thus, it is likely that different mechanisms are involved in the uncoupling effect of fatty acids under the different conditions.

REFERENCES

[1] B.C. Pressman, H.A. Lardy, Effect of surface active agents on the latent ATPase of mitochondria, Biochim. Biophys. Acta 21 (1956) 458-466.

[2] B. Cannon, O. Lindberg, Mitochondria from brown adipose tissue: Isolation and properties, Methods Enzymol. 55 (1979) 65-78.

[3] J. Nedergaard, The relationship between extramitochondrial Ca^{2+} concentration, respiratory rate, and the membrane potential in mitochondria from brown adipose tissue of the rat, Eur. J. Biochem. 133 (1983) 185-91.

[4] G.V. Richieri, A. Anel, A.M. Kleinfeld, Interactions of long-chain fatty acids and albumin: Determination of free fatty acid levels using the fluorescent probe ADIFAB, Biochemistry 32 (1993) 7574-7580.

62

A KINETIC MODEL OF MITOCHONDRIAL CA^{2+} EXCITABILITY

Vitalii A. Selivanov[*†], *François Ichas*[*‡] *and Jean-Pierre Mazat*[*¶]

[*]Université Bordeaux 2 and CJF-INSERM 97-05, F-33076 Bordeaux cedex, France.
[†] Belozersky Institute, Moscow State University, Moscow, 119899, Russia.
[‡] Present address : CNR Center for the Study of Biomembranes, Department of Biomedical Sciences, Laboratory of Biophysics and Membrane Biology, University of Padova, Viale G. Colombo 3, I-35121 Padova, Italy
[¶] corresponding author

Keywords : mitochondria, Cell calcium signalling, Model of calcium oscillations and spikes,
mitochondrial calcium-induced-calcium-release, Permeability Transition Pore

Abbreviations: $\Delta\Psi$, mitochondrial membrane potential; mCICR, mitochondrial Ca^{2+}-induced Ca^{2+} release; pH$_i$, mitochondrial matrix pH; PTP, permeability transition pore.

INTRODUCTION

In many cells, the information provided by external stimuli, either electrical, hormonal, photochemical, or mechanical, is conveyed within the cytoplasm by Ca^{2+} signals that take the form of Ca^{2+} oscillations and waves [1]. The information is encoded by the spatiotemporal organization of these signals (frequency, amplitude, etc...) and determines the subsequent cellular responses (AM or/and FM calcium signalling) [2, 3]. The main mechanism underlying the organization of the cytosolic Ca^{2+} signals is autocatalytic and termed "Ca^{2+}-induced Ca^{2+} release" (CICR) [1,4,5]. The CICR machinery is usually identified with the sole endoplasmic reticulum (ER), and thought to rely principally on Ca^{2+}-activable Ca^{2+} channels of the ER membrane, i.e., the inositol 1,4,5-trisphosphate (IP$_3$) and ryanodine receptors (repectively IP$_3$R and RyR) [1,4,5]. However, when Ca^{2+} is released from the ER at locally high concentration, the neighbouring mitochondria take up some of it [6]. This results in a modification of the spatiotemporal organization of the Ca^{2+} signals [7, 8, 9]. We have shown that a Ca^{2+}-induced calcium release can also be evidenced in mitochondria (mCICR) and that it contributes to the cytosolic Ca^{2+} raise [10,11]. This mechansimdepends on the transient opening of the PTP by mitochondrial Ca^{2+} uptake which and results in Ca^{2+} spikes (10) and oscillations [13, 14] *in vitro*..

We have already presented a theoretical analysis of mCICR providing direct information on the mitochondrial determinants of mCICR [15, 16]. We based our mathematical model on the following observations: (i) extra-mitochondrial Ca^{2+} is taken-up electrophoretically by mitochondria through the ruthenium red-sensitive Ca^{2+} uniporter [17], (ii) mitochondrial Ca^{2+} uptake causes a transitory drop in $\Delta\Psi$ that results in respiration activation [17], (iii) activation of respiration, which corresponds to an increased H$^+$ extrusion, results in the akalinization of the mitochondrial matrix [17], (iv) matrix alcalinization activates the PTP [18], and thus triggers various ion fluxes - among those, Ca^{2+} efflux - according to their electrochemical potential, (v) PTP activation also causes a relative respiration inhibition [13] that contributes to matrix acidification, (vi) matrix acidification inactivates the PTP [18]. The sequence of these events is described in Fig. 1.

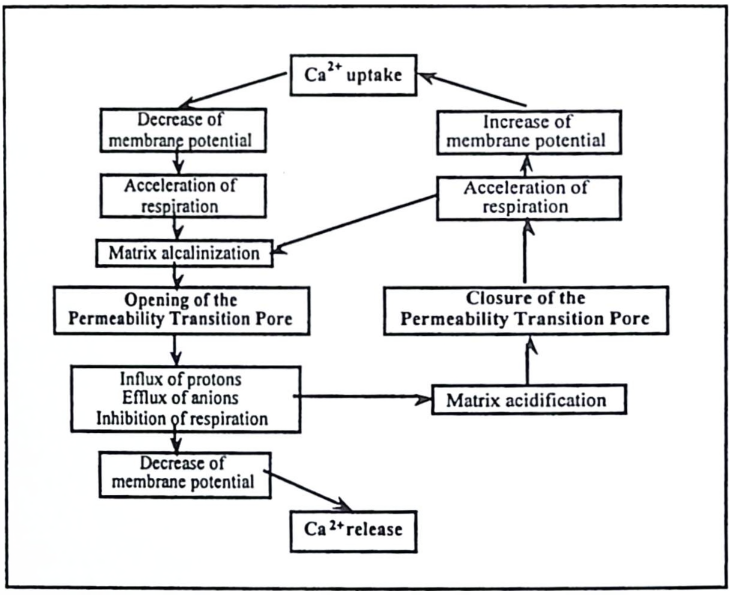
Ca^{2+} uptake
Decrease of membrane potential
Acceleration of respiration
Matrix alcalinization
Opening of the Permeability Transition Pore
Influx of protons
Efflux of anions
Inhibition of respiration
Decrease of membrane potential
Ca^{2+} release
Increase of membrane potential
Acceleration of respiration
Closure of the Permeability Transition Pore
Matrix acidification

Figure 1. Sequence of events leading to mCICR.

We showed that two factors are crucial to account for the various mCICR profiles that can be observed experimentally : (i) the dependence of PTP opening and closure on matrix pH (pHi), and (ii) the relative inhibition of the respiratory rate after PTP opening. These two factors are dependent upon three parameters in the model : k_{AH}, P_{An} and P_A. Fig. 2 gives a schematic description of the model components.

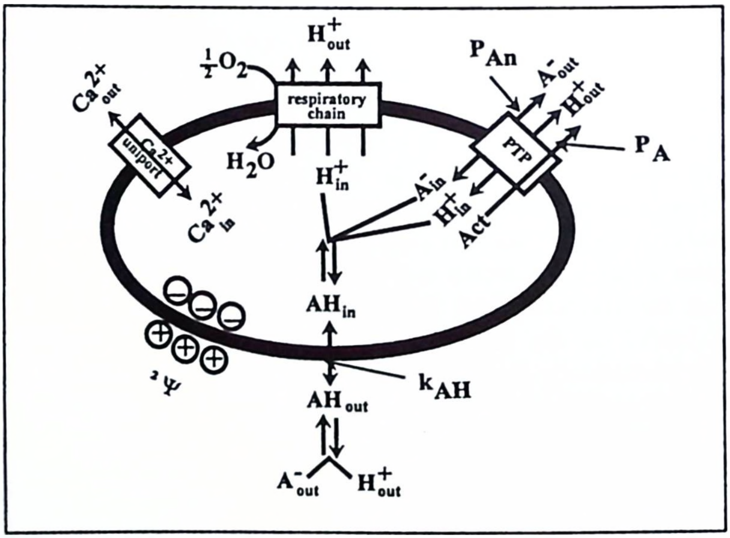

Figure 2. Schematic representation of the model components.

During mCICR, the electroneutral flux of weak organic acids, i.e., principally succinate under the reference *in vitro* conditions [10,13], allows the recovery of pH_i after H^+ respiratory efflux, due to the dissociation of the transported acids inside the matrix according to the equation : $J_{AH} = k_{AH} \times (H_{in} - H_{out})$ where we set H_{out} to 0.1µM (pH=7).

P_{An} is the permeability of anion through the opened PTP. It allows a rapid efflux of Ca^{2+} by charges compensation. We have considered anion concentration, inside as well as outside, as a constant An= 10 mM. In these conditions, the flux of anions through the PTP is described by the equation : $J_{An} = -P_{An}\, T^{op}\, \Delta\Psi\, An$ [16].

It was shown that the respiration rate undergoes a relative inhibition consecutive to PTP opening, while $\Delta\Psi$ is decreased [19]. The factor, which induces this inhibition is still unknown. We supposed in the model the existence of an activator of respiration, such that the respiration rate is proportional to its intra-mitochondrial concentration. We further assumed that the relative inhibition of respiration during PTP opening is due to the efflux of activator through the opened PTP. The efflux of activator (J_A) is proportional to its relative amount inside mitochondria, and to the PTP opening state:

$J_A = P_A \times [T^{op}] \times [A]$

In this study, the permeability coefficient P_A is set to $100 min^{-1}$.

The production of activator (V_A) is supposed to be dependent on the relative amount of activator inside mitochondria (between 0 and 1). The production is stopped when the activator concentration reaches the relative maximal level of 1 and it linearly increases when the concentration decreases:

$V_A = k_A \times (1 - A)$ where k_A is a constant set to $0.3 min^{-1}$.

In this short paper we have studied the different patterns of calcium movements when two of these three parameters are varied : k_{AH} and P_{An}. P_A is set to $100 min^{-1}$. The other equations of the model, particularly the differential equations are described in 16.

RESULTS AND DISCUSSION

Fig. 3 describes all the behaviours that are observed when k_{AH} and P_{An} are varied and Fig. 4 gives some examples of these behaviours after a 33 µM calcium pulse, following the path indicated in Fig. 3, with mainly a variation of P_{An}. In case (I), k_{AH} is great and changes in pH_i are rapidely compensated by the electroneutral flux of AH and thus PTP does not open. For PTP to open, k_{AH} has to be decreased (Fig. 4, (II)); in this case, Ca^{2+} efflux is rather low and all Ca^{2+} can be reaccumulated. When Ca^{2+} efflux is larger as a consequence of P_{An} increase, (Fig. 4 (III)), during the re-uptake phase, the pH_i threshold of PTP opening is reached once again, and a second smaller spike is observed with then, a complete re-uptake similar to the one of Fig. 4 (II). As P_{An} is further increased damped oscillations (Fig. 4 (IV)) and then sustained oscillations (Fig4. (V)) are observed.

Finally, a larger increase in P_{An} value lead to a very rapid Ca^{2+} efflux with a big change in pH_n which can no longer be compensated and the PTP remains open causing a complete and irreversible Ca^{2+} efflux (Fig4. (VI)).

Fig. 4 describes all the behaviours that can be observed in this system. This shows that our two hypotheses of (i) PTP opening in a low conductance mode [11], triggered by pH i and (ii) the inhibition of respiration when the PTP opens as experimentally observed are enough to account for all the behaviours experimentally observed.

A complete exploration according ro the variation of k_{AH} and P_{An} and P_A is under way in our laboratory.

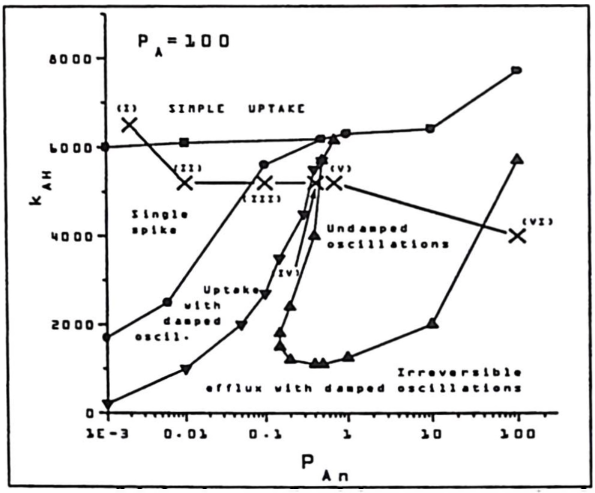

Figure 3. Different type of behaviours of calcium movements through mitochondrial membrane as a function of the parameters k_{AH} and P_{An}. P_A is set constant at 100min^{-1}.

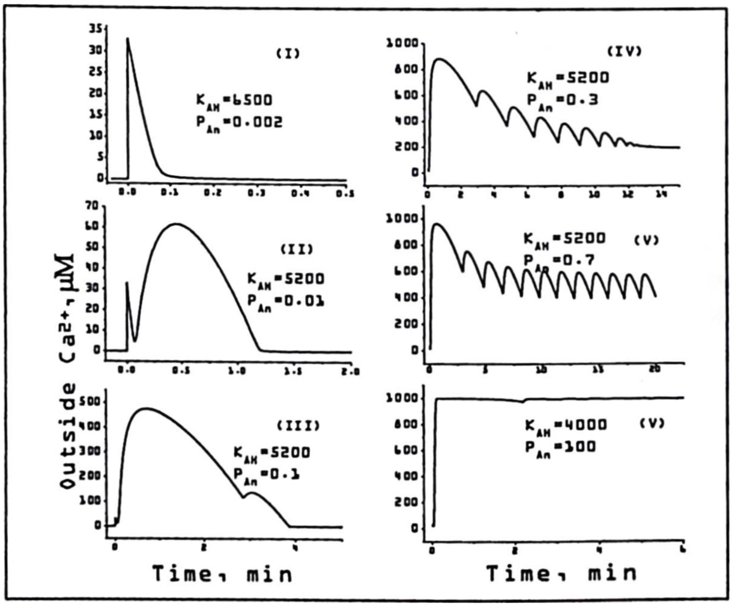

Figure 4. Some examples of the different type of behaviours of calcium movements through mitochondrial membrane after a 33 µM calcium pulse. The numbers of the different Fig. 4 correspond to the same numbers on the path of Fig. 3, with the corresponding values of the parameters.

ACKNOWLEDGEMENTS

This work was funded by la Ligue Contre le Cancer (L.C.C.), l'AFM, la Région Aquitaine, and la FRM. V. S. was supported by the Univsersity Bordeaux 2 and INSERM.

REFERENCES

1. S. Miyazaki, Curr. Opin. Cell Biol. 7 (1995) 190-196.
2. X. Gu and N.C. Spitzer Nature 375 (1995) 759-760.
3 . M.J. Berridge, Nature 386 (1997) 315
4. M.J. Berridge, Nature 361 (1993) 315.
5. J.D. Lechleiter and D.E. Clapham, Cell 69 (1992) 283.
6. R. Rizzuto, M. Brini, M.Murgia and T. Pozzan, Science 262, (1993) 744.
7. L.S. Jouaville, F. Ichas, E.L. Holmuhamedov, P. Camacho and J.D. Lechleiter, Nature 377 (1995) 438.
8. S.L. Budd and D.G. Nicholls, J. Neurochem. 66 (1996) 403.
9. P.B. Simpson and J.T. Russel, J. Biol. Chem., 271 (1996) 33493.
10. F. Ichas, L.S. Jouaville, S.S. Sidash, J.-P. Mazat and E.L. Holmuhamedov, FEBS Lett. 348 (1994) 211.
11. F. Ichas, L.S. Jouaville and J.-P. Mazat, Cell 89 (1997) 1145.
12. D.D. Friel and R.W. Tsien, (1994) J. Neurosci. 14 (1994) 4007.
13. Y.U. Evtodienko, V.V. Teplova, J.Khawaja and N.E.L Saris, Cell Calcium 15 (1994) 143.
14. Y.V. Kim, L.Y. Kudzina, V.P. Zinchenko and Y.V. Evtodienko, Eur. J. Biochem., 153 (1985) 503.
15. V. Selivanov, F. Ichas, E. L. Holmuhammedov, L. S. Jouaville, Y.V. Evtodienko and J.-P. Mazat in Biothermokinetics of living cell. Eds Westerhoff, H.V., Snoep, F.E., Sluse, F.E., Wijker, J.E., Kholodenko, B.N. Amsterdam, 1996 268-273.
16. V. Selivanov, F. Ichas, E. L. Holmuhammedov, L. S. Jouaville, Y.V. Evtodienko and J.-P. Mazat Biophys. Chem. 72 (1998), 111-121
17. T.E. Gunter, K.K. Gunter, S.S. Sheu, and C.E. Gavin, Am. J. Physiol. 267 (1994) C313.
18. M. Zoratti and I. Szabò, Biochim. Biophys. Acta, 1241 (1995) 139.
19. F. Ichas (1997) PhD Thesis

CHLORIDE IN SKELETAL MUSCLE FIBRES: VOLUME CONTROL OR REGULATION?

Jan Siegenbeek van Heukelom, Harald G.J. van Mil and Remco J. Geukes Foppen.

Institute of Neurosciences, Cell Biophysics, Faculty of Biology, University of Amsterdam, Amsterdam, The Netherlands, Tel.: +31(0)20 5257642; Fax.: 31(0)20 6659125; e-mail: siegenbeek@bio.uva.nl

INTRODUCTION

Because skeletal muscle's primary function is contraction, it is most likely that this does not occur at constant volume. Additionally, the energy for contraction is provided directly by ATP-hydrolysis and indirectly by oxidative phosphorylation: therefore it is most likely that osmolality in the muscle fibre does not remain constant. Taking both arguments together one has good reasons to suppose that skeletal muscle fibres possess means to cope with volume and osmolality variations. It is now sufficiently clear that mammalian skeletal muscle fibres possess an electroneutral Na/K/2Cl cotransport system in the membrane importing Cl^- energised by the Na^+-gradient[1]. In other cellular systems this import-mechanism is directly related with the volume regulatory increase, occurring after cell shrinkage in reaction to hypertonic media.

A peculiarity of skeletal muscle fibres is that the chloride permeability (P_{Cl}) is extremely high, promoting equilibration of Cl^- across the cell membrane. This couple, electroneutral Cl^- import and electrogenic Cl^- efflux, makes that in the cell Cl^- is slightly out of equilibrium: $E_{Cl} = (RT/F)\ln(Cl_i/Cl_o) = -70.5$ mV and $V_m = -74$ mV.

Being the only major permeable anion, chloride can provide osmotic strength additional to the impermeable anions in the cell. For each excess chloride ion electroneutrality condition will always provide an additional cation. So, whereas under isotonic conditions Cl_i is low (about 9-10 mM), in hypertonic situations additional osmotic strength will be provided by increase in Cl_i. If the import through the cotransporter is the only way of "up-hill" transport one can study the control of this mechanism by blocking the cotransporter by using the specific blocker bumetanide.

Blocking the import will unveil the influence of chloride-handling by these two transport systems: import by the Na/K/2Cl cotransporter and electrogenic efflux through chloride channels. We measured the influence of bumetanide electrophysiologically in mouse skeletal muscle between 270 and 344 mOsm, the (patho)physiologically range found in mammals. From this response one can deduce the change in intracellular chloride concentration and consequently the osmolality.

These data and information published earlier we shall use to estimate how chloride controls or regulates intracellular osmolality.

MATERIALS AND METHODS

Measurements were made in Krebs-Henseleit solutions, with intracellular microelectrodes. For a more detailed description of materials and methods one is referred to the contribution of Geukes Foppen et al. in this volume.

Hypotonicity was obtained by leaving out small amounts of NaCl (total 12.5 mM), thus reducing the activities of Na and Cl to values still much higher than the half-maximal values of the cotransporter. Hypertonicity was obtained by adding the impermeable and uncharged PolyEthyleneGlycol (MW 400): PEG 400. Bumetanide was used in the concentration of 75 μM.

RESULTS

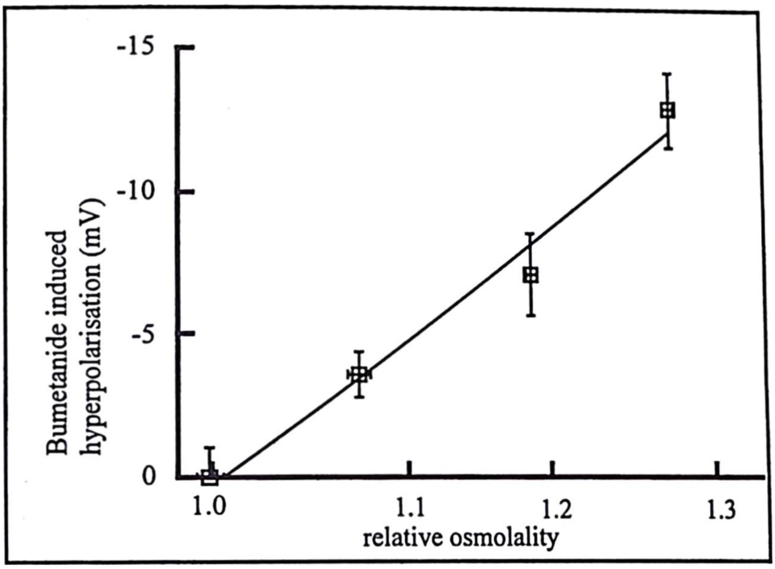

In the Figure the hyperpolarizations induced by bumetanide are presented as a function of the relative osmolality. Apparently at 270 mOsm the induced hyperpolarization is vanishing and we took this value as 1.0. To ascertain that this is not due the reduction of NaCl in the medium, we added to this hypotonic solution 20 mOsm PEG 400 and obtained in this special 290 mOsm-solution the same bumetanide induced hyperpolarization as in the normal control medium.

A problem arising at osmolalities higher than 360 mOsm, was that the cell did not survive such high osmolalities ànd bumetanide. The membrane potential decreased to about - 45 mV, responses disappeared and, on microscopical examination, the cell appeared to die.

DISCUSSION

From the graph one can calculate the control of the cotransporter on the membrane potential, the intracellular chloride concentration and the power of the cell to cope with osmotic and/or volume changes.

Evaluating from the slope of the membrane potential as function of the osmolality the control value gives:

$(\Delta V_m/\Delta \mathrm{Osm})(\mathrm{Osm}/V_m) = -0.61$

V_m can be written[1,2] expressed as a sum of the contribution of the three major ions each weighted with their own weight:

$V_m = t_K E_K + t_{Cl} E_{Cl} + t_{Na} E_{Na} = 0.368 E_K + 0.611 E_{Cl} + 0.021 E_{Na}$

As accumulation of cations leads to more negative values of their equilibrium potentials, the minimal change in E_{Cl} one obtains on taking the relative contribution of chloride as the transport number t_{Cl} (= 61 %) time V_m:

$(\Delta E_{Cl}/\Delta Osm)(Osm/E_{Cl}) = - 1.00$

Because E_{Cl} is a logarithmic transform of Cl_i, linearity is not preserved over the total range and the change in Cl_i is solved by adjusting $Cl_i = Cl_o \exp\{E_{Cl}F/0.611RT)$ to make V_m fit the experimentally found value: -61.7 mV for 344 mOsm. This gives an increase in Cl_i of approximately 10 mM (i.e. doubling of the concentration). To compensate charge the cation concentration should increase equally. Close scrutiny of the dependence of V_m on the two other terms, learn that their influences are small. If all cations would be K+ the value Ki would increase from 150 mM to 160 mM and E_K would increase - 1.7 mV of which would be observed 1 mV in V_m. If all cations would be Na+ then Nai rises from 14 to 24 mM and E_{Na} would become 14.2 mV more negative, but due to the small transport number (t_{Na}) V_m would hyperpolarize only 0.3 mV.

This rough calculation shows that only 20 mOsm can be explained by this analysis starting with the change in V_m from - 74 mV to - 61 mV. One can also invert the analysis: to cope with the increase in medium osmolality, from 290 to 344 mOsm, Cl_i must increase 27 mM, leading to a depolarisation of E_{Cl} to - 28 mV and of V_m to - 51 mV. This last value is much lower than what was found experimentally. So, we conclude that this mechanism can not explain straightforward the response of V_m to hypertonic solutions. The differences are too large to be bridged by introducing correction terms such as activity coefficients. The transport number t_{Cl} used here is low compared with values, as is suggested by others. Introducing such values would have reduced the amount of intracellular osmolality compensation that can be explained.

Now we can return to the original question: "Is the cotransporter designed for osmoregulation in this tissue?" To be safe one can answer: "If it should be answered "yes", it functions poorly, because it can explain only 50 % or less." One should keep in mind that membrane potentials are related to concentration gradients and not to amounts of ions in the cell; so a concomitant cell shrinkage does not change the analysis presented here.

However, the observation, that beyond 360 mOsm hypertonicity and bumetanide killed the cell, demonstrates that the cotransporter serves a vital role, at least in hypertonic media. In the presentation by Geukes Foppen et al. we suggest that the high value op P_{Cl} is necessary for conservation of the t-tubules in the fibres. Such explanation and this analysis would put in perspective experiments with shocks of high osmotic strength[3], that lead to rupture of the t-tubules. So, the proper function of the t-tubule might be the regulated entity instead of the volume or osmolality of the muscle fibre itself.

REFERENCES

1. Siegenbeek van Heukelom, J., Van Mil, H.G.J., Geukes Foppen, R.J., in "Biothermokinetics of the living cell", 1996, 112-118.
2. Siegenbeek van Heukelom, J., 1991, J. Physiol. 434, 549-560.
3. Krolenko, S.A., Amos, W.B., Lucy, J.A., 1995, J. Muscle Res. Cell. Motil. 16, 401-411

MODELLING AND QUANTIFICATION OF CARBON FLUXES IN PHOTOSYNTHESIZING CELLS OF INTACT PLANT LEAVES *IN VIVO*

Olav Keerberg and Tiit Pärnik

Institute of Experimental Biology at the Estonian Agricultural University, EE3051 Harku, Estonia, Phone +372 2 512 489, Fax +372 2 512 489
E-mail olav@ebi.ee (O.K), tiit@ebi.ee (T.P.)

INTRODUCTION

Investigations during last decades have elucidated the chemistry and the basic control mechanisms of the photosynthetic carbon metabolism. The sequence and compartmentalization of partial reactions as well as mechanisms of the intracellular transport of metabolites have become clear. The main subsystems involved in photosynthetic carbon metabolism are the reductive pentose phosphate cycle (Calvin cycle), the glycolate cycle and pathways of end product synthesis including reactions of respiration (glycolysis and the tricarboxylic acid cycle).

Biochemical knowledge in this field has been obtained, in its major part on the subcellular level and by means of model systems, i.e. *in vitro*. As to quantitative biochemical studies on the level of the integrated photosynthetic apparatus, intact leaf *in vivo*, these are less advanced. In this report we present a method for the determination of carbon fluxes and pool sizes of metabolites involved in photosynthetic carbon metabolism on the level of intact plant leaf. The method is based on the interpretation analysis of the kinetics of ^{14}C incorporation into the products of steady-state photosynthesis of leaves in the medium of $^{14}CO_2$. The application of the method is illustrated by the results of an experiment with leaves of barley.

METHODS

Young leaves of barley were placed into leaf chamber [1] and illuminated until the steady rate of CO_2 fixation was achieved. After that the leaves were exposed to $^{14}CO_2$ (300 µL/L) for different time intervals ranging from 5 s to 10 min. Exposures were performed under saturating light at 25°C. After the exposure leaves were killed in liquid nitrogen. Labeled photosynthates were extracted with perchloric acid and separated by paper chromatography combined with additional separation of phosphorylated compounds in Partisil columns and amino acids with automatic analyzer AAA 339 (Mikrotechna, Czech Republic). Radioactivity of individual compounds was determined and plotted against the duration of exposure to $^{14}CO_2$. The radioactivity of compounds was expressed in absolute (µg-atom C.m^{-2}) and in relative (per cent total radioactivity fixed by leaves) units.

Principally the experimental kinetic curves contain the information about rates of carbon fluxes and pool sizes of metabolites studied. To extract this information the following three-step procedure was used.

1. Choice of the model of subsystem under investigation. The model must embrace, in a generalized form, all the information available concerning the structure of the

system, pathways of synthesis and conversion of metabolites involved. The qualitative knowledge is an inevitable prerequisite for quantification.

2. Derivation of analytical functions $P(t) = f(t, c_i, R_i)$, which theoretically describe the dependence of radioactivity $P(t)$ of the model components upon the duration of tracer feeding t. Parameters of the functions must represent pool sizes c_i and carbon fluxes R_i, i.e. the values to be determined.
3. Determination of the values of parameters c_i and R_i by fitting functions $P(t)$ to experimental kinetic curves by means of nonlinear regression procedure. Degree of coincidence of theoretical and experimental data shows the adequacy of the model adopted.

RESULTS AND DISCUSSION

The procedure above was applied at quantitative description of different subsystems of the photosynthetic metabolism. Results of the analysis of kinetic data in an experiment with barley leaves are shown in Table 1 and Fig. 1.

Table 1. THE RATES OF CARBON FLUXES IN THE REACTION SYSTEM OF PHOTOSYNTHETIC CARBON METABOLISM IN LEAVES OF BARLEY
The data represent mean values of the rates derived from analysis of the curves of absolute and relative radioactivity.

Carbon fluxes	µg-atom C.m^{-2}.s^{-1}	Per cent true photosynthesis
True photosynthesis	14.76 ±0,74	
Carbon flux through the glycolate cycle	7,38 ±2,07	50,0
Decarboxylation of glycine		
calculated	1,85 ±0,52	12,5
measured	2,27 ±0,09	16,2
Synthesis of		
malate	0,33 ±0,02	2,2
aspartate	0,04 ±0,01	0,3
alanine	0,12 ±0,01	0,8
Accumulation of		
sucrose	10,67 ±0,22	72,3
starch	1,04 ±0,03	7,0
glucose and fructose	0,23 ±0,01	1,5
malate	0,10 ±0,01	0,7
CO_2 of photorespiration	1,89 ±0,05	12,8
other compounds	0,49 ±0,04	3,4
End products of photosynthesis – total	14,42 ±0,23	97,6
Decarboxylation of malate		
calculated	0,23 ±0,03	1,5
measured	0,21 ±0,06	1,4

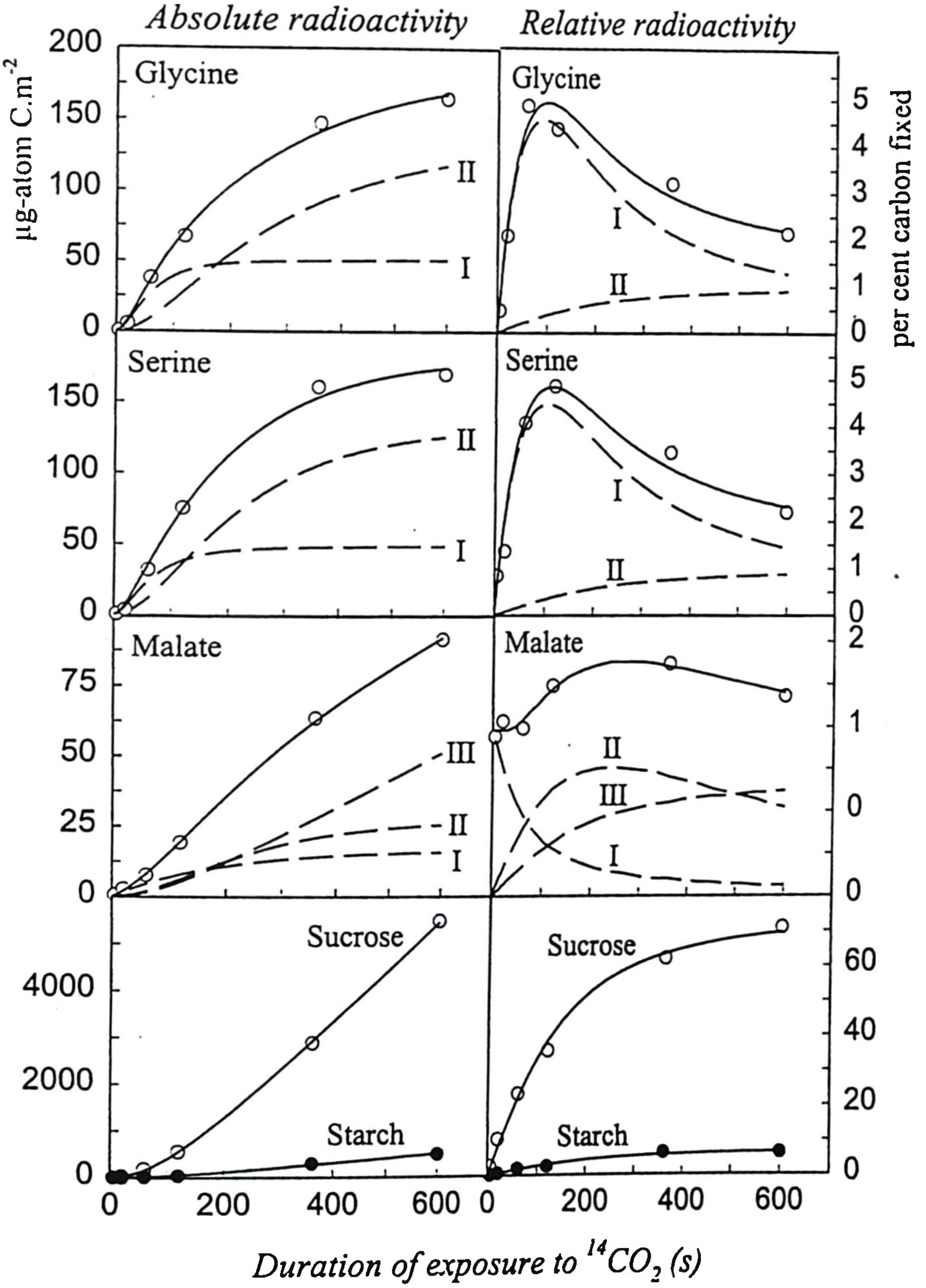

Fig.1. Kinetics of ^{14}C incorporation into the metabolites of photosynthetic $^{14}CO_2$ assimilation in barley leaves.Circles represent the experimental values. Solid lines are theoretical functions derived from models and fitted to experimental data.

Dashed lines show the calculated kinetics of ^{14}C incorporation into different pools of respective metabolites.

The model used in the calculations of the glycolate cycle [2] presumes that intermediates of the cycle (glycolate, glycine, serine) have two metabolic pools with different labeling kinetics: active pools with rapid turnover in organellae (peroxisomes and mitochondria) and less mobile pools in the cytosol (Fig. 1). At steady state photosynthesis these pools are in diffusional equilibrium. Using this model the rate of carbon flux through the glycolate cycle and the rate of glycine decarboxylation in this cycle were calculated. The results were compared with direct measurements of photorespiratory decarboxylation of primary photosynthates by means of a radiogasometric method [3]. Calculated and measured rates of glycine decarboxylation coincide in the limits of experimental deviations (Table 1).

Two-pool model was used also in the analysis of the labeling kinetics of C_3- and C_4-acids (malate, aspartate, and alanine) [4]. The model presumes the existence of active pools of these compounds localized in cytosol and organellae, and vacuolar pools with the kinetics of end product labeling. According to the two-pool model of malate turnover the kinetics of its labeling was divided into three components describing (I) the incorporation of ^{14}C into C-4 atom of malate molecule, (II) incorporation of ^{14}C from triose phosphates into C-1, C-2 and C-3 atoms of malate and (III) accumulation of malate as an end product of photosynthesis (dashed lines in Fig. 1). Using the non-linear regression procedure the model was fitted to the experimental data and the components of malate turnover were calculated. The results in Table 1 demonstrate that rate of synthesis of malate exceeds that of its accumulation. The difference of these rates may be regarded as the rate of decarboxylation malate in the reactions of glycolysis and Krebs cycle. The calculated value of decarboxylation is in good agreement with the result of direct measurement of respiratory decarboxylation (Table 1).

Table 1 shows the rates of accumulation also for other products of photosynthesis. The labeling kinetics of sucrose and starch is plotted in Fig. 1. The total rate of carbon accumulation in the end products of photosynthesis is approximately equal to the rate of true photosynthesis, the fact confirming the validity of kinetic calculations.

REFERENCES

1. Pärnik, T.R., Keerberg, O.F. and Jürisma, E.J. (1987) Plant Physiol. (Moscow) **34**, 837-845.
2. Keerberg, O.F. and Viil, J.A. (1988) in Photosynthesis and Production Process, (Nichiporovich, A.A., ed.), pp. 40-53. Nauka, Moscow.
3. Pärnik, T. and Keerberg, O. (1995) J. Exptl Bot. **46**, 1439-1447.
4. Ivanova, H., Keerberg, O. and Pärnik, T. (1993) Proc. Estonian Acad. Sci. Chem. **42**, 185-197.

AN INCREASE IN NAD$^+$ CONCENTRATION AFFECTS FLUXES THROUGH GLYCOLYSIS AND NEOGLUCOGENESIS IN ISOLATED RAT LIVER CELLS

*Anne Devin, Bernard Guérin and Michel Rigoulet**

Institut de Biochimie et Génétique Cellulaires du CNRS, Université de Bordeaux 2, 1 rue Camille Saint Saëns, 33 077 Bordeaux cedex. FRANCE
*To whom correspondence should be addressed. Tel : 33 5 56 99 90 40: Fax : 33 5 56 99 90 59. E-mail : Michel.Rigoulet@ibgc.u-bordeaux2.fr

INTRODUCTION

By focusing on the thermodynamic relationships between adenine and pyridine nucleotides, two of the most important components of the energy transforming mechanisms in the cell, the issue of free pools may be considered [1-3]. Indeed, free pyridine nucleotide ratio are widely accepted to be a marker of the reducing or oxidising power of these nucleotides and ATP/ADP ratio *via* phosphate potential is a marker of the energy status of the cell. However, both free and bound forms of the pyridine nucleotides are essential reagents in dehydrogenase reactions. The thermodynamics is determined by free nucleotides while the velocity is determined by bound forms [4]. Moreover, for a given amount of nucleotides, bound and free pools are interconnected.

We have previously reported that at steady state and in isolated hepatocytes, nicotinamide nucleotide content is increased by a rise in the ATP content of the whole cell under physiological conditions [5]. It is a straight line relationship when only ATP and NAD$^+$ are considered. Moreover, when regarding the compartmentation of this phenomenon, it appears that the linear relationship between ATP and NAD$^+$ occurs only in the cytosol.

The purpose of the present work was to investigate whether such a dependence could be a supplementary mechanism of regulation between various metabolic pathways in the liver cell. Thus, we increased the NAD$^+$ content of isolated hepatocytes by the use of nicotinamide, one of NAD+ precursors and investigated the influence of this increase on both glycolysis and neoglucogenesis. For this study, we used either dihydroxyacetone whose metabolism is mainly controlled by ATP/ADP ratio or glycerol whose metabolism is mainly controlled by cytosolic redox state [6]. We show that with glycerol as substrate, when considering substrate consumption flux, the rate of glycolysis and neoglucogenesis, it appears that the main influence of an increase in the NAD$^+$ content of the liver cell lies at the level of cytosolic glycerol-3-phosphate dehydrogenase.

MATERIAL AND METHODS

Preparation and perifusion of hepatocytes

Hepatocytes from male Wistar rats starved overnight were isolated by the collagenase method of Berry and Friend [7] as modified by Groen et al. [8].
Liver cells (20-30mg/ml) were perifused by the method of van der Meer and Tager [9] as modified by Groen et al.[10]. Hepatocytes were perifused at 37°C at a flow rate of

5ml/min with continuously gassed Krebs-bicarbonate buffer pH 7.4, saturated with O2/CO2 (19:1) and containing 1.3mM calcium. Cells were continuously perifused with either 10mM dihydroxyacetone or 5mM glycerol and nicotinamide 5mM was perifused as indicated in the figures. Samples of perifusate were taken at the time indicated on the figures for subsequent determination of glucose, lactate and pyruvate. Proteins in the perifusate were denatured by heating the samples at 80°C for 10 min before centrifugation [11]. Cellular content was separated from the extra cellular medium by centrifugation of the cell suspension through a layer of silicone oil as described previously[10].

Measurements of adenine nucleotides and NAD^+

Adenine nucleotides and NAD^+ were measured in neutralised HClO4 extracts [12]. ATP, ADP and AMP were measured by HPLC using a reverse phase (Spherisorb, ODS II, 5µM) column (0.46x25 cm) at 30°C. Elution was performed with a 25mM sodium pyrophosphate/ pyrophosphoric acid buffer (pH 5.75) at a flow rate of 1.2 ml/min. Adenine nucleotide detection was performed at 254 nm. NAD^+ determination was performed fluorimetrically with alcohol dehydrogenase as described in [13].

Metabolite determination

Glucose, lactate and pyruvate were measured spectrophotometrically as described in Bergmeyer [14]. Dihydroxyacetone phosphate and glycerol-3-phosphate were measured fluorimetrically as described in Bergmeyer [14].

RESULTS AND DISCUSSION

We have previously shown that in addition to their relationships in terms of potential (i.e. thermodynamic relationships), nicotinamide and adenine nucleotides can be linked in terms of concentration [5]. There is a linear relationship in isolated hepatocytes between [ATP] and [NAD^+], however the ATP content of the cell is manipulated (i.e. various cellular substrates, respiratory chain uncoupling or inhibition). Moreover, we have shown that this relation between ATP and NAD^+ is cytosolic. Here, we investigate whether this could be a new way to regulate the metabolism. To answer this question, we have increased the NAD^+ content of isolated hepatocytes by way of one of its precursors and measured its metabolic consequences on the fluxes through glycolysis and neoglucogenesis.

When Glycerol (5mM) is used as substrate, the perifusion of 5mM nicotinamide inducing an increase in the total NAD^+ content of the cell (Fig. 1a) slightly stimulates glycolysis and inhibits neoglucogenesis (Fig. 1b). This occurs in such a way that the glycerol consumption flux is drastically inhibited by an increase in the NAD^+ content of the cell (Fig. 1b). Moreover, when DHA (10mM) is used as substrate, the perifusion of 5mM nicotinamide inducing an increase in the NAD^+ content of the cell induces a reorientation of DHA metabolism : glycolysis is stimulated whereas neoglucogenesis is inhibited (not shown). However this occurs in such a way that DHA consumption flux is unaffected (Fig. 1b).

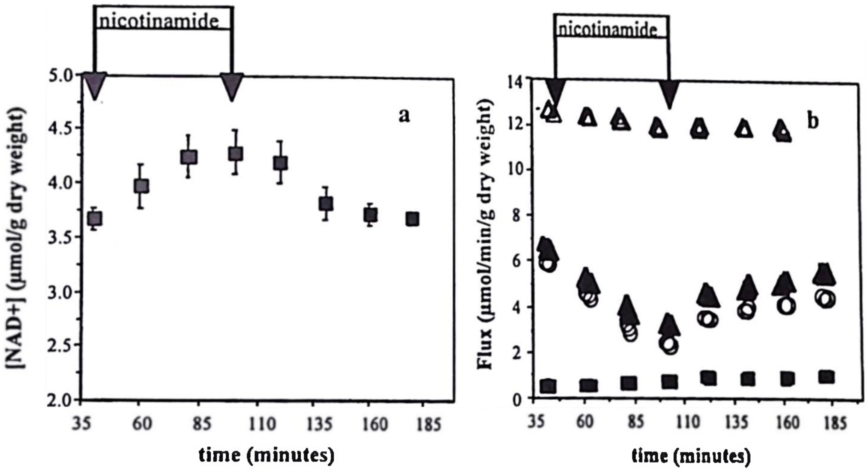

Figure 1: Perifusion of isolated hepatocytes in the presence or absence of nicotinamide. (a) Increase in NAD$^+$ content induced by nicotinamide addition to isolated hepatocytes perifused with 5mM glycerol. Nicotinamide was added as indicated on the figure. (b) Substrate consumption flux (glycerol ▲, DHA △) and flux through glycolysis : lactate+pyruvate (■) and neoglucogenesis : glucose (○) with 5 mM glycerol as substrate. Nicotinamide was added as indicated on the figure.

These flux modifications occur without any significant change in either cellular ATP/ADP ratio or cytosolic redox potential (i.e. lactate/pyruvate ratio which is an indicator of free nicotinamide adenine nucleotide ratio in the cytosol assessed by the lactic dehydrogenase near-equilibrium, see figure 2a). This tends to show that such flux variations are linked to the increase in the NAD$^+$ content of the liver cell. Substrate consumption flux is inhibited only when glycerol is used as substrate whereas DHA consumption flux is two times higher than glycerol consumption flux. Moreover, considering that the difference between DHA and glycerol metabolism lies at the level of glycerol-3-phosphate dehydrogenase, the inhibition of glycerol consumption flux could be linked to an inhibition at the level of this enzyme. This is indeed reflected by an increase in both glycerol-3-phosphate concentration and glycerol-3-phosphate/dihydroxyacetone phosphate ratio when the NAD$^+$ concentration of the cell increases (Fig. 2b).

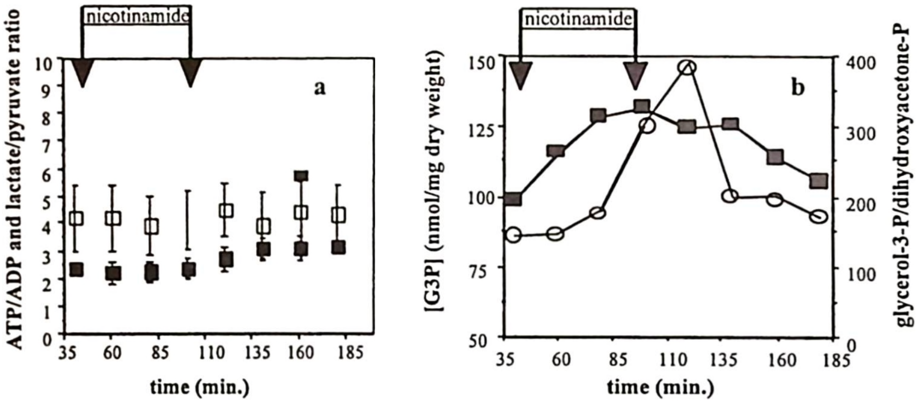

Figure 2: (a) Cellular ATP/ADP ratio (■) and cytosolic lactate/pyruvate ratio (□) when hepatocytes are perifused with 5mM glycerol as substrate and in the presence or absence of 5 mM nicotinamide. (b) Glycerol-3-phosphate concentration (■) and G3P/DHAP ratio (○)when hepatocytes are perifused with 5mM glycerol as substrate and in the presence or absence of 5 mM nicotinamide. Cellular content was separated as described in Material and Methods section, glycerol-3-phosphate (G3P or glycerol-3-P) and dihydroxyacetone phosphate (dihydroxyacetone-P) were determined as described in Material and Methods section.

We checked that the inhibition at the level of cytosolic glycerol-3-phosphate dehydrogenase was not linked to the effect of nicotinamide which induced only 10% inhibition of the functionally isolated enzyme at a concentration of 10mM (not shown). Moreover, when cytosolic glycerol-3-phosphate dehydrogenase was functionally isolated, it was almost insensitive to an increase in NAD^+ concentration in the range we measured in isolated hepatocytes. It could be hypothesised that when NAD^+ concentration increases, and the lactate/pyruvate ratio is constant, the total NADH concentration of the cell also increases, and this increase could have an inhibitory effect on the activity of the cytosolic glycerol-3-phosphate dehydrogenase. Experiments are in progress in order to assess this question.

It should be noticed that whereas the inhibition of neoglucogenesis is indeed associated with an increase in the NAD^+ content of the cell and is suppressed when nicotinamide is no longer perifused thus inducing a decrease in NAD^+ content, the stimulation of glycolysis is not reversible and is maintained while the NAD^+ content of the cell decreases. This could be linked to an intermediary metabolite accumulation when glycolysis is stimulated. Experiments are in progress in order to assess this question. However, glycolysis stimulation is low compared to neoglucogenesis inhibition, which occurs essentially at the level of glycerol-3-phosphate dehydrogenase when glycerol is used as substrate.

CONCLUSION

Our study of the influence of an increase in cellular NAD^+ content on flux through glycolysis and neoglucogenesis with both dihydroxyacetone and glycerol as substrates indicates two distinct phenomena. Firstly, an increase in total NAD^+ and/or NADH concentration inhibits cytosolic glycerol-3-phosphate dehydrogenase, which explains the decrease in glycerol consumption flux. Secondly, the distribution between neoglucogenesis and glycolysis is affected whatever the substrate used, with a constant cytosolic ATP/ADP ratio and cytosolic redox potential. Experiments are under way in order to assess this problem.

ACKNOWLEDGEMENTS

The authors wish to thank Dr. R. Cooke for his contribution to the editing of the manuscript. This work was supported by grants from the Pôle Médicament d'Aquitaine and the Région Aquitaine.

REFERENCES

[1] Nakazawa, J. and Nunokawa, T. (1977) J. Biochem. 82, 1575-1583.

[2] Wilson, D. F., Stubbs, M., Veech, R. L., Erecinska, M. and Krebs, H. A. (1974) Biochem. J. 140, 57-64.

[3] Boschmann, M., Halangk, W., Bohnensack, R. (1996) Biochim. Biophys. Acta 1273, 223-230.

[4] Veech, R. L., Randolph Lawson, J. W., Cornell, N. W. and Krebs, H. A. (1979) J. Biol. Chem. 254, 6538-6547.

[5] Devin, A;, Guérin, B. and Rigoulet, M. (1997) FEBS Lett. 410, 329-332.

[6] Williamson, D. H. , Veloso, D., Ellington, E. V. and Krebs, H. A. (1969) Biochem. J. 114, 575-584.

[7] Berry, M.N. and Friend, D.S. (1969) J. Cell. Biol. 43, 506-520.

[8] Groen, A.K., Sips, H.J., Vervoorn, R.C. & Tager, J.M. (1982) Eur. J. Biochem. 122, 87-93.

[9] van der Meer, R. and Tager, J. M. (1976) FEBS Lett. 67, 36-40

[10] Groen, A. K., Vervoon, R. C., van der Meer and Tager, J. M. (1983) J. Biol. Chem. 258, 14346-14353.

[11] Leverve, X. M., Verhoeven, A. J., Groen, A. K., Meijer, A. J. and Tager, J. M. (1986) Eur. J. Biochem. 155, 551-556.

[12] Bergmeyer, H.U. (ed) (1970) Methods of Enzymatic Analysis, 2nd ed., Verlag Chemie, Academic Press, London.

[13] Methods of enzymatic analysis, vol.VII, (Bergmeyer H.U. et al., eds), pp.255, VCH Publishers

[14] Bergmeyer, H.U. (ed) (1974) Methods of Enzymatic Analysis, pp 468, 1196, 1314, 1415, 1446, 1464, 1836, and 1840, Academic Press, London.

66

AEROBIC-ANOXIC TRANSITIONS AND REGULATION OF MITOCHONDRIAL OXYGEN FLUX

B. Lassnig, A. V. Kuznetsov, R. Margreiter, E. Gnaiger

Department of Transplant Surgery, D. Swarovski Research Laboratory, University Hospital Innsbruck, Anichstraße 35, A-6020 Innsbruck, Austria, Tel: +43 512 504 4624, Fax: +43 512 504 4625, E-mail: barbara.lassnig@uibk.ac.at

INTRODUCTION

We applied high-resolution respirometry to study the control of mitochondrial respiration by oxygen. In the closed respirometer chamber, oxygen is depleted by mitochondrial respiratory flux, and hyperbolic relationships are found between oxygen flux and oxygen pressure [1-4]. Hyperbolic fitting to flux/pressure plots results in the two parameters p_{50} and J_{max}. p_{50} is comparable to the apparent Michaelis-Menten-Constant, K_{m}', which is used for isolated enzymes [5], whereas p_{50} is a parameter for the complex system of enzymes in the mitochondrial respiratory chain. These parameters of steady-state kinetics should yield information about the physiological role of intracellular steady state oxygen levels. Application of steady-state kinetics to transitions in a closed system or to initial rates may be criticized when the possible influence of pre-steady-state transitions is ignored and therefore could lead to wrong interpretations [6]. The relevance of our results obtained by the measurement of aerobic-anoxic transitions for physiological steady state conditions is corroborated by a large data base and specifically designed test experiments showing the high stability of the kinetic parameters over a wide range of transition times in which dynamic equilibrium is obtained.

METHODS

Oxygen dependence of respiration of isolated rat liver mitochondria was studied in series of aerobic-anoxic transitions in the presence of rotenone (0.5 μM), succinate (10 mM) and ATP (1 mM), and after further addition of ADP. Mitochondrial protein concentrations ranged from 0.1 to 0.8 $\text{mg}\cdot\text{cm}^{-3}$. The incubation medium consisted of 200 mM sucrose, 20 mM HEPES, 0.5 mM EGTA, 1 g/l BSA (essentially fatty acid free), 3 mM $MgCl_2$, 20 mM taurine and 10 mM KH_2PO_4, ~300 mosm, pH 7.1 at 30°C. To obtain different oxygen levels the measuring chamber was opened to allow gas exchange to selected levels. Alternatively reoxygenations were performed in the presence of catalase by the addition of hydrogen peroxide, which is immediately converted to oxygen. The high sensitivity of the OROBOROS oxygraph, the use of inert materials and special mathematical corrections provided the basis for oxygen kinetic measurements at correspondingly low oxygen levels [1]. Data acquisition at 1 s sampling intervals and data analysis were performed with the software DatLab (OROBOROS, Innsbruck, Austria). Volume-specific fluxes at kinetic oxygen saturation were always kept below an instrumental and statistical threshhold level above which resolution of oxygen kinetics becomes distorted [4, 7].

RESULTS

The p_{50} was dependent on metabolic state. Oxygen pressure at half-maximum respiratory activity, p_{50}, increased from 0.02 kPa (0.2 µM, 0.15 Torr) in the passive state without ADP, up to 0.06 kPa (0.6 µM, 0.45 Torr) in the active state after the addition of ADP (Fig. 1, [4]). J_{max} increased proportional to mitochondrial protein concentration. The transition time between kinetic oxygen saturation at 1.1 kPa and anoxia varied as a function of metabolic state and mitochondrial density. p_{50} was independent of transition time in any metabolic state (Fig. 1).

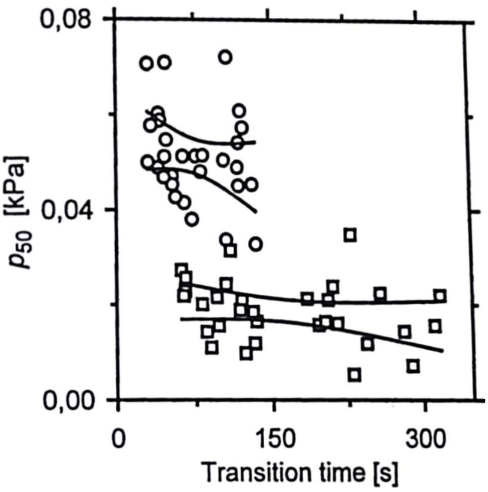

Figure 1. Oxygen pressure at half-maximum respiration, p_{50}, was independent of the transition time, the time until oxygen pressure declined from 1.1 kPa to zero. Squares show mitochondria respiring in the presence of ATP without ADP, circles represent highly active mitochondria after the addition of 1 mM ADP. Lines show the 95% confidence interval.

The change of respiratory capacity with time (Fig. 2) was small compared to the oxygen dependent change of respiratory flux during aerobic-anoxic transitions and therefore did not exert any distorting effect on the calculation of oxygen affinities. Respiratory activity declined when incubation times extended up to 2.5 h (Fig. 2). Dependent on the oxygen levels after reoxygenations and the presence or absence of catalase, differences in the loss of respiratory activity were observed. Preliminary experiments indicated that permanent exposure to unphysiological high oxygen (> 80 µM) results in a more severe decline than incubation at lower oxygen levels with short intermittent intervals of anoxia. High initial oxygen levels resulted in a slightly higher respiratory flux compared to reoxygenations to low p_{O_2}, but led to a more severe decline in respiration during extended incubation periods. Addition of cytochrome *c* restored part of the initial respiration. Uncoupling with FCCP led to a further increase of the respiratory rate.

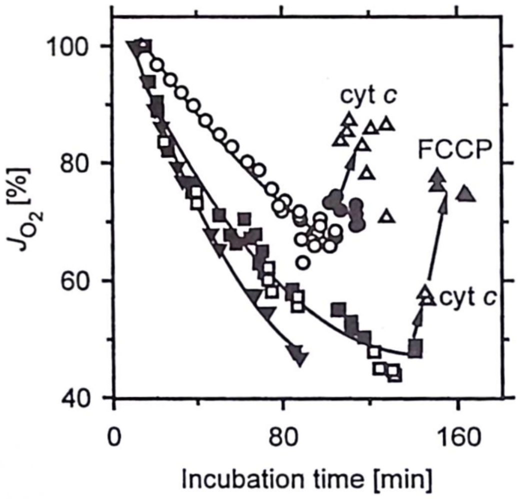

Figure 2. Respiratory flux at kinetic oxygen saturation, J_{O_2}, is shown as a function of incubation time in the measuring chamber. Rat liver mitochondria were respiring in the presence of succinate, ATP and ADP. In series of aerobic-anoxic transitions (circles and squares) reoxygenations were performed to low (<25 µM, open symbols) or high oxygen levels (>25 µM, closed symbols) or the oxygen concentration was always kept above 80 µM (downward triangles). The presence of catalase (circles) and low oxygen levels improved preservation of respiratory rate. Non-linear fits combine experiments with identical conditions. Addition of 10 µM cytochrome *c* (opened upward triangles) partly restored the initial respiration. A further increase of the respiratory rate was obtained after uncoupling by 2 µM FCCP (closed upward triangles).

DISCUSSION

The importance of oxygen in the regulation of mitochondrial activity becomes obvious when our p_{50} values are compared to average p_{O_2} levels in the intracellular microenvironment of tissues. Contrary results or non-hyperbolic relations [8–10] are most probably due to instrumental artefacts. Especially in active states at high ADP concentration, when the oxygen affinity, $1/p_{50}$, decreases compared to resting states without ADP, the regulating role of oxygen must not be underestimated. For heart an average intracellular p_{O_2} of ~ 0.3 kPa (c. 1 to 2% of air saturation) is obtained from measurement of oxygen saturation of myoglobin. [10, 11]. Under these conditions mitochondria work at 70 to 90% of their maximum capacity [3, 4]. Therefore limitations in oxygen supply to mitochondria are of major importance, especially under pathological conditions, e.g. in case of mitochondrial disorders or loss of functional enzyme during aging [7].

The rapid adaptation of mitochondrial function to altered metabolic conditions and the stability of our kinetic parameters, p_{50} and J_{max}, over a range of transition times, .confirm the physiological relevance of our oxygen kinetic measurements (compare Refs. [12, 13]).

The significant decline of the initial respiratory rate observed during prolonged incubation may be due to suboptimal incubation conditions and temperature, and damaging effects of high oxygen [14, 15]. Part of the irreversible decline with incubation time could be explained by cytochrome *c* release, resulting from disruption of the outer mitochondrial membrane. The elevation of respiratory flux after uncoupling indicates a defect of the phosphorylation system, including ATP-synthase and adenylate translocase.

Most bioenergetic studies are performed at nonphysiological high p_{O_2}, whereby the influence of oxidative stress is frequently ignored. A compromise of sufficient support with oxygen for the production of high energy phosphates and a restriction of the production of oxygen radicals is made by the maintenance of low intracellular oxygen levels. Protective effects of low oxygen and added catalase might explain the higher stability of the respiratory rate.

ACKNOWLEDGEMENTS

Supported by a research grant of the University of Innsbruck. A.K. was supported by an OROBOROS Research Award.

REFERENCES

[1] Gnaiger, E., Steinlechner-Maran, R., Méndez, G., Eberl, T., Margreiter, R. (1995) J. Bioenerg. Biomembr. 27 (6), 583-596.

[2] Steinlechner-Maran, R., Eberl, T., Kunc, M, Margreiter, R., Gnaiger, E. (1996) Am. J. Physiol. 271, C2053-C2061.

[3] Gnaiger, E., Lassnig, B., Kuznetsov, A., Rieger, G. and Margreiter, R. (1998) J. Exp. Biol. 201, 1129-1139.

[4] Gnaiger, E., Lassnig, B., Kuznetsov, A., Rieger, G. and Margreiter, R. (1998) Biochim. Biophys. Acta, EBEC issue (in press).

[5] Minnaert, K. (1961) Biochim. Biophys. Acta 50, 23-34.

[6] Cornish-Bowden, A. (1995) Fundamentals of enzyme kinetics. Portland Press, London.

[7] Lassnig, B., Kuznetsov, A., Margreiter, R. and Gnaiger, E. (1998) in prep.

[8] Cole, R.C., Sukanek, P.C., Wittenberg, J.B. and Wittenberg, B.A. (1982) J. Appl. Physiol. 53, 1116-1124.

[9] Petersen, L.C., Nicholls, P. and Degn, H. (1974) Biochem. J. 142, 247-252.

[10] Wittenberg, B.A., Wittenberg, J.B. (1989) Annu. Rev. Physiol. 51, 857-878.

[11] Wagner, P.D. (1996) Annu. Rev. Physiol. 58, 21-50.

[12] Wilson, D.F., Rumsey, W.L., Green, T.J. and Vanderkooi, J. (1988) J. Biol. Chem. 263, 2712-2718.

[13] Rumsey, W.L., Schlosser, C., Nuutinen, E.M., Robiolio, M. and Wilson, D.F. (1990) J. Biol. Chem. 265, 15392-15399.

[14] Richter, C., Schweizer, M. (1997) Oxidative Stress and the Molecular Biology of Antioxidant Defenses, Cold spring Harbor Laboratory Press, 169-200.

[15] Dykens, J.A. (1997) in Mitochondria and free radicals in neurodegenerative diseases (Beal, M.F., Howell, N. and Bodis-Wollner, I., ed.), pp. 29-55, Wiley-Liss, New York.

ENERGY-DEPENDENT MAINTENANCE OF CELL REDOX POTENTIALS

M.N. Berry, A.R. Grivell, M.B. Grivell, J.W. Phillips

Department of Medical Biochemistry, Flinders University, GPO Box 2100 Adelaide 5001, Australia

INTRODUCTION

Normal liver, when exposed to a constant concentration of lactate, maintains a steady [lactate]/[pyruvate] ratio which, if perturbed by further addition of a bolus of lactate or pyruvate, is gradually restored to close to its previous value [1]. It has been proposed by several groups that this regulation of the [lactate]/[pyruvate] ratio results from the maintenance of the components of the reaction catalysed by lactate dehydrogenase (LDH), as well as those of reactions catalysed by a number of other NAD-linked dehydrogenases, in a state of near-equilibrium as part of a network of close-to-equilibrium reactions that exists within the cytoplasmic compartment of the cell (see [2] for review). In view of this equilibration it has been considered feasible to use the steady state mass action ratio of the substrates of the reaction catalysed by LDH to determine the redox state or potential (E_{hc}) of cytoplasmic free ([NAD$^+$]/[NADH]). Similar considerations have allowed the determination of the hepatic mitochondrial NAD-linked potential (E_{hm}) from the measurement of the steady state mass action ratio of the reaction catalysed by 3-hydroxybutyrate dehydrogenase, which is confined to the mitochondrial compartment.

Thus, published data implies that E_{hc} and E_{hm} are individually held close to equilibrium, yet in terms of energy state, some 60 mV apart. This would be feasible if the two NAD pools were totally segregated, but it is well established that, despite this apparent energy barrier, reducing equivalents flow freely between the two compartments [3-5]. This apparent paradox has prompted us to re-examine the interrelationships of E_{hc} and E_{hm}. We conclude that E_{hc} and E_{hm}, as calculated by conventional means, represent not near-equilibrium potentials but rather energised far-from-equilibrium steady states.

MATERIALS AND METHODS

Sources of chemicals, inhibitors of oxidative phosphorylation, collagenase and enzymes necessary for the assay of metabolites, as well as incubation procedures and analytical techniques are described elsewhere [6]. A stock solution of palmitic acid was neutralised and dissolved in isotonic saline containing 9% (w/v) defatted bovine serum albumin (fraction V). Hepatocytes were prepared from 24-h fasted male Hooded Wistar rats of body mass 280-320 g as described in [7]. In preliminary studies hepatocytes were separated from the incubation medium by centrifugation, and analyses performed on the pellet and supernatant. These showed that the intracellular concentrations of lactate, pyruvate, 3-hydroxybutyrate and acetoacetate were consistently within 10% of extracellular values. The rate of oxygen uptake (J_O) was measured manometrically on a Gilson differential respirometer and inner mitochondrial "membrane potential" ($\Delta\Psi$) was determined with [^{14}C]TPMP$^+$ [8]. The cytoplasmic and mitochondrial NAD-linked redox potentials were calculated according to [2]. The difference between the mitochondrial and cytoplasmic redox potentials, designated as E_{hdiff}, represents $E_{\mathrm{hc}} - E_{\mathrm{hm}}$.

RESULTS

Relationship between cytoplasmic and mitochondrial redox potentials

When hepatocytes from fasted rats were exposed to 10 mM lactate, it took about 40 min for the [lactate]/[pyruvate] ratio to approach a value near 6/1 as lactate was consumed and pyruvate accumulated [9] (Fig. 1A). The ratio attained at any time point was found to be dependent on the initial concentration of added lactate. For example, if this concentration was 5 mM the [lactate]/[pyruvate] ratio at 40 min was less than 5/1. On the other hand, initial concentrations of 15 or 20 mM lactate yielded [lactate]/[pyruvate] ratios of about 7.5/1 and 10/1 respectively (Fig. 1A, inset). All these ratios declined further as the incubation was continued for another 20 min, but remained significantly different. The corresponding values for E_{hc} at 50 min, for the four different initial lactate concentrations employed, indicate a spread of 9 mV (Table 1). Changes occurring concomitantly in the [3-hydroxybutyrate]/[acetoacetate] ratio over the incubation period are shown in Fig. 1B. Due to the lack of added fatty acid in the incubation medium these ratios were very low and at 50 min all were below 0.35/1; the corresponding values for E_{hm} spanned about 8 mV (Table 1). Because the variations in E_{hc} and E_{hm} were of the same order and direction, E_{hdiff} remained almost constant for the different concentrations of added lactate (Table 1).

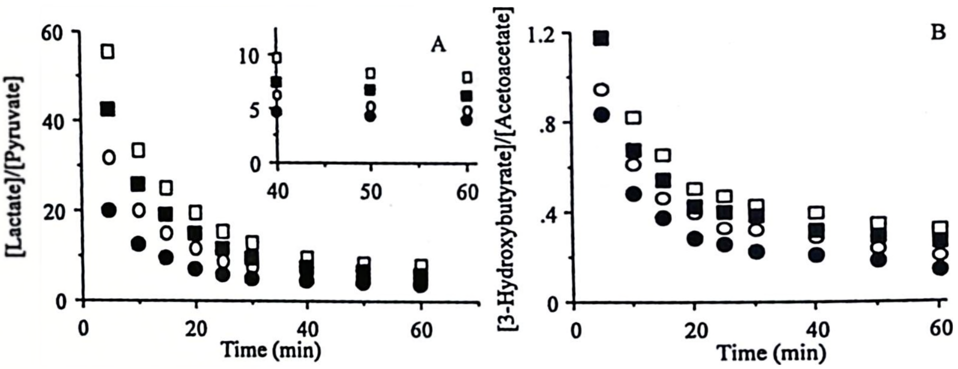

Figure 1A and 1B. Relationships between the starting concentration of lactate and [lactate]/[pyruvate] (1A) or [3-hydroxybutyrate]]/[acetoacetate] (1B) attained during the course of an incubation. Hepatocytes were incubated with 5, 10, 15 or 20 mM lactate (●,○,■,□) at 37°C. The data presented are from a representative experiment.

TABLE 1

Effect of initial lactate concentration on $-E_{hc}$, $-E_{hm}$ and E_{hdiff}

Lactate (mM)	$-E_{hc}$ (mV)	$-E_{hm}$ (mV)	E_{hdiff} (mV)
5	235	275	39
10	238	278	40
15	241	281	40
20	244	283	39

Hepatocytes were incubated with 5, 10, 15 or 20 mM lactate at 37°C for 50 min.

The [lactate]/[pyruvate] ratio can be altered by exposing hepatocytes to palmitate [10]. Because the fatty acid is rapidly metabolised by the liver at a rate that is concentration-dependent [11], and the amount that can be added is limited due to its poor solubility, hepatocytes are normally incubated with palmitate complexed with albumin. Saturating concentrations of unbound fatty acid that induce maximal rates of acetoacetate plus 3-hydroxybutyrate ("ketone bodies") formation are obtained when hepatocytes from fasted rats are exposed to 2 mM palmitate complexed with 2.25% albumin [12]. Lower non-saturating concentrations of free palmitate can be achieved by complexing the fatty acid with higher concentrations of albumin [10]. In the present studies, we employed four albumin concentrations between 2% and 9%, which confirmed that the greater the concentration of unbound palmitate to which the hepatocytes were exposed, the faster the rate of ketone body production and the higher the corresponding E_{hc} and E_{hm} attained (Table 2). Nevertheless, because E_{hc} and E_{hm} increased by about the same extent for each individual free palmitate concentration tested, E_{hdiff} remained virtually constant.

TABLE 2

Effect of albumin addition on the rate of acetoacetate + 3-hydroxybutyrate formation, $-E_{hc}$, $-E_{hm}$ and E_{hdiff}

Albumin	Ketone Body Formation (µmol.min^{-1}.g^{-1} wet wt)	$-E_{hc}$ (mV)	$-E_{hm}$ (mV)	E_{hdiff} (mV)
2.2%	1.11	255	299	44
4.5%	0.74	251	294	43
8.9%	0.42	244	289	44

Hepatocytes were incubated with lactate 8 mM and palmitate 2 mM (as described in Methods) at 37°C and E_{hc} and E_{hm} were measured at 40 min. The results are from a representative experiment.

Energy-dependence of cellular redox potentials

These studies indicated that hepatocytes exposed to lactate alone or in combination with palmitate were capable of maintaining an approximately constant potential difference between E_{hc} and E_{hm}, even though the individual redox potentials were substantially altered in the presence of different initial substrate concentrations.

Furthermore, there appeared to be significant interaction between the two potentials in that the presence of the cytoplasmic substrate, lactate, elevated E_{hm} as well as E_{hc}, whilst the mitochondrial substrate, palmitate, raised not only E_{hm} but also E_{hc}. These observations confirm that bidirectional reducing-equivalent flow and equilibration of hepatocyte cytoplasmic and mitochondrial NAD pools readily occur in the intact liver, despite the calculated 60 mV difference between the two potentials, equivalent to a hundredfold difference in redox state (mitochondria more negative). Because previous studies had indicated that reducing-equivalent transfer between cytoplasmic and mitochondrial compartments involves energy-dependent mechanisms [3,4,13] we examined the effects of uncoupling agents on the interrelationships of E_{hc} and E_{hm}.

TABLE 3
Effect of FCCP addition on ΔΨ, $-E_{hc}$, $-E_{hm}$, E_{hdiff}, ATP concentration and the rate of oxygen utilisation$_{\Delta\Psi}$

FCCP (μM)	(mV)	$-E_{hc}$ (mV)	$-E_{hm}$ (mV)	E_{hdiff} (mV)	[ATP] (μmol. g^{-1} wet wt)	J_O (μmol.min^{-1}. g^{-1} wet wt)
0	168	252	299	45	2..3	6.6
10	162	248	294	45	2.1	7.5
20	157	248	289	41	1.8	7.0
30	147	249	285	36	1.5	8.5
40	137	255	278	23	1.0	8.5
60	118	267	269	2	0.4	6.9

Hepatocytes were incubated with 10 mM lactate, 2 mM palmitate and 2 mM asparagine. Results are the mean of 4-7 expts. Measurements were made at 30 min.

Table 3 illustrates the effects of increasing concentrations of the uncoupling agent FCCP on J_O, [ATP] and potentials when cells were incubated with lactate and palmitate. In these experiments asparagine was present as a source of shuttle components. In the absence of added asparagine the hepatocytes were grossly damaged at relatively low concentrations of FCCP, as indicated by trypan blue uptake and lactate dehydrogenase leakage. The almost complete abolition of E_{hdiff} induced by the highest concentration of FCCP was the result of a substantial fall in E_{hm} and a lesser rise in E_{hc}. Similar results were obtained with the ionophore, valinomycin (data not shown).

Since [ATP] and ΔΨ fell in parallel as E_{hdiff} decreased, it was not clear from these experiments whether the energy-dependent decline in E_{hdiff} was due solely to the fall in [ATP] or to a general mitochondrial de-energisation. To investigate this we incubated hepatocytes with lactate and palmitate together with carboxyatractyloside or oligomycin both of which maintain ΔΨ whilst greatly depleting cellular [ATP]. The results set out in Table 4 show that E_{hdiff} was elevated rather than decreased in the presence of these inhibitors, and hence its maintenance is not dependent on [ATP].

TABLE 4
Effect of oligomycin or carboxyatractyloside addition on $-E_{hc}$, $-E_{hm}$, E_{hdiff}, ATP concentration and $\Delta\Psi$.

Inhibitor	$-E_{hc}$ (mV)	$-E_{hm}$ (mV)	E_{hdiff} (mV)	[ATP] (μmol. g^{-1} w w)	$\Delta\Psi$ (mV)
None	252	299	45	2.3	168
Oligomycin (0.6 μM)	258	323	65	0.78	169
Carboxyatractyloside (100 μM)	264	324	61	0.34	161

Hepatocytes were incubated with 10 mM lactate, 1 mM pyruvate and 2 mM palmitate. Measurements were made at 30 min.

TABLE 5
Effect of rotenone addition on the rate of oxygen utilisation and glucose formation, $\Delta\Psi$, ATP concentration, $-E_{hc}$, $-E_{hm}$ and E_{hdiff}.

Rotenon	J_O	$J_{Glucose}$	$\Delta\Psi$	[ATP]	$-E_{hc}$	$-E_{hm}$	E_{hdiff}
(μM)	(μmol.min^{-1}.g^{-1} wet wt)		(mV)	(μmol. g^{-1} w w)	(mV)	(mV)	(mV)
0	5.7	1.5	169	2.48	256	298	42
0.1	5.3	1.3	158	2.32	258	303	45
0.25	5.2	1.1	158	2.17	262	307	45
0.5	4.8	0.8	157	2.07	265	311	46
1	4.1	0.4	156	1.91	268	316	47
2	3.1	0.1	147	1.54	273	323	50

Hepatocytes were incubated with 10 mM lactate, 1 mM pyruvate and 2 mM palmitate. Results are from a representative experiment. Measurements were made at 40 min.

The relationship between mitochondrial electron flow and E_{hdiff} was further studied by exposing hepatocytes to graded concentrations of the respiratory inhibitor, rotenone. The results in Table 5 show that the inhibition of O_2-uptake by increasing rotenone concentrations was associated with decreasing mitochondrial energisation as indicated by a decline in $\Delta\Psi$, [ATP] and the rate of glucose synthesis, but there was a rise in both E_{hc} and E_{hm} and maintenance of E_{hdiff}. This implies that the creation of an apparent redox potential difference between the mitochondrial and cytoplasmic compartments is not directly dependent on the generation of $\Delta\Psi$ or ΔG_p, as reflected by [ATP], but rather, like $\Delta\Psi$, may be produced as an immediate and independent consequence of the utilisation of free energy arising during electron transport.

An energy-dependent mechanism that could be involved in the maintenance of E_{hdiff} is "reversed electron transfer", a process described in animal mitochondria more than 25 years ago [14], but the physiological significance of which, in animal cells, has been discounted. It is noteworthy that rotenone, which does not inhibit flavin-linked oxidations and is therefore not a potent suppressor of fatty acid oxidation, did not diminish, but actually increased E_{hdiff}. These findings suggest that whereas a general mitochondrial inner membrane de-energising agent, such as the uncoupler FCCP, can interfere with all energy-dependent processes including generation of $\Delta\mu H^+$, ATP synthesis and reversed electron transfer, inhibitors which specifically act at a single locus within the electron transport complex may be less broad in their actions on energy transduction. These studies and others previously reported [6,15,16] confirm that close correlations can exist under certain conditions between the magnitudes of $\Delta\Psi$, ΔG_p, E_{hc} and E_{hm} and rates of metabolic synthesis, but indicate that these correlations are not the result of a direct linkage between the various cellular potentials. Rather they may reflect a connection with, and dependence on, a more fundamental energisation of the mitochondria arising as a consequence of substrate oxidation and electron flow down the electrochemical gradient to oxygen. What factors determine the absolute value of the cellular potentials, or the mechanisms by which the redox potentials in the various cell compartments are energetically linked, remain to be elucidated.

ACKNOWLEDGMENTS

This work was supported in part by a grant from the National Health and Medical Research Foundation and the Flinders Medical Centre Foundation.

REFERENCES

1 Hems, R., Ross, B.D., Berry, M.N. and Krebs, H.A. (1966) *Biochem. J.* **101**, 284-292.

2 Sies, H. (1982) in *Metabolic compartmentation* (Sies, H., ed.), pp. 205-231, Academic Press Inc. (London) Limited, London.

3 Meijer, A.J. and Williamson, J.R. (1974) *Biochim. Biophys. Acta* **333**, 1-11.

4 Berry, M.N. (1971) Biochem. *Biophys. Res. Commun.* **44**, 1449-1456.

5 Berry, M.N., Phillips, J.W., Gregory, R.B., Grivell, A.R. and Wallace, P.G. (1992) *Biochim Biophys. Acta* **1136**, 223-230.

6 Berry, M.N., Gregory, R.B., Grivell, A.R., Henly, D.C., Phillips, J.W., Wallace, P.G. and Welch, G.R. (1987) *FEBS Lett.* **224**, 201-207.

7 Berry, M.N. and Friend, D.S. (1969) *J. Cell Biol.* 43, 506-520.

8 Hoek, J.B., Nicholls, D.G. and Williamson, J.R. (1980) *J. Biol. Chem.* **255**, 1458-1464.

9 Efthivoulou, M-A., Berry, M.N. and Phillips, J.W. (1995) *Biochim. Biophys. Acta* **1244**, 303-310.

10 Berry, M.N., Clark, D.G., Grivell, A.R. and Phillips, J.W. (1991) Evidence for cytoplasmic organization derived from studies of energy-dependent mitochondrial-cytoplasmic interactions. In *"Regulation of hepatic function. Metabolic and structural"*, pp. 179-192, Munksgaad, Copenhagen.

11 Ontko, J.A. (1972) *J. Biol. Chem.* **247**, 1788-1800.

12 Berry, M.N., Clark, D.G., Grivell, A.R. and Wallace, P.G. (1983) *Eur. J. Biochem.* **131**, 205-214.

13 LaNoue, K.F., Bryla, J. and Bassett, D.J. (1974) *J. Biol. Chem.* **249**, 7514-7521.

14 Chance, B. and Hollunger, G. (1961) *J. Biol. Chem.* **236**, 1577-1584.

15 Berry, M.N., Gregory, R.B., Grivell, A.R., Henly, D.C., Nobes, C.D., Phillips, J.W. and Wallace, P.G. (1988) *Biochim. Biophys. Acta* **936**, 294-306.

16 Berry, M.N., Gregory, R.B., Grivell, A.R., Henly, D.C., Phillips, J.W., Wallace, P.G. and Welch, G.R. (1988) *FEBS Lett.* **231**, 19-24.

IS THE GLYCOLYTIC FLUX CONDITIONALLY CONTROLLED BY THE ATP CONCENTRATION IN *SACCHAROMYCES CEREVISIAE*?

Larsson C., Nilsson A., Påhlman I.-L., Blomberg A., Gustafsson L.

General and Marine Microbiology, Lundberg Laboratory, Box 462, S-405 30 Göteborg, Sweden. Phone: +46 31 773 2579; Fax: 46 31 773 2599
E-mail: Christer.Larsson@gmm.gu.se

INTRODUCTION

The rate of glycolysis can potentially be regulated at several steps, including sugar transport, and by different mechnisms (*eg.* 2, 3, 4, 7, 20, 21). Enzymes may be regulated both by allosteric control of existing enzymes as well as by changes in the amount of glycolytic enzymes. However, attempts to improve flux by increasing the amount of certain key enzymes has in general proved unsuccessful (6). The regulation of glycolytic rate as well as rate of respiration involves nucleotides and especially adenine nucleotides (2, 3, 4, 7). The adenine nucleotides act as allosteric effectors but they are also taking part as substrates and products of glycolysis. Therefore, both their absolute concentration as well as their mass action ratios may be of importance for the regulation of glycolysis.

The rate of energy production in the catabolic pathways are not always correlated by the anabolic energy requirements, *i.e.* more ATP is produced than needed by biosynthetic and maintenance demands (11, 13, 20). During growth of *S. cerevisiae* in a glucose limited chemostat, the cells are facing an energy limitation (19, 24). Consequently, under such conditions a low extent of uncoupling is to be expected. A nitrogen limitation, on the other hand, may provoke metabolic uncoupling since this represents an energy excess situation. Indeed, this has been reported for aerobic chemostat cultures of *S. cerevisiae* where a gradual change from glucose (energy) limitation to nitrogen limitation and energy excess was studied (11). The primary response during energy excess was an increased respiratory activity. When the maximum respiratory activity was reached also the rate of fermentation increased (11). In a recent chemostat study by Larsson et al. (12), changes in the glycolytic flux were brought about by imposing on the cells a gradually increasing nitrogen limitation, and hence increasing surplus of energy, *i.e.* by inducing different degrees of metabolic uncoupling. To reach even higher fluxes of both glycolysis and respiration at a constant rate of growth, we also took advantage of the uncoupling effect of weak organic acids, *e.g.* acetic- and benzoic acid.. The glycolytic flux was thereby increased by 100% (at a constant growth rate of 0.10 h^{-1}).

This system was used in order to (*i*) investigate the levels of intracellular nucleotides and glycolytic enzymes at different glycolytic fluxes and to (*ii*) check whether there is any correlation between any of these concentrations and rate of glycolysis. In order to study the regulation of glycolysis in more detail we are presently harvesting cells from the chemostat and subsequently permeabilizing the cells by a technique using nystatin. The aim of the study is to determine to which extent different nucleotides exert control on glycolytic flux.

MATERIAL AND METHODS

The Baker's yeast strain, supplied by the Swedish Baker's yeast manufacturer (Jästbolaget AB, Rotebro, Sweden) and W303-1A (*ade2, his3, leu2,trp1, ura3, can1-100*) strain was used. Cells were cultured in a defined medium described by Albers *et al.* (1) with $(NH_4)_2SO_4$ as the nitrogen source. In experiments with the auxotrophic mutant the necessary amino acids and bases were added to the medium at a concentration of 120 mg/l or concerning leucine 240 mg/l. The glucose concentration was kept constant at 20 g/l whereas the ammoniumsulphate concentration was varied in order to obtain medium C/N ratios ranging from 10 - 640 (gC/gN). In the experiments with acetic acid and benzoic acid addition a feed medium concentration of 5 mM was used.

The chemostat cultures were conducted at a constant dilution rate of 0.10 h^{-1} in a 2 liter CMF mini fermenter (Chemap AG, Volketswil, Switzerland). The working volume was 1.5 l, the temperature was 30°C, the stirring rate was 500 rpm (anaerobic) or 600 rpm (aerobic) and the pH was controlled at 5.0 by addition of 1 M NaOH. Anaerobic conditions were obtained by flushing the fermentor with N_2 at a rate of 0.2 vol/vol/min by using a mass flow controller (Bronkhorst High-Tech B.V., Ruurlo, The Netherlands). Samples (2 x 1.5 ml) were centrifuged for 2 min at 15,000 x g and the supernatants were stored in the freezer (-20°C). Concentrations of substrates and products were determined with enzyme combination kits (Biochemica Test Combination; Boehringer Mannheim GmbH, Mannheim Germany).

For determination of intracellular nucleotides, samples (2 x 1 ml) were extracted using a TCA method previously described (9). Analysis was performed by ion-pair reversed phase HPLC. The column was hypersil BDS C18 (Hewlett Packard Company, Camas, WA) 250 x 4.6 mm and a particle size of 5 µm. The mobile phase consisted of 60 mM $NH_4H_2PO_4$ + 5 mM of tetrabutylammoniumdihydrogen phosphate (pH 6.50). The acetonitrile concentration was linearly increased from 0 to 8% during the first 15 min and this concentration was maintained until the end of the run. The temperature was 42°C and the flow rate 1 ml/min. Detection was performed by measuring the absorbance at 254 nm.

For determination of total protein content of the cells, samples (2 x 10 ml) were centrifuged at 5,000 x g for 5 min and washed twice with 0.9 % (wt/vol) NaCl. The pellet was resuspended in 3 ml of NaOH and total protein was determined by a modified biuret method (24) using bovine serum albumin as a standard. The protein composition was determined by two-dimensional (2D) poly-acrylamide gel electrophoresis. The 2D-PAGE gels were run as described with first dimensional separation in an immobilised 3 - 10 pH gradient subsequently resolved on SDS containing 10% acrylamide gels (16). Identification of resolved proteins have earlier been performed by micro-sequencing (16) and image-data can be found on our www - server (http://yeast-2DPAGE.gmm.gu.se). Silver staining of the proteins were performed according to a silver nitrate based protocol with prior treatment of the gels with dithiothreitol (15). In order to properly quantify the stained 2D resolved proteins, a calibration strip with step-wise increased concentrations of BSA was simultaneously stained and utilised in the computer aided image analysis. By applying this quantification procedure the silver staining technology showed both a linear and protein invariant response (Norbeck and Blomberg; unpublished data). 2D resolved proteins were automatically quantified by image analysis by the PDQUEST software (v. 5. 1), which is a commercial variant of the QUESTsystem (8).

For further experimental details see (12).

RESULTS

In order to study whether the changes in glycolytic flux was accompanied by changes in the levels of glycolytic enzymes, 2D-PAGE analysis was used. There seemed to be a general trend in that the relative amount of glycolytic enzymes decreased when the conditions changed from energy limitation to energy excess (Fig. 1A). However, also the actin content decreased and if the results were normalized to actin concentration it was only HXK2 and ENO1 which still showed a significant decrease in abundance during energy excess (Fig. 1B).

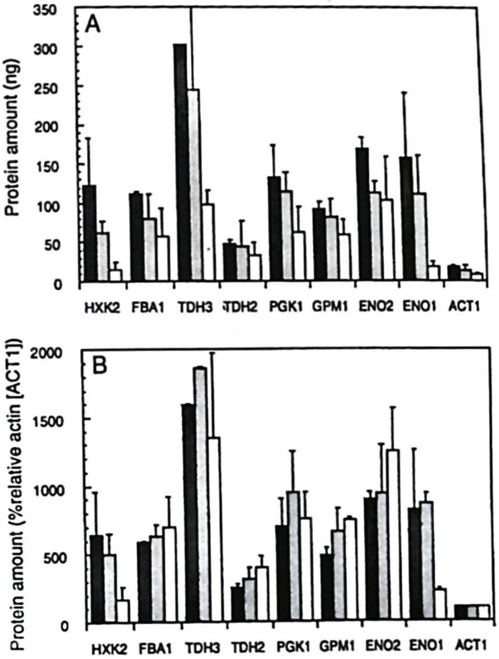

Figure 1. Changes in the level of glycolytic enzymes analyzed by 2D-gel electrophoresis during anaerobic chemostat cultures of *S. cerevisiae* at a dilution rate of 0.10 h^{-1} and a feed medium C/N ratio of 10 (black bars), 80 (grey bars) and 320 (open bars). (A) protein amount per 20 μg total protein and (B) amount of protein in percent of actin. Printed from Larsson et al. (12), copyright ©American Society of Microbiology.

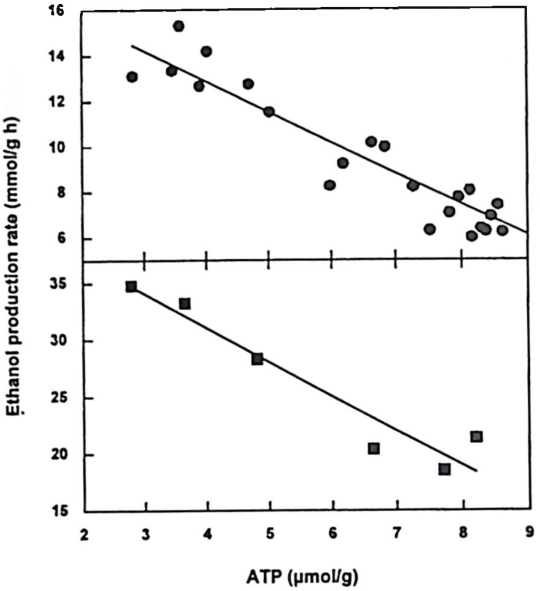

Figure 2. The correlation between glycolytic rate and intracellular ATP content during anaerobic chemostat cultures of *S. cerevisiae* at a dilution rate of 0.10 h^{-1} with and without addition of 5 mM of benzoic acid. No addition (●) and 5 mM benzoic acid (■). The results without addition of weak acid are based on two entirely separate experiments using the Baker's yeast strain and one experiment with the W303-1A strain. The correlation coefficient, r^2 was 0.85 and the t value -10.9 (n = 22). Benzoic acid additions were performed with the Baker's yeast strain. The correlation coefficient, r^2 was 0.92 and the t value -6.8 (n = 6). Printed from Larsson et al. (12), copyright © American Society for Microbiology.

For each series of varying C/N ratio there was a strong negative correlation between glycolytic flux and intracellular ATP content, *i.e.* the higher the ATP content the lower the rate of glycolysis, both during anaerobic (Fig. 2) and aerobic (see 12) conditions. No correlation could be found with the other nucleotides tested (ADP, GTP, UTP) or with the ATP/ADP ratio (data not shown). However, the same intracellular ATP content yielded a much higher glycolytic flux in the presence of benzoic acid than without addition (Fig. 2). A different response was also found when anaerobic and aerobic conditions were compared. Anaerobically the glycolytic flux was higher at the same ATP content than during aerobic conditions.

DISCUSSION

It is clear that uncoupling between anabolic energy demands and catabolic energy production can occur in *S. cerevisiae* (11, 12, 13, 22). Anaerobically, when the nitrogen feed was decreased and energy excess was introduced, the catabolic activity of the cells increased (at a constant growth rate) until an ethanol production rate of about 15 mmol/g h was reached (12). However, the presence of benzoic acid somehow enabled the cells to increase the fermentation rate above what seemed to be a saturation level. Similar effects have earlier been reported on respiratory activity under aerobic conditions where oxygen consumption rates of 19-21 mmol /g h were recorded in the presence of benzoic acid (23). This value is much higher than the maximum respiratory rate reported by, *e.g.* Rieger *et al.* (18) for *S. cerevisiae*. The feature of allowing uncoupling of catabolism and anabolism in *S. cerevisae*, enables the glycolytic rate to be separated from the growth rate (12). This feature was used in the here presented studies of the correlation between glycolytic rate and different potential factors that may be involved in the control of the glycolytic rate.

The strong negative correlation between intracellular ATP content and the rate of glycolysis suggests that ATP levels are involved in the control of the glycolytic rate (no correlation could be found with the other nucleotides tested or with the ATP/ADP ratio). The other explanation would be that the rate of glycolysis in combination with the energy demand determine the ATP levels. However, if this would be the case it ought to be a positive correlation between ATP content and glycolytic flux. Instead, our study (12) showed that the highest rates of glycolysis was obtained during energy excess and low ATP levels (Fig. 2). The clear correlation between intracellular ATP content and glycolytic flux is probably a reflection of allosteric regulation of glycolysis. Also the possibility that glycolytic flux may be regulated by adjustment of the level of glycolytic enzymes was studied (12). However, this seems not to be the case since the enhanced glycolytic flux obtained under energy excess was in fact accompanied with a decrease in the amount of glycolytic enzymes, most notably HXK2 and ENO1 (Fig. 1). Hexokinase (HXK) and phosphofructokinase (PFK) are considered as key enzymes in the control of glycolytic flux. PFK is subject to a number of allosteric regulators including an inhibition by ATP (7, 17). Reibstein *et al.* (17) reported that PFK activity did decrease when the ATP concentration was changed from 1.5 to 3.1 mM and different ADP concentrations was without effect. However, PFK activity was said to be virtually independent of ATP concentrations ranging from 2 to 5 mM (17). Similarly, Caubet *et al.* (5) showed a very low effect on PFK activity when the ATP concentration was raised above 0.5 mM. By assuming an intracellular volume of 2 µl/mg (14) the ATP concentrations in the present study ranged from approximately 1.1 - 4.6 mM. In other words, by extrapolating these *in vitro* data, the measured ATP concentrations seem to be higher than the range where it controls PFK activity. Concerning HXK2 it has been reported that the activity of this enzyme is inhibited by ATP concentrations above 2 mM ATP (10). When the conditions changed gradually from energy limitation to energy excess the resulting increased glycolytic flux might be due to an increased HXK2 activity regulated by the ATP level. However, this is based on *in vitro* data and it might very well be that *in vivo* ATP exerts control of glycolytic flux by regulating the activity of HXK2 as well as PFK (or even more enzymes). Furthermore, the control of glycolytic rate is more complex than just involving ATP. For instance, benzoic acid addition or transition from anaerobic to aerobic conditions changed the relation between ATP content and rate of glycolysis implying that more factors are involved in this control.

ACKNOWLEDGEMENTS

Financial support from Nordic Industrial Fund (NIF) and Swedish National Board for Technical Development (NUTEK) are gratefully acknowledged.

REFERENCES

1. Albers, E., C. Larsson, G. Lidén, C. Niklasson, and L. Gustafsson (1996) Appl. Environ. Microbiol. 62, 3187-3195.
2. Beauvoit, B., M. Rigoulet, O. Bunoust, G. Raffard, P. Canioni, and B. Guérin (1993) Eur. J. Biochem. 214, 163-172.
3. Blazquez, M. A., R. Lagunas, C. Gancedo, and J. M. Gancedo (1993) FEBS Lett. 329, 51-54.
4. Campbell-Burk, S. L., and R. G. Shulman (1987) Ann. Rev. Microbiol. 41, 595-616.
5. Caubet, R., B. Guerin, and M. Guerin (1988) Arch. Microbiol. 149, 324-329.
6. Fell, D. (1997) Understanding the control of metabolism. Portland Press, London.
7. Gancedo, C., and R. Serrano (1989) Energy-yielding metabolism, p. 206-259. *In* A. H. Rose and J. S. Harrison (ed.), The yeasts, vol. 3. Academic Press Limited, London.
8. Garrels, J. J. (1989) J. Biol. Chem. 264, 5269-5282.
9. Gustafsson, L. (1979) Arch. Microbiol. 120, 15-23.
10. Kopetzki, E., and K. E. Entian (1985) Eur. J. Biochem. 146, 657-662.
11. Larsson, C., U. von Stockar, I. Marison, and L. Gustafsson (1993) J. Bacteriol. 175, 4809-4816.
12. Larsson, C., Nilsson A., Blomberg, A., and L. Gustafsson (1997) J. Bacteriol. 179, 7243-7250.
13. Liden, G., A. Persson, L. Gustafsson, and C. Niklasson (1995) Appl. Microbiol. Biotechnol. 43, 1034-1038.
14. Meredith, S. A., and A. H. Romano (1977) Biochem. Biophys. Acta. 497, 745-759.
15. Morrisey, J. H. (1981) Anal. Biochem. 117, 307-310.
16. Norbeck, J., and A. Blomberg (1997) Yeast. Accepted.
17. Reibstein, D., J. A. den Hollander, S. J. Pilkis, and R. G. Shulman (1986) Biochemistry. 25, 219-227.
18. Rieger, M., O. Käppeli, and A. Fiechter (1983) J. Gen. Microbiol. 129, 653-661.
19. Roels, J. A. (1983) Energetics and kinetics in biotechnology. Elsevier Biomedical Press, Amsterdam.
20. Teusink, B., Diderich, J.A., Westerhoff, H.V., van Dam, K. and M.C. Walsh (1998) J. Bacteriol. 180, 556-562.
21. Thevelein, J.M. and S. Hohmann (1995) TIBS 20, 3-10.
22. van Urk, H., P. R. Mak, W. A. Scheffers, and J. P. van Dijken (1988) Yeast. 4, 283-291.
23. Verduyn, C., E. Postma, W. A. Scheffers, and J. P. van Dijken (1992) Yeast. 8, 501-517.
24. Verduyn, C., A. H. Stouthamer, W. A. Scheffers, and J. P. van Dijken (1991) Antonie van Leeuwenhoek. 59, 49-63.

69

MODULATION OF RATS DIGESTIVE GLANDS RESISTANCE TO ACTION OF IONIZING RADIATION BY MEANS OF SODIUM ALFA-KETOGLUTARATE

N.Kurgaliuk, O.Goryn

Department of Physiology, Biology Faculty, Ivan Franko Lviv State University, Lviv 290005, Hrushevsky Str. 4, Ukraine, (0322) 794786, e-mail: natalia@mitoch.lviv.ua

Keywords: ADP-dependent respiration, alfa-ketoglutarate (KG), ionizing radiation

INTRODUCTION

Regulation of organism neurohormonal status during irradiation and other time periods after it can be one of the ways of functional influence on organizm radioresistance. Numerous investigation performed in our laboratory showed that injection of Citric Acid Cycle (CAC) intermediates can influence autonomic nervous system status. Succinate (SC) injection has proved to increase adrenergetic nervous system activity [1]. Significant role in increasing the organizm resistance to extremal environment conditions belongs to cholynergic influences. Our investigations showed the injection of cholynomimetic substance (karbacholine) (30 min befor irradiation) to make normal change postirradiation disfunctions of respiration and oxidative phosphorylation processes in mitochondria (MCH) of hepato- and enterocytes towards normalization [2]. The KG injection activates cholynergic regulation mechanism connected with correlation changes in acetylcholin-cholinesterase system [3]. However, KG influence on the organizm resistance to high-dose irradiation has not been studied.

METHODS

Influence of high-dose irradiation was modeled by RUM-17. The animal group (235 white rats) was totally irradiated by dose 259 mKl/kg. Half of the group was injected KG (20 mg/100g body weight) 1 hour after irradiation. Another half was injected a similar volume of saline solution for control. Animals were decapitated 1, 2, 3, 24 and 72 hours after KG injection. MCH of hepatocytes and enterocytes were extracted by differential centrifuging and respiration was measured by polarographyc method in different metabolic states. Enzymes activity was measured spectrophotometrically by using Osadcha technique (alanine-, aspartateaminotransferase) and according to Eschenko-Volsky technique (succinatedehydrogenase) in samples freesed in liquid nitrogenium. The obtained results were statistically procesed and a mean statistic value M and mean statistic error m were defined. Students` criterion was used.

RESULTS AND DISCUSSION

The KG injection 30 min befor irradiation aggravated irradiation damage influence the rat organizm. On the 30th day after irradiation animals mortality was 92% ($p<0{,}001$). The same symptoms of intestinal form of irradiation desease were observed in the animal group which received KG 3 hours after irradiation. However injection made 1 and 2 hours after X-ray treatment resulted in the increasing of rats vitality. The effect of KG injection made 1 hour after irradiation was more pronounced.

Our preliminary studies showed that KG injection at early terms after ionizing irradiation in minimal lethal dose decrease intensity of oxygen consumption through the activation of cholynergic regulation mechanism. However, sodium of KG normalized cell energy metabolism thruogh increasing the coupling respiration and oxidative phosphorylation [4].

Total irradiation depressed ADP-dependent respiration, decreased ADP phosphorylation during SC and KG oxidation. Coupling of respiration and oxidative phosphorylation during KG oxidation decrease significantly. By the end of the first twenty-four hours after irradiation the speed of ADP-stimulated respiration was reduced by 25% during KG oxidation and by 13,3% during SC as compared to unirradieted control. Effectiveness of ADP-phosphorylation was 20% lower for SC. Activity of alanine- and aspartateaminotransferase in digestive organs tissues (liver, pancreas, mucos intestinum tenue) were siggnificatly decreased. However, succinatedehydrogenase actyvity was increased.

The parentheral KG injection 1 hour after irradiation in minimal lethal dose improved indices of oxidative phosphorylation in the hepatocytes and enterocytes MCH already 2 hours after irradiation when both CAC substrates were used. As a result, the speed of phosphorylative respiration during SC and KG oxidation increased even more then the same in nonirradiated animals; coupling of respiration and phosphorylation became normal.

We observed a similar KG normalization effect on MCH processes twenty-four hours after irradiation. The speed of phosphorylative respiration increased by 22,6% and 32,7% during KG and SC oxidation accordingly as compered to irradiation without KG injection.

Many experiments demonstrated that irradiation in lethal doses provoked sharp discoupling of respiration and phosphorylation processes in rabit and rat liver MCH 1 hour after irradiation. It is connected with disfunction electron and proton transportation in respirative chain [2]. With the help of specific inhibitors of electron transportationit was determined that 2 points of macroergs synthesis connected with SC oxidation damage by irradiation influence. Irradiation provokes structure-functional changes in MCH, activates MCH ATP-ase. These changes result in the decrease of ATP content and swelling of MCH.

A great role in oxygen consumption during exogenic KG oxidation, is known, to belong to endogenic KG generated from SC. That is why we studied phosphorylative respiration while adding malonic acid (succinatedehydrogenase inhibitor). Addition of KG and malonic acid to MCH suspension decreased KG oxidation> However, activating influence of KG injection on mitochondrial KG oxidation was better. Thus while stimulation of ADP-dependent respiration 24-hours after KG injection into irradiated rats was 6,3%, with malonic acid it was 41,2%. Under these condions stimulating effect of KG on SC oxidation (24 hour after irradiation) was blocked by addition of rotenone into incubation mixture (inhibitor of electron transport in respirative chane of MCH). The above obviously demonstrates the fact of contribution of NAD-dependentsubstrates of oxidation to stimulation of respiration during SC oxidation.

Session 5

Metabolic Modeling
& Applications

The influence of KG on energy metabolism in MCH of irradiated animals can occurs in several ways. The first way is the activating influence of KG on glutamate-malate mixture oxidation (152,3%, p< 0,01) and glutamate-pyruvate mixture (124,1%, p<0,05) as compared to irradiated animals.This causes the increase of endogenic KG synthesis as a result of aminotransferases reactions and to the increase of anabolic methabolism level. Shuch fact to cofirm by increasing of alanine- and aspartateaminotransferase activity in tissues of digestive organs (liver, pancreas, mucos intestinum tenue) during 72 hour after KG injection.

The second way is two-fold increase of GTP concentration [5] as a result phosphorylation on substrate level during KG oxidation. Increasing GTP concentration leads to decreasing cAMP/cGMP correlation. Such condition is favourable for realization of cholynergic nervous system influences increasing radioresistance and vitality of animal organizms.

Consequently, we can make a conclusion that KG injection 1 hour after irradiation of rats in minimal lethal dose results in a considerable activation of energy processes in MCH of irradiated animals towards their normalization. It is important for energy support of the functional activity of the organizm to the influence of stress irritants, specifically to ionizing irradiation.

REFERENCES

1.Babsky, A.M., Doliba, N.M., Shostakovskaya, I.V. (1990) VI-th Eur.Bioenerg.Conf. Reports 92.
2. Doliba,N.M. at all (1989) Radiobiology Meeting Reports 5, 1026-1027
3. Kurgaliuk, N.M. (1996) EBEC Short Reports 9,179
4. Doliba at all (1993) 39,5-6, 65-70.
5. Lozinskaya, I.N. at all (1992) Radiobiology 32, 4 534-539.

ELEMENTARY MODES ANALYSIS ILLUSTRATED WITH HUMAN RED CELL METABOLISM

Stefan Schuster[1,2,*], *David A. Fell*[3], *Thomas Pfeiffer*[2,4], *Thomas Dandekar*[1,5] *and Peer Bork*[1,5]

[1]Max Delbrück Center for Molecular Medicine, D-13125 Berlin-Buch, Germany
[2]Humboldt University Berlin, Institute of Biology, D-10115 Berlin, Germany
[3]School of Biological and Molecular Sciences, Oxford Brookes University, Headington, Oxford OX3 0BP, U.K.
[4]Universidad Complutense de Madrid, Depto. de Bioquímica y Biología Molecular I, E-28040 Madrid, Spain
[5]EMBL, Biocomputing Unit, Meyerhofstr. 1, D-69012 Heidelberg, Germany
[*]Corresponding author, phone +49-30-94063125, FAX +49-30-94062834, e-mail schuster@bp.biologie.hu-berlin.de

INTRODUCTION

Analysing the topology of metabolic charts has recently attracted renewed interest in the light of functional genomics [1,2]. A widely used method for assigning genes to enzyme functions is sequence comparison and the search for orthologous genes in the organism under study and a better characterised organism [1,3]. However, a significant proportion of the genes still remain unidentified. Given these uncertainties it seems promising to go beyond the purely genetic approach and put the individual proteins into the context of higher-order processes such as metabolic pathways.

Methods for the structural (topological) analysis of metabolic pathways have been improved considerably in the last decade [4 8]. A modern approach in this analysis is by detecting basic biochemical production routes. These routes are referred to as "biochemical pathways" [4], "elementary flux modes" [6,9], or "basic reaction modes" [7].

Roughly speaking, an elementary flux mode is a flux pattern which can be accomplished at steady state (with all the irreversible reactions proceeding in the appropriate direction) and cannot be decomposed into two simpler flux distributions. Such a mode can be characterised by indicating the enzymes involved and the proportions of fluxes carried by these enzymes. The modes correspond to routes through, or cycles within, the system. All steady-state flux distributions in a reaction network are superpositions of elementary modes. A mathematically sound definition of this concept and an algorithm for computing all elementary modes for systems of any complexity have been given earlier [10]. The approach has been used, for example, in determining optimal routes in the synthesis of precursors of aromatic amino acids [7] and in the investigation of optimal stoichiometric structures in carbohydrate metabolism [8].

In the present paper, we apply the elementary modes approach to the human red blood cell. We have chosen this cell as an exemplifying system because its metabolism is very simple and very well known. For the same reason, this cell has been the subject of intense kinetic modelling [9,11–13]. Since during maturation of the human erythrocyte, the nucleus is eliminated, this cell might, at first sight, be of no interest in the context of genome analysis. However, the enzymes operating in mature erythrocytes originate, after all, from gene translation. The approach can then be ported to more complex cells (harbouring genetic information) in a straightforward way.

METHODS

As for the metabolites and other substances, it is usual practice in modelling to make a technical distinction between external and internal metabolites. External metabolites (sources and sinks) are buffered by connection to reservoirs. The internal metabolites, by contrast, do not participate in reactions other than those included in the model. For these metabolites, it is sensible to apply a quasi-steady-state hypothesis.

The erythrocyte is a prominent example of a cell whose metabolism operates at a stationary state. In our analysis, we use the reaction scheme shown in Fig. 1. On the basis of a slightly simpler scheme, Joshi and Palsson [11] and Ni and Savageau [13] developed the most comprehensive kinetic models of human erythrocyte metabolism so far existing.

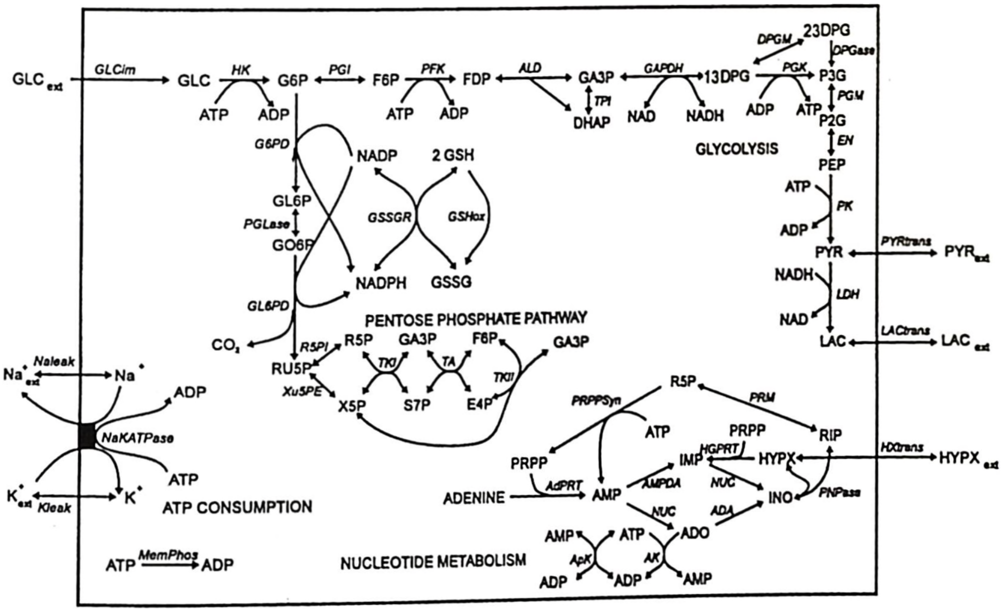

Figure 1. Scheme of the main reactions proceeding in human red blood cells. All metabolites with the subscript ext as well as adenine and CO_2 are considered as external substances. Reversible reactions are indicated by double arrow-heads. The abbreviation MemPhos is used for a group of enzymes responsible for the phosphorylation of membrane lipids and proteins and for establishing the lipid asymmetry in the bilayer membrane.

The algorithm for computing all elementary modes for reaction systems of any complexity [10] has been implemented as computer programs in Turbo-Pascal by Claus Hilgetag (Newcastle) and SmallTalk by John Woods (Oxford). Recently, one of the authors (T.P.) wrote a program in C (GNU - public license) which runs under UNIX and can easily be included in larger simulation packages. Using pointer variables, it can readily cope with the varying size of intermediate tableaux in the course of the algorithm. The reaction equations (or optionally the stoichiometry matrix) and the information about which reactions are irreversible are required as the only inputs. Care should be taken where an enzymic protein catalyses more than one reaction, whether the same chemical reaction with alternate substrates at a single active site, or different reactions at separate active sites. In the system shown in Fig. 1, this concerns 5'-nucleotidase (NUC), which dephosphorylates both IMP and AMP, DPGM and DPGase, which reside on the same protein (cf. [14]), and the two functions of transketolase (TKI and TKII).

RESULTS

Running any one of the above-mentioned computer programs for the scheme of erythrocyte metabolism shown in Fig. 1 gives the 21 elementary modes listed in Table 1.

These elementary modes can be interpreted in terms of biochemical function. For example, mode 8 represents glycolysis plus the Na^+ and K^+ transport across the erythrocyte membrane. So the ATP produced in glycolysis is utilized by the Na^+/K^+-ATPase. Mode 21 represents the pentose phosphate pathway (PPP) in a certain combination with several reactions of glycolysis (which form the link to the surroundings of the cell). Interestingly, there are different combinations of the PPP and glycolysis. While in mode 21, PGI is not involved while PFK is, it is the other way round in mode 19, with PGI proceeding backwards.

Some of the calculated modes differ only slightly from each other. For example, modes (4) and (6) coincide apart from the exchange of AMPDA and ADA. The modes (7), (8) and (11) only differ in the way of utilization of the ATP produced in glycolysis. Whereas in mode (7), ATP is used for membrane phosphorylation, it is used for Na^+ and K^+ transport in mode (8) and for driving the futile cycle formed by AMP and AK in mode (11). It is therefore sensible to group the modes. An objective criterion for this grouping is the overall stoichiometry for the external metabolites. By inspecting the 21 elementary modes, we see that there are 6 different overall stoichiometries for the erythrocyte system.

It is worth noting that none of the modes calculated contains pyruvate export. This is because in the network considered [11,13], the steady state condition requires that the NADH formed by GAPDH must be reduced by LDH. However, part of the NADH is actually used to reduce the methemoglobin permanently generated by autoxidation of hemoglobin. If this reaction were included, modes involving pyruvate transport would arise. So detection of elementary modes is a helpful tool in testing the completeness of a model system.

Another field of application is provided by the enzyme deficiencies important in medicine. These are in fact related to the issue of missing links in bacterial metabolism.

For analysing enzymopathies, it is necessary first to decide which cell functions are compulsory. In erythrocytes, these are at least the generation of redox capacity for coping with the oxidative stress as well as the Na^+/K^+-ATPase activity for establishing the osmotic balance. Other functions, probably of lesser importance, are membrane phosphorylation and maintenance of the lipid asymmetry and of the level of 2,3DPG, which is an important modulator of oxygen binding to hemoglobin. For fulfilling the latter function, for example, at least one of the modes 19–21 involving DPGM and DPGase is physiologically desirable, although they give a lower ATP yield than the modes involving PGK. Complete lack of DPGM/DPGase is not critical, though, but leads to mild erythrocytosis to compensate for the increased affinity of hemoglobin to oxygen [14].

As all the modes computed involve HK and PK, one can substantiate the well-known result that severe HK or PK deficiencies lead to hemolytic anemia [14]. Our results are also in agreement with the finding that an absence of ADA is non-critical [15]. Indeed, any mode involving ADA has a counterpart involving AMPDA with the same overall stoichiometry.

G6PD defects (favism) belong to the most wide-spread enzymopathies in man and are notorious for causing side-effects in drug therapy. This enzyme is indispensable to protect cells against even mild oxidative stress (cf. [12,16]). Lack of G6PD impedes operation of all modes but the ones numbered 7–12 and 20. These modes do not involve the glutathione oxidation reaction, which is necessary for meeting the oxidative stress. Pandolfi and coworkers [16] stated that in the absence of G6PD, there is still a pathway leading from glucose to ribose via the TK and TA reactions. We have checked this by calculating the flux modes in a system where G6PD is blocked and ribose-5-phosphate (R5P) is considered external. This gives 20 modes, with one of them actually performing a transformation from glucose to R5P:

4 GLC ---> 3 R5P + 3 LACext {4HK 4PGI 2PFK 2ALD 2TPI 3GAPDH 3PGK 3PGM 3EN 3PK 3LDH 3LACex 2R5PI –2Xu5PE –TKI –TKII –TA}.

The effects of erythrocyte enzymopathies have been studied earlier on the basis of a smaller reaction scheme, lacking the adenine nucleotide metabolism and considering PRPP as an external metabolite [12]. It was concluded that complete deficiencies of DPGM, Xu5PE, TK or TA could be tolerated. It was stated, however, that the importance of the enzymes of the nonoxidative PPP were possibly underestimated because the salvage pathway was neglected in the model. This issue can easily be tested by our approach. In the reaction scheme shown in Fig. 1, blocking of any one of the enzymes Xu5PE, TK and TA suppresses all modes in which the NADPH producing enzymes G6PD and GL6PD are involved. This leads to the conclusion that the enzymes of the nonoxidative PPP are indispensable.

Elementary modes analysis allows one to detect all means of ATP utilization in the system, by treating ATP and ADP as externals and all other substances as internals. For the system considered, this gives the following four modes: {MemPhos}, {–2KLeak 3NaLeak NaKATPase}, {AMPase AK}, and {–ApK NUC PNPase PRM PRPPsyn HGPRT}. The latter two of these are futile cycles, with the last one hardly detectable by inspection.

Table 1. Elementary modes for the reaction scheme of erythrocyte metabolism given in Fig. 1. The enzyme names written in braces indicate the enzymes used in the respective mode. Negative values indicate the reaction is used in the reverse sense.

(1) GLCext —> LACext + 3 CO2 {GLCim HK -2PGI GAPDH PGK PGM EN PK LDH LACtrans MemPhos 3G6PD 3PGLase 3GL6PD 6GSSGR 6GSHox R5PI 2Xu5PE TKI TKII TA}

(2) GLCext —> LACext + 3 CO2 {GLCim HK -2PGI GAPDH PGK PGM EN PK LDH LACtrans 3G6PD 3PGLase 3GL6PD 6GSSGR 6GSHox R5PI 2Xu5PE TKI TKII TA -2KLeak 3NaLeak NaK-ATPase}

(3) 2 GLCext —> 2 LACext + 6 CO2 {GLCim 2HK -4PGI 2GAPDH 2PGK 2PGM 2EN 2PK 2LDH 2LACtrans -ApK 6G6PD 6PGLase 6GL6PD 12GSSGR 12GSHox 2R5PI 4Xu5PE 2TKI 2TKII 2TA NUC PNPase PRM PRPPsyn HGPRT}

(4) 2 GLCext + Adenine —> HYPXext + 2 LACext + 6 CO2 {2GLCim 2HK -4PGI 2GAPDH 2PGK 2PGM 2EN 2PK 2LDH 2LACtrans -ApK AMPDA AdPRT 6G6PD 6PGLase 6GL6PD 12GSSGR 12GSHox 2R5PI 4Xu5PE 2TKI 2TKII 2TA NUC PNPase PRM PRPPsyn HXtrans}

(5) GLCext —> LACext + 3 CO2 {GLCim HK -2PGI GAPDH PGK PGM EN PK LDH LACtrans NUC AK 3G6PD 3PGLase 3GL6PD 6GSSGR 6GSHox R5PI 2Xu5PE TKI TKII TA}

(6) 2 GLCext + Adenine —> HYPXext + 2 LACext + 6 CO2 {2GLCim 2HK -4PGI 2GAPDH 2PGK 2PGM 2EN 2PK 2LDH 2LACtrans NUC ADA -ApK AdPRT 6G6PD 6PGLase 6GL6PD 12GSSGR 12GSHox 2R5PI 4Xu5PE 2TKI 2TKII 2TA PNPase PRM PRPPsyn HXtrans}

(7) GLCext —> 2 LACext {GLCim HK PGI PFK ALD TPI 2GAPDH 2PGK 2PGM 2EN 2PK 2LDH 2LACtrans 2MemPhos}

(8) GLCext —> 2 LACext {GLCim HK PGI PFK ALD TPI 2GAPDH 2PGK 2PGM 2EN 2PK 2LDH 2LACtrans -4KLeak 6NaLeak 2NaK-ATPase}

(9) GLCext —> 2 LACext {GLCim HK PGI PFK ALD TPI 2GAPDH 2PGK 2PGM 2EN 2PK 2LDH 2LACtrans -ApK NUC PNPase PRM PRPPsyn HGPRT}

(10) GLCext + Adenine —> HYPXext + 2 LACext {GLCim HK PGI PFK ALD TPI 2GAPDH 2PGK 2PGM 2EN 2PK 2LDH 2LACtrans -ApK AMPDA AdPRT NUC PNPase PRM PRPPsyn HXtrans}

(11) GLCext —> 2 LACext {GLCim HK PGI PFK ALD TPI 2GAPDH 2PGK 2PGM 2EN 2PK 2LDH 2LACtrans 2NUC 2AK}

(12) GLCext + Adenine —> HYPXext + 2 LACext {GLCim HK PGI PFK ALD TPI 2GAPDH 2PGK 2PGM 2EN 2PK 2LDH 2LACtrans NUC ADA -ApK AdPRT PNPase PRM PRPPsyn HXtrans}

(13) 3 GLCext —> 5 LACext + 3 CO2 {3GLCim 3HK 2PFK 2ALD 2TPI 5GAPDH 5PGK 5PGM 5EN 5PK 5LDH 5LACtrans 5MemPhos 3G6PD 3PGLase 3GL6PD 6GSSGR 6GSHox R5PI 2Xu5PE TKI TKII TA}

(14) 3 GLCext —> 5 LACext + 3 CO2 {3GLCim 3HK 2PFK 2ALD 2TPI 5GAPDH 5PGK 5PGM 5EN 5PK 5LDH 5LACtrans 3G6PD 3PGLase 3GL6PD 6GSSGR 6GSHox R5PI 2Xu5PE TKI TKII TA -10KLeak 15NaLeak 5NaK-ATPase}

(15) 6 GLCext —> 10 LACext + 6 CO2 {6GLCim 6HK 4PFK 4ALD 4TPI 10GAPDH 10PGK 10PGM 10EN 10PK 10LDH 10LACtrans -5ApK 6G6PD 6PGLase 6GL6PD 12GSSGR 12GSHox 2R5PI 4Xu5PE 2TKI 2TKII 2TA 5NUC 5PNPase 5PRM 5PRPPsyn 5HGPRT}

(16) 6 GLCext + 5 Adenine —> 5 HYPXext + 10 LACext + 6 CO2 {6GLCim 6HK 4PFK 4ALD 4TPI 10GAPDH 10PGK 10PGM 10EN 10PK 10LDH 10LACtrans -5ApK 5AMPDA 5AdPRT 6G6PD 6PGLase 6GL6PD 12GSSGR 12GSHox 2R5PI 4Xu5PE 2TKI 2TKII 2TA 5NUC 5PNPase 5PRM 5PRPPsyn 5HXtrans}

(17) 3 GLCext —> 5 LACext + 3 CO2 {3GLCim 3HK 2PFK 2ALD 2TPI 5GAPDH 5PGK 5PGM 5EN 5PK 5LDH 5LACtrans 5NUC 5AK 3G6PD 3PGLase 3GL6PD 6GSSGR 6GSHox R5PI 2Xu5PE TKI TKII TA}

(18) 6 GLCext + 5 Adenine —> 5 HYPXext + 10 LACext + 6 CO2 {6GLCim 6HK 4PFK 4ALD 4TPI 10GAPDH 10PGK 10PGM 10EN 10PK 10LDH 10LACtrans 5NUC 5ADA -5ApK 5AdPRT 6G6PD 6PGLase 6GL6PD 12GSSGR 12GSHox 2R5PI 4Xu5PE 2TKI 2TKII 2TA 5PNPase 5PRM 5PRPPsyn 5HXtrans}

(19) GLCext —> LACext + 3 CO2 {GLCim HK -2PGI GAPDH DPGM DPGase PGM EN PK LDH LACtrans 3G6PD 3PGLase 3GL6PD 6GSSGR 6GSHox R5PI 2Xu5PE TKI TKII TA}

(20) GLCext —> 2 LACext {HK PGI PFK ALD TPI 2GAPDH 2DPGM 2DPGase 2PGM 2EN 2PK 2LDH 2LACtrans}

(21) 3 GLCext —> 5 LACext + 3 CO2 {3GLCim 3HK 2PFK 2ALD 2TPI 5GAPDH 5DPGM 5DPGase 5PGM 5EN 5PK 5LDH 5LACtrans 3G6PD 3PGLase 3GL6PD 6GSSGR 6GSHox R5PI 2Xu5PE TKI TKII TA}

An important application is blood banking. It was observed that blood could be preserved longer when stored in the presence of adenosine or inosine (cf. [17]). This is firstly due to retardation of the progressive loss of adenine nucleotides. Secondly, it might be speculated that the ribose moiety involved in adenosine could be used as a carbon source. We therefore computed the elementary modes for the case where GLCim is blocked (which is equivalent to glucose starvation) and adenosine (ADO) is treated as an external metabolite. This gives rise to 36 modes. 13 of them perform the transformation ADO ---> HYPX + 2 CO2 + LACext. As in the modes given in Table 1, production of lactate and CO_2 is accompanied with regeneration of ATP and NADPH, respectively. For example, there exists the following mode: {–2PGI GAPDH PGK PGM EN PK LDH LACex AK AMPDA 2G6PD 2PGLase 2GL6PD 4GSSGR 4GSHox 2Xu5PE TKI TKII TA NUC PNPase PRM –2KLeak 3NaLeak NaKATPase}. When inosine (INO) instead of adenosine is treated as external, 24 modes arise. 9 of them realize the transformation INO ---> HYPX + 2 CO2 + LACext, while 7 of them have the overall stoichiometry 3 INO ---> 3 HYPX + 5 LACext.

Our analysis can be used as a guideline in the reconstruction of bacterial metabolism. For example, it appears that in *Mycoplasma hominis*, PFK and ALD are absent. Moreover, the first three enzymes of the PPP (G6PD, PGLase and GL6PD) are absent from *M. hominis* and many other Mollicutes except *Acholeplasma* species [18,19]. Pollack *et al.* argued that "Nonglycolytics, such as *My. hominis*, bypass these two enzyme deficiencies: PFK and aldolase... G6P enters the PPP and eventually appears as glyceraldehyde-3-phosphate that enters the EMP below... This may be a great advantage because by reentering the EMP without reacting with PFK, an equivalent of one ATP is saved." [19, pp.291-292]. However, it can be seen in Table 1 that there is no mode lacking PFK, ALD, and the enzymes of the oxidative PPP (not even one lacking PFK and G6PD only). We have checked this by calculating the modes when these enzymes are absent. The set of elementary modes is then actually empty. This is understandable because several intermediates of the PPP such as E4P would not be regenerated in any mode bypassing these five enzymes. So the above finding of Pollack and coworkers has to be critically reexamined, either by biochemical assays or by function assignment of sequenced genes.

DISCUSSION

An elementary mode is a minimal set of enzymes that can operate at steady state. It can be interpreted as a biochemical pathway with a specific biological function. By detecting these modes, the stoichiometric feasibility of observed, desired or hypothesized biotransformations can be tested. In medical applications, intricate consequences of inherited or acquired enzyme deficiencies with respect to substrate flows can be assessed. These are not always obvious from inspection of the metabolic map. As for the assignment of enzyme functions to newly sequenced genes, the method may provide missing links in the reconstructed pathways.

The present paper is devoted to the pathway analysis of the human erythrocyte. We have detected all routes through the metabolic network and showed how to detect futile cycles. Although this cell lives on a single carbon substrate, its metabolism represents a superposition of elementary flux modes. The proportions of the modes in this combination depend on conditions such as oxidative stress (the higher this stress is, the higher will be the proportion of the modes involving the PPP), osmotic pressure of the extracellular medium, glucose starvation, oxygen pressure (depending, for example, on altitude), coagulation, malaria infection etc. Even if pure modes are not realizable in this cell, their detection is in line with the classical scientific methodology based on analysis, which in Greek means 'decomposition.' An illustrative analogy is the decomposition of sounds into pure harmonics.

REFERENCES

[1] R.L. Tatusov, A.R. Mushegian, P. Bork et al., Metabolism and evolution of Haemophilus influenzae deduced from a whole-genome comparison with Escherichia coli, Curr. Biol. 6, (1996) 279-291.

[2] E. Selkov, N. Maltsev, G.J. Olsen, R. Overbeek, W.B. Whitman, A reconstruction of the metabolism of *Methanococcus janaschii* from sequence data, Gene 197 (1997) GC11-GC26.

[3] M. Huynen, Y. Diaz-Lazcoz, P. Bork, Differential genome display, Trends Genet. 13 (1997) 389-390.

[4] M.L. Mavrovouniotis, G. Stephanopoulus, G. Stephanopoulus, Computer-aided synthesis of biochemical pathways, Biotechnol. Bioeng. 36 (1990) 1119-1132.

[5] D.A. Fell, Substrate cycles: theoretical aspects of their role in metabolism, Comm. Theor. Biol. 6 (1990) 1-14.

[6] S. Schuster, C. Hilgetag, On elementary flux modes in biochemical reaction systems at steady state, J. Biol. Syst. 2 (1994) 165-182.

[7] J.C. Liao, S.-Y. Hou, Y.-P. Chao, Pathway analysis, engineering, and physiological considerations for redirecting central metabolism, Biotechnol. Bioeng. 52 (1996) 129-140.

[8] J.C. Nuño, I. Sánchez-Valdenebro, C. Pérez-Iratxeta, E. Meléndez-Hevia, F. Montero, Network organization of cell metabolism: monosaccharide interconversion, Biochem. J. 324 (1997) 103-111.

[9] R. Heinrich, S. Schuster, The Regulation of Cellular Systems, Chapman & Hall, New York, 1996.

[10] S. Schuster, C. Hilgetag, J.H. Woods, D.A. Fell, Elementary modes of functioning in biochemical networks, in: Computation in Cellular and Molecular Biological Systems (R. Cuthbertson, M. Holcombe, R., Paton, eds), World Scientific, Singapore., 1996, pp. 151-165.

[11] A. Joshi, B.O. Palsson, Metabolic dynamics in the human red cell. I. A comprehensive kinetic model, J. Theor. Biol. 141 (1989) 515-528.

[12] R. Schuster, H.-G. Holzhütter, Use of mathematical models for predicting the metabolic effect of large-scale enzyme activity alterations. Eur. J. Biochem. 229 (1995) 403-418.

[13] T.-C. Ni, M.A. Savageau, Application of Biochemical Systems Theory to metabolism in human red blood cells, J. Biol. Chem. 271 (1996) 7927-7941.

[14] K.R. Tanaka, D.E. Paglia, Pyruvate kinase and other enzymopathies of the erythrocyte, in: The Metabolic and Molecular Bases of Inherited Disease, Vol III (C.R. Scriver et al., eds), McGraw-Hill, New York, 1995, pp. 3485-3511.

[15] E.H. Chen, B.S. Mitchell, Hereditary overexpression of adenosine deaminase in

erythrocytes: Studies in erythroid cell lines and transgenic mice, Blood 84 (1994) 2346-2353.

[16] P. Pandolfi, F. Sonati, R. Rivi, et al. Targeted disruption of the housekeeping gene encoding glucose 6-phosphate dehydrogenase (G6PD): G6PD is dispensable for pentose synthesis but essential for defense against oxidative stress, EMBO J. 14 (1995) 5209-5215.

[17] D.E. Paglia, W.N. Valentine, A.P. Tartaglia, et al., Control of red blood cell adenine nucleotide metabolism. Studies of adenosine deaminase, in: The Red Cell: Fourth Ann Arbor Conference, Alan R. Liss, New York, 1978, pp. 319-335.

[18] D. DeSanits, V.V. Tryon, J.D. Pollack, Metabolism of Mollicutes: the Embden-Meyerhof-Parnas pathway and the hexose-monophosphate shunt, J. Gen. Microbiol. 135 (1989) 683-688.

[19] J.D. Pollack, M.V. Williams, R.N. McElhaney, The comparative metabolism of the Mollicutes (*Mycoplasmas*): The utility for taxonomic classification and the relationship of putative gene annotation and phylogeny to enzymatic function in the smallest free-living cells, Crit. Rev. Microbiol. 23 (1997) 269-354.

RETRO-REGULATION OF THE BACTERIAL PHOSPHOTRANSFERASE SYSTEM: A KINETIC MODEL

Johann M. Rohwer[a,*], *Jan-Hendrik S. Hofmeyr*[a], *Pieter W. Postma*[b]

[a] Dept. of Biochemistry, Univ. of Stellenbosch, Private Bag X1, 7602 Matieland, South Africa
[b] E.C. Slater Institute, BioCentrum, University of Amsterdam, Plantage Muidergracht 12, NL-1018 TV Amsterdam, The Netherlands
[*] Corresponding author. Tel.: +27-21-8083029, Fax: +27-21-8083022, Email: jr@land.sun.ac.za

INTRODUCTION

Glucose uptake in enteric bacteria is catalysed by the phosphotransferase system (PTS), a complex system of proteins responsible for the sequential transfer of a phosphoryl group from phosphoenolpyruvate (PEP) to the glucose molecule, which is phosphorylated concomitantly with the uptake process (reviewed in [1]). The glucose PTS consists of three cytoplasmic proteins (Enzyme I or EI, HPr and $\mathrm{IIA^{Glc}}$) and a membrane-bound protein ($\mathrm{IICB^{Glc}}$), the actual glucose "permease". The five phosphotransfer reactions of the PTS can be summarised as follows, with "P" representing a phosphoryl group:

(a) $\mathrm{EI + PEP \leftrightarrow EI \cdot P + pyruvate}$

(b) $\mathrm{EI \cdot P + HPr \leftrightarrow HPr \cdot P + EI}$

(c) $\mathrm{HPr \cdot P + IIA^{Glc} \leftrightarrow IIA^{Glc} \cdot P + HPr}$

(d) $\mathrm{IIA^{Glc} \cdot P + IICB^{Glc} \leftrightarrow IIA^{Glc} + IICB^{Glc} \cdot P}$

(e) $\mathrm{IICB^{Glc} \cdot P + Glc_{out} \leftrightarrow IICB^{Glc} + Glc6P_{in}}$

Each PTS component can thus exist in a phosphorylated and an unphosphorylated form. Apart from catalysing glucose uptake, the PTS component $\mathrm{IIA^{Glc}}$ is also a signal transducing protein. The phosphorylated form activates adenylate cyclase, whereas the unphosphorylated form inhibits proteins involved in the uptake systems for lactose, maltose, melibiose and glycerol by stoichiometric binding to these target proteins. This prevents the alternative carbon sources from entering the cell and inducing their own catabolic operons; hence the inhibition process is named "inducer exclusion". Activation of adenylate cyclase and inducer exclusion together account for catabolite repression and the preferential use of PTS carbohydrates above non-PTS carbon sources by enteric bacteria [1,2].

In the case of the glycerol uptake system, $\mathrm{IIA^{Glc}}$ binds to the target protein glycerol kinase [3–5]. (Because glycerol is taken up by facilitated diffusion [6], inhibition of glycerol kinase, the first enzyme in the catabolic pathway, will prevent the intracellular accumulation and metabolism of glycerol.) The crystal structure shows that four $\mathrm{IIA^{Glc}}$ molecules bind to a glycerol kinase tetramer [7] with a Zn(II) ion coordinated in the binding site [8]. Because $\mathrm{IIA^{Glc}}$ sequestered in a complex with glycerol kinase is unable to partake in the phosphotransfer reactions of the PTS, we recently investigated experimentally whether the PTS in turn could be inhibited by glycerol owing to decreased amounts of available $\mathrm{IIA^{Glc}}$. Indeed, the extent of inhibition of PTS-mediated uptake correlated with intracellular levels of glycerol kinase [9,10], demonstrating a "retro-regulation" of the PTS and extending the notion of dominance by the PTS in regulating carbohydrate metabolism to one of multidirectional signal transduction.

In this report we extend our previous kinetic model of the PTS ([9]; Rohwer, J.M., Meadow, N.D, Roseman, S. and Postma, P.W., in preparation) to include binding of IIA^{Glc} to glycerol kinase. We show that, when K_d values in line with experimental literature data are assumed for this binding equilibrium, significant inhibition of the calculated PTS flux occurs with increasing total glycerol kinase concentrations.

METHODS

All numerical simulations were performed on an IBM-compatible PC with the metabolic modelling package SCAMP [11], and the results were checked with Gepasi [12]. Our previous detailed kinetic model of PTS-mediated uptake [9] was extended by including four binding equilibria between a glycerol kinase tetramer (GlpK) and unphosphorylated IIA^{Glc}. The intrinsic dissociation constants for these steps are K_1 to K_4, as follows:

$$\begin{aligned}
&\mathrm{GlpK}\cdot\mathrm{IIA}^{\mathrm{Glc}} \xleftrightarrow{K_1} \mathrm{GlpK}+\mathrm{IIA}^{\mathrm{Glc}}\\
&\mathrm{GlpK}\cdot\left(\mathrm{IIA}^{\mathrm{Glc}}\right)_2 \xleftrightarrow{K_2} \mathrm{GlpK}\cdot\mathrm{IIA}^{\mathrm{Glc}}+\mathrm{IIA}^{\mathrm{Glc}}\\
&\mathrm{GlpK}\cdot\left(\mathrm{IIA}^{\mathrm{Glc}}\right)_3 \xleftrightarrow{K_3} \mathrm{GlpK}\cdot\left(\mathrm{IIA}^{\mathrm{Glc}}\right)_2+\mathrm{IIA}^{\mathrm{Glc}}\\
&\mathrm{GlpK}\cdot\left(\mathrm{IIA}^{\mathrm{Glc}}\right)_4 \xleftrightarrow{K_4} \mathrm{GlpK}\cdot\left(\mathrm{IIA}^{\mathrm{Glc}}\right)_3+\mathrm{IIA}^{\mathrm{Glc}}
\end{aligned} \tag{1}$$

First, the binding sites were assumed to be independent, and all the intrinsic dissociation constants were taken equal to an average dissociation constant K_d. Next, positive cooperativity in binding was simulated by modulating the intrinsic dissociation constants K_i with a factor α as follows:

$$\begin{aligned}
&K_1 \to K_1\alpha^2 \qquad &&K_2 \to K_2\alpha\\
&K_3 \to K_3/\alpha \qquad &&K_4 \to K_4/\alpha^2
\end{aligned} \tag{2}$$

This leaves the average dissociation constant $K_d=\sqrt[4]{K_1K_2K_3K_4}$ unchanged. The model was used to calculate the PTS activity as a function of increasing total glycerol kinase concentrations for $\alpha = 1$ (no cooperativity), 2 (moderate cooperativity) and 100 (approximating "infinite" cooperativity between the binding sites of the glycerol kinase subunits). We verified that the results for $\alpha = 100$ closely matched those of a Hill mechanism (i.e., a single binding equilibrium in which four IIA^{Glc} species bind simultaneously to a GlpK tetramer with a dissociation constant of K_d^4).

RESULTS AND DISCUSSION

The dissociation constant for IIA^{Glc} and glycerol kinase has not been determined experimentally, but K_i values of glycerol kinase for IIA^{Glc} have been reported [8]. Although it is not immediately apparent what such a K_i value means in terms of the binding of four IIA^{Glc} molecules to a glycerol kinase tetramer, we equated K_i with K_d (the average dissociation constant) for simulation purposes. Furthermore, the above K_i value has been shown to decrease from 16.6 to 0.28 μM as the Zn(II) concentration in the assay was increased from zero to 0.1 mM [8], confirming a role for Zn(II) in the binding site.

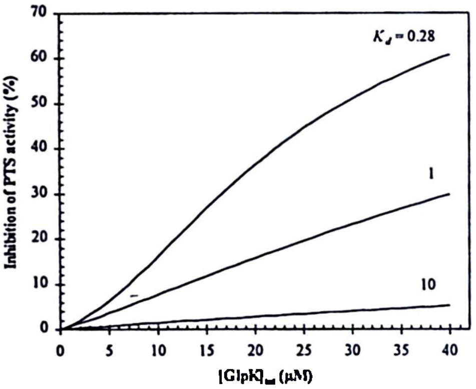

Figure 1. Calculated inhibition of PTS activity with increasing total glycerol kinase concentrations. The interaction of glycerol kinase and IIA$^{\text{Glc}}$ was simulated as described under Methods for the indicated values (in µM) of the average dissociation constant K_d. Other model parameters are taken from [9]. The uninhibited reference flux was 25.9 mM min^{-1}.

First, we calculated the inhibition of PTS activity as a function of increasing total glycerol kinase concentration using different values of the average dissociation constant K_d (Fig. 1). In this simulation we assumed the binding sites on the glycerol kinase tetramer to be independent and not to exhibit cooperativity. The model shows that significant inhibition of PTS activity (i.e., around 60 %, which was also found experimentally [9,10]) was only observed when the K_d equalled 0.28 µM. Hardly any inhibition was observed when K_d was taken as 10 µM. Of course, the extent of inhibition might have been greater if we had increased the total glycerol kinase concentration to higher levels. However, it seems unlikely that the intracellular glycerol kinase concentration should increase above that of IIA$^{\text{Glc}}$ (40 µM) after growing the cells on glycerol for only 3 h as in the experimental protocol [9,10]. The modelling result thus confirms that tight enough binding between glycerol kinase and IIA$^{\text{Glc}}$ requires the presence of Zn(II) ions.

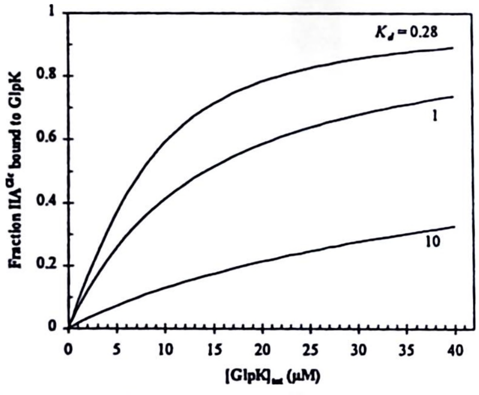

Figure 2. Sequestration of IIA$^{\text{Glc}}$ by glycerol kinase. The fraction of IIA$^{\text{Glc}}$ bound to glycerol kinase is shown for the different K_d values. Simulation conditions were as in Fig. 1. The total IIA$^{\text{Glc}}$ concentration was kept constant at 40 µM.

Next, we calculated the fraction of the total amount of IIA$^{\text{Glc}}$ that was bound to glycerol kinase for the different K_d values (Fig. 2). Although some 32 % of the total IIA$^{\text{Glc}}$ was sequestered at a total glycerol kinase concentration of 40 µM for a K_d of 10 µM, the PTS activity was almost unaffected (Fig. 1). This illustrates the important point that the flux-response coefficient [13] of IIA$^{\text{Glc}}$ in PTS-mediated uptake is zero at normal levels of this enzyme, as determined experimentally [14] and verified by kinetic modelling [9]. In order for the PTS activity to be inhibited by any significant extent—i.e., for IIA$^{\text{Glc}}$ to become flux-controlling—at least 70 % of the total IIA$^{\text{Glc}}$ must be sequestered into an inactive complex with glycerol kinase (cf. Figs. 1 and 2).

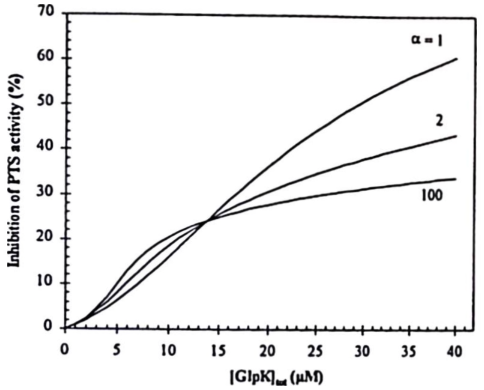

Figure 3. Effect of cooperative binding between IIA^{Glc} and glycerol kinase on the inhibition of PTS activity. Dissociation constants were modulated with the cooperativity factor α as described under Methods. $K_d = 0.28$ μM. Other parameters were as in Fig. 1.

The fact that four IIA^{Glc} molecules bind to a glycerol kinase tetramer suggests that the binding process may be cooperative. Indeed, a sigmoidal curve was obtained when determining the inhibition of glycerol uptake as a function of varying IIA^{Glc} concentrations *in vivo* [15]. Simulation of cooperative binding by increasing the factor α resulted in a steeper inhibition curve for the lower glycerol kinase concentrations but a lower maximal extent of inhibition at higher glycerol kinase concentrations (Fig. 3). The sigmoidal nature of the inhibition curve also increased with greater cooperativity. The experimental inhibition data [9,10] could be approximated equally well by a straight line or a slightly sigmoidal curve, but not by a strongly sigmoidal curve (cf. Fig. 3 for α = 100). While some cooperativity in binding may thus be present, the model seems to rule out strong or infinite cooperativity in the binding of IIA^{Glc} to glycerol kinase.

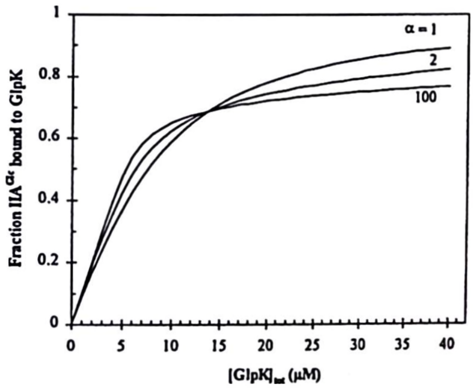

Figure 4. Effect of cooperative binding on the sequestration of IIA^{Glc} by glycerol kinase. The fraction of IIA^{Glc} bound to glycerol kinase is shown for different values of the cooperativity factor α. Simulation conditions were as in Fig. 3.

To analyse the effect of cooperativity in more detail, we calculated how changes in the cooperativity factor α would affect the fraction of IIA^{Glc} sequestered by glycerol kinase (Fig. 4). Stronger cooperativity resulted in a sharper increase in the amount of IIA^{Glc} sequestered in an inactive complex at the lower glycerol kinase concentrations, but the maximal amount of IIA^{Glc} sequestered was lower (Fig. 4 for α = 100). This was in agreement with the lower maximal extent of inhibition of PTS activity (Fig. 3).

To summarise, we have been able to mimic experimental results of inhibition of PTS activity by glycerol kinase with a detailed kinetic model using realistic parameters. This provides further insight into the mechanism responsible for such a mode of inhibition, i.e., sequestration of the PTS component IIA^{Glc} into an inactive complex. Indeed, these results may serve as a general example for analysing regulation through sequestration of enzymes by protein-protein interactions in signal transduction pathways. In contrast to a hierarchical mode of regulation, we observe that the regulator can be regulated itself.

REFERENCES

[1] Postma, P.W., Lengeler, J.W. and Jacobson, G.R. (1993) Microbiol. Rev. 57, 543–594.

[2] Saier Jr., M.H. (1989) Microbiol. Rev. 53, 109–120.

[3] De Boer, M., Broekhuizen, C.P. and Postma, P.W. (1986) J. Bacteriol. 167, 393–395.

[4] Novotny, M.J., Frederickson, W.L., Waygood, E.B. and Saier Jr., M.H. (1985) J. Bacteriol. 162, 810–816.

[5] Postma, P.W., Epstein, W., Schuitema, A.R.J. and Nelson, S.O. (1984) J. Bacteriol. 158, 351–353.

[6] Sweet, G., Gandor, C., Voegele, R., Wittekindt, N., Beuerle, J., Truniger, V., Lin, E.C.C. and Boos, W. (1990) J. Bacteriol. 172, 424–430.

[7] Hurley, J.H., Faber, H.R., Worthylake, D., Meadow, N.D., Roseman, S., Pettigrew, D.W. and Remington, S.J. (1993) Science 259, 673–677.

[8] Feese, M., Pettigrew, D.W., Meadow, N.D., Roseman, S. and Remington, S.J. (1994) Proc. Natl. Acad. Sci. USA 91, 3544–3548.

[9] Rohwer, J.M. (1997) Ph.D. Thesis, University of Amsterdam.

[10] Rohwer, J.M., Bader, R., Westerhoff, H.V. and Postma, P.W. (1998) Mol. Microbiol., in the press.

[11] Sauro, H.M. (1993) Comput. Appl. Biosci. 9, 441–450.

[12] Mendes, P. (1997) Trends Biochem. Sci. 22, 361–363.

[13] Fell, D. (1996) Understanding the Control of Metabolism. Portland Press, London.

[14] Van der Vlag, J., van't Hof, R., van Dam, K. and Postma, P.W. (1995) Eur. J. Biochem. 230, 170–182.

[15] Van der Vlag, J., van Dam, K. and Postma, P.W. (1994) J. Bacteriol. 176, 3518–3526.

NUMERICAL OPTIMISATION AND SIMULATION FOR RATIONAL METABOLIC ENGINEERING

Pedro Mendes & Douglas B. Kell

Institute of Biological Sciences, Cledwyn Building, University of Wales, Aberystwyth
SY23 3DD, U. K., Phone: + 44 1970 622353; Fax: + 44 1970 622354
Email: prm@aber.ac.uk, dbk@aber.ac.uk, http://gepasi.dbs.aber.ac.uk/home.htm

INTRODUCTION

Dating from the work of Chakrabarty [1], there is much current interest in what has become known as *Metabolic Engineering* (e.g. [2-5]), i.e. in increasing by a directed mechanism (usually by rDNA technology, [6]) the concentrations or activities of enzymes in a pathway of interest, with a view to increasing the flux towards desirable products (or eliminating undesirable ones). However, if this is to be done rationally, one must have a way of targeting those metabolic steps that are to have the greatest effect on the fluxes of interest. Metabolic control analysis (MCA) seems to be one good candidate for such a purpose [7-12]. Notwithstanding the power and utility of these approaches, however, their take-up amongst biotechnologists has been less than widespread, due arguably to three main factors: *i)* some of the mathematics underpinning MCA is rather recondite from a biochemical point of view, *ii)* MCA is exact only for small changes in parameters such as enzyme concentrations (although in favourable cases its approximations for "large" changes may be good, [13, 14]), and *iii)* it is normally necessary to perform an extensive series of experiments to find out the distribution of the control of flux in a metabolic pathway between different enzymes before knowing which one(s) might be best to clone (see e.g. [15-18]). Here we show that a practical way of overcoming these limitations is to analyse the properties of an appropriate model of the pathway of interest using computer simulation. We have developed [19, 20] and are currently extending a user-friendly metabolic simulator (Gepasi) that is suitable for performing "what if?" experiments *in numero* prior to undertaking a series of difficult and possibly misguided experiments. The full specification of this software and related material is available over the Internet at *http://gepasi.dbs.aber.ac.uk/softw/gepasi.html*. There are numerous uses for a friendly simulator of this type, including those in education. Here we illustrate how numerical optimisation methods, recently introduced in Gepasi, can be used as a tool for rational metabolic engineering through the analysis of the steady-state behaviour of a hypothetical model of a branched pathway.

MODEL AND METHODS

We analyse the branched pathway depicted in Fig. 1. Our interest is to find conditions for which the flux towards P1 is high. We note that the structure of this pathway and the kinetics of its enzymes are such that it is almost impossible to guess the behaviour of this system by intuition. Apart from the conservation of the cofactor moiety ([A]+[AH]=constant), the first enzyme on the branch of interest is substrate-inhibited and the AH form of the cofactor is a modifier of the first enzyme of the other branch (following the Botts-Morales mechanism [21], AH can be either an activator or inhibitor depending on the values of the kinetic constants).

For this study we assume that we possess the technology to change enzyme concentrations (by cloning) and to do site-directed mutagenesis on the enzymes so that we could manipulate their kinetic parameters. The problem is what parameters to manipulate to obtain *i*) high flux to P1 with low flux to P2 and *ii*) high flux to P1 without affecting the flux to P2. In both cases we limit the adjustable parameters by specifying upper and lower boundaries, in addition *ii*) is also constrained by a fixed value of the flux towards P2. We defined the pathway in Gepasi, attributed arbitrary numerical values to the various parameters, simulated its steady state and took this as the reference state (our wild type strain). Then we selected 35 parameters to be potential targets for manipulation: all the enzyme concentrations, the total concentration of the cofactor plus 28 kinetic parameters (all those for the ordered Bi Bi enzymes, and all those related to the action of M2 as inhibitor of E3 and AH as modifier of E6. We allow these parameters to be adjusted to values within 3 orders of magnitude on either side of the "wild type" value.

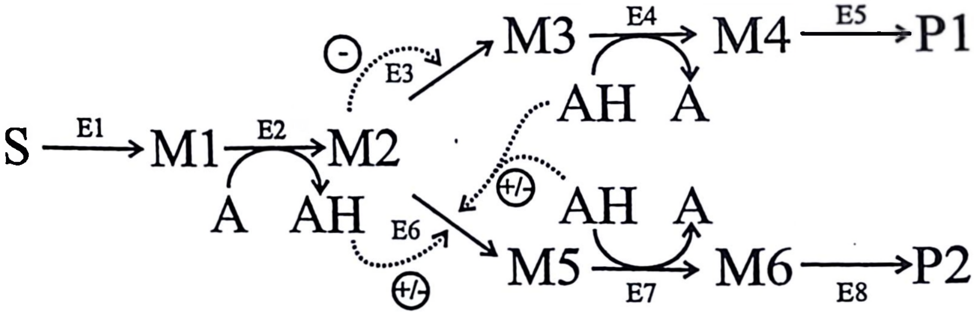

Figure 1 - Scheme of pathway analysed in the text. Arrows represent the enzymatic steps and point to the forward direction of flux, all reactions are chemically reversible. Dotted arrows represent regulatory effects, the symbol +/- indicates that the effect can be either of activation or inhibition. E1, E5 and E6 follow reversible Michaelian kinetics; E2, E4 and E7 follow ordered Bi Bi kinetics in which the cofactor is always the first to bind and the last to be released (this mechanism has 10 kinetic parameters); E3 is inhibited by its own substrate (i.e. M2 binds both the active and an inhibitory sites) and E6 follows the general Botts-Morales modifier-type kinetics, in which the modifier can be an inhibitor or activator depending on the values of the kinetic parameters (7 in total). We took the reference state to have all kinetic constants, enzyme concentrations and total concentration of the cofactor ([A]+[AH]) equal to 1. The equilibrium constants of all steps are also 1, and are not changed in any simulation. All values are in arbitrary units.

In the most recent version of Gepasi we have devised an interface that allows the program to combine numerical optimisation algorithms with steady state or time course simulations. Apart from applications of the type described here, this also allows the program to carry out *robust* parameter estimation (fitting). This combination of optimisation and simulation has been implemented in such a way that many different optimisation algorithms can be used to attempt to solve a problem. This is an advantage as in numerical optimisation there is no single algorithm that is best for all kinds of problems [22]. The ability to apply several of these is then almost a necessity for any moderately complex problem. In particular when the number of adjustable parameters is large (e.g. more than 10) or when the property to optimise is non-linear there is the high probability that there will be many local optima. For the pathway of Fig. 1 we have applied the following optimisation methods: random search, the Hooke and Jeeves direct search [23], steepest descent, a limited memory bounds-constrained quasi-Newton method (L-BFGS-B) [24], and a genetic algorithm [25-27].

RESULTS AND DISCUSSION

We want to maximise the steady-state flux of step 5 (J5) subject only to bound constraints on the adjustable parameters. Using the new version of Gepasi we applied 5 different optimisation algorithms to this problem. Analysis of the results summarised in Table 1 reveals that the best estimate for the maximum (J5=294.24) is 5 orders of magnitude higher than the "wild type" and it was obtained with the direct search method of Hooke and Jeeves. This is a local optimisation method that does not require information from the gradient of the objective function; rather at each iteration it generates a new search direction using a heuristic based on the results of a few previous iterations. The second best solution was obtained with the genetic algorithm, with a value of J5 only 2% lower than the best estimate. This method required only 10% the number of simulations carried out by the Hooke and Jeeves method. The two gradient descent methods (steepest descent and L-BFGS-B) performed very badly (albeit still ten-fold higher than the "wild type").

Table 1 - Performance of several optimisation methods for the maximisation of the flux to P1 (J5) with simple bound constraints on the adjustable parameters. The *wild type* entry refers to the initial state before applying the optimisation. The last column lists the number of simulations that the optimisation method required to reach the solution.

Method	**J5**	**J8**	**[A]/[AH]**	**Simulations**
Wild type	0.021139	0.033821	0.17651	1
Steepest descent	0.23389	0.060530	0.28111	308
L-BFGS-B	0.34677	0.31353	0.61628	1715
Hooke & Jeeves	294.24	1.3310×10^{-3}	0.60946	154195
Genetic algorithm	288.44	0.0050157	0.60550	10100
Random search	3.5908	0.012252	0.57515	10100

Comparing the parameter values of the "wild type" with our best solution we conclude that the optimal value of J5 was obtained by setting the concentration of all enzymes to their upper boundary value (1000) except E6 which was set to its lower boundary value (0.1). Interestingly this results in the finding that the only enzyme of the branch to P2 to have control over J8 is E6 (with a unity flux-control coefficient). However E1-E5 also control J8 but their flux-control coefficients cancel each other. If one were to engineer this pathway to increase the flux by 5 orders of magnitude *for the same concentration of substrate* one would have to: *i*) over-express all enzymes except E6 which must be under-expressed, *ii*) engineer all enzymes such that they become as sensitive as possible to their substrates *and* products (i.e. K_m as low as possible), *iii*) engineer the three Bi Bi enzymes such that their inhibition constants of the second substrate and the first product are increased 1000-fold, but the one of the first substrate only 100-fold *iv*) reduce the strength of inhibition of E3 by its own substrate, *v*) increase the sensitivity of E6 towards its modifier (AH) and in such a way that it becomes an inhibitor.

Table 2 - Performance of several optimisation methods for the maximisation of the flux to P1 (J5) subject to the constraint of flux towards P2 to be within 5% of the wild type value.

Method	J5	J8	[A]/[AH]	Simulations
Wild type	0.021139	0.033821	0.17651	1
Genetic algorithm	23.385	0.033653	0.58172	100200
Random search	1.0846	0.033334	0.33144	100000

More interesting, from a biological point of view, is the case where we want to maximise the flux towards P1 while keeping the competing flux to P2 essentially unchanged. In this case we have a constraint on one of the variables of the model and unfortunately only a couple of the optimisation methods can deal with this (random search and genetic algorithms). To implement this constraint we have instructed Gepasi only to allow solutions for which $0.032<J8<0.034$ (roughly the "wild type" value +/- 5%). Our best estimate for the maximum is 3 orders of magnitude higher (but this may actually be far from the true maximum) which is a considerable improvement. The genetic algorithm performed much better than the random search, as we anticipated. Interestingly, for this constrained solution the concentration of both E6 and E8 is reduced but not that of E7. The latter has a substrate and product common to the flux being maximised.

Optimisation of biochemical models is inherently a hard process due to the high dimensionality of the search space. If one were to examine the model above with a brute-force method (that examines all combinations of *n* values of each parameter) one would have to execute n^{35} simulations. It is obvious that such a solution is prohibitive, even on the fastest computers and for small *n*. Additionally, in such a high dimensional search space there are almost certainly numerous local optima, due to the high non-linearity of some of the kinetic functions. Even if multiple optima are not present, there will be large flat regions of parameter space where methods based on gradients will halt. We have reasons to believe that this is what happened with the gradient descent methods in our first example (see Table 1).

We hope that the by making available our software, biochemists who do not necessarily wish to develop this level of expertise in numerical analysis and computer programming can still benefit from the use of simulation-optimisation strategies.

ACKNOWLEDGEMENT

We are indebted to the UK BBSRC for financial support.

REFERENCES

1 Chakrabarty, A.M. (1974) United States patent no. 3,813,316

2 Bailey, J.E., Birnbaum, S., Galazzo, J.L., Khosla, C. and Shanks, J.V. (1990) Ann. N. Y. Acad. Sci. 589, 1-15.

3 Bailey, J.E. (1991) Science 252, 1668-1675.

4 Stephanopoulos, G. and Vallino, J.J. (1991) Science 252, 1675-1681.
5 Cameron, D.C. and Tong, I. (1993) Appl. Biochem. Biotechnol. 38, 105-140.
6 Skatrud, P.L., Tietz, A.J., Ingolia, T.D., Cantwell, C.A., Fisher, D.L., Chapman, J.L. and Queener, S.W. (1989) Bio/Technology 7, 477-485.
7 Kell, D.B. and Westerhoff, H.V. (1986) Trends Biotechnol. 4, 137-142.
8 Kell, D.B. and Westerhoff, H.V. (1986) FEMS Microbiol. Rev. 39, 305-320.
9 Westerhoff, H.V. and Kell, D.B. (1987) Biotech. Bioeng. 30, 101-107.
10 Kell, D.B., van Dam, K. and Westerhoff, H.V. (1989) Symp. Soc. Gen. Microbiol. 44, 61-93.
11 Cornish-Bowden, A., Hofmeyr, J.-H.S. and Cárdenas, M.L. (1995) Bioorg. Chem. 23, 439-449.
12 Westerhoff, H.V. and Kell, D.B. (1996) J. Theoret. Biol. 182, 411-420.
13 Small, J.R. and Kacser, H. (1993) Eur. J. Biochem. 213, 613-624.
14 Small, J.R. and Kacser, H. (1993) Eur. J. Biochem. 213, 625-640.
15 Niederberger, P., Prasad, R., Miozzari, G. and Kacser, H. (1992) Biochem. J. 287, 473-479.
16 Hofmeyr, J.H.S., Cornish-Bowden, A. and Rohwer, J.M. (1993) Eur. J. Biochem. 212, 833-837.
17 Cornish-Bowden, A. and Hofmeyr, J.H.S. (1994) Biochem. J. 298, 367-375.
18 Giersch, C. (1994) J. Theoret. Biol. 169, 89-99.
19 Mendes, P. (1997) Trends Biochem. Sci. 22, 361-363.
20 Mendes, P. (1993) Comput. Appl. Biosci. 9, 563-571.
21 Botts, J. and Morales, M. (1953) Trans. Farad. Soc. 49, 696-707.
22 Wolpert, D.H. and Macready, W.G. (1997) IEEE Trans. Evol. Comput. 1, 67-82.
23 Hooke, R. and Jeeves, T.A. (1961) J. Ass. Comput. Mach. 8, 212-229.
24 Byrd, R.H., Lu, P., Nocedal, J. and Zhu, C. (1995) SIAM J. Sci. Comput. 16, 1190-1208.
25 Bäck, T., Fogel, D.B. and Michalewicz, Z. (1997), IOPPublishing/Oxford University Press, Oxford.
26 Michalewicz, Z. (1994) Genetic algorithms + data structures = evolution programs, 3rd ed., Springer-Verlag, Berlin.
27 Mitchell, M. (1995) An Introduction to Genetic Algorithms, MIT Press, Boston.

A KINETIC MODEL OF INTERLEAFLET TRANSPORT OF LIPIDS MEDIATED BY PORE-FORMING PROTEINS

Stephan Frickenhaus, Reinhart Heinrich

Humboldt University Berlin, Biology / Theoretical Biophysics, Invalidenstr. 42D-10115
Berlin, Phone +49-30-2093-8698; Fax +49-30-2093-8813;
fric@bp.biologie.hu-berlin.de

INTRODUCTION

Recently, experimental evidence has been presented for an accelerated interleaflet transport of lipids through pores formed by membrane integral peptides [1,2]. This type of transport may contribute to the fluxes of passive transmembrane movements determining the steady-state asymmetric lipid distribution between the two membrane monolayers. We investigate a kinetic model for such a transport mechanism, which shows some correspondence to *classical* models of *single-file diffusion*, that is, of particles moving in a spatially ordered way in the direction of transport [3,4]. Our *modified* model is based on a rather different picture of single-file transport which may fit better for the phenomenon of lipid translocation. A linear arrangement of lipids along the pore is assumed, which is not subject to diffusion of empty volume. Besides the hardcore repulsion between the lipids, there are no energy wells along the pore, that is, the restrictions of movement are alone due to the ordering inside the pore, and the entering and leaving of the lipids from and to the adjacent leaflets, respectively. Furthermore, exchange of the positions of neighboured lipids inside the pore are allowed at specified rates. The pore is considered to be formed by either $l-1$ or l lipids interacting with the membrane spanning protein. The kinetic constants are assumed to be independent of the species. Hence, changes of content and ordering inside the pore leaves the rate constants unchanged. A quasi-steady-state approximation for all different forms of the pores allows to derive expressions for the pore-mediated fluxes of lipids. For the case of a narrow pore, where no neighbour exchanges occur, a closed expression for the lipid fluxes is given for an arbitrary pore-capacity l and an arbitrary number of lipid species.

METHODS

From the above given basic assumptions the following kinetic scheme for the pore involved processes emerges:

$$P_X^{l-1} + j^c \underset{k_c^-}{\overset{k_c^+}{\rightleftarrows}} P_{jX}^l , \qquad P_X^{l-1} + j^e \underset{k_e^-}{\overset{k_e^+}{\rightleftarrows}} P_{Xj}^l \tag{1a,b}$$

$$P_{XijY}^{l-1} \underset{p}{\overset{p}{\rightleftarrows}} P_{XjiY}^{l-1} , \qquad P_{XijY}^{l} \underset{q}{\overset{q}{\rightleftarrows}} P_{XjiY}^{l} \tag{1c,d}$$

where $i,j=1...s$. The upper index of the pore symbol P refers to the number of lipids contained in the pore. The upper indices c and e of the lipid species symbol j denotes the leaflet in which the lipid is located (c=cytoplasmic, e=external). The symbols X and Y denote (sub-)sequences of species indices. Taking into account the processes depicted in scheme (1a) one arrives at the following differential equation for the time dependence of the concentrations of the lipids in the cytoplasmic leaflet

$$\frac{d}{dt}N_i^c = -N_i^c k_c^+ \sum_Z P_Z^{l-1} + k_c^- \sum_X P_{iX}^l \quad . \tag{2}$$

Besides an analogue differential equation for the concentrations in the external leaflet *e*, further kinetic equations arise from processes (1a-d) for the concentrations of the different forms of the pore. Making a quasi-steady-state assumption for all forms of the pore allows for derivation of kinetic equations for the lipids by computer algebra, for example, with MATHEMATICA.

RESULTS

The complexity of the kinetics is very much increasing with the pore capacity *l*. However, at vanishing neighbour-exchange ($p = q = 0$) the kinetic equations simplify for arbitrary pore capacity to an expression

$$J_i^P = P\frac{\left(k_c^- k_e^+ N^e\right)^l N_i^e/N^e - \left(k_c^+ k_e^- N^c\right)^l N_i^c/N^c}{\left(k_c^- + k_e^- + k_c^+ N^c + k_e^+ N^e\right)\sum\limits_{j=0}^{l-1}\left(k_e^- k_c^+ N^c\right)^j \left(k_c^- k_e^+ N^e\right)^{l-j-1}} \quad , \tag{5}$$

which is linear in the lipid specific concentrations $N_i^{c,e}$ and non-linear (for $l>1$) in the total leaflet concentrations $N^{c,e} = \sum N_i^{c,e}$. Assuming constant, species independent mechanical forces during jumps into and out of the pore, one may include the effects of lipid compression under transport due to volume (surface area) restrictions of the leaflets in a symmetrical way as

$$k_{c,e}^+ = k^+ e^{\mp X^{mech}/4RT} \quad , \quad k_{c,e}^- = k^- e^{\pm X^{mech}/4RT} \quad . \tag{6}$$

$X^{mech} = -2\alpha\left(N^c - N^e\right)/N$ represents the mechanical force of lateral compression due to translocation of lipids [5,6]. Simulation of lipid redistribution through pores is done with the use of Eq. (5), taking into account a further type of passive transport as well as active inward transport of aminophospholipids [7]. This additional passive transport is considered to be a pore-independent lipid flip-flop [8], which is described by

$$J_i^{flip-flop} = k_i^+ N_i^e - k_i^- N_i^c \quad . \tag{7}$$

The flip-flop rate constants $k_i^\pm$ obey modifications of their mechanical equilibrium values k_i^{ff} as (see [6])

$$k_i^\pm = k_i^{ff} e^{\mp X^{mech}/2RT} \, . \tag{8}$$

Active transport of phosphatidylserine (PS) and phosphatidylethanolamine (PE) by a translocase is (for simplicity linearly) modelled with uni-directional fluxes as

$$J_i^{act} = l_i^+ N_i^e \quad , \quad i = PS, PE \; . \tag{9}$$

For the cytoplasmic lipid concentrations the kinetic equation

$$\frac{dN_i^c}{dt} = J_i^{act} + J_i^{flip-flop} + J_i^P \tag{10}$$

is used for simulation of the redistribution of lipids upon activation of the translocase, as well as after its inhibition (setting $l_{PS,PE}^+ = 0$ at $t > 10000\,\text{min}$). The resulting time-course of normalised cytoplasmic lipid concentrations, obtained from numerical integration of Eq. (10), is displayed in the figure. All parameter values and further abbreviations are given in the table. The requirement for a slow movement of SM, which is assumed to have almost no pore independent flip-flop, restricts the capacity of the pore to be $l \approx 7$. This estimation is based on a relation between diffusion- and coupling-coefficients of linear flux-force relations (see [5]), which is obtained by linearization of Eq. (5) near equilibrium (more details for different kinetic schemes presented in [6]). The dash-dotted line represents the deviation of the flip-flop rate constants from their symmetrical equilibrium value due to mechanical effects (see Eq. (8))

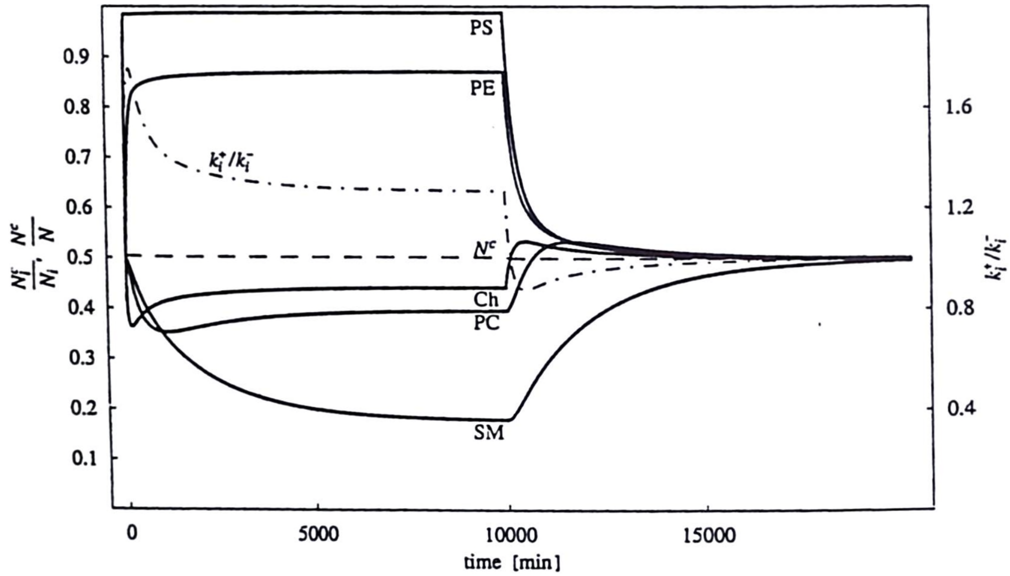

Parameter values for the simulation of the human erythrocyte lipid asymmetry			
l_{PS}^+	$1/6.82\,\text{min}^{-1\,\dagger}$	N_{PS}	$0.55\text{ mM}^{\dagger}$
l_{PE}^+	$1/90\,\text{min}^{-1\,\dagger}$	N_{PE}	$1.12\text{ mM}^{\dagger}$
$k_{PS,PE}^{ff}$	$1/700\,\text{min}^{-1}$	N_{PC}	$1.24\text{ mM}^{\dagger}$
k_{PC}^{ff}	$1/1312\,\text{min}^{-1}$	N_{SM}	$1.04\text{ mM}^{\dagger}$
k_{SM}^{ff}	$1/84000\,\text{min}^{-1}$	N_{Ch}	$3.5\text{ mM}^{\dagger}$
k_{Ch}^{ff}	$1\,\text{min}^{-1}$	α	$35\,RT^{\dagger,\ddagger}$
l	7	† see [5] ‡ modifications due to [6]	
P	$N/100$		
$k^- = k^+ N$	$1/4\,\text{min}^{-1}$	**Abbr.** *PC*: phosphatidylcholine, *SM*: sphingomyelin, *Ch*: cholesterol	

DISCUSSION

The resulting expressions for the fluxes in Eq. (5) open a route for experimentalists to determine pore-capacities by analysing fluxes of various particle species and their non-linear dependencies on the difference of the total leaflet lipid concentrations. The presented procedure for an incorporation of lateral mechanical compression into kinetic constants of translocation is highly relevant for an explanation of the recent experimental findings of an enhancement of lipid flip-flop under mechanical manipulations [9]. Probably the imbalance of flip- and flop-rate constants of PC [10] may be due to the described mechanical effects. The very low steady-state flux of SM to the cytoplasmic leaflet [11] is explained by the fact that pores are primarily involved in counter-directed fluxes. The model may easily be generalised for particle fluxes through membrane pores connecting two solvent compartments, provided that no localised particle-pore interaction (binding sites) exists. For this, transmembrane electric potential differences and hydrostatic pressure differences should be incorporated in an analogue way as presented for the mechanical compression forces. Furthermore, the model gives a kinetic interpretation of the positive coupling of fluxes, which has been demonstrated to yield a realistic simulation by a thermodynamic modelling approach [5]. After linearization, expressions of the fluxes through the pore, caused by a net difference in total leaflet lipid concentrations, have similar a structure as the previously introduced *compensatory fluxes* [12].

REFERENCES

[1] E. Fattal, S. Nir, R. A. Parente, F. C. Szoka, Jr., Pore-forming peptides induce rapid phospholipid flip-flop in membranes, Biochemistry 33: (1994) 6721-6731

[2] K. Matsuzaki, O. Murase, N. Fujii, K. Miyajima, An antimicrobial peptide, magainin 2, induced rapid flip-flop of phospholipids coupled with pore formation and peptide translocation, Biochemistry 35 (1996) 11361-11368

[3] A. L. Hodgkin, R. D. Keynes, The potassium permeability of giant nerve fibre, J. Physiol. 128 (1955) 61-88

[4] H-H. Kohler, K. Heckmann, Unidirectional fluxes in saturated single-file pores of biological and artificial membranes, J. theor. Biol. 85 (1980) 575-595

[5] R. Heinrich, M. Brumen, A. Jaeger, P. Müller, A. Herrmann, Modelling of phospholipid translocation in the erythrocyte membrane: A combined kinetic and thermodynamic approach, J. theor. Biol. 185 (1997) 295-312

[6] S. Frickenhaus, R. Heinrich, Kinetic and thermodynamic aspects of lipid translocation in biological membranes, submitted to Biophys. J. (1998)

[7] M. Seigneuret, P. F. Devaux, ATP-dependent asymmetric distribution of spin-labeled phospholipids in the human erythrocyte membrane: relation to shape changes, Proc. Natl. Acad. Sci. USA. 81 (1984) 3751-3755

[8] R. D. Kornberg, H. M. McConnell, Inside-outside transitions of phospholipids in vesicle membranes, Biochemistry 10 (1971) 1111-1120

[9] M. R. Raphael, R. E. Waugh, Accelerated transport of phosphatidylcholine molecules in membranes under deformation, Biophys. J. 71 (1996) 1374-1388

[10] M. Bitbol, P. F. Devaux, Measurement of outward translocation of phospholipids across human erythrocyte membrane, Proc. Natl. Acad. Sci. USA. 85 (1988) 6783-6787

[11] G. Morrot, P. Hervé, A. Zachowski, P. Fellmann, P. F. Devaux, Aminophospholipid translocase of human erythrocytes: phospholipid substrate specificity and effect of cholesterol, Biochemistry 28 (1988) 3456-3462

[12] M. Brumen, R. Heinrich, A. Herrmann P. Müller, Mathematical modeling of lipid transbilayer movement in the human erythrocyte plasma membrane, Eur. Biophys. J. 22 (1993) 213-223.

COMBINED EFFECTS OF CA-DEPENDENT POTASSIUM CHANNELS AND ADENYLATE METABOLISM IN HUMAN ERYTHROCYTES VOLUME STABILIZATION

Michael V. Martinov, Victor M. Vitvitsky & Fazoil I. Ataullakhanov

Research Center for Hematology, 125167 Moscow, Russia, Phone: 7(095) 212-55-31, 212-35-22. Fax: 7(095) 212-88-70. E-mail: fazli@bioscience.msk.su

INTRODUCTION

Human erythrocytes stabilize its volume precisely [1]. Despite numerous experimental and theoretical studies on regulation of erythrocyte volume regulation [2,3] the mechanisms of its stabilization are not understood well. Our previous model studies examined the effects of putative involvement of Ca dependent potassium channels (K-channels) [4] and adenylate metabolism [5] in stabilization of erythrocyte volume against non-selective changes of membrane permeability for cations. This study is an attempt to combine the two mechanisms of human erythrocyte volume stabilization in one mathematical model. We considered the effects of adenylate metabolism and K-channels on transmembrane ion fluxes as schematically shown in Fig. 1.

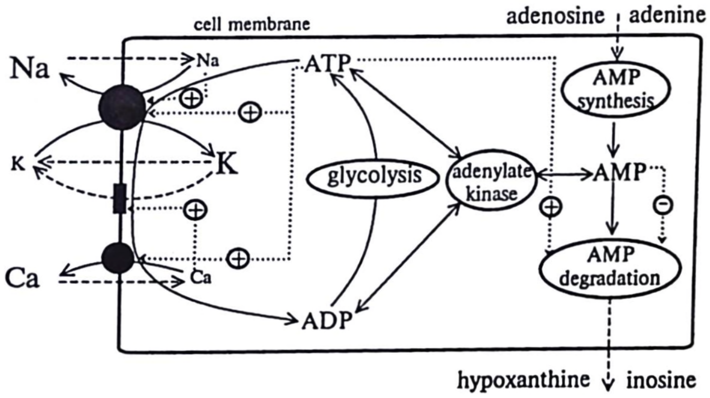

Figure 1. Schematic representation of the effects of adenylate metabolism and K-channels on transmembrane ion fluxes in human erythrocytes. Black circles stand for Na/K and Ca ATPases. The rectangle denotes a K-channel. Solid lines show active ion fluxes and fluxes of metabolites. Dashed lines indicate passive ion and metabolite fluxes. Dotted lines indicate regulatory interactions. Plus and minus denote positive and negative influence, respectively.

Mathematical Model

Ion balance and erythrocyte volume are described by a set of equations which was taken from [4]. Model includes equations for fluxes of Na, K and Ca across erythrocyte membrane, osmotic equilibrium in the system, electroneutrality and equilibrium distribution of permeable anions.

The expression $P_{CH} = P_{max}\left(\frac{[Ca^{2+}]}{[Ca^{2+}] + K_{CH}}\right)^N$

shows how the permeability of K-channels depends on the concentration of Ca. It was obtained on the basis of the data described in [6,7].The parameters N and K_{CH} were varied when analyzing the model.

Glycolysis is described by the following set of equations:

$$\frac{d}{dt}\left(C_i \frac{V}{V_0}\right) = U_i^+ - U_i^-$$

Ci - concentrations of metabolites from G6P to PEP.

U^+_i, U^-_i - rates of metabolite synthesis and degradation, respectively.

The expressions for rates of enzymatic reactions in this model were taken from [5,8].

In the model, adenylate metabolism is represented by a reaction of irreversible AMP synthesis and two irreversible reactions of AMP degradation. The dynamics of adenylate concentrations can be described by solving the following set of equations if we take into account the adenylate kinase equilibrium:

$$\frac{d}{dt}\left(e \frac{V}{V_0}\right) = \upsilon_{GLYCOLYSIS} - \upsilon_{ATPASES} - 2\upsilon_{AMP\_SYNTHESIS}$$

$$\frac{d}{dt}\left(a \frac{V}{V_0}\right) = \upsilon_{AMP\_SYNTHESIS} - \upsilon_{AMPP} - \upsilon_{AMPD}$$

Here e = 2[ATP]+[ADP] - energy pool, a = [ATP]+[ADP]+[AMP] - adenylate pool. $\upsilon_{AMP\_SYNTHESIS}$ is assumed to be constant (0.04 mM/h). This low rate of adenylate metabolism in human erythrocytes is optimum for maintaining the stable state of cellular metabolism [9]. υ_{AMPP} and υ_{AMPD} denote the rates of AMP phosphatase and AMP deaminase. Regulation of the adenylate pool is assumed to be based on that AMP phosphatase is inhibited by AMP and activated by ATP [9]. This regulation provides an increase in adenilate pool under increase in activity of ATP-consuming processes.The AMP deaminase rate sharply increases with increasing AMP. This determines the greatest possible value of the adenylate pool.

RESULTS

Role of Ca-dependent potassium channels in erythrocyte volume stabilization.

The contribution of K-channels into erythrocyte volume stabilization can be evaluated by setting rates of AMP synthesis and degradation equal to 0, because this excludes adenylate metabolism from the model. K-channels provide volume stabilization when the cell membrane permeability to cations changes in a wide range of its values. The stabilization effect is based on intracellular Ca concentration increase at non-selective increase of cell membrane permeability. Sequentially, K efflux from the cell increases and cell volume decreases. The volume stabilization range increases with increase in K-channel cooperativity and strongly depends on the K-channel affinity for Ca (Fig. 2). While the cell volume remains almost constant in erythrocytes containing K-channels, their intracellular Na, K, Ca and ATP concentrations change appreciably with changes of membrane permeability. The characteristic time of operation of the calcium mechanism of stabilization is several seconds; this time is required for the cell to establish a new intracellular Ca concentration. The volume approaches its stationary value monotonically, without overshooting.

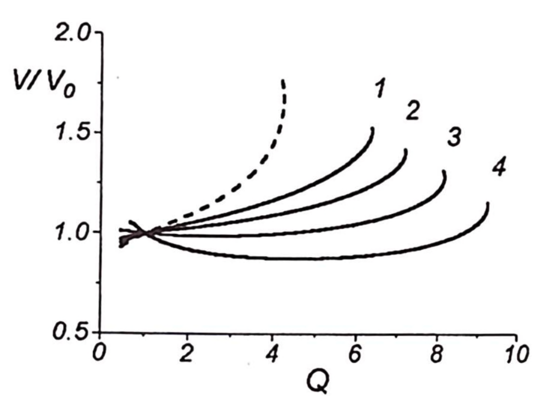

Fig. 2. Dependence of the stationary erythrocyte volume on the normalized value of cell membrane permeability to cations (Q) for various values of the K-channel parameters and a constant value of the adenylate pool: N=4, K_{CH}=0.35, 0.33, 0.25, and 0.22 μM for curves 1, 2, 3, and 4, respectively. The dashed line shows the results of solving the model from which equations describing adenylate metabolism and K-channels were excluded.

Role of adenylate metabolism in erythrocyte volume stabilization

The contribution of adenylate metabolism into erythrocyte volume stabilization can be evaluated by setting P_{CH}=0 and excluding equation for calcium exchange from the model. Over a wide range of changes in the membrane permeability, the stationary value of erythrocyte volume can be stabilized efficiently through regulation of adenylate metabolism (Fig. 3A). In this case, volume stabilization

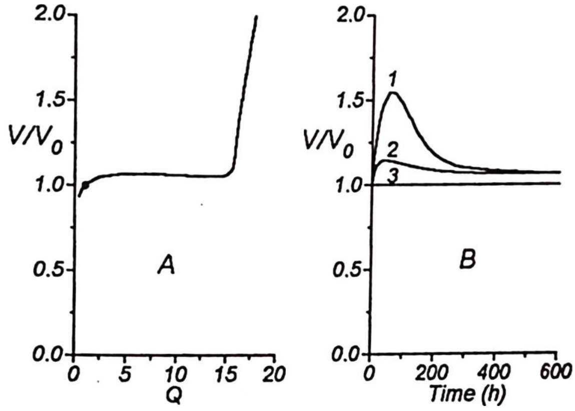

Fig. 3. Erythrocyte volume stabilization achievable through regulation of adenylate metabolism (K-channels are excluded from the model). (A): Dependence of the stationary erythrocyte volume on the normalized passive permeability of the cell membrane to cations. Circle on curve indicate the physiological stationary state.
(B): Kinetics of erythrocyte volume changes after an instantaneous increase in the cell membrane permeability at t=0 by 12-fold (1) 8-fold (2), without permeability increase (3).

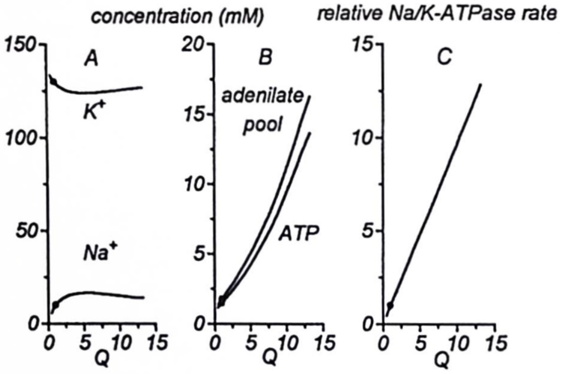

Fig. 4. Dependence of the stationary values of intracellular variables on the normalized value of cell membrane permeability to cations simulated using the model from which equation describing K-channels were excluded: (A) K and Na concentrations, (B) the adenylate pool and ATP concentration, and (C) the relative rate of Na/K ATPase. Circles on curves indicate the physiological stationary state.

results from stabilization of intracellular Na and K concentrations (Fig. 4A), which is achieved through regulation of the rate of Na/K ATPase. The important model assumption is that this rate depends on the ATP concentration. If the adenylate pool changes, ATP concentration and the rate of ATPase also changes (Fig. 4B, 4C).

The volume stabilization effect of adenylate pool regulation is excellent only if the membrane permeability changes slowly, because the rate of adenylate metabolism in erythrocytes is slow. If the membrane permeability changes abruptly, the erythrocyte volume takes transient values that can be far apart from its stationary value, which is stabilized in erythrocytes (Fig. 3B).

Combined effects of potassium channels and adenylate metabolism

The model of volume stabilization describing contributions of both K-channels and adenylate metabolism does not differ from the previous models in the efficiency of stabilization of the stationary volume (Fig. 5A), but provides much less pronounced overshooting in the cell volume response to abrupt changes in the membrane permeability (Fig. 5B). This model also describes the stabilization of the stationary values of intracellular ion concentrations, which is provided by the effect of stimulation of transport ATPases by increased ATP concentrations. The dynamic stabilization of cell volume during transient processes elicited by an abrupt change in the cell membrane permeability is possible in the model due to the operation of K-channels, whereas the stabilization of the stationary values of intracellular ion concentrations is maintained due to adenylate metabolism control.

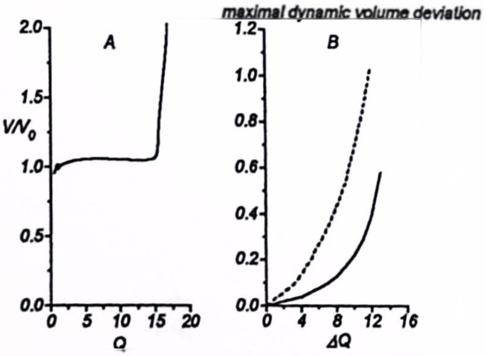

Fig. 5. Erythrocyte volume stabilization in the model describing the contributions of both K-channels and adenylate metabolism control. (A): Dependence of the stationary erythrocyte volume on the normalized passive permeability of the cell membrane to cations. The circle on the curve indicates the physiological stationary state. (B): Effect of an abrupt change in the membrane permeability (ΔQ) on the maximum increase in the erythrocyte volume during transient processes (a solid line). The dashed line illustrates the results obtained with the model from which K-channels were excluded.

Interestingly, the functional roles of K-channels and adenylate metabolism in erythrocytes are still unclear. The results obtained confirm the hypothesis proposed earlier [4,5] that these systems are of primary importance in erythrocytes, because they function to stabilize the erythrocyte volume and thereby provide the functional integrity and viability of erythrocytes.

REFERENCES

[1] Lew, V.L., Raftos, J.E., Sorette, M., Bookchin, R.M., Mohandas, N. (1995) *Blood* **86**, 334-341.

[2] Hoffmann, E.K. & Simonsen, L.O. (1989) *Physiol. Reviews* **69**, 315-382.

[3] Sarkadi, B. & Parker, J.C. (1991). *Biochim. Biophys. Acta* **1071**, 407-427.

[4] Ataullakhanov, F.I., Martinov, M.V., Vitvitsky, V.M., Kiyatkin, A.B. & Pichugin, A.V. (1996). *in: Biothermokinetics of the Living Cell.* (Westerhoff, H.V., Snoep, J.L., Wijker, J.E. & Kholodenko, B.N. eds.) BioThermoKinetics Press, Amsterdam, 80-84.

[5] Ataullakhanov, F.I., Komarova, S.V., Martinov, M.V. & Vitvitsky, V.M. (1996). *J. Theor. Biol.* **183**, 307-316.

[6] Simons, T.J.B. (1976). *J. Physiol.* **256**, 227-244.

[7] Leinders, T., Van Kleef, R.G.D.M. & Vijverberg, H.P.M. (1992) *Biochim. Biophys. Acta* **1112**, 67-74.

[8] Erlich, L.I., Ataullakhanov, F.I., Vitvitsky, V.M., Zhabotinsky, A.M., Pichugin, A.V. & Kholodenko, B.N. (1985). *Izvestiia Academii Nauk SSSR (seriya biologicheskaya)* **5**, 754-766.

[9] Ataullakhanov, F.I., Komarova, S.V. & Vitvitsky, V.M. (1996) *J. Theor. Biol.* **179**, 75-86.

CAN DEFICIENCY OF NON-KEY GLYCOLYTIC ENZYMES IN ERYTHROCYTES LEAD TO HEMOLYTIC ANEMIA?: A MATHEMATICAL MODEL.

Vitvitsky V.M., Martinov M.V., Plotnikov A.G., Ataullakhanov F.I.

Research Center for Hematology, Moscow, 125167 Russia, Tel: 7(095)2123522,
Fax: 7(095)2128870, E-mail: victor@blood.ru

INTRODUCTION

The only abnormality found in many patients with nonspherocytic hemolytic anemia was a deficiency of one of glycolytic enzymes [1-3]. A decrease in GPI, TPI, and PGK activities was often reported. These enzymes are the so-called non-key enzymes whose normal activities are about 1000-fold higher than the rate of glycolytic flux. Surprisingly, but the activities of GPI, TPI, and PGK decrease by only 5-20-fold in hemolytic anemia. In other words, their activities are still higher by at least 50-fold than the rate of glycolytic flux. Therefore, it is unclear whether the deficiency observed is actually the cause of anemia. Earlier, the effects of glycolytic enzyme deficiency on the viability of erythrocytes have been studied by means of mathematical modelling [4,5]. The criteria for cell death used in these models were somewhat arbitrary. They included a considerable decrease in ATP and appreciable accumulation of glycolytic intermediates. Analysis of these models showed that the activities of HK, PK, and sometimes PFK and PGK decreased to the level observed in patients with nonspherocytic hemolytic anemia can actually lead to death of erythrocytes. On the other hand, the values of GPI, TPI, and, in certain cases, PGK activities in patients appeared much higher than the minimum predicted by the models at which cells remain viable (1% of the normal activity or less). Hence, a *per se* decrease in activities of these enzymes observed in anemia cannot be the cause of erythrocyte destruction. However, the discrepancy between the calculated permissible minimum values of activities of non-key enzymes and the values determined experimentally in anemia can be eliminated by the assumption that the deficient enzyme is unstable [4].

This study is an attempt to estimate the permissible minima of glycolytic enzyme activities and activity of Na/K-ATPase in erythrocytes using a model describing all reactions of glycolysis, adenylate metabolism, ionic balance, and osmotic regulation of the cell volume. The natural criterion for cell viability is such an increase in cell volume that impairs the rheology of erythrocytes and leads to their sequestration from the circulation or even lysis. We chose a 10% and 50%-values for this increase. Note that in the population of circulating erythrocytes, the maximum change in their volume observed experimentally was 10% of the normal mean value [6,7]. A 50% increase in the volume corresponds to osmotic lysis of the erythrocyte [6,7].

Mathematical model

The model is a set of differential and algebraic equations describing ionic balance on extra- and intracellular concentration variables, glycolysis, and adenylate metabolism. The description of ionic balance includes differential equations for Na and K fluxes across the cell membrane and equations for the electroneutrality, osmotic equilibrium, and equilibrium partition of permeating anions between the cell and its milieu [8]. The description of glycolysis includes differential equations for all intermediates (except pyruvate) [4,8,9]. The concentrations of pyruvate, lactate, orthophosphate, and the sum of NAD and NADH concentrations are considered as constant. The adenylate metabolism is described by differential equations for ATP, ADP, and AMP and an equation for their equilibrium in adenylate kinase reaction. The equation for AMP describes its synthesis at a low constant rate and degradation, which is assumed to be proportional to the [ATP]/[AMP] ratio at physiological AMP concentrations [8] and to be accelerated greatly at high AMP concentrations.

The equation for the *i*-th metabolite is taken in the following general form in the model:

$$\frac{d}{dt}\left(\frac{XiV}{Vo}\right)=\sum_{n}U^{+}_{in}-\sum_{k}U^{-}_{ik}$$

Here, Xi is the concentration of the *i*-th metabolite in the cytoplasm; V and Vo denote the current and normal (physiological) volumes of the erythrocyte, respectively. The functions U^{+}_{in} and U^{-}_{ik} describe the dependencies of the production and utilisation rates for the *i*-th metabolite on the concentrations of enzymes and metabolites [4,8,9].

The DBSolve package, which was kindly provided by Dr. I. Goryanin, was used to analyse the model.

RESULTS AND DISCUSSION

Analysis of the model showed that the erythrocyte volume increases after any of the glycolytic enzymes (except DPGM) drops to a certain minimum. The volume can increase because either the steady state is lost due to the inability of glycolysis to power active transport of ions (in HK, GPI, and PFK deficiencies) or the stationary concentrations of osmotically active metabolites of glycolysis increase (in TPI, PGK, DPGP, PGM, ENO and PK deficiencies). In ALD, GAPDH, and LDH deficiencies, an 10%-increase in the volume results from accumulation of glycolytic intermediates, whereas a 50%-increase is a consequence of the loss of the steady state. If DPGM activity diminishes to zero, the erythrocyte metabolism and volume almost do not change. If ATPase activity decreases, the stationary Na and K gradients decrease, and the erythrocyte increase in volume. However, if ATPase activity increases (even considerably), the Na and K gradients change only slightly, producing almost no effect on the erythrocyte volume and metabolism. Table 1 shows (1) the minimum critical values of ATPase and glycolytic enzyme activities calculated for stable deficient enzymes whose activity is low and constant in time and (2) mean ATPase and glycolytic enzyme activities for erythrocyte populations with unstable deficient enzymes (their activities vary from normal values to minimum critical values with time). Interestingly, the critical minimum values of glycolytic enzyme activities obtained in this study and those calculated in [4,5] are similar, despite the different criteria for the viability of erythrocytes used. In hemolytic anemia with HK and PK deficiencies, the enzymatic activities measured in patients' erythrocytes appeared close to the calculated critical minimum values. By contrast, the enzymatic activities measured in erythrocytes of patients with hemolytic anemia and GPI, PFK, TPI, or PGK deficiency were much greater, as a rule, than their calculated minimum values. Thus, these enzyme deficiencies are unlikely to be the cause of erythrocyte destruction and development of anemia if the deficient enzyme is stable. However, the discrepancy between the calculated and observed values can be explained if we assume that the enzyme is unstable. Suppose that entering the circulation, erythrocytes have normal activity of the deficient enzyme, which decays exponentially with a time constant T from the initial value (α_o) to the critical minimum (α_c)

$\alpha = \alpha_o \exp(-t/T)$

When the enzymatic activity reaches the critical minimum, an erythrocyte dies. If this is the case, the measured activity is the cell population mean, which can be significantly greater than the critical minimum. Under the assumptions made, the mean value can be expressed as:

$\alpha_m = (\alpha_o - \alpha_c)/\ln(\alpha_o / \alpha_c)$

Table 1 shows that the PFK and non-key enzyme deficiencies can result in destruction of erythrocytes and development of anemia only if these enzymes are unstable. The suggestion that their activity decreases exponentially is not critical. This decrease can follow an arbitrary law. Actually, the instability of the deficient enzyme can be found in most cases of

Table 1. Comparison of ATPase and glycolytic enzyme activities for which the model predicts the erythrocyte destruction and those measured in erythrocytes of patients with hemolytic anemia: Normalised minimum critical values for stable enzymes (α_c / α_o) and mean values for unstable enzymes (α_m / α_o).

Enzyme	Model results				Experimental data [1-3]
	V/Vo = 1.1		V/Vo = 1.5		
	Stable enzyme (α_c / α_o)	Unstable enzyme (α_m / α_o)	Stable enzyme (α_c / α_o)	Unstable enzyme (α_m / α_o)	(α / α_o)
HK	0.39	0.65	0.39	0.65	0.15-0.75
GPI	0.015	0.23	0.015	0.23	0.05-0.40
PFK	0.011	0.22	0.011	0.22	0.06-0.60
ALD	0.0006	0.13	0.0005	0.13	0.04-0.16
TPI	0.00046	0.13	0.00039	0.13	0.016-0.20
GAPDH	0.14	0.44	0.13	0.43	0.20-50
PGK	0.0069	0.20	0.0033	0.17	0.05-0.20
DPGP	0.32	0.60	0.11	0.40	-
PGM	0.022	0.26	0.0074	0.20	-
ENO	0.47	0.70	0.20	0.50	0.06-0.50
PK	0.48	0.71	0.22	0.52	0.03-0.40
LDH	0.016	0.24	0.015	0.23	-
ATPase	0.36	0.63	0.11	0.40	0.20-0.60

Abbreviations. HK, hexokinase; GPI, glucosephosphate isomerase; PFK, phosphofructokinase; ALD, aldolase; TPI, triosephosphate isomerase; GAPDH, glyceraldehyde phosphate dehydrogenase; PGK, phosphoglycerate kinase; DPGM, diphosphoglycerate mutase; DPGP, diphosphoglycerate phosphatase; PGM, phosphoglycerate mutase; ENO, enolase; PK, pyruvate kinase; LDH, lactate dehydrogenase; ATPase, transport Na,K-ATPase; DAP, dihydroxyaceton phosphate.

hemolytic anemia associated with glycolytic enzyme deficiencies [1-3]. The suggestion that the deficient enzyme is unstable also accounts for certain changes in metabolite concentrations observed in erythrocytes (e.g., extremely high DAP concentration in TPI deficiency; Table 2).

The measured activity is sometimes lower than the calculated critical minimum (HK, ENO, and PK deficiencies). This can be explained by the low rate of erythrocyte destruction in the circulation. The characteristic time of changes in the erythrocyte volume is about 100 h in the model. Therefore, even if the activity of the deficient enzyme is several times lower than the calculated critical minimum, the time it takes an erythrocyte to swell to the critical volume is on the order of several days (Table 3).

Table 2. DAP concentrations and cell volume for various TPI activities in erythrocytes. Mean values for unstable TPI were calculated under the assumption that the concentrations of metabolites change quasistationarily as the enzyme activity decreases; I and II denotes the means calculated for $\alpha_c/\alpha_o=0.00046$ and $\alpha_c/\alpha_o=0.00039$, respectively.

Parameter	Model results								Experimental data [10]	
	Stable enzyme, steady-state values						Unstable enzyme, mean values			
							I	II		
α/α_o	1.0	0.10	0.01	0.001	0.00046	0.00039	0.13	0.13	0.028	0.022
$\frac{[DAP]}{[DAP]_o}$	1.0	1.09	2.05	17.6	121	419	16.1	46.2	23.2	36.3
V/V_o	1.0	1.0	1.0	1.01	1.10	1.50	1.01	1.05	-	-

Table 3. Time it takes erythrocytes to swell to the critical volume values after the PK activity have dropped abruptly from the normal value to the value indicated.

α/α_o		0.4	0.2	0.1	0.05
Time (h)	$V=1.1V_o$	278	52	25	19
	$V=1.5V_o$	-	700	132	115

These results demonstrate that the existing mathematical models describe the erythrocyte glycolysis adequately and can be used for analysis of impairments caused by glycolytic enzyme deficiencies. It is important for this analysis that the potential instability of the deficient enzymes and the distribution of experimentally determined parameters in cell population were taken into consideration.

REFERENCES

1. Waller, H.D. and Benohr, H.C. (1974) In: Cellular and molecular biology of erythrocytes (Yoshikawa, H. and Rapoport, S.M., eds.), pp. 377-407, University of Tokyo Press, Tokio.
2. Beutler, E. (1978) Hemolytic anemia in disorders of red cell metabolism, Plenum Medical Book Company, New York.
3. Tanaka, K.R. and Zerez, C.R. (1990) Sem. Hematol. 27, 165-185.
4. Erlich, L.I., Ataullakhanov, F.I., Vitvitsky, V.M., Zhabotinsky, A.M., Pichugin, A.V. and Kholodenko, B.N. (1985) Izvestiya Akademii Nauk SSSR. Seriya Biologicheskaya No. 5, 754-766. (in Russian)
5. Schuster, R. and Holzhutter, H.-G. (1995) Eur. J. Biochem. 229, 403-418.
6. Linderkamp, O. and Meiselman, H.J. (1982) Blood 59, 1121-1127.
7. Lew, V.L., Raftos, J.E., Sorette, M., Bookchin, R.M. and Mohandas, N. (1995) Blood 86, 334-341.

8. Ataullakhanov, F.I., Komarova, S.V., Martynov, M.V. and Vitvitsky, V.M. (1996) J. theor. Biol. 183, 307-316.
9. Joshi, A. and Palsson, B.O. (1990) J. theor.Biol. 142, 41-68.
10. Orosz, F., Vertessy, B.G., Hollan, S., Horanyi, M. and Ovadi, J. (1996) J. theor. Biol. 182, 437-447.

76

HOW DO MITOCHONDRIAL ENZYMES CONTROL THE RESPIRATION AND SUPEROXIDE PRODUCTION RATES?

O.V. Demin[1,2], *H.V. Westerhoff*[3,4], *Jan B. Hoek*[5] *and B.N. Kholodenko*[3,5]

[1]A.N. Belozersky Institute of Physico-Chemical Biology, Moscow State University, 119899, Vorobjovy Gory, Moscow, Russia, [2]M.M. Shemyakin and Yu.A. Ovchinikov Institute of Bioorganic Chemistry, Moscow, Russia, [3]Department of Microbial Physiology, Vrije Universiteit, De Boelelaan 1087, 1081 HVAmsterdam, The Netherlands, [4]E.C.Slater Institute, BioCentrum Amsterdam,University of Amsterdam, The Netherlands, [5]Department of Pathology, Anatomy and Cell Biology, Thomas Jefferson University, 1020 Locust St., 271, JAH, Philadelphia, PA 19107, E-mail: oleg@energ.genebee.msu.su, FAX: (7 095) 939-3181

INTRODUCTION

Non-enzymatic oxidation of semiquinone by oxygen in the Q-cycle is a major source of superoxide radicals (O_2^-) in mitochondria respiring on succinate. Increase in semiquinone concentration increases the rate of superoxide production. The transmembrane electric potential, $\Delta\Psi$, inhibits the oxidation of semiquinone to ubiquinone in the Q-cycle (see Fig.1) by suppressing the electron transfer between hemes of bc_1 complex (and, consequently, respiration rate). Thus, inhibition of $\Delta\Psi$-consuming reactions leads to an increase in superoxide production rate and a decrease in the respiration rate. Such a situation occurs, e.g., during State 3 - State 4 transition. To study how the ability to produce O_2^- depends on $\Delta\Psi$ and to understand how the concentrations of mitochondrial enzymes can be adjusted to minimize O_2^- production and maximize the respiration, we developed a mathematical model of oxidative phosphorylation in mitochondria. Using this model, we described the mitochondrial State 3 - State 4 transition and calculate control coefficients of all enzymes of energy metabolism over two selected fluxes: the respiration and superoxide production.

MATHEMATICAL MODEL

A mathematical model of mitochondria respiring on succinate consists of the $\Delta\mu_H$ producing reactions of the respiratory chain including succinate ubiquinone reductase (SUR), bc_1 complex, cytochrome oxidase and the following $\Delta\mu_H$ consuming processes: (1) ATP synthesis, catalyzed by H^+-ATP-synthase; (2) translocation of adenine nucleotides, catalyzed by the adenine nucleotide translocator; (3) symport of inorganic phosphate and a proton, catalyzed by the phosphate carrier; (4) H^+ - leakage; (5) K^+ - leakage; (6) electroneutral exchange of K^+ for H^+; catalyzed by K^+/H^+-antiporter. The model assumes that there are four electrogenic steps in the Q-cycle (Fig.1). One corresponds to the intramembrane electron transfer from heme b_{556} (low potential heme b_l) to heme b_{560} (high potential heme b_h) and contributes 80% of the total electrogenesis. Three other steps account for the proton translocations in reactions of semiquinone dismutation and ubiquinol oxidation and contribute 20% only [1,2]. In addition, we took into consideration the electrogenic steps in cytochrome c oxidase reaction and in the processes (1) - (5) listed above [3,4]. The present model of mitochondrial free-energy transduction also considers ion balances and the buffering of the proton concentration by mitochondrial matrix proteins [3,4]. The description of the reaction rates and the parameter values are given elsewhere [5,6].

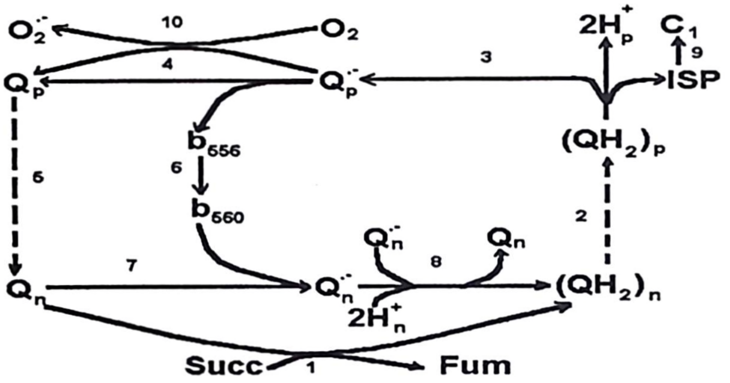

FIGURE 1. Kinetic scheme of the initial segment of the respiratory chain. Q_p, $Q_p^{\bullet-}$, $(QH_2)_p$ and Q_n, $Q_n^{\bullet-}$ $(QH_2)_n$ are quinone species at the external positive (p) and internal negative (n) side of the inner mitochondrial membrane, respectively. b_{556}, b_{560} are the low and high potential hemes of cytochrome b. Iron sulphur protein (ISP) and cytochrome c_1 are shown.

RESULTS AND DISCUSSION

The external ADP concentration was a parameter, which varied from 0 to 20 μM to model the State 4 - State 3 transition. Fig.2A shows how the level of ΔΨ changes with variation of ADP. Fig.2B shows how the respiration and superoxide production rate varied with the electric potential. The results suggest that O_2^{-}-production rates increases dramatically with increase in ΔΨ in the range from 150 to 180 mV and at state 4 this rate should be much higher than in state 3.

To study the ability of mitochondrial enzymes to control the oxygen consumption and superoxide production rates, we determined the control coefficients of these enzymes over the corresponding fluxes. The control exerted by ATP/ADP translocator over the respiratory flux is positive (Fig. 3A) and it is negative over O_2^{-}-production flux (Fig. 3B). The control coefficient of proton leak over oxygen consumption increases with ΔΨ and becomes substantially positive (Fig. 3A) and the control coefficient of proton leak but over superoxide production is negative and close to zero (Fig. 3B). Therefore, activation of these enzymes leads to an increase in oxygen consumption and to a decrease in superoxide production. One can explain this results by a decrease in ΔΨ due to the activation of ATP/ADP translocation or the proton leak. As shown in Fig.2B, a decrease in ΔΨ leads to an increase in the oxygen consumption and to a decrease in superoxide production.

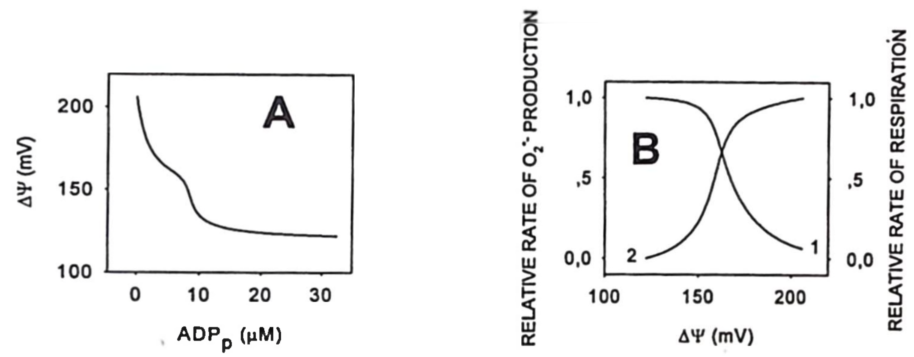

FIGURE 2. Oxidative phosphorylation and O_2^--production in coupled mitochondria: A - dependence of ΔΨ on external ADP concentration; B - dependence of the relative rate of respiration (1) and of the relative rate of superoxide production (2) on ΔΨ

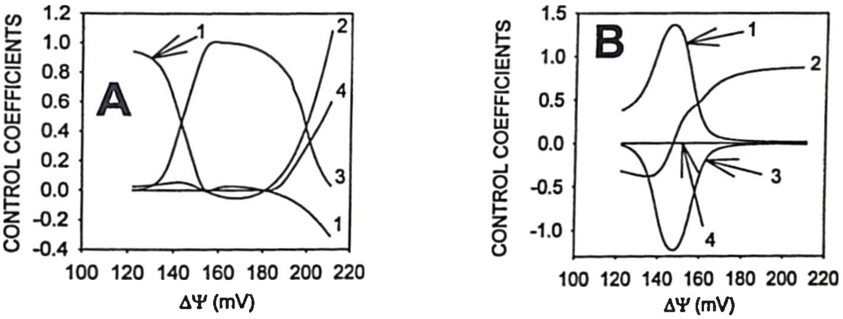

FIGURE 3. Control coefficients over oxygen consumption (A) and superoxide production (B) with respect to SUR (1), bc_1 complex (2), ATP/ADP translocator (3) and H^+-leak (4).

For respiratory enzymes, we found that control coefficients of the complex III over both superoxide production flux and oxygen consumption flux changed the sign and became substantially positive when ΔΨ increased (Fig. 3). The control exerted by SUR on O_2^--production rate was positive in the entire range of ΔΨ (Fig.3B). Control coefficient of SUR over oxygen consumption rate changed from positive to negative values at very high ΔΨ (Fig.3A). To explain this phenomenon of negative control, we note that the reduction of Q_n to $(QH_2)_n$ proceeds by two competing routes, i.e., either via succinate oxidation by SUR (step 1 in Fig. 1) or by taking electrons from the high potential heme, b_h, of bc_l complex (step 7). At very high ΔΨ, the rate of the electron transfer between the hemes b_l and b_h is strongly inhibited, and the bc_l complex completely limits the respiration rate (the control coefficient is 1, Fig. 3A). An increase in SUR activity decreases the steady-state concentration of Q_n regardless of whether external ADP concentration is low (Fig.4A) or high (Fig.4B). However, at high ΔΨ (Fig.4A), a decrease in Q_n becomes critical for a further inhibition of Q-cycle and, consequently, the respiration rate. Fig. 4A shows that even a decrease in ΔΨ, accompanying a decrease in the respiration rate cannot release an inhibitory effect of a decrease in Q_n at high ΔΨ. At low and normal ΔΨ an increase in SUR activity increases the rate of respiration (Figs. 3a and 4b).

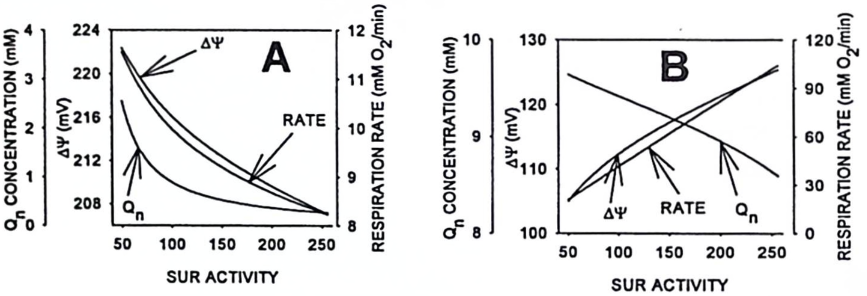

FIGURE 4. Dependence of Q_n concentration, membrane potential (ΔΨ) and respiration rate (RATE) on SUR activity at low (0.12 μM - 1) and high (12 μM - 2) concentration of external ADP.

Our analysis revealed the enzymes mainly contributing to the control of oxygen consumption and superoxide production at different mitochondria states. At low ΔΨ, i.e. in the range from 120 mV to 145 mV (State 3), SUR controls both oxygen consumption and superoxide production: the corresponding control coefficients are near unity. When ΔΨ is in the range from 145 mV to 190 mV, ATP/ADP translocator limits the oxygen consumption, its control coefficient approximately equals unity [cf. 6]. There are four enzymes, which significantly contribute to the control of superoxide production flux, namely SUR, ATP/ADP translocator, bc_1 complex and cytochrome oxidase. Control coefficients of SUR and ATP/ADP translocator are approximately identical and differ by sign (SUR exerts a positive control) and sum of positive control coefficients with respect to complex III and cytochrome oxidase are approximately equal to unity. At high potential values, i.e. in the range from 190 mV to 220 mV, bc_1 complex controls both oxygen consumption and superoxide production fluxes.

ACKNOWLEDGMENT.

We acknowledge NIH grant AA11689, RFFR grant N 98-04-48868, EU Copernicus grant IC15-CT96-0307 and NWO for the support of this work.

REFERENCES

[1] Drachev, L.A., Kaurov, B.S., Mamedov, M.D., Mulkidjanian, A.Y., Semenov, A.Y., Shinkarev, V.P., Skulachev, V.P. and Verkhovsky, M.I. (1989), BBA, 973, 189-197.

[2] Semenov, A.Y. (1993) FEBS Lett., 321, 1-5.

[3] Kholodenko, B.N. and Erlich, L.I. (1985) Biophysics (USSR), 30, 837-843 (Engl. transl. 30, 911-919).

[4] Kholodenko, B.N. (1988) D.Sc. Thesis. Moscow State University.

[5] Demin, O.V., Westerhoff, H.V. and Kholodenko, B.N. (1998) Biochemistry (Moscow) 63, No 6, 37-53

[6] Kholodenko, B., Zilinskiene V., Borutaite V., Ivanoviene L., Toleikis A. & Praskevicius A. (1987) FEBS Lett. 223,247-250.

HEART AND NON-SYNAPTIC BRAIN MITOCHONDRIAL H_2O_2 PRODUCTION DOES NOT INCREASE IN PROPORTION TO O_2 CONSUMPTION DURING THE STATE 4 TO STATE 3 TRANSITION. MAIN FREE RADICAL GENERATION AT COMPLEX I.

Asunción Herrero, Susana Cadenas and Gustavo Barja

Department of Animal Biology-II (Animal Physiology), Faculty of Biology, Complutense University, Madrid 28040, Spain, Tel.: +34-1-394 4987, Fax: +34-1-394 4935

INTRODUCTION

Early studies found that succinate-supported free radical production of heart mitochondria is stopped after the addition of sufficient ADP to cause the energy transition from the resting State 4 to the respiratorily active State 3 [1,2]. This finding generated the widespread notion that mitochondria only produce free radicals in the resting State 4 condition. A lack of free radical generation in State 3 would eliminate the implication of mitochondrial reactive oxygen species in tissue damage during exercise and hypermetabolism. Nevertheless, increases in free radical concentration have been detected by direct ESR techniques in muscle during exercise [3-5] and in neurons during hypermetabolic excitotoxicity [6,7]. This constitutes a first "exercise" paradox.

The simple idea that the rate of mitochondrial free radical production increases in proportion to the rate of oxygen consumption is frequently assumed without evidence about it. It is then difficult to understand how muscles could avoid a massive oxidative damage during an acute exercise bout -a situation which does not take place- if free radical production would immediately increase by 23-fold during exercise (as human skeletal muscle oxygen consumption does from rest to heavy work). This constitutes a second "exercise" paradox. In this work the control by ADP of free radical production and free radical leak were studied using both Complex II (succinate) and Complex I (pyruvate/malate)-linked substrates in rat heart and nonsynaptic brain mitochondria.

METHODS

Isolation of heart and non-synaptic brain mitochondria

Ventricles were rinsed, chopped and homogenized in a Dounce with loose fitting pestle in 10 ml of isolation buffer (200 mM mannitol, 70 mM sucrose, 1 mM EDTA, 10 mM Tris-HCl, pH 7.4) containing 5 mg of nagarse and 25 mg of fatty acid-free albumin. After standing for 1 min, 25 ml of additional isolation buffer containing 25 mg of albumin were added and homogenization was performed again with a tighter-fitting pestle. Mitochondria were isolated by a serial centrifugations at 700 *g* during 10 min (obtaining supernatants) and at 8,000 *g* during 10 min (obtaining pellets). The final mitochondrial pellets were resuspended in 1 ml of isolation buffer. Non-synaptic brain mitochondria were isolated by centrifugation in discontinuous 3%/6% Ficoll gradients following the method of Lai and Clark (1979) [8] with minor modifications [9]. Isolation procedures were performed at 5°C. Mitochondrial protein was measured by the Biuret method.

Mitochondrial oxygen consumption

The rate of oxygen consumption was measured at 30°C in a water-thermostted incubation chamber with a Clark-type O_2 electrode and O_2 electrode and O_2 control box (CB1-D Hansatech) as described elsewhere [9]. After correction for nonmitochondrial oxygen consumption, respiratory control ratios higher than 5.0 (pyruvate/malate) and between 2.3 and 3.4 (succinate) were obtained.

Mitochondrial oxygen radical production

The rate of mitochondrial free radical production was measured following the linear increase in fluorescence (excitation at 312 nm, emission at 420 nm) due to enzymatic oxidation of homovalinic acid by H_2O_2 in the presence of horseradish peroxidase [10], modified to kinetically follow the rate of production of reactive oxygen species by isolated mitochondria [9] in a LS50B computer-controlled Perkin-Elmer fluorometer.

Mitochondrial free radical leak

The percent free radical leak was calculated as the rate of free radical production divided by two times the rate of O_2 consumption, and the result was multiplied by 100.

Statistical analysis

Differences were statistically analyzed with Student's *t* test. The minimum level of statistical significance was set at $p < 0.05$ in all the analyses.

RESULTS AND DISCUSSION

Addition of ADP increased rat heart and nonsynaptic brain mitochondria oxygen consumption by releasing the phosphorylating State 3 respiration (data not shown). This ADP addition resulted in a strong decrease in the rate of succinate-supported free radical production of heart mitochondria in State 3 (Fig. 1A). A direct tracing showing the stop of rat heart mitochondrial free radical production induced by the ADP addition during the State 4 to State 3 transition is shown in Fig. 2A.

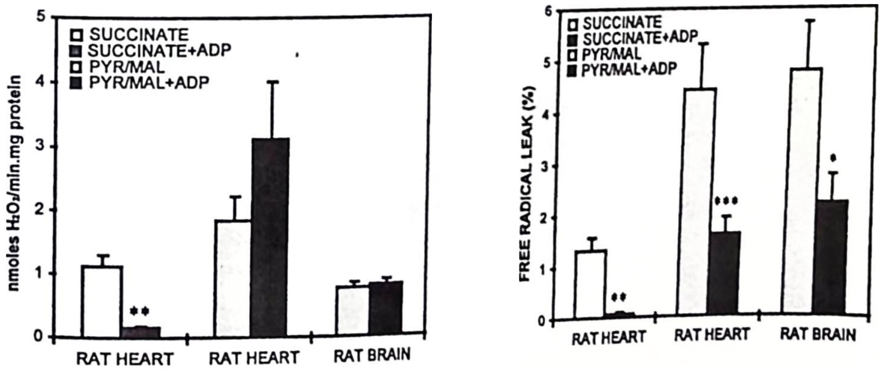

A)

B)

Figure 1. Rates of free radical production (A) and free radical leak (%) (B) of State 4 (substrate alone) and State 3 (substrate plus ADP) heart and nonsynaptic brain mitochondria supplemented with Complex I or Complex II-linked substrates. Values are means ± SEM from 6 to 7 rats; $^{*}p < 0.05$; $^{**}p < 0.01$; $^{***}p < 0.001$.

Contrary to what happened with succinate as substrate, the rate of free radical production of pyruvate/malate-supplemented heart mitochondria was not stopped by addition of ADP (Fig. 1A). Fig. 2B shows a direct tracing from a sample showing increases in pyruvate/malate supplemented free radical production after ADP additon.

Nonsynaptic brain mitochondria supplemented with succinate produced very low levels of free radicals which were near to the limit of detection or did not generate detectable free radicals (results not shown). Similarly to what happened in heart mitochondria, addition of ADP to pyruvate/malate-supplemented nonsynaptic brain mitochondria did not significantly change the rates of free radical production (Fig. 1A). Measurement of mitochondrial free radical production has routinely been performed in the absence of ADP in many previous works, whereas ADP is present in resting tissues *in vivo* al low μM concentrations as calculated from ^{31}P-NMR data [11]. This stresses the relevance of the observation of free radical production even in the presence of saturating ADP levels (500 μM) in pyruvate/malate supported mitochondria.

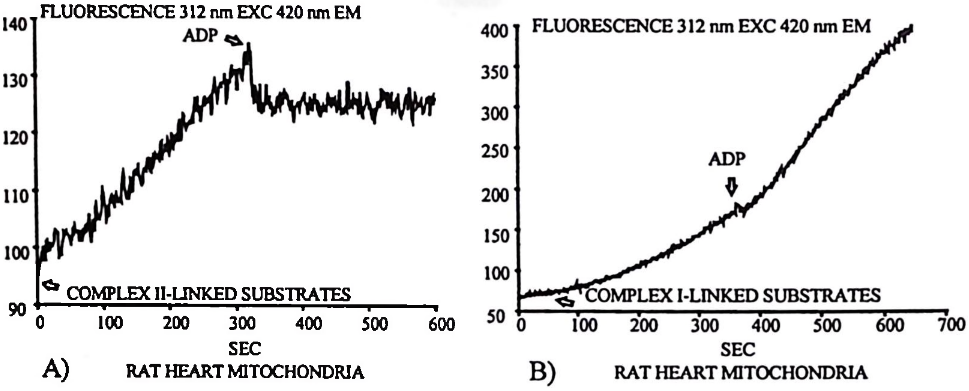

Figure 2. Direct tracings showing the effect of ADP on free radical production of rat heart mitochondria with Complex II (A) or Complex I-linked (B) substrates during the stimulation of oxygen consumption from State 4 to State 3.

Addition of ADP strongly decreased the free radical leak of heart mitochondria with both kinds of substrates and nonsynaptic brain mitochondria with pyruvate/malate (Figure 1B). This was due to the decrease (succinate) or moderate or no increase (pyruvate/malate) of free radical production together with the strong stimulation of oxygen consumption during the State 4 to State 3 transition. The decreased free radical leak in State 3 can be a protecting factor against acute oxidative stress during intense increases in respiration of aerobic tissues. The global effects of ADP on free radical production with both kinds of substrates can possibly explain in part the two apparent exercise (or hypermetabolic) paradoxes: a) there can be some oxidative damage during acute exercise -especially if untrained- and tissue activation because State 3 mitochondria produce free radicals with Complex I-linked substrates; b) oxidative damage is not massive during activity, in spite of the strong increment in mitochondrial oxygen consumption and the low antioxidant capacity of muscles [5,12], heart [13], and brain [14], because the mitochondrial free radical leak strongly decreases during the

State 4 to State 3 transition. The lack of massive increases in mitochondrial free radical production in State 3 would be consistent with the observation that chronic exercise does not decrease longevity neither in rodents [15] or in humans [16].

It is well established that the rate of mitochondrial free radical production rises strongly when the degree of reduction of the respiratory chain electron carriers is increased [1,2]. The degree of reduction of the respiratory chain strongly decreases during the State 4 to State 3 transition at the same time that the rate of electron flow is increased [17]. Our results show that pyruvate/malate supplemented heart and nonsynaptic brain mitochondria avoid massive increases in free radical production during State 3 active respiration owing to their strong decrease in free radical leak. This probably results to a large extent from a lower degree of reduction of the Complex I free radical generator during intense electron flow in State 3. Free radical production with Complex I-linked substrates is maintained at comparable rates in States 3 and 4 since the decrease in free radical leak compensates for the increase in electron flow in State 3.

In conclusion, since ADP stops free radical production with succinate but not with pyruvate/malate, Complex I must be the main or only source of oxygen radicals in State 3. Thus, Complex I is a main free radical generator both in the resting (State 4) and in the active (State 3) mitochondrial state. The results obtained here, showing that a moderate free radical production occurs with Complex I-linked substrates during ADP-stimulated mitochondrial active respiration (State 3), can help to explain the two exercise or hypermetabolic paradoxes.

ACKNOWLEDGMENTS

This work was supported by a grant from the National Research Foundation of the Spanish Ministry of Health (FISss No. 96/1253).

REFERENCES

[1] Loschen, G., Flohé, L. and Chance, B. (1971) FEBS Lett. 18, 261-264

[2] Boveris, A., Oshino, N. and Chance, B. (1972) Biochem. J. 128, 617-630

[3] Davies, J.A., Quintanilha, A.T., Brooks, G.A. and Packer, L. (1982) Biochem. Biophys. Res. Commun. 107, 1198-1205

[4] Jackson, M.J., Edwards, R.H.T. and Symons, M.C.R. (1985) Biochim. Biophys. Acta 847, 185-190

[5] Barja de Quiroga, G. (1992) Free Rad. Biol. Med. 13, 325-340

[6] Dugan, L.L., Sensi, S.L., Cancionero, L.M.T., Handran, S.D., Rothman, S.M., Lin, T.S. and Goldberg, M.P. (1995) J. Neurosci. 15, 6377-6388

[7] Reynolds, I.J. and Hastings, T.G. (1995) J. Neurosci. 15, 3318-3327

[8] Lai, C.K. and Clark, J.B. (1979) Meth. Enzymol. 55, 51-60

[9] Barja, G. (1998) in Methods in Aging Research (Yu, B.P., ed.), Chapter 23, CRC Press, Boca Raton, Florida, USA (in press)

[10] Ruch, W., Cooper, P.H. and Baggiolini, M. (1983) J. Immunol. Meth. 63, 347-357

[11] Kemp, G.J., Taylor, D.J. and Radda, G.K. (1993) NMR Biomed. 6, 66-72

[12] Jenkins, R.R., Friedland, R. and Howland, H. (1985) Int. J. Sports Med. 5, 11-14

[13] Rojas, C., Cadenas, S., López-Torres, M., Pérez-Campo, R. and Barja, G. (1996) Free Rad. Biol. Med. 21, 907-915

[14] Barja de Quiroga, G., Pérez, R. and López, M. (1990) Biochem. J. 272, 247-250

[15] Goodrick, C.L. (1980) Gerontology 26, 22-33

[16] Paffenbarger, R.S., Hyde, R.T., Wing, A.L. and Hsie, C. (1986) New Engl. J. Med. 314, 605-613
[17] Tzagoloff, A. (1982) Mitochondria, pp.136-137, Plenum Press, New York.

SIMULATION OF THE EPIDERMALGROWTH FACTOR SIGNAL TRANSDUCTION PATHWAY

Frances A. Brightman & David A. Fell

School of Biological and Molecular Sciences, Oxford Brookes University, Gipsy Lane, OXFORD, OX3 0BP,Great Britain, Tel: +44 1865 483964, Fax: +44 1865 484017email: francesb@bms.brookes.ac.ukdaf@bms.brookes.ac.uk

A number of aspects of signal transduction have been investigated from a theoretical perspective, through the development of mathematical models describing the interactions of the various components of the system [1, 2, 3, 4]. These approaches have so far yielded only a 'static' view of the properties of signalling systems. Thus, in order to provide a dynamic simulation of the behaviour of signal transduction networks, the application of computer simulation techniques has been proposed [5].

A kinetic model of a signal transduction pathway is currently being developed, using existing biochemical kinetics simulation software (SCAMP, Gepasi) [6, 7]. The epidermal growth factor (EGF) transduction pathway has been selected as a suitable model system, as this represents the best characterised signal transduction cascade [8]. We are currently working on the simulation of the interaction of EGF with the EGF receptor, and the subsequent activation of the receptor.

EGF is a polypeptide hormone that exerts its mitogenic effect through interaction with a specific membrane receptor (EGFR), which has intrinsic protein tyrosine kinase activity [9, 10]. The mechanism whereby EGF binding activates EGFR remains unresolved [8]. Two types of model have been proposed for the activation of the EGFR, both of which are supported by experimental evidence [11]. One is an intramolecular model [12], which asserts that the external binding of EGF induces a conformational change in the receptor that is transmitted through the transmembrane domain and activates the cytoplasmic tyrosine kinase activity [13, 14].

The alternative, more generally accepted model, is an intermolecular mechanism, in which the receptor is viewed as a membrane-associated allosteric enzyme [10], activation of which is controlled by aggregation [15]. Ligand-induced receptor oligomerisation is a property common to all growth factor receptors with tyrosine kinase activity [15, 10]. The precise molecular details of the phenomenon are still not entirely clear, although models for EGF-induced EGFR dimerisation have been developed, in which the dimer is formed by two monomeric EGF-EGFR complexes [16, 17, 18].

Central to the allosteric activation model is the premise that the dimerised receptor possesses elevated tyrosine kinase activity and enhanced affinity for EGF [15]. Evidence has been presented that dimerisation parallels receptor activation and increases the affinity of EGFR for EGF [19, 20, 21, 22, 23]. Furthermore, it has been suggested that the high affinity state is predominant in mediating EGF signal transduction [19, 24, 25].

Scatchard analysis of EGF-EGFR equilibrium binding assays generally results in a plot showing negative curvature, which is usually associated with negatively co-operative binding [11]. However, non-linearity can also arise is if there is heterogeneity in the binding affinities of the receptors. Hence, this curvature is frequently ascribed to the existence of two populations of the receptor which differ in their binding affinity for the ligand [15, 26]; a small population with high affinity for EGF and a large population with lower affinity [27]. Similarly, studies investigating the kinetics of EGF-EGFR interaction have suggested the presence of at least two affinity classes of EGF receptors [28, 25, 29, 30, 31].

These observations appear to support the conclusion that the high affinity state represents the dimeric form of the receptor whilst the low affinity state constitutes the monomeric form [15, 22, 23]. This interpretation may however be incorrect [11], as there is no direct evidence for two stable populations of EGFR with different affinities for EGF [25], and because such a model predicts that a Scatchard plot will exhibit curvature characteristic of positive cooperativity [16, 17], which is clearly inconsistent with the majority of experimental evidence [11]. Moreover, evidence has been presented which suggests that the emergence of high-affinity binding sites is independent of the oligomeric state of the receptor [32].

In order to account for the more typical negative curvature of the Scatchard binding plot, a model which is based upon negative cooperativity within a ligand-induced receptor dimer has been proposed [11]. Since aggregation is not an absolute requirement for receptor activation [12, 33], the assumption that ligand-induced dimerisation is a prerequisite for tyrosine kinase activation may be questionable [34]. Furthermore, high affinity receptors can be activated by EGF [24], hence dimerisation may not necessarily result in receptor activation. To account for this, a non-allosteric model has been presented [8] in which the high affinity subclass is proposed to consist of dimeric receptors in an intermediary inactive state, which can be fully activated only upon EGF binding [35]. Finally, a ternary complex binding model of EGFR activation has also been proposed [28], in which the high affinity state is equated with the association of the EGF-EGFR complex with a cell surface interaction molecule.

It is apparent that there is some controversy surrounding the issue of binding to the high affinity EGFR, receptor dimerisation and activation, although experimental evidence clearly demonstrates a link between these events. In an attempt to address this issue, we are developing parallel simulations of EGF-EGFR interaction, based upon the allosteric model for EGFR activation and a number of the alternatives, in order to investigate any differences between them in terms of kinetic behaviour and regulatory properties. This approach may resolve the controversy, or at least provide supporting evidence for the most probable mechanism of EGFR activation.

REFERENCES

1 Stadtman, E.R. and Chock, P.B. (1978) Curr. Topics Cell. Reg. 13, 53-95.
2 Goldbeter, A. and Koshland, D.E. (1984) J. Biol. Chem. 259 (23), 14441-14447.
3 Shacter, E., Chock, P.B., Rhee, S.G. and Stadtman, E.R. (1986) The Enzymes. 17, 21-42.
4 Huang, C.Y. and Ferrell, J.E. (1996) Proc. Natl. Acad. Sci. USA, 93, 10078-10083.
5 Schamel, W.W.A. and Dick, T.P. (1996) Med. Hypoth. 47, 249-255.
6 Sauro, H. (1993) CABIOS 9, 441-450.
7 Mendes, P. (1997) Trends Biochem. Sci. 22, 361-363.
8 Gadella, W.J. and Jovin, T.M. (1995) J. Cell Biol. 129 (6), 1543-1558
9 Carpenter, G. and Cohen, S. (1990) J. Biol. Chem. 265, 7709-7712.
10 Ullrich, A. and Schlessinger, J. (1990) Cell 61, 203-212.
11 Wofsy, C., Goldstein, B., Lund, K. and Wiley, H.S. (1992) Biophys. J. 63, 98-110.

12 Koland, J.G. and Cerione, R.A. (1988) J. Biol. Chem. 263, 2230-2237.

13 Weber, W., Bertics, P.J. and Gill, G.N. (1984) J. Biol. Chem. 259 (23), 14631-14636.

14 Bertics, P.J. and Gill, G.N. (1985) J. Biol. Chem. 260, 14642-14647.

15 Schlessinger, J. (1988) Biochemistry 27, 3119-3123.

16 Sherrill, J.M. and Kyte, J. (1996) Biochemistry 35, 5705-5718.

17 Lemmon, M.A., Bu, Z., Ladbury, J.E., Zhou, M., Pinchasi, D., Lax, I., Engelman, D.M. and Schlessinger, J. (1997) EMBO J. 16 (2), 281-294.

18 Odaka, M., Kohda, D., lax, I., Schlessinger, J. and Inagaki, F. (1997) J. Biochem. 122, 116-121.

19 Yarden, Y. and Schlessinger, J. (1987) Biochemistry 26, 1434-1442.

20 Yarden, Y. and Schlessinger, J. (1987) Biochemistry 26, 1443-1451.

21 Boni-Schetzler, M. and Pilch, P.F. (1987) Proc. Natl. Acad. Sci., USA. 84, 7832-7836.

22 Zhou, M., Felder, S., Rubinstein, M., Hurwitz, D.R., Ullrich, A., Lax, I. and Schlessinger, J. (1993) Biochemistry 32, 8193-8198.

23 Sorokin, A., Lemmon, M.A., Ullrich, A. and Schlessinger, J. (1994) J. Biol. Chem. 269 (13), 9752-9759.

24 Defize, L.H.K., Boonstra, J., Meisenhelder, J., Kruijer, W., Tertoolen, L.G.J., Tilly, B.C., Hunter, T., van Bergen en Henegouwen, P.M.P., Moolenaar, W.H. and de Laat, S.W. (1989) J. Cell Biol. 109, 2495-2507.

25 Bellot, F., Moolenaar, W., Kris, R., Mirakhur, B., Verlaan, I., Ullrich, A., Schlessinger, J. and Felder, S. (1990) J. Cell Biol. 110, 491-502

26 Carpenter, G. (1987) Ann. Rev. Biochem. 56, 881-914.

27 Gill, G.N., Bertics, P.J. and Stanton, J.B. (1987) Mol. Cell. Endocrinol. 51, 169-186.

28 Mayo, K.H., Nunez, M., Burke, C., Starbuck, C., Lauffenburger, D. and Savage, C.R. (1989) J. Biol. Chem. 264 (30), 17838-17844.

29 Waters, C.M., Oberg, K.C., Carpenter, G. and Overholser, K.A. (1990) Biochemistry 29, 3563-3569.

30 Berkers, J.A.M., van Bergen en Henegouwen, P.M.P. and Boonstra, J. (1992) J. Receptor Research 12 (1), 71-100.

31 Rousseau, D.L., Staros, J.V. and Beechem, J.M. (1995) Biochemistry 34, 14508-14518.

32 Northwood, I.C. and Davis, R.J. (1989) J. Biol. Chem. 264 910), 5746-5750.

33 Northwood, I.C. and Davis, R.J. (1988) J. Biol. Chem. 263, 7450-7453.

34 Carraway III, K.L. and Cerione, R.A. (1993) Biochemistry 32, 12039-12045.

35 Spargaaren, M., Defize, L.H.K., Boonstra, J. and de Laa, S.W. (1991) J. Biol. Chem. 266 (3), 1733-1739.

THE CONTROL OF GLUCOSE TRANSPORT ON GLYCOLYSIS IN THE YEAST *SACCHAROMYCES BAYANUS.*

Diderich, Jasper, A.[1]*; Valkier, Jeroen*[1]*; Anjos, Jorge*[2]*; Spencer-Martins, Isabel*[2]*; Van Dam, Karel*[1]*; Walsh, Michael, C.*[1]

[1] E.C. Slater Institute, BioCentrum, University of Amsterdam, Plantage Muidergracht 12, NL-1018 TV Amsterdam, The Netherlands, Telephone: +31 20 525 5069,
Fax: +31 20 525 5124, E-mail: jad@chem.uva.nl
[2] Biotechnology Unit, Faculty of Sciences and Technology, New University of Lisbon, P-2825 Monte de Caparica, Portugal

INTRODUCTION

The extent to which the transport of glucose across the cell membrane controls the glycolytic flux is defined as the relative change in the glycolytic flux as a result of a relative change in glucose transport activity under a defined set of conditions. In this study we took glucose consumption as a measure of the glycolytic flux. Consequently, we determined the control of the glucose transport step on the flux through the glucose transporters.

Two characteristics of glucose transport have been used to change the transport activity specifically:

- Maltose competitively inhibits glucose transport in *Saccharomyces bayanus.*
- Extracellular glucose, the substrate of the glucose transporters, can be varied to modulate glucose transport activity [1], [2], [3].

Two approaches have been followed to derive the flux control coefficient of glucose transport from the experimental data:

- Comparison of the steady state glycolytic flux with the zero *trans*-influx of glucose.
- Determination of the response of the glycolytic flux to a change in the mathematically derived steady state glucose transport activity.

When extracellular glucose is used to modulate the glucose transport activity, the control of glucose transport on the glycolytic flux may be written as:

$$C^{J}_{v_{trans}} = \frac{d\ln J}{d\ln G_{out}} \Big/ \frac{\partial \ln v_{trans}}{\partial \ln G_{out}} = R^{J}_{G_{out}} \Big/ \varepsilon^{v_{trans}}_{G_{out}} \qquad (1)$$

The first term in equation 1 is the response coefficient and involves the determination of the glycolytic flux (J) as a function of extracellular glucose (G_{out}). The second term, the elasticity coefficient, can be derived from the kinetic parameters of glucose transport. Under the conditions studied the kinetics of glucose transport fitted to a system with two components. Assuming two symmetric four-state-carriers, the rate equation of glucose uptake (i.e. the steady state activity of glucose transport) can be written as:

$$v_{trans} = V_{max1} \frac{\frac{1}{K_{m1}}(s-p)}{1+\frac{s}{K_{m1}}+\frac{p}{K_{m1}}+\alpha\frac{sp}{K_{m1}^{2}}} + V_{max2} \frac{\frac{1}{K_{m2}}(s-p)}{1+\frac{s}{K_{m2}}+\frac{p}{K_{m2}}+\alpha\frac{sp}{K_{m2}^{2}}} \qquad (2)$$

The s and p in this rate equation are the concentrations of the substrate and product of the carrier, i.e. glucose outside and inside the cell, respectively. It is assumed that the glucose transport step is only connected to the rest of metabolism by the pool of intracellular glucose [4]. V_{max} is the maximal transport activity of the corresponding component and K_m the Michaelis-Menten constant for glucose of the corresponding component. The "interactive constant" α is a constant relating the mobilities of the free and the loaded sugar carriers. The interactive constant is set to 0.91 [5]. The elasticity coefficient can now be derived by calculating the effect of a small change in extracellular glucose (s) on the steady state activity of glucose transport (v_{trans}), keeping terms that are connected to other steps in glycolysis (in this case intracellular glucose) constant. The flux control coefficient of glucose transport on the glycolytic flux is obtained by dividing the response coefficient by the elasticity coefficient (equation1).

METHODS

Strain and growth conditions

Cells of *Saccharomyces bayanus* IGC 4565 (CBS 378) were grown in batch on a rotary shaker (200 rpm) at 30°C, in 2% (w/v) Yeast Extract, 1% (w/v) Peptone and 2% (w/v) glucose to diauxic shift.

Glucose consumption assay

Cultured yeast cells (approximately 10g protein/l) were preincubated for 5 minutes in a stirred thermostated vessel at 30°C; then an equal volume of a glucose/maltose mixture in phosphate buffer (pH 6.5) was added. Samples were taken at different times by adding a volume of the glucose metabolising cells to an equal volume of 10% (w/v) TCA which was kept on ice. After centrifugation and dilution, total glucose was determined.

Zero *trans*-influx assay

Zero *trans*-influx of glucose was determined in 5 seconds uptake experiments according to Walsh et al. [6]. Maltose inhibition of glucose transport was determined by adding maltose and glucose simultaneously. Kinetic parameters of glucose transport were derived by using Enzfittter software.

RESULTS AND DISCUSSION

A. Competitive inhibition of glucose transport by maltose in the yeast Saccharomyces bayanus

In fig. 1, zero *trans*-influx of glucose, in cells of *Saccharomyces bayanus* grown on glucose to the diauxic shift, was measured over a range of glucose concentrations with and without the simultaneous addition of maltose. In the absence of maltose the zero trans-influx of glucose showed a curved Eadie-Hofstee plot, which indicates the presence of more than one component of glucose transport. Glucose transport could be fitted to a two component system with apparent kinetic characteristics that can be described by assuming two distinct Michaelis-Menten type carriers; a high affinity component with a K_m of 1.55 (± 0.15) mM and a V_{max} of 277 (± 25) nmol $\cdot$ min^{-1} $\cdot$ (mg protein)$^{-1}$ and a low affinity component with a K_m of 33.7 (± 10.2) mM and V_{max} of 339 (± 23) nmol $\cdot$ min^{-1} $\cdot$ (mg protein)$^{-1}$. In the presence of maltose, it was not possible to (accurately) distinguish two components of glucose transport, under these conditions glucose transport was best fitted to a one component system with a K_m of 9.75 (± 0.40) mM and a V_{max} of 600 (± 19) nmol · min^{-1} · (mg protein)$^{-1}$. Apparently, maltose has the characteristics of a competitive inhibitor towards glucose transport in *Saccharomyces bayanus*: the V_{max} remains constant while the K_m increases.

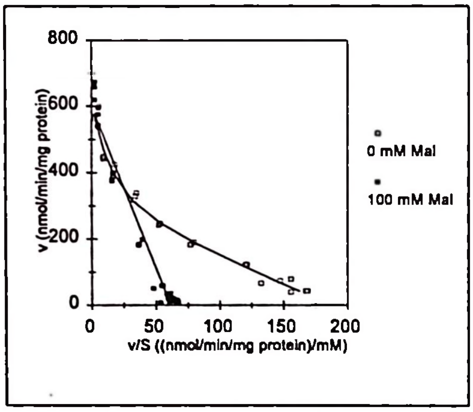

Figure 1. Eadie-Hofstee plot of the inhibition of the zero trans-influx of glucose by maltose in *Saccharomyces bayanus*. Cells of *Saccharomyces bayanus* (IGC 4565) were grown on YEP, 2% glucose to the diauxic shift. Zero *trans*-influx of glucose was measured as described in Materials and Methods in the absence and presence of 100 mM maltose.

B. Comparison of zero trans-influx of glucose and glucose consumption

The rate of glucose consumption was measured at different concentrations of glucose with and without the addition of 100 mM maltose. To compare glucose consumption at a certain glucose concentration with the zero *trans*-influx of glucose at that extracellular glucose concentration, the zero *trans*-influx of glucose at that extracellular glucose concentration was calculated from the kinetic data fitted to a system with two Michaelis-Menten enzymes for glucose transport in the absence of maltose and a system with one component for glucose transport in the presence of maltose.

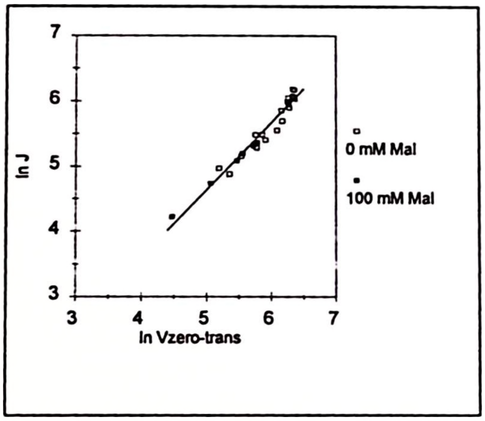

Figure 2. Comparison of the zero *trans*-influx of glucose $v_{zero\text{-}trans}$ with the rate of glucose consumption (J). The zero *trans*-influx of glucose and flux were modulated by varying glucose and maltose. Cells of *Saccharomyces bayanus* (IGC 4565) were grown on YEP, 2% glucose to the diauxic shift. The rate of glucose consumption (J) and the zero *trans*-influx of glucose were measured as described in Materials and Methods in the absence and presence of 100 mM maltose. The consumption rate (J) and the zero *trans*-influx (v) are expressed in nmol · min^{-1} · (mg protein)$^{-1}$.

In fig. 2, the ln($v_{zero\text{-}trans}$) versus ln(J)-plot gives a slope of 1.04 (± 0.04), which suggests all the control of the glycolytic flux to be in the glucose transport step, in other words glucose transport as the rate-limiting step. In the approach used above the glycolytic flux was compared to the zero *trans*-influx of glucose. However, the zero *trans*-influx of glucose is not the actual steady state activity of glucose transport.

C. Determination of the response of the glycolytic flux to a change in the mathematically derived steady state glucose transport activity

The control of the actual glucose transport activity can be derived mathematically, using experimental data (figure 1 and 2), assuming that glucose transport is only connected to the rest of metabolism by the pool of intracellular glucose. Also ATP and G6P have been suggested to effect the glucose transport activity, although no direct evidence has been presented (see for refs. 4). To determine the control of glucose transport activity on the glycolytic flux one has to determine the effect of a small change of the actual steady state glucose transport activity on the glycolytic flux. The actual steady state glucose transport activity was calculated assuming two four state carriers which are only connected to the rest of metabolism by the pool of intracellular glucose (equation 2). The flux control coefficient (figure 3) can now be derived from the division of the response coefficient by the elasticity coefficient (equation 1).

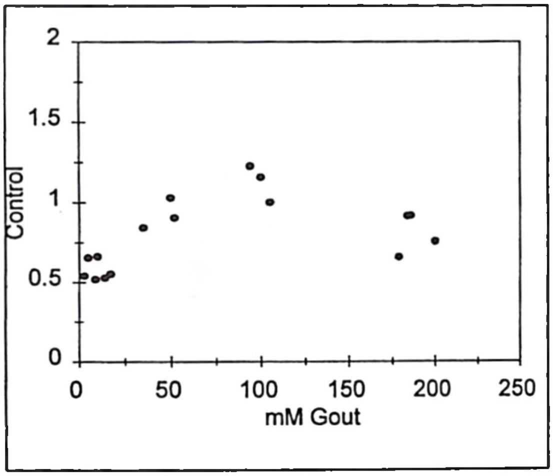

Figure 3. The flux control coefficient ($C^{J}_{v_{trans}}$) of glucose transport activity on the rate of glucose consumption (glycolytic flux) as a function of extracellular glucose (s). Cells of *Saccharomyces bayanus* (IGC 4565) were grown on YEP, 2% glucose to the diauxic shift. The flux control coefficient was obtained by dividing the flux response coefficient by the elasticity coefficient.

The flux control coefficient of the glucose transport step on the glycolytic flux is high (fig. 3). At every extracellular glucose concentration measured at least half of the control of the glycolytic flux is in glucose transport. Flux control coefficients of more than 1 were obtained, however these were probably a consequence of errors in the fitting of the kinetic characteristics of glucose transport and the determination of the rate of glucose consumption. If we varied the concentration of intracellular glucose in the calculation of the elasticity coefficient between 0 and 20% of the extracellular glucose concentration, no considerable effects on the flux control coefficients were obtained. We concluded that the derivation of the flux control coefficient is dependent on the concentration of intracellular glucose, however the flux control coefficient of glucose transport is certainly high (i.e. more than half of the control is in the glucose transport step), under these conditions.

Glucose transport has often been described as an important rate-limiting step of glycolysis in yeast [7], [8], [9], [10], [11]. Strong evidence for this was the demonstration that overproduction of different glycolytic enzymes in the yeast *Saccharomyces cerevisiae* did not result in an increased glycolytic flux [12], [13]. In addition, overexpression of the glycolytic enzymes did not result in significant differences in the concentrations of intracellular metabolites [13]. Also in the present study we confirm, on a more quantitative basis, that the control of glucose transport on the glycolytic flux is high. Both approaches followed show that in cells of *Saccharomyces bayanus*, grown on glucose and harvested at the diauxic shift, most control of the glycolytic flux resides in the transport of glucose across the cell membrane.

ACKNOWLEDGEMENTS

This work was supported by the Foundation for Chemical Research (SON), which is subsidized by the Netherlands Organization for Scientific Research (NWO), and the Netherlands Association for Biotechnological Research Centers (ABON). We also acknowledge the financial support of the European Union, grant no. BIO4 CT950107 of the BIOTECH program.

REFERENCES

1 Kacser, H. and Burns, J.A. (1973) Symp. Soc. Exp. Biol. 27, 65-104.
2 Fell, D.A. (1992) Biochemical J. 286, 313-330.
3 Teusink, B., Walsh, M.C., Van Dam, K., Gustafsson, L. and Westerhoff, H.V. (1996) In 7th International Meeting on Biothermokinetics; p. 417-421; Westerhoff, H.V., Snoep, J.L., Wijker, J.E., Sluse, F.E. and Khlolodenko, B.N. (eds.); BioThermoKinetics Press, Amsterdam.
4 Teusink, B., Diderich, J. A., Westerhoff, H. V., Van Dam, K. & Walsh, M. C. (1998) J. Bacteriol. 180, 556-562.
5 Kotyk, A. (1967) Biochim. Biophys. Acta 135, 112-119.
6 Walsh, M.C., Smits, H.P., Scholte, M. and Van Dam, K. (1994) J. Bacteriol. 176, 953-958.
7 Kotyk, A. and Kleinzeller, A. (1967) Biochim. Biophys. Acta 135, 106 -111.
8 Does, A.L. and Bisson, L.F. (1989) J. Bacteriol. 171, 1303-1308.
9 Gancedo, C. and Serrano, R. (1989) In The yeast; p. 205-259; A.H.Rose and J.S. Harrison (eds.); Academic Press; London.
10 Oehlen, L.J.W.M., Scholte, M.E., De Koning, W. and Van Dam, K. (1994) Microbiol. 140, 1891-1898.
11 Pedler, S., Wallace, P.G., Wallace, J.C. and Berry, M.N. (1997) Yeast 13, 119-125.
12 Heinisch, J. (1986) Mol. Gen. Genet. 202, 75-82.
13 Schaaff, I., Heinisch, J. and Zimmermann, F.K. (1989) Yeast 5, 285-290.

MODELING THE FLUXES OF REDUCING EQUIVALENTS IN MICROAEROBIC RQ-CONTROLLED CONTINUOUS CULTURES OF *SACCHAROMYCES CEREVISIAE*

Carl Johan Franzén and Claes Niklasson

Dept. of Chemical Reaction Engineering, Chalmers University of Technology, S-412 96
Göteborg, Sweden. Ph: +46-(0)31-772 30 96, Fax: +46-(0)31-772 30 35,
Email address: franzen@cre.chalmers.se

INTRODUCTION

Metabolic flux analysis (MFA) is a metabolic modeling method in which the stoichiometry of intracellular reactions is coupled to measurements of a number of steady-state conversion rates, to give information about unknown intracellular reaction rates and net production rates. MFA is one of several tools that can be used in metabolic engineering, or the rational design or improvement of metabolic pathways [1, 2]. When used in conjunction with controlled perturbations of cultivation conditions, MFA can be used for identifying possible rigid branchpoints, identifying the existence of alternative pathways, predicting the effects of introducing new pathways on whole-cell metabolism, and calculation of maximum theoretical yields [2, 3].

In this work, metabolic flux analysis was used to gain detailed information about changes in the intracellular flux distribution as a consequence of variations in the oxygen uptake rate in RQ-controlled microaerobic continuous cultures [4, 5].

METHODS

Experimental

The yeast *Saccharomyces cerevisiae* CBS 8066 was grown on a synthetic medium containing antifoam, ergosterol and oleic acid, with glucose (40 g/l) as carbon and energy source [6]. The respiratory quotient (RQ), defined as the carbon dioxide production rate divided by the oxygen uptake rate, was controlled at values between 6.2 and 50, using the inlet gas composition as control variable [6]. The dilution rate was set between 0.07 h^{-1} and 0.36 h^{-1}. Analyses included the concentrations of 12 extracellular metabolites, total biomass concentration, and cellular contents of protein, RNA, and carbohydrate [5].

Calculations

In metabolic flux analysis, the rates of intracellular reactions, as well as some unknown net production rates, can be calculated from measurements of a number of net production rates. In this work, the reaction network model consisted of 80 metabolites participating in 77 intracellular reactions. 17 metabolites were consumed or produced at nonzero rates, and 63 metabolites were considered to be in pseudo steady state, *i.e.* with net production rates equal to zero. Typically, these were intermediates in various reaction sequences. The model was compartmentalized in a cytosolic and a mitochondrial part. NADH and NADPH consumption and production must be balanced in each compartment [5, 7].

Assuming steady-state conditions, the vector of net specific production rates, **q**, can be calculated from the vector of rates of the intracellular reactions, **r**, by

$$\mathbf{q} = \mathbf{T}^T \mathbf{r} \qquad (1)$$

where **T** is the total stoichiometric matrix, containing the stoichiometric coefficients for all metabolites in the intracellular reactions. In this work, the vector **r** was estimated by minimization of the weighted sum of squares

$$Z = \mathbf{E}^T \mathbf{V}^{-1} \mathbf{E} \qquad (2)$$

where **V** is a diagonal matrix containing the variances of the measured conversion rates, and **E** is the vector of residuals, given by

$$\mathbf{E} = \hat{\mathbf{q}}_m - \mathbf{q}_m . \qquad (3)$$

$\hat{\mathbf{q}}_m$ is the part of the vector of estimated net production rates (Eqn. 1), that corresponds to the measured conversion rates, $\mathbf{q}_m$. The metabolic reaction network was solved by quadratic programming using the minimization routine CONSTR in MATLAB™. Constraints were primarily of the pseudo-steady state asssumption type. Additionally, irreversibility constraints were put on the isocitrate dehydrogenase (IDH) and α-ketoglutarate dehydrogenase reactions, and the net conversion rates of metabolites not initially present in the medium were constrained to be positive.

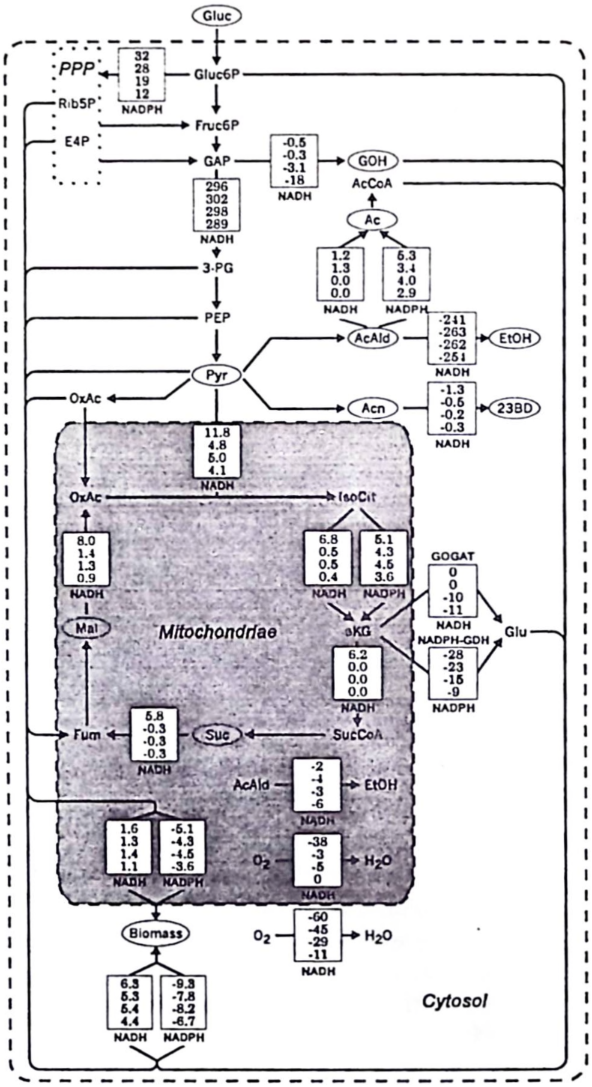

Figure 1. Fluxes of reducing equivalents (mmol g^{-1} h^{-1}) in continuous cultures of S. cerevisiae at 0.15 h^{-1}. Numbers represent (top to bottom) RQ 6.2, 12.5, 17, and 50, and are normalized to a glucose uptake rate of 1 C-mol g^{-1} h^{-1}. Circled metabolites are measured in the culture broth.

RESULTS AND DISCUSSION

Steady-state flux estimations at RQ 6.2, 12.5, 17, and 50, at a dilution rate of 0.15 h^{-1} are shown in Fig. 1, in which the production and consumption of the reducing equivalents NADH and NADPH are presented. With increasing RQ (less aerobic conditions), the activities of the TCA cycle and the pentose phosphate pathway decrease. Whereas NADP-IDH remains active to furnish biosynthesis with mitochondrial NADPH at all RQ values, the activity of NAD-IDH decreases substantially with increasing RQ. At RQ values above 12, malate and succinate are formed from fumarate released in the biosynthesis of amino acids and nucleotides. Moreover, at higher RQ values, glycerol formation commences, and the model predicts an increase in the proportion of glutamate formation via the tentatively active GS-GOGAT system [8-10]. Total respiration decreases with increasing RQ, but the proportion of respiration of cytosolic NADH, via the external NADH dehydrogenase, increases [11]. Furthermore, a slight increase in the mitochondrial alcohol dehydrogenase (ADH) is also predicted, facilitating a balanced mitochondrial NADH pool [7].

Clearly, a wealth of information can be obtained from these calculations. However, these results can also be used to illustrate some of the limitations of MFA. The equation system in Eqn. 1 can, under certain conditions, be solved analytically. Furthermore, if the system is overdetermined and the magnitude of the errors in the measured rates are known, the maximum-likelihood estimate can be found [12, 13]. A problem with these solution methods is that additional constraints, other than the pseudo-steady state assumptions, cannot be included. Minor products, such as acetate, may very well be predicted to be taken up from a medium in which they are not present, or even produced. Furthermore, violations of irreversibility constraints must be dealt with by removing the reaction in question from the network – thus a single model may not be sufficient when operating conditions vary.

To avoid these problems, constrained optimization should be used to solve the system. Since the original problem is a linear equation system, linear optimization is often used. The objective function is often chosen as maximum biomass production rate. Measurements are included as constraints, together with maximum and/or minimum rates and pseudo-steady state assumptions. The solution to a linear programming problem lies on the boundary of at least one variable or constraint, and it is therefore difficult to allow for potential measurement errors in all measured variables. However, for prediction of the effects of *e.g.* genetic changes, this methodology works very well.

Minimizing a quadratic objective function, such as the one used in this work, by means of a nonlinear constrained optimization routine enables the inclusion of all these kinds of constraints, and furthermore, allows for distribution of errors over all estimated production rates. It also makes it possible to test the effects of alternative pathways while still obeying irreversibility constraints – the 'best' network would result in the lowest value of the objective function.

Parallel reactions sometimes become difficult to resolve by MFA. In this work, there are two sets of parallel reactions proceeding with different cofactors, and two sets of reactions proceeding in both compartments. The activity of NADP-IDH is directly governed by the cellular need for mitochondrial NADPH, so the split between NADP-IDH and NAD-IDH is easily determined. However, the split between NAD- and NADP-coupled AlDH is not straightforward. Hypothetically, cytosolic NADPH production can be fully explained by PPP activity. Thus, the split between the two

AlDHs must be resolved by other means. One alternative is to use an NADH balance. In our case, reproducible results (*i.e.*, insensitive to initial guess) could be obtained by adding a penalty for the GOGAT activity in the objective function. This forces the solution towards minimal GOGAT activity [7, 8], and minimizes cytosolic NADH formation, which causes the AlDH activity to move towards NADP-coupled activity at elevated RQ values.

Respiration and ADH activity are present in the mitochondrial as well as in the cytosolic compartments. Therefore, the distribution of respiration between the mitochondrial and external NADH dehydrogenases cannot be uniquely determined. However, omitting any one of these reactions from the network is in contradiction to published data [7, 11, 14].

Validation of a model is a fundamental part of any modeling procedure, and has recently been discussed also in relation to MFA [15, 16]. However, measuring intracellular reaction rates *in vivo* is indeed a complicated task. Enzyme activity measurements, immunoblotting and Northern blotting techniques may give a clue to the presence or absence of certain enzymes and reactions, but cannot be used to give solid support for the actual flux distribution, since both allosteric regulation and concentration effects, *e.g.* the [NADH] / [NADPH] ratio, are neglected in these measurements. Measuring the fractional enrichment of ^{13}C [17] or the isotopomer distributions in intracellular metabolites [18] may facilitate the validation of intracellular reaction rates.

Thus, the information gathered by a metabolic flux analysis should be treated with some caution before solid conclusions can be drawn. Nonetheless, it is a very valuable tool for identifying key areas of metabolism where research efforts must be intensified.

ACKNOWLEDGEMENT

The authors are grateful to Dr. Gunnar Lidén for valuable constructive critique.

REFERENCES

1 Bailey, J.E. (1991) Science 252, 1668-1675.

2 Nielsen, J. (1998) Biotechnol. Bioeng. 58, 125-132.

3 Stephanopoulos, G. and Vallino, J.J. (1991) Science 252, 1675-1681.

4 Franzén, C.J. (1997) Ph.D Thesis, Department of Chemical Reaction Engineering, Chalmers University of Technology, Göteborg, Sweden. ISBN 91-7197-551-9.

5 Franzén, C.J. and Niklasson, C. Biotechnol. Bioeng., Submitted.

6 Franzén, C.J., Albers, E. and Niklasson, C. (1996) Chem. Engng. Sci. 51, 3391-3402.

7 Nissen, T.L., Schulze, U., Nielsen, J., Villadsen, J. (1997) Microbiology 143, 203-218.

8 Avendano, A., Deluna, A., Olivera, H., Valenzuela, L. and Gonzalez, A. (1997) J. Bacteriol. 179, 5594-5597.

9 Filetici, P., Martegani, M.P., Valenzuela, L., Gonzalez, A. and Ballario, P. (1996) Yeast 12, 1359-1366.

10 Folch, J.-L., Antaramamian, A., Rodriguez, L., Bravo, A., Brunner, A. and Gonzalez, A. (1989) J. Bacteriol. 171, 6776-6781.

11 von Jagow, G., Klingenberg, M. (1970) Eur. J. Biochem. 12, 583-592.

12 Nielsen, J. and Villadsen, J. (1994) Bioreaction Engineering Principles, Plenum Press, New York, USA.

13 Tsai, S.P., Lee, Y.H. (1988) Biotechnol. Bioeng. 32, 713-715.

14 Wiesenfeld, M., Schimpfessel, L. and Crokaert, R. (1975) Biochim. Biophys. Acta 405, 500-512.

15 Vanrolleghem, P.A., de Jong-Gubbels, P., van Gulik, W.M., Pronk, J.T., van Dijken, J.P., Heijnen, S. (1996) Biotechnol. Prog. 12, 434-448.

16 Vanrolleghem, P.A. and Heijnen, J.J. (1998) Biotechnol. Bioeng. 58, 133-138.

17 Marx, A., de Graaf, A.A., Wiechert, W., Eggeling, L. and Sahm, H. (1996) Biotechnol. Bioeng. 49, 111-129.

18 Schmidt, K., Carlsen, M., Nielsen, J. and Villadsen, J. (1997) Biotechnol. Bioeng. 55, 8311-840.

MATHEMATICAL MODELLING OF BIOCHEMICAL PATHWAYS

Jens Nielsen

Center for Process Biotechnology, Department of Biotechnology, Building 223,
Technical University of Denmark, DK-2800 Lyngby, Denmark
Tel: +45 4525 2696; Fax: +45 4588 4148; e-mail: jn@ibt.dtu.dk

Metabolic engineering

The concept of metabolic pathway manipulation for the purpose of improving living cells to perform better, in the course of process development, has been used extensively in the past. Thus, improved brewing strains of *Saccharomyces* were obtained through classical methods of sexual hybridization and genetic recombination, and in the production of penicillin by *Penicillium chrysogenum* the productivity increased by more than 10,000 times through repeated rounds of mutation and selection of new strains. With the introduction of recombinant DNA technology it became possible to utilize a more rational approach to strain improvement, since directed genetic modificaton enables more selective breeding to be carried out, without the transference of undesirable characteristics.

The general designation metabolic engineering, which was defined by Bailey (1991) as the improvement of cellular activities by manipulation of enzymatic transport and regulatory functions of the cell with the use of recombinant DNA technology, may well be extended to encompass changes of the process conditions leading to re-orientations of metabolic fluxes. The application of genetic engineering support metabolic engineering by allowing:

1) the insertion of new pathways in microorganisms with the aim of producing novel metabolites (*e.g.* production of polyketides by *Steptomyces*), degrading toxic compounds (*e.g.* in bioremediation), or constructing a novel biotransformation system;
2) the production of heterologous peptides of pharmaceutical interest (*e.g.* human insulin, erythropoitin and tPA) or industrial enzymes (*e.g.* lipases and cellulases);
3) the improvement of pathway fluxes in the direction of the desired product (e.g. increasing the flux towards antibiotic or primary metabolites production, including biomass).

Metabolic engineering implies an integrated approach to the complete study of any living organism as a cell factory and it is, therefore, instrumental in the future development of new bioprocesses as well as in the optimization of the existing ones. What characterizes metabolic engineering is the rational approach to select the cellular and genetic targets upon which to act. As with all other fields of engineering it consists of two steps: *analysis* and *synthesis* (Stephanopoulos *et al.*, 1998). To reach its objectives, it is fundamental to have the concerted input of different disciplines: cell biology, physiology, biochemistry, molecular biology, analytical chemistry and chemical engineering. Identification of the proper genetic changes require a meticulous mapping of the cellular metabolism at different operating conditions. The genetic plasticity of the organism and lack of understanding the complex interactions between entangled metabolic pathways present major complications and have prevented real breakthroughs and more rapid progress in this field.

As a consequence of the difficulties in performing detailed analysis of cellular metabolism, the focus in the recent past has been mainly on synthesis, *e.g.* expression of new genes in various host cells, amplification of endogenous enzymes, and deletion of genes or modulation of enzyme activities. With the steadily refining analytical techniques it is now possible to perform detailed analysis of the cellular functions both through *in vitro* and, mostly important, *in vivo* measurements. Thus there are several examples of *in vivo* measurement of intracellular metabolites using NMR and based on experiments with ^{13}C-enriched carbon sources followed by measurements of the fractional enrichment of ^{13}C in cellular amino acids it is possible to quantify intracellular flux distributions with a high precision. Furthermore, using high performance bioreactors equipped with on-line flow injection analyzers it is possible to monitor cellular metabolism, *i.e.* uptake of substrates and secretion of metabolites, with a high precision and high frequency. Finally, novel sampling techniques now allow rapid sampling and quenching of cellular activity which may lead to precise measurement of intracellular metabolites and co-factors. Thus, with the present techniques it is possible to quantify the two groups of variables that supplies the most fundamental physiological information: *intracellular metabolites* and *metabolic fluxes*. It is expected that with these tools in hands it will in the near future be possible to construct reliable models (both verbal and mathematical models) for even complex pathway networks - at least for a few model organisms. Hereby one can obtain the true integration of the many intracellular reactions that it needed in order to metabolic engineer the cellular function to suit a specific need.

The role of MCA in metabolic engineering

One of the most important aspects of metabolic engineering is *control of flux*, *i.e.* how the rates of synthesis and conversion of metabolites are kept in close balance over a very wide range of external conditions without catastrophic rises or falls in the metabolite concentrations. A powerful technique for evaluation of flux control within biochemical pathways is metabolic control analysis. Its foundation is the so-called elasticity coefficients and flux control coefficients (FCCs). Whereas the elasticity coefficients are properties of the individual enzymes the FCCs are properties of the system. The FCCs can be determined by many different methods, but in this presentation there will be emphasis on the application of mathematical models for analysis of flux control. Using mathematical models for biochemical pathways it is possible not only to calculate the FCCs, but it is also possible to evaluate the effect of introducing large changes in the enzyme activities or to investigate the influence of variations in the substrate concentration.

The application of mathematical models in analysis of flux control has been illustrated by an analysis of the penicillin biosynthetic pathway. Based on a kinetic model for the enzymes in this pathway the FCCs were calculated at different stages of fed-batch cultivations, and a drastic shift in the flux control was observed (Nielsen and Jørgensen, 1995; Pissarra *et al.*, 1996). During the first part of the cultivation the flux control was mainly at the first step in the pathway, *i.e.* the formation of the tripeptide LLD-ACV by ACV synthetase (ACVS), whereas later in the cultivation flux control shifted to the second step in the pathway, *i.e.* the conversion of LLD-ACV to isopenicillin N by isopenicillin N synthetase (IPNS). This shift in flux control was due to intracellular accumulation of LLD-ACV which has been shown to be an inhibitor of ACVS (Theilgaard *et al.* 1997). Obviously it makes no sense to talk about a "rate limiting step" or a "bottleneck enzyme" in this process. Besides the shift in flux control it is interesting to note that most of the flux control was at the two first step in the pathway. Furthermore, through analysis of the kinetic model it was found that the value of the FCCs depends on the dissolved oxygen concentration, which is a substrate in the IPNS catalyzed reaction (Henriksen *et al.*, 1997). In the presentation the model will be extended to include formation of bis-ACV from the free thiol ACV, and the distribution of flux control in the pathway will be calculated with this new model structure.

References

Bailey, J. E. 1991. Science **252**:1668-1674

Henriksen, C. M.; Nielsen, J:; Villadsen, J. 1997. *Biotechnol. Prog.* **13**:776-782

Nielsen, J.; Jørgensen, H. S. 1995. Biotechnol. Prog. **11**:299-305

Pissarra, P. N.; Nielsen, J.; Bazin, M. J. 1996. Biotechnol. Bioeng. **51**:168-176

Theilgaard, H. B. Aa.; Henriksen, C. M.; Kristiansen, K.; Nielsen, J.. 1997. *Biochem. J.* **327**:185-191

LIST OF PARTICIPANTS

Albers, Eva
Dept. Chemical Reaction Engineering,
Chalmers University of Technology, Göteborg,
412 96 Göteborg, Sweden
Tel: 46 31 7723096
Fax: 46 31 7723035
E-mail: eva@cre.chalmers.se
Author pages: 277

AlipQur, Homan
General and Marine Microbiology, Göteborg
University, Lundberglaboratoriet, Box 462, 405
30 Göteborg, Sweden
Tel: 46 31 7732568
Fax: 46 31 7732599
E-mail: homan.alipour@gmm.gu.se
Author pages:

Averet, Nicole
IBGC-CNRS, 1 rue Camille Saint-Saëns 33077
Bordeaux cedex, France
Tel: 33 556 999033
Fax: 33 556 999059
E-mail: Averet@ibgc.u-bordeaux2.fr
Author pages:

Bakker, Barbara, M.
Kluyver Laboratory of Biotechnology, Delft
University of Technology, Julianalaan 67 NL-
2628 BC Delft, The Netherlands
Tel: 31 20 4447228
Fax: 31 20 4447229
E-mail: barbara@chem.uva.nl or
jwijker@bio.vu.nl
Author pages: 66, 240

Beauvoit, Bertrand
IBGC-CNRS, 1 rue Camille Saint-Saëns 33077
Bordeaux cedex, France
Tel: 33 556 999033
Fax: 33 556 999059
E-mail: beauvoit@ibgc.u-bordeaux2.fr
Author pages: 226

Berry, Michael N.
Dept. of Medical Biochemistry, School of
Medicine, Faculty of Health Sciences, Flinders
University, G.P.O. Box 2100, Adelaide 5001,
Australia
Tel: 61 8 82044015
Fax: 61 8 83740139
E-mail: Michael.Berry@flinders.edu.au
Author pages: 317

Blomberg, Anders
Göteborgs Universitet Allmän och Marin
Mikrobiologi, Lundberglaboratoriet Box 462
405 30 Göteborg, Sweden
Tel: 46 31 7732589
Fax: 46 31 7732599
E-mail: Anders.Blomberg@gmm.gu.se
Author pages: 323

Boogerd, Fred C.
Institute for Molecular Biological Sciences,
BioCentrum Amsterdam, Vrije Universiteit, De
Boelelaan 1087 NL-1081 HV Amsterdam, The
Netherlands
Tel: 31 20 4447194
Fax: 31 20 4447229
E-mail: fcb@bio.vu.nl
Author pages: 117

Boubekeur, Samira
IBGC-CNRS, 1 rue Camille Saint-Saëns 33077
Bordeaux cedex, France
Tel: 33 556 999033
Fax: 33 556 999059
E-mail: Boubekeur@ibgc.u-bordeaux2.fr
Author pages: 268

Brand, Martin, D.
Department of Biochemistry, University of
Cambridge, Tennis Court Road, Cambridge,
CB2 1QW, U.K.
Tel: 44 1223 333648
Fax: 44 1223 333345
E-mail: M.D.Brand@Bioc.cam.ac.uk
Author pages: 128, 192

Brightman, Frances
School of Biological and Molecular Sciences,
Oxford Brookes University, Headington,
Oxford, OX3 0BP, U.K.
Tel: 44 1865 483964
Fax: 44 1865 484017
E-mail: 97102742@brookes.ac.uk
Author pages: 375

Bronnikov, Gennady
Stockholm University, Wenner-Gren Institute,
The Arrhenius Lab. F3; Stockholm University,
S-106 91 Stockholm, Sweden
Tel: 46 8 164125
Fax: 46 8 156756
E-mail: gennady@molbio.su.se
Author pages: 231

Brown, Guy C.
Department of Biochemistry, University of
Cambridge, Tennis Court Road , Cambridge
CB2 1QW, U.K.
Tel: 44 1223 333342
Fax: 44 1223 333345
E-mail: gcb@mole.bio.cam.ac.uk
Author pages: 31, 102

Cadenas, Susana
Department of Biochemistry, University of
Cambridge, Tennis Court Road, Cambridge
CB2 1QW, U.K.
Tel: 44 1223 333649
Fax: 44 1223 333345
E-mail: SC268@mole.bio.cam.ac.uk
Author pages: 370

de Winde, J.H.
Laboratory for Molecular Cell Biology, Dept of
Biology, Catholic University of Leuven,
Kardinaal Mercierlaan 92 B-3001 Leuven-
Heverlee, Belgium
Tel: 32 16 321516
Fax: 32 16 321979
E-mail: han.dewinde@bio.kuleuven.ac.be
Author pages: 250

Demin, Oleg
A.N. Belozersky Institute of Phys.-Chem.
Biology, Moscow State University, Dept. of
Bioenergetics, Bldg. A. Vorobjovy Gory ,
Moscow 119899, Russia
Tel: 7 95 9395408
Fax: 7 95 9393181
E-mail: bkhol@energ.genebee.msu.su
Author pages: 196, 211, 365

Devin, Anne
IBGC-CNRS, 1 rue Camille Saint-Saëns 33077
Bordeaux cedex, France
Tel: 33 556 999033
Fax: 33 556 999059
E-mail: Anne.Devin@ibgc.u-bordeaux2.fr
Author pages: 152, 307

Diderich, Jasper
EC Slater Institute, Plantage Muidergracht 12,
NL-1018 TV Amsterdam, The Netherlands
Tel: 31 20 5255069
Fax: 31 20 5255124
E-mail: jad@chem.uva.nl
Author pages: 378

Diolez, Philippe
RMSB, UMR 5536 CNRS / Bordeaux 2, 146
rue Léo-Saignant, F-33076 Boreaux cedex,
France
Tel: 33 557571018
Fax: 33 556961341
E-mail: diolez@rmsb.u-bordeaux2.fr
Author pages: 18

Eaton, Simon
Unit of Paediatric Surgery, Institute of Child
Health & Great Ormond Street Hospital for
Children NHS Trust, University College
London Medical School, 30 Guilford Street,
London WC1N 1EH, U.K.
Tel: 44 171 242 9789, 44 171 242 0719
Fax: 44 171 404 6181
E-mail: s.eaton@ich.ucl.ac.uk
Author pages: 113, 287

Elliot, Keith
School of Biological Sciences, University of
Manchester, Stopford Building, Oxford Road,
Manchester M13, 9PT, U.K.
Tel: 44 161 2755634
Fax: 44 161 2755456
E-mail: keith.elliott@man.ac.uk
Author pages: 113

Fell, David A
School of Biological & Molecular Sciences,
Oxford Brookes University, Gipsy Lane
Headington, Oxford OX3 0BP, UK
Tel: 44 1865 483247
Fax: 44 1865 484017
E-mail: daf@bms.brookes.ac.uk
Author pages: 41, 46, 332, 375

Franzén, Carl Johan
Dept. Chemical Reaction Engineering,
Chalmers University of Tecnology, S-412 96
Göteborg, Sweden
Tel: 46 31 7723096
Fax: 46 31 7723035
E-mail: franzen@cre.chalmers.se
Author pages: 383

Fuchs, Anita
OROBOROS / Bioenergetics and Biomedical
Instruments, Schoepfstr. 18, A-6020 Innsbruck,
Austria
Tel: 43 512 566796
Fax: 43 512 566796
E-mail: anita.fuchs@uibk.ac.at
Author pages: 89

Garlid, Keith D.
Oregon Graduate Institute of Science and
Technology, P.O. Box 91000, Portland, OR
97291-1000, USA
Tel: 1 503 690 1680
Fax: 1 503 690 1464
E-mail: garlid@bmb.ogi.edu
Author pages:

Geukes, Foppen R.J.
Institute of Neurosciences, Fac. of Biology,
University of Amsterdam, Kruislaan 320, 1098
SM Amsterdam, The Netherlands
Tel: 31 20 5257642
Fax: 31 20 6659125
E-mail: foppen@bio.uva.nl
Author pages: 221, 300

Giersch, Christoph
Institut für Botanik, Technische Universitaet,
Schnittspahnstr. 3-5, D-64287 Darmstadt,
Germany
Tel: 49 6151 16 4024
Fax: 49 6151 16 4630
E-mail: giersch@bio.tu-darmstadt.de
Author pages: 76

Gnaiger, Erich
Department of Transplant Surgery, D.
Swarovski Research Laboratory, Anichstr. 35,
University Hospital Innsbruck, A-6020
Innsbruck, Austria
Tel: 43 512 504 4623
Fax: 43 512 504 4625
E-mail: erich.gnaiger@uibk.ac.at
Author pages: 81, 89, 273, 312

Goryanin, Igor
ATI, 6F207, Glaxo Wellcome, Research
Medicine Centre, Gunnels Wood Road,
Stevenage, Herts, SG1 2NY, U.K.
Tel: 44 1438 764022
Fax: 44 1438 763082
E-mail: gzz78923@ggr.co.uk
Author pages:

Goryn, Oksana
Ivan Franko Lviv State University, Str. I.
Franko 48 # 7 290005 Lviv, Ukraine
Tel: 380 322745637
Fax:
E-mail: oksana@mitoch.lviv.ua
Author pages: 329

Gustafsson, Lena
Göteborgs Universitet Allmän och Marin
Mikrobiologi, Lundberglaboratoriet Box 462
405 30 Göteborg, Sweden
Tel: 46 31 7732597
Fax: 46 31 7732599
E-mail: Lena.Gustafsson@gmm.gu.se
Author pages: 277, 323

Görgens, Johann F.
Teknisk Mikrobiologi, Lunds Universitet, P.O.
Box 124, S-221 00 Lund, Sweden
Tel: 46 46 2228325
Fax: 46 46 2224203
E-mail: johann.gorgens@tmb.lth.se
Author pages:

Haberichter, Thomas
Institute of Biology, Humboldt University,
Theoretical Biophysics, Invalidenstrasse 42,
10115 Berlin, Germany
Tel: 49 30 20938694
Fax: 49 30 20938813
E-mail: haberich@bp.biologie.hu-berlin.de
Author pages: 96

Heinrich, Reinhart
Institute of Biology, Humboldt University,
Theoretical Biophysics, Invalidenstrasse 42,
10115 Berlin, Germany
Tel: 49 30 20938698
Fax: 49 30 20938813
E-mail: reinhart=heinrich@rz.hu-berlin.de
Author pages: 71, 96, 186, 350

Hoerter, Jacqueline
INSERM U-446, Faculté Pharmacie, 5 rue J.B.
Clément, F-92296 Châtenay Malabry, France
Tel: 33 146 835759
Fax: 33 146 835475
E-mail: Jacqueline.Hoerter@cep.u-psud.fr
Author pages:

Hofmeyr, Jan-Hendrik Servaas
Dept. of Biochemistry, University of
Stellenbosch, Private Bag X1, Matieland 7602,
South Africa
Tel: 27 21 8083039
Fax: 27 21 8083022
E-mail: jhsh@maties.sun.ac.za
Author pages: 7, 340

Jeneson, Jeroen A.L.
Dept. of Radiology, University of Washington
Medical Center, School of Medicine, Box
357115, Seattle WA 98195 USA
Tel: 1 206 685 2805
Fax: 1 206 543 3495
E-mail: utrecht@u.Washington.edu
Author pages: 179, 183

Jensen R. Peter
Department of Microbiology, The Technical
University of Denmark, Building 301, DK-2800
Lyngby, Denmark.
Tel: 45 4525 2510
Fax: 45 4593 2809
E-mail: PRJ@im.dtu.dk
Author pages: 11, 117, 157, 171, 205, 215, 261

Keerberg, Olav
Institute of Experimental Biology,Estonian
Agricultural University, EE 3051 Harku,
Estonia
Tel: 372 2 512489
Fax: 372 2 512489
E-mail: olav@ebi.ee
Author pages: 303

Kell, Douglas B.
Cledwyn Building, Institute of Biological
Sciences, University of Wales, Aberystwyth
SY23 3DA, U.K.
Tel: 44 1970 622334
Fax: 44 1970 622354
E-mail: dbk@aber.ac.uk
Author pages: 345

Kemp, Graham J.
Dept. of Orthopaedic & Accident Surgery,
University of Liverpool, Liverpool L69 3GA,
U.K.
Tel: 44 151 706 4124
Fax: 44 151 706 5815
E-mail: gkemp@liv.ac.uk
Author pages: 200

Keyhani, Ezzatollah
Institute for Biochemistry and Biophysics,
University of Tehran, P.O. Box 13148 - 1384
Tehran, I.R. Iran
Tel: 8 21 611 3373
Fax: 8 21 640 4680
E-mail: Keyhanie@ibb.ut.ac.ir
Author pages: 175, 236

Kholodenko, Boris N.
Dept. of Pathology Anatomy and Cell Biology,
Thomas Jefferson University, Jefferson Alumni
Hall, Rm 271 1020 Locust Street, Philadelphia,
PA 19107-6799, USA
Tel: 1 215 5035022 1 215 5035016
Fax: 1 215 9232218
E-mail: Kholode1@jeflin.tju.edu
Author pages: 1, 50, 102, 108, 137, 365

Klipp, Edda
Institute of Biology, Humboldt University,
Theoretical Biophysics, Invalidenstrasse 42,
10115 Berlin, Germany
Tel: 49 30 20938383
Fax: 49 30 20938813
E-mail: edda=klipp@rz.hu-berlin.de
Author pages: 27

Koefoed, Sarah
Dept. of Molecular Cell Physiology,
BioCentrum, Faculty of Biology, Vrije
Universiteit, De Boelelaan 1087 NL-1081 HV
Amsterdam, The Netherlands
Tel: 31 20 4447192
Fax: 31 20 4447229
E-mail: saark@bio.vu.nl
Author pages: 171

Komarova, Svetlana
NASA Ames Research Center, M-S 236-7
Moffett Field, CA 94035-1000, USA
Tel: 1 650 6046390
Fax: 1 650 6045931
E-mail: skomarova@mail.arc.nasa.gov
Author pages: 58, 62

Korzeniewski, Bernard
Institute of Molecular Biology, Jagiellonian
University, al. Mickiewicza 3, 31-120 Krakov,
Poland
Tel: 48 12 6341305
Fax: 48 12 6336907
E-mail: benio@mol.uj.edu.pl
Author pages:

Krauss, Stefan
Dept. of Biochemistry, University of
Cambridge, Tennis Court Road, Cambridge,
CB2 1QW, U.K.
Tel: 44 1223 333649
Fax: 44 1223 333345
E-mail: sk@mole.bio.cam.ac.uk
Author pages: 128

Kunz, Wolfram S.
Department of Epileptology, University of Bonn
Medical Center, Sigmund - Freud Str. 25, D-53105 Bonn, Germany
Tel: 49 228 2876110
Fax: 49 228 2876294
E-mail: Kunz@mailer.meb.uni-bonn.de
Author pages: 123

Kurgaliuk, Natalia
Biology Department, Ivan Franko Lviv State
University, Hrushevsky Str. 4 Lviv 290005
Ukraine
Tel: 380 322794786
Fax:
E-mail: natalia@mitoch.lviv.ua
Author pages: 329

Kushmerick, Martin J.
Departements of Radiology, Bioengineering,
Physiology and Biophysics, UW Mail Box
357115, University Washington Medical
Center, Room AA 010K1959 NE Pacific Ave,
Seattle, WA 98195-7115, USA
Tel: 1 206 543 3762
Fax: 1 206 543 3495
E-mail: kushmeri@u.washington.edu
Author pages: 179

Kuznetzov, Andrey
Department of Transplant Surgery, D.
Swarovski Research Laboratory, Anichstr. 35,
University Hospital Innsbruck, A-6020
Innsbruck, Austria
Tel: 43 512504 4626
Fax: 43 512 504 4625
E-mail: andrei.kuznetsov@uibk.ac.at
Author pages: 81, 89, 273, 312

Köbmann, Brian J.
Department of Microbiology, The Technical
University of Denmark, Building 301, DK-2800
Lyngby, Denmark.
Tel: 45 4525 2497
Fax: 45 4593 2809
E-mail: bk@im.dtu.dk
Author pages: 11, 205

Lankelma, Jan
Dept. Medical Oncology, Free University
Hospital, Room BR230, P.O. Box 7057, 1007
MB Amsterdam, The Netherlands
Tel: 31 20 4442603
Fax: 31 20 4443844
E-mail: J.Lankelma@azvu.nl
Author pages: 163

Larsson, Christer
Göteborgs Universitet, Allmän och Marin
Mikrobiologi, Lundberglaboratoriet Box 462,
405 30 Göteborg, Sweden
Tel: 46 31 7732579
Fax: 46 31 7732599
E-mail: Christer.Larsson@gmm.gu.se
Author pages: 323

Lassnig, Barbara
Department of Transplant Surgery, D.
Swarovski Research Laboratory, Anichstr. 35,
University Hospital Innsbruck, A-6020
Innsbruck, Austria
Tel: 43 512 504 4624
Fax: 43 512 504 4625
E-mail: barbara.lassnig@uibk.ac.at
Author pages: 81, 89, 273, 312

Lebedeva, Galina
Biological Department, Section of Biophysics
Moscow State University, Vorobjovy Gory,
Moscow 119 899 Russia
Tel: 7 95939 1963
Fax: 7 95 939 1115
E-mail: lebed@biophys.msu.ru
Author pages: 196

Leducq, Nathalie
RMSB, UMR 5536 CNRS / Bordeaux 2, 146
rue Léo-Saignant, F-33076 Boreaux cedex,
France
Tel: 33 557571018
Fax: 33 556961341
E-mail: leducq@rmsb.u-bordeaux2.fr
Author pages: 18

Lidén, Gunnar
Dept. Chemical Reaction Engineering,
Chalmers University of Technology, Göteborg,
412 96 Göteborg, Sweden
Tel: 46 31 7723039
Fax: 46 31 7723035
E-mail: liden@cre.chalmers.se
Author pages:

Malgat, Monique
INSERM CJF 9705, Université Bordeaux 2, 146
rue Leo-Saignat F-33076 Bordeaux - Cedex,
France
Tel: 33 557 571379
Fax: 33 557 571612
E-mail: m.malgat@gesbi.u-bordeaux2.fr
Author pages:

Martinov, Michael V.
Russian Research Center for Hematology,
Novozykovsky proezd 4a, 125167 Moscow,
Russia
Tel: 7 95 2123522
Fax: 7 95 2128870
E-mail: MICK@BLOOD.RU
Author pages: 355, 360

Matthias, Anita
Stockholm University, The Wenner-Gren
Institute, The Arrhrenius Lab. F3; S-106 91
Stockholm, Sweden
Tel: 46 8 164122
Fax: 46 8 156756
E-mail: anita@zoofys.su.se
Author pages: 291

Mazat, Jean-Pierre
INSERM CJF 9705, Université Bordeaux 2, 146
rue Leo-Saignat F-33076 Bordeaux - Cedex,
France
Tel: 33 557 571379
Fax: 33 557 571612
E-mail: jpm@u-bordeaux2.fr
Author pages: 295

Mendes, Pedro
Institute of Biological Sciences, University of
Wales, Aberystwyth, Ceredigion SY23 3DD,
U.K.
Tel: 44 1970 622353
Fax: 44 1970 622354
E-mail: prm@aber.ac.uk
Author pages: 345

Mildaziene, Vida
Institute of Biomedical Research, Kaunas
Biomedical Academy, Eiveniu st 4, 3007
Kaunas, Lithuania
Tel: 370 7 734614
Fax: 370 7 796498
E-mail: bioch@kma.lt
Author pages: 137, 147

Nartsissov, Yaroslav R.
Medical Scientific & Production Complex
"Biotics", P.O. Box 39, Moscow 113 452 Russia
Tel:
Fax: 7 95 3220074
E-mail: yarosl@biotic.dol.ru
Author pages: 50, 54

New, Karen
c/o Quant Patti Ann, Unit of Paediatric
Surgery,Institute of Child Health & Great
Ormond Street Hospital for Children NHS,
Trust, University College London Medical
School 30 Guilford Street, London WC1N 1EH,
U.K.
Tel: 44 171 242 9782, 44 171 242 2254
Fax: 44 171 4046181
E-mail: k.new@ich.ucl.ac.uk
Author pages: 113

Nicholls, Peter
Dept. of Biological Sciences, Central Campus,
University of Essex, Wivenhoe Park, Colchester
Essex, CO4 3SQ, U.K.
Tel: 44 1206 873776
Fax: 44 1206 872592
E-mail: pnicholl@essex.ac.uk
Author pages: 282

Nielsen, Jens
Center for Process Biotechnology, Dept. of
Biotechnology, Building 223, Technical
University of Denmark, DK-2800 Lyngby,
Denmark
Tel: 45 4525 2696
Fax: 45 4588 4148
E-mail: jn@ibt.dtu.dk
Author pages: 22, 35, 388

Niklasson, Claes
Dept. Chemical Reaction Engineering,
Chalmers University of Technology, Göteborg,
412 96 Göteborg, Sweden
Tel: 46 31 7723027
Fax: 46 31 7723035
E-mail: claes@cre.chalmers.se
Author pages: 383

Nilsson, Annika
Göteborgs Universitet Allmän och Marin Mikrobiologi, Lundberglaboratoriet Box 462
405 30 Göteborg, Sweden
Tel: 46 31 7732585
Fax: 46 31 7732599
E-mail: Annika.Nilsson@gmm.gu.se
Author pages: 323

Nogueira, Veronique
Laboratoire de Bioenergetique Fundamentale et Appliquee, Universite' Joseph Fourier Bat 72, Biologie, BP 53X - 38041, Grenoble Cedex
France,
Tel: 33 67 6635625
Fax: 33 67 6514218
E-mail: Veronique.Nogueira@ujf-grenoble.fr
Author pages: 152

Olsson, Lisbeth
Center for Process Biotechnology, Dept.of Biotechnology, Building 223, Technical University of Denmark, DK-2800 Lyngby,
Denmark
Tel: 45 4525 2677
Fax: 45 4588 4148
E-mail: LO@IBT.DTU.DK
Author pages: 22

Otten, Marijke F.
Dept. of Molecular Cell Physiology, BioCentrum, Faculty of Biology, Vrije Universiteit, De Boelelaan 1087 NL-1081 HV
Amsterdam, The Netherlands
Tel: 31 20 4447183
Fax: 31 20 4447229
E-mail: mfotten@bio.vu.nl
Author pages: 142

Patil, Kalpana
Unit of Paediatric Surgery, Institute of Child Health & Great Ormond Street Hospital for Children NHS Trust, University College London Medical School, 30 Guilford Street,
London WC1N 1EH, U.K.
Tel: 44 181 672 1255
Fax: 44 181 672 5304
E-mail:
Author pages: 287

Paulik, Mark
Glaxo Wellcome, Inc, 3-2075, 5 Moore Drive,
Research Triangle Park, NC 27509, USA
Tel: 1 919 483 5854
Fax: 1 919 483 5691
E-mail: map16209@glaxowellcome.com
Author pages: 256

Pedersen , Martin Bastian
Department of Microbiology, The Technical University of Denmark, Building 301, DK-2800
Lyngby, Denmark.
Tel: 45 4525 2281
Fax: 45 4593 2809
E-mail: mbp@im.dtu.dk
Author pages: 11, 215, 261

Pokhilko, Alexandra
Research Center for Hematology,
Novozykovskij pr. 4a, Moscow, 125167 Russia
Tel: 70952125531
Fax: 70952128870
E-mail: fazli@blood.ru
Author pages:

Påhlman, Anna-Karin
Göteborgs Universitet Allmän och Marin Mikrobiologi, Lundberglaboratoriet Box 462,
495 30 Göteborg, Sweden
Tel: 46 31 7732580
Fax: 46 31 7732599
E-mail: Anna-Karin.Pahlman@gmm.gu.se
Author pages:

Påhlman, Inga-lill
Göteborgs Universitet Allmän och Marin Mikrobiologi, Lundberglaboratoriet Box 462,
405 30 Göteborg, Sweden
Tel: 46 31 7732581
Fax: 46 31 7732599
E-mail: Inga-lill.Pahlman@gmm.gu.se
Author pages: 323

Quant, Patti Ann
Unit of Paediatric Surgery, Institute of Child Health & Great Ormond Street Hospital for Children NHS Trust, University College London Medical School, 30 Guilford Street, London WC1N 1EH, U.K.
Tel: 44 171 2429789, 44 171 2422136
Fax: 44 171 4046181
E-mail: P.Quant@ich.ucl.ac.uk
Author pages: 113, 287

Raamsdonk, Leonie
E.C. Slater Institute, University of Amsterdam, Plantage Muidergracht 12, 1018 TV Amsterdam, The Netherlands
Tel: 31 20 5255069
Fax: 31 20 5255124
E-mail: Leonie@chem.uva.nl
Author pages: 167

Rabkin, Brian
NASA Ames Research Center, M-S 236-7
Moffett Field, CA 94035-1000, USA
Tel: 1 650 604 6390
Fax: 1 650 604 3159
E-mail:
Author pages: 58, 62

Reijenga, C.A.
Dept. of Molecular Cell Physiology, BioCentrum, Faculty of Biology, Vrije Universiteit, De Boelelaan 1087 NL-1081 HV Amsterdam, The Netherlands
Tel: 31 20 4447195
Fax: 31 20 4447229
E-mail: reijenga@bio.vu.nl
Author pages: 246

Rigoulet, Michel
IBGC-CNRS, 1 rue Camille Saint-Saëns F-33077 Bordeaux cedex, France
Tel: 33 5 56 999040
Fax: 33 5 56 999059
E-mail: Michel.Rigoulet@ibgc.u-bordeaux2.fr
Author pages: 152, 226, 268, 307

Rohwer, Johann M.
Dept. of Biochemistry, University of Stellenbosch, Private Bag X1, Matieland 7602, South Africa
Tel: 27 21 8083029
Fax: 27 21 8083022
E-mail: jr@land.sun.ac.za
Author pages: 7, 340

Rossignol, Rodrique
INSERM CJF 9705, Université Bordeaux 2, 146, rue Leo-Saignat 33076 Bordeaux - Cedex, France
Tel: 33 5 57 571379
Fax: 33 5 57 571612
E-mail: rossig@hippocrate.u-bordeaux2.fr
Author pages:

Schuster, Stefan
Max Delbrück Center for Molecular Medicine, Dept. of Bioinformatics, Robert-Rössle-Str.10, D-13 125 Berlin-Buch, Germany
Tel: 49 30 94063125
Fax: 49 30 94062834
E-mail: schuster@bp.biologie.hu-berlin.de
Author pages: 332

Selivanov, Vitalii A.
INSERM CJF 9705, Université Bordeaux 2, 146 rue Leo-Saignat F-33076 Bordeaux - Cedex, France
Tel: 33 5 57 571379
Fax: 33 5 57 571612
E-mail: seliv@u-Bordeaux2.fr
Author pages: 295

Siegenbeek van Heukelom J.
Institute of Neurosciences, Fac. Biology, University of Amsterdam, Kruislaan 320, 1098 SM Amsterdam, The Netherlands
Tel: 31 20 5257642
Fax: 31 20 6659125
E-mail: siegenbeek@bio.uva.nl
Author pages: 221, 300

Nilsson, Annika
Göteborgs Universitet Allmän och Marin
Mikrobiologi, Lundberglaboratoriet Box 462
405 30 Göteborg, Sweden
Tel: 46 31 7732585
Fax: 46 31 7732599
E-mail: Annika.Nilsson@gmm.gu.se
Author pages: 323

Nogueira, Veronique
Laboratoire de Bioenergetique Fundamentale et
Appliquee, Universite' Joseph Fourier Bat 72,
Biologie, BP 53X - 38041, Grenoble Cedex
France,
Tel: 33 67 6635625
Fax: 33 67 6514218
E-mail: Veronique.Nogueira@ujf-grenoble.fr
Author pages: 152

Olsson, Lisbeth
Center for Process Biotechnology, Dept.of
Biotechnology, Building 223, Technical
University of Denmark, DK-2800 Lyngby,
Denmark
Tel: 45 4525 2677
Fax: 45 4588 4148
E-mail: LO@IBT.DTU.DK
Author pages: 22

Otten, Marijke F.
Dept. of Molecular Cell Physiology,
BioCentrum, Faculty of Biology, Vrije
Universiteit, De Boelelaan 1087 NL-1081 HV
Amsterdam, The Netherlands
Tel: 31 20 4447183
Fax: 31 20 4447229
E-mail: mfotten@bio.vu.nl
Author pages: 142

Patil, Kalpana
Unit of Paediatric Surgery, Institute of Child
Health & Great Ormond Street Hospital for
Children NHS Trust, University College
London Medical School, 30 Guilford Street,
London WC1N 1EH, U.K.
Tel: 44 181 672 1255
Fax: 44 181 672 5304
E-mail:
Author pages: 287

Paulik, Mark
Glaxo Wellcome, Inc, 3-2075, 5 Moore Drive,
Research Triangle Park, NC 27509, USA
Tel: 1 919 483 5854
Fax: 1 919 483 5691
E-mail: map16209@glaxowellcome.com
Author pages: 256

Pedersen , Martin Bastian
Department of Microbiology, The Technical
University of Denmark, Building 301, DK-2800
Lyngby, Denmark.
Tel: 45 4525 2281
Fax: 45 4593 2809
E-mail: mbp@im.dtu.dk
Author pages: 11, 215, 261

Pokhilko, Alexandra
Research Center for Hematology,
Novozykovskij pr. 4a, Moscow, 125167 Russia
Tel: 70952125531
Fax: 70952128870
E-mail: fazli@blood.ru
Author pages:

Påhlman, Anna-Karin
Göteborgs Universitet Allmän och Marin
Mikrobiologi, Lundberglaboratoriet Box 462,
495 30 Göteborg, Sweden
Tel: 46 31 7732580
Fax: 46 31 7732599
E-mail: Anna-Karin.Pahlman@gmm.gu.se
Author pages:

Påhlman, Inga-lill
Göteborgs Universitet Allmän och Marin
Mikrobiologi, Lundberglaboratoriet Box 462,
405 30 Göteborg, Sweden
Tel: 46 31 7732581
Fax: 46 31 7732599
E-mail: Inga-lill.Pahlman@gmm.gu.se
Author pages: 323

Quant, Patti Ann
Unit of Paediatric Surgery, Institute of Child Health & Great Ormond Street Hospital for Children NHS Trust, University College London Medical School, 30 Guilford Street, London WC1N 1EH, U.K.
Tel: 44 171 2429789, 44 171 2422136
Fax: 44 171 4046181
E-mail: P.Quant@ich.ucl.ac.uk
Author pages: 113, 287

Raamsdonk, Leonie
E.C. Slater Institute, University of Amsterdam, Plantage Muidergracht 12, 1018 TV Amsterdam, The Netherlands
Tel: 31 20 5255069
Fax: 31 20 5255124
E-mail: Leonie@chem.uva.nl
Author pages: 167

Rabkin, Brian
NASA Ames Research Center, M-S 236-7
Moffett Field, CA 94035-1000, USA
Tel: 1 650 604 6390
Fax: 1 650 604 3159
E-mail:
Author pages: 58, 62

Reijenga, C.A.
Dept. of Molecular Cell Physiology, BioCentrum, Faculty of Biology, Vrije Universiteit, De Boelelaan 1087 NL-1081 HV Amsterdam, The Netherlands
Tel: 31 20 4447195
Fax: 31 20 4447229
E-mail: reijenga@bio.vu.nl
Author pages: 246

Rigoulet, Michel
IBGC-CNRS, 1 rue Camille Saint-Saëns F-33077 Bordeaux cedex, France
Tel: 33 5 56 999040
Fax: 33 5 56 999059
E-mail: Michel.Rigoulet@ibgc.u-bordeaux2.fr
Author pages: 152, 226, 268, 307

Rohwer, Johann M.
Dept. of Biochemistry, University of Stellenbosch, Private Bag X1, Matieland 7602, South Africa
Tel: 27 21 8083029
Fax: 27 21 8083022
E-mail: jr@land.sun.ac.za
Author pages: 7, 340

Rossignol, Rodrique
INSERM CJF 9705, Université Bordeaux 2, 146, rue Leo-Saignat 33076 Bordeaux - Cedex, France
Tel: 33 5 57 571379
Fax: 33 5 57 571612
E-mail: rossig@hippocrate.u-bordeaux2.fr
Author pages:

Schuster, Stefan
Max Delbrück Center for Molecular Medicine, Dept. of Bioinformatics, Robert-Rössle-Str.10, D-13 125 Berlin-Buch, Germany
Tel: 49 30 94063125
Fax: 49 30 94062834
E-mail: schuster@bp.biologie.hu-berlin.de
Author pages: 332

Selivanov, Vitalii A.
INSERM CJF 9705, Université Bordeaux 2, 146 rue Leo-Saignat F-33076 Bordeaux - Cedex, France
Tel: 33 5 57 571379
Fax: 33 5 57 571612
E-mail: seliv@u-Bordeaux2.fr
Author pages: 295

Siegenbeek van Heukelom J.
Institute of Neurosciences, Fac. Biology, University of Amsterdam, Kruislaan 320, 1098 SM Amsterdam, The Netherlands
Tel: 31 20 5257642
Fax: 31 20 6659125
E-mail: siegenbeek@bio.uva.nl
Author pages: 221, 300

Snoep, Jacky
Dept. of Molecular Cell Physiology,
BioCentrum, Faculty of Biology, Vrije
Universiteit, De Boelelaan 1087 NL-1081 HV
Amsterdam, The Netherlands
Tel: 31 20 4447192
Fax: 31 20 4447229
E-mail: js@bio.vu.nl
Author pages: 97, 157, 171, 205, 240, 246

Soboll, Sibylle
Institut für Physiologische Chemie I, Heinrich
Heine Universität, Universitätsstrasse 1, 40225
Düsseldorf, Germany
Tel: 49 211 81 3029
Fax: 49 211 81 2834
E-mail: Sibylle.soboll@uni-duesseldorf.de
Author pages:

Somsen, Oscar
Dept. of Molecular Cell Physiology, Faculty of
Biology, Vrije Universiteit, De Boelelaan 1087
NL-1081 HV Amsterdam, The Netherlands
Tel: 31 20 4447195
Fax: 31 20 4447229
E-mail: oscar@bio.vu.nl
Author pages: 1, 97

Stephani, Amadeus
Institute of Biology, Humboldt University,
Theoretical Biophysics, Invalidenstrasse 42,
10115 Berlin, Germany
Tel: 49 30 20938381
Fax: 49 30 20938813
E-mail: amadeus=stephani@rz.hu-berlin.de
Author pages: 186

Teusink, Bas
EC Slater Institute, Plantage Muidergracht 12,
NL-1018 TV Amsterdam, The Netherlands
Tel: 31 20 5255069
Fax: 31 20 5255124
E-mail: a311bt@chem.uva.nl
Author pages: 240, 246

Theilgaard, Hanne Aae
Center for Process Biotechnology, Dept. of
Biotechnology, Building 223, Technical
University of Denmark, DK-2800 Lyngby,
Denmark
Tel: 45 4525 2681
Fax: 45 4588 4148
E-mail: ht@ibt.dtu.dk
Author pages: 35

Thomas, Simon
School of Biological and Molecular Sciences,
Oxford Brookes University, Gipsy Lane,
Headington, Oxford, OX3 0BP, U.K.
Tel: 44 1865 483964
Fax: 44 1865 484017
E-mail: simon@bms.brookes.ac.uk
Author pages: 41, 46

Thornton, Roy J
E & J Gallo Winery P.O. Box 1130, Modesto,
CA 95355, USA
Tel: 1 209 341 7054
Fax: 1 209 341 7067
E-mail: Roy.Thornton@ejgallo.com
Author pages:

Valadi, Hadi
Göteborgs Universitet Allmän och Marin
Mikrobiologi, Lundberglaboratoriet Box 462
405 30 Göteborg, Sweden
Tel: 46 31 7732585
Fax: 46 31 7732599
E-mail: Hadi.valadi@gmm.gu.se
Author pages:

van Dam, Karel
EC Slater Institute, Plantage Muidergracht 12,
NL-1018 TV Amsterdam, The Netherlands
Tel: 31 20 5255125
Fax: 31 20 5255124
E-mail: a311vdam@chem.uva.nl
Author pages: 167, 240, 378

van der Gugten, Anton
Netherlands Cancer Institute, Plesmanlaan 121,
NL-1066 CX Amsterdam, The Netherlands
Tel: 31 20 5122024
Fax: 31 20 5122029
E-mail: tgugt@nki.nl
Author pages:

Vasenko, Andrew
A.N. Belozersky Institute of Phys.-Chem.
Biology, Moscow State University, Dept. of
Bioenergetics, Vorobjovy Gory , Moscow
119899, Russia
Tel:
Fax: 7 95 9393181
E-mail: bkhol@energ.genebee.msu.su
Author pages: 211

Westerhoff, Hans V.
Dept. of Molecular Cell Physiology,
BioCentrum, Faculty of Biology, Vrije
Universiteit, De Boelelaan 1087 NL-1081 HV
Amsterdam, The Netherlands
Tel: 31 20 4447228, 31 20 4447230
Fax: 31 20 4447229
E-mail: hw@bio.vu.nl
Author pages: 1, 66, 97, 102, 108, 142, 157,
163, 167, 171, 179, 205, 240, 246, 365

Winterberg, Andersen Heidi
Department of Microbiology, The Technical
University of Denmark, Building 301, DK-2800
Lyngby, Denmark.
Tel: 45 4525 2527
Fax: 45 4588 2660
E-mail: hwa@im.dtu.dk
Author pages: 11, 157, 215, 261

Wiseman, Robert W.
Dept. of Radiology, University of Washington
Medical Center, Scool of Medicine, Box
357115, Seattle WA 98195 - USA
Tel: 1 206 685 1262
Fax: 1 206 543 3495
E-mail: rwiseman@u.washington.edu
Author pages: 179, 183

Vitvitsky, Victor M.
Russian Research Center for Hematology,
Novozykovsky proezd 4a, 125167 Moscow,
Russia
Tel: 7 95 2123522
Fax: 7 95 2128870
E-mail: victor@blood.ru
Author pages: 355, 360

Wolf, Jana
Institute of Biology, Humboldt University,
Theoretical Biophysics, Invalidenstrasse 42,
10115 Berlin, Germany
Tel: 49 30 20938494
Fax: 49 30 20938813
E-mail: jana=Wolf@rz.hu-berlin.de
Author pages: 71

Zarnitsina, Veronika
Scientific Center for Hematology,
Novozykovsky 4a, Moscow, 125167 Russia
Tel: 7 95 2123522
Fax: 7 95 2128870
E-mail: inf@issep.msk.su
Author pages: 132

Östergaard, Simon
Center for Process Biotechnology, Department
of Biotechnology, Building 223, Technical
University of Denmark, DK-2800 Lyngby,
Denmark
Tel: 45 4522 683
Fax: 45 4588 4148
E-mail: SIOS@IBT.DTU.DK
Author pages: 22